



Durham E-Theses

Mechanism-Guided Studies of Brønsted Acid and Base Organocatalysis

LINDSAY, ANITA,GERALDINE

How to cite:

LINDSAY, ANITA,GERALDINE (2010) *Mechanism-Guided Studies of Brønsted Acid and Base Organocatalysis*, Durham theses, Durham University. Available at Durham E-Theses Online: <http://etheses.dur.ac.uk/314/>

Use policy

The full-text may be used and/or reproduced, and given to third parties in any format or medium, without prior permission or charge, for personal research or study, educational, or not-for-profit purposes provided that:

- a full bibliographic reference is made to the original source
- a [link](#) is made to the metadata record in Durham E-Theses
- the full-text is not changed in any way

The full-text must not be sold in any format or medium without the formal permission of the copyright holders.

Please consult the [full Durham E-Theses policy](#) for further details.

Academic Support Office, Durham University, University Office, Old Elvet, Durham DH1 3HP
e-mail: e-theses.admin@dur.ac.uk Tel: +44 0191 334 6107
<http://etheses.dur.ac.uk>

Mechanism-Guided Studies of Brønsted Acid and Base Organocatalysis

By

Anita G. Lindsay

B. Sc. (Hons), Chemistry (2005)

University College Dublin

Submitted to the Department of Chemistry

In Partial Fulfilment of the Requirements for the

Degree of Doctor of Philosophy

at

Durham University



2010

Table of Contents

<i>Abbreviations</i>	<i>vi</i>
<i>Acknowledgements</i>	<i>ix</i>
<i>Dedication</i>	<i>xi</i>
<i>Abstract</i>	<i>xii</i>
Chapter 1	14
1.0 Foreword.	15
1.1 Organocatalysis	16
1.1.1 Historical background & classification.....	18
1.1.2 Azolium ions as precursors to Brønsted base organocatalysts.	21
1.1.2.1 Structure and background.	21
1.1.2.2 NHCs as organocatalysts.	22
1.1.3 Organocatalysis by chiral Brønsted acids.	26
1.2 The Mannich reaction.	34
1.2.1 Asymmetric organocatalysis of the Mannich reaction.....	34
1.2.1.1 Catalysis of the Mannich reaction by chiral phosphoric acids.	38
Chapter 2	43
2.0 Foreword.	44
2.1 Introduction.	45
2.1.1 The Classical Mannich reaction.....	45
2.1.2 Brønsted acid-base catalysis.	47
2.1.2.1 The Brønsted law.	48
2.1 Results	51
2.1.1 Synthesis	51
2.1.2 Evaluation of the enantioselectivity of the Mannich reaction.....	56
2.1.3 Determination of pK_a values of iminium ions	58
2.1.3.1 Attempted determination of aqueous pK_a values.	58
2.1.3.2 Determination of pK_a values of iminium ions in dimethyl sulfoxide.	80
2.1.3.3 Investigations of iminium ion pK_a values in acetonitrile.	98
2.1.4 Determination of pK_a values of phosphoric acid catalysts.....	98
2.1.4.1 Attempted determination of aqueous pK_a values.	99
2.1.4.2 Investigations of pK_a values of phosphoric acid catalysts in acetonitrile. ..	101

2.1.4.3	Determination of pK_a values of (thio)phosphoric acids in DMSO.	103
2.1.5	Kinetic studies of the Mannich reaction.	124
2.1.5.1	Uncatalysed Mannich reactions.	124
2.1.5.2	Catalysed Mannich reactions.	145
2.2	Discussion.	147
2.2.1	Synthesis.	147
2.2.1.1	Preparation of <i>N</i> -Boc imines.	147
2.2.1.2	Synthesis of (thio)phosphoric acid catalysts.	150
2.2.2	Enantioselectivity of the Mannich reaction.	153
2.2.3	Attempted determination of aqueous pK_a values of iminium ions.	159
2.2.4	Determination of pK_a values of iminium ions in dimethyl sulfoxide.	169
2.2.5	pK_a values of (thio)phosphoric acid catalysts.	172
2.2.6	Kinetics of the Mannich reaction.	175
Chapter 3	177
3.0	Foreword.	178
3.1	Introduction.	178
3.1.1	Acid-base chemistry of azolium ions.	178
3.1.2	Kinetic acidities of azolium ions.	179
3.1.3	Thermodynamic acidities of azolium ions.	184
3.2.	Results.	188
3.2.1	Deuterium exchange reactions of triazolium ions followed by ^1H NMR spectroscopy.	188
3.2.1.1	2-Phenyl-6,7-dihydro-5H-pyrrolo[2,1-c][1,2,4]triazol-2-ium tetrafluoroborate (179).	191
3.2.1.2	4-Methoxyphenyl-6,7-dihydro-5H-pyrrolo[2,1-c][1,2,4]triazol-2-ium tetrafluoroborate (180).	196
3.2.1.3	Pentafluorophenyl-6,7-dihydro-5H-pyrrolo[2,1-c][1,2,4]triazol-2-ium tetrafluoroborate (181).	198
3.2.1.4	1,3,4-Triphenyl-4H-1,2,4-triazol-1-ium tetrafluoroborate (182).	200
3.2.2	Determination of second-order rate constants for deuterioxide ion-catalysed exchange k_{DO} ($\text{M}^{-1}\text{s}^{-1}$).	202
3.2.3	Estimation of k_{HO} and pK_a values.	214
3.2.4	Deuterium exchange reactions of imidazolium ions followed by ^1H NMR spectroscopy.	218
3.2.4.1	1-Butyl-3-methylimidazolium hexafluorophosphate (185).	220

3.2.4.2	1-Hexyl-3-methylimidazolium hexafluorophosphate (186).....	222
3.2.4.3	1-Octyl-3-methylimidazolium bromide (187).....	225
3.2.5	Estimation of k_{HO} and $\text{p}K_{\text{a}}$ values.....	228
3.3	Discussion.....	232
3.3.1	Deuterium exchange reactions.....	232
3.3.2	Acidity of 1,2,4-triazolium ions.....	238
3.3.2.1	Substituent effects on kinetic acidities, k_{DO} ($\text{M}^{-1}\text{s}^{-1}$), of triazolium ions.	238
3.3.2.2	Substituent effects on carbon acid $\text{p}K_{\text{a}}$ values of triazolium ions.....	241
3.3.3	Acidity of imidazolium ions.....	242
3.3.3.1	Substituent effects on kinetic acidities, k_{DO} ($\text{M}^{-1}\text{s}^{-1}$), of imidazolium ions.	242
3.3.3.2	The effect of counter ion on the kinetic acidity of imidazolium ions.....	243
3.4	Summary.....	246
Chapter 4.....		248
4.0	Foreword.....	249
4.1	General instrumentation.....	249
4.2	Synthesis of compounds for kinetic study.....	251
4.2.1	Synthesis of <i>N</i> -Boc imines.....	251
4.2.1.1	<i>N</i> -(<i>tert</i> -butoxycarbonyl)- α -(phenylsulfonyl)benzylamine (198).....	251
4.2.1.2	Benzaldehyde <i>N</i> -(<i>tert</i> -butoxycarbonyl)imine (121).....	252
4.2.1.3	<i>N</i> -(<i>tert</i> -butoxycarbonyl)- α -(phenylsulfonyl)-4-methylbenzylamine (199).	253
4.2.1.4	<i>p</i> -Methylbenzaldehyde <i>N</i> -(<i>tert</i> -butoxycarbonyl)imine (120).....	253
4.2.1.5	<i>N</i> -(<i>tert</i> -butoxycarbonyl)- α -(phenylsulfonyl)-4-methoxybenzylamine (200).	254
4.2.1.6	<i>p</i> -Methoxybenzaldehyde <i>N</i> -(<i>tert</i> -butoxycarbonyl)imine (119).....	255
4.2.1.7	<i>N</i> -(<i>tert</i> -butoxycarbonyl)- α -(phenylsulfonyl)-3-methoxybenzylamine (201).	255
4.2.1.8	<i>m</i> -Methoxybenzaldehyde <i>N</i> -(<i>tert</i> -butoxycarbonyl)imine (202).....	256
4.2.1.9	<i>N</i> -(<i>tert</i> -butoxycarbonyl)- α -(phenylsulfonyl)-4-bromobenzylamine (203).....	257
4.2.1.10	<i>p</i> -Bromobenzaldehyde <i>N</i> -(<i>tert</i> -butoxycarbonyl)imine (122).....	257
4.2.1.11	<i>N</i> -(<i>tert</i> -butoxycarbonyl)- α -(phenylsulfonyl)-4-fluorobenzylamine (204).....	258
4.2.1.12	<i>p</i> -Fluorobenzaldehyde <i>N</i> -(<i>tert</i> -butoxycarbonyl)imine (123).....	259
4.2.1.13	<i>N</i> -(<i>tert</i> -butoxycarbonyl)- α -(phenylsulfonyl)-4-nitrobenzylamine (205).....	259
4.2.1.14	<i>p</i> -Nitrobenzaldehyde <i>N</i> -(<i>tert</i> -butoxycarbonyl)imine (206).....	260

4.2.1.15	<i>N</i> -(<i>tert</i> -butoxycarbonyl)- α -(phenylsulfonyl)-4- <i>tert</i> -butylbenzylamine (207).	260
4.2.1.16	4- <i>tert</i> -Butylbenzaldehyde <i>N</i> -(<i>tert</i> -butoxycarbonyl)imine (129).	261
4.2.1.17	<i>N</i> -(<i>tert</i> -butoxycarbonyl)- α -(phenylsulfonyl)-4-chlorobenzylamine (208).	262
4.2.1.18	<i>N</i> -(<i>tert</i> -butoxycarbonyl)- α -(phenylsulfonyl)-4-(methylthio)benzylamine (209).	262
4.2.1.19	<i>N</i> -(<i>tert</i> -butoxycarbonyl)- α -(phenylsulfonyl)-4-cyanobenzylamine (210).	263
4.2.2	Synthesis of phosphoric acid catalysts and thiophosphoryl analogues.	264
4.2.2.1	(<i>R</i>)-2,2'- <i>Bis</i> (ethoxymethoxy)-1,1'-binaphthyl (109).	265
4.2.2.2	(<i>R</i>)-3,3'-Dibromo-2,2'- <i>Bis</i> (ethoxymethoxy)-1,1'-binaphthyl (110).	266
4.2.2.3	General Procedure A: preparation of 3,3'-diaryl-2,2'- <i>bis</i> (ethoxymethoxy)-1,1'-binaphthyls (211)-(214).	267
4.2.2.4	General Procedure B: preparation of 3,3'-disubstituted-2,2'-dihydroxy-1,1'-binaphthyls (146), (147), (215)-(217).	271
4.2.2.5	General Procedure C: preparation of 3,3'-disubstituted-1,1'-binaphthyl-2,2'-diyl hydrogenphosphates (7), (84), (133), (135), (136) and (218).	276
4.2.2.6	General Procedure D: preparation of 3,3'-disubstituted-1,1'-binaphthyl-2,2'-diyl thiophosphates (137), (138), (219)-(222).	282
4.2.3	General Procedure for phosphoric acid-catalysed direct Mannich reactions.	287
4.2.3.1	(2-Acetyl-3-oxo-1-phenyl-butyl)-carbamic acid <i>tert</i> -butyl ester (141).	288
4.2.3.2	[2-Acetyl-1-(4-methoxyphenyl)-3-oxo-butyl]-carbamic acid <i>tert</i> -butyl ester (139).	288
4.2.3.3	(2-Acetyl-3-oxo-1-4-tolyl-butyl)-carbamic acid <i>tert</i> -butyl ester (140).	289
4.2.3.4	[2-Acetyl-1-(4-fluorophenyl)-3-oxo-butyl]-carbamic acid <i>tert</i> -butyl ester (143).	289
4.3	Materials	290
4.4	Preparation of solutions	291
4.4.1	Preparation of solutions for ¹ H NMR kinetic experiments.	291
4.4.1.1	¹ H NMR exchange experiments	291
4.4.1.2	¹ H NMR studies of the Mannich reaction.	291
4.4.2	Preparation of solutions for UV-Vis spectrophotometric experiments.	291
4.4.2.1	Kinetics of imine hydrolysis.	291
4.4.2.2	Determination of p <i>K</i> _a values in dimethyl sulfoxide.	292
4.4.3	Preparation of solutions for stopped-flow spectrophotometric measurements.	292

4.5 Kinetic methods	293
4.5.1 ¹ H NMR exchange reactions.....	293
4.5.2 ¹ H NMR studies of the Mannich reaction.....	296
4.5.3 UV-Vis spectrophotometric measurements.....	297
4.5.3.1 Kinetics of imine hydrolysis.....	297
4.5.3.2 Determination of p <i>K</i> _a values.....	297
4.5.4 Stopped-flow spectrophotometric measurements.....	297
Chapter 5	298
References.....	303
Appendices.....	308
Appendix A Kinetics of imine hydrolysis	A1
Appendix B Determination of the p<i>K</i>_a value of anilinium ion (130') in DMSO.....	B1
Appendix C Kinetics of the uncatalysed Mannich reaction	C1
Appendix D Determination of p<i>K</i>_a values of azolium ions.....	D1
Appendix E Supplementary NMR spectra	E1

Abbreviations

Å	angstrom(s)
Abs	absorbance
Ac	acetyl
Acac	acetylacetone
Ad	adamantyl
Ar	aryl
A_{max}	absorbance maximum
A_{min}	absorbance minimum
aq.	aqueous
Biph	biphenyl
br.	broad (spectral)
Bu	butyl
cat.	catalyst
°C	degree centigrade
cm⁻¹	wavenumbers
¹³C NMR	carbon 13 nuclear magnetic resonance
δ	chemical shift
d	doublet
DBU	1,8-diazabicyclo[5.4.0]undec-7-ene
DCM	dichloromethane
DME	dimethoxyethane
DMSO	dimethyl sulfoxide
D₂O	deuterium oxide
ee	enantiomeric excess
Et	ethyl
EtOAc	ethyl acetate
equiv	equivalent
g	gram(s)
HCl	hydrochloric acid
HIn	Indicator in neutral form
¹H NMR	proton nuclear magnetic resonance

hr	hour(s)
Hz	hertz
In⁻	Indicator in anionic form
ⁱPr	isopropyl
IR	infra red
<i>J</i>	coupling constant
<i>k</i>	rate constant
<i>K</i>	equilibrium constant
<i>K_a</i>	acidity constant
kcal	kilocalorie(s)
kJ	kilojoule(s)
λ	wavelength
L	litre(s)
LFER	linear free energy relationship
lit.	literature
ln	natural logarithm
log	logarithm
M	moles/litre (Molar)
<i>m-</i>	<i>meta</i>
m	multiplet (spectral)
Me	methyl
MeO	methoxy
Mes	mesityl
μg	microgram
μL	microlitre(s)
min	minute(s)
mL	millilitre(s)
mm	millimetre(s)
mmol	millimole(s)
mol	mole(s)
ms	millisecond(s)
m/z	mass per unit charge
NaOH	sodium hydroxide
NHC	<i>N</i> -Heterocyclic carbene

<i>o-</i>	<i>ortho</i>
<i>p-</i>	<i>para</i>
Ph	phenyl
ppm	parts per million
ps	picoseconds
R	alkyl substituents
R_f	retention factor
r.t.	room temperature
ρ	reaction constant
σ	substituent constant
sec, s	second(s)
s	singlet (spectral)
t	triplet (spectral)
<i>tert-</i>	tertiary
THF	tetrahydrofuran
TLC	thin layer chromatography
TS	transition state
UV	ultraviolet
Vis	visible
wt.	Weight.

Acknowledgements

Firstly I would like to extend my sincere gratitude to my supervisor Dr. AnnMarie O'Donoghue for giving me the wonderful opportunity of coming to Durham and conducting my PhD research under her instruction. The guidance, support, patience and repeated explanations were invaluable and I couldn't have asked for a better supervisor on both a personal and professional level.

I would also like to thank past and present members of Team AMOD, Barry, Chuks, Lami, Eleanor, Shelley, Terry, Enrique and numerous Richards for all the fun and banter along the way. Particular thanks to Barry for lots of laughs over the years and to Rich Delley, your speedy distillation skills and syringe cleaning came in very handy when time was running out. You can dismantle the Anita-Dog now!

To the Durham tea groups, especially those who were so welcoming when we first set up the lab; Andzrej, Emma, Kiran, Alan, Blondie, Ed, Ollie, Markus, Khairul, Seb, Lucas, Doncadh, Chris H., Chris McPake, Graham, Ian, Matt, Andy, Ricky, Helen, Emma, Dave. Thanks to the fluorine group for adopting me when things were quiet on our side of CG 115, in particular to Chris and Ian for keeping me entertained. Big thanks to Chris for being a great friend when times were hard, I'll miss the Simpsons quotes and Friday pints! To Will and Mark for lots of fun over the years, Hallgarth '08 was so much fun! Thanks too for putting me up during my trips back to Durham.

To all the analytical staff in Durham particularly Dr. Alan Kenwright, Mr. Ian McKeag and Ms Catherine Heffernan for all the NMR access and troubleshooting and Dr. Aileen Congreve for help with chiral HPLC. Thanks to Kelvin in the mechanical workshop for keeping our spectrometers up and running.

Sincere gratitude to Dr. Mike Crampton for stepping in when AnnMarie was on maternity leave and helping me get the pK_a determinations off the ground. Your help was invaluable and much appreciated! Also thanks to Dr. David Hodgson for useful conversations and good advice over the years.

To my amazing friends in Dublin, Cara, Edel, Ruth, Suzy, Sarah, Laura, Dawson, Alan, Annie and Billy for all the support while I was away and good times when I was home and in particular for keeping my spirits up during the long writing up process. Especially to Cara and Edel, you're the best friends I could ask for, thanks for always being there!

To my wonderful family, I couldn't have completed my PhD without you all. Thanks to Karen and Darren for numerous lifts to the airport, extra large glasses of wine and for helping me get to Durham in one piece (albeit in a pie van). I never would have lasted past the first weekend if it wasn't for you Kaz! Thanks for all the chats and advice especially at the end when I was so stressed and for giving us Seán, the best little distraction from writing up! To Austin, for formatting tips, printing, binding and saving me so much stress and to Neil for sensible advice at the end. To Grace, not only my twin but my best friend, thanks for all the laughs and keeping me sane for the last few years. You made Edinburgh a great get-away for me whenever I needed a break! Finally thank you to my parents, Rita and Austin. Your encouragement and love has gotten me through all the difficult times and I am so grateful. Thank you for always telling me I could achieve what ever I wanted to in life. This thesis is dedicated to you both.

Do mo thuismitheoirí

Abstract

We have studied the mechanism of the reaction of *N*-Boc imines and acetylacetone in the presence and absence of chiral phosphoric acid catalysts. In order to gain mechanistic insight into the asymmetric Mannich reaction, a structurally homologous series of *N*-Boc imines and BINOL-derived phosphoric acid and thiophosphoric acid catalysts were synthesised. The degree of asymmetric catalysis was evaluated by chiral HPLC analysis of the products of catalysed Mannich reactions.

Knowledge of the acidity difference between the phosphoric acid catalysts and the iminium ions is essential in order to determine the likely extent of proton transfer, full or partial, between these two species in the course of the Mannich reaction. The determination of aqueous pK_a values of iminium ions was attempted by construction of pH-rate profiles for hydrolysis using UV-Vis spectrophotometry. Estimates of the second-order rate constant for acid-catalysed hydrolysis (k_H , $M^{-1}s^{-1}$) and the first-order rate constant for the solvent reaction (k_0 , s^{-1}) for each imine were extracted from the rate-profiles, however, pK_a values could not be obtained for reasons that will be discussed. Iminium ion pK_a values were determined in dimethyl sulfoxide by adopting a bracketing indicator method with use of UV-Vis spectrophotometry and pK_a values in the range 0.65-1.61 were observed for the series of *N*-Boc aryl iminium ions. The pK_a values of (thio)phosphoric acid catalysts were also estimated in dimethyl sulfoxide using this approach and values in the range 2.21-3.86 were obtained. The determination of pK_a values of phosphoric acids in water and acetonitrile was unsuccessful due to the poor solubility of the catalyst in these media.

Rate constants for the uncatalysed Mannich reaction of each imine with acetylacetone have been quantified using 1H NMR spectroscopy in CD_2Cl_2 , $CDCl_3$ and CD_3CN . It was found that the solvent effect on the rate of the Mannich reaction was small, with the fastest reaction occurring in CD_3CN . Altering the imine substituent was found to have a larger effect on the rate. We also aimed to determine rate constants for the catalysed Mannich reaction using 1H NMR spectroscopy. However, in all cases complete hydrolysis of the imine substrate occurred before the first time-point could be obtained. All efforts to suppress hydrolysis proved unsuccessful.

Azolium ion organocatalysts were also investigated. These are the conjugate acids of *N*-heterocyclic carbenes, a class of highly successful nucleophilic/Brønsted base organocatalysts. As these carbenes are generated *in situ* from azolium ions during organocatalytic reactions, knowledge of the acidity of the parent ion is much sought after. This thesis describes the determination of aqueous pK_a values of imidazolium and triazolium ions using a kinetic approach. Second-order rate constants for the deprotonation of these azolium ions by deuterioxide ion (k_{DO} , $M^{-1}s^{-1}$) in D_2O at 25 °C were determined by 1H NMR spectroscopy. These k_{DO} values could be used to calculate values for k_{HO} ($M^{-1}s^{-1}$), the second-order rate constant for deprotonation of the azolium ion by hydroxide ion to give the carbene/ylide in water. Evidence is presented that the reverse rate constant for carbene protonation by solvent water is limited by solvent reorganisation and occurs with a rate constant of $k_{HOH} = k_{reorg} = 10^{11} s^{-1}$. Values for k_{HO} and k_{HOH} permitted the calculation of reliable carbon acid pK_a values for ionisation of the azolium ions in water. The effects of the *N*-substituents and counter ion on k_{HO} and pK_a values are discussed. Of the triazolium ions studied, k_{DO} values of 3.66×10^7 - $6.47 \times 10^8 M^{-1}s^{-1}$ were observed with corresponding pK_a values of 16.6-17.8. For *N,N*-dialkylated imidazolium ions, k_{DO} values of 1.03×10^2 - $1.07 \times 10^2 M^{-1}s^{-1}$ were obtained which yielded pK_a values of 23.3-23.4.

Chapter 1

Introduction

1.0 Foreword.

Organocatalysis is the acceleration of a rate of reaction by a sub-stoichiometric amount of a small organic molecule, which does not contain a metal at its' active centre.¹ This is an attractive technology for chemists, particularly in industry, given the high cost of purchase and disposal of metal analogues. As such, recent years have witnessed a rapid increase in research focussing on this area.¹⁻⁴ Highly efficient and selective variants of a range of transformations are reported in the literature, although the success of a given catalyst is highly substrate and solvent dependent. Currently there exists a dearth of kinetic and mechanistic studies on organocatalysed reactions, which hampers the rational design of improved and more broadly applicable organocatalysts. This aim of this thesis is to gain mechanistic insight into organocatalysed reactions using physical organic techniques. In particular, Brønsted acids and *N*-heterocyclic carbene catalysts are investigated. This chapter provides an overview of the field of enantioselective organocatalysis, reviewing previous work relevant to these studies.

1.1 Organocatalysis.

The development of new methodologies for the production of optically active building blocks is of vital importance, given the demand for single enantiomers as intermediates in the synthesis of pharmaceuticals. Asymmetric catalytic processes offer an attractive solution to the chemical industry, avoiding problems such as the waste involved in the resolution of racemic mixtures. The term catalysis is commonly equated to transition metal-mediated transformations or those involving enzymes but it is now apparent that small organic molecules can also promote highly efficient enantioselective reactions. As catalysts, these small organic molecules have a number of advantages over biocatalysts and organometallic compounds as they are generally robust, relatively inexpensive and non-toxic. Organocatalysis is a particularly useful tool for the preparation of pharmaceutical compounds which do not tolerate metal contamination. In many instances, the organocatalyst is inert towards air and moisture and the need for demanding reaction conditions such as low temperatures, inert atmosphere and absolute solvents may be avoided. A clear benefit is the readily available multitude of enantiopure compounds, such as amino acids and carbohydrates, provided by nature from which catalysts may be developed.

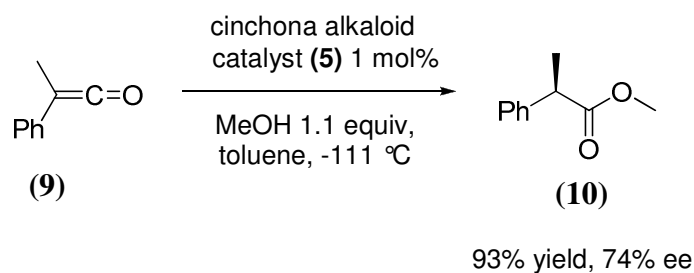
In order for a successful enantioselective reaction to occur, it is clear that stereoselectivity must be controlled by a well-organised transition state. In organometallic systems, it is the metal which activates the substrates and governs chirality transfer in the transition state. In an organocatalytic system, the transition state is a result of binding interactions between the catalyst and substrate. A distinction can be made between processes which involve the formation of covalent adducts between the catalyst and substrate in the catalytic cycle and those which rely on non-covalent interactions such as hydrogen bonding. These interactions are termed covalent and non-covalent catalysis respectively.⁵ For many organocatalytic transformations, it is hydrogen bonding which provides rigid three dimensional stereoselectivity-determining structures allowing successful asymmetric transformations to occur.

Alder reaction respectively.¹⁰ Stronger Brønsted acids include chiral phosphoric acid (7) developed independently by Akiyama and Terada and the BINOL-derived *N*-triflyl phosphoramidate (8) made by Yamamoto and co-workers. These catalysts have been used for a multitude of asymmetric transformations including Mannich¹¹ and Diels-Alder¹² reactions respectively.

1.1.1 Historical background & classification.

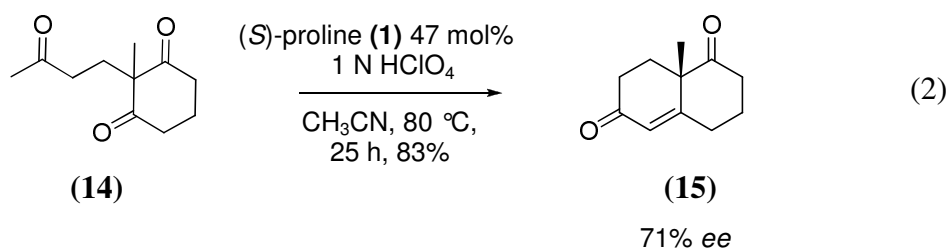
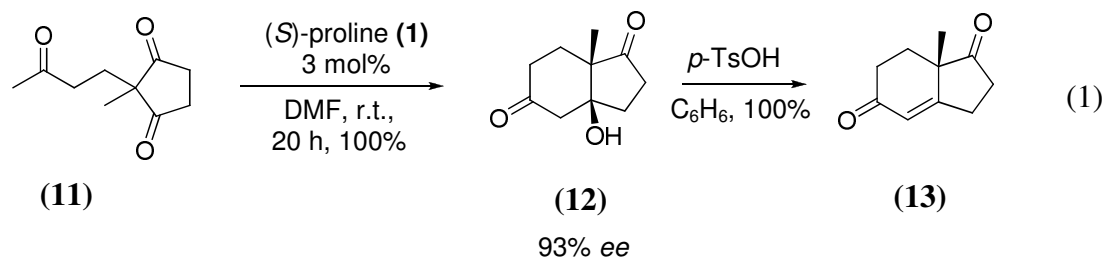
The use of small organic molecules as catalysts in chemical transformations was reported as early as the beginning of the 20th century with Bredig's modestly enantioselective alkaloid-catalysed cyanohydrin synthesis.¹³ Several decades later, Pracejus reported a highly enantioselective addition of methanol to phenylmethylketene, again using a cinchona alkaloid catalyst (Scheme 1.1).¹⁴

Scheme 1.1:



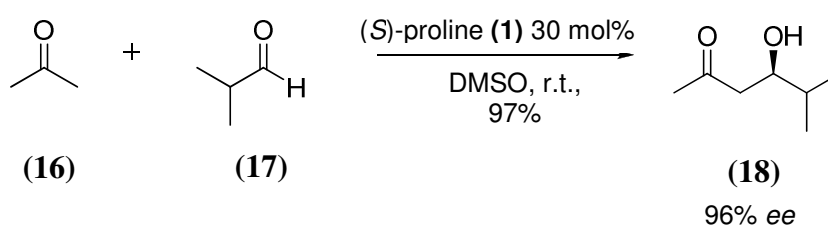
The next milestone in the history of organocatalysis came in the 1970s with the development of the Hajos-Parrish-Eder-Sauer-Wiechert reaction¹⁵⁻¹⁷ by two industrial groups. Hajos and Parrish reported the intramolecular aldol reaction of achiral triketones which proceeded in good yield and *ee* (Scheme 1.2-1). Acid-catalysed dehydration furnished condensation products (13) in a second step. Eder, Sauer and Wiechert isolated the cyclised aldol condensation product (15) in one step, using proline and an acid co-catalyst (Scheme 1.2-2).

Scheme 1.2:

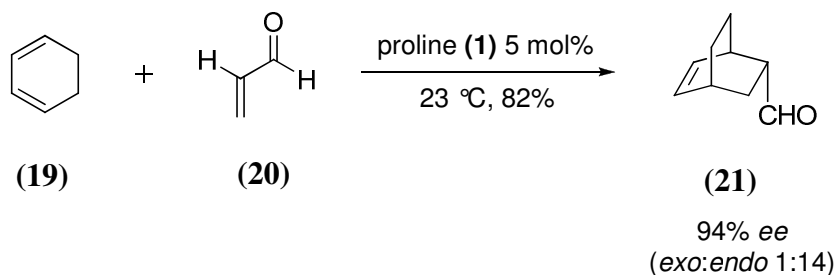


Although used in natural product and steroid synthesis, the full scope of this chemistry was not explored until 2000 when pioneering papers were published by the groups of List and MacMillan, reporting organocatalysed intermolecular aldol^{6,7} (Scheme 1.3) and Diels-Alder¹⁸ reactions (Scheme 1.4) respectively. These significant studies revealed the potential of organocatalysts to rival the efficiency and selectivity of organometallic counterparts, prompting an explosion of research into new catalysts and methodologies.

Scheme 1.3:

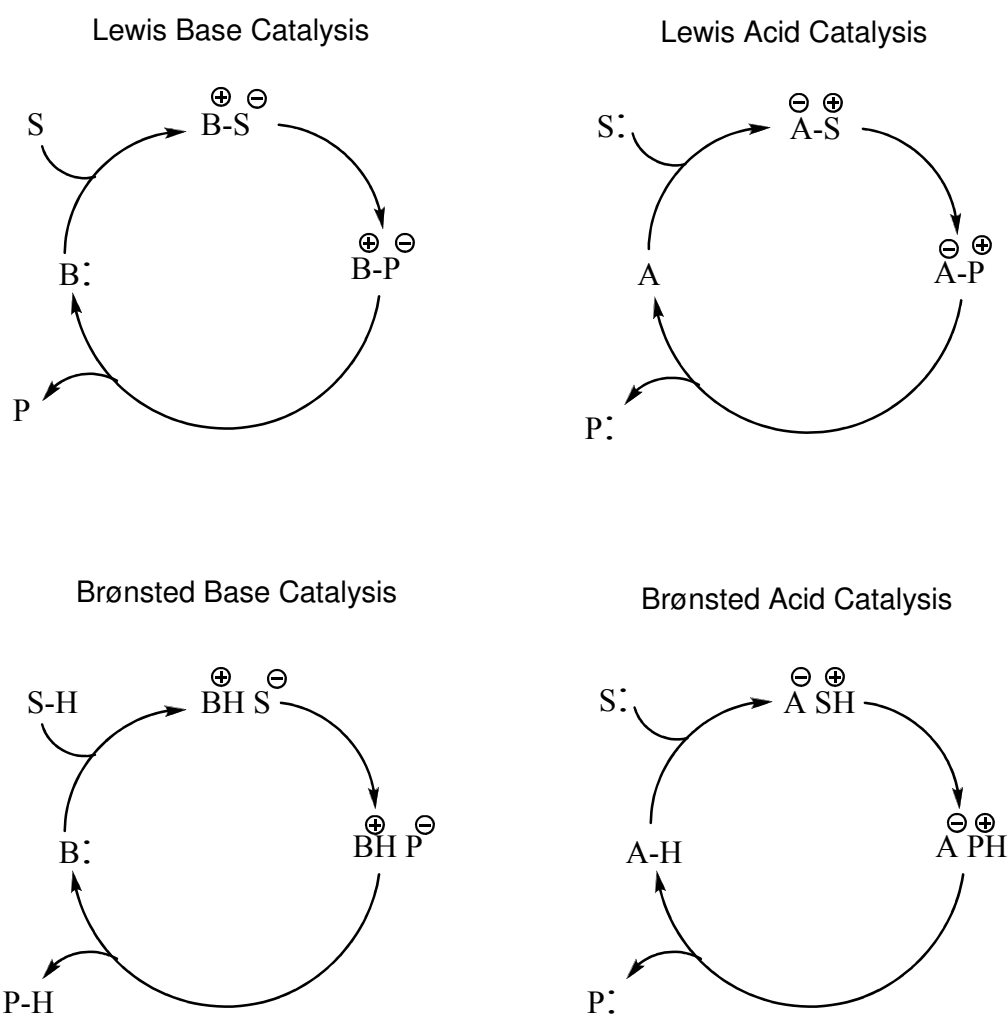


Scheme 1.4:



List broadly classifies organocatalysts based on their mechanisms as being Lewis bases, Lewis acids, Brønsted acids and Brønsted bases. Simplified catalytic cycles are shown in Scheme 1.5. The usefulness of this classification system can be limited as the mechanism of some organocatalytic reactions remains unclear.

Scheme 1.5: Organocatalytic cycles.



Lewis acid and base catalysts initiate the catalytic cycle by electrophilic or nucleophilic addition to substrates (S), respectively. The resulting complex undergoes reaction and product (P) and catalyst are subsequently released. Brønsted acid and base catalytic cycles are initiated by (partial) protonation or deprotonation, respectively.

1.1.2 Azolium ions as precursors to Brønsted base organocatalysts.

To date, azolium ions have been the subject of much synthetic interest as deprotonation provides access to stable carbenes. These species have emerged as useful ligands in asymmetric organometallic chemistry¹⁹ and have found application as organocatalysts in the benzoin condensation and a variety of other transformations.²⁰ As a result, knowledge of their basicity and nucleophilicity has become increasingly sought after. The following section provides a brief introduction to carbenes and an overview of their application as organocatalysts.

1.1.2.1 Structure and background.

Carbenes are neutral compounds with a divalent carbon atom and six valence electrons. Four of these electrons are involved in bonds to other atoms, with the other two electrons remaining on carbon. These electrons may be in the same orbital (singlet state) or different orbitals (triplet state) (Figure 1.2).

Figure 1.2:

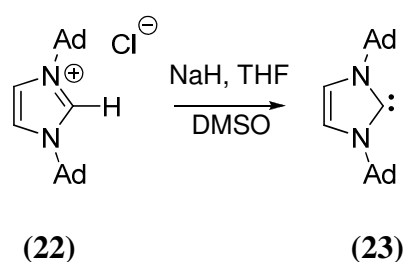


The first evidence of the existence of carbenes is found in the pioneering studies of Buchner, Curtis, Staudinger and Kupfer in the late 19th and early 20th century. However, due their pronounced reactivity, they could not be isolated and were regarded as reactive intermediates.

Studies by Breslow²¹ and Wanzlick²² reawakened interest in the field in the 1950s and 60s and illustrated the dramatically increased stability of carbenes with α -amino substituents. These so-called push-pull substituents stabilise the carbene lone pair by the inductive effect of the two electronegative nitrogen atoms while the carbene electron deficiency is reduced by π -donation of the nitrogen lone pairs.²³ In 1970 Wanzlick reported that deprotonation of imidazolium salts by potassium *tert*-

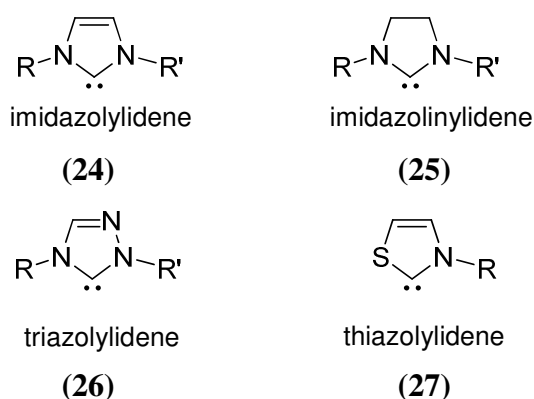
butoxide could result in the corresponding imidazole-2-ylidenes although these were trapped as metal containing dimers and not isolated.^{23,24} Decisive progress in the field of carbene chemistry came with the groundbreaking reports of Bertrand *et al.*²⁵ and Arduengo *et al.*²⁶, who presented compounds that were stable at room temperature and regarded as carbenes. As there was some doubt concerning the extent of the carbene character of Bertrand's phosphinocarbene, the imidazol-2-ylidene synthesised by Arduengo *et al.* in 1991 became widely recognised as the first stable carbene to be isolated and characterised (Scheme 1.6).

Scheme 1.6:



This landmark prompted a surge of interest in the preparation of free carbenes and the development of their metal complexes. A number of stable *N*-heterocyclic carbenes have been successfully isolated and characterised by different groups. The general structures of commonly used carbenes are summarised in Figure 1.3.

Figure 1.3:

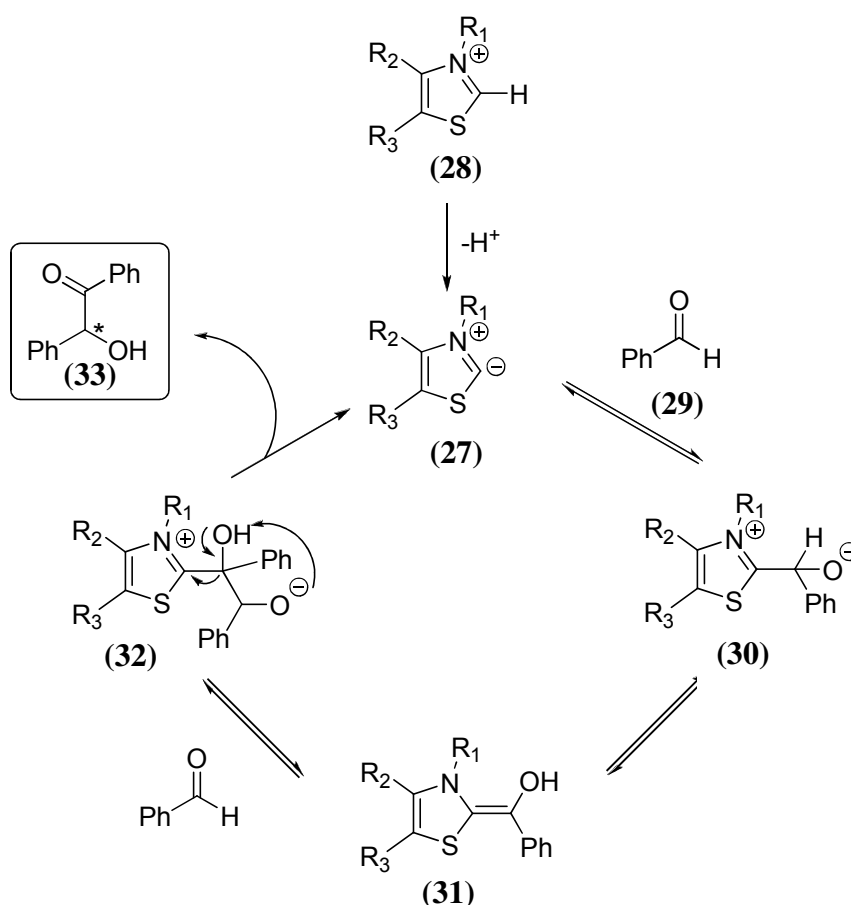


1.1.2.2 NHCs as organocatalysts.

Carbene catalysis offers the opportunity to alter conventional reactivity patterns by pursuing the concept of umpolung (polarity reversal). A prominent example of this is

the benzoin condensation catalysed by *N*-heterocyclic carbenes. This reaction has been the subject of intense investigation. A mechanistic model for the reaction was proposed by Breslow in a seminal report in 1958²⁷ and is illustrated in Scheme 1.7. In this mechanism, the catalytically active species is thiazolin-2-ylidene (**27**) which is formed *in situ* by deprotonation of the thiazolium salt (**28**). The carbene nucleophilically attacks the aldehyde carbonyl group, forming thiazolium adduct (**30**). Deprotonation, reprotonation leads to the active aldehyde in the form of the resonance-stabilised Breslow intermediate (**31**). This reacts again with an electrophilic substrate such as the carbonyl group of a second aldehyde molecule. Finally, benzoin (**33**) is eliminated and the carbene catalyst is regenerated.

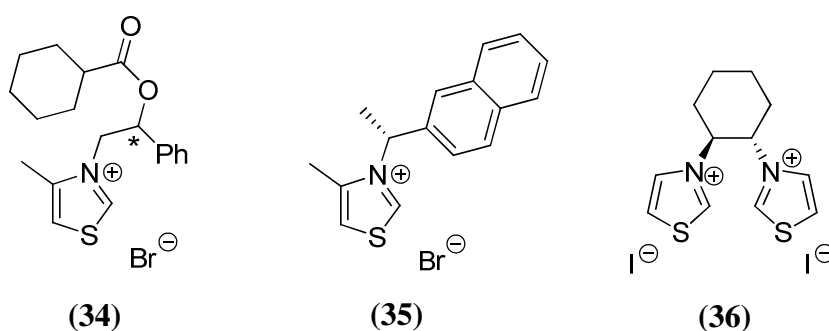
Scheme 1.7: Proposed catalytic cycle of the benzoin condensation.



In addition to creating a carbon-carbon bond, a new stereogenic centre is formed. As such, this reaction became the benchmark to evaluate the potential of chiral azolium salts as catalysts. A large variety of structurally diverse thiazolium, imidazolium and

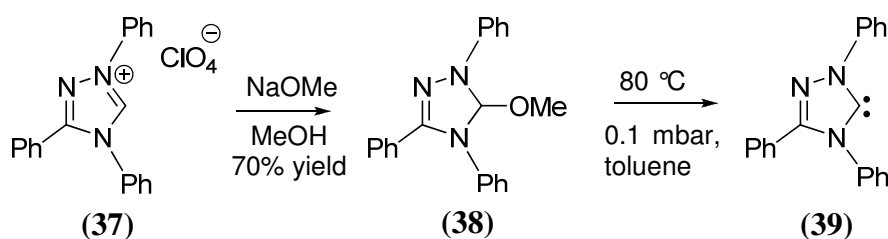
thiazolium salts have been developed which has resulted in improved selectivity and yields.

Following these studies, attention was focussed on the development of an asymmetric variant of the benzoin condensation. Early studies dealt with implementing chirality in thiazolium scaffolds. In 1966, Sheehan and Hunneman presented the first example of an asymmetric benzoin condensation utilising a thiazolium salt as a pre-catalyst (**34**). The resulting *ee* was 22%.²⁸ Modification of the thiazolium salt (**35**) improved the *ee* up 51%, but with very low yields of 6%.²⁹ Many years later Rawal developed this protocol and obtained enantiomeric excesses of up to 48% and with improved yields.³⁰ In 1993, Lopez Calahorra and co-workers synthesised a bithiazolium salt catalyst (**36**) which afforded benzoin product in 27% *ee* and a yield of 21%.



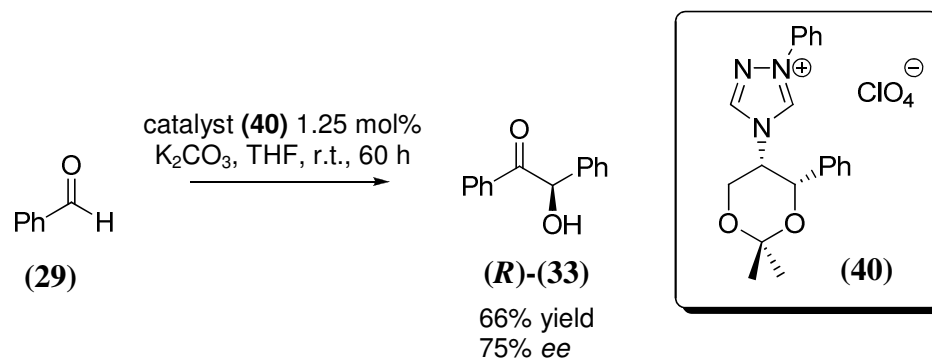
High yields and enantioselectivity remained elusive until triazole heterocycles were investigated as an alternative core structure. In 1995, Enders *et al.* developed the first commercially available carbene, which was found to be stable at temperatures up to 150 °C in the absence of air and moisture.³¹ The triazolium salt (**37**) was treated with sodium methoxide in methanol, forming 5-methoxytriazole (**38**) which underwent thermal elimination of methanol *in vacuo* to form carbene (**39**) (Scheme 1.8).

Scheme 1.8:



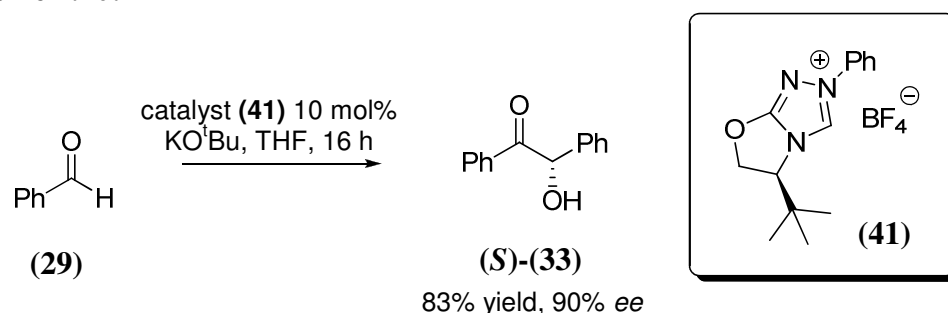
A range of chiral triazolium salts were applied to the benzoin condensation with slight changes in the substitution pattern of the triazolium system leading to profound effects on catalytic activities. The development of triazolium ion pre-catalysts has played a crucial role in improving catalytic activity in the asymmetric benzoin condensation, providing significantly higher yields (66%) and *ees* (75%) than the previously investigated thiazolium salts (Scheme 1.9).³²

Scheme 1.9:



Apart from higher reactivity over thiazolium counterparts, triazolium salts allow the introduction of a second group of varying steric demand at the formerly unfunctionalised position of sulfur and also the integration of the triazole core within cyclic scaffolds of enhanced rigidity. Leeper and Knight developed novel bicyclic triazolium salts capable of providing aromatic acyloins with up to 83% *ee*.^{33,34} Bicyclic triazolium salts were also applied by Enders *et al.* to the asymmetric benzoin condensation, achieving high yields and *ees* (Scheme 1.10).³⁵

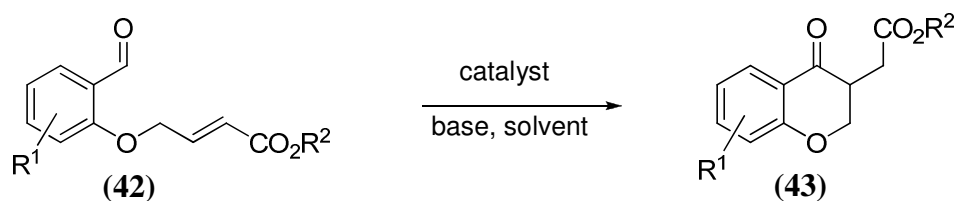
Scheme 1.10:



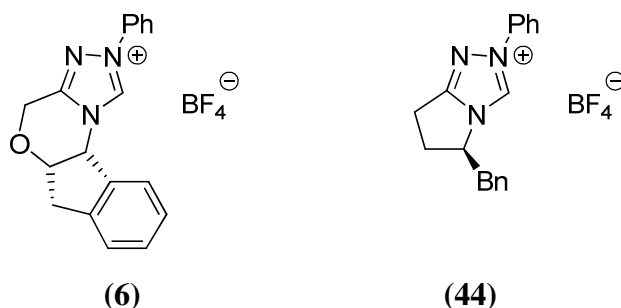
The application of azolium salts to formoin reactions to give C2 to C6 building blocks has also been investigated. 1,2,4-Triazolium ions were found to be much more active than their thiazolium and imidazolium ion counterparts.³⁶

The benzoin condensation was extended to Michael acceptors in the 1970s, creating a new pathway for the preparation of 1,4-bifunctional molecules.³⁷ This reaction is commonly known as the Stetter reaction and the first reports involved cyanide as a catalyst. An asymmetric version of the intramolecular Stetter reaction was developed by Enders *et al.* and utilised triazolium ion (**40**) to deliver 1,4-ketoesters in good yield and moderate selectivity (41-74% *ee*).³⁸ This reaction is commonly used as a benchmark to evaluate catalytic efficiency (Scheme 1.11).

Scheme 1.11:



Rovis *et al.* achieved greater asymmetric induction using salts in which the chiral group is fused to a second ring.^{39,40} Only by application of these types of catalysts have *ee* values of over 90% be obtained.



The triazolium catalysts perform less effectively in the intermolecular Stetter reaction, which is thus restricted to the less active and selective thiazolium catalysts (*ee* up to 39%).

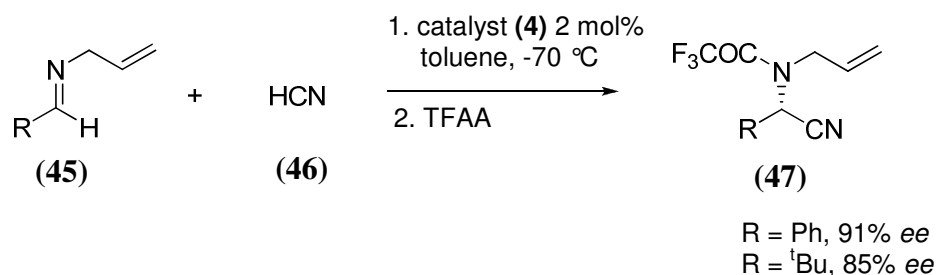
1.1.3 Organocatalysis by chiral Brønsted acids.

Activation of substrates using Brønsted acids has long been one of the most common and straightforward approaches to promoting reactions and has been utilised in a multitude of organic transformations. Research has focussed on the development of

superacids which are capable of electrophilic activation of carbonyl substrates, generating highly reactive protonated intermediates. The realisation that many reactions which are known to be susceptible to general acid catalysis involving prochiral substrates could potentially be carried out in the presence of a chiral Brønsted acid with some degree of stereoinduction, prompted a surge of interest in this area. The key to achieving enantioselective catalysis by chiral Brønsted acids is the design of a catalyst capable of stabilising the transition state of a rate-determining, stereocentre-forming step by hydrogen-bonding/partial proton transfer while preventing access to one enantiotopic face of substrate. The organic reaction could proceed under the chiral environment provided by the chiral conjugate base of the catalyst which exists in the vicinity of the (partially) protonated substrate. Hydrogen bonds, although relatively weak interactions are capable of forming the rigid supramolecular structures vital to transition states of asymmetric transformations. The weaker binding interaction means that product inhibition, often found with stronger Lewis acids, is much less of a problem.

The first example of catalysis by a chiral Brønsted acid was the asymmetric Strecker reaction catalysed by peptide-based thiourea derivatives reported by Jacobsen and co-workers.⁹ This transformation involves the addition of hydrogen cyanide to imines in the presence of a thiourea derivative, affording amino nitriles in high enantiomeric excess (Scheme 1.12).

Scheme 1.12:

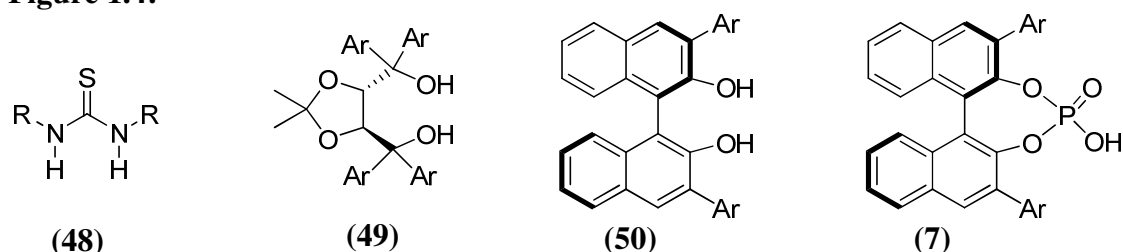


This work illustrated that a chiral Brønsted acid could discriminate between enantiotopic faces of an imine substrate by hydrogen bonding. Since this seminal study, the field of Brønsted acid organocatalysis has become the focus of intense research and has emerged as a powerful methodology in synthetic chemistry.

Compared to carbonyl compounds, imines are relatively strong and directional H-bond acceptors and are therefore among the best potential substrates for enantioselective H-bond donor catalysis. In this context it is unsurprising that addition reactions of imines have proven to be attractive targets for application of Brønsted acid organocatalysts. Nucleophilic addition to imines generally results in an increase in basicity at the heteroatom in the transition state. Also the enantioenriched protected amine products are often of high synthetic utility.

The three main modes of activation of carbonyl compounds and/or imines include Brønsted acid catalysis, single hydrogen bonding and double hydrogen bonding. Depending on their mode of activation, these catalysts are generally classed as being either hydrogen bonding catalysts or stronger Brønsted acids (Figure 1.4). However there is no clear boundary between the two, owing to the sparse mechanistic information and relative pK_a data available for many organocatalytic reactions.

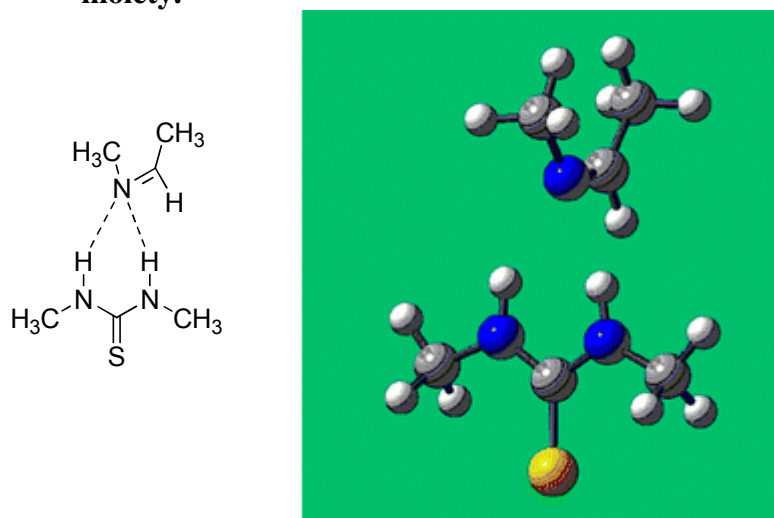
Figure 1.4:



Hydrogen bonding Catalysis \longrightarrow *Stronger Brønsted Acid Catalysis*

Pertinent studies include Jacobsen's report on the mechanism of the asymmetric Strecker reaction in 2002. This investigation was based on NMR, kinetic, structure-activity and theoretical studies and revealed that the thiourea moiety was responsible for catalytic activity and that the imine interacts with the catalyst via a dual hydrogen bond to the urea protons (Figure 1.5).⁴¹

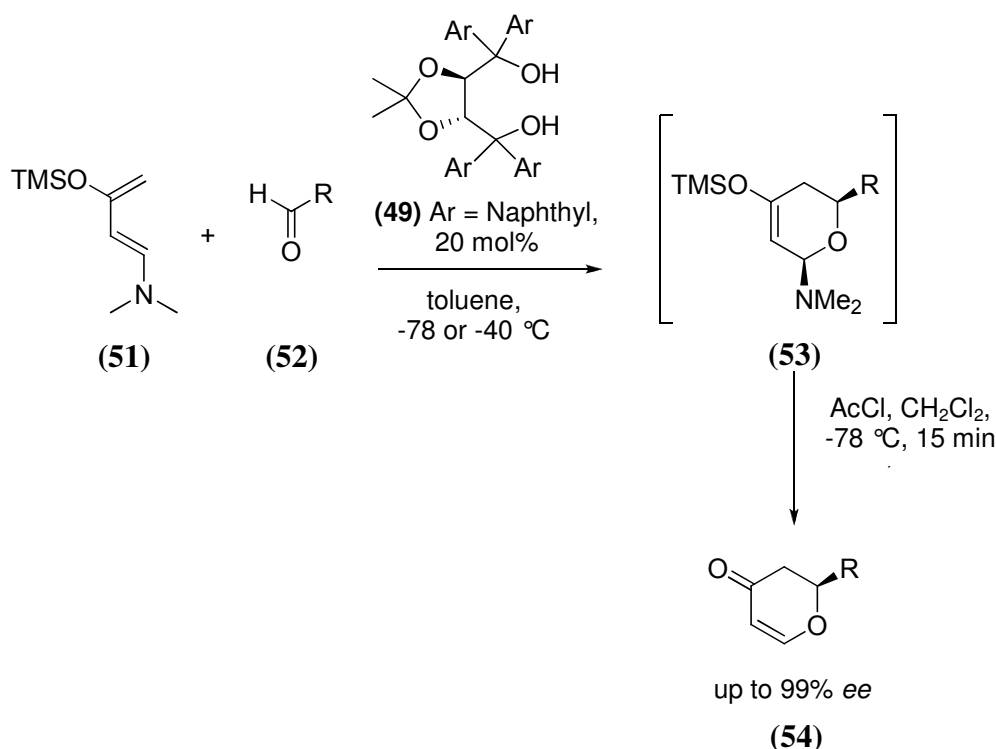
Figure 1.5: Hydrogen bonding interaction of the imine and thiourea moiety.



(Reproduced with the permission of ACS publications)

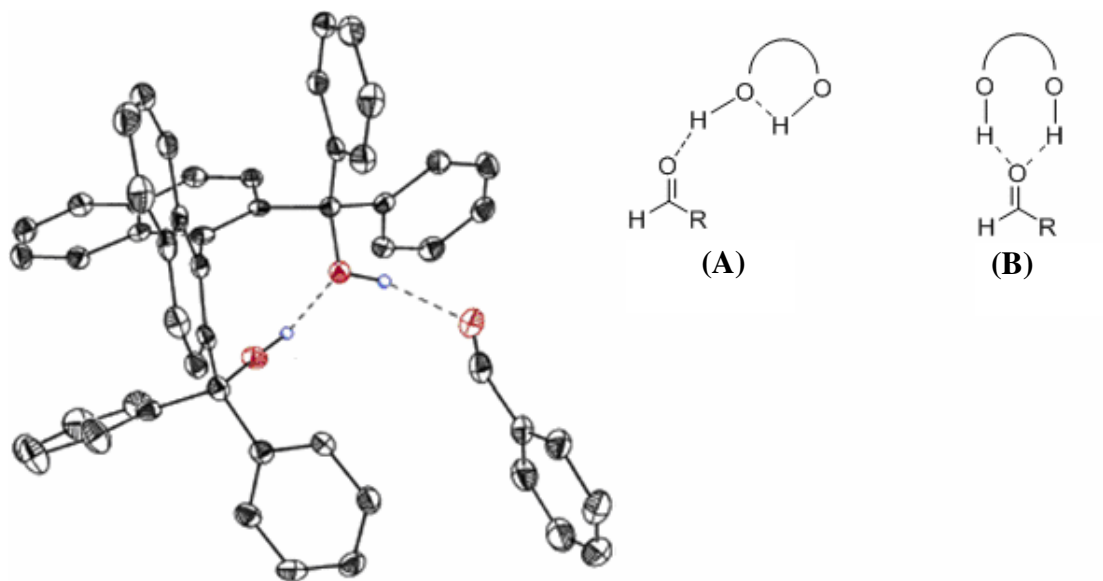
The results of theoretical investigations suggested that the catalyst – aminonitrile product complex features a weaker and singly-bonded interaction which provides an explanation for the basis of the catalyst turnover. This study helped to establish that simple H-bond donors could act serve as useful asymmetric catalysts.

Following Jacobsen's pioneering report, compounds such as TADDOL (*tetraaryl-1,3-dioxolane-4,5-dimethanol*), which was previously used as a chiral ligand for organometallic chemistry⁴², were investigated as potential hydrogen-bonding organocatalysts. TADDOL proved to be an efficient and selective catalyst when applied to a range of transformations⁴³ including the hetero-Diels-Alder reaction¹⁰ (Scheme 1.13).

Scheme 1.13: TADDOL-catalysed hetero-Diels-Alder reaction.

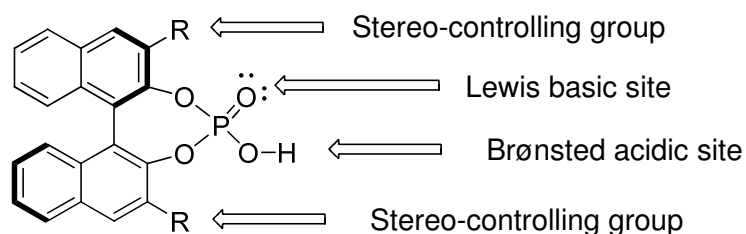
Hydrogen-bonding to the carbonyl group results in a highly enantioselective reaction. The reaction did not proceed in the absence of catalyst and use of monomethyl and dimethylether derivatives of (49) had a detrimental effect on catalytic activity. This evidence indicates the importance of the hydrogen-bonding capability of the catalyst.

Rawal also showed the axially chiral 1,1-biaryl-2,2-dimethanol (BAMOL) scaffold to be a highly effective catalyst for this reaction.⁴⁴ In an effort to shed light on the factors responsible for asymmetric induction, an X-ray structure of an inclusion complex of a simple member of the BAMOL family of catalysts (2,2'-bis-(diphenylhydroxymethyl)binaphthylene) and benzaldehyde was obtained (Figure 1.6). This structure not only shows a 1:1 association between BAMOL and benzaldehyde (29), but also reveals the presence of an *intramolecular* hydrogen bond between the two hydroxyls and an *intermolecular* hydrogen bond to the carbonyl oxygen of benzaldehyde, at least in the solid-state structure. The complex suggests that carbonyl activation is through a single-point hydrogen bond, as was postulated for TADDOL catalysis. The single point activation proposed here (A) differs from the double point activation (B) previously discussed.

Figure 1.6: Inclusion complex of BAMOL and benzaldehyde.

(Reproduced with the permission of ACS publications)

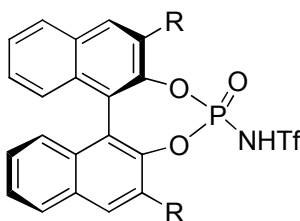
In 2004, the research groups of Akiyama⁴⁵ and Terada¹¹ independently reported the development of a new class of chiral Brønsted acids which represent a significant departure from the thio(urea)-based catalysts in terms of design principle (Figure 1.7). These chiral phosphoric acid diesters are derived from BINOL and are conformationally rigid, relying on a single proton and axially chiral substituents for the transfer of stereochemical information to the substrate. The presence of the Lewis acidic phosphoryl moiety in proximity to the acidic proton potentially allows for bifunctional catalysis. The application of these phosphoric acids to the asymmetric Mannich reaction will be discussed in detail in Section 1.2.

Figure 1.7: Structural features of chiral phosphoric acid catalysts

(55) R = 4-NO₂-C₆H₄

(56) R = 4-(β-naphthyl)-C₆H₄

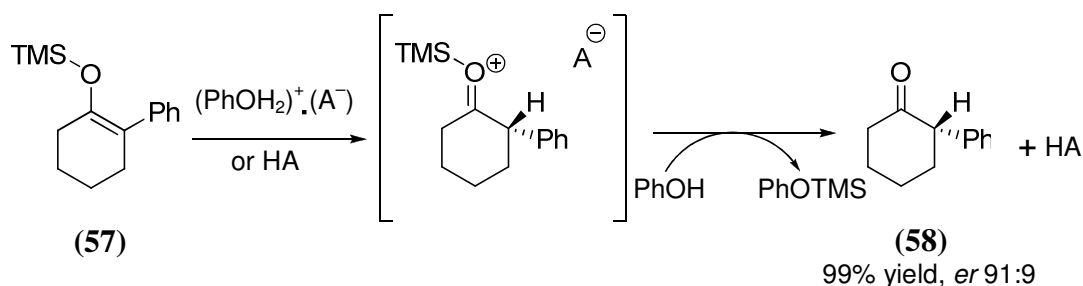
Following these milestone studies, it soon became apparent that chiral phosphoric acids possessed tremendous potential for development of novel asymmetric transformations. The utility of these catalysts has been limited to nitrogen-based electrophiles such as imines and the activation of aldehydes and ketones has been rare. Incorporation of the *N*-trifluoromethanesulfonyl (NTf) group into the phosphoric acid catalyst (**8**) has made the activation of carbonyl compounds possible. This stronger chiral phosphoric acid has been applied to the asymmetric Diels-Alder reaction.¹²



(**8**) R = 1,3,5-(ⁱPr)₃-C₆H₂

It was thought that substitution of the oxygen atom in the P=O bond in an *N*-triflyl phosphoramidate with sulfur or selenium would further decrease the p*K*_a of the catalyst and broaden the scope of Brønsted acid organocatalysis.⁴⁶ These phosphoric acids were found to be successful in the enantioselective protonation of prochiral enol derivatives. This is an attractive route for the preparation of optically active α -carbonyl compounds. An achiral proton source was essential for the success of this transformation. It was proposed that the protonation reaction proceeds through a two-step sequence (Scheme 1.14).

Scheme 1.14:



Initially proton transfer occurs from the chiral Brønsted acid or achiral oxonium ion pair, generated by rapid proton transfer between the chiral Brønsted acid and the achiral proton source PhOH, to the silyl enol ether. This forms an intermediary chiral

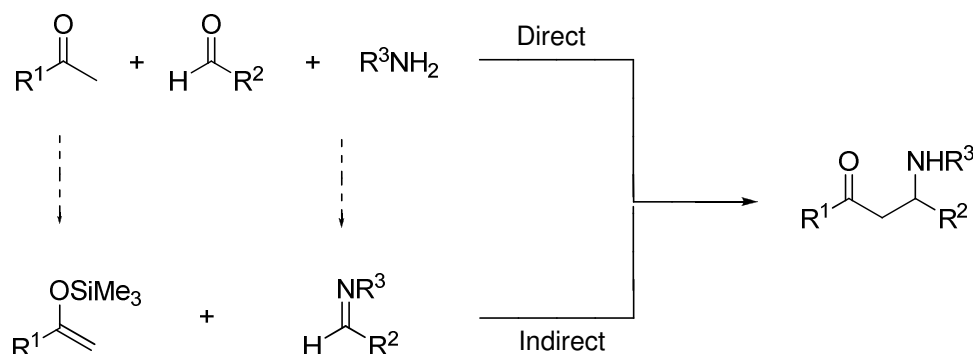
ion pair. Desilylation with phenol forms the corresponding ketone (**58**) and the silylated achiral proton source whilst regenerating the Brønsted acid. The reactivity of this Brønsted acid is particularly appealing for chiral phosphoric acid catalysis as the catalyst loading can be decreased up to 0.05 mol% without any detrimental effect on *ee*. Thiophosphoryl analogues were also investigated but were found to be inactive for this transformation, with only trace amounts of product formed after 96 hours.

It is clear that hydrogen bonding and strong Brønsted acid catalysts developed to date differ greatly in structure. Mechanisms for electrophilic activation and catalysis by these compounds are varied. There is however a common design feature: a dual or single hydrogen bond donor site flanked by sites for secondary interactions with substrates such as aromatic, basic or acidic functionalities.

1.2 The Mannich reaction.

The Mannich reaction is an important carbon-carbon bond forming reaction which yields β -amino carbonyl compounds. These products, also known as Mannich bases, are of particular interest due to their application as synthetic building blocks and precursors of biologically active compounds. There are both direct and indirect variants of this transformation (Figure 1.8). The indirect Mannich reaction involves the addition of a preformed enolate equivalent to an imine, whereas the direct Mannich reaction utilises unmodified ketone donors. In either case, the imine may be preformed, or the aldehyde and amine precursors used. Three component Mannich reactions where the imine has not been preformed may be complicated by the potential for a competitive aldol pathway.

Figure 1.8: Direct and indirect Mannich reaction pathways.



There are abundant examples of both direct and indirect Mannich reactions reported in the literature.^{7,47}

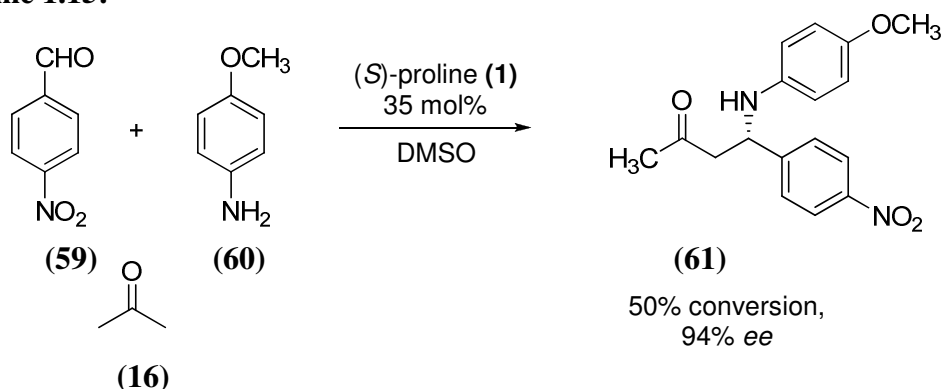
1.2.1 Asymmetric organocatalysis of the Mannich reaction.

Although the Mannich reaction was discovered in 1912, it was at the end of the last century that the first highly successful asymmetric variants were reported. These indirect Mannich reactions involved the addition of preformed enolate equivalents, typically silyl enol ethers and silyl ketene acetals, to imines. Intense research into catalytic indirect Mannich reactions followed. Further investigations focussed on

direct Mannich reactions which avoided the problem of preparation and stability of enolate equivalents and as such are a more attractive option for synthetic chemists. The direct Mannich reaction may be catalysed by both organometallic complexes and organocatalysts.

In 2000, List reported the highly successful proline-catalysed Mannich reaction with *N*-aryl imines (Scheme 1.15). Proline (**1**) is among the simplest possible chiral bifunctional catalysts, bearing both an acidic carboxyl group and a basic amine moiety. This one-pot three-component reaction involving a ketone, aldehyde and a primary amine provided the Mannich product in high *ee* (up to 99%). The corresponding aldol product also formed but in significantly lower yield (< 20%)⁴⁸ A clear advantage of this approach is that the catalyst is readily available in both enantiomeric forms.

Scheme 1.15:

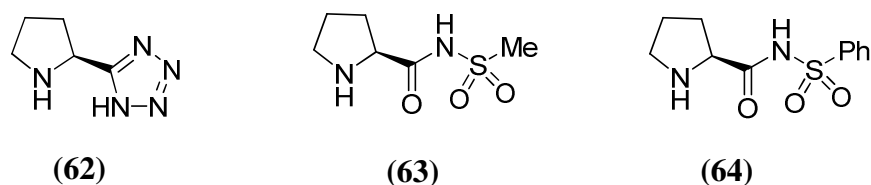


Shortly afterwards Barbas reported the development of an analogous proline-catalysed three-component Mannich reaction.⁴⁹

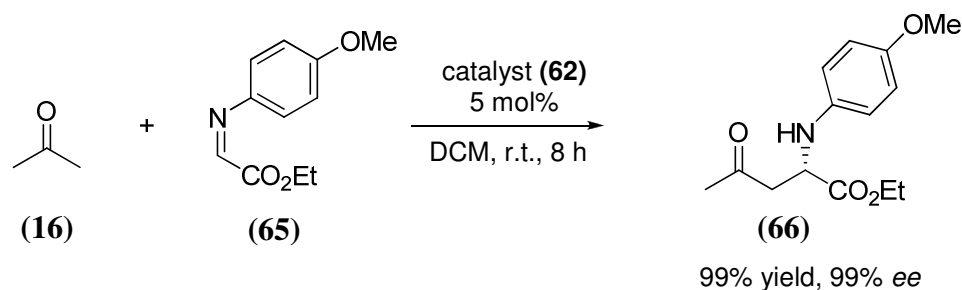
Enders *et al.* reported the first example of *tert*-butoxycarbonyl (Boc) as an imine protecting group in proline-catalysed Mannich reactions, achieving good yields and selectivity. Soon thereafter Cordova and List independently reported extensive studies on the use of *N*-Boc imines in Mannich reactions. Cordova's study showed that both proline and hydroxyproline were able to stereoselectively promote the reaction between *N*-Boc aryl imines and aliphatic aldehydes in high yields (73-85%) and selectivity (*ee* up to 99%).⁵⁰

List's report dealt with the synthesis of *N*-Boc amino aldehydes employing proline as the catalyst. It was found that acetone could also be used as the Mannich donor. There are certain limitations as aliphatic imines are not tolerated by the process and the imines must be pre-formed.⁵¹

Despite the fact that proline has been often shown to catalyse reactions in high enantio- and diastereoselectivity, there are a few drawbacks to the use of proline. The proline-catalysed reaction is generally performed in solvents such as DMF, dioxane and DMSO due to the relatively good solvation of the catalyst in these polar solvents. Recently, Ley and co-workers developed substituted proline catalysts (**62**)-(**64**) which have proven to work efficiently in more apolar solvents such as CH₂Cl₂ at significantly lower catalyst loadings (Scheme 1.16).⁵²

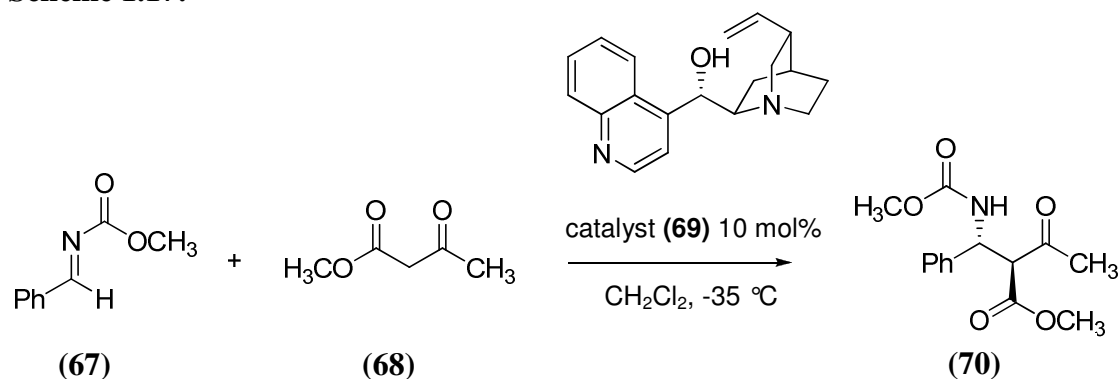


Scheme 1.16:



Asymmetric Mannich reactions of malonates and β -ketoesters are attractive transformations for synthetic chemists as the products are readily transformed into β -amino acid derivatives. Schaus and co-workers employed cinchonine in the highly enantioselective Mannich reaction of β -ketoesters with aryl methyl carbamate imines (Scheme 1.17).⁵³

Scheme 1.17:

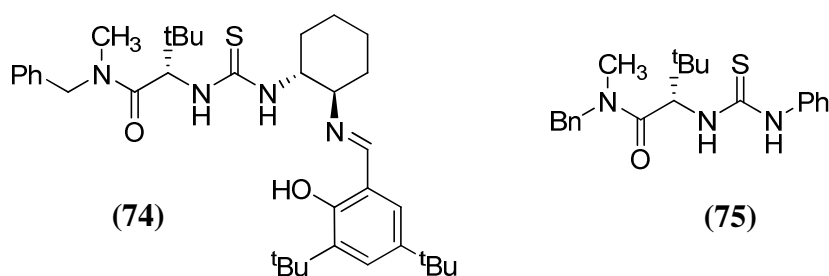
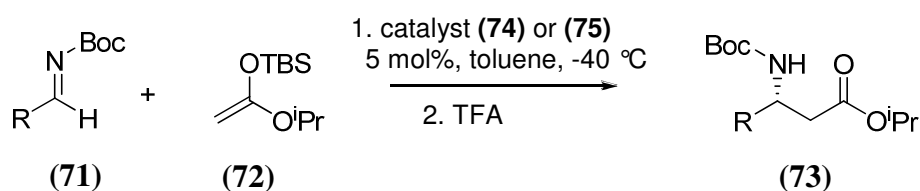


94% ee, 20:1 dr
99% yield

Deng and co-workers applied quinine-derived thiourea catalysts to the direct Mannich reaction of malonate compounds and *N*-Boc imines, achieving high enantioselectivity. The protocol was expanded to include alkyl *N*-Boc imines but required stoichiometric amounts of catalyst to achieve high enantiomeric excess.⁵⁴

Jacobsen reported the successful Mannich reaction of silyl ketene acetals and *N*-Boc aldimines in 2002.⁵⁵ This methodology provides a convenient route to Boc-protected β -amino acid derivatives. Subsequent systematic investigation of the efficiency of thiourea derivatives in the asymmetric Mannich reaction revealed that a significantly simplified thiourea (**75**) displays comparable reactivity and selectivity to catalyst (**74**) (Scheme 1.18).⁵⁶

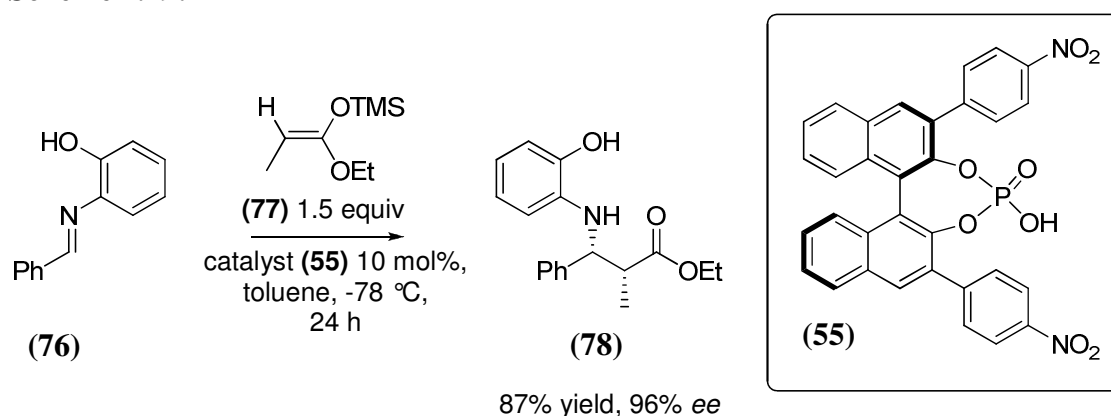
Scheme 1.18:



1.2.1.1 Catalysis of the Mannich reaction by chiral phosphoric acids.

It is clear that significant progress has been made in the field of hydrogen bonding catalysis. However, the acidity of thiourea⁵⁷ and aliphatic alcohol⁵⁸ functionalities is relatively weak (pK_a 20 to 30 in DMSO). Stronger Brønsted acids have also proven to be successful organocatalysts. Akiyama had previously reported that Mannich-type reactions proceeded smoothly in the presence of a catalytic amount of a strong Brønsted acid (HBF_4)⁵⁹ and postulated that use of a chiral Brønsted acid in which the proton is surrounded by bulky substituents, may lead to effective asymmetric induction. This was achieved using phosphoric acid (**55**) which successfully catalysed the Mannich reaction of *N*-aryl imines with silyl ketene acetals in high enantiomeric excess (Scheme 1.19).⁴⁵ It was thought that these Brønsted acids acted as stronger electrophilic activators by protonating the imine substrate to some extent.

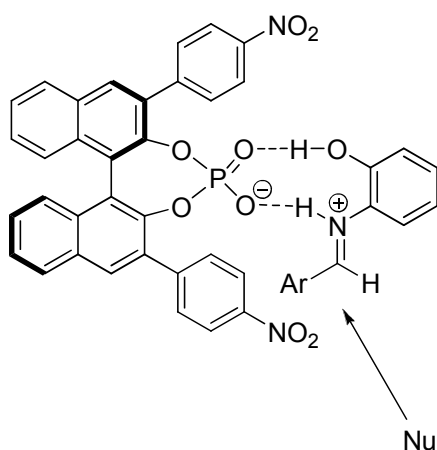
Scheme 1.19:



However, the success of this reaction proved highly substrate and solvent dependent. Only aromatic solvents were tolerated with ether, dichloromethane and ethanol giving distinctly lower *ees* (30%, 13% and 0% respectively). It was found that 3,3'-substitution of the catalyst framework enhanced the enantioselectivity of the reaction. Use of the un-substituted analogue gave a racemic mixture after 22 hours. The aldimine could not be substituted for aliphatic derivatives and use of *N*-benzylideneaniline lowered the *ee* to 39%, indicating that the presence of the hydroxy group in the *ortho* position of the aldimine is essential for the success of this particular transformation. It was thought that the 2-hydroxy group would hydrogen bond to the phosphoryl oxygen to form a nine-membered cyclic transition state.

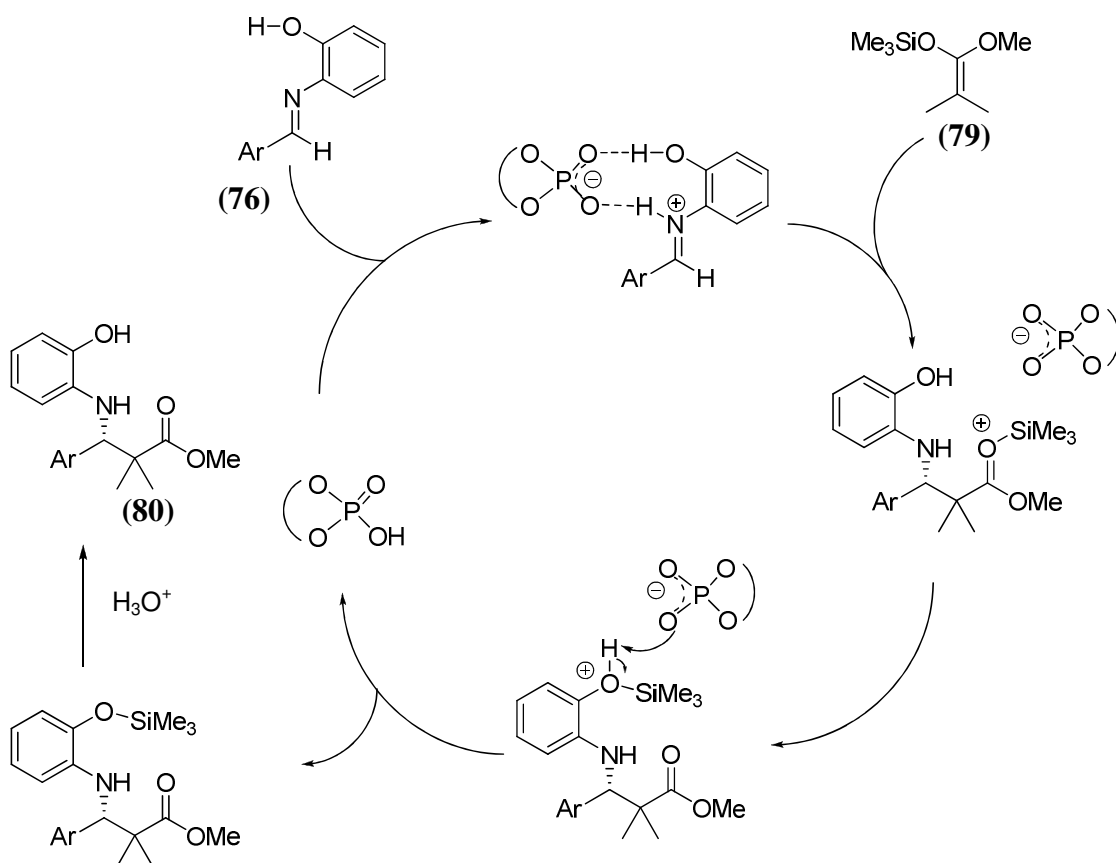
The mechanism of this reaction was probed in a DFT study by Akiyama in 2007.⁶⁰ Two possible reaction pathways were explored (mono and dicoordination). This theoretical study elucidated that this reaction proceeds via a dicoordination pathway through a zwitterionic nine-membered transition state involving the phosphoric acid and the aldimine (Figure 1.9).

Figure 1.9: Proposed nine-membered cyclic transition state.



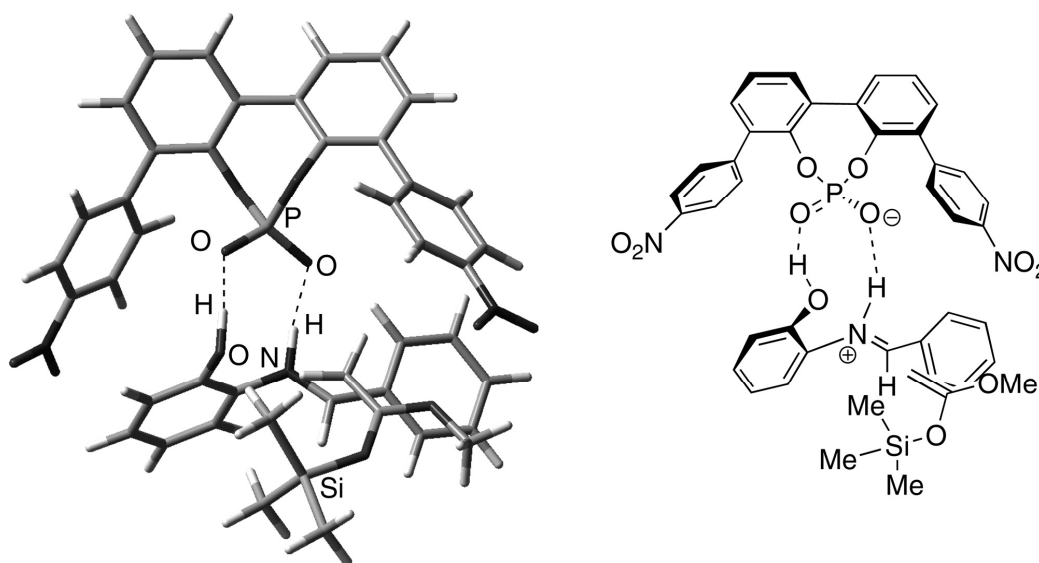
A possible reaction mechanism was proposed (Scheme 1.20).

Scheme 1.20:



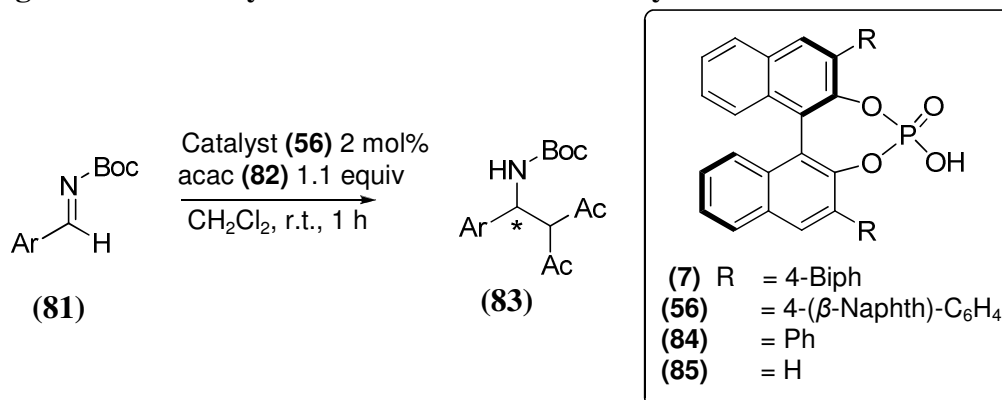
The *re*-facial selectivity was also well rationalised theoretically. The nine-membered cyclic structure and aromatic stacking interaction between the 4-nitrophenyl group and the *N*-aryl group would fix the geometry of the aldimine in the transition state. The *si*-facial alternative is structurally less favoured due to repulsive interactions of the 3,3'-substituents. The transition state model was calculated using a structurally simpler biphenyl-derived phosphoric acid (Figure 1.10).⁶¹

Figure 1.10: Zwitterionic cyclic transition state for the Mannich reaction.



(Reproduced with the permission of ACS publications)

Terada independently reported the efficient and selective phosphoric acid-catalysed direct Mannich reaction of *N*-Boc imines with acetylacetone in the same year (Figure 1.11).¹¹ Again, 3,3'-substitution was found to be essential for high enantioselectivity, with use of (**56**) giving up to 98% *ee*. This direct Mannich reaction is particularly attractive as it is performed under mild reaction conditions (ambient temperature) and acetylacetone, a readily enolisable unmodified ketone donor, is used instead of a preformed enolate equivalent. Whilst the *ortho*-substituted aryl imine was deemed essential for the success Akiyama's asymmetric Mannich reaction, Terada's system utilised *N*-Boc imines with no detrimental effect on *ee* (Table 1.1).

Figure 1.11: Asymmetric Brønsted acid-catalysed direct Mannich reaction.**Table 1.1:**

Entry	Ar	Yield (%)	ee (%)
1.	<i>p</i> -MeO- C_6H_4	93	90
2.	<i>p</i> -Me- C_6H_4	98	94
3.	<i>p</i> -Br- C_6H_4	96	98
4.	<i>p</i> -F- C_6H_4	94	96
5.	<i>o</i> -Me- C_6H_4	94	93
6.	1-Naphthyl	99	92

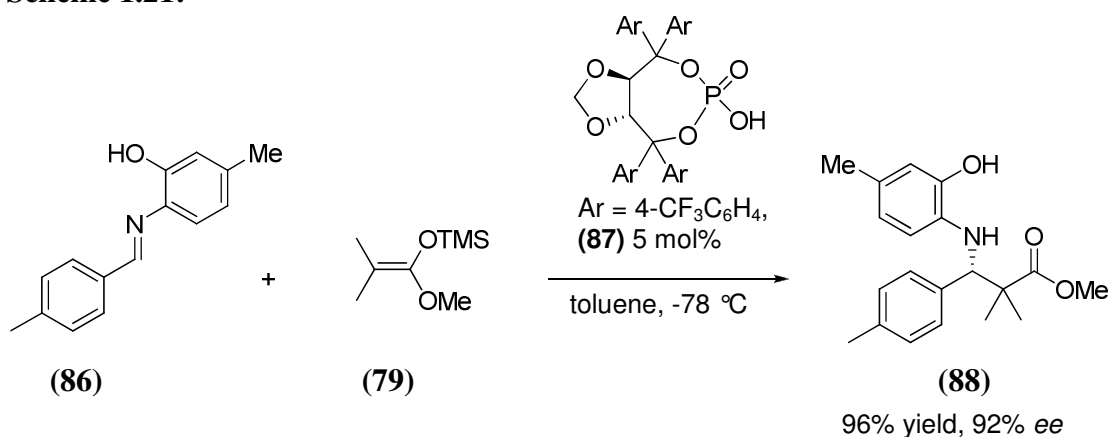
This reaction was found to proceed in high yield and *ee* and tolerated a range of substituted aldimines. Only 2 mol% catalyst is required and catalyst can be recovered in high yield.

Gridnev and Terada studied a complex derived from (*S*)-**(7)** and *N*-Boc imine **(81)** using computational methods in order to rationalise the origin of the enantioselectivity.⁶² It was concluded in this study that although the acidic proton interacts strongly with the nitrogen atom of the imine, it remains connected to the chiral phosphoric acid. The formation of simple hydrogen-bonded associates between the chiral phosphoric acid and imine is finely regulated by steric interactions of the catalyst with the substrate. The configuration of the hydrogen-bonded associate is suitable for stereospecific nucleophilic attack. One side of the imine double bond is shielded by a biphenyl substituent, whereas the other face is open for the approach of the nucleophile. Terada postulated that the asymmetric Mannich reaction proceeded through a hydrogen-bonding network in which the phosphoric acid catalyst electrophilically activates the imine through the acidic proton, with the phosphoryl oxygen interacting with the intramolecularly hydrogen-bonded proton of

the enol form of **(82)**. This leads to formation of the Mannich product and regeneration of the acid catalyst.

Chiral phosphoric acids are not restricted to those developed from BINOL. A TADDOL based phosphoric acid was developed by Akiyama *et al.* and applied to the Mannich reaction (Scheme 1.21).⁶³ It was found that the aryl substituents of the catalyst strongly affected both the chemical yield and the enantioselectivity.

Scheme 1.21:



As for the BINOL phosphoric acid-catalysed Mannich reaction, a nine-membered transition state was proposed, wherein the phosphate hydrogen activated the imine and the phosphoryl oxygen interacted with the imine hydroxyl group by hydrogen bonding.

It is clear that organocatalysis has emerged as a highly active and exciting field of research in recent years. In particular, many efficient and selective Brønsted acid-catalysed reactions have been developed. However, many transformations are highly substrate and solvent dependent and few broadly successful catalysts exist. The development of improved catalysts is hampered in many cases by a lack of mechanistic insight. This work aims to probe the mechanism of Brønsted acid organocatalysis of the Mannich reaction. The results of these investigations are presented and discussed in Chapter 2.

Chapter 2

Mechanism-guided investigations of the Mannich reaction

2.0 Foreword.

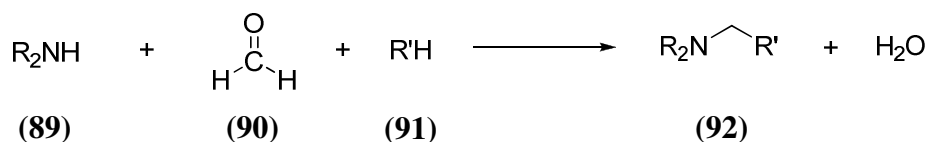
This chapter describes investigations of the asymmetric Mannich reaction. In Section 2.1 a brief review of relevant literature pertaining to mechanistic studies of the Mannich reaction is presented. Section 2.2 describes the results obtained from our studies of Brønsted acid organocatalysis of the Mannich reaction. This includes the synthesis of compounds for kinetic study (Section 2.2.1), evaluation of the success of phosphoric acid catalysts and thiophosphoryl analogues in the asymmetric Mannich reaction by chiral HPLC analysis of the reaction products (Section 2.2.2), determination of the pK_a values of iminium ions and BINOL-derived catalysts (Sections 2.2.3-2.2.4) and kinetic studies of the Mannich reaction (Section 2.2.5). These results are discussed in Section 2.3.

2.1 Introduction.

2.1.1 The Classical Mannich reaction.

As mentioned in Chapter 1, the Mannich reaction is an important carbon-carbon bond forming reaction that involves the addition of carbon nucleophiles to imines. In the original and most widely recognised form, the Mannich reaction consists of three components: (i) an amine; (ii) a non-enolisable aldehyde, usually formaldehyde; and (iii) an active methylene compound (Scheme 2.1). The active hydrogen compound, R'H, is most frequently a ketone, an acid or an ester. These compounds condense with release of water to produce a new base, known as a "Mannich base", in which the active hydrogen is replaced by an aminomethyl group.

Scheme 2.1:

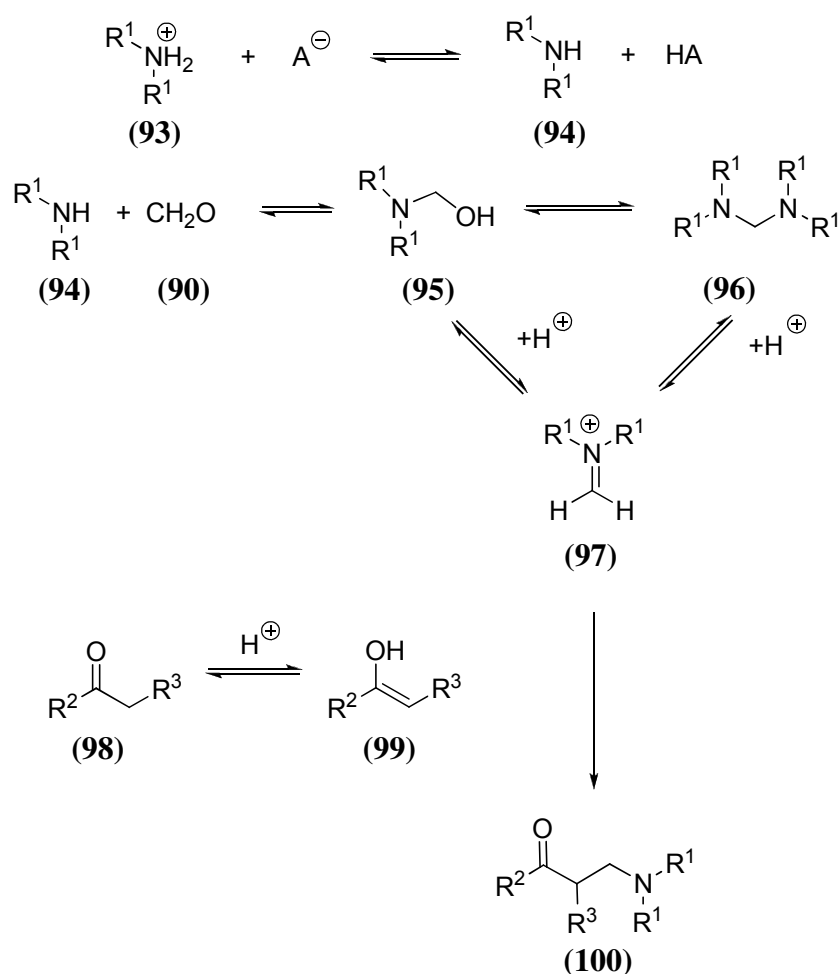


The formation of these nitrogenous molecules makes the Mannich reaction an attractive transformation for synthetic chemists. As a result the classical Mannich reaction has been thoroughly studied.⁶⁴⁻⁶⁶ and the reaction mechanism has been the subject of considerable discussion.⁶⁷⁻⁷⁰

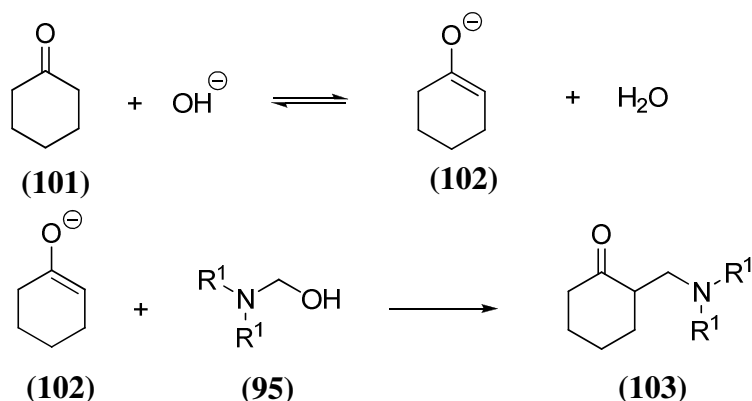
The Mannich reaction is most commonly performed in protic solvents and involves acid catalysis (usually by employing the amine component in the hydrochloride salt form). Under these conditions, the amine is in equilibrium with the salt form. The mechanism is thought to involve the intermediacy of a highly reactive, positively charged iminium ion, which reacts with the active enol form of the methylene component to produce the Mannich base. Formation of the iminium ion occurs by decomposition of methylenediamine or hydroxymethylamine, both of which are generated reversibly by condensation of the aldehyde and amine components. *N*-hydroxymethylamines may be obtained from aqueous formaldehyde and the amine with cooling. Methylenediamines are formed exclusively when formaldehyde and amine are reacted without cooling. Both classes of compound are very acid sensitive

and follow a well defined reaction course in acid hydrolysis from the symmetrical methylenediamine.⁷¹ Acid catalysis not only promotes the decomposition of the hydroxymethylamine to the iminium ion, but also the enolisation of the active methylene component (Scheme 2.2). Protic solvents also support the formation of the charged iminium species by virtue of their high dielectric constant.

Scheme 2.2: Mechanism of the classical Mannich reaction in an acidic medium.



Studies of the reaction kinetics of the classical Mannich reaction indicate that there is a change in mechanism with changing pH. The proposed mechanism for the Mannich reaction in basic media does not suggest the formation of the iminium ion, which indeed should only be present in acidic media. Aminomethylation in base-catalysed Mannich reactions, as shown for cyclohexanone in Scheme 2.3, is believed to occur by an $\text{S}_{\text{N}}2$ mechanism in which the enolate displaces hydroxide from dialkylaminomethanol.

Scheme 2.3: Mechanism of the classical Mannich reaction in a basic medium.

There has been no in-depth kinetic analysis of the addition of acetylacetone to *N*-Boc imines to date, despite the wide synthetic use of this transformation. While mechanistic studies of the classical Mannich reaction have utilised aqueous reaction media, modern catalysed Mannich reactions are more frequently performed in organic solvent. Moreover, many common substrates such as *N*-Boc imines are hydrolytically labile. There is dearth of kinetic data pertaining to enantioselective Mannich reactions and corresponding background reactions which hampers the elucidation of reaction mechanisms and rational design of improved processes.

2.1.2 Brønsted acid-base catalysis.

As mentioned previously Brønsted acid-base catalysis is a very common form of catalysis in organic chemistry. In Brønsted acid-base catalysis, a proton or hydroxide becomes involved in the reaction mechanism, lowers the energy of the transition state(s), accelerates the reaction and finally is regenerated. The two classes of Brønsted acid-base catalysis are identified as specific and general catalysis.

Specific acid catalysis refers to a process in which proton transfer is fast and takes place in a pre-equilibrium rather than as part of the rate determining step. The rate of reaction depends upon the concentration of hydronium ion. General acid catalysis refers to a process in which proton transfer is involved in the rate determining step and is not involved in a pre-equilibrium step. In the case of general acid catalysis, the nature and concentration of all acids present in solution affect the rate of the reaction.

2.1.2.1 The Brønsted law.

The Brønsted relationship is one of the earliest examples of a linear free energy relationship. This relationship is between the catalytic constants for a reaction catalysed by a family of general acids or bases and the relevant pK_a values for these acid/base catalysts. The Brønsted law is described by Equations 2.1-2.2, where k_{HA} is the catalytic constant and K_{HA} is the acid dissociation constant. Since general catalysis arises when proton transfer from/to an acid or base occurs in the rate-determining step, the rates of the reactions depend on the intrinsic reactivity of the acid or base acting as the catalyst *i.e.* the observed rate constant depends on the concentrations of the catalysts and also their structure. For example, a general acid catalysed reaction proceeds at a faster rate if a stronger acid is used.

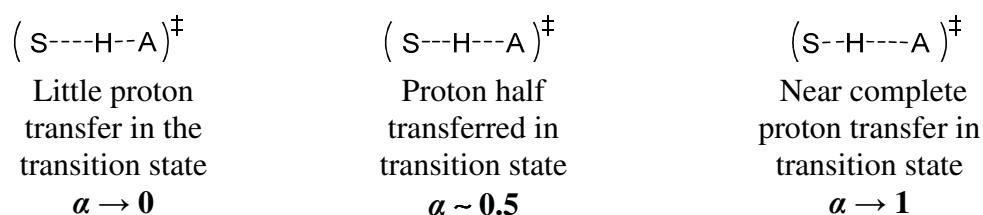
$$\log k_{HA} = \alpha \log K_{HA} + C = -\alpha pK_{HA} + C \quad (\text{Equation 2.1})$$

$$\log k_{A^-} = -\beta \log K_{A^-} + C = \beta pK_{A^-} + C \quad (\text{Equation 2.2})$$

The magnitude of the Brønsted coefficients, α and β , gives mechanistic insight into general acid- and general base-catalysed reactions. In the simplest cases, these reflect the extent of proton transfer in the transition state of the rate-determining step. Brønsted coefficients can be determined from a logarithmic plot of the catalytic constants k_{HA} or k_{A^-} against the pK_a values of the catalytic acids or bases.

For a general acid-catalysed reaction, if the extent of proton transfer is minimal in the transition state, then a poor proton donor will be as effective as a good proton donor resulting in a small value of α . Alternatively if proton transfer at the transition state is almost complete a stronger acid will be a much more effective catalyst and α will have a value close to unity (Figure 2.1).

Figure 2.1: Proton transfer progression at the transition state.



Obtaining Brønsted coefficients that do not lie between 0-1 is clearly conflict with the hypothesis that α or β is equal to the degree of proton transfer at the transition state. Negative proton transfer or more than complete proton transfer can have no real meaning. However these values typically result from transition-state imbalances and are now well understood.

Deviations from linearity may be observed in Brønsted plots. The rate of an acid-catalysed reaction cannot continue to increase indefinitely. As the acid increases in strength, the rate will only increase until the proton transfer process begins to approach the diffusion controlled limit. At this point the rate can no longer increase proportionally with the introduction of stronger acids and curvature in the Brønsted plot is exhibited, with a plateau at $\alpha = 0$.

Although there have been significant advances in the field of Brønsted acid organocatalysis, mechanistic investigations have been comparatively sparse. While Terada and Akiyama have provided some studies on the mechanism of the asymmetric Mannich reaction, further work is certainly required to fully understand the transfer of chirality in the transition state for the reaction. Previous studies have made use of computational chemistry, but to date there have been no systematic structure-activity investigations. If indeed chirality transfer occurs by proton transfer to a single enantiotopic face of substrate, the extent of proton transfer has not been experimentally quantified. Application of the Brønsted linear free energy relationship to the asymmetric Mannich reaction could shed light on these unanswered mechanistic questions. This chapter presents results towards this aim.

A number of possibilities exist. If proton transfer to/from the catalyst is involved in the transition state for the rate-determining step, a change in catalytic constant would be observed upon use of a structurally homologous series of acids of varying pK_a values ($\alpha = 0-1$). Conversely, if proton transfer to/from the catalyst is not involved in the transition state for the rate-determining step, there would be no change in the catalytic constant upon use of catalysts with different pK_a values ($\alpha = 0$).

There is also a possibility that the conjugate base of the catalyst could act as a general base and activate the enolate for reaction with the protonated imine. This corresponds

to a mechanism of specific acid catalysis followed by general base catalysis, which would be kinetically observed as general acid catalysis. In this situation, the catalytic constant would show a dependence on changing acid ($\alpha = 0-1$).

In order to apply the Brønsted linear free energy relationship to the Mannich reaction, a structurally homologous series of imines and catalysts must be prepared and overall rates of reaction measured. Correlation of the rate data with pK_a values of phosphoric acid catalysts and iminium ions would provide Brønsted coefficients which could be interpreted in terms of the reaction mechanism.

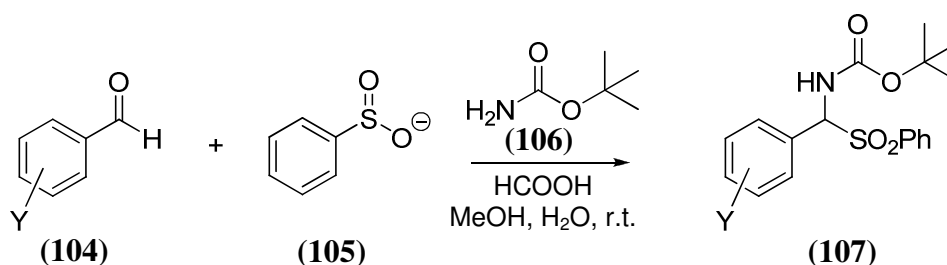
2.1 Results

2.1.1 Synthesis

A rigorous physical organic study of mechanistic aspects of the Mannich reaction requires the synthesis of a structurally homologous series of substrates and catalysts. This was achieved using established literature protocols with slight modifications in some cases for the improvement of purity or yield.

N-Boc imines (**81**) were synthesised in two steps according to literature procedures.⁷² Reaction of *tert*-butyl carbamate (**106**), benzene sulfonic acid sodium salt (**105**) and formic acid with various *para*- or *meta*- substituted benzaldehydes (**104**) yielded sulfone product (**107**). Reaction times varied according to the aldehyde used from 24 to 72 h (Scheme 2.4). Isolation of pure sulfone required trituration with ice-cold water followed by diethyl ether. Further crops of product were obtained from the filtrate. The sulfones were dried rigorously under high vacuum before further reaction.

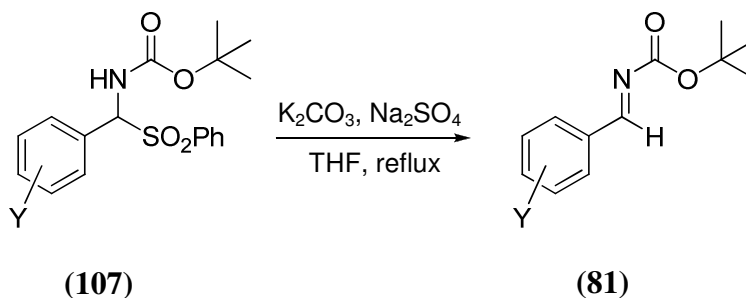
Scheme 2.4:



Y = *p*MeO, *m*MeO, *p*Me, H, *p*F, *p*Br, *p*Cl, *p*NO₂, *p*^tBu, *p*MeS

The exclusion of adventitious water was essential to the success of the second step. The sulfone precursors were reacted with dried potassium carbonate in the presence of sodium sulfate in dry THF to give imines (**81**) in high yield and purity (Scheme 2.5).

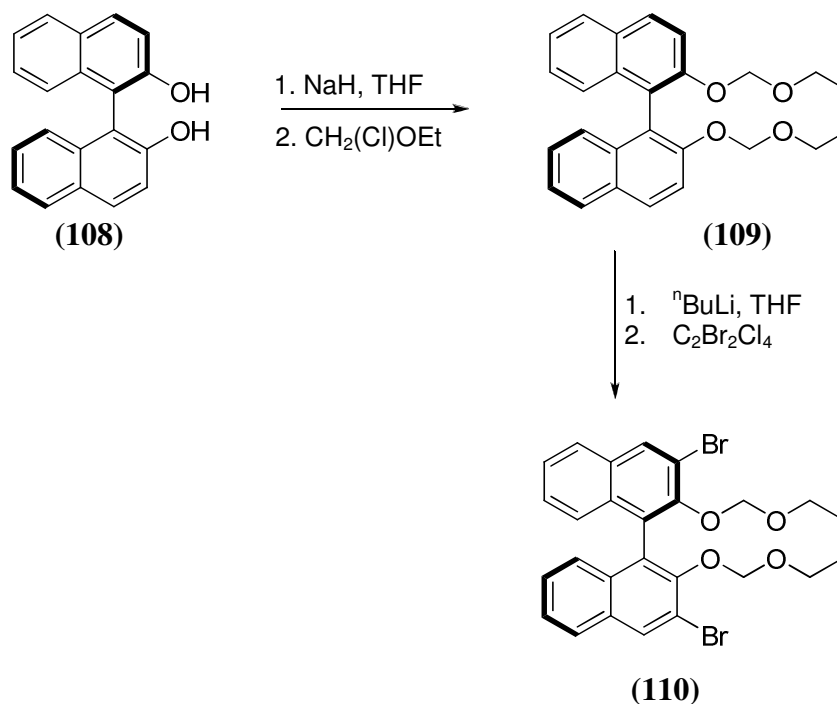
Scheme 2.5:



Y = *p*MeO, *m*MeO, *p*Me, H, *p*F, *p*Br, *p*NO₂, *p*^tBu

BINOL-derived phosphoric acid catalysts were synthesised in five steps as described in the literature.⁷³ Initially, (*R*)-BINOL (**108**) was deprotonated using NaH and protected using chloromethyl ethyl ether. The product (**109**) was isolated in high yield by column chromatography. This was followed by *ortho*-metalation using ⁿBuLi and dibromotetrachloroethane which afforded pure product (**110**) after column chromatography and recrystallisation (Scheme 2.6).

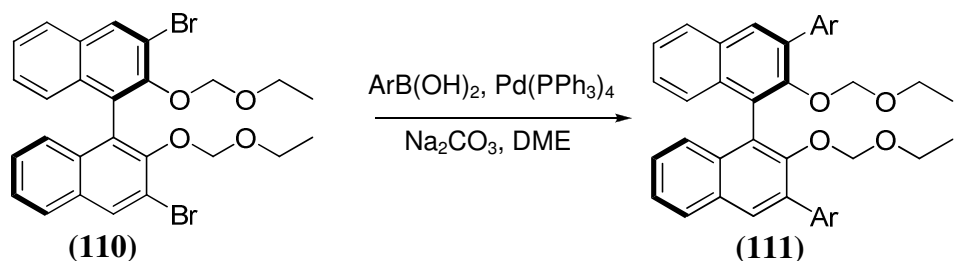
Scheme 2.6:



It was reported by Terada that 3,3'-substitution with aromatic moieties induced higher enantioselectivity in the Mannich reaction.⁷⁴ Therefore, standard Suzuki cross-coupling conditions were employed to extend the aromatic backbone and provide a

range of 3,3'-substituted compounds for kinetic study (Scheme 2.7). This reaction proceeded in good yield using DME or toluene as the solvent. Column chromatography was again required to isolate pure product (**111**).

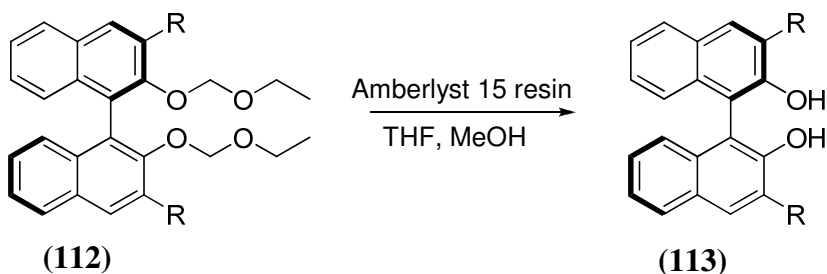
Scheme 2.7:



Ar = Ph, *p*MeOPh, Naphth, Biph

Removal of the methoxyethyl protecting groups was achieved by reflux with Amberlyst 15 resin (Scheme 2.8). Column chromatography followed by recrystallisation afforded pure diol products (**113**).

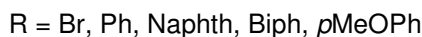
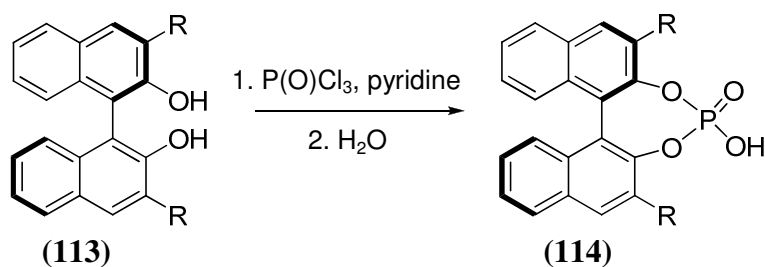
Scheme 2.8:



R = Br, Ph, *p*MeOPh, Naphth, Biph

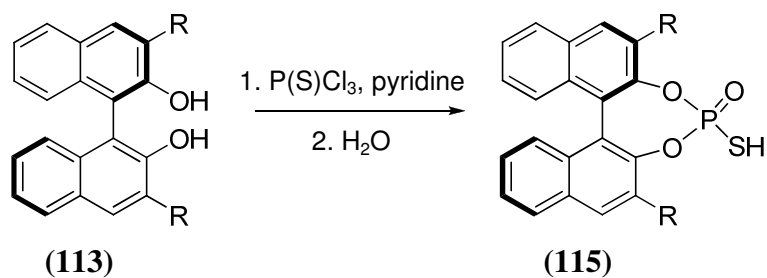
The final step was reaction of the diols with phosphorus oxychloride in dry pyridine followed by water (Scheme 2.9). Pyridine was removed by acid work-up. Purification of the resulting phosphoric acids (**114**) was achieved by column chromatography.

Scheme 2.9:



Although there are many examples of the use of BINOL-derived phosphoric acid catalysts in the literature, the application of thiophosphoryl analogues in asymmetric organocatalysis has not been explored. In order to evaluate their success in asymmetric Mannich reactions and potentially gain mechanistic insight, we synthesised a series of BINOL-derived thiophosphoric acid compounds. This was achieved by substitution of phosphorus oxychloride for thiophosphoryl chloride in the final step of the synthesis (Scheme 2.10). The exact positioning of the proton in these compounds is unknown. Analysis of the IR spectra did not allow us to differentiate between a carbon-sulfur double bond and a carbon-oxygen double bond. Clearly distinct P=O or P=S stretches would indicate which form was present, however the spectra obtained were not of sufficient quality to distinguish separate P=O or P=S stretches and were difficult to interpret. Yamamoto independently developed thiophosphoric acid catalysts for use in asymmetric protonation reactions in 2008 and reports the structure with a carbon-oxygen double bond.⁴⁶ A study by Frey and Sammons on phosphorothioate anion concludes that the P-S bond is a single bond with negative charge localised on sulfur, while the P-O bond order for the non-bridging oxygen approaches two. Their conclusions for this example and related anions are based on a review of bond length data from X-ray crystallography and electron diffraction.⁷⁵ In the absence of physical data to provide evidence for the existence of either form, the structures will be presented with a carbon-oxygen double bond throughout this thesis although this is tentatively assigned.

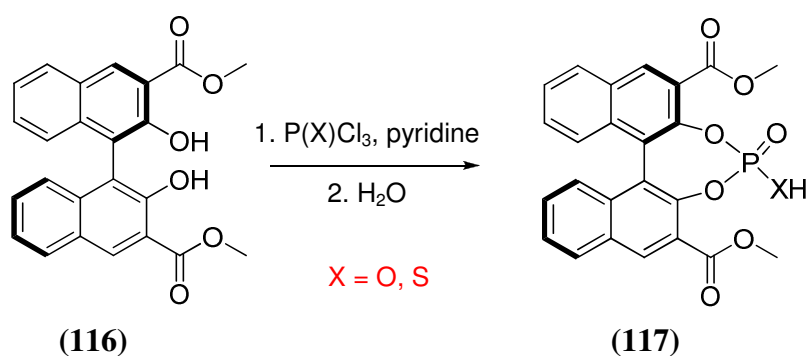
Scheme 2.10:



R = H, Br, Ph, Naphth, Biph

A commercially available BINOL derivative (116) was (thio)phosphorylated in order to access another two catalysts for our investigation (Scheme 2.11). Dilute acid was used in the reaction workup to ensure that the ester side chains remained intact.

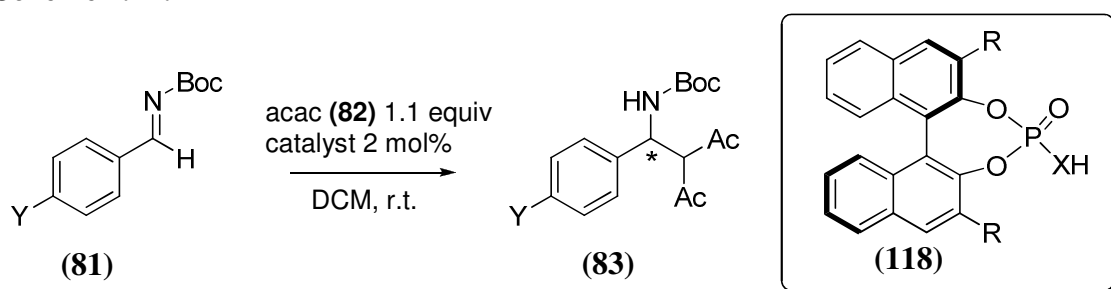
Scheme 2.11:



2.1.2 Evaluation of the enantioselectivity of the Mannich reaction

Each catalyst was used in the Mannich reaction of *N*-Boc imines (**81**) and acetylacetone (**82**) in order to assess their efficiency relative to those used by Terada⁷⁴ according to Scheme 2.12. Although the same reaction conditions were employed, it was impossible to isolate Mannich products in yields above 70% for the catalysed reactions examined. The remaining ~ 30% was identified as aldehyde which is the product of a competitive hydrolysis reaction.

Scheme 2.12:



Racemic samples were prepared by conducting the reactions without catalyst present. The Mannich bases were then examined by chiral HPLC in order to determine the enantiomeric excess (*ee*). The results of these investigations are presented in Table 2.1.

Table 2.1:

Entry	Imine ^a	Catalyst	Additive ^b	Yield ^c (%)	<i>ee</i> ^d (%)
1.	Y = Me	R = H, X = O	-	71	0.5
2.	Y = F	R = H, X = O	-	68	19
3.	Y = Me	R = H, X = S	-	67	10
4.	Y = MeO	R = H, X = S	-	65	12
5.	Y = F	R = H, X = S	-	68	2
6.	Y = MeO	R = Ph, X = O	4Å MS	67	75
7.	Y = MeO	R = Ph, X = O	Na ₂ SO ₄	68	75
8.	Y = MeO	R = Ph, X = S	-	68	3
9.	Y = MeO	R = Naphth, X = O	-	64	74
10.	Y = F	R = Naphth, X = S	-	65	3
11.	Y = MeO	R = Naphth, X = S	-	63	2
12.	Y = MeO	R = Biph, X = O	-	64	72
13.	Y = MeO	R = Biph, X = S	-	65	51
14.	Y = MeO	R = ester, X = O	4Å MS	68	63
15.	Y = MeO	R = Br, X = O	-	65	33
16.	Y = MeO	R = <i>p</i> MeOPh, X = O	4Å MS	65	47

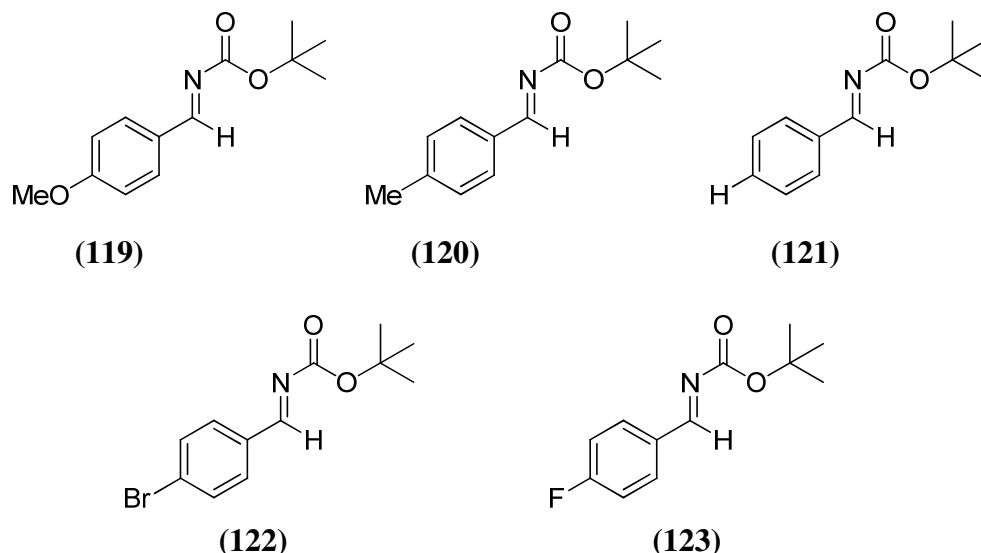
(a) The concentration of imine used was 0.1 mmol. (b) Drying agent added to attempt to reduce hydrolysis of imine substrate. (c) Isolated yield after column chromatography. (d) Separated on a Chiralpak IA column at 10 °C using 90:10, hexane:ethanol as the mobile phase. Absorbance was monitored at 254 nm. Each *ee* value is the average of two runs.

2.1.3 Determination of pK_a values of iminium ions

This section describes investigations of pK_a values of *N*-Boc aryl iminium ions both in water and organic solvent using UV-Vis spectrophotometry. Determination of aqueous pK_a values was complicated by the hydrolytic lability of the imine substrates. As such, a pH rate profile for hydrolysis was constructed, according to the method of Cordes and Jencks.⁷⁶ Investigations of pK_a values in organic solvent were conducted using a bracketing indicator method.⁷⁷

2.1.3.1 Attempted determination of aqueous pK_a values.

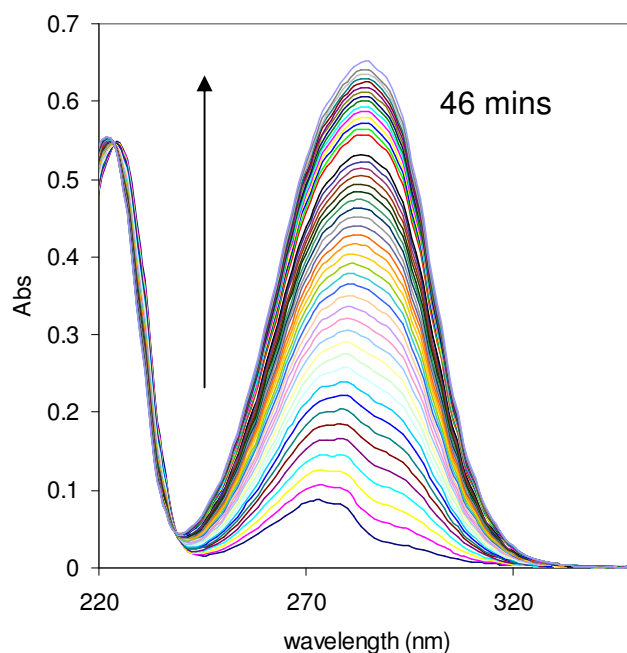
In recent years, *N*-Boc imines have proven to be synthetically useful in a wide variety of asymmetric transformations providing a convenient route to optically active nitrogenous products. Despite this popularity, there is a dearth of literature data concerning the pK_a values of these iminium ions. This may be the result of the hydrolytic lability of these compounds, which complicates the determination of pK_a values. A systematic study by Jencks in the 1960s on a series of *N*-alkyl imines gave pK_a values between 5.4 and 7.7.⁷⁶ The effect of substitution of the alkyl chain for a Boc group will likely be to reduce the pK_a value and it was therefore predicted that pK_a values of *N*-Boc iminium ions lay between 2 and 4. Unfortunately hydrolysis of the imine is prominent in the pH region of interest and occurs with rate constants of between $1 \times 10^{-1} \text{ s}^{-1}$ and $7 \times 10^{-4} \text{ s}^{-1}$. This precluded pK_a measurements by conventional UV-Vis spectrophotometric methods. Instead, the method of Cordes and Jencks⁷⁶ was adopted and pH-rate profiles for hydrolysis were constructed with the aim of gaining information about the iminium ion pK_a values. Rate constants for hydrolysis of a series of substituted *N*-Boc aryl imines (**119**)-(**123**) to the corresponding aldehydes were determined using a combination of UV-Vis spectrophotometry and stopped-flow spectrophotometry, in a range of aqueous buffers and HCl solutions. In all cases, reactions were conducted at 25 °C with ionic strength maintained at 1.0 with potassium chloride.



Typically, stock solutions of imines in acetonitrile were prepared to a concentration of 6 mM and reactions were initiated by a 1/120 dilution of these stock solution into the relevant buffer or acid solution which had been thermostated at 25 °C for ten minutes.

A representative repetitive scan of the hydrolysis reaction of *p*-methoxybenzaldehyde *N*-(*tert*-butoxycarbonyl)imine (**119**) at pH 4.10 at 25 °C and $I = 1.0$ (KCl) is shown in Figure 2.2. As the reaction proceeds, there is an increase in absorbance corresponding to aldehyde formation at 284 nm. The products of the hydrolysis reaction were verified by mass spectrophotometric analysis of the reaction solution and by comparison of the final absorbance with that of the same concentration of an authentic sample of aldehyde. ¹H NMR spectroscopic analysis also confirmed the presence of aldehyde as the product of hydrolysis for each imine with characteristic peaks visible at ~10 ppm. There was no evidence of hydrolysis occurring at the Boc carbonyl group of the imine in the pH range investigated.

Figure 2.2: Representative repetitive scan of *p*-methoxybenzaldehyde *N*-(*tert*-butoxycarbonyl)imine (119) in acetic acid buffer (pH 4.10) at 25 °C and I = 1.0 (KCl).



Experimental pseudo-first-order rate constants for hydrolysis, k_{obs} (s^{-1}), were obtained from semi-logarithmic plots of $\Delta A = A_{\infty} - A_t$ against time, where A_{∞} is the maximum absorbance and A_t is the absorbance at time t .

The observed experimental first-order rate constant can potentially be the sum of rate constants for several parallel hydrolysis processes, including a pH independent (k_0), specific acid catalysed (k_{H}) and general acid catalysed (k_{HA}) reaction. Higher order dependency on a general acid is a possibility (e.g. $k_{\text{HA}}'[\text{HA}]^2$ where $[\text{HA}]$ is the concentration of the general acid).

The rate constant for hydrolysis (k_{obs} , s^{-1}) is defined as in Equation 2.3.

$$k_{\text{obs}} = k_0 + k_{\text{H}}[\text{H}^+] + k_{\text{HA}}[\text{HA}] \quad \text{(Equation 2.3)}$$

The contribution of general acid catalysis was investigated by conducting experiments at fixed pH and constant buffer acid/base ratio, whilst varying the absolute buffer concentration. In general, a higher concentration of general acid ($[\text{HA}]$) was found to increase the rate constant (k_{obs} , s^{-1}) at fixed pH. The dependency of k_{obs} on $[\text{HA}]$ was

linear. No upward curvature was observed which would have been indicative of a higher order dependence on [HA]. Buffer-independent rate constants for hydrolysis, $k_{\text{hyd}} \text{ (s}^{-1}\text{)}$, were obtained by extrapolation to a buffer-independent y-axis intercept of a plot of $k_{\text{obs}} \text{ (s}^{-1}\text{)}$ against buffer concentration [HA].

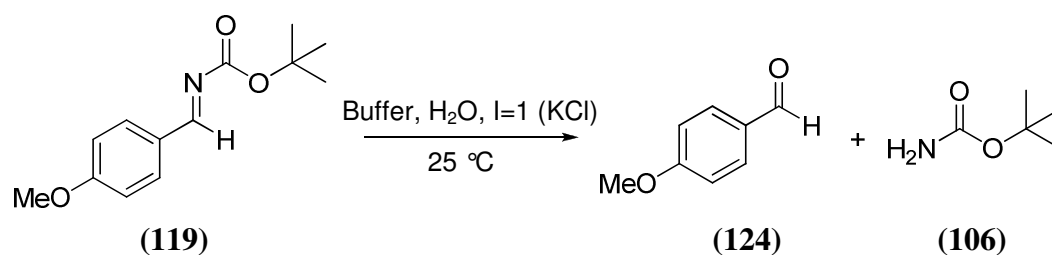
$$k_{\text{hyd}} = k_0 + k_{\text{H}}[\text{H}^+] \quad \text{(Equation 2.4)}$$

Buffer-independent rate constants, $k_{\text{hyd}} \text{ (s}^{-1}\text{)}$, were used in the construction of pH-rate profiles for imine hydrolysis (Equation 2.4).

2.1.3.1.1 *p*-Methoxybenzaldehyde *N*-(*tert*-butoxycarbonyl)imine (119).

The hydrolysis reaction of *p*-methoxybenzaldehyde *N*-(*tert*-butoxycarbonyl)imine (**119**) in a range of aqueous buffer and HCl solutions was investigated using a combination of UV-Vis and stopped-flow spectrophotometry (Scheme 2.13).

Scheme 2.13: Hydrolysis reaction of *p*-methoxybenzaldehyde *N*-(*tert*-butoxycarbonyl)imine (**119**).



A representative repetitive scan of the hydrolysis reaction of imine (**119**) in acetic acid buffer is shown in Figure 2.2. As the reaction proceeds, an increase in absorbance at $\lambda_{\text{max}} = 284 \text{ nm}$ is seen which corresponds to formation of *p*-methoxybenzaldehyde (**124**). The analytical wavelength, $\lambda = 284 \text{ nm}$, was chosen for kinetic study.

Figure 2.3 shows a typical kinetic trace of absorbance (abs) versus time data obtained at 284 nm for imine (**119**). The first-order rate constant for hydrolysis at this pH and different buffer concentrations, $k_{\text{obs}} \text{ (s}^{-1}\text{)}$, could be obtained as the slope of a semi-logarithmic plot of $\Delta A = A_{\infty} - A_t$ against time (Figure 2.4).

Figure 2.3: Hydrolysis of *p*-methoxybenzaldehyde *N*-(*tert*-butoxycarbonyl)imine (119) in acetic acid buffer (75% f_B , pH 5.09) at 25 °C and $I = 1.0$ (KCl); plot of absorbance against time.

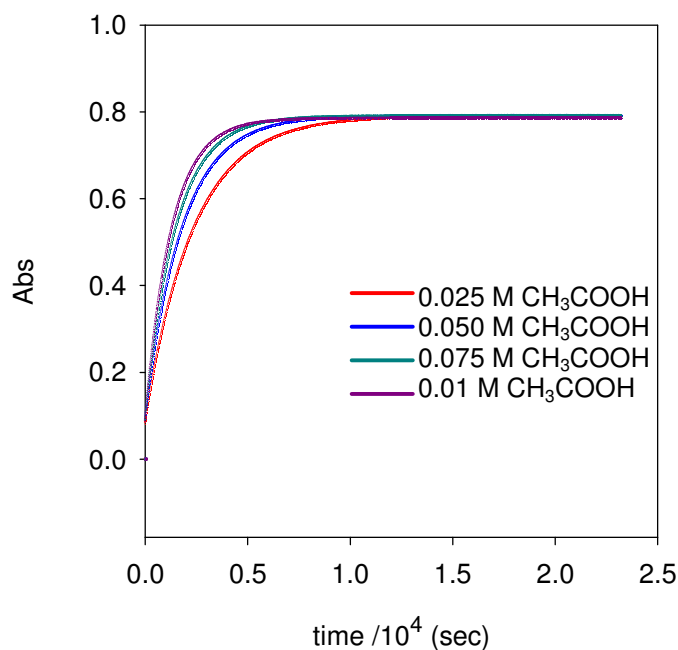
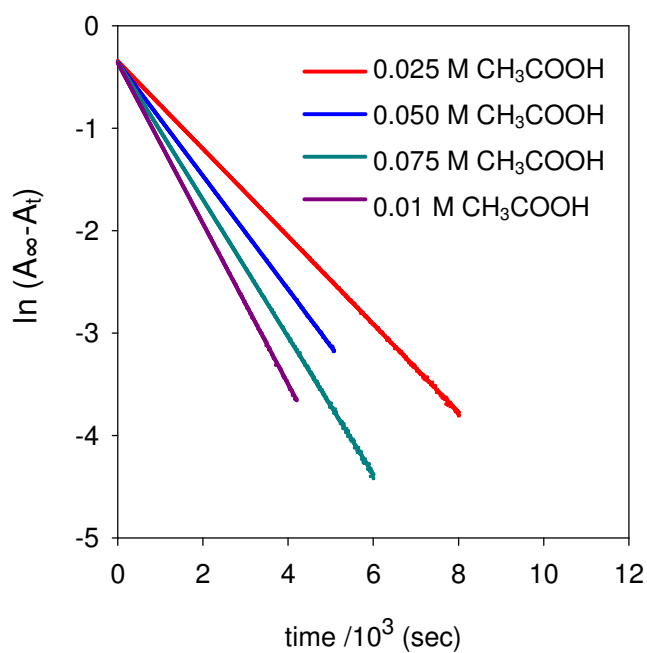
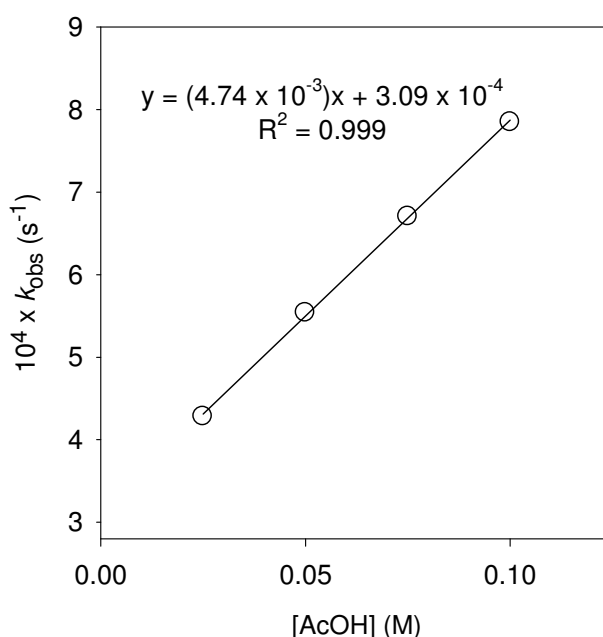


Figure 2.4: Semi-logarithmic plot of $(A_{\infty}-A_t)$ against time for the hydrolysis of *p*-methoxybenzaldehyde *N*-(*tert*-butoxycarbonyl)imine (119) in acetic acid buffer (75% f_B , pH 5.09) at 25 °C and $I = 1.0$ (KCl).



The second-order rate constant for general acid-catalysed hydrolysis (k_{HA} , $\text{M}^{-1}\text{s}^{-1}$) could be obtained as the slope of a plot of the k_{obs} values against the concentration of general acid, acetic acid (Figure 2.5). As mentioned previously, a value for k_{hyd} (s^{-1}), the first-order rate constant for buffer-independent hydrolysis, can be obtained as the y-axis intercept of this plot. As can be observed in Figure 2.5, this plot is linear and thus a higher order dependence on the concentration of acetic acid is not observed.

Figure 2.5: Hydrolysis of *p*-methoxybenzaldehyde *N*-(*tert*-butoxycarbonyl)imine (**119**) in acetic acid buffer (75% f_{B} , pH 5.09); plot of k_{obs} against the concentration of acetic acid, $[\text{CH}_3\text{COOH}]$.



Hydrolysis of imine (**119**) was followed in acetic acid buffers at pH 3.61, 4.10, 4.65, 5.09 and 5.58. The hydrolysis of imine (**119**) was also monitored in chloroacetic acid buffers (pH 3.19), phosphate buffers (pH 5.86, 6.54) and imidazole buffers (pH 7.24, 7.71, 8.18). All remaining first and second-order plots for the hydrolysis of imine (**119**) are presented in Appendix A (Figures A2-A11). Reaction data for these plots is also tabulated in Appendix A (Tables A2-A4). For reactions in acetic acid, chloroacetic acid and phosphate buffers, pseudo-first-order rate constants for hydrolysis were observed to increase linearly with an increase in concentration of general acid. For reactions in imidazole buffer a decrease in k_{obs} was observed as the concentration of imidazolium ion ($[\text{ImH}^+]$) increased.

Reactions in HCl solution were monitored using stopped-flow spectrophotometry and first-order rate constants (k_{hyd} , s^{-1}) were obtained directly by least squares analysis of absorbance versus time data. A representative example of a kinetic trace with a first-order exponential fit and corresponding residuals is shown in Figure 2.6. All further plots and reaction data are shown in Figure A1 (a)-(k) and Table A1 respectively (Appendix A).

Figure 2.6: Hydrolysis of *p*-methoxybenzaldehyde *N*-(*tert*-butoxycarbonyl)imine (119) in HCl solution (pH 1.45) at 25 °C and I = 1.0 (KCl).

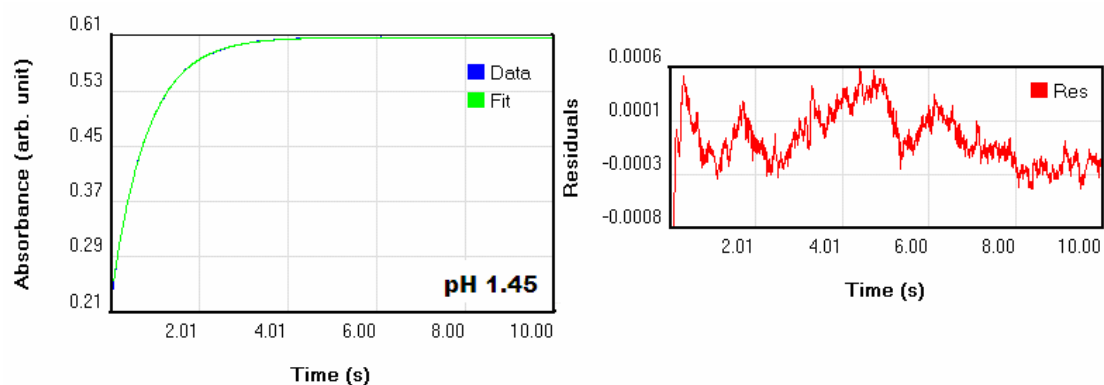


Table 2.2 summarises the reaction data for the hydrolysis of *p*-methoxybenzaldehyde *N*-(*tert*-butoxycarbonyl)imine (**119**).

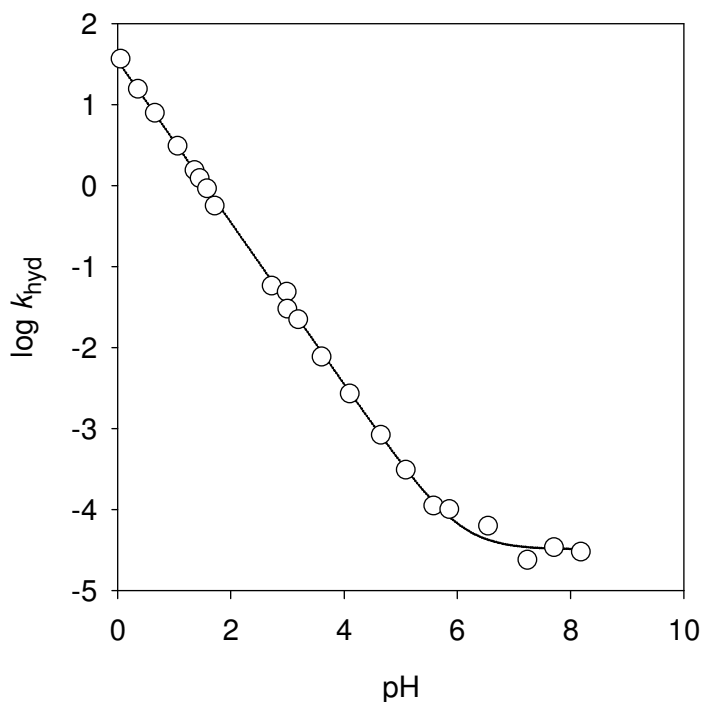
Table 2.2: Rate constants for the hydrolysis of *p*-methoxybenzaldehyde *N*-(*tert*-butoxycarbonyl)imine (**119**) in buffer and HCl solution at 284 nm, 25 °C and I = 1.0 (KCl).^a

pH	k_{HA}^{b} ($\text{M}^{-1}\text{s}^{-1}$)	$k_{\text{hyd}}^{\text{c}}$ (s^{-1})	$\log k_{\text{hyd}}$
0.057	-	$3.67 \times 10^{1\text{d}}$	1.56
0.36	-	$1.57 \times 10^{1\text{d}}$	1.20
0.66	-	7.87^{d}	8.96×10^{-1}
1.06	-	3.09^{d}	4.90×10^{-1}
1.36	-	1.55^{d}	1.90×10^{-1}
1.45	-	1.23^{d}	8.99×10^{-2}
1.58	-	$9.25 \times 10^{-1\text{d}}$	-3.38×10^{-2}
1.72	-	$5.60 \times 10^{-1\text{d}}$	-2.52×10^{-1}
2.72	-	$5.80 \times 10^{-2\text{d}}$	-1.24
2.99	-	$3.57 \times 10^{-2\text{d}}$	-1.45
3.00	-	$3.01 \times 10^{-2\text{d}}$	-1.52
3.19	3.15×10^{-2}	2.22×10^{-2}	-1.65
3.61	7.27×10^{-3}	7.71×10^{-3}	-2.11
4.10	5.08×10^{-3}	2.68×10^{-3}	-2.57
4.65	4.58×10^{-3}	8.30×10^{-4}	-3.08
5.09	4.74×10^{-3}	3.09×10^{-4}	-3.51
5.58	4.79×10^{-3}	1.13×10^{-4}	-3.95
5.86	2.61×10^{-3}	1.01×10^{-4}	-4.00
6.54	2.47×10^{-3}	6.29×10^{-5}	-4.20
7.24	2.44×10^{-5}	2.38×10^{-5}	-4.62
7.71	1.77×10^{-4}	3.48×10^{-5}	-4.46
8.18	4.90×10^{-4}	3.00×10^{-5}	-4.52

(a) Measurements were made at an initial substrate concentration of 5×10^{-5} M. (b) The value of the second-order rate constant for general acid-catalysed hydrolysis, (k_{HA} , $\text{M}^{-1}\text{s}^{-1}$), was obtained as the slope of the plot of k_{obs} against concentration of general acid in Figures A2-A11 (Appendix A). (c) The value of the first-order rate constant, k_{hyd} (s^{-1}), was obtained as the y-axis intercept of the plot of k_{obs} against the concentration of general acid in Figures A2-A11 (Appendix A). (d) The value of the first-order rate constant, k_{hyd} (s^{-1}), was obtained directly from least squares analysis of absorbance versus time data in Figure A1 (a)-(k) (Appendix A).

Shown below is the pH rate profile obtained for the hydrolysis of *p*-methoxybenzaldehyde *N*-(*tert*-butoxycarbonyl)imine (**119**) (Figure 2.7).

Figure 2.7: pH-Rate profile for hydrolysis of imine (**119**) at 25 °C and I = 1.0 (KCl).



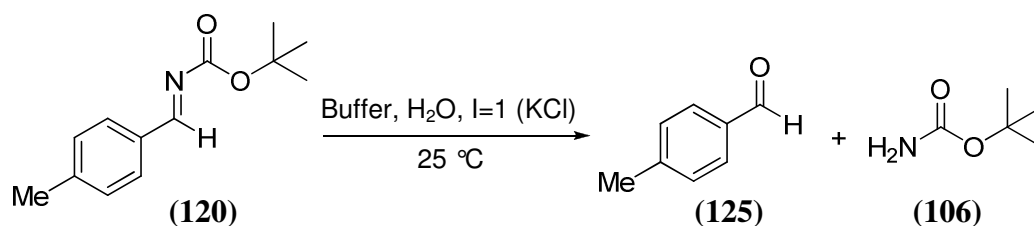
Estimates of the second-order rate constant for acid-catalysed hydrolysis, k_{H} ($\text{M}^{-1}\text{s}^{-1}$), and the first-order rate constant for buffer-independent hydrolysis, k_0 (s^{-1}), were obtained by non-linear least squares analysis. The experimental data, shown as (○), was fitted to Equation 2.5 where $x = \text{pH}$.

$$F = \log k_{\text{hyd}} = \log(k_{\text{H}}10^{-x} + k_0) \quad \text{(Equation 2.5)}$$

For imine (**119**), values of $k_{\text{H}} = 3.50 \times 10^1 \text{ M}^{-1}\text{s}^{-1}$ and $k_0 = 3.20 \times 10^{-5} \text{ s}^{-1}$ were obtained.

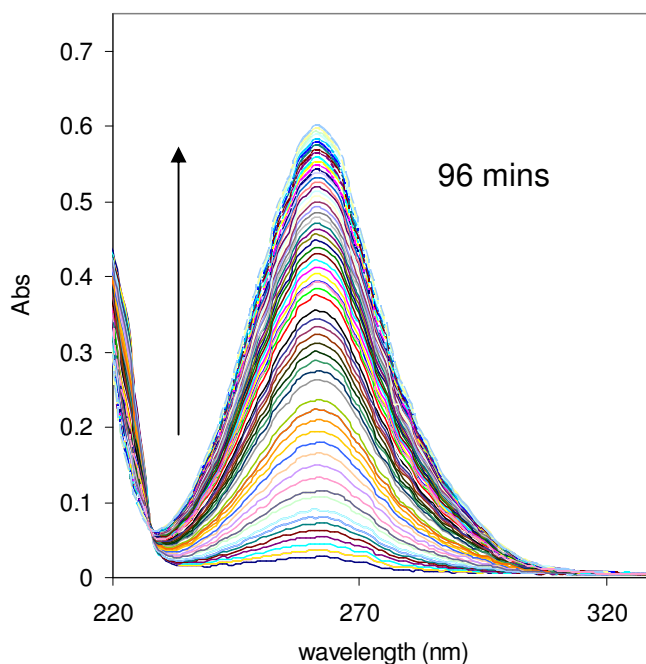
2.1.3.1.2 *p*-Methylbenzaldehyde *N*-(*tert*-butoxycarbonyl)imine (120).

Kinetic studies of the hydrolysis of *p*-methylbenzaldehyde *N*-(*tert*-butoxycarbonyl)imine (120) (Scheme 2.14) were conducted as per Section 2.1.3.1.1.

Scheme 2.14: Hydrolysis reaction of *p*-methylbenzaldehyde *N*-(*tert*-butoxycarbonyl)imine (120).

A representative repetitive scan of the hydrolysis reaction of imine (120) in acetic acid buffer is shown in Figure 2.8. As the reaction proceeds, an increase in absorbance at $\lambda_{\text{max}} = 260 \text{ nm}$ is seen which corresponds to formation of *p*-tolualdehyde (125). The analytical wavelength, $\lambda = 260 \text{ nm}$, was chosen for kinetic study.

Figure 2.8: Repetitive scan of the hydrolysis reaction of *p*-methylbenzaldehyde *N*-(*tert*-butoxycarbonyl)imine (120) in acetic acid buffer (pH 4.12) at 25 °C and I = 1.0 (KCl).



First and second-order plots and reaction data are presented in Appendix A (Figures A12-A22 and Tables A5-A7 respectively).

A summary of reaction data obtained for the hydrolysis reaction of *p*-methylbenzaldehyde *N*-(*tert*-butoxycarbonyl)imine (**120**) is presented in Table 2.3.

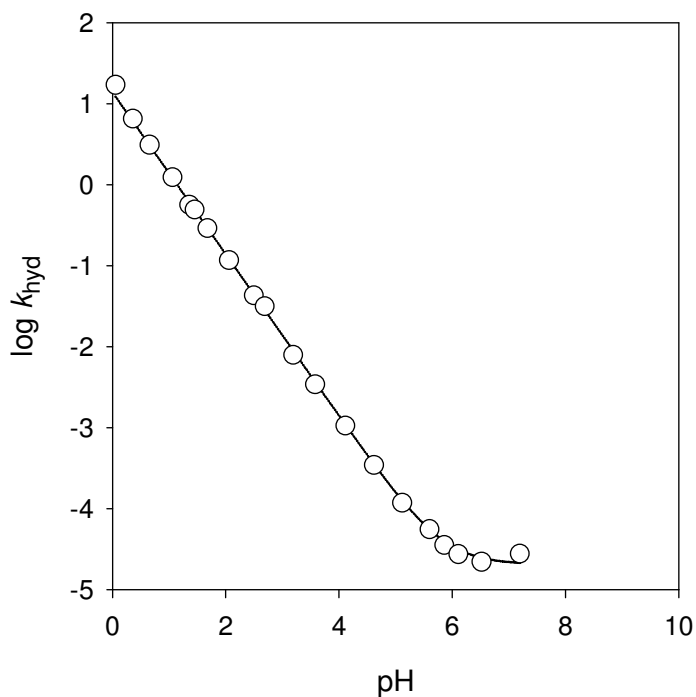
Table 2.3: Rate constants for the hydrolysis of *p*-methylbenzaldehyde *N*-(*tert*-butoxycarbonyl)imine (**120**) in aqueous buffer and HCl solution at 260 nm, 25 °C and I = 1.0 (KCl).^a

pH	k_{HA}^{b} ($\text{M}^{-1}\text{s}^{-1}$)	$k_{\text{hyd}}^{\text{c}}$ (s^{-1})	$\log k_{\text{hyd}}$
0.057	-	$1.69 \times 10^{1\text{d}}$	1.23
0.36	-	6.49^{d}	8.12×10^{-1}
0.66	-	3.10^{d}	4.91×10^{-1}
1.06	-	1.23^{d}	8.99×10^{-2}
1.36	-	$5.66 \times 10^{-1\text{d}}$	-2.47×10^{-1}
1.45	-	$4.90 \times 10^{-1\text{d}}$	-3.10×10^{-1}
1.68	-	$2.88 \times 10^{-1\text{d}}$	-5.40×10^{-1}
2.06	-	$1.17 \times 10^{-1\text{d}}$	-9.32×10^{-1}
2.50	-	$4.30 \times 10^{-2\text{d}}$	-1.37
2.69	-	$3.13 \times 10^{-2\text{d}}$	-1.50
3.19	3.66×10^{-3}	7.86×10^{-3}	-2.10
3.58	3.08×10^{-3}	3.41×10^{-3}	-2.47
4.12	3.10×10^{-3}	1.05×10^{-3}	-2.98
4.62	2.73×10^{-3}	3.45×10^{-4}	-3.46
5.12	2.67×10^{-3}	1.17×10^{-4}	-3.93
5.60	2.57×10^{-3}	5.54×10^{-5}	-4.26
5.86	1.77×10^{-3}	3.55×10^{-5}	-4.45
6.11	1.81×10^{-3}	2.59×10^{-5}	-4.59
6.52	1.71×10^{-3}	2.19×10^{-5}	-4.66
7.19	2.25×10^{-3}	2.75×10^{-5}	-4.56

(a) Measurements were made at an initial substrate concentration of 5×10^{-5} M. (b) The value of the second-order rate constant for general acid-catalysed hydrolysis, (k_{HA} , $\text{M}^{-1}\text{s}^{-1}$), was obtained as the slope of the plot of k_{obs} against the concentration of general acid in Figures A13-A22 (Appendix A). (c) The value of the first-order rate constant, k_{hyd} (s^{-1}), was obtained as the y-axis intercept of the plot of k_{obs} against the concentration of the general acid in Figures A13-A22 (Appendix A). (d) The value of the first-order rate constant, k_{hyd} (s^{-1}), was obtained directly from least-squares analysis of absorbance versus time data in Figure A12 (a)-(j), (Appendix A).

The pH-rate profile obtained for the hydrolysis of imine (**120**) is shown in Figure 2.9.

Figure 2.9: pH-Rate profile for hydrolysis of imine (**120**) at 25 °C and I = 1.0 (KCl).

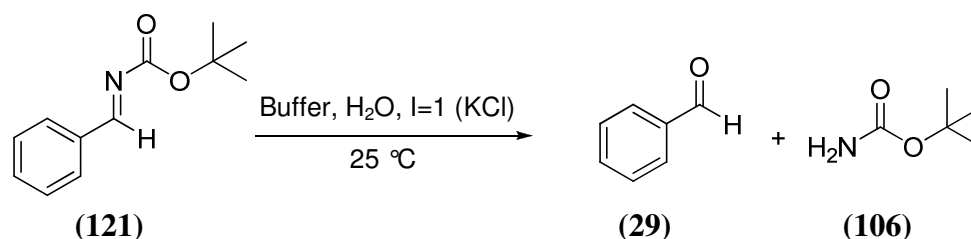


Estimates of the second-order rate constant for acid-catalysed hydrolysis, k_{H} ($\text{M}^{-1}\text{s}^{-1}$), and the first-order rate constant for buffer-independent hydrolysis, k_0 (s^{-1}), were obtained by non-linear least squares analysis. The experimental data, shown as (○), was fitted to Equation 2.5 where $x = \text{pH}$.

For imine (**120**), $k_{\text{H}} = 1.39 \times 10^1 \text{ M}^{-1}\text{s}^{-1}$ and $k_0 = 2.03 \times 10^{-5} \text{ s}^{-1}$.

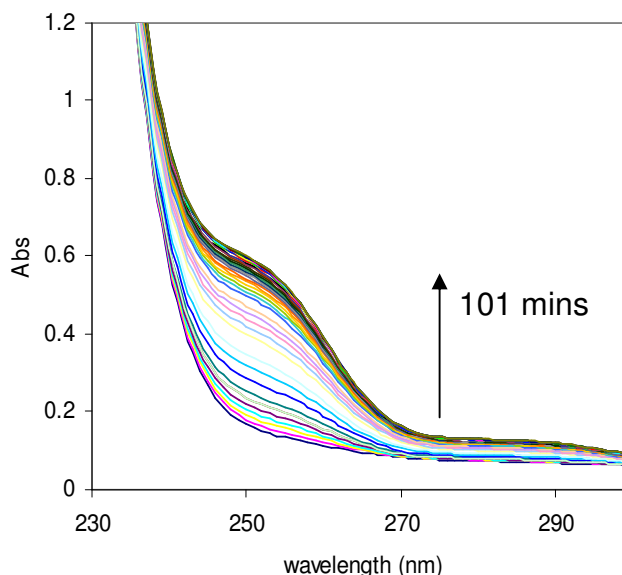
2.1.3.1.3 Benzaldehyde *N*-(*tert*-butoxycarbonyl)imine (121).

Kinetic studies of the hydrolysis of benzaldehyde *N*-(*tert*-butoxycarbonyl)imine (**121**) (Scheme 2.15) were conducted as per Section 2.1.3.1.1.

Scheme 2.15: Hydrolysis reaction of benzaldehyde *N*-(*tert*-butoxycarbonyl)imine (121).

A representative repetitive scan of the hydrolysis reaction of imine (**121**) in acetic acid buffer is shown in Figure 2.10. As the reaction proceeds, an increase in absorbance at $\lambda_{\text{max}} = 249 \text{ nm}$ is seen which corresponds to formation of benzaldehyde (**29**). The analytical wavelength, $\lambda = 249 \text{ nm}$, was chosen for kinetic study.

Figure 2.10: Repetitive scan of the hydrolysis reaction of benzaldehyde *N*-(*tert*-butoxycarbonyl)imine (121) in acetic acid buffer (pH 4.11) at 25 °C and I = 1.0 (KCl).



First and second-order plots and reaction data are presented in Appendix A (Figures A23-A31 and Tables A8-A10 respectively).

Table 2.4 summarises the reaction data obtained for the hydrolysis reaction of benzaldehyde *N*-(*tert*-butoxycarbonyl)imine (**121**).

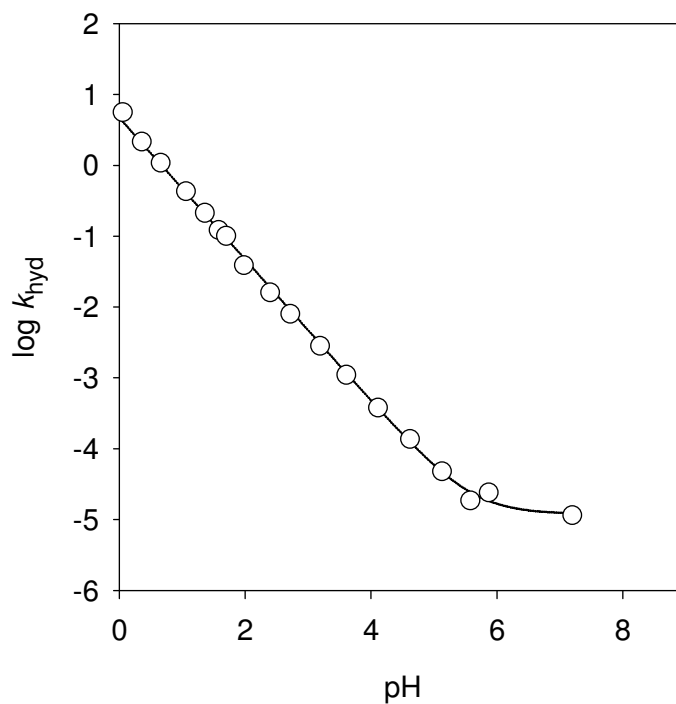
Table 2.4: Rate constants for the hydrolysis of benzaldehyde *N*-(*tert*-butoxycarbonyl)imine (**121**) in aqueous buffer and HCl solution at 249 nm, 25 °C and I = 1.0 (KCl).^a

pH	k_{HA}^{b} ($\text{M}^{-1}\text{s}^{-1}$)	$k_{\text{hyd}}^{\text{c}}$ (s^{-1})	$\log k_{\text{hyd}}$
0.057	-	5.58^{d}	7.47×10^{-1}
0.36	-	2.15^{d}	3.32×10^{-1}
0.66	-	1.08^{d}	3.34×10^{-2}
1.06	-	$4.28 \times 10^{-1\text{d}}$	-3.68×10^{-1}
1.36	-	$2.12 \times 10^{-1\text{d}}$	-6.74×10^{-1}
1.58	-	$1.22 \times 10^{-1\text{d}}$	-9.15×10^{-1}
1.70	-	$1.01 \times 10^{-1\text{d}}$	-9.96×10^{-1}
1.98	-	$3.88 \times 10^{-2\text{d}}$	-1.41
2.40	-	$1.59 \times 10^{-2\text{d}}$	-1.80
2.71	-	$8.00 \times 10^{-3\text{d}}$	-2.10
3.19	1.62×10^{-2}	2.82×10^{-3}	-2.55
3.61	2.18×10^{-3}	1.10×10^{-3}	-2.96
4.11	1.97×10^{-3}	3.79×10^{-4}	-3.42
4.62	1.71×10^{-3}	1.37×10^{-4}	-3.86
5.12	1.87×10^{-3}	4.76×10^{-5}	-4.32
5.58	1.91×10^{-3}	1.87×10^{-5}	-4.73
5.87	1.31×10^{-3}	2.40×10^{-5}	-4.62
7.20	1.27×10^{-3}	1.14×10^{-5}	-4.94

(a) Measurements were made at an initial substrate concentration of 5×10^{-5} M. (b) The value of the second-order rate constant for general acid-catalysed hydrolysis, k_{HA} ($\text{M}^{-1}\text{s}^{-1}$), was obtained as the slope of the plot of k_{obs} against the concentration of the general acid in Figures A24-A31 (Appendix A). (c) The value of the first-order rate constant, k_{hyd} (s^{-1}), was obtained as the y-axis intercept of the plot of k_{obs} against the concentration of the general acid in Figures A24-A31 (Appendix A). (d) The value of the first-order rate constant, k_{hyd} (s^{-1}), was obtained directly from least-squares analysis of absorbance versus time data in Figure A23 (a)-(j) (Appendix A).

Shown below is the pH-rate profile obtained for the hydrolysis of imine (**121**) (Figure 2.11).

Figure 2.11: pH-Rate profile for hydrolysis of benzaldehyde *N*-(*tert*-butoxycarbonyl)imine (**121**).

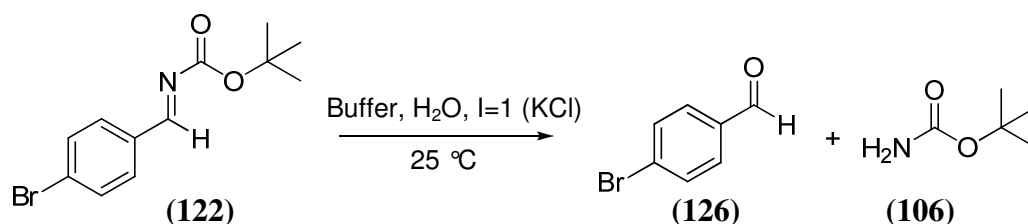


Estimates of the second-order rate constant for acid-catalysed hydrolysis, k_{H} ($\text{M}^{-1}\text{s}^{-1}$), and the first-order rate constant for buffer-independent hydrolysis, k_0 (s^{-1}), were obtained by non-linear least squares analysis. The experimental data, shown as (○), was fitted to Equation 2.5 where $x = \text{pH}$.

For imine (**121**), $k_{\text{H}} = 4.68 \text{ M}^{-1}\text{s}^{-1}$ and $k_0 = 1.19 \times 10^{-5} \text{ s}^{-1}$.

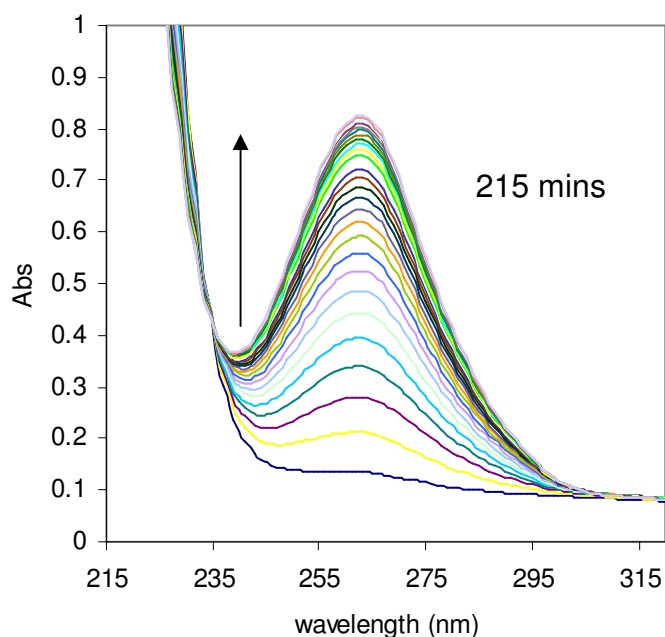
2.1.3.1.4 *p*-Bromobenzaldehyde *N*-(*tert*-butoxycarbonyl)imine (**122**).

Kinetic studies of *p*-bromobenzaldehyde *N*-(*tert*-butoxycarbonyl)imine (**122**) (Scheme 2.16) were conducted as per Section 2.1.3.1.1.

Scheme 2.16: Hydrolysis of *p*-bromobenzaldehyde *N*-(*tert*-butoxycarbonyl)imine (**122**).

A representative repetitive scan of the hydrolysis reaction of imine (**122**) in acetic acid buffer is shown in Figure 2.12. As the reaction proceeds, an increase in absorbance at $\lambda_{\text{max}} = 262 \text{ nm}$ is seen corresponding to formation of *p*-bromobenzaldehyde (**126**). The analytical wavelength, $\lambda = 262 \text{ nm}$, was chosen for kinetic study.

Figure 2.12: Repetitive scan of the hydrolysis reaction of *p*-bromobenzaldehyde *N*-(*tert*-butoxycarbonyl)imine (**122**) in acetic acid buffer (pH 4.12) at 25 °C and I = 1.0 (KCl).



First and second-order plots and reaction data are presented in Appendix A (Figures A32-A37 and Tables A11-A13 respectively).

Table 2.5 summarises the reaction data obtained for the hydrolysis reaction of imine (122).

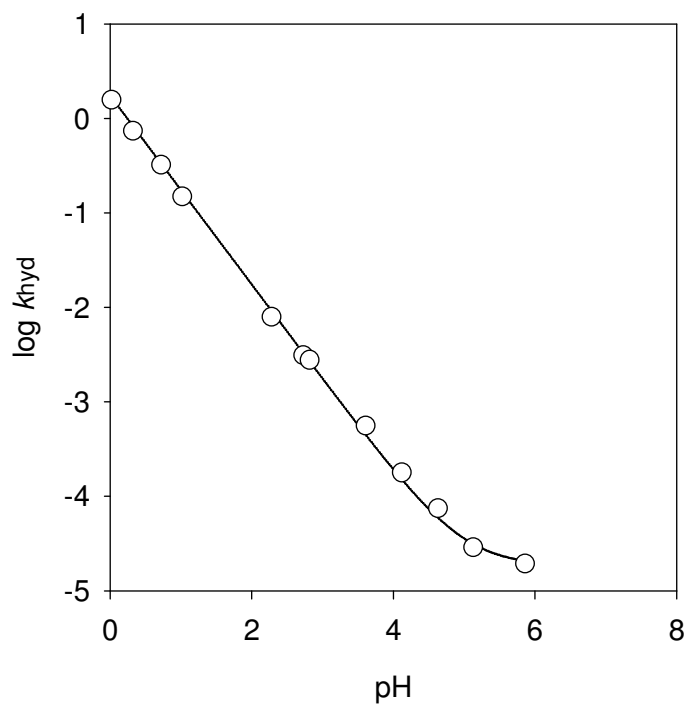
Table 2.5: Rate constants for the hydrolysis of *p*-bromobenzaldehyde *N*-(*tert*-butoxycarbonyl)imine (122) in aqueous buffer and HCl solution at 262 nm, 25 °C and I = 1.0 (KCl).

pH	k_{HA}^{a} ($\text{M}^{-1}\text{s}^{-1}$)	$k_{\text{hyd}}^{\text{b}}$ (s^{-1})	$\log k_{\text{hyd}}$
0.02	-	1.57 ^c	1.96×10^{-1}
0.32	-	$7.35 \times 10^{-1\text{c}}$	-1.34×10^{-1}
0.72	-	$3.21 \times 10^{-1\text{c}}$	-4.93×10^{-1}
1.02	-	$1.50 \times 10^{-1\text{c}}$	-8.24×10^{-1}
2.28	-	$7.96 \times 10^{-3\text{c}}$	-2.10
2.73	-	$3.10 \times 10^{-3\text{c}}$	-2.51
2.82	-	$2.78 \times 10^{-3\text{c}}$	-2.56
3.61	1.32×10^{-3}	5.58×10^{-4}	-3.25
4.12	1.38×10^{-3}	1.79×10^{-4}	-3.75
4.63	1.28×10^{-3}	7.45×10^{-5}	-4.12
5.13	1.46×10^{-3}	2.87×10^{-5}	-4.54
5.86	1.01×10^{-3}	1.94×10^{-5}	-4.71

(a) Measurements were made at an initial substrate concentration of 5×10^{-5} M. (b) The value of the second-order rate constant for general acid-catalysed hydrolysis, k_{HA} ($\text{M}^{-1}\text{s}^{-1}$), was obtained as the slope of the plot of k_{obs} against the concentration of the general acid in Figures A33-A37 (Appendix A). (c) The value of the first-order rate constant, k_{hyd} (s^{-1}), was obtained as the y-axis intercept of the plot of k_{obs} against the concentration of general acid in Figures A33-A37 (Appendix A). (d) The value of the first-order rate constant, k_{hyd} (s^{-1}), was obtained directly from least-squares analysis of absorbance versus time data in Figure A32 (a)-(g) (Appendix A).

Shown below is the pH-rate profile obtained for the hydrolysis of imine (**122**).

Figure 2.13: pH-Rate profile for the hydrolysis reaction of *p*-bromobenzaldehyde *N*-(*tert*-butoxycarbonyl)imine (**122**).

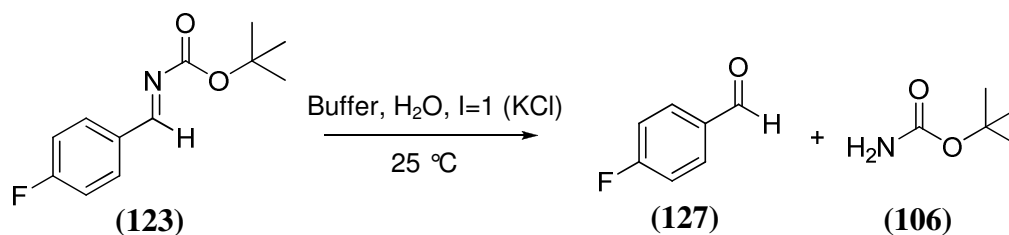


Estimates of the second-order rate constant for acid-catalysed hydrolysis, k_{H} ($\text{M}^{-1}\text{s}^{-1}$), and the first-order rate constant for buffer-independent hydrolysis, k_0 (s^{-1}), were obtained by non-linear least squares analysis. The experimental data, shown as (O), was fitted to Equation 2.5 where $x = \text{pH}$.

For imine (**122**), $k_{\text{H}} = 1.74 \text{ M}^{-1}\text{s}^{-1}$ and $k_0 = 1.82 \times 10^{-5} \text{ s}^{-1}$.

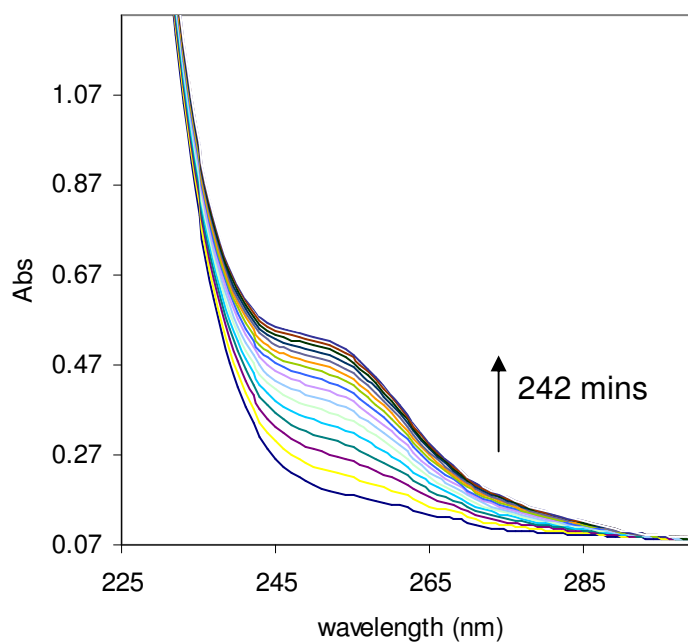
2.1.3.1.5 *p*-Fluorobenzaldehyde *N*-(*tert*-butoxycarbonyl)imine (123).

Kinetic studies of *p*-fluorobenzaldehyde *N*-(*tert*-butoxycarbonyl)imine (**123**) (Scheme 2.17) were conducted as per Section 2.1.3.1.1.

Scheme 2.17: Hydrolysis reaction of *p*-fluorobenzaldehyde *N*-(*tert*-butoxycarbonyl)imine (123**).**

A representative repetitive scan of the hydrolysis reaction of imine (**123**) in acetic acid buffer is shown in Figure 2.14. As the reaction proceeds, an increase in absorbance at $\lambda_{\text{max}} = 250 \text{ nm}$ is seen which corresponds to formation of *p*-fluorobenzaldehyde (**127**). The analytical wavelength, $\lambda = 250 \text{ nm}$, was chosen for kinetic study.

Figure 2.14: Repetitive scan of the hydrolysis reaction of *p*-fluorobenzaldehyde *N*-(*tert*-butoxycarbonyl)imine (**123**) in acetic acid buffer (pH 4.10) at 25 °C and I = 1.0 (KCl).



First and second-order plots as well as reaction data are presented in Appendix A (Figures A38-A44 and Tables A14-A16 respectively).

Table 2.6 summarises the reaction data obtained for the hydrolysis reaction of imine (123).

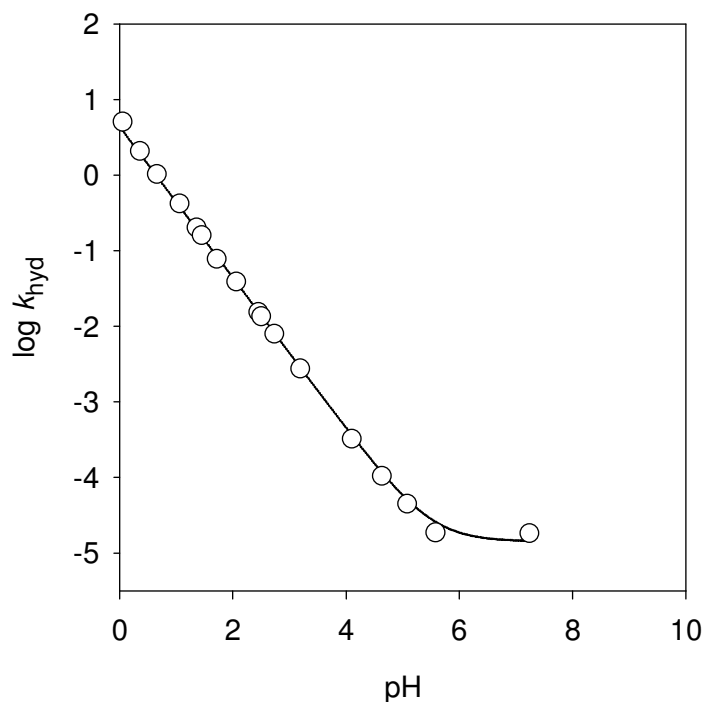
Table 2.6: Rate constants for the hydrolysis of *p*-fluorobenzaldehyde *N*-(*tert*-butoxycarbonyl)imine (123) in aqueous buffer and HCl solution at 250 nm, 25 °C and I = 1.0 (KCl).

pH	k_{HA}^{a} ($\text{M}^{-1}\text{s}^{-1}$)	$k_{\text{hyd}}^{\text{b}}$ (s^{-1})	$\log k_{\text{hyd}}$
0.057	-	5.09 ^c	7.07×10^{-1}
0.36	-	2.08 ^c	3.18×10^{-1}
0.66	-	1.03 ^c	1.28×10^{-2}
1.06	-	$4.19 \times 10^{-1\text{c}}$	-3.77×10^{-1}
1.36	-	$2.03 \times 10^{-1\text{c}}$	-6.93×10^{-1}
1.45	-	$1.60 \times 10^{-1\text{c}}$	-7.96×10^{-1}
1.72	-	$7.78 \times 10^{-2\text{c}}$	-1.11
2.06	-	$3.89 \times 10^{-2\text{c}}$	-1.41
2.45	-	$1.54 \times 10^{-2\text{c}}$	-1.81
2.50	-	$1.35 \times 10^{-2\text{c}}$	-1.87
2.73	-	$8.00 \times 10^{-3\text{c}}$	-2.10
3.19	1.45×10^{-2}	2.74×10^{-3}	-2.56
4.10	1.38×10^{-3}	3.27×10^{-4}	-3.49
4.63	1.30×10^{-3}	1.04×10^{-4}	-3.98
5.08	1.33×10^{-3}	4.50×10^{-5}	-4.35
5.58	1.31×10^{-4}	1.85×10^{-5}	-4.73
7.24	2.76×10^{-5}	1.81×10^{-5}	-4.74

(a) Measurements were made at an initial substrate concentration of 5×10^{-5} M. (b) The value of the second-order rate constant for general acid-catalysed hydrolysis, k_{HA} ($\text{M}^{-1}\text{s}^{-1}$), was obtained as the slope of the plot of k_{obs} against the concentration of general acid in Figures A39-A44 (Appendix A). (c) The value of the first-order rate constant, k_{hyd} (s^{-1}), was obtained as the y-axis intercept of the plot of k_{obs} against the concentration of general acid in Figures A39-A44 (Appendix A). (d) The value of the first-order rate constant, k_{hyd} (s^{-1}), was obtained from least-squares analysis of absorbance versus time data in Figure A38 (a)-(k) (Appendix A).

Shown below is the pH-rate profile obtained for the hydrolysis of imine (**123**).

Figure 2.15 pH-Rate profile for hydrolysis of imine (**123**) at 25 °C and I = 1.0 (KCl).



Estimates of the second-order rate constant for acid-catalysed hydrolysis, k_H ($M^{-1}s^{-1}$), and the first-order rate constant for buffer-independent hydrolysis, k_0 (s^{-1}), were obtained by non-linear least squares analysis. The experimental data, shown as (○), was fitted to Equation 2.5 where $x = \text{pH}$.

For imine (**123**), $k_H = 4.39 M^{-1}s^{-1}$ and $k_0 = 1.41 \times 10^{-5} s^{-1}$.

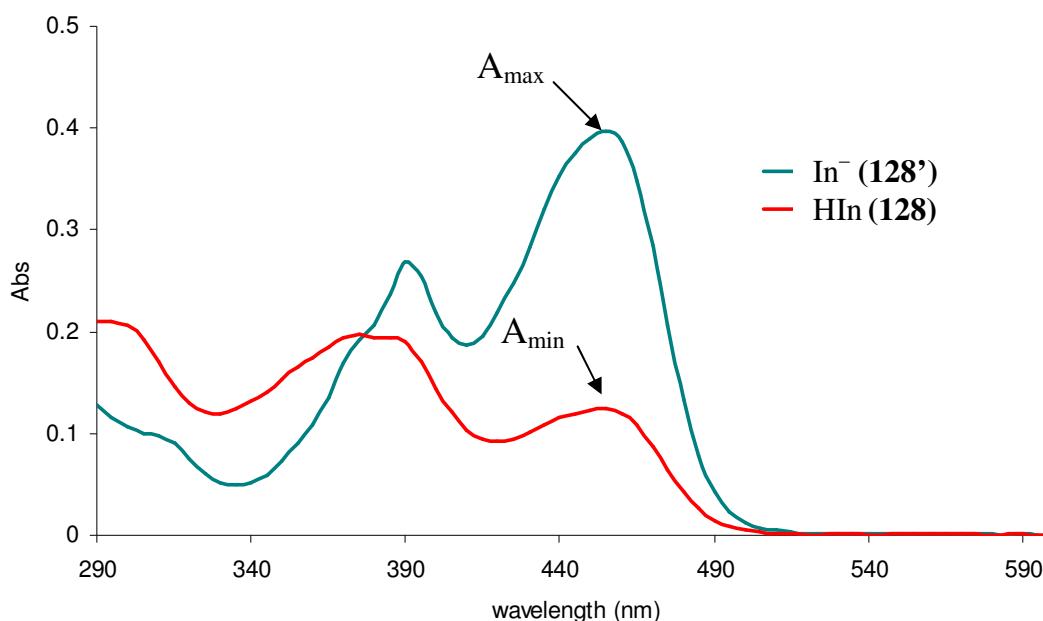
No levelling off at low pH was exhibited in any of the pH-rate profiles for hydrolysis of imines (**119**)-(123). Therefore, the aqueous $\text{p}K_a$ values of the iminium ions could not be estimated. These results suggest that the aqueous $\text{p}K_a$ values of this series of iminium ions lie at least below 2 units.

2.1.3.2 Determination of pK_a values of iminium ions in dimethyl sulfoxide.

As the hydrolytic lability of *N*-Boc iminium ions hampers the determination of their aqueous pK_a values, it was envisaged that measurements performed in organic solvent would minimise this unwanted decomposition of the substrate and allow dissociation constants to be estimated. Dimethyl sulfoxide was chosen for our purposes for its' excellent solvation properties. Bordwell has applied a spectrophotometric method using overlapping indicators in this solvent and produced extensive data covering the range 0-32 pK_a units.^{78,79}

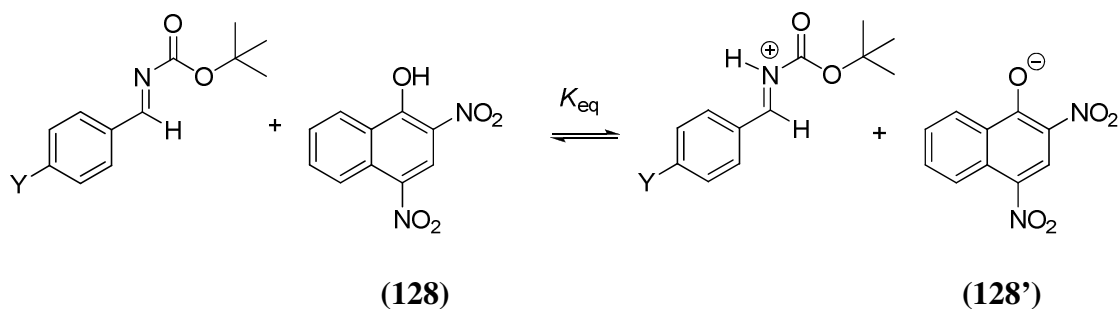
We applied the spectrophotometric method of Bordwell with modifications by Crampton⁷⁷ in order to measure ionisation constants for *N*-Boc iminium ions, taking as our reference point the indicator 2,4-dinitronaphthol (**128**) which has a pK_a value of 2.11 ± 0.04 in DMSO.⁷⁸ A pronounced change in the UV-Visible spectrum of this indicator is observed upon ionisation. Formation of the indicator anion (**128'**) resulted in an increase in absorbance at $\lambda_{\max} = 454$ nm which was chosen as the analytical wavelength. UV-Vis spectra of the neutral and ionised indicator are shown in Figure 2.16 and were obtained by addition of acid and base respectively to solutions of indicator (**128**) in DMSO.

Figure 2.16: UV-Vis scans of solutions containing indicator (3×10^{-5} M) (**128**) in DMSO, in the presence of acid (HCl, 100 mM) (—) and base (DBU, 6mM) (—).



In a typical experiment, spectra were recorded with a constant concentration (3×10^{-5} M) of indicator in solutions buffered with neutral and protonated forms of the imine. The iminium ion was formed by adding varying amounts of HCl in ether to imine solution, such that the final concentration of ether was $< 2\%$. Measurements were made with a constant salt concentration of 0.01 M. Imine and indicator solutions were incubated at 25 °C for several minutes prior to the addition of the acid solution.

Scheme 2.18 and Equation 2.6 define an equilibrium constant, K_{eq} , for the overall conversion of indicator (**128**) to the deprotonated form (**128'**) by the respective imine.

Scheme 2.18: Equilibrium between imine substrate and indicator.

$$K_{\text{eq}} = \frac{K_{\text{a}}^{\text{HIn}}}{K_{\text{a}}^{\text{ImineH}^+}} = \frac{[\text{ImineH}^+][\text{In}^- \text{(128'')}]}{[\text{Imine}][\text{HIn} \text{(128)}]} \quad \text{(Equation 2.6)}$$

As the main absorbing species at the analytical wavelength ($\lambda = 454 \text{ nm}$) is the indicator anion (128''), Equation 2.6 may be written as Equation 2.7 and the equilibrium constant K_{eq} can therefore be obtained from absorbance measurements.

$$K_{\text{eq}} = \frac{[\text{ImineH}^+] (\text{Abs} - A_{\text{min}})}{[\text{Imine}] (A_{\text{max}} - \text{Abs})} \quad \text{(Equation 2.7)}$$

A_{min} = absorbance without substrate (neutral indicator (128) only).

The value of A_{min} was obtained from a spectrum of the indicator in the presence of an excess of acid (Figure 2.16).

A_{max} = absorbance without substrate (indicator anion (128'') only).

The value of A_{max} was obtained from a spectrum of the indicator in the presence of an excess of base (Figure 2.16).

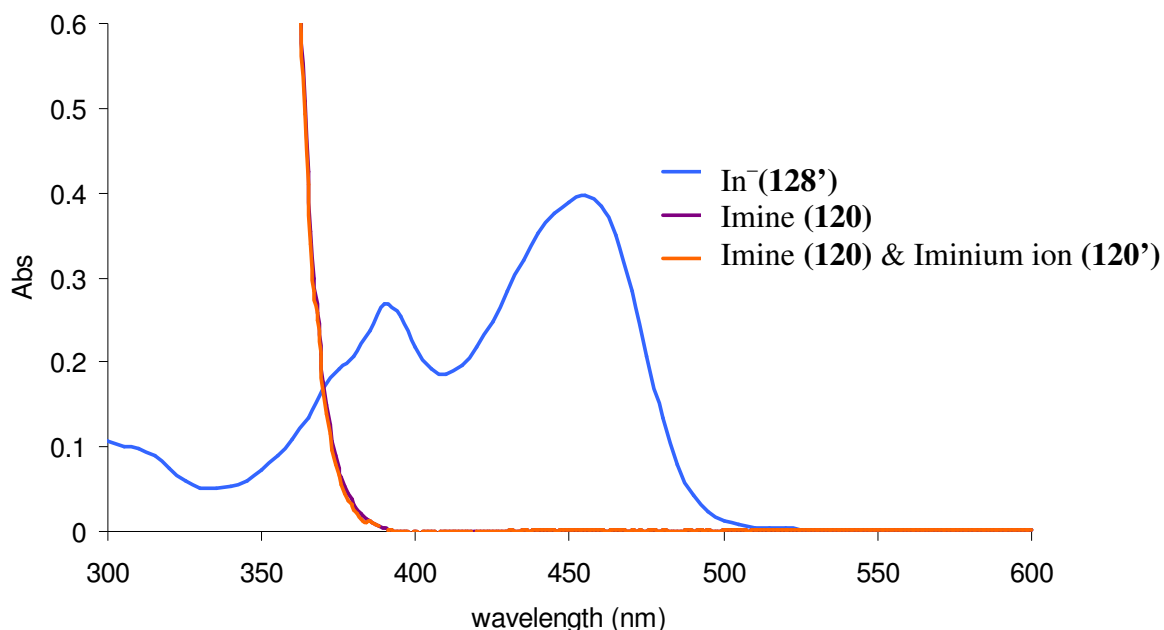
$[\text{ImineH}^+]$ = initial concentration of iminium ion.

$[\text{Imine}]$ = initial concentration of imine.

Abs is the absorbance at 454 nm for a given mixture of indicator and imine.

There was no interfering absorbance of imine or iminium ion at the analytical wavelength. Representative scans of both species are shown in Figure 2.17.

Figure 2.17: UV-Vis scans of indicator anion (**128'**) (3×10^{-5} M), imine (**120**) only (0.01 M) and imine (0.01 M) in the presence of HCl (4.5×10^{-3} M) in DMSO.



The concentration of imine/iminium ion is kept in large excess over the concentration of indicator. As such, the extent of indicator ionisation had a negligible effect on imine/iminium ion concentration.

The equilibrium constant for the ionisation of an iminium ion is given by Equation 2.8.

$$K_a^{\text{ImineH}^+} = \frac{[\text{Imine}][\text{H}^+]}{[\text{ImineH}^+]} \quad (\text{Equation 2.8})$$

In these measurements, the iminium ion was generated in solution by addition of acid.

$$\begin{aligned} [\text{ImineH}^+] &= [\text{H}^+]_{\text{added}} \\ [\text{Imine}] &= [\text{Imine}]_{\text{total}} - [\text{ImineH}^+] \end{aligned}$$

However, analysis of the pH-rate profiles for the hydrolysis of the imine substrates indicated that the aqueous pK_a values of the iminium ions were < 2 and similarly low pK_a values in DMSO could be predicted. In general relative pK_a values in DMSO and water depend on the nature of the acid and conjugate base and the extent of delocalisation in both species. Typically pK_a values in water and DMSO are similar for compounds which form highly delocalised ions. For example, the aqueous pK_a value of 4-chloro-2,6-dinitrophenol is 3.0⁷⁹ while the pK_a value in DMSO is 3.56⁷⁸. Acidities of

anilinium ion are also similar in both media. The aqueous pK_a value was determined as 4.58⁷⁷, while the pK_a value in DMSO is 3.82.⁷⁷ Low pK_a values of the iminium ions require that the natural ionisation of the iminium ion has to be factored into the estimation of $[\text{ImineH}^+]$. In order to account for this high acidity, the concentration of free H^+ ions at equilibrium, x , was calculated and the values of the concentrations of imine and iminium ion were adjusted accordingly.

$$[\text{ImineH}^+] = [\text{H}^+]_{\text{added}} - x \quad (\text{where } x \text{ is the concentration of free } \text{H}^+ \text{ ions at equilibrium due to the ionisation of } \text{ImineH}^+).$$

Also,

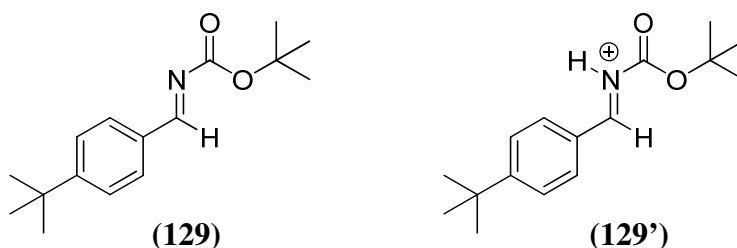
$$[\text{Imine}] = [\text{Imine}]_{\text{total}} - ([\text{H}^+]_{\text{added}} - x).$$

An estimated value of K_a was used to solve Equation 2.9 and provide a value for x , which was used to adjust the concentrations of imine and iminium ion. The value of K_a chosen was in order to give the smallest variation in resulting K_{eq} values.

$$K_a^{\text{ImineH}^+} = \frac{([\text{Imine}]_{\text{total}} - [\text{H}^+]_{\text{added}} + x)x}{([\text{H}^+]_{\text{added}} - x)} \quad (\text{Equation 2.9})$$

An illustrative example of uncorrected data obtained in these investigations is presented in Table 2.7.

Table 2.7: Absorbance data for 2,4-dinitronaphthol^a (128) in DMSO containing imine (129) and iminium ion^b (129') at 454 nm and 25 °C.



Spectrum number	[ImineH ⁺] (M)	[Imine] (M)	Abs	[In ⁺]/[HIn] ^c	$K_{eq}^{uncorr\ d}$
1.	1.50×10^{-3}	8.60×10^{-3}	0.493	3.74	0.65
2.	2.00×10^{-3}	8.10×10^{-3}	0.476	3.04	0.75
3.	2.50×10^{-3}	7.60×10^{-3}	0.458	2.50	0.82
4.	3.00×10^{-3}	7.10×10^{-3}	0.447	2.23	0.94
5.	4.00×10^{-3}	6.10×10^{-3}	0.430	1.89	1.24
6.	5.00×10^{-3}	5.10×10^{-3}	0.408	1.54	1.51
7.	7.00×10^{-3}	3.10×10^{-3}	0.377	1.17	2.65
8.	8.00×10^{-3}	2.10×10^{-3}	0.369	1.09	4.17
9.	9.00×10^{-3}	1.10×10^{-3}	0.356	0.98	8.00

(a) The final concentration of 2,4-dinitronaphthol was 3×10^{-5} M. (b) Iminium ion was generated by addition of HCl in ether solution in DMSO such that the final concentration of ether was < 2%. (c) The ratio of phenolate to phenol was obtained using the relationship $Abs - A_{min} / A_{max} - Abs$.

(d) Calculated as $\frac{[ImineH^+]}{[Imine]} \cdot \frac{(Abs - 0.126)}{(0.591 - Abs)}$

The large variation in K_{eq} values is clear when the natural ionisation of the iminium ion is not accounted for in the estimation of imine and iminium ion concentrations (Table 2.7).

The final K_{eq} was estimated using Equation 2.10.

$$K_{eq} = \frac{([H^+]_{added} - x)}{([Imine]_{total} - [H^+]_{added} + x)} \cdot \frac{(Abs - A_{min})}{(A_{max} - Abs)} = \frac{K_a^{HIn}}{K_a^{ImineH^+}} \quad \text{(Equation 2.10)}$$

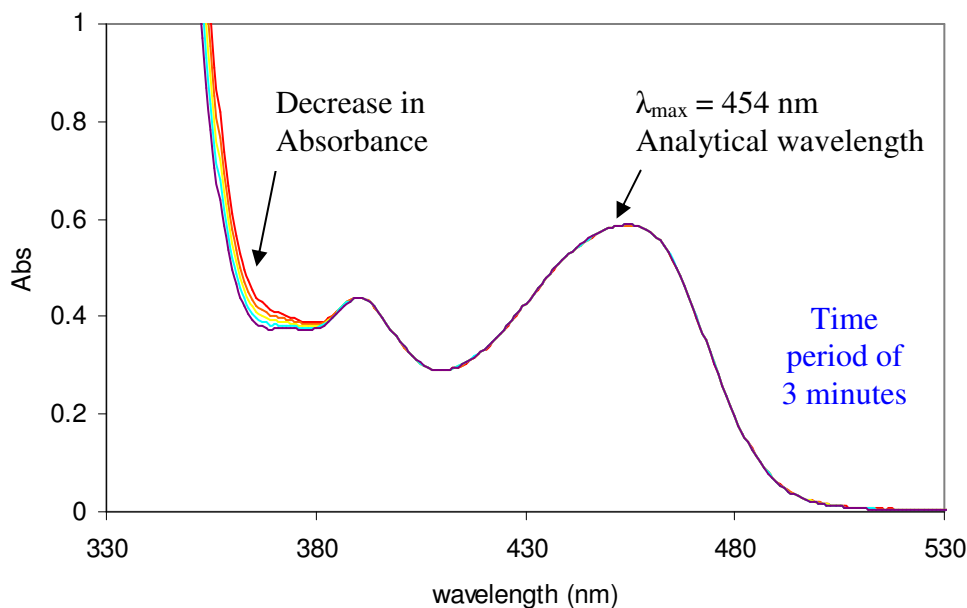
The pK_a values of iminium ions were related to $\log_{10}K_{eq}$ and the pK_a value of the indicator by Equation 2.11.

$$pK_a(\text{ImineH}^+) = \log_{10}K_{eq} + pK_a(2,4\text{-dinitronaphthol}) \quad \text{(Equation 2.11)}$$

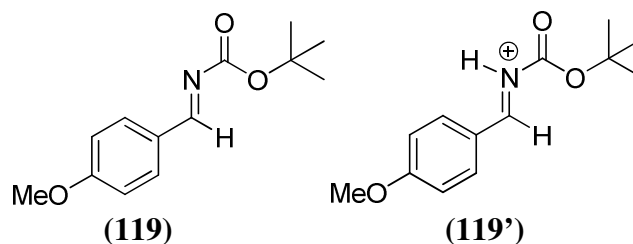
The mean values of K_{eq} and pK_a are presented followed by the standard deviation in parentheses as an indication of the error in the measurements.

Repetitive scans of mixtures of indicator and imine in the presence of HCl over longer periods of time revealed hydrolysis was occurring as spectral changes were visible between 250 - 300 nm. Changes in the absorbance value at the analytical wavelength were negligible during the time interval of the measurement (Figure 2.18). ^1H NMR spectroscopic investigation confirmed that competitive hydrolysis was insignificant at the highest concentration of acid used over the short period of measurement employed. These measurements could not be performed for the determination of the pK_a value of *p*-fluoro-substituted iminium ion (**123'**) due to the insolubility of the imine in DMSO at the concentrations required to buffer the indicator in 100-fold excess.

Figure 2.18: Repetitive UV-Vis scan of indicator in DMSO with imine in the presence of HCl.



In order to confirm the validity of this method for determination of pK_a values, analogous measurements were performed on a compound whose pK_a in DMSO is known. Measurement of the pK_a value of anilinium ion (**130'**) in DMSO provided a value of 3.84 ± 0.16 which compares well with the literature pK_a value of 3.82.⁷⁷ 4-Chloro-2,6-dinitrophenol was used as the indicator as the pK_a of this compound is known to be 3.56 in DMSO. The pK_a value of anilinium ion is greater than 3 units and so the natural ionisation did not need to be factored in to the concentrations of aniline and anilinium ion. The results of this measurement are presented in Appendix B.

2.1.3.2.1 *p*-Methoxybenzaldehyde *N*-(*tert*-butoxycarbonyl)iminium ion (119')

UV-Visible spectra of 2,4-dinitronaphthol (**128**) (3×10^{-5} M) in DMSO solutions containing *p*-methoxybenzaldehyde *N*-(*tert*-butoxycarbonyl)imine (**119**) and *p*-methoxybenzaldehyde *N*-(*tert*-butoxycarbonyl)iminium ion (**119'**) were recorded at 25 °C. These are shown in Figure 2.19, with scans 1-9 corresponding to the conditions given in Table 2.8.

Figure 2.19: UV-Visible spectra of 2,4-dinitronaphthol (**128**) in DMSO containing imine (**119**) and iminium ion (**119'**) at 25 °C.

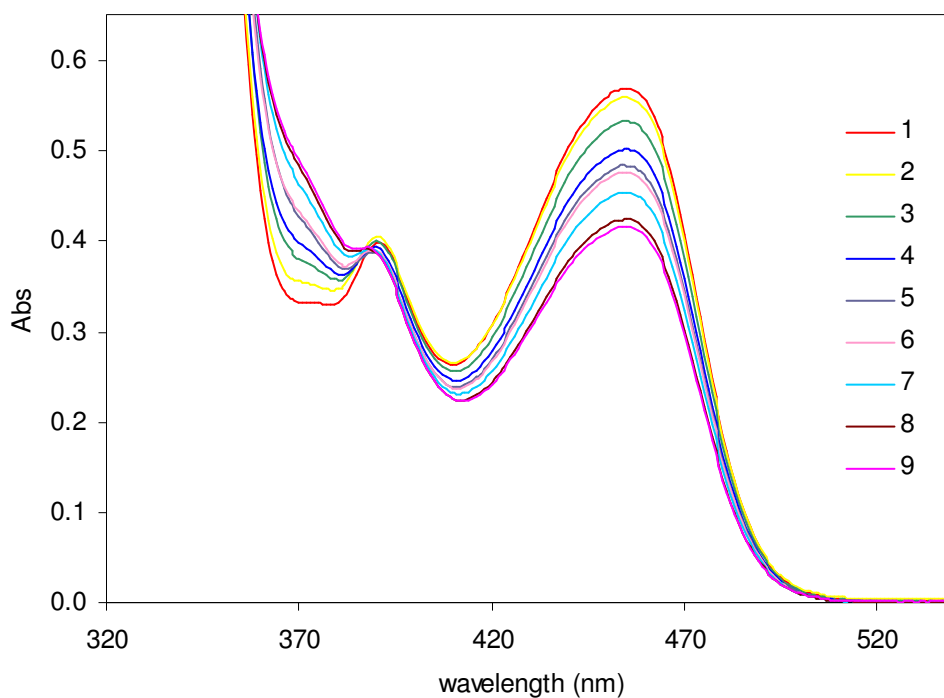


Table 2.8: Absorbance data for 2,4-dinitronaphthol^a (128) in DMSO containing imine (119) and iminium ion^b (119') at 454 nm and 25 °C.

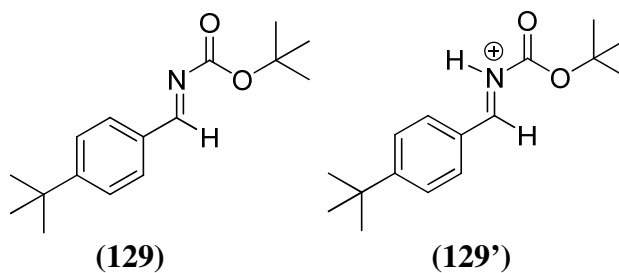
Spectrum number	x ^c (M)	[ImineH ⁺] (M)	[Imine] (M)	Abs	[In ⁻]/[HIn] ^d	K _{eq} ^e
1.	1.02 × 10 ⁻³	4.84 × 10 ⁻⁴	9.52 × 10 ⁻³	0.570	5.96	0.30
2.	1.36 × 10 ⁻³	6.38 × 10 ⁻⁴	9.36 × 10 ⁻³	0.558	4.93	0.34
3.	1.71 × 10 ⁻³	7.88 × 10 ⁻⁴	9.21 × 10 ⁻³	0.531	3.44	0.29
4.	2.06 × 10 ⁻³	9.36 × 10 ⁻⁴	9.06 × 10 ⁻³	0.518	2.97	0.31
5.	2.42 × 10 ⁻³	1.08 × 10 ⁻³	8.92 × 10 ⁻³	0.498	2.40	0.29
6.	2.78 × 10 ⁻³	1.22 × 10 ⁻³	8.78 × 10 ⁻³	0.482	2.06	0.29
7.	3.14 × 10 ⁻³	1.36 × 10 ⁻³	8.64 × 10 ⁻³	0.475	1.93	0.30
8.	4.25 × 10 ⁻³	1.75 × 10 ⁻³	8.25 × 10 ⁻³	0.451	1.55	0.33
9.	5.00 × 10 ⁻³	2.00 × 10 ⁻³	8.00 × 10 ⁻³	0.432	1.32	0.33
10.	5.76 × 10 ⁻³	2.24 × 10 ⁻³	7.76 × 10 ⁻³	0.423	1.22	0.35

(a) The final concentration of 2,4-dinitronaphthol was 3 × 10⁻⁵ M. (b) Iminium ion was generated by addition of HCl in ether solution in DMSO such that the final concentration of ether was < 2%. (c) The concentration of free H⁺ ions at equilibrium, x, was calculated using Equation 2.9 with K_a = 2.0 × 10⁻². The value of K_a was chosen to give the least variation in values of K_{eq}. (d) The ratio of phenolate to phenol was obtained using the relationship Abs-A_{min}/A_{max}-Abs.

(e) Calculated as
$$\frac{[\text{ImineH}^+]}{[\text{Imine}]} \cdot \frac{(\text{Abs} - 0.159)}{(0.669 - \text{Abs})}$$

An average value of K_{eq} was calculated, K_{eq} = 0.32 (± 0.02).

The pK_a value was calculated using Equation 2.11. In this case, pK_a = 1.61 (± 0.03).

2.1.3.2.2 *p*-*tert*-Butylbenzaldehyde *N*-(*tert*-butoxycarbonyl)iminium ion (129').

UV-Visible spectra of 2,4-dinitronaphthol (**128**) (3×10^{-5} M) in DMSO solutions containing *p*-*tert*-butylbenzaldehyde *N*-(*tert*-butoxycarbonyl)imine (**129**) and *p*-*tert*-butylbenzaldehyde *N*-(*tert*-butoxycarbonyl)iminium ion (**129'**) were recorded at 25 °C. These are shown in Figure 2.20, with scans 1-9 corresponding to the conditions given in Table 2.9.

Figure 2.20: UV-Visible spectra of 2,4-dinitronaphthol (**128**) in DMSO containing imine (**129**) and iminium ion (**129'**) at 25 °C.

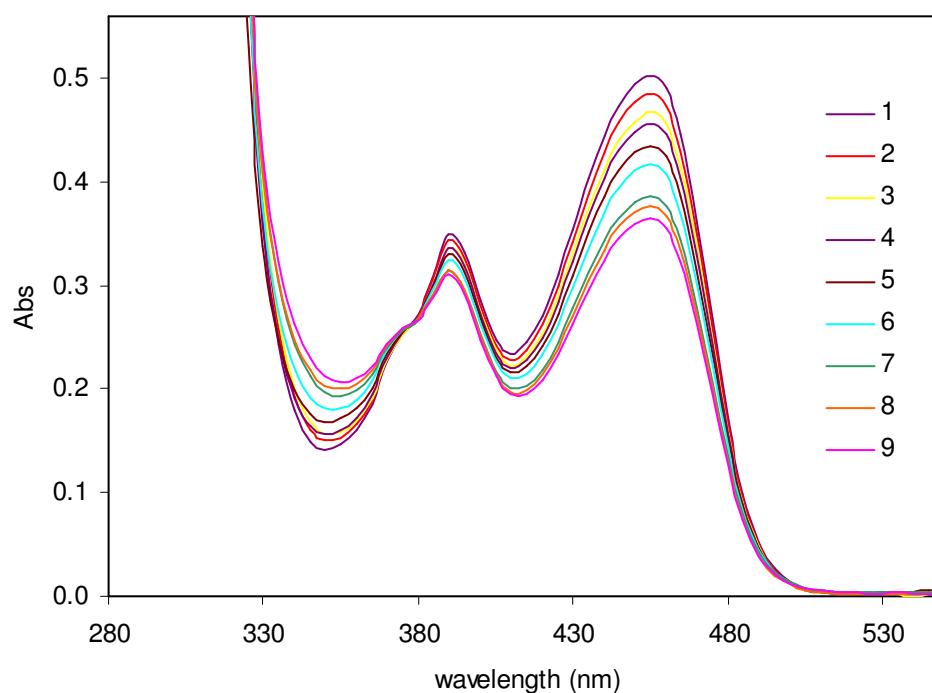


Table 2.9: Absorbance data for 2,4-dinitronaphthol^a (128) in DMSO containing imine (129) and iminium ion^b (129') at 454 nm and 25 °C.

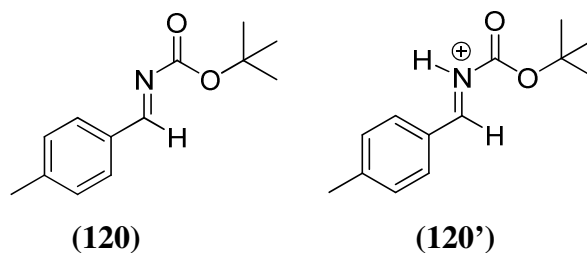
Spectrum number	x ^c (M)	[ImineH ⁺] (M)	[Imine] (M)	Abs	[In ⁻]/[HIIn] ^d	K _{eq} ^e
1.	1.15 × 10 ⁻³	9.75 × 10 ⁻³	3.54 × 10 ⁻⁴	0.493	3.74	0.14
2.	1.53 × 10 ⁻³	9.63 × 10 ⁻³	4.68 × 10 ⁻⁴	0.476	3.04	0.15
3.	1.92 × 10 ⁻³	9.52 × 10 ⁻³	5.79 × 10 ⁻⁴	0.458	2.50	0.15
4.	2.31 × 10 ⁻³	9.41 × 10 ⁻³	6.89 × 10 ⁻⁴	0.447	2.23	0.16
5.	3.10 × 10 ⁻³	9.20 × 10 ⁻³	9.03 × 10 ⁻⁴	0.430	1.89	0.19
6.	3.89 × 10 ⁻³	8.99 × 10 ⁻³	1.11 × 10 ⁻³	0.408	1.54	0.19
7.	5.50 × 10 ⁻³	8.60 × 10 ⁻³	1.50 × 10 ⁻³	0.377	1.17	0.20
8.	6.32 × 10 ⁻³	8.42 × 10 ⁻³	1.68 × 10 ⁻³	0.369	1.09	0.22
9.	7.14 × 10 ⁻³	8.24 × 10 ⁻³	1.86 × 10 ⁻³	0.356	0.98	0.22

(a) The final concentration of 2,4-dinitronaphthol was 3 × 10⁻³ M. (b) Iminium ion was generated by addition of HCl in ether solution in DMSO such that the final concentration of ether was < 2%. (c) The concentration of free H⁺ ions at equilibrium, x, was calculated using Equation 2.9 with K_a = 3.16 × 10⁻². The value of K_a was chosen to give the least variation in values of K_{eq} (d) The ratio of phenolate to phenol was obtained using the relationship Abs-A_{min}/A_{max}-Abs.

(e) Calculated as
$$\frac{[\text{ImineH}^+]}{[\text{Imine}]} \cdot \frac{(\text{Abs} - 0.126)}{(0.591 - \text{Abs})}$$

An average value of K_{eq} was calculated, K_{eq} = 0.18 (± 0.03).

The pK_a value was calculated using Equation 2.11. In this case, pK_a = 1.37 (± 0.08).

2.1.3.2.3 *p*-Methylbenzaldehyde *N*-(*tert*-butoxycarbonyl)imine (120) and *N*-(*tert*-butoxycarbonyl)iminium ion (120').

UV-Visible spectra of 2,4-dinitronaphthol (**128**) (3×10^{-5} M) in DMSO solutions containing *p*-methylbenzaldehyde *N*-(*tert*-butoxycarbonyl)imine (**120**) and *p*-methylbenzaldehyde *N*-(*tert*-butoxycarbonyl)iminium ion (**120'**) were recorded at 25 °C. These are shown in Figure 2.21, with scans 1 – 10 corresponding to the conditions given in Table 2.10.

Figure 2.21: UV-Visible spectra of 2,4-dinitronaphthol (**128**) in DMSO containing imine (**120**) and iminium ion (**120'**) at 25 °C.

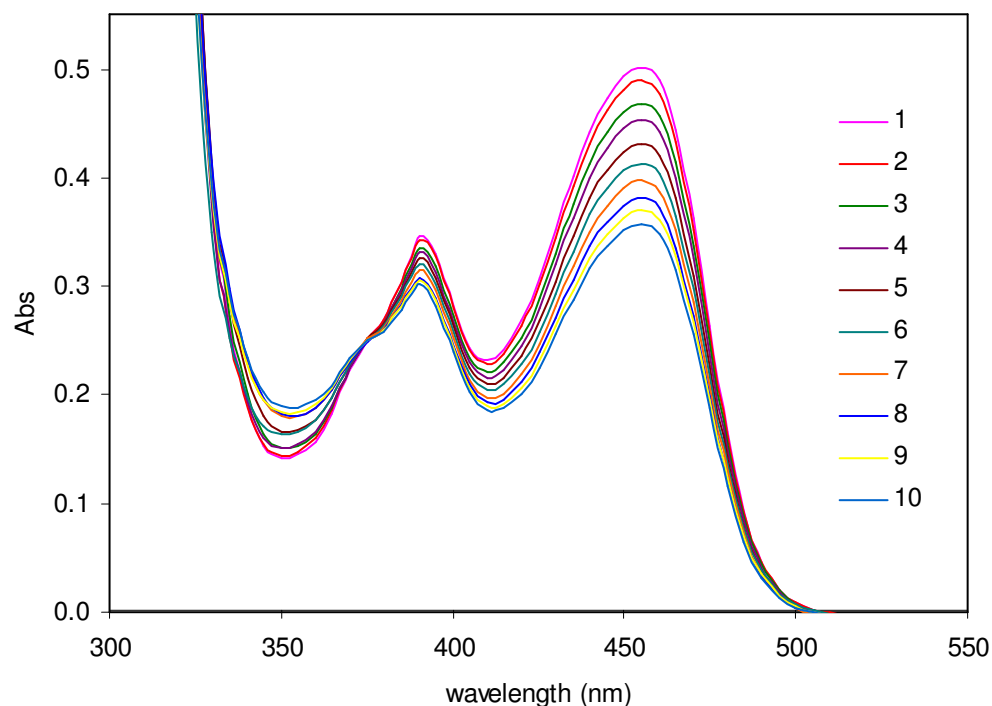


Table 2.10: Absorbance data for 2,4-dinitronaphthol^a (128) in DMSO containing imine (120) and iminium ion^b (120') at 454 nm and 25 °C.

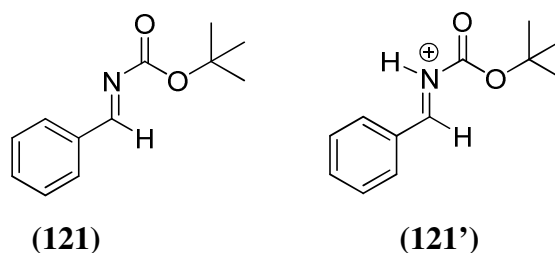
Spectrum number	x ^c (M)	[ImineH ⁺] (M)	[Imine] (M)	Abs	[In ⁻]/[HIn] ^d	K _{eq} ^e
1.	1.25 × 10 ⁻³	2.50 × 10 ⁻⁴	9.95 × 10 ⁻³	0.503	4.28	0.11
2.	1.67 × 10 ⁻³	3.33 × 10 ⁻⁴	9.87 × 10 ⁻³	0.490	3.60	0.12
3.	2.09 × 10 ⁻³	4.12 × 10 ⁻⁴	9.79 × 10 ⁻³	0.470	2.84	0.12
4.	2.51 × 10 ⁻³	4.88 × 10 ⁻⁴	9.71 × 10 ⁻³	0.456	2.44	0.12
5.	3.36 × 10 ⁻³	6.44 × 10 ⁻⁴	9.56 × 10 ⁻³	0.433	1.94	0.13
6.	4.21 × 10 ⁻³	7.91 × 10 ⁻⁴	9.41 × 10 ⁻³	0.415	1.64	0.14
7.	5.06 × 10 ⁻³	9.38 × 10 ⁻⁴	9.26 × 10 ⁻³	0.399	1.42	0.14
8.	5.92 × 10 ⁻³	1.08 × 10 ⁻³	9.12 × 10 ⁻³	0.382	1.22	0.14
9.	6.78 × 10 ⁻³	1.22 × 10 ⁻³	8.98 × 10 ⁻³	0.372	1.12	0.15
10.	7.65 × 10 ⁻³	1.35 × 10 ⁻³	8.85 × 10 ⁻³	0.358	1.00	0.15

(a) The final concentration of 2,4-dinitronaphthol was 3 × 10⁻⁵ M. (b) Iminium ion was generated by addition of HCl in ether solution in DMSO such that the final concentration of ether was < 2%. (c) The concentration of free H⁺ ions at equilibrium, x, was calculated using Equation 2.9 with K_a = 5.01 × 10⁻². The value of K_a was chosen to give the least variation in values of K_{eq} (d) The ratio of phenolate to phenol was obtained using the relationship Abs-A_{min}/A_{max}-Abs.

(e) Calculated as
$$\frac{[\text{ImineH}^+]}{[\text{Imine}]} \cdot \frac{(\text{Abs} - 0.126)}{(0.591 - \text{Abs})}$$

An average value of K_{eq} was calculated, K_{eq} = 0.13 (± 0.01).

The pK_a value was calculated using Equation 2.11. In this case, pK_a = 1.24 (± 0.05).

2.1.3.2.4 Benzaldehyde *N*-(*tert*-butoxycarbonyl)iminium ion (121').

UV-Visible spectra of 2,4-dinitronaphthol (**128**) (3×10^{-5} M) in DMSO solutions containing benzaldehyde *N*-(*tert*-butoxycarbonyl)imine (**121**) and benzaldehyde *N*-(*tert*-butoxycarbonyl)iminium ion (**121'**) were recorded at 25 °C. These are shown in Figure 2.22, with scans 1-13 corresponding to the conditions given in Table 2.11.

Figure 2.22: UV-Visible spectra of 2,4-dinitronaphthol (**128**) in DMSO containing imine (**121**) and iminium ion (**121'**) at 25 °C.

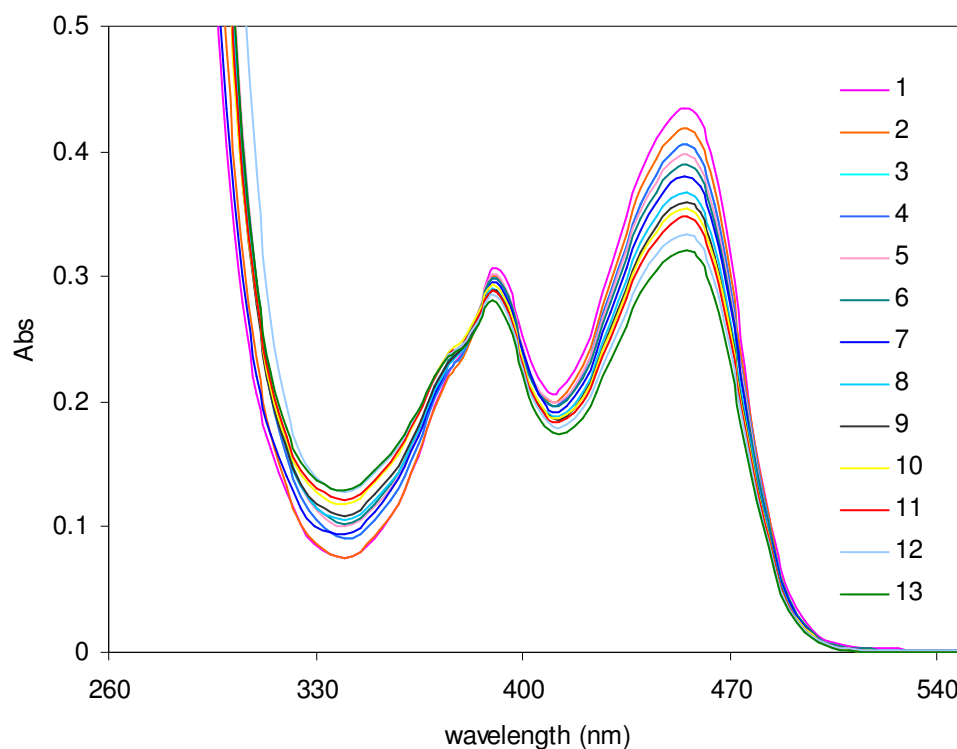


Table 2.11: Absorbance data for 2,4-dinitronaphthol^a (128) in DMSO containing imine (121) and iminium ion^b (121') at 454 nm and 25 °C.

Spectrum number	x ^c (M)	[ImineH ⁺] (M)	[Imine] (M)	Abs	[In ⁻]/[HIIn] ^d	K _{eq} ^e
1.	1.61 × 10 ⁻³	3.90 × 10 ⁻⁴	9.65 × 10 ⁻³	0.418	1.69	0.068
2.	2.02 × 10 ⁻³	4.84 × 10 ⁻⁴	9.55 × 10 ⁻³	0.404	1.49	0.075
3.	2.42 × 10 ⁻³	5.76 × 10 ⁻⁴	9.46 × 10 ⁻³	0.397	1.40	0.085
4.	2.84 × 10 ⁻³	6.64 × 10 ⁻⁴	9.37 × 10 ⁻³	0.389	1.30	0.092
5.	3.26 × 10 ⁻³	7.38 × 10 ⁻⁴	9.30 × 10 ⁻³	0.380	1.20	0.096
6.	3.65 × 10 ⁻³	8.46 × 10 ⁻⁴	9.19 × 10 ⁻³	0.367	1.08	0.099
7.	4.07 × 10 ⁻³	9.31 × 10 ⁻⁴	9.10 × 10 ⁻³	0.359	1.00	0.103
8.	4.48 × 10 ⁻³	1.02 × 10 ⁻³	9.02 × 10 ⁻³	0.354	0.96	0.108
9.	4.90 × 10 ⁻³	1.10 × 10 ⁻³	8.94 × 10 ⁻³	0.347	0.91	0.112
10.	5.74 × 10 ⁻³	1.18 × 10 ⁻³	8.85 × 10 ⁻³	0.345	0.89	0.119
11.	5.74 × 10 ⁻³	1.26 × 10 ⁻³	8.77 × 10 ⁻³	0.334	0.81	0.117
12.	6.16 × 10 ⁻³	1.31 × 10 ⁻³	8.73 × 10 ⁻³	0.334	0.81	0.122
13.	6.58 × 10 ⁻³	1.42 × 10 ⁻³	8.61 × 10 ⁻³	0.321	0.72	0.119

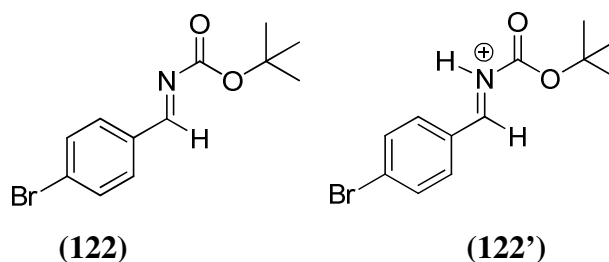
(a) The final concentration of 2,4-dinitronaphthol was 3 × 10⁻⁵ M. (b) Iminium ion was generated by addition of HCl in ether solution in DMSO such that the final concentration of ether was < 2%. (c) The concentration of free H⁺ ions at equilibrium, x, was calculated using Equation 2.9 with K_a = 3.98 × 10⁻². The value of K_a was chosen to give the least variation in values of K_{eq}. (d) The ratio of phenolate to phenol was obtained using the relationship Abs-A_{min}/A_{max}-Abs.

(e) Calculated as

$$\frac{[\text{ImineH}^+]}{[\text{Imine}]} \cdot \frac{(\text{Abs} - 0.126)}{(0.591 - \text{Abs})}$$

An average value of K_{eq} was calculated, K_{eq} = 0.101(± 0.02).

The pK_a value was calculated using Equation 2.11. In this case, pK_a = 1.11 (± 0.08).

2.1.3.2.5 *p*-Bromobenzaldehyde *N*-(*tert*-butoxycarbonyl)iminium ion (122'**).**

UV-Visible spectra of 2,4-dinitronaphthol (**128**) (3×10^{-5} M) in DMSO solutions containing *p*-bromobenzaldehyde *N*-(*tert*-butoxycarbonyl)imine (**122**) and *p*-bromobenzaldehyde *N*-(*tert*-butoxycarbonyl)iminium ion (**122'**) were recorded at 25 °C. These are shown in Figure 2.23, with scans 1-11 corresponding to the conditions given in Table 2.12.

Figure 2.23: UV-Visible spectra of 2,4-dinitronaphthol (**128**) in DMSO containing imine (**122**) and iminium ion (**122'**) at 25 °C.

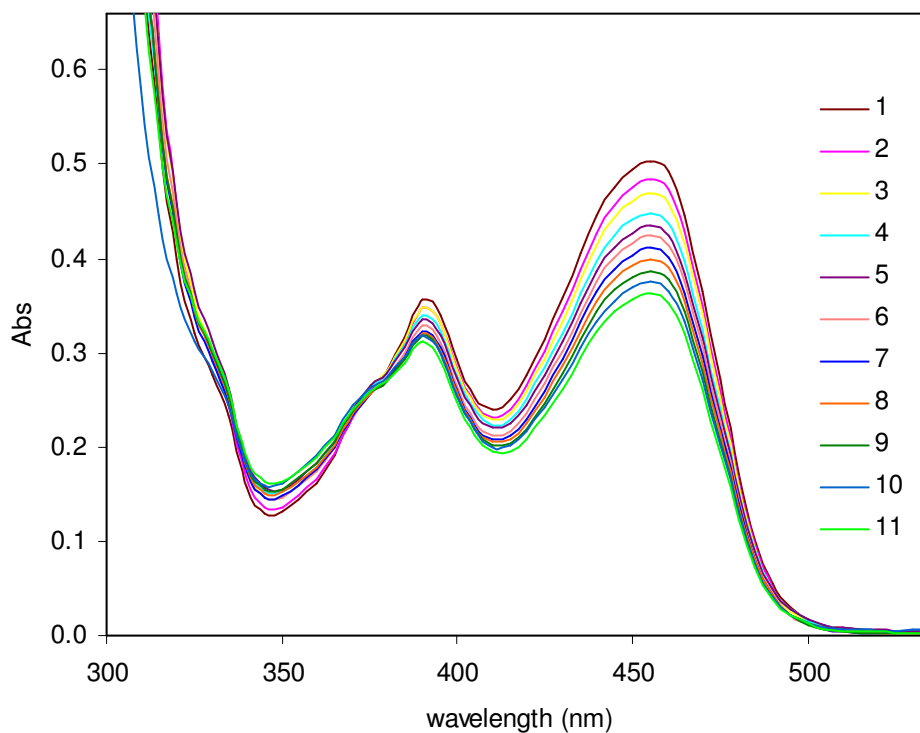


Table 2.12: Absorbance data for 2,4-dinitronaphthol^a (128) in DMSO containing imine (122) and iminium ion^b (122') at 454 nm and 25 °C.

Spectrum number	x^c (M)	[ImineH ⁺] (M)	[Imine] (M)	Abs	[In ⁻]/[HIn] ^d	K_{eq}^e
1.	1.43×10^{-3}	7.35×10^{-5}	9.97×10^{-3}	0.493	3.74	0.028
2.	1.90×10^{-3}	9.55×10^{-5}	9.95×10^{-3}	0.475	3.01	0.029
3.	2.38×10^{-3}	1.18×10^{-4}	9.93×10^{-3}	0.460	2.55	0.030
4.	2.86×10^{-3}	1.42×10^{-4}	9.90×10^{-3}	0.446	2.21	0.032
5.	3.81×10^{-3}	1.89×10^{-4}	9.86×10^{-3}	0.425	1.80	0.035
6.	4.29×10^{-3}	2.12×10^{-4}	9.84×10^{-3}	0.416	1.66	0.036
7.	4.77×10^{-3}	2.34×10^{-4}	9.81×10^{-3}	0.402	1.46	0.035
8.	5.72×10^{-3}	2.79×10^{-4}	9.77×10^{-3}	0.390	1.31	0.038
9.	6.68×10^{-3}	3.25×10^{-4}	9.72×10^{-3}	0.378	1.18	0.039
10.	7.63×10^{-3}	3.69×10^{-4}	9.68×10^{-3}	0.366	1.07	0.041
11.	8.59×10^{-3}	4.14×10^{-4}	9.63×10^{-3}	0.356	0.98	0.042

(a) The final concentration of 2,4-dinitronaphthol was 3×10^{-5} M. (b) Iminium ion was generated by addition of HCl in ether solution in DMSO such that the final concentration of ether was < 2%. (c) The concentration of free H⁺ ions at equilibrium, x , was calculated using Equation 2.9 with $K_a = 2.00 \times 10^{-1}$. The value of K_a was chosen to give the least variation in values of K_{eq} . (d) The ratio of phenolate to phenol was obtained using the relationship $Abs - A_{min} / A_{max} - Abs$.

(e) Calculated as

$$\frac{[\text{ImineH}^+]}{[\text{Imine}]} \cdot \frac{(\text{Abs} - 0.126)}{(0.591 - \text{Abs})}$$

An average value of K_{eq} was calculated, $K_{eq} = 0.035 (\pm 0.005)$.

The pK_a value was calculated using Equation 2.11. In this case, $pK_a = 0.65 (\pm 0.06)$.

2.1.3.3 Investigations of iminium ion pK_a values in acetonitrile.

Studies of iminium ion pK_a values were undertaken in acetonitrile. Solutions of imines and 2,4-dinitrophenol (**131**) (1×10^{-4} M) were mixed in a 1:1 ratio and scanned using UV-Vis spectrophotometry. The resulting spectra were observed to change significantly over time and reliable absorbance data could not be obtained. Further investigations in acetonitrile were not pursued as the imines were not soluble in acetonitrile in concentrations required to buffer the in indicator in large excess, according to the method adopted for the study of pK_a values in DMSO.

2.1.4 Determination of pK_a values of phosphoric acid catalysts.

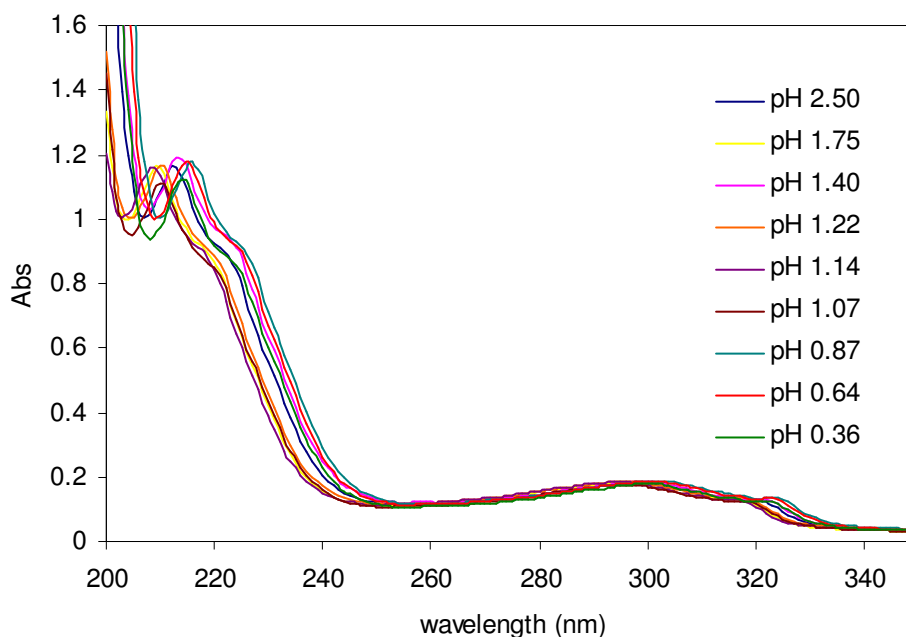
For the purposes of detailed structure-activity analysis, the pK_a values of a structurally homologous series of catalysts are required. While simple phosphate esters are the focus of considerable research due to their role as models for more complex biological systems, there are no values reported for BINOL-derived phosphoric acids. It has been assumed that these compounds have an aqueous pK_a value of 1.29 (that of dimethyl phosphate⁸⁰). This dearth of relevant literature data made it necessary to determine the solution pK_a values of a range of phosphoric acid catalysts and thiophosphoryl analogues. The results of these investigations are presented in the following section.

2.1.4.1 Attempted determination of aqueous pK_a values.

The simplest method for the determination of thermodynamic pK_a values of strong Brønsted acids (pK_a 0-14) is to measure the equilibrium concentration of acid versus conjugate base in aqueous solution. However, it was found that these compounds were sparingly soluble, presumably due to the presence of the bulky aromatic framework. Attempts were made at determining the pK_a values using pH titrations however, no clear endpoint was obtained. Similarly, ^{31}P NMR spectroscopic titrations were unsuccessful as the small amount of compound in solution was not sufficient to give signals of appropriate intensity. The compound precipitated out of solution at concentrations required to provide reasonable results for both methods.

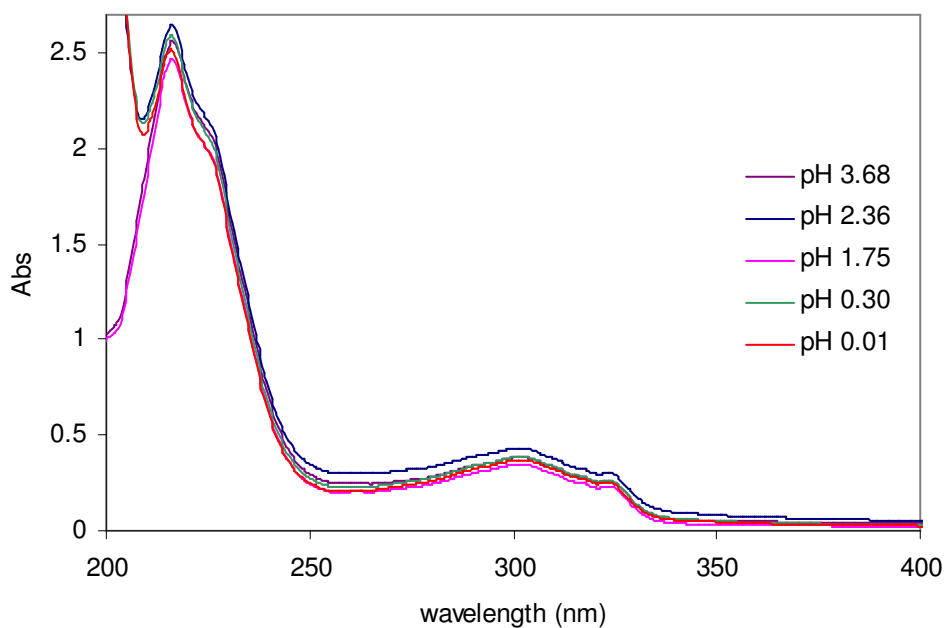
With this in mind, UV-Vis spectrophotometry was employed as a more sensitive experimental technique. Spectra were obtained in a range of aqueous solutions at different pHs, constant ionic strength ($I = 1.0$ KCl) and 25°C according to conventional spectrophotometric techniques for determination of pK_a values. As illustrated in Figure 2.24, very small changes in absorbance were observed over the pH range investigated.

Figure 2.24: UV-Visible spectra of phosphoric acid catalyst (85) in HCl solutions at $I = 1.0$ (KCl) and 25°C .



In order to amplify these spectral changes, this experiment was repeated at increased catalyst concentration and using acetonitrile as a co-solvent (5%). This resulted in precipitation of the compound and gave inconsistent results with no visible isosbestic point (Figure 2.25). Further investigation of aqueous pK_a values of phosphoric acids was not undertaken.

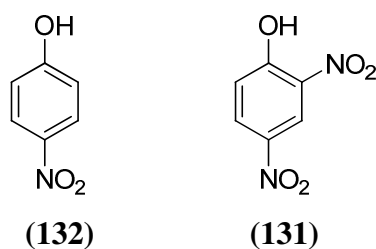
Figure 2.25: UV-Visible spectra of phosphoric acid catalyst (85) in HCl and buffer solutions at $I = 1.0$ (KCl) and $25\text{ }^\circ\text{C}$.



2.1.4.2 Investigations of pK_a values of phosphoric acid catalysts in acetonitrile.

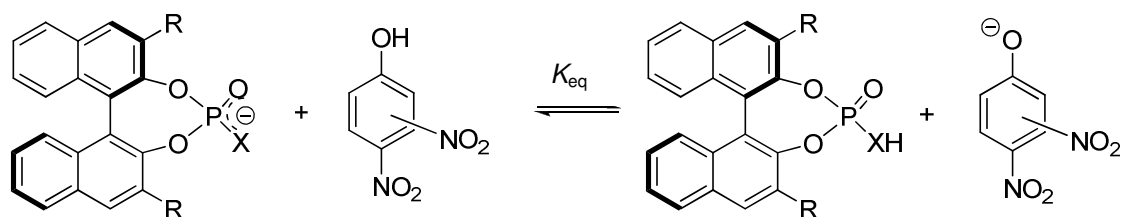
As poor solubility of the phosphoric acids hampered the measurement of aqueous pK_a values, such determinations were limited to the use of organic solvents.

Initial studies focussed on bracketing pK_a values of phosphoric acid catalysts using acetonitrile as a solvent and UV-Vis spectrophotometry. A selection of catalysts was mixed in a 1:1 ratio with substituted phenol indicators of known pK_a .



The resulting equilibrium is described in Scheme 2.19.

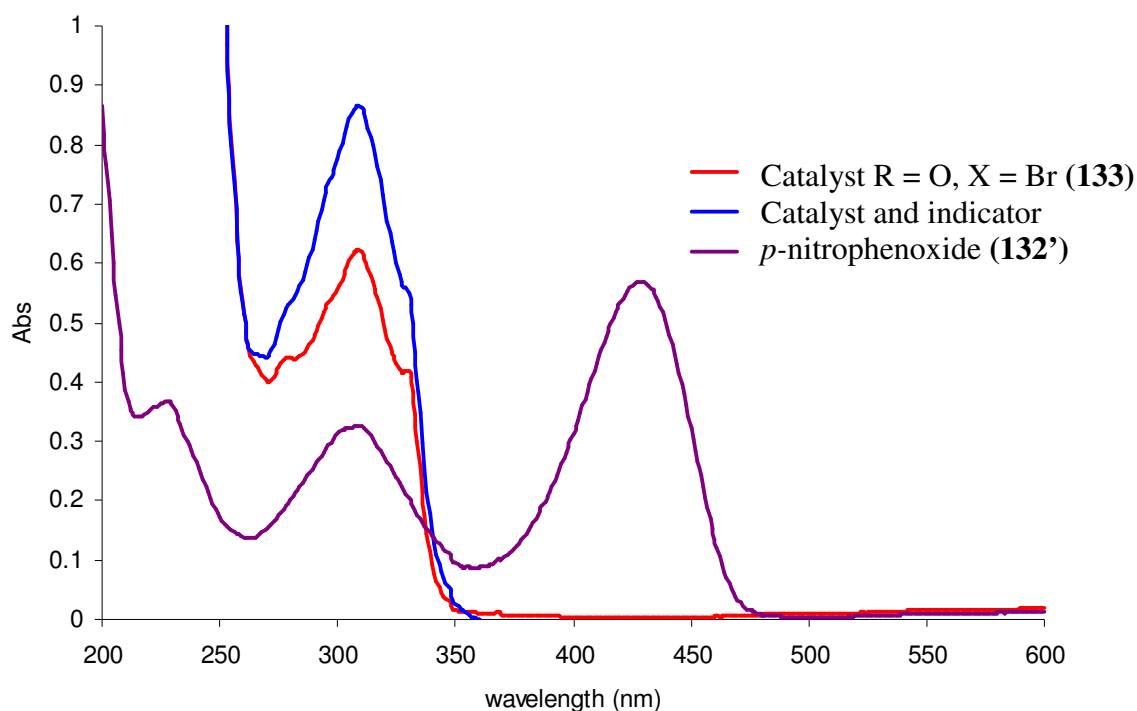
Scheme 2.19:



X = O, S
R = H, Br, Ph, Naphth, Biph

It was found that when each catalyst was mixed with *p*-nitrophenol (**132**), complete quenching of the absorbance of the nitrophenoxide species was observed (Figure 2.26). This indicated that the catalyst pK_a values were below 20.7⁸¹ in acetonitrile.

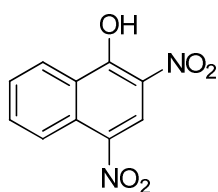
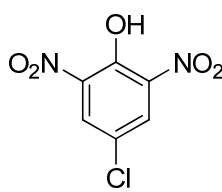
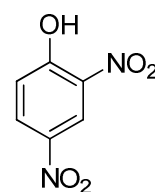
Figure 2.26: UV-Vis spectra of indicator anion (**132'**) (1.2×10^{-4} M), catalyst (**133**) (1.2×10^{-4} M) and an equimolar solution of (**133**) and (**132'**) in DMSO.



Further investigations involved the use of 2,4-dinitrophenol (**131**) which has a pK_a of 16.66 in acetonitrile⁸². Upon mixing this indicator with catalyst (R=H, X=O) (**85**) in a 1:1 ratio, complete quenching of phenolate absorbance was not observed. This indicates that the catalyst pK_a is within 2 units of that of the indicator. Further investigations in acetonitrile were not undertaken as the phosphoric acid catalysts had limited solubility in this solvent at the concentrations required to buffer the indicator in 100-fold excess.

2.1.4.3 Determination of pK_a values of (thio)phosphoric acids in DMSO.

It was anticipated that the effect of the bulky aromatic backbone would be to increase the pK_a values of BINOL-derived phosphoric acid catalysts relative to that of simple dimethyl phosphate which has an aqueous pK_a value of 1.29. With this in mind, the initial indicators screened were in the pK_a range of 2.11-5.12.⁷⁸ The indicators used in this study were a series of substituted phenols shown below.

**(128)****(134)****(131)**

$$pK_a (\text{DMSO}) = 2.11 \pm 0.04$$

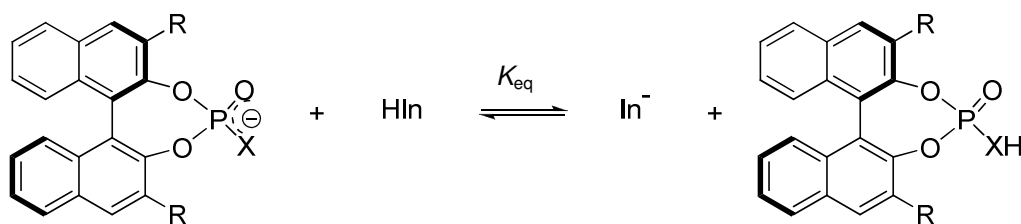
$$3.56 \pm 0.02$$

$$5.12 \pm 0.04$$

Each indicator is colourless in the neutral form. A pronounced change in the UV-Visible spectrum is observed upon ionisation to give a brightly yellow-orange coloured anion in each case. In a typical experiment, spectra were recorded with a constant concentration (3×10^{-5} M) of indicator in solutions buffered with the phosphoric acid and the conjugate base anion. The anion was formed by adding varying amounts of a sodium hydroxide in DMSO solution to the phosphoric acid solution, such that the final concentration of water was $< 2\%$. Measurements were made with a constant salt concentration of 0.01 M.

Initially each catalyst was screened with the substituted phenoxides in order to bracket the pK_a . It was found that when each phosphoric acid was mixed with 2,4-dinitrophenoxide (**131**) complete quenching of the absorbance resulted. This indicated that the pK_a values of the phosphoric acids were lower than 5.12 units. Further screening revealed 2,4-dinitronaphthol (**128**) and 4-chloro-2,6-dinitrophenol (**134**) to be of appropriate acidity, as complete quenching of the indicator anion to the neutral phenol was not observed when these indicators were mixed with the phosphoric acids.

Scheme 2.20 and Equation 2.12 define an equilibrium constant, K_{eq} , for the overall conversion of indicator (HIn) to the deprotonated form (In⁻) by the respective (thio)phosphoric acid catalyst.

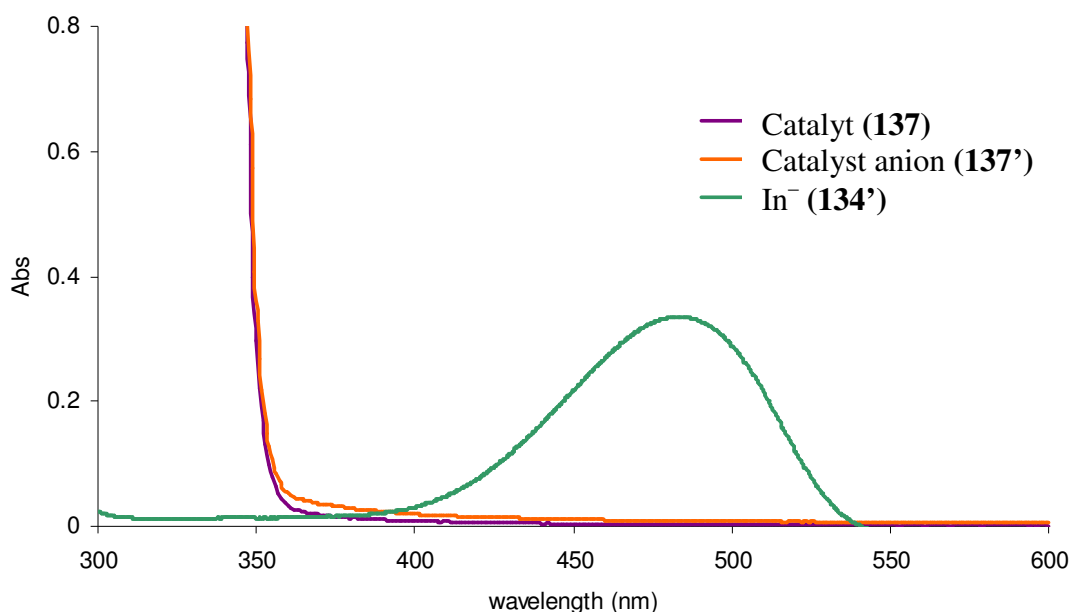
Scheme 2.20: Equilibrium between the catalyst and indicator.

X = O, S

$$K_{\text{eq}} = \frac{K_{\text{a}}^{\text{HIn}}}{K_{\text{a}}^{\text{Cat}}} = \frac{[\text{Cat}] [\text{In}^-]}{[\text{Cat}^-] [\text{HIn}]} \quad (\text{Equation 2.12})$$

Initial studies of the equilibrium constants showed that 4-chloro-2,6-dinitrophenol (**134**) and 2,4-dinitronaphthol (**128**) were the most suitable indicators for the range of phosphoric acids investigated. 4-Chloro-2,6-dinitrophenol (**134**) proved to be of appropriate pK_{a} for use in measurements with catalysts (**7**), (**84**), (**85**), (**133**), (**135**)-(**137**). Ionisation of this indicator to form (**134'**) results in an increase in absorbance at $\lambda_{\text{max}} = 480 \text{ nm}$ which was chosen as the analytical wavelength. In general, no interfering absorbance from the phosphoric acid or the conjugate base anion was observed at this wavelength. Representative scans are shown in Figure 2.27.

Figure 2.27: UV-Vis spectra of indicator anion (134'**) ($3 \times 10^{-5} \text{ M}$), catalyst (**137**) (0.01 M) and catalyst anion (**137'**) (0.01 M) in DMSO.**



As the indicator anion is the main absorbing species at the analytical wavelength, Equation 2.12 may be written as Equation 2.13.

$$K_{\text{eq}} = \frac{[\text{Cat}] (\text{Abs} - A_{\text{min}})}{[\text{Cat}^-] (A_{\text{max}} - \text{Abs})} \quad (\text{Equation 2.13})$$

A_{min} = absorbance of the neutral form of indicator only.

This was obtained from a spectrum of the indicator in the presence of an excess of acid (Figure 2.28).

A_{max} = absorbance of indicator anion.

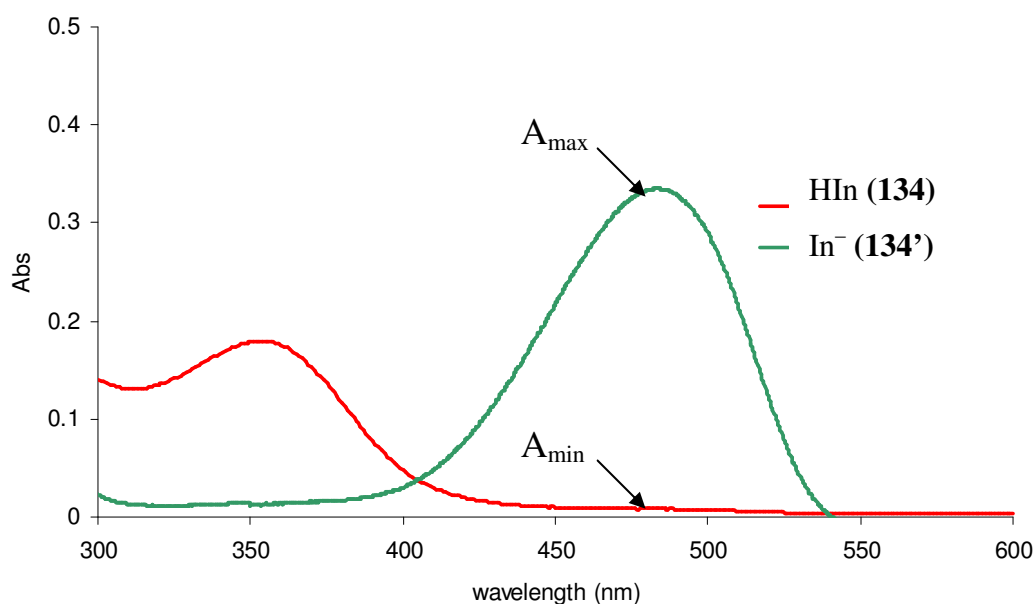
This was obtained from a spectrum of the indicator in the presence of an excess of base (Figure 2.28).

$[\text{Cat}^-]$ = initial concentration of the catalyst anion ($[\text{Cat}^-] = [\text{OH}^-]_{\text{added}}$).

$[\text{Cat}]$ = initial concentration of neutral catalyst ($[\text{Cat}] = [\text{Cat}]_{\text{total}} - [\text{Cat}^-]$).

Abs is the absorbance of at the analytical wavelength for a given mixture of indicator and catalyst.

Figure 2.28: UV-Visible spectra of indicator (3×10^{-5} M) (134) in the presence of acid (HCl, 100 mM) (—) and base (DBU, 6mM) (—) in DMSO.



In a typical experiment, spectra were recorded with a constant concentration (3×10^{-5} M) of indicator in solutions buffered with neutral and ionised forms of the BINOL-

derived catalyst. The catalyst was ionised by addition of a solution of sodium hydroxide in DMSO. The resulting mixture was incubated at 25 °C for several minutes prior to the addition of the indicator. The indicator was added last in order to prevent the direct reaction of sodium hydroxide with the substituted phenol (**134**). Scans and absorbance measurements at the analytical wavelength were recorded over a period of 5 mins.

The pK_a values of the BINOL-derived catalysts were related to $\log_{10}K_{eq}$ and the pK_a value of the indicator by Equation 2.14.

$$pK_a(\text{Cat}) = \log_{10}K + pK_a(4\text{-chloro-2,6-dinitrophenol}) \quad (\text{Equation 2.14})$$

The most acidic catalysts of the range investigated required the use of 2,4-dinitronaphthol (**128**) as the indicator. Ionisation of this indicator to form (**128'**) results in an increase in absorbance at $\lambda_{\text{max}} = 454$ nm which was chosen as the analytical wavelength. The absorbance values of the neutral (A_{min}) and ionised indicator (A_{max}) were measured by recording spectra of the indicator (**128**) in the presence of an excess of acid and base respectively. Examples of the spectra obtained are shown in Figure 2.15, Section 2.1.3.2). For those (thio)phosphoric acids with pK_a values < 3 , the natural ionisation of the compound must also be taken into account. A small adjustment of the values of the concentrations of the catalyst and the conjugate base anion was therefore required to account for the high acidity. The dissociation constant of the phosphoric acid catalyst is defined by Equation 2.15.

$$K_a^{\text{Cat}} = \frac{[\text{Cat}^-][\text{H}^+]}{[\text{Cat}]} \quad (\text{Equation 2.15})$$

$$[\text{Cat}^-] = [\text{OH}^-]_{\text{added}} + x \quad (\text{where } x \text{ is the concentration of free } \text{H}^+ \text{ ions at equilibrium due to the ionisation of the catalyst}).$$

$$[\text{Cat}] = [\text{Cat}]_{\text{total}} - [\text{Cat}^-]$$

Solving Equation 2.16 using an estimated value of K_a gave a value for x , which was used to adjust the concentrations of catalyst and catalyst anion. The value of K_a was chosen so as to give the smallest variation in the final values of K_{eq} .

$$K_a^{\text{Cat}} = \frac{([\text{OH}^-]_{\text{added}} + x)x}{([\text{Cat}]_{\text{total}} - ([\text{OH}^-]_{\text{added}} + x))x} \quad (\text{Equation 2.16})$$

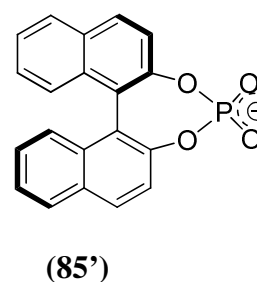
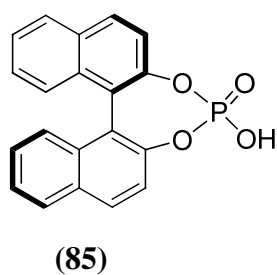
The final K_{eq} was estimated using Equation 2.17.

$$K_{\text{eq}} = \frac{([\text{Cat}]_{\text{total}} - ([\text{OH}^-]_{\text{added}} + x)) \cdot (\text{Abs} - A_{\text{min}})}{([\text{OH}^-]_{\text{added}} + x) \cdot (A_{\text{max}} - \text{Abs})} = \frac{K_a^{\text{HIn}}}{K_a^{\text{Cat}}} \quad (\text{Equation 2.17})$$

The $\text{p}K_a$ values of the catalysts were related to $\log_{10}K_{\text{eq}}$ and the $\text{p}K_a$ value of the indicator by Equation 2.18.

$$\text{p}K_a(\text{Cat}) = \log_{10}K_{\text{eq}} + \text{p}K_a(2,4\text{-dinitronaphthol}) \quad (\text{Equation 2.18})$$

The mean values of K_{eq} and $\text{p}K_a$ are presented followed by the standard deviation in parentheses as an indication of the error in the measurements.

2.1.4.3.1 (*R*)-1,1'-Binaphthyl-2,2'-diyl hydrogenphosphate (**85**).

UV-Visible spectra of 4-chloro-2,6-dinitrophenol (**134**) (3×10^{-5} M) in DMSO solutions containing (*R*)-1,1'-binaphthyl-2,2'-diyl hydrogenphosphate (**85**) and the conjugate base anion (**85'**) were recorded at 25 °C. These are shown in Figure 2.29, with scans 1- 8 corresponding to the conditions given in Table 2.13.

Figure 2.29: UV-Visible spectra of 4-chloro-2,6-dinitrophenol (**134**) in DMSO containing phosphoric acid (**85**) and conjugate base anion (**85'**) at 25 °C.

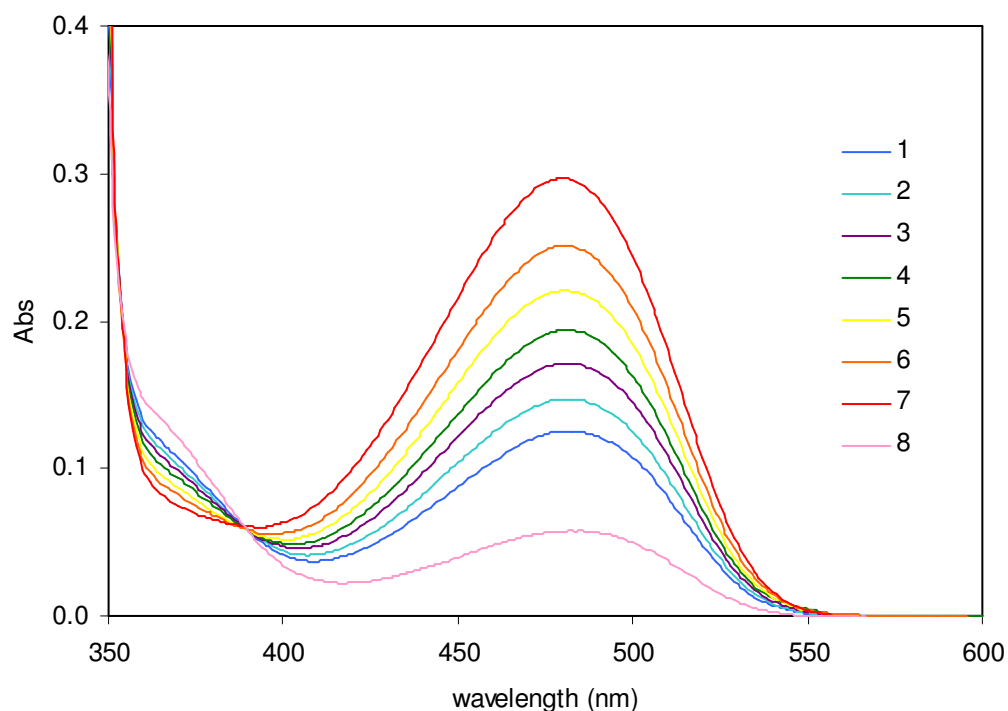


Table 2.13: Absorbance data for 4-chloro-2,6-dinitrophenol (134)^a in DMSO containing phosphoric acid (85) and conjugate base anion^b (85') at 480 nm and 25 °C.

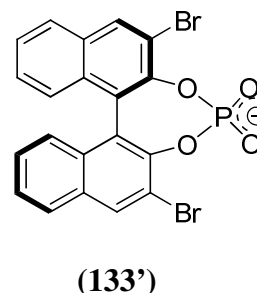
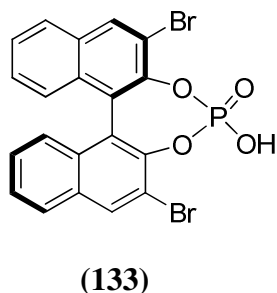
Spectrum number	[Cat ⁻] (M)	[Cat] (M)	[Indicator] (M)	Abs	[In ⁻]/[HIn] ^c	<i>K</i> _{eq} ^d
1.	3.33×10^{-3}	6.67×10^{-3}	3.00×10^{-5}	0.121	0.39	0.78
2.	4.17×10^{-3}	5.83×10^{-3}	3.00×10^{-5}	0.143	0.51	0.72
3.	5.00×10^{-3}	5.00×10^{-3}	3.00×10^{-5}	0.167	0.68	0.68
4.	5.83×10^{-3}	4.17×10^{-3}	3.00×10^{-5}	0.189	0.86	0.61
5.	6.67×10^{-3}	3.33×10^{-3}	3.00×10^{-5}	0.215	1.13	0.56
6.	7.50×10^{-3}	2.50×10^{-3}	3.00×10^{-5}	0.246	1.58	0.53
7.	8.33×10^{-3}	1.67×10^{-3}	3.00×10^{-5}	0.296	2.93	0.59
8.	-	1.00×10^{-2}	3.00×10^{-5}	0.059	-	-

(a) The concentration of 4-chloro-2,6-dinitrophenol was 3×10^{-5} M. (b) Catalyst anion was generated by addition of a solution of NaOH in DMSO such that the final concentration of water was < 2%. (c) The ratio of phenolate to phenol was obtained using the relationship $\text{Abs} - A_{\text{min}} / A_{\text{max}} - \text{Abs}$.

(d) Calculated as $\frac{[\text{Cat}]}{[\text{Cat}^-]} \cdot \frac{(\text{Abs} - 0.015)}{(0.392 - \text{Abs})}$

An average value of *K*_{eq} was calculated, *K*_{eq} = 0.64 (± 0.09).

The p*K*_a value was calculated using Equation 2.14. In this case, p*K*_a = 3.37 (± 0.06).

2.1.4.3.2 **(*R*)-3,3'-Dibromo-1,1'-binaphthyl-2,2'-diyl hydrogenphosphate (133).**

UV-Visible spectra of 4-chloro-2,6-dinitrophenol (**134**) (3×10^{-5} M) in DMSO solutions containing (*R*)-3,3'-dibromo-1,1'-binaphthyl-2,2'-diyl hydrogenphosphate (**133**) and the conjugate base anion (**133'**) were recorded at 25 °C. These are shown in Figure 2.30, with scans 1-9 corresponding to the conditions given in Table 2.14.

Figure 2.30: UV-Visible spectra of 4-chloro-2,6-dinitrophenol (**134**) in DMSO containing phosphoric acid (**133**) and conjugate base anion (**133'**) at 25 °C.

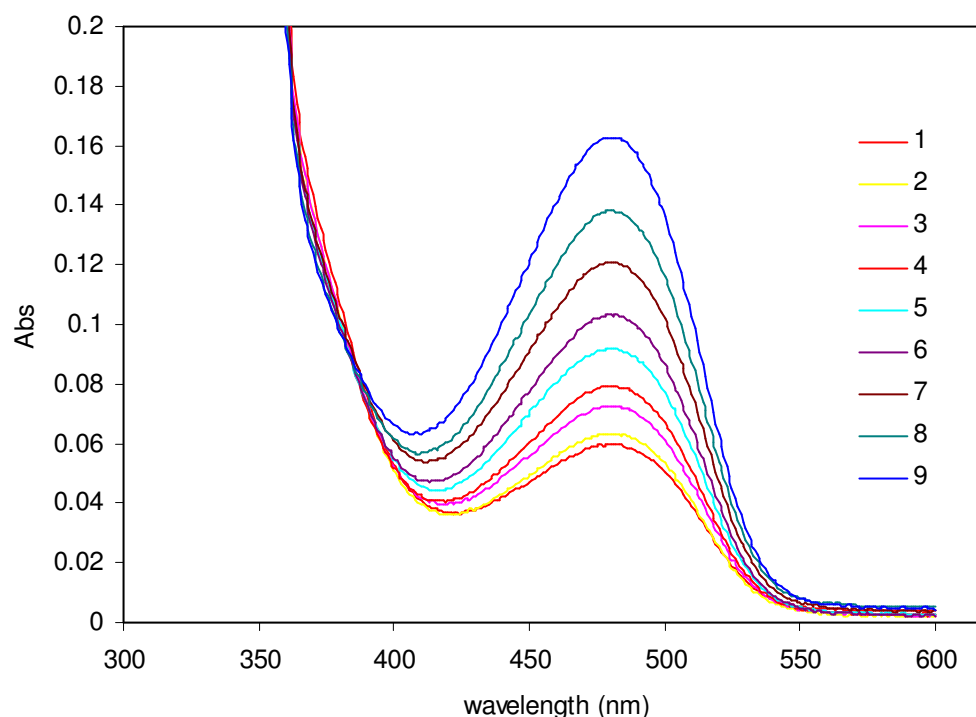


Table 2.14: Absorbance data for 4-chloro-2,6-dinitrophenol^a (134) in DMSO containing phosphoric acid (133) and conjugate base anion^b (133') at 480 nm and 25 °C.

Spectrum number	x ^c (M)	[Cat ⁻] (M)	[Cat] (M)	Abs	[In ⁻]/[HIIn] ^d	K _{eq} ^e
1.	1.37 × 10 ⁻³	5.37 × 10 ⁻³	4.63 × 10 ⁻³	0.055	0.23	0.20
2.	1.20 × 10 ⁻³	5.70 × 10 ⁻³	4.30 × 10 ⁻³	0.059	0.25	0.19
3.	1.04 × 10 ⁻³	6.04 × 10 ⁻³	3.96 × 10 ⁻³	0.068	0.31	0.20
4.	8.94 × 10 ⁻⁴	6.39 × 10 ⁻³	3.61 × 10 ⁻³	0.074	0.36	0.20
5.	7.61 × 10 ⁻⁴	6.76 × 10 ⁻³	3.24 × 10 ⁻³	0.088	0.47	0.22
6.	6.36 × 10 ⁻⁴	7.14 × 10 ⁻³	2.86 × 10 ⁻³	0.099	0.57	0.23
7.	5.22 × 10 ⁻⁴	7.52 × 10 ⁻³	2.48 × 10 ⁻³	0.116	0.76	0.25
8.	4.12 × 10 ⁻⁴	7.91 × 10 ⁻³	2.09 × 10 ⁻³	0.134	1.02	0.27
9.	2.24 × 10 ⁻⁴	8.72 × 10 ⁻³	1.28 × 10 ⁻³	0.159	1.53	0.22

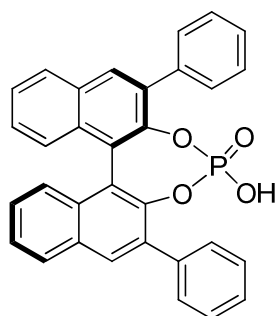
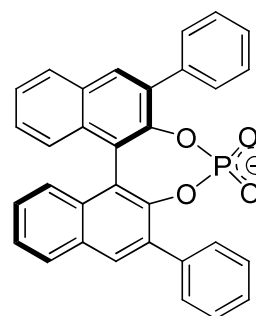
(a) The final concentration of 4-chloro-2,6-dinitrophenol was 3 × 10⁻³ M. (b) Catalyst anion was generated by addition of a solution of NaOH in DMSO such that the final concentration of water was < 2%. (c) The concentration of free H⁺ ions at equilibrium, x, was calculated using Equation 2.16 with K_a = 1.58 × 10⁻³. The value of K_a was chosen so as to give the smallest variation in the resulting K_{eq} values. (d) The ratio of phenolate to phenol was obtained using the relationship Abs-A_{min}/A_{max}-Abs.

(e) Calculated as

$$\frac{[\text{Cat}]}{[\text{Cat}^-]} \cdot \frac{(\text{Abs} - 0.009)}{(0.257 - \text{Abs})}$$

An average value of K_{eq} was calculated, K_{eq} = 0.22 (± 0.03).

The pK_a value was calculated using Equation 2.14. In this case, pK_a = 2.90 (± 0.05).

2.1.4.3.3 **(R)-3,3'-Diphenyl-1,1'-binaphthyl-2,2'-diyl hydrogenphosphate (84).****(84)****(84')**

UV-Visible spectra of 4-chloro-2,6-dinitrophenol (**134**) (3×10^{-5} M) in DMSO solutions containing (R)-3,3'-diphenyl-1,1'-binaphthyl-2,2'-diyl hydrogenphosphate (**84**) and the conjugate base anion (**84'**) were recorded at 25 °C. These are shown in Figure 2.31, with scans 1-8 corresponding to the conditions given in Table 2.15.

Figure 2.31: UV-Visible spectra of 4-chloro-2,6-dinitrophenol (**134**) in DMSO containing phosphoric acid (**84**) and conjugate base anion (**84'**) at 25 °C.

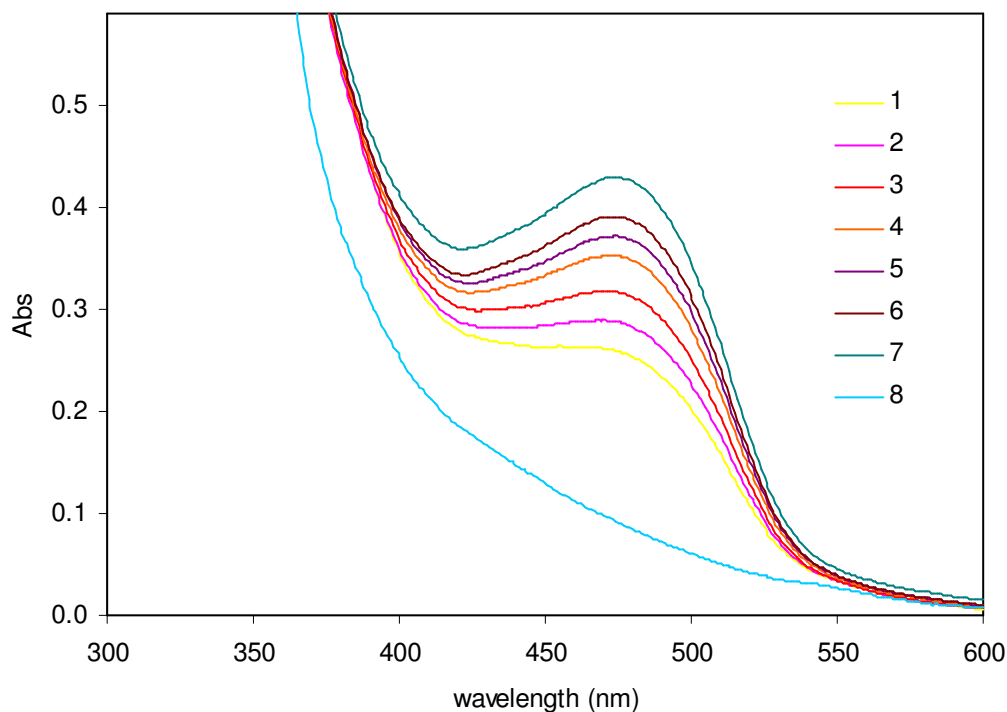


Table 2.15: Absorbance data for 4-chloro-2,6-dinitrophenol (134) in DMSO containing phosphoric acid (84) and conjugate base anion^a (84') at 500 nm and 25 °C.

Spectrum number	[Cat ⁻] (M)	[Cat] (M)	[Indicator] (M)	Abs ^b	[In ⁻]/[HIn] ^c	K _{eq} ^d
1.	2.00 × 10 ⁻³	8.00 × 10 ⁻³	3.00 × 10 ⁻⁵	0.139	0.65	2.59
2.	3.00 × 10 ⁻³	7.00 × 10 ⁻³	3.00 × 10 ⁻⁵	0.165	0.89	2.08
3.	4.00 × 10 ⁻³	6.00 × 10 ⁻³	3.00 × 10 ⁻⁵	0.190	1.21	1.81
4.	5.00 × 10 ⁻³	5.00 × 10 ⁻³	3.00 × 10 ⁻⁵	0.220	1.75	1.75
5.	5.50 × 10 ⁻³	4.50 × 10 ⁻³	3.00 × 10 ⁻⁵	0.237	2.20	1.80
6.	6.00 × 10 ⁻³	4.00 × 10 ⁻³	3.00 × 10 ⁻⁵	0.252	2.74	1.83
7.	7.00 × 10 ⁻³	3.00 × 10 ⁻³	3.00 × 10 ⁻⁵	0.274	4.84	2.08
8.	-	1.00 × 10 ⁻²	-	0.070	-	-

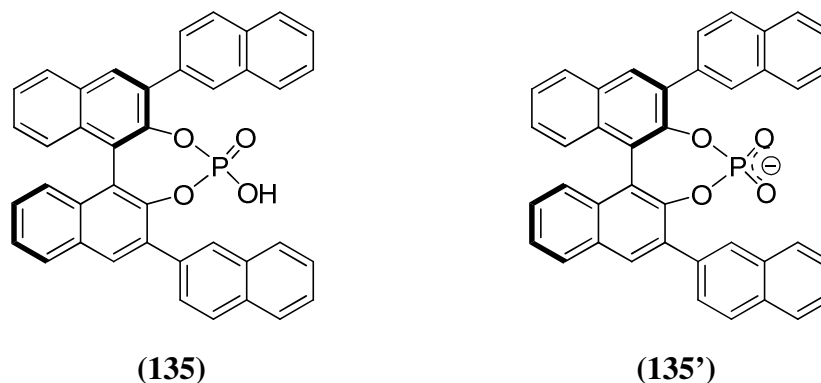
(a) Catalyst anion was generated by addition of a solution of NaOH in DMSO such that the final concentration of water was < 2%. (b) A small correction was made to account for background absorbance of the catalyst at the analytical wavelength. There was no change in absorbance of the catalyst upon deprotonation at this wavelength. (c) The ratio of phenolate to phenol was obtained using the relationship $\text{Abs} - A_{\text{min}} / A_{\text{max}} - \text{Abs}$.

(d) Calculated as
$$\frac{[\text{Cat}]}{[\text{Cat}^-]} \cdot \frac{(\text{Abs} - 0.008)}{(0.341 - \text{Abs})}$$

An average value of K_{eq} was calculated, $K_{\text{eq}} = 1.99 (\pm 0.29)$.

The $\text{p}K_{\text{a}}$ value was calculated using Equation 2.14. In this case, $\text{p}K_{\text{a}} = 3.86 (\pm 0.06)$.

2.1.4.3.4 (*R*)-3,3'-Bis(2-naphthyl)-1,1'-binaphthyl-2,2'-diyl hydrogenphosphate (**135**).



UV-Visible spectra of 4-chloro-2,6-dinitrophenol (**134**) (3×10^{-5} M) in DMSO solutions containing (*R*)-3,3'-bis(2-naphthyl)-1,1'-binaphthyl-2,2'-diyl hydrogenphosphate (**135**) and the conjugate base anion (**135'**) were recorded at 25 °C. These are shown in Figure 2.32, with scans 1-7 corresponding to the conditions given in Table 2.16.

Figure 2.32: UV-Visible spectra of 4-chloro-2,6-dinitrophenol (**134**) in DMSO containing phosphoric acid (**135**) and conjugate base anion (**135'**) at 25 °C.

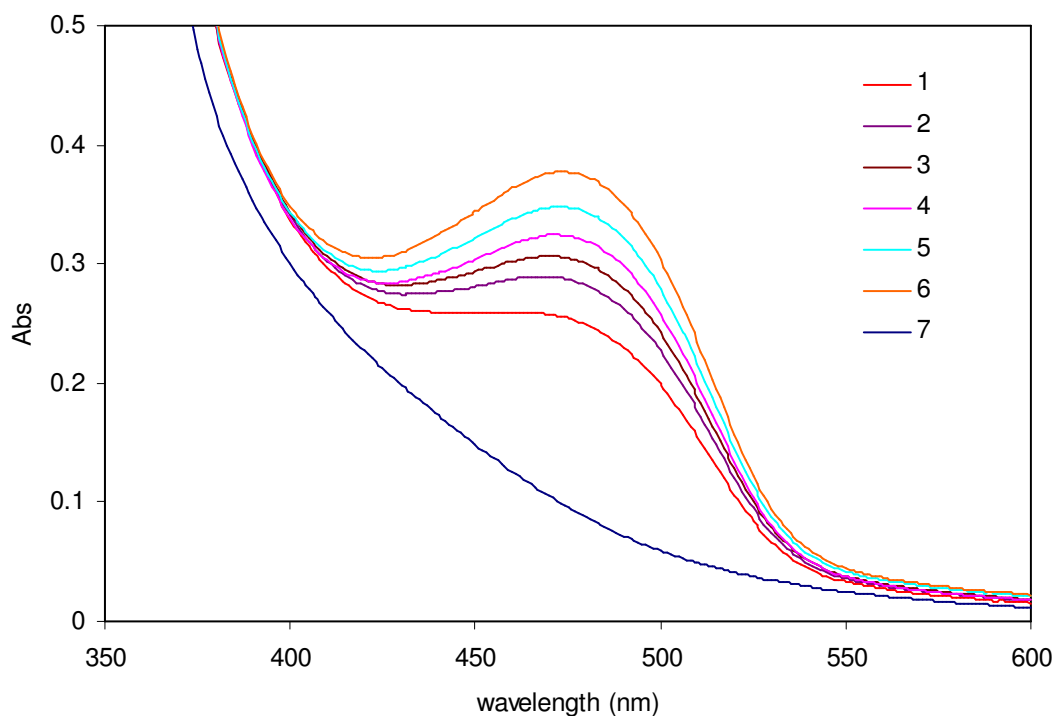


Table 2.16: Absorbance data for 4-chloro-2,6-dinitrophenol (134) in DMSO containing phosphoric acid (135) and conjugate base anion^a (135') at 480 nm and 25 °C.

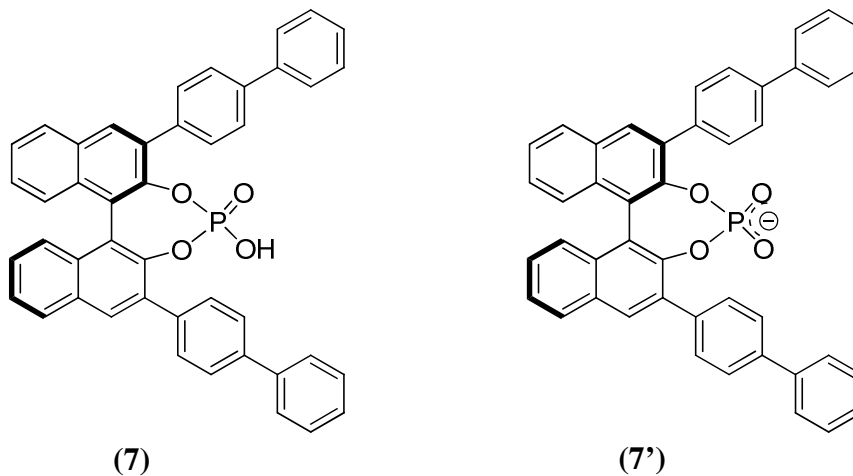
Spectrum number	[Cat ⁻] (M)	[Cat] (M)	[Indicator] (M)	Abs ^b	[In ⁻]/[HIn] ^c	K _{eq} ^d
1.	3.50 × 10 ⁻³	5.07 × 10 ⁻³	3 × 10 ⁻⁵	0.140	0.78	1.13
2.	3.75 × 10 ⁻³	4.82 × 10 ⁻³	3 × 10 ⁻⁵	0.169	1.16	1.49
3.	4.00 × 10 ⁻³	4.57 × 10 ⁻³	3 × 10 ⁻⁵	0.185	1.45	1.66
4.	4.50 × 10 ⁻³	4.07 × 10 ⁻³	3 × 10 ⁻⁵	0.204	1.91	1.73
5.	5.00 × 10 ⁻³	3.57 × 10 ⁻³	3 × 10 ⁻⁵	0.223	2.53	1.81
6.	5.50 × 10 ⁻³	3.07 × 10 ⁻³	3 × 10 ⁻⁵	0.249	3.55	1.98
7.	-	8.57 × 10 ⁻³	3 × 10 ⁻⁵	0.057		

(a) Catalyst anion was generated by addition of a solution of NaOH in DMSO such that the final concentration of water was < 2%. (b) A small correction was made to account for background absorbance of the catalyst at the analytical wavelength. There was no change in absorbance of the catalyst upon deprotonation at this wavelength. (c) The ratio of phenolate to phenol was obtained using the relationship $\text{Abs} - A_{\text{min}} / A_{\text{max}} - \text{Abs}$.

(d) Calculated as
$$\frac{[\text{Cat}]}{[\text{Cat}^-]} \cdot \frac{(\text{Abs} - 0.009)}{(0.355 - \text{Abs})}$$

An average value of K_{eq} was calculated, $K_{\text{eq}} = 1.63 (\pm 0.29)$.

The $\text{p}K_{\text{a}}$ value was calculated using Equation 2.14. In this case, $\text{p}K_{\text{a}} = 3.77 (\pm 0.08)$.

2.1.4.3.5 **(*R*)-3,3'-Bis(4-biphenyl)-1,1'-binaphthyl-2,2'-diyl hydrogenphosphate (7).**

UV-Visible spectra of 4-chloro-2,6-dinitrophenol (**134**) (3×10^{-5} M) in DMSO solutions containing (*R*)-3,3'-bis(4-biphenyl)-1,1'-binaphthyl-2,2'-diyl hydrogenphosphate (**7**) and the conjugate base anion (**7'**) were recorded at 25 °C. These are shown in Figure 2.33, with scans 1-9 corresponding to the conditions given in Table 2.17.

Figure 2.33: UV-Visible spectra of 4-chloro-2,6-dinitrophenol (**134**) in DMSO containing phosphoric acid (**7**) and conjugate base anion (**7'**) at 25 °C.

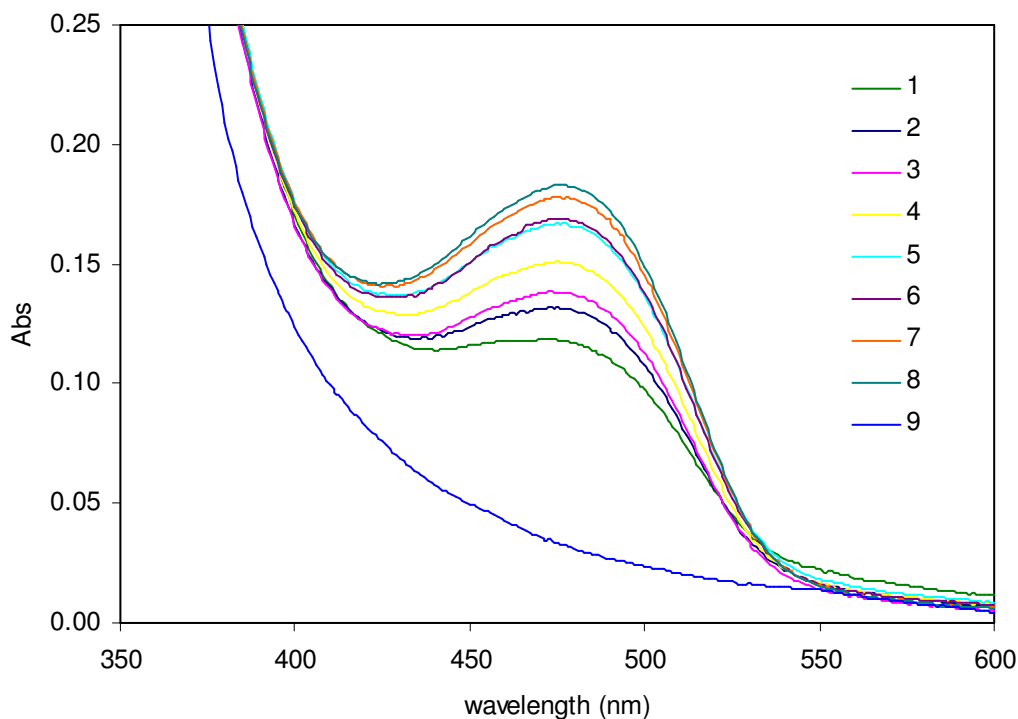


Table 2.17: Absorbance data for 4-chloro-2,6-dinitrophenol (134) in DMSO containing phosphoric acid (7) and conjugate base anion^a (7') at 480 nm and 25 °C.

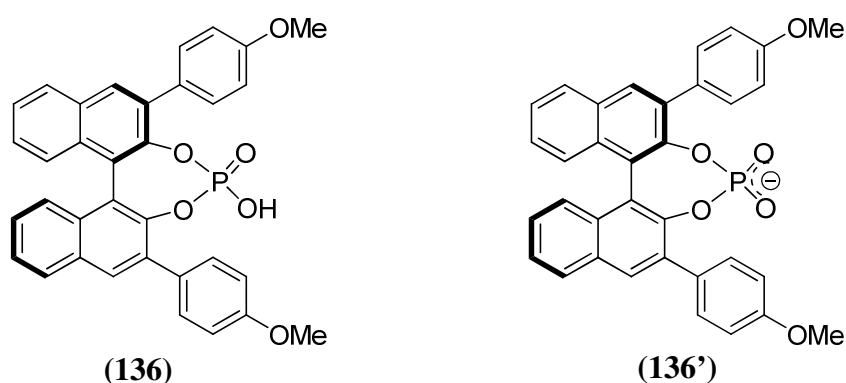
Spectrum number	[Cat ⁻] (M)	[Cat] (M)	[Indicator] (M)	Abs ^b	[In ⁻]/[HIn] ^c	K _{eq} ^d
1.	3.00 × 10 ⁻³	7.05 × 10 ⁻³	3.00 × 10 ⁻⁵	0.085	0.45	1.06
2.	4.00 × 10 ⁻³	6.05 × 10 ⁻³	3.00 × 10 ⁻⁵	0.099	0.58	0.88
3.	4.50 × 10 ⁻³	5.55 × 10 ⁻³	3.00 × 10 ⁻⁵	0.108	0.81	0.82
4.	5.00 × 10 ⁻³	5.05 × 10 ⁻³	3.00 × 10 ⁻⁵	0.118	1.22	0.82
5.	5.50 × 10 ⁻³	4.55 × 10 ⁻³	3.00 × 10 ⁻⁵	0.134	1.05	0.87
6.	5.75 × 10 ⁻³	4.30 × 10 ⁻³	3.00 × 10 ⁻⁵	0.137	1.37	0.83
7.	6.00 × 10 ⁻³	4.05 × 10 ⁻³	3.00 × 10 ⁻⁵	0.143	0.68	0.84
8.	6.25 × 10 ⁻³	3.80 × 10 ⁻³	3.00 × 10 ⁻⁵	0.150	1.10	0.83
9.	-	1.00 × 10 ⁻²	-	0.031	-	-

(a) Catalyst anion was generated by addition of a solution of NaOH in DMSO such that the final concentration of water was < 2%. (b) A small correction was made to account for background absorbance of the catalyst at the analytical wavelength. There was no change in absorbance of the catalyst upon deprotonation at this wavelength. (c) The ratio of phenolate to phenol was obtained using the relationship $Abs - A_{min} / A_{max} - Abs$.

(d) Calculated as $\frac{[Cat]}{[Cat^-]} \cdot \frac{(Abs - 0.009)}{(0.253 - Abs)}$

An average value of K_{eq} was calculated, $K_{eq} = 0.87 (\pm 0.08)$.

The pK_a value was calculated using Equation 2.14. In this case, $pK_a = 3.54 (\pm 0.04)$.

2.1.4.3.6 **(*R*)-3,3'-Bis(4-methoxyphenyl)-1,1'-binaphthyl-2,2'-diyl hydrogenphosphate (136).**

UV-Visible spectra of 4-chloro-2,6-dinitrophenol (**134**) (3×10^{-5} M) in DMSO solutions containing (*R*)-3,3'-bis(4-methoxyphenyl)-1,1'-binaphthyl-2,2'-diyl hydrogenphosphate (**136**) and the conjugate base anion (**136'**) were recorded at 25 °C. These are shown in Figure 2.34, with scans 1-8 corresponding to the conditions given in Table 2.18.

Figure 2.34: UV-Visible spectra of 4-chloro-2,6-dinitrophenol (**134**) in DMSO containing phosphoric acid (**136**) and conjugate base anion (**136'**) at 25 °C.

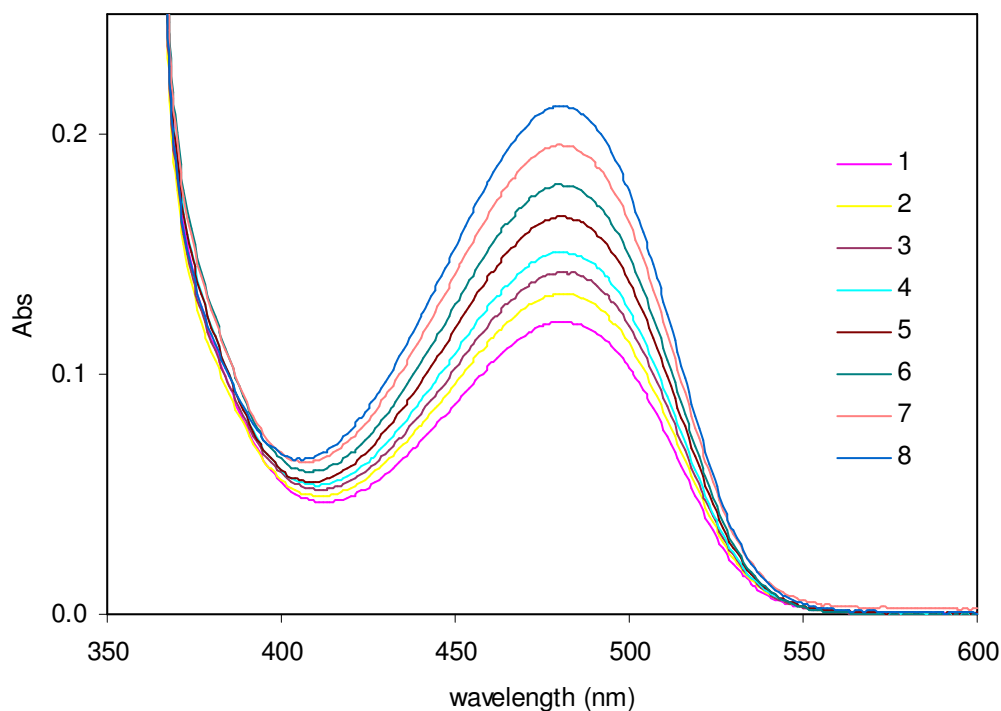


Table 2.18: Absorbance data for 4-chloro-2,6-dinitrophenol^a (134) in DMSO containing phosphoric acid (136) and conjugate base anion^b (136') at 480 nm and 25 °C.

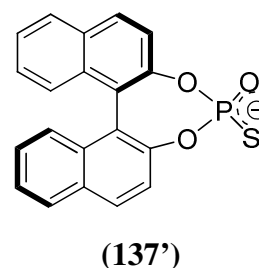
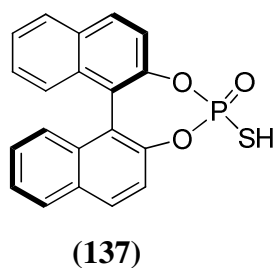
Spectrum number	[Cat ⁻] (M)	[Cat] (M)	Abs	[In ⁻]/[HIn] ^c	K_{eq} ^d
1.	3.50×10^{-3}	6.59×10^{-3}	0.122	0.48	0.91
2.	3.75×10^{-3}	6.34×10^{-3}	0.133	0.56	0.94
3.	4.00×10^{-3}	6.09×10^{-3}	0.142	0.62	0.95
4.	4.50×10^{-3}	5.59×10^{-3}	0.151	0.70	0.86
5.	5.00×10^{-3}	5.09×10^{-3}	0.166	0.83	0.85
6.	5.50×10^{-3}	4.59×10^{-3}	0.179	0.97	0.81
7.	6.00×10^{-3}	4.09×10^{-3}	0.195	1.16	0.79
8.	6.50×10^{-3}	3.59×10^{-3}	0.211	1.40	0.77

(a) The concentration of 4-chloro-2,6-dinitrophenol was 3×10^{-5} M. (b) Catalyst anion was generated by addition of a solution of NaOH in DMSO such that the final concentration of water was < 2%. (c) The ratio of phenolate to phenol was obtained using the relationship $Abs - A_{min} / A_{max} - Abs$.

(d) Calculated as $\frac{[Cat]}{[Cat^-]} \cdot \frac{(Abs - 0.009)}{(0.355 - Abs)}$

An average value of K_{eq} was calculated, $K_{eq} = 0.86 (\pm 0.07)$.

The pK_a value was calculated using Equation 2.14. In this case, $pK_a = 3.49 (\pm 0.03)$.

2.1.4.3.7 (R)-1,1'-Binaphthyl-2,2'-diyl hydrogenthiophosphate (137).

UV-Visible spectra of 4-chloro-2,6-dinitrophenol (**134**) (3×10^{-5} M) in DMSO solutions containing (*R*)-1,1'-binaphthyl-2,2'-diyl hydrogenthiophosphate (**137**) and the conjugate base anion (**137'**) were recorded at 25 °C. These are shown in Figure 2.35, with scans 1-10 corresponding to the conditions given in Table 2.19.

Figure 2.35: UV-Visible spectra of 4-chloro-2,6-dinitrophenol (**134**) in DMSO containing phosphoric acid (**137**) and conjugate base anion (**137'**) at 25 °C.

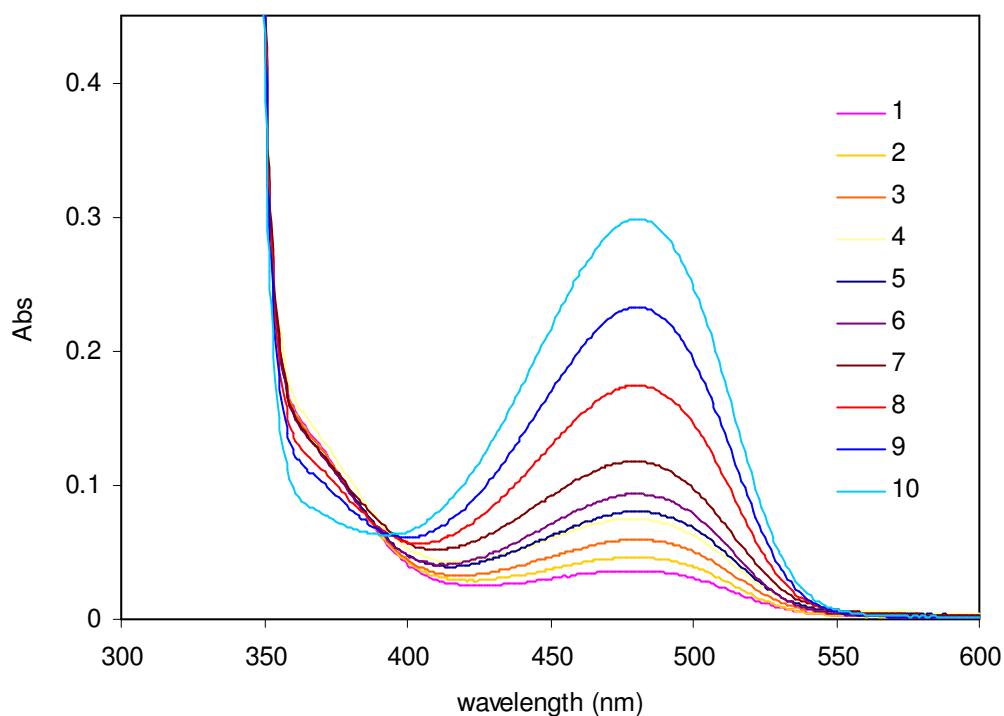


Table 2.19: Absorbance data for 4-chloro-2,6-dinitrophenol^a (134) in DMSO containing phosphoric acid (137) and conjugate base anion^b (137') at 480 nm and 25 °C.

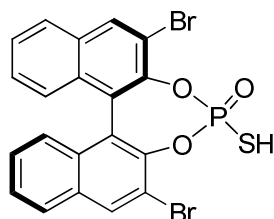
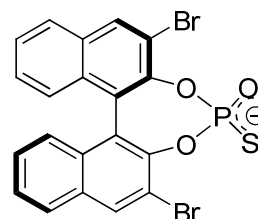
Spectrum number	[Cat ⁻] (M)	[Cat] (M)	Abs	[In ⁻]/[HIn] ^c	K_{eq} ^d
1.	1.50×10^{-3}	8.53×10^{-3}	0.036	0.08	0.48
2.	3.00×10^{-3}	7.03×10^{-3}	0.050	0.13	0.32
3.	4.00×10^{-3}	6.03×10^{-3}	0.060	0.17	0.26
4.	4.50×10^{-3}	5.53×10^{-3}	0.074	0.23	0.28
5.	5.00×10^{-3}	5.03×10^{-3}	0.081	0.26	0.26
6.	5.50×10^{-3}	4.53×10^{-3}	0.094	0.33	0.27
7.	6.00×10^{-3}	4.03×10^{-3}	0.114	0.44	0.29
8.	7.00×10^{-3}	3.03×10^{-3}	0.176	0.93	0.40
9.	7.50×10^{-3}	2.53×10^{-3}	0.234	1.86	0.32
10.	8.00×10^{-3}	2.03×10^{-3}	0.296	4.86	0.30

(a) The concentration of 4-chloro-2,6-dinitrophenol was 3×10^{-5} M. (b) Catalyst anion was generated by addition of a solution of NaOH in DMSO such that the final concentration of water was < 2%. (c) The ratio of phenolate to phenol was obtained using the relationship $Abs - A_{min} / A_{max} - Abs$.

(d) Calculated as $\frac{[Cat^-]}{[Cat]} \cdot \frac{(Abs - 0.009)}{(0.355 - Abs)}$

An average value of K_{eq} was calculated, $K_{eq} = 0.32 (\pm 0.07)$.

The pK_a value was calculated using Equation 2.14. In this case, $pK_a = 3.07 (\pm 0.09)$.

2.1.4.3.8 (R)-3,3'-Dibromo-1,1'-binaphthyl-2,2'-diyl hydrogenthiophosphate (138).**(138)****(138')**

UV-Visible spectra of 2,4-dinitronaphthol (**128**) (3×10^{-5} M) in DMSO solutions containing (R)-3,3'-dibromo-1,1'-binaphthyl-2,2'-diyl hydrogenthiophosphate (**138**) and the conjugate base anion (**138'**) were recorded at 25 °C. These are shown in Figure 2.36, with scans 1-8 corresponding to the conditions given in Table 2.20.

Figure 2.36: UV-Visible spectra of 2,4-dinitronaphthol (**128**) in DMSO containing phosphoric acid (**138**) and conjugate base anion (**138'**) at 25 °C.

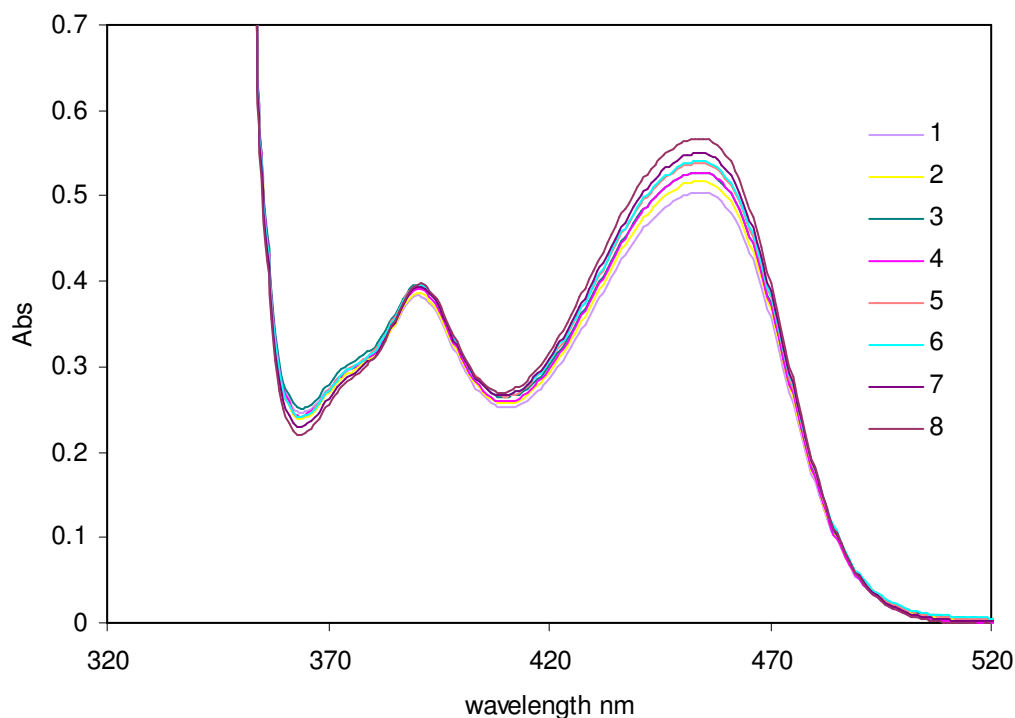


Table 2.20: Absorbance data for 2,4-dinitronaphthol (128) in DMSO containing phosphoric acid (138) and conjugate base anion (138') at 454 nm and 25 °C.

Spectrum number	x^c (M)	$[\text{Cat}^-]$ (M)	$[\text{Cat}]$ (M)	Abs	$[\text{In}^-]/[\text{HIn}]^d$	K_{eq}^e
1.	2.35×10^{-3}	6.85×10^{-3}	3.20×10^{-3}	0.503	2.57	1.20
2.	1.96×10^{-3}	6.96×10^{-3}	3.09×10^{-3}	0.516	2.95	1.31
3.	1.97×10^{-3}	7.22×10^{-3}	2.83×10^{-3}	0.527	3.35	1.31
4.	1.85×10^{-3}	7.35×10^{-3}	2.70×10^{-3}	0.527	3.35	1.23
5.	1.73×10^{-3}	7.48×10^{-3}	2.57×10^{-3}	0.537	3.78	1.30
6.	1.61×10^{-3}	7.61×10^{-3}	2.44×10^{-3}	0.539	3.88	1.24
7.	1.38×10^{-3}	7.88×10^{-3}	2.17×10^{-3}	0.547	4.31	1.19
8.	1.16×10^{-3}	8.16×10^{-3}	1.89×10^{-3}	0.566	5.73	1.33

(a) The final concentration of 2,4-dinitronaphthol was 3×10^{-3} M. (b) Catalyst anion was generated by addition of a solution of NaOH in DMSO such that the final concentration of water was $< 2\%$. (c) The concentration of free H^+ ions at equilibrium, x , was calculated using Equation 2.16 with $K_a = .501 \times 10^{-3}$. The value of K_a was chosen so as to give the smallest variation in the resulting K_{eq} values. (d) The ratio of phenolate to phenol was obtained using the relationship $\text{Abs} - A_{\text{min}} / A_{\text{max}} - \text{Abs}$.

(e) Calculated as $\frac{[\text{Cat}^-]}{[\text{Cat}]} \cdot \frac{(\text{Abs} - 0.159)}{(0.637 - \text{Abs})}$

An average value of K_{eq} was calculated, $K_{\text{eq}} = 1.26 (\pm 0.05)$.

The $\text{p}K_a$ value was calculated using Equation 2.18. In this case, $\text{p}K_a = 2.21 (\pm 0.02)$.

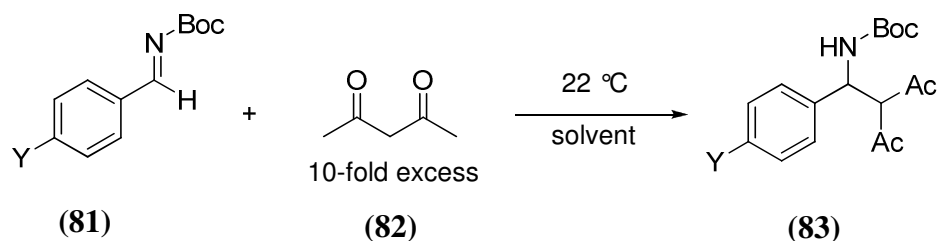
Unfortunately, shortage of material and time constraints dictated that determination of $\text{p}K_a$ values of the remaining catalysts was not possible during these investigations.

2.1.5 Kinetic studies of the Mannich reaction.

2.1.5.1 Uncatalysed Mannich reactions.

An appropriate $k_{\text{cat}}/k_{\text{uncat}}$ ratio is vital for the success of an asymmetric transformation and as such, it can be instructive to examine rates of uncatalysed reactions. To date, there have been no kinetic studies of the uncatalysed reaction of *N*-Boc imines and acetylacetone. Rate constants for the background reaction of a family of imines with an excess of acetylacetone were measured in three solvents using ^1H NMR spectroscopy as part of our investigations of the Mannich reaction.

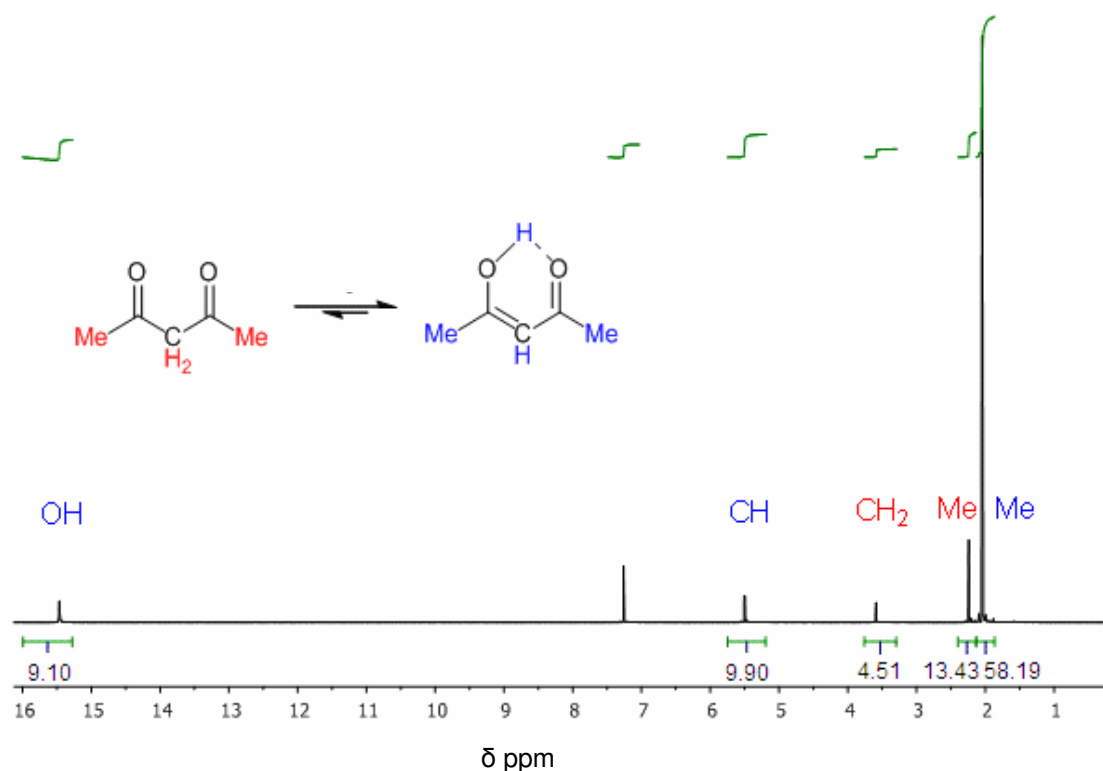
Scheme 2.21: Uncatalysed Mannich reaction.



The reactions were performed under pseudo-first-order conditions with a 10-fold excess of acetylacetone over imine substrate as illustrated in Scheme 2.21. A typical experiment involved a final imine concentration of 5-10 mM, depending on solubility in a given solvent. Reactions were initiated by direct addition of the required amount of imine stock solution to an acetylacetone solution. The reaction was conducted in an NMR tube with spectra recorded at various intervals throughout the time-course. The sample remained in a thermostated water bath in between NMR spectroscopic measurements. Each ^1H NMR spectrum was recorded over a period of 6 minutes (16 transients) with the reaction time t calculated from the time at the midpoint of these analyses.

A typical ^1H NMR spectrum, obtained during the Mannich reaction of a particular imine substrate (**81**) with acetylacetone (**82**) at 22 °C consists of a number of peaks. Acetylacetone and other relatively acidic β -diketones exist in both keto and enol forms in solution. The interconversion is slow on the NMR timescale and thus signals for both species are visible in the ^1H NMR spectrum (Figure 2.37). The enol form has two tautomers, incorporating an intramolecular hydrogen bond. In this case the rate of exchange of the two tautomers is much faster than the NMR time scale and a single set of signals is observed for the enol form.

Figure 2.37: ^1H NMR spectrum of acetylacetone (**82**) (100 mM) in CDCl_3 at 22 °C.



Solvent polarity is also very important in determining the percentage of both tautomeric forms. The enol form is less polar than the keto tautomer because of the intramolecular hydrogen bonding. Thus, an increase in solvent polarity favours the more polar keto form. Table 2.21 summarises the proportion of enol present in each solvent used in this study. The ratio of the two tautomers is calculated by integration of relevant signals in ^1H NMR spectra of acetylacetone (100 mM) recorded at 22 °C.

Table 2.21: Enolisation of acetylacetone (82) in deuterated NMR solvent at 22 °C.

Solvent	Integrated Area ^a		% enol ^b
	Methylene	Vinyl	
Chloroform-d ₁	4.51	9.90	81
Dichloromethane-d ₂	4.60	11.86	84
Acetonitrile-d ₃	7.35	5.92	62

(a) Integrated relative to internal standard (tetramethylsilane) at 0 ppm. (b) Calculated by $A_p^{\text{Enol}}/(A_p^{\text{Enol}} + A_p^{\text{Keto}})$, where $A_p^{\text{Keto}} = A_p^{\text{methylene}}/2$ and $A_p^{\text{Enol}} = A_p^{\text{vinyl}}$.

In ¹H NMR spectra of the reaction mixture the signal due to the imine hydrogen is visible as a singlet at ~9.0 ppm. Over time the area of this signal decays due to the formation of the product (**83**). The signal due to the twelve methyl hydrogens of the internal standard, tetramethylsilane, appears as a singlet at 0 ppm.

The progress of the Mannich reactions for imines (**119**)-(**123**) was determined from the change in the integrated area of the singlet at ~9.0 ppm ($A_s^{9\text{ppm}}$), due to the imine hydrogen over time relative to that of a peak at ~0 ppm due to the twelve non-exchanging methyl hydrogens of the internal standard (A_{std}). The appearance of a broad doublet at ~4 ppm due to the NHCHCH of product as well as changing aromatic protons were also monitored and gave results within experimental error ($\pm 10\%$) of those obtained using the imine hydrogen peak at 9 ppm. The peak due to the imine hydrogen was more conveniently followed as this region of the spectrum has no interfering peaks.

The fraction of substrate remaining $f(s)$, for imines (**119**)-(**123**) is determined from Equation 2.19.

$$f(s) = \frac{(A_s^{9\text{ppm}}/A_{\text{std}})_t}{(A_s^{9\text{ppm}}/A_{\text{std}})_{t=0}} \quad \text{(Equation 2.19)}$$

The observed pseudo-first-order rate constant for Mannich reaction of imines (**119**)-(**123**) was then determined from semi-logarithmic plots of $f(s)$ against time (Equation 2.20). These plots were linear for the half-lives examined with 4 - 12 data points.

$$\ln f(s) = -k_{\text{obs}} t \quad \text{(Equation 2.20)}$$

2.1.5.1.1 The Mannich reaction in acetonitrile at 25 °C.

As part of initial investigations, the Mannich reactions of *N*-Boc imines (**119**)-(**123**) and acetylacetone (**82**) in acetonitrile- d_3 at 25 °C were monitored by 500 MHz ^1H NMR spectroscopy. Semi-logarithmic analysis of the fraction of un-reacted substrate over time by application of Equations 2.19 and 2.20 yielded rate constants for the Mannich reaction. The results of these studies are summarised in Figures 2.38-2.39 and Table 2.22.

Figure 2.38: Semi-logarithmic plot of the fraction of remaining imine hydrogen against time for the Mannich reaction of imines (**120**, \blacktriangle)-(**121**, \blacklozenge) and acetylacetone (**82**) in CD_3CN at 25 °C.

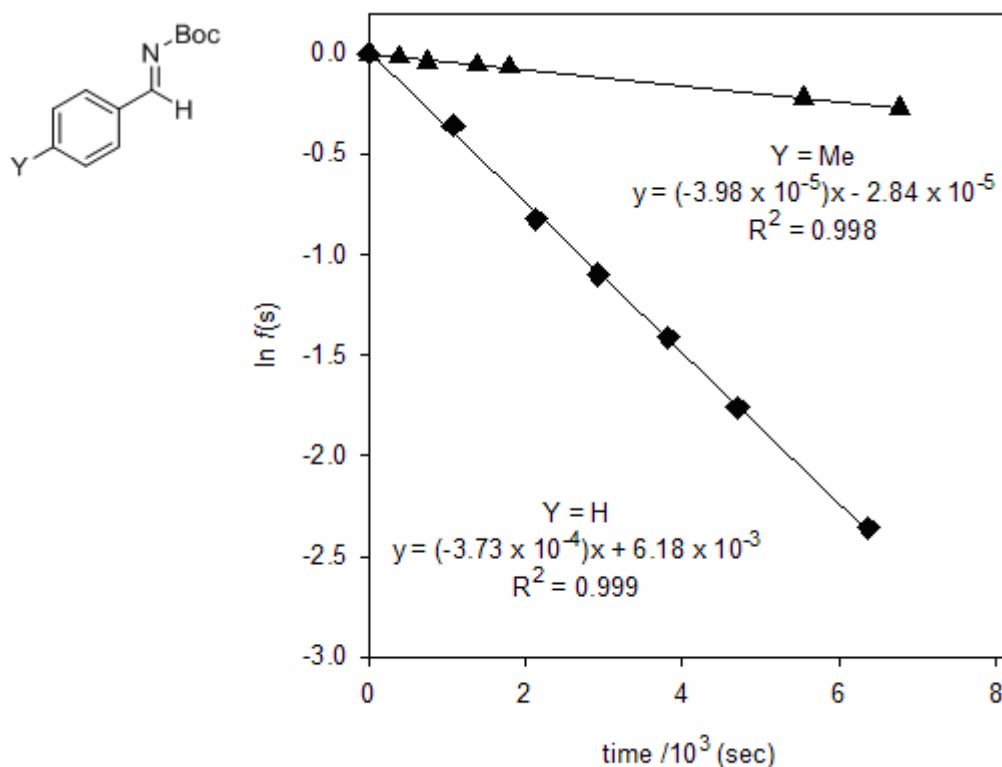


Figure 2.39: Semi-logarithmic plot of the fraction of remaining imine hydrogen against time for the Mannich reaction of imine (122,■)-(123,●) and acetylacetone (82) in CD₃CN at 25 °C.

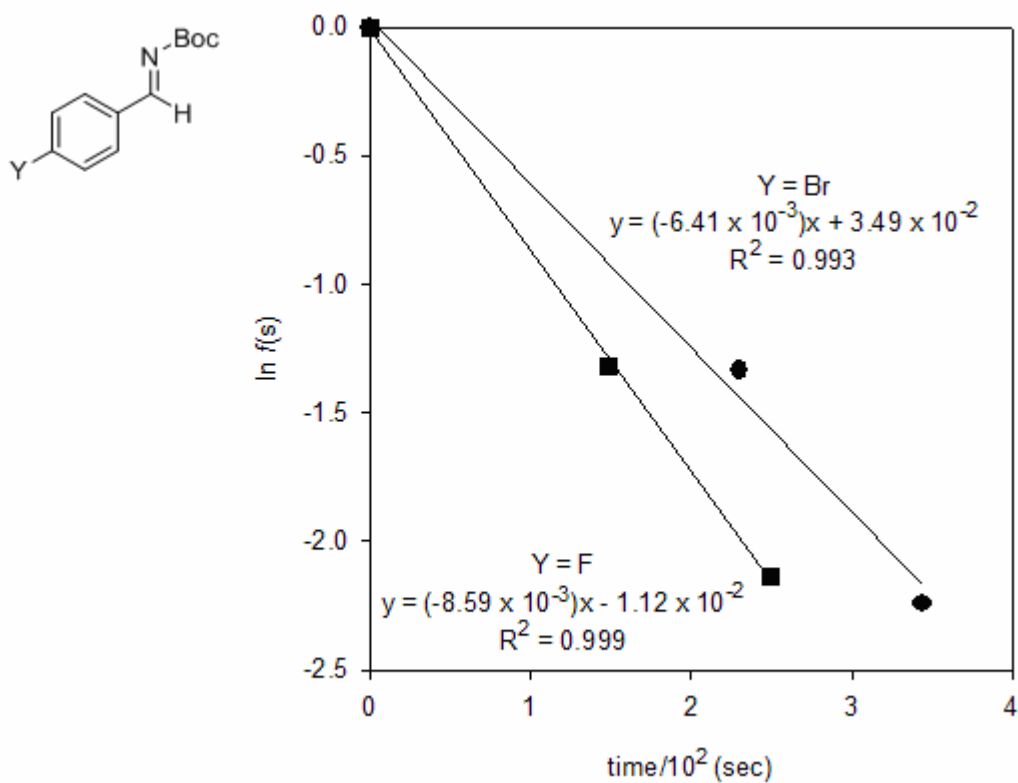


Table 2.22 : First-order rate constants for the uncatalysed Mannich reaction of imines (120)-(123) (10 mM) with acetylacetone (82) (100 mM) at 25 °C in CD₃CN.

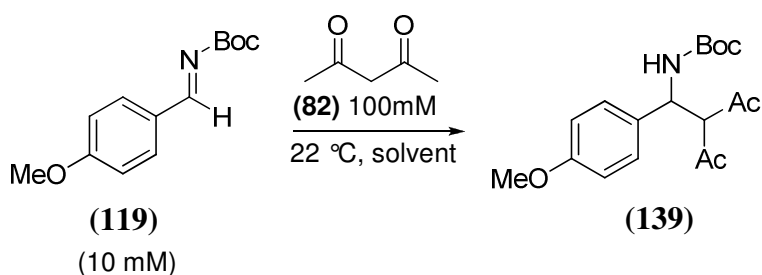
Imine	Time (s)	$f(s)^a$	$\ln f(s)$	k_{obs}^b (s ⁻¹)
Y = Me	0	1.000	0.000	3.98×10^{-5}
	387	0.988	-0.012	
	744	0.961	-0.040	
	1394	0.949	-0.052	
	1800	0.935	-0.067	
	5550	0.802	-0.221	
	6774	0.763	-0.270	
Y = H	0	1.000	0.000	3.73×10^{-4}
	1079	0.700	-0.357	
	2134	0.439	-0.824	
	2931	0.333	-1.099	
	3814	0.244	-1.409	
	4703	0.172	-1.759	
	6369	0.094	-2.360	
Y = F	0	1.000	0.000	6.41×10^{-3}
	230	0.263	-1.334	
	344	0.106	-2.240	
Y = Br	0	1.000	0.000	8.59×10^{-3}
	149	0.267	-1.320	
	249	0.118	-2.135	

(a) The fraction of substrate remaining, $f(s)$ was calculated according to Equation 2.19. (b) The value of the first-order rate constant (k_{obs} , s⁻¹) was obtained as the slope of the plot of $\ln f(s)$ against time in Figure 2.38 and 2.39.

2.1.5.1.2 Investigations of the background Mannich reaction at 22 °C.

After studies in acetonitrile revealed the background Mannich reaction to occur with rates of up to 10^{-3} s^{-1} , further investigations were undertaken in two additional solvents to ascertain the most appropriate for use in kinetic study. A slower background rate would potentially allow for a better $k_{\text{cat}}/k_{\text{uncat}}$ ratio.

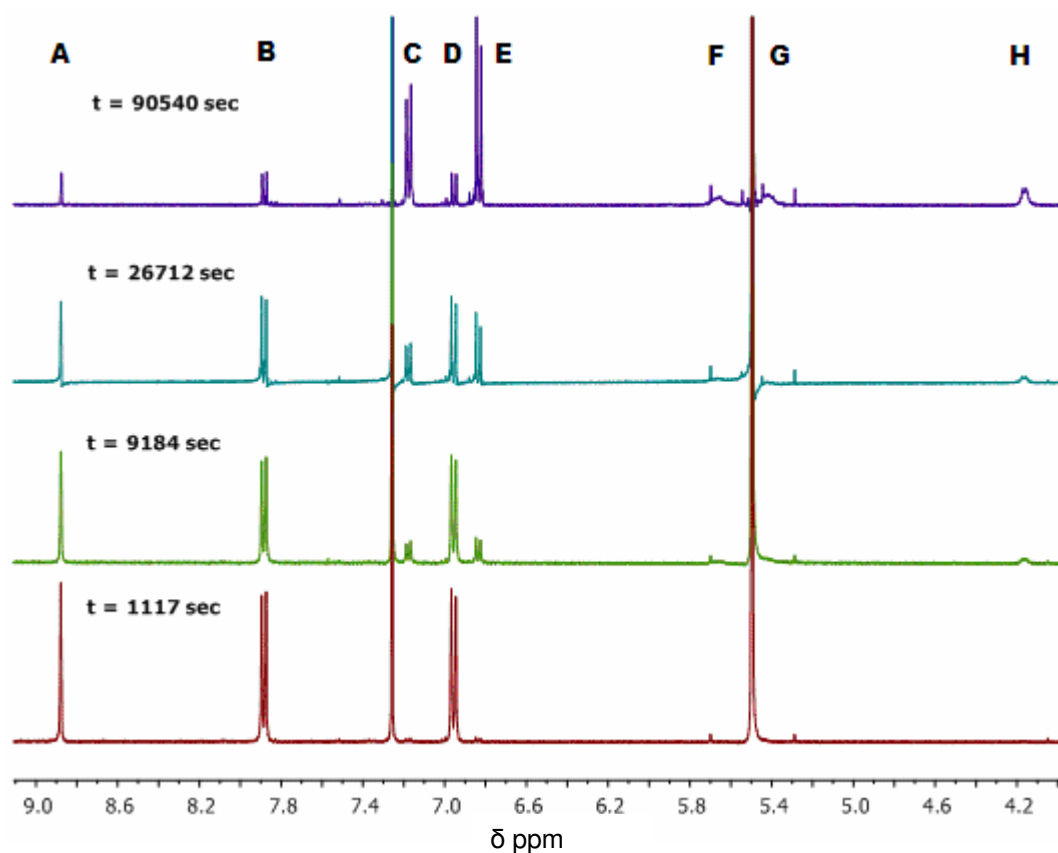
2.1.5.1.2.1 *p*-Methoxybenzaldehyde *N*-(*tert*-butoxycarbonyl)imine (**119**).



Rate constants for the uncatalysed Mannich reaction of *p*-methoxybenzaldehyde *N*-(*tert*-butoxycarbonyl)imine (**119**) and acetylacetone to form β -amino carbonyl compound (**139**) were determined by 400 MHz ^1H NMR spectroscopy. Reactions were conducted in both chloroform- d_1 and dichloromethane- d_2 .

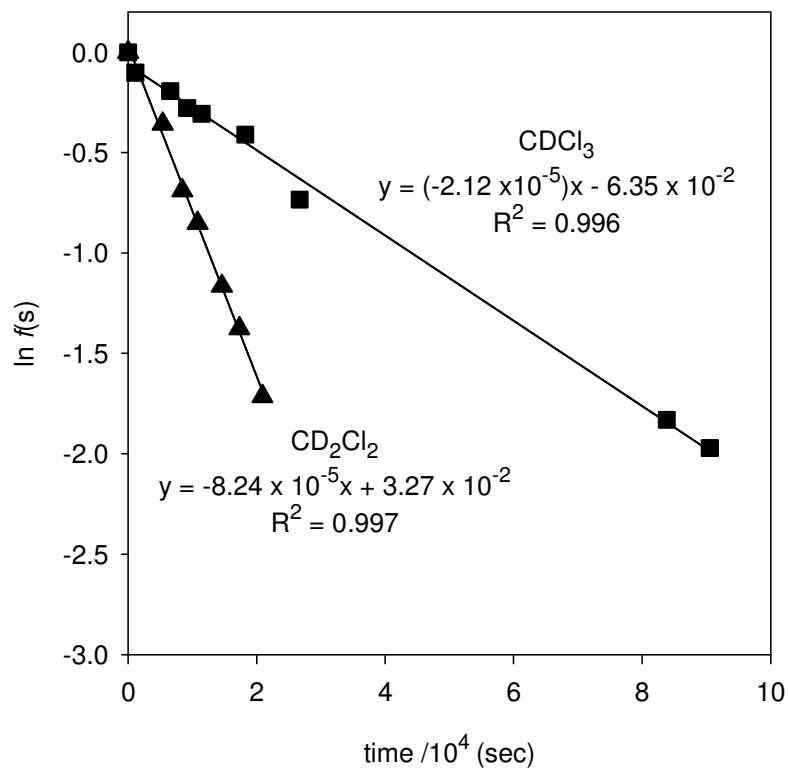
Figure 2.40 shows representative ^1H NMR spectra illustrating the background Mannich reaction of imine (**119**) and acetylacetone (10 mM and 100 mM respectively) at 22 °C in CDCl_3 . As the reaction proceeds, the singlet peak due to the imine hydrogen at 8.88 ppm (A) disappears. The two doublets at 7.90 ppm (B) and 6.97 ppm (D) are due to the imine PhHs. As the reaction proceeds, these signals decrease and two doublets due to the product (**139**) aryl protons appear at 7.18 ppm (C) and 6.85 ppm (E) along with two broad singlets due to the NH and NHCH at 5.67 ppm (F) and 5.42 ppm (G) and a broad doublet increases at 4.17 ppm due to the NHCHCH proton (H). The singlet peaks due to the imine ArOCH_3 and *tert*-butyl protons occur at 3.88 ppm and 1.58 ppm respectively. Over the course of the reaction the corresponding product signals appear at 3.77 ppm and 1.41 ppm. The peaks due to the product COCH_3 protons appear as two singlets at 2.14 and 2.12 ppm. No additional peaks due to other products were identified during the timescale for complete conversion of the imine. The decaying signal due to imine hydrogen was integrated relative to the twelve methyl protons of the internal standard peak at 0 ppm.

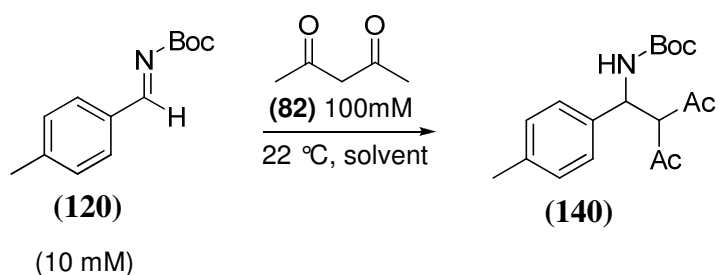
Figure 2.40: Representative ^1H NMR spectra at 400 MHz of the Mannich reaction of imine (119) (10 mM) and acetylacetone (82) (100 mM) in CDCl_3 at 22 °C. The time elapsed is indicated above each spectrum in seconds.



Values for experimental first-order rate constants for the uncatalysed Mannich reaction (k_{obs} , s^{-1}) were obtained as the slopes of semi-logarithmic plots (Figure 2.41) of $f(s)$ against time. Reaction data and first-order rate constants (k_{obs} , s^{-1}) are shown in Appendix C, Table C1.

Figure 2.41: Semi-logarithmic plot of the fraction of remaining imine hydrogen against time for the Mannich reaction of imine (119) with acetylacetone (82) at 22 °C: (■) CDCl_3 ; (▲) CD_2Cl_2 .



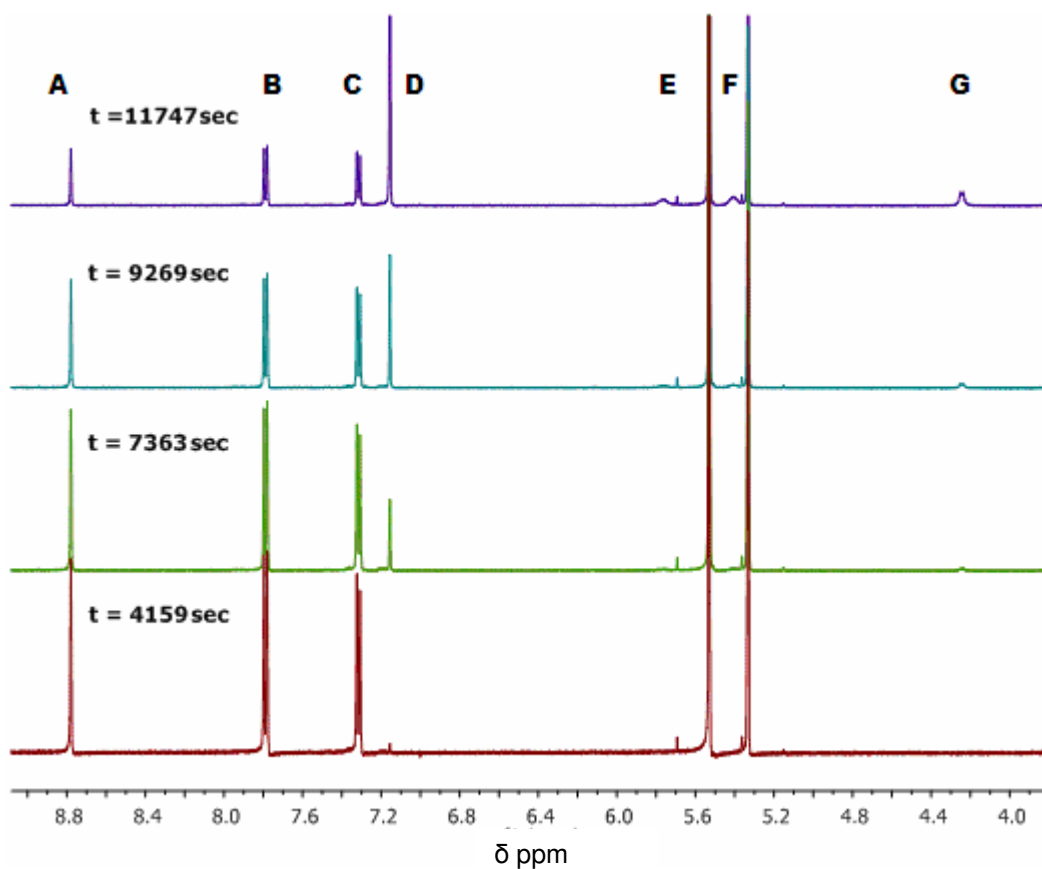
2.1.5.1.2.2 *p*-Methylbenzaldehyde *N*-(*tert*-butoxycarbonyl)imine (**120**).

Rate constants for the uncatalysed Mannich reaction of *p*-methylbenzaldehyde *N*-(*tert*-butoxycarbonyl)imine (**120**) and acetylacetone to form β -amino carbonyl compound (**140**) were determined by 400 MHz ^1H NMR spectroscopy.

Figure 2.42 shows representative ^1H NMR spectra illustrating the background Mannich reaction of imine (**120**) and acetylacetone (**82**) (10 mM and 100 mM respectively) at 22 °C in CD_2Cl_2 . As the reaction proceeds, the singlet peak due to the imine hydrogen at 8.79 ppm (A) disappears. The two doublets at 7.80 ppm (B) and 7.29 ppm (C) are due to the imine PhHs. As the reaction proceeds, these signals decrease and a signal due to the product (**140**) aryl protons appears at 7.11 ppm (D) along with two broad singlets due to the NH and NHCH at 5.72 ppm (E) and 5.41 ppm (F) and a broad doublet increases at 4.19 ppm due to the NHCHCH proton (G). The singlet peaks due to the imine ArCH₃ and *tert*-butyl protons occur at 2.42 ppm and 1.58 ppm respectively. Over the course of the reaction the corresponding product signals appear at 2.31 ppm and 1.35 ppm. The peaks due to the product COCH₃ protons appear as two singlets at 2.18 and 2.12 ppm. No additional peaks due to other products were identified during the timescale for complete conversion of the imine.

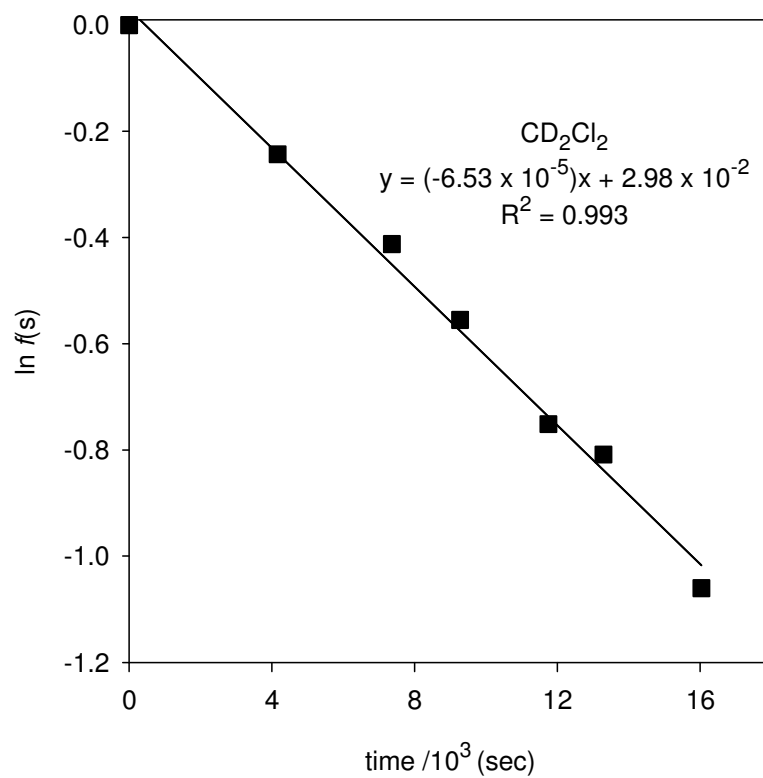
The decaying signal due to imine hydrogen was integrated relative to the twelve methyl protons of the internal standard peak at 0 ppm.

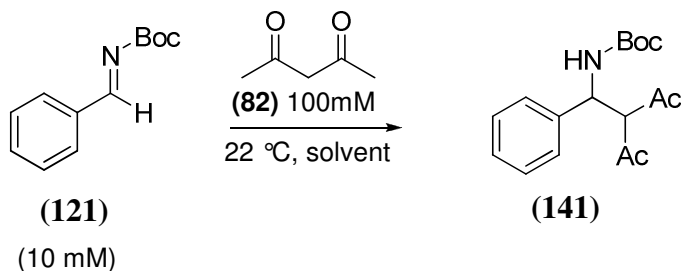
Figure 2.42: Representative ^1H NMR spectra at 400 MHz of the Mannich reaction of imine (120) (10 mM) and acetylacetone (82) (100 mM) in CD_2Cl_2 at 22 °C. The time elapsed is indicated above each spectrum in seconds.



The values for the experimental first-order rate constant for the uncatalysed Mannich reaction (k_{obs} , s^{-1}) was obtained as the slope of a semi-logarithmic plot (Figure 2.43) of $f(s)$ against time. Reaction data and the first-order rate constant (k_{obs} , s^{-1}) are shown in Appendix C, Table C2.

Figure 2.43: Semi-logarithmic plot of the fraction of remaining imine hydrogen against time for the Mannich reaction of imine (120) with acetylacetone (82) at 22 °C in CD₂Cl₂.

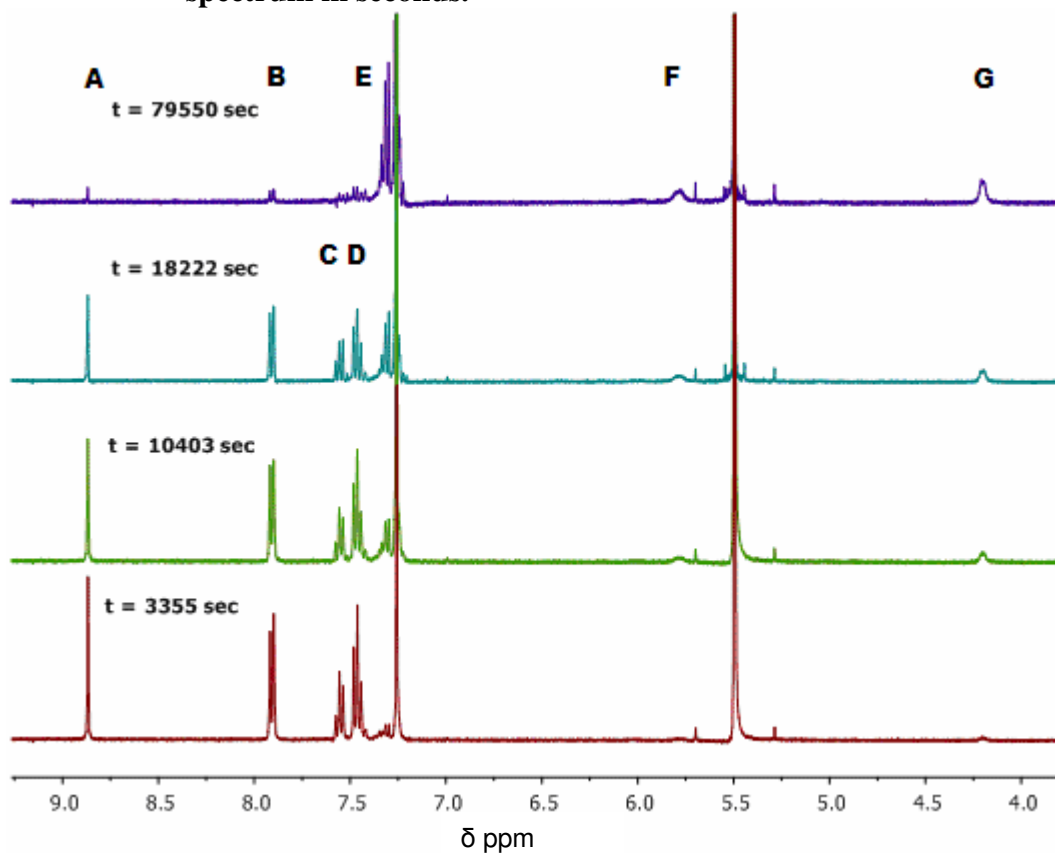


2.1.5.1.2.3 Benzaldehyde *N*-(*tert*-butoxycarbonyl)imine (**121**).

Rate constants for the uncatalysed Mannich reaction of benzaldehyde *N*-(*tert*-butoxycarbonyl)imine (**121**) and acetylacetone to form β -amino carbonyl compound (**141**) were determined by 400 MHz ^1H NMR spectroscopy.

Figure 2.44 shows representative ^1H NMR spectra illustrating the background Mannich reaction of imine (**121**) and acetylacetone (**82**) (10 mM and 100 mM respectively) at 22 °C in CDCl_3 . As the reaction proceeds, the singlet peak due to the imine hydrogen at 8.88 ppm (A) disappears. The multiplets at 7.90-7.93 ppm (B), 7.54-7.57 ppm (C) and 7.43-7.49 ppm (D) are due to the imine PhHs. As the reaction proceeds, these signals decrease and a multiplet due to the product (**141**) aryl protons appears at 7.24-7.34 ppm (E) along with two broad singlets due to the NH and NHCH at 5.82 ppm (F) and 5.45 ppm and a broad doublet increases at 4.20 ppm due to the NHCHCH proton (G). The singlet peak due to the imine *tert*-butyl protons occurs at 1.59 ppm. Over the course of the reaction the corresponding product signal appears at 1.39 ppm. The peaks due to the product COCH_3 protons appear as two singlets at 2.18 and 2.11 ppm. No additional peaks due to other products were identified during the timescale for complete conversion of the imine.

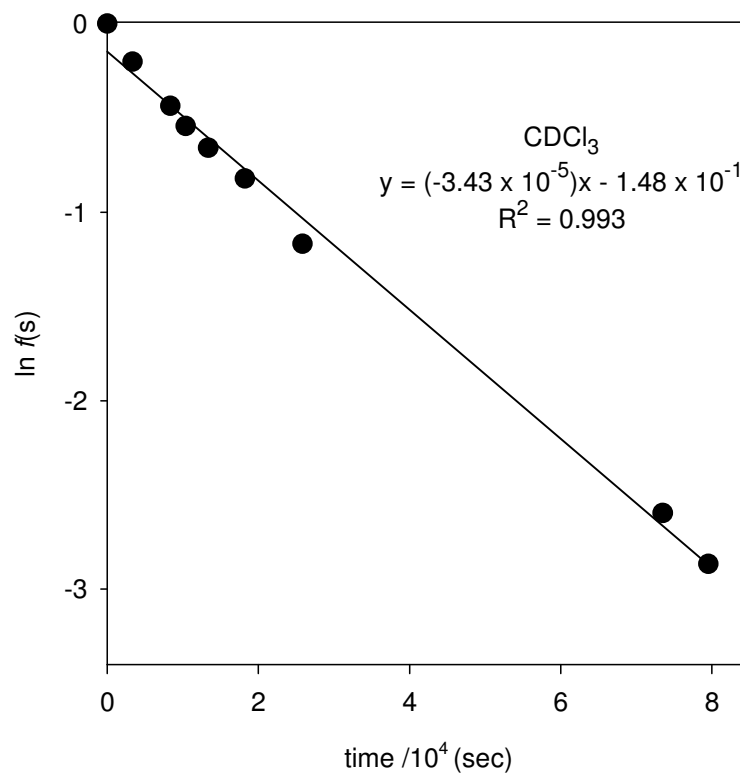
Figure 2.44: Representative ^1H NMR spectra at 400 MHz of the Mannich reaction of imine (121) (10 mM) and acetylacetone (82) (100 mM) in CDCl_3 at 22 °C. The time elapsed is indicated above each spectrum in seconds.

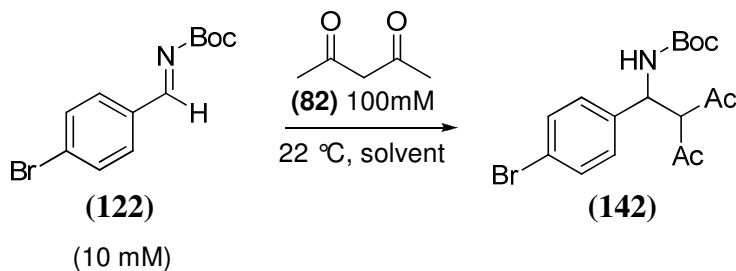


The decaying signal due to imine hydrogen was integrated relative to the twelve methyl protons of the internal standard peak at 0 ppm.

The value for the experimental first-order rate constant for the uncatalysed Mannich reaction (k_{obs} , s^{-1}) was obtained as the slope of a semi-logarithmic plot (Figure 2.45) of $f(s)$ against time. Reaction data and the first-order rate constant (k_{obs} , s^{-1}) are shown in Appendix C, Table C3.

Figure 2.45: Semi-logarithmic plot of the fraction of remaining imine hydrogen against time for the Mannich reaction of imine (121) with acetylacetone (82) at 22 °C in CDCl_3 .



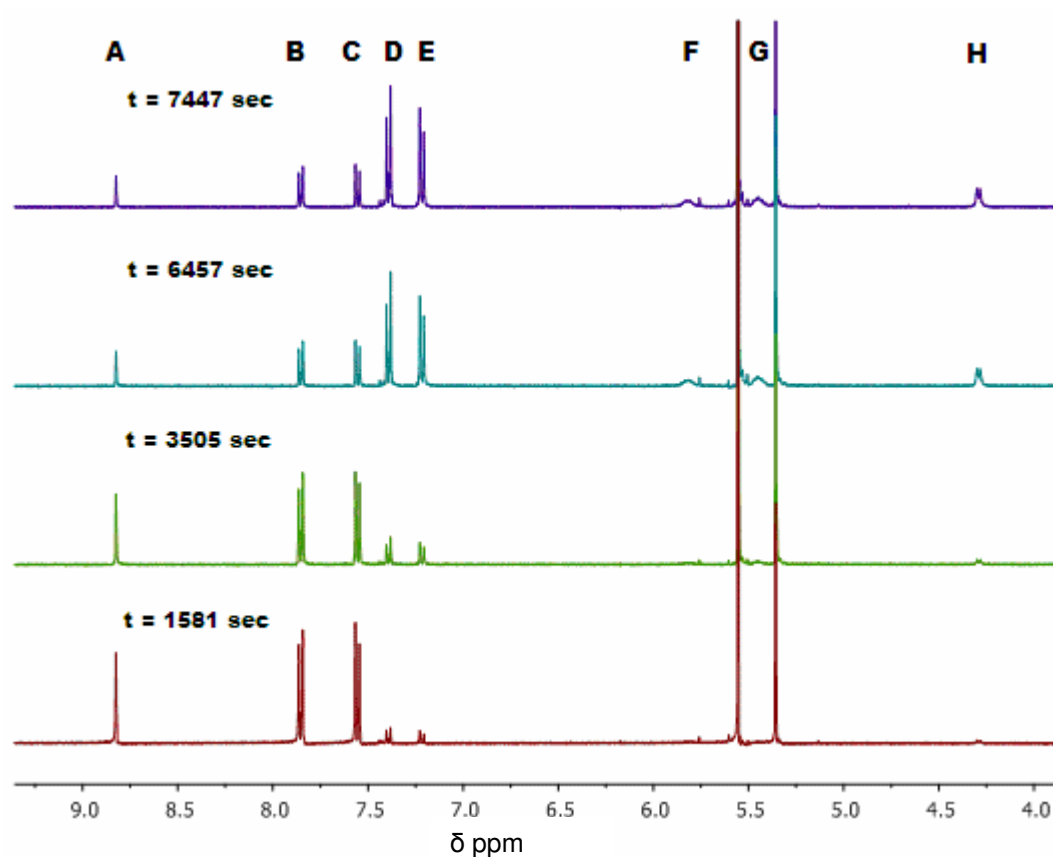
2.1.5.1.2.4 *p*-Bromobenzaldehyde *N*-(*tert*-butoxycarbonyl)imine (**122**).

Rate constants for the uncatalysed Mannich reaction of *p*-bromobenzaldehyde *N*-(*tert*-butoxycarbonyl)imine (**122**) and acetylacetone (**82**) to form β -amino carbonyl compound (**142**) were determined by 400 MHz ^1H NMR spectroscopy.

Figure 2.46 shows representative ^1H NMR spectra illustrating the background Mannich reaction of imine (**122**) and acetylacetone (10 mM and 100 mM respectively) at 22 °C in CD_2Cl_2 . As the reaction proceeds, the singlet peak due to the imine hydrogen at 8.80 ppm (A) disappears. The doublets at 7.78 ppm (B) and 7.54 ppm (C) and are due to the imine PhHs. As the reaction proceeds, these signals decrease and two doublets appear due to the product (**142**) aryl protons at 7.42 (D) and 7.16 ppm (E) along with two broad singlets due to the NH and NHCH at 5.75 ppm (F) and 5.45 ppm (G) and a broad doublet increases at 4.21 ppm due to the NHCHCH proton (H). The singlet peak due the imine *tert*-butyl protons occurs at 1.59 ppm. Over the course of the reaction the corresponding product signal appears at 1.37 ppm. The peaks due to the product COCH_3 protons appear as two singlets at 2.18 and 2.08 ppm. No additional peaks due to other products were identified during the timescale for complete conversion of the imine.

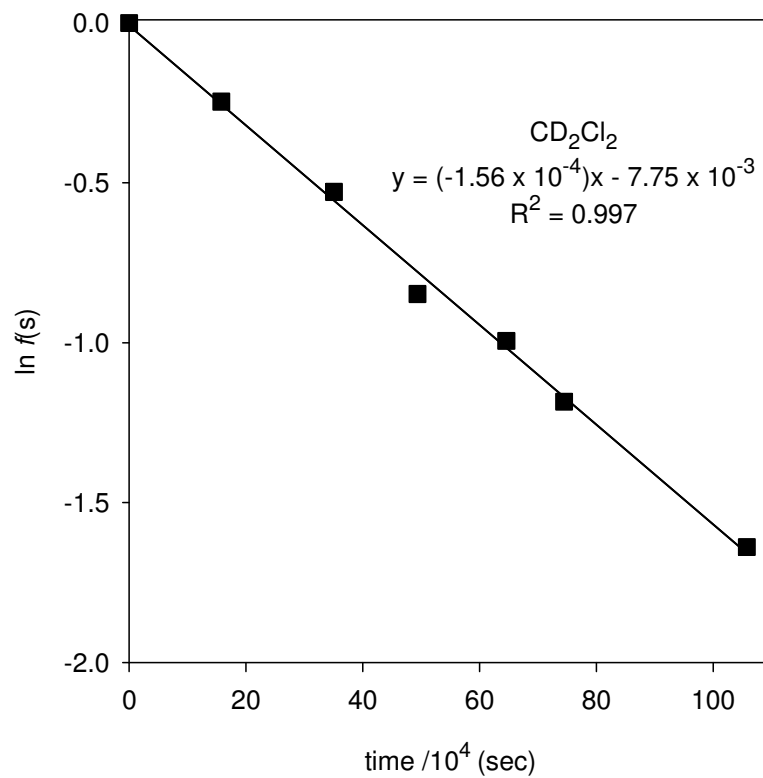
The decaying signal due to imine hydrogen was integrated relative to the twelve methyl protons of the internal standard peak at 0 ppm.

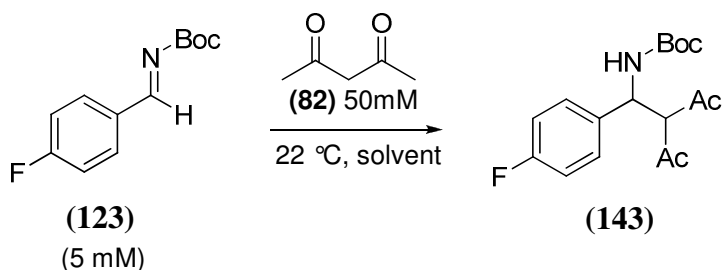
Figure 2.46: Representative ^1H NMR spectra at 400 MHz of the Mannich reaction of imine (122) (10 mM) and acetylacetone (82) (100 mM) in CD_2Cl_2 at 22 °C. The time elapsed is indicated above each spectrum in seconds.



The value for the experimental first-order rate constant for the uncatalysed Mannich reaction (k_{obs} , s^{-1}) was obtained from the slope of a semi-logarithmic plot (Figure 2.47) of $f(s)$ against time. Reaction data and first-order rate constant (k_{obs} , s^{-1}) are shown in Appendix C, Table C4.

Figure 2.47: Semi-logarithmic plot of the fraction of remaining imine hydrogen against time for the Mannich reaction of imine (122) with acetylacetone (82) at 22 °C in CD₂Cl₂.



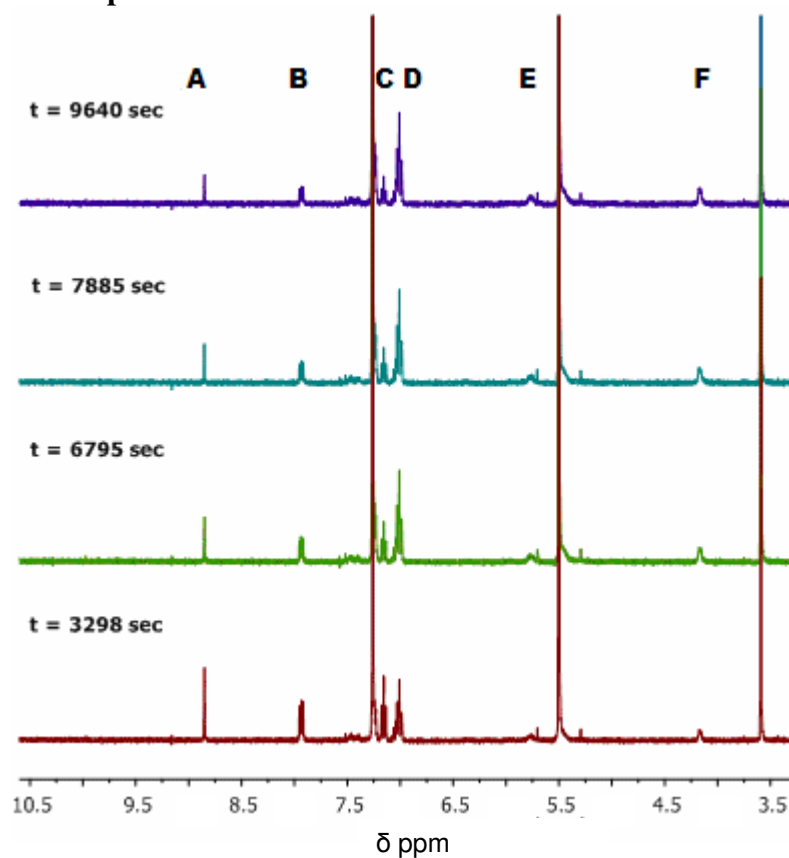
2.1.5.1.2.7 *p*-Fluorobenzaldehyde *N*-(*tert*-butoxycarbonyl)imine (**123**).

Rate constants for the uncatalysed Mannich reaction of *p*-fluorobenzaldehyde *N*-(*tert*-butoxycarbonyl)imine (**123**) and acetylacetone to form β -amino carbonyl compound (**143**) were determined by 400 MHz ¹H NMR spectroscopy.

Figure 2.48 shows representative ¹H NMR spectra illustrating the background Mannich reaction of imine (**123**) and acetylacetone (**82**) (5 mM and 50 mM respectively) at 22 °C in CDCl₃. As the reaction proceeds, the singlet peak due to the imine hydrogen at 8.85 ppm (A) disappears. The multiplets at 7.90-7.96 ppm (B), 7.12-7.18 ppm (C) are due to the imine PhHs. As the reaction proceeds, these signals decrease and two multiplets due to the product (**143**) aryl protons appear at 7.15-7.27 ppm and 6.92-7.02 ppm (D) along with two broad singlets due to the NH and NHCH at 5.67 ppm (E) and 5.35 ppm and a broad doublet increases at 4.09 ppm due to the NHCHCH proton (F). The singlet peak due to the imine *tert*-butyl protons occurs at 1.58 ppm. Over the course of the reaction the corresponding product signal appears at 1.36 ppm. The peaks due to the product COCH₃ protons appear as two singlets at 2.16 and 2.09 ppm. No additional peaks due to other products were identified during the timescale for complete conversion of the imine.

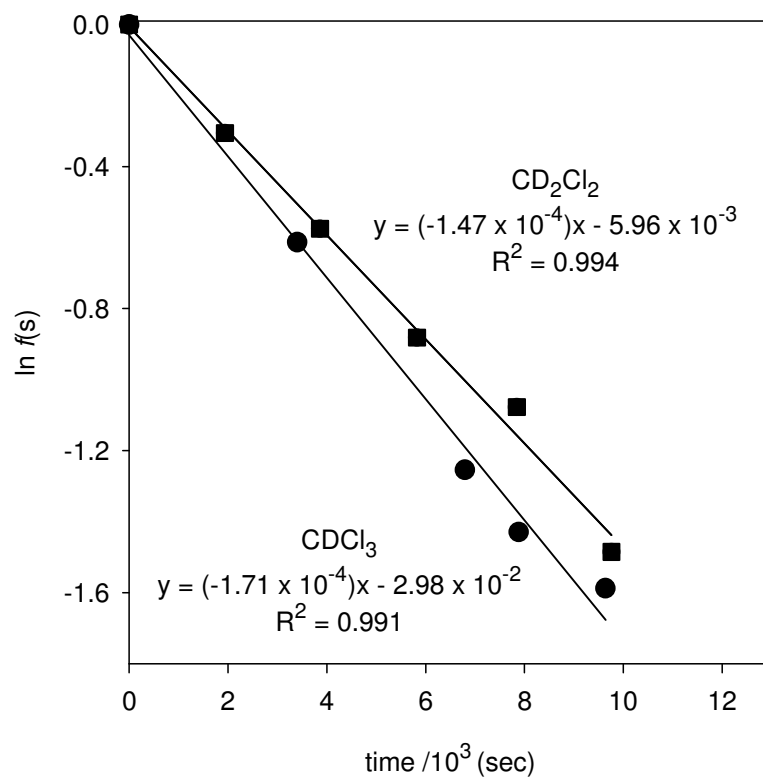
The decaying signal due to imine hydrogen was integrated relative to the twelve methyl protons of the internal standard peak at 0 ppm.

Figure 2.48: Representative ^1H NMR spectra at 400 MHz of the Mannich reaction of imine (123) (5 mM) and acetylacetone (82) (50 mM) in CD_2Cl_2 at 22 °C. The time elapsed is indicated above each spectrum in seconds.



The value for the experimental first-order rate constant for the uncatalysed Mannich reaction (k_{obs} , s^{-1}) were obtained as the slope of a semi-logarithmic plot (Figure 2.49) of $f(s)$ against time. Reaction data and the first-order rate constant (k_{obs} , s^{-1}) are shown in Appendix C, Table C5.

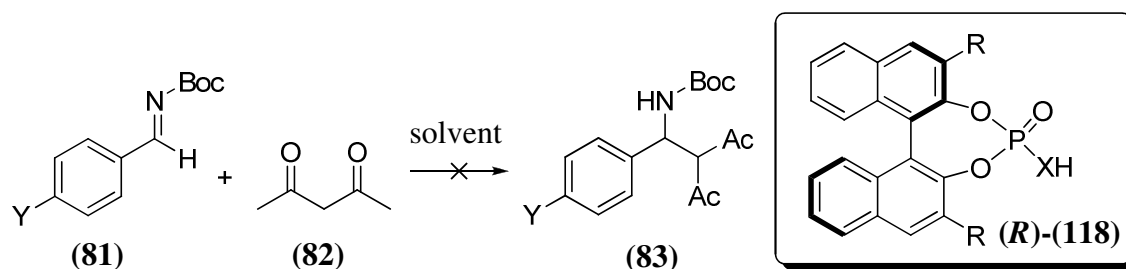
Figure 2.49: Semi-logarithmic plot of the fraction of remaining imine hydrogen against time for the Mannich reaction of imine (123) with acetylacetone (82) at 22 °C: (■), CD₂Cl₂; (●), CDCl₃.



2.1.5.2 Catalysed Mannich reactions.

Measurements of rate constants of phosphoric-acid catalysed Mannich reactions were attempted in chloroform-d₁, dichloromethane-d₂, acetonitrile-d₃ and toluene-d₈. It was found that the background Mannich reactions of *N*-Boc imines with acetylacetone could be performed with no detectable hydrolysis of substrate under the conditions employed. For the catalysed Mannich reaction, however, in all cases complete hydrolysis of imine substrates occurred before the first ¹H NMR spectrum could be recorded (< 6 minutes). Efforts to eliminate sources of adventitious water/acid were made but were ultimately unsuccessful. The conditions used in these attempts are presented in Table 2.23.

Table 2.23: Conditions for the attempted phosphoric acid-catalysed Mannich reaction of *N*-Boc imines and acetylacetone.



Imine ^a (10 mM)	Cat ^b	[Cat] (M)	[acac] ^c (M)	Temp (°C)	Solvent
Y = Me	R = H, X = O	6×10^{-5}	1×10^{-2}	25	CD ₂ Cl ₂
Y = Me	R = H, X = O	1×10^{-5}	1×10^{-2}	25	CD ₂ Cl ₂
Y = H	R = H, X = O	1.5×10^{-5}	1×10^{-2}	25	CD ₂ Cl ₂
Y = H	R = H, X = O	1×10^{-5}	1×10^{-2}	25	CD ₂ Cl ₂
Y = MeO	R = H, X = O	6×10^{-5}	1×10^{-2}	25	CD ₂ Cl ₂
Y = MeO	R = H, X = O	1×10^{-5}	1×10^{-2}	25	CD ₂ Cl ₂
Y = F ^d	R = H, X = O	2×10^{-5}	5×10^{-3}	25	CD ₂ Cl ₂ ^e
Y = F ^d	R = H, X = O	5×10^{-6}	5×10^{-3}	25	CD ₂ Cl ₂ ^e
Y = F ^d	R = H, X = O	2.5×10^{-6}	5×10^{-3}	25	CD ₂ Cl ₂ ^e
Y = Me	R = H, X = O	6×10^{-5}	1×10^{-2}	25	CD ₃ CN
Y = Me	R = H, X = O	4×10^{-5}	1×10^{-2}	25	CD ₃ CN
Y = Me	R = H, X = O	2×10^{-5}	1×10^{-2}	25	CD ₃ CN
Y = MeO	R = H, X = O	1×10^{-5}	1×10^{-2}	25	CD ₃ CN
Y = H	R = H, X = O	3×10^{-5}	1×10^{-2}	25	CD ₃ CN
Y = H	R = H, X = O	1×10^{-5}	1×10^{-2}	25	CD ₃ CN
Y = H	R = H, X = O	5×10^{-6}	1×10^{-2}	25	CD ₃ CN
Y = F ^d	R = H, X = O	2×10^{-5}	5×10^{-3}	25	CD ₃ CN
Y = F ^d	R = H, X = O	1×10^{-5}	5×10^{-3}	25	CD ₃ CN

Y = MeO	R = H, X = O	6×10^{-5}	1×10^{-2}	22	CDCl ₃
Y = MeO	R = H, X = O	4×10^{-5}	1×10^{-2}	22	CDCl ₃
Y = MeO	R = H, X = O	2×10^{-5}	1×10^{-2}	22	CDCl ₃
Y = Me	R = H, X = O	2×10^{-5}	1×10^{-2}	22	CDCl ₃
Y = F ^d	R = H, X = O	1×10^{-5}	5×10^{-3}	22	CDCl ₃
Y = Br	R = H, X = O	6×10^{-5}	1×10^{-2}	22	CDCl ₃
Y = Br	R = H, X = O	2×10^{-5}	1×10^{-2}	22	CDCl ₃
Y = MeO	R = H, X = O	6×10^{-5}	1×10^{-2}	22	CDCl ₃ ^e
Y = MeO	R = H, X = O	4×10^{-5}	1×10^{-2}	22	CDCl ₃ ^e
Y = MeO	R = H, X = O	2×10^{-5}	1×10^{-2}	22	CDCl ₃ ^e
Y = MeO	R = H, X = O	6×10^{-5}	1×10^{-2}	22	CDCl ₃ ^f
Y = MeO	R = H, X = O	4×10^{-5}	1×10^{-2}	22	CDCl ₃ ^f
Y = MeO	R = H, X = O	2×10^{-5}	1×10^{-2}	22	CDCl ₃ ^f
Y = Me	R = H, X = O	2×10^{-5}	1×10^{-2}	22	CDCl ₃ ^e
Y = Me	R = H, X = O	2×10^{-5}	1×10^{-2}	22	CDCl ₃ ^g
Y = MeO	R = H, X = S	2×10^{-5}	1×10^{-2}	22	CDCl ₃
Y = MeO	R = Ph, X = O	2×10^{-5}	1×10^{-2}	22	CDCl ₃
Y = MeO	R = Naphth, X = O	2×10^{-5}	1×10^{-2}	22	CDCl ₃
Y = MeO	R = H, X = O	2×10^{-5}	1×10^{-2}	22	C ₇ D ₈
Y = MeO	R = H, X = O	6×10^{-5}	-	22	C ₇ D ₈
Y = MeO	R = H, X = O	4×10^{-5}	-	22	C ₇ D ₈
Y = MeO	R = H, X = O	2×10^{-5}	-	22	C ₇ D ₈

(a) The imines were dried under high vacuum overnight and then placed in a vacuum dessicator in the presence of phosphorus pentoxide for several hours. The imines were stored in dry bags in the freezer when not in use. (b) The catalyst was dried under high vacuum overnight and placed in a vacuum dessicator in the presence of phosphorus pentoxide for several hours. (c) The acetylacetone was > 99.9% pure and was dried under high vacuum for several hours before use. (d) The concentration of fluoro-substituted imine used was 5 mM due to the limited solubility of this compound in the solvents used in this study. (e) The solvent was dried over molecular sieves (4 Å) before use. (f) The solvent was dried over Na₂SO₄ before use (g) Acetylacetone was stored over molecular sieves (4 Å) before use.

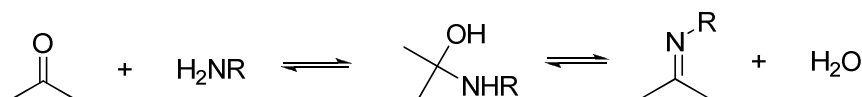
2.2 Discussion.

2.2.1 Synthesis.

2.2.1.1 Preparation of *N*-Boc imines.

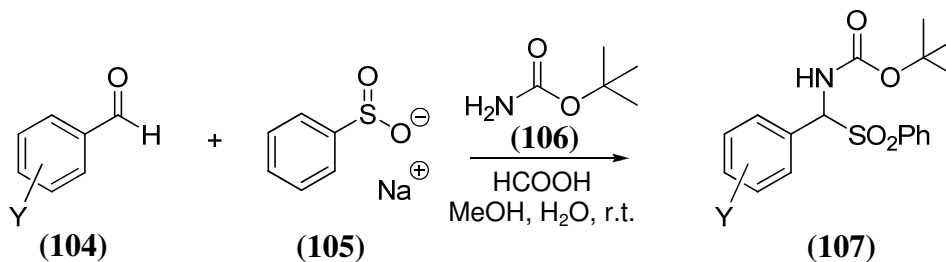
Imines may be formed by the reaction of carbonyl compounds with primary amines (RNH_2). Addition of amines to carbonyls involves two steps, the first of which is the nucleophilic attack of the amine to form a carbinolamine intermediate. Dehydration via the iminium ion leads to the imine (Scheme 2.22).

Scheme 2.22:



Alkyl imines are not very stable with the equilibrium shown in Scheme 2.22 lying significantly to the left. Imines with one or more aryl substituents on the carbon or nitrogen are more stable and are termed Schiff bases. Since imines are not always readily isolable, alternative syntheses have been developed. The method mostly commonly adopted for the preparation of *N*-Boc imines involves a two-step protocol. Firstly, a sulfone is prepared from a substituted benzaldehyde, *tert*-butylcarbamate and benzenesulfinic acid sodium salt in aqueous methanol with formic acid (Scheme 2.23). After stirring at room temperature for between 1-3 days, crude product could be isolated by filtration. Purification was achieved by trituration with ice-cold water followed by diethyl ether, providing sulfones in moderate yields. The trituration process had to be repeated several times in order to obtain pure product in the case of the bromo-substituted sulfone, resulting in a lower yield (53%). Cyano- and nitro-substituted sulfones were not successfully purified by trituration and recrystallisation was employed.

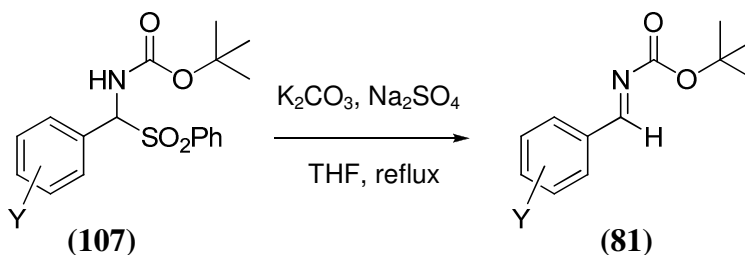
Scheme 2.23:



Y =	<i>p</i> MeO	Yield =	68%	Y =	<i>p</i> Cl	Yield =	68%
	<i>m</i> MeO		64%		<i>p</i> Br		53%
	<i>p</i> ^t Bu		69%		<i>p</i> NO ₂		60%
	<i>p</i> Me		64%		<i>p</i> F		64%
	H		68%		<i>p</i> MeS		61%

The pure sulfone **(107)** was further reacted with potassium carbonate in the presence of sodium sulfate to provide the imine in high yield and purity following filtration of the reaction mixture and concentration of the filtrate (Scheme 2.24). It was found that reflux of the reaction mixture for more than 15 hours resulted in a lower yield.

Scheme 2.24:



Y =	<i>p</i> MeO	Yield =	94%	Y =	H	Yield =	95%
	<i>m</i> MeO		95%		= <i>p</i> Br		91%
	<i>p</i> Me		96%		= <i>p</i> NO ₂		75%
	<i>p</i> ^t Bu		87%				

The hydrolytic lability of these compounds was particularly problematic. Slow filtration of the final imine reaction mixture or use of the rotary evaporator for concentration resulted in hydrolysis of the imine. It was found that if hydrolysis did occur to some extent, the aldehyde contamination could be effectively removed by percolation of the product solution through a bed of Celite. However, this approach was not adopted as it was anticipated that the use of slightly acidic Celite could cause formation of the iminium ion to some extent and interfere with measurements. Attempts at purification by preparative scale TLC or flash column chromatography resulted in decomposition of the imine.

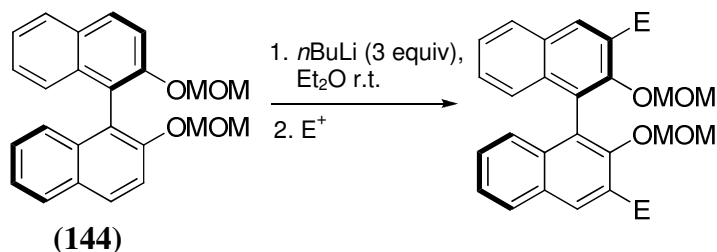
Certain precautions were required for the general handling of imines in order to prevent hydrolysis. When not in use, the imines were stored under argon in dry bags containing calcium chloride in the freezer. When required, the bags were removed from the freezer and warmed to room temperature before removing the flask. It was found that some sources of CDCl_3 would rapidly hydrolyse the imine sample before an NMR spectrum could be obtained. It was therefore necessary to store deuterated solvent used to analyse the imines over potassium carbonate to remove any traces of acid or water.

A range of imines with electron-donating and withdrawing substituents were successfully prepared. While sulfones derived from chlorobenzaldehyde and 4-(methylthio)benzaldehyde were synthesised, further reaction to form the corresponding imines was not undertaken due to time constraints. Attempts were made at preparation of nitro- and cyano-substituted imines. The nitro-substituted imine was successfully formed following reaction of the corresponding sulfone as indicated by a ^1H NMR spectrum of the reaction product. Unfortunately the imine rapidly hydrolysed before further characterisation data could be obtained. Only hydrolysis product was isolated from the reaction of the cyano-substituted sulfone. It appears that electron-withdrawing substituents on the imine increases susceptibility to hydrolysis.

2.2.1.2 Synthesis of (thio)phosphoric acid catalysts

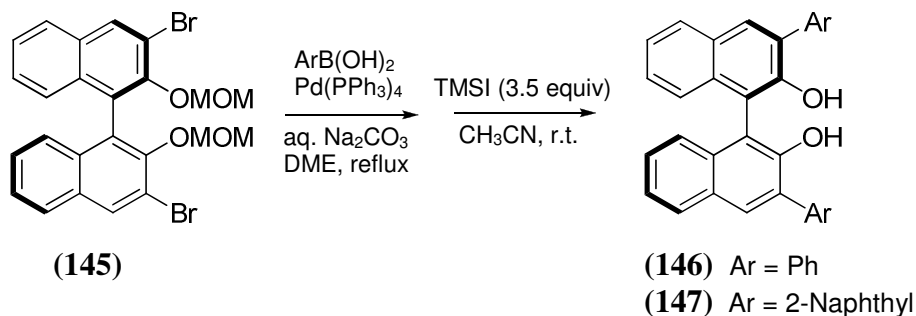
BINOL (**108**) and its derivatives are some of the mostly widely used classes of ligands in asymmetric synthesis, and are utilised in a broad array of transformations. As such, expedient and efficient routes to substituted BINOL compounds have been developed. Substituents at the 3,3'-positions of BINOL are normally introduced via a protocol that involves treatment of a suitably protected BINOL with an organolithium reagent followed by reaction with an electrophile. Snieckus and co-workers prepared a series of 3,3'-substituted 1,1-bi-2-naphthols by directed *ortho*-metalation and Suzuki cross-coupling methods (Scheme 2.25-2.26).⁸³ 3-Substituted or 3,3'-disubstituted products can be obtained by controlling the amount of the organolithium reagent (BuLi). The generation of the dianion of methoxymethyl (MOM)-BINOL was optimally achieved using 3 equivalents of ⁿBuLi in Et₂O at room temperature. The dianion can be further treated with diverse electrophiles *in situ* to form the desired 3,3'-disubstituted BINOL derivatives in good to excellent yields with no loss of enantiomeric purity.

Scheme 2.25:



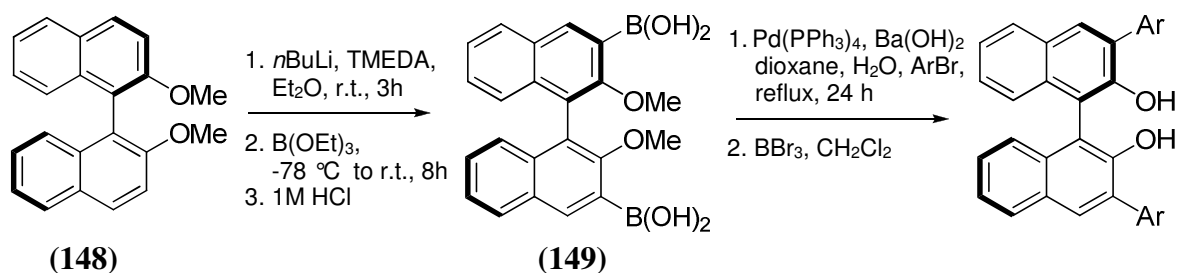
Treatment of (**145**) with phenyl- or 2-naphthylboronic acid under Suzuki conditions followed by deprotection gave (**146**) and (**147**) in high yield (85-87%) (Scheme 2.26).

Scheme 2.26:



Jørgensen *et al.* reported another synthetic route to toward 3,3'-diaryl-BINOLs by the reaction of the 3,3'-boronic acid of *bis*(methoxy)-BINOL (**148**) with commercially available aromatic bromides by a Suzuki cross-coupling reaction (Scheme 2.27) with good overall yields (65-73%).⁸⁴

Scheme 2.27:



The synthetic routes developed by Snieckus and Jørgensen are both facile approaches to the preparation of 3,3'-substituted BINOLs. The method of Snieckus and co-workers achieved higher yields and utilised mild reaction conditions and so was adopted during these investigations with slight modifications. The protection of BINOL was achieved using methoxyethyl groups, rather than methoxy methyl groups with no detrimental effect on yield or complications with deprotection. Column chromatography was required to separate the desired product from a small amount of mono-protected (*R*)-BINOL. A suitable precursor for Suzuki cross-coupling was generated by bromination at the 3,3'-positions of the binaphthyl backbone. Column chromatography and recrystallisation were required to isolate pure product. Suzuki coupling proceeded in good yields (85-95%) for reactions with various substituted boronic acids. It was found that small amounts of mono-coupled derivatives were formed in each case and column chromatography was therefore required to isolate pure product. Removal of the protecting groups was achieved in high yield (85-96%) by reacting with Amberlyst 15 resin in methanol:THF at reflux. The brominated BINOL derivative was also deprotected in order to access a catalyst with an electron-withdrawing substituent in the 3,3'-position.

The phosphorylation of substituted BINOLs is generally achieved using phosphorus oxychloride and pyridine. Literature procedures suggest reaction times of 2-6 hours before the addition of water.^{11,85,86} However, in this work a significant amount of

starting material was observed after 6 hours by TLC analysis of the reaction mixtures and as such, the reactions were run overnight before the addition of water. Despite the extension of the reaction times, a small amount of starting material usually remained and had to be separated using column chromatography. The phosphoric acids are polar compounds and stick to the baseline during column chromatography on silica. As such, the columns were performed on a small scale, using the minimum amount of silica and required ~ 10% alcohol in the mobile phase in order to elute the product.

Thiophosphoryl analogues were synthesised using thiophosphoryl chloride instead of phosphorus oxychloride in the final step. Again, longer reaction times were required in order to obtain high yields.

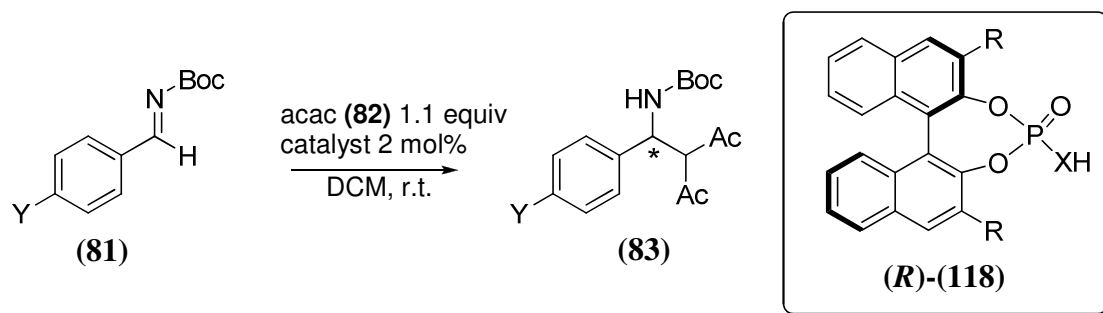
A commercially available BINOL derivative with ester groups at the 3,3'-positions (**116**) was also (thio)phosphorylated successfully. Care had to be taken not to hydrolyse the ester groups and a lower concentration of acid (0.1 M HCl) was used in the work-up.

2.2.2 Enantioselectivity of the Mannich reaction.

Products of Mannich reactions catalysed by the (thio)phosphoric acids synthesised in this work were analysed by chiral HPLC in order to evaluate the degree of enantioselection. The catalysed Mannich reactions were performed using imine (0.1 mmol), acetylacetone (1.1 equiv.) and (thio)phosphoric acid catalysts (2 mol%). The reaction mixture was stirred at room temperature before the product was isolated by column chromatography. It was found that 100% conversion of the imine was achieved in all cases, with isolated yields of 63-71%. The remaining material was identified as imine hydrolysis product. Efforts were made to minimise the competing hydrolysis reaction. All glassware was oven-dried before use and the reactions were performed under argon. The solvent used was obtained from an Innovative Technology Inc. solvent purification system with typical residual H₂O levels of 16.1 ppm for dichloromethane as shown by Karl Fischer titration. The unsubstituted *N*-Boc imine which is an oil, was used as a representative substrate for the catalysed Mannich in Terada's study. In our investigations we focused on the methyl and methoxy-substituted imines which were solids and therefore easier to dry and also weigh out quickly.

The catalysts and imines were dried under high vacuum overnight and placed in a vacuum desiccator in the presence of phosphorus pentoxide for several hours before use. Attempts were made with additives such as molecular sieves or sodium sulfate included in the reaction mixture as well as utilising solvents and acetylacetone which had been stored over molecular sieves. Hydrolysis of the imine was observed to a certain extent despite these measures, however good yields of Mannich product were also obtained. The product was isolated in each case after a reaction time of one hour by flash column chromatography through a short path of silica. The results obtained were presented in Table 2.1 which is repeated below for clarity.

Table 2.1:



Entry	Imine ^a	Catalyst	Additive ^b	Yield ^c (%)	ee ^d (%)
1.	Y = Me	R = H, X = O	-	71	0.5
2.	Y = F	R = H, X = O	-	68	19
3.	Y = Me	R = H, X = S	-	67	10
4.	Y = MeO	R = H, X = S	-	65	12
5.	Y = F	R = H, X = S	-	68	2
6.	Y = MeO	R = Ph, X = O	4Å MS	67	75
7.	Y = MeO	R = Ph, X = O	Na ₂ SO ₄	68	75
8.	Y = MeO	R = Ph, X = S	-	68	3
9.	Y = MeO	R = Naphth, X = O	-	64	74
10.	Y = F	R = Naphth, X = S	-	65	3
11.	Y = MeO	R = Naphth, X = S	-	63	2
12.	Y = MeO	R = Biph, X = O	-	64	72
13.	Y = MeO	R = Biph, X = S	-	65	51
14.	Y = MeO	R = ester, X = O	4Å MS	68	63
15.	Y = MeO	R = Br, X = O	-	65	33
16.	Y = MeO	R = <i>p</i> MeOPh, X = O	4Å MS	65	47

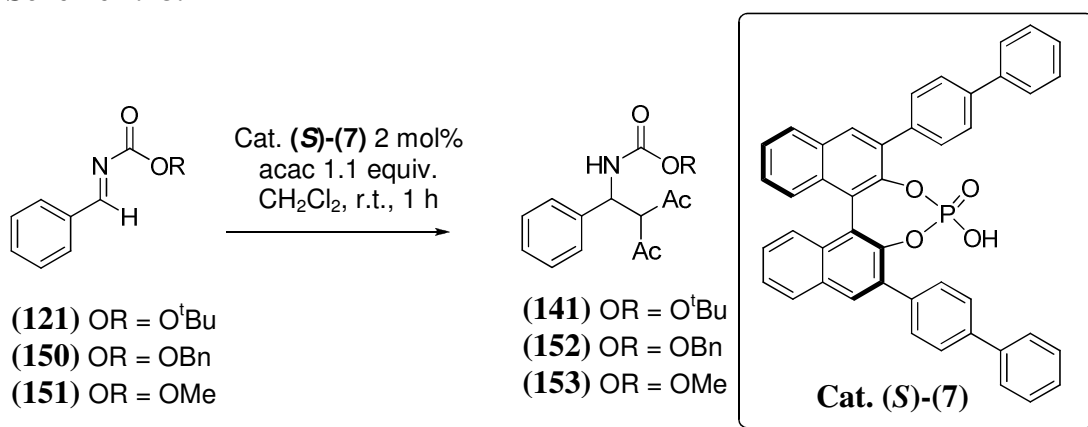
(a) The concentration of imine used was 0.1 mmol. (b) Drying agent added to attempt to reduce hydrolysis of imine substrate. (c) Isolated yield after column chromatography. (d) Separated on a Chiralpak IA column at 10 °C using 90:10, hexane:ethanol as the mobile phase. Absorbance was monitored at 254 nm. Each *ee* value is the average of two runs.

From these results it is clear that 3,3'-substitution of the BINOL framework with aromatic moieties has a beneficial effect on the enantiomeric excess of the Mannich product. The highest *ees* were obtained using phenyl, naphthyl and biphenyl substituents on the phosphoric acid. Lower levels of enantioselection were observed for ester- and bromo-substituted catalysts, with unsubstituted catalysts giving the lowest *ees*. All (thio)phosphoric acids investigated in this study proved to be effective catalysts of the Mannich reaction and good yields of 63-71% were obtained after a

reaction time of one hour. However significant decreases in *ees* were observed when thiophosphoric acids were employed. For the phenyl-substituted phosphoric acid an *ee* of 74% was obtained with the methoxy-substituted imine (**119**), however, use of the same imine with the sulfur analogue resulted in an *ee* of 3%.

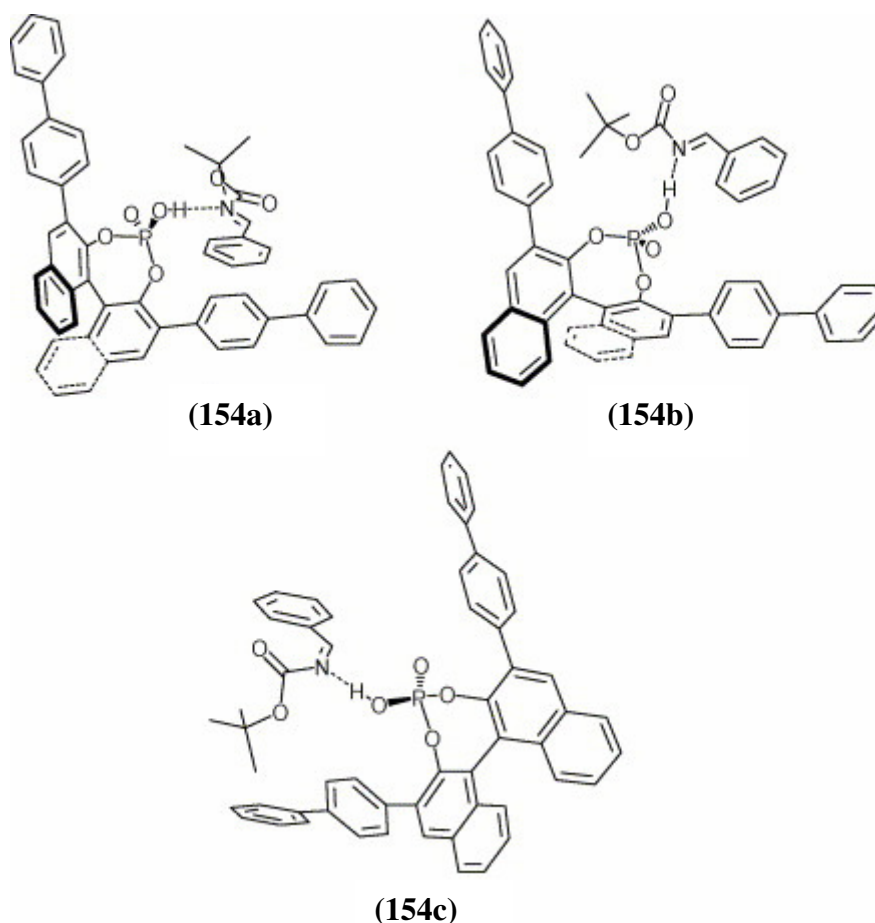
Terada also observed that increased *ee* values were obtained using phosphoric acids with aromatic groups in the 3,3'-positions¹¹ and subsequently used computational methods to probe which conformations of catalyst and *N*-Boc imine would lead to higher *ees* and the (*S*)-configured Mannich product.

Scheme 2.28:



It was predicted by Gaussian calculations that the formation of 1:1 adducts between the catalyst **(S)-7** and imine **(121)** is sterically controlled by the bulky substituents of the phosphoric acid. Three different configurations of H-bonded associates were investigated (**154a-c**), with only **(154a)** deemed pertinent for the stereospecific nucleophilic attack (Figure 2.50). In this associate one side of the $\text{C}=\text{N}$ double bond is effectively shielded by a biphenyl substituent while the other side is completely open for the approach of the nucleophile. If enantioselection occurs via reaction of this associate the selective formation of the *S* form of the Mannich base would be observed, as is the case. Inspection of the other structures shows that the $\text{C}=\text{N}$ double bond is equally shielded from both sides and therefore reaction of a nucleophile with either **(154b)** or **(154c)** would proceed in a non-stereospecific manner. The calculated interatomic distances of the H-bonded associates indicate that the acidic proton in **(154a-c)** remains connected to the chiral phosphoric acid.

Figure 2.50: 2D representation of 3D structures for the optimised geometries (at the B3LYP/6-31G* level of theory) of the H-bonded associates (154a-c).



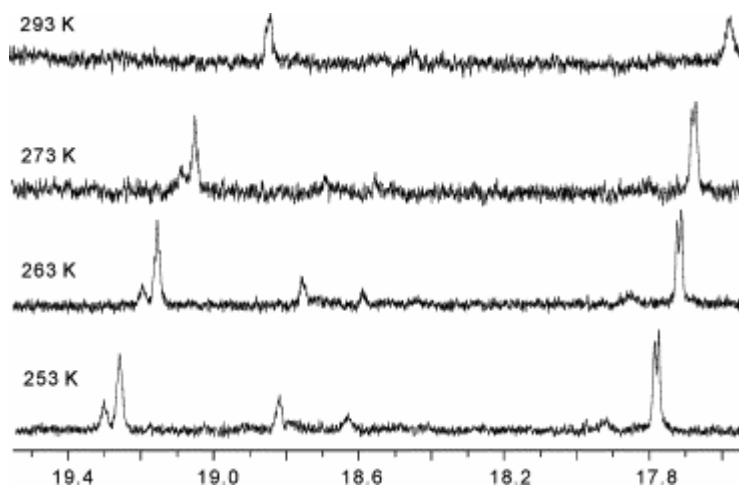
(Reproduced with the permission of Elsevier Limited)

The bulky *tert*-butyl substituent was found to be important for effective stereoselection. In associate (154a), free rotation around the hydrogen bond is not possible due to the close contacts of the *tert*-butyl group with the biphenyl substituent of the catalyst. It was postulated that a reduction in this hindrance would result in a dramatic decrease in the enantioselectivity of the reaction. This was tested by altering the Boc substituent on the imine and applying these analogues (150)-(151) in the phosphoric acid-catalysed Mannich reaction. A significant decrease in product *ee* was observed when the imine with the benzyl substituent (150) was used and the reaction became only slightly stereoselective with imine (151).

Computational studies had predicted the signals for the acidic protons in the H-bonded associates as occurring at 12-13 ppm. In order to probe this, Terada undertook ^1H

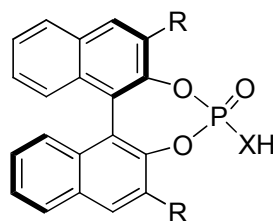
NMR spectroscopic studies of 1:10 mixtures of the chiral phosphoric acid (*S*)-(7) and imine (121). These measurements were performed temperatures ranging from at -20 - 20 °C (Figure 2.51).

Figure 2.51: Low field ^1H NMR spectra of catalyst (*S*)-(7) and imine (121) in deuteriotoluene.



(Reproduced with the permission of Elsevier Limited)

Deuterated toluene was used in these experiments as trace amounts of water can more readily be removed from this solvent and it has been demonstrated that the phosphoric acid-catalysed Mannich reaction also proceeds with a high degree of enantioselection in this medium. Significantly low field chemical shifts of the acidic proton were observed in the spectra and indicate a strong interaction with the nitrogen of atom of the imine that must provide the necessary activation of the imine molecule. The observed chemical shifts are somewhat higher than the computed ones which is possibly because solvent effects were neglected. Doublet splitting was observed for one of these signals at 17.2 ppm due to coupling with phosphorus. The low field signals immediately disappeared from the spectrum when acetylacetone was added to the sample.



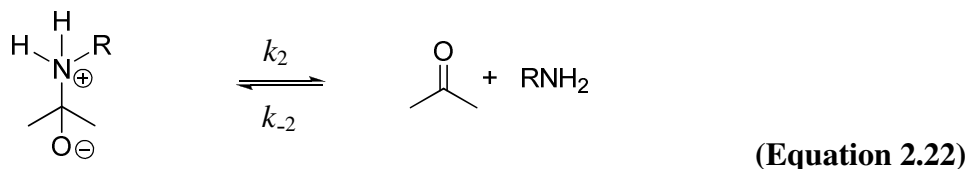
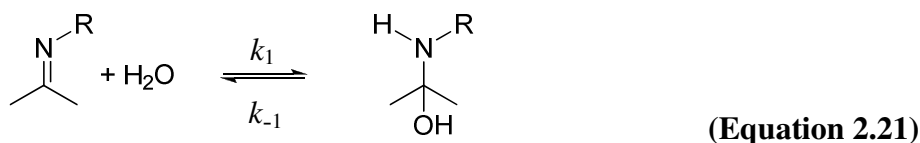
(118)

Application of BINOL-derived thiophosphoric acids (**118**) (X=S) in the Mannich reaction resulted in lower *ees* than those obtained with phosphoric acid analogues. For example, where for catalyst (**118**) where R=phenyl and X=S, the resulting *ee* is 3% while that obtained with the corresponding oxygen analogue is 75%. Similar reductions in enantioselectivity are observed for sulfur analogues where R=biphenyl and R=naphthyl. The steric effect of the group in the 3,3'-position of the catalyst as well as sulfur/oxygen substitution appear to play an important role in the enantioselectivity of the asymmetric Mannich reaction. It is clear that while the thiophosphoric acids accelerate the rate of the Mannich reaction, selectivity is poor. This could be a result of the larger sulfur atom, which may enable more flexible interactions or rotation in the H-bonded associates. It has been shown that the pK_a values of (thio)phosphoric acids are relatively invariant for the series investigated. The NMR evidence of hydrogen-bonded associates indicates that full proton transfer does not occur from the catalyst to the imine in toluene. This is consistent with the relative pK_a values of catalysts and iminium ions determined in this work (see Section 2.1.3.3 and 2.1.4.3) as the pK_a values of the *N*-Boc iminium ions are only 1-3 units lower than those of the catalysts. In contrast, a larger pK_a difference would promote complete proton transfer.

2.2.3 Attempted determination of aqueous pK_a values of iminium ions.

N-Boc protected imines are widely used in a variety of organocatalytic transformations. Application of the Brønsted linear free energy relationship to the Mannich reaction of acetylacetone with *N*-Boc imines requires the pK_a values of the iminium ions to be known. Despite their frequent use in synthetic chemistry there are no literature pK_a values of *N*-Boc iminium ions. This is likely owing to the hydrolytic lability of this class of imine which precludes the use of conventional techniques for determination of pK_a values. An alternative approach is to investigate the imine hydrolysis reaction and construct pH rate profiles from which acidity constants could potentially be estimated.

Following the detailed kinetic work by Jencks and co-workers^{76,87} the formation and hydrolysis of a number of imines as well as oximes, semicarbazones and related compounds is now well understood and has been shown to proceed through Equations 2.21-2.22.

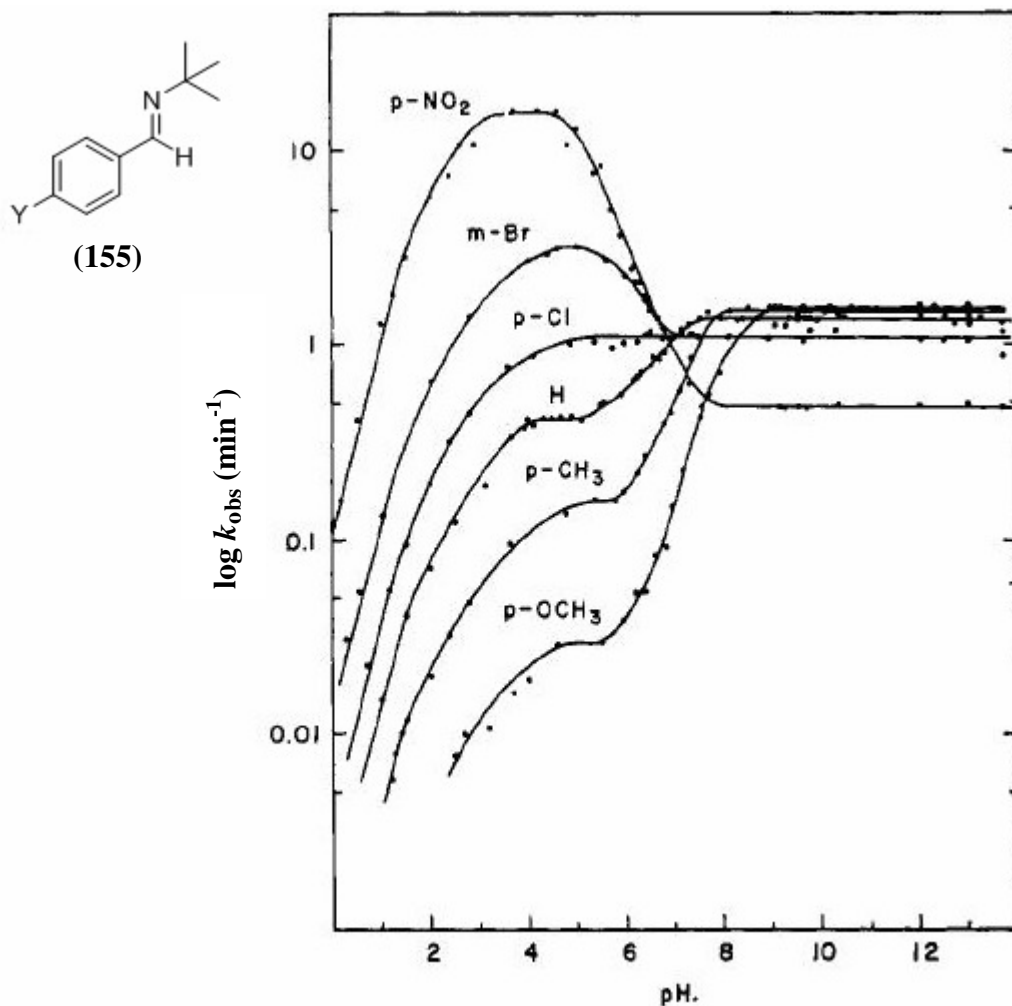


The pH dependence of the rate constant for imine hydrolysis has been well established and a plot of this rate constant against pH typically displays a break towards the acidic region which is consistent with a change in rate-determining step.

At neutral and alkaline pH values, carbinolamine formation is rate determining (Equation 2.21 k_1). At more acidic pH values, loss of amine from the carbinolamine addition intermediate becomes rate-determining (Equation 2.22, k_2).

In a study by Cordes and Jencks in 1963, analysis of pH rate profiles for the hydrolysis of *N*-benzylidene-*tert*-butylamines (**155**) (Figure 2.52) allowed the estimation of acidity constants of the iminium ions (Table 2.26)⁷⁶.

Figure 2.52: Logarithm of first-order rate constants for the hydrolysis of substituted benzylidene-*tert*-butylamines (**155**) as a function of pH in aqueous buffered solution at 25 °C and $I = 0.5$.

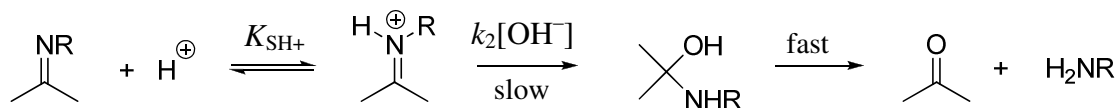


(Reproduced with the permission of ACS publications)

At alkaline pH values (9-14) there is only a small amount of variation in the rate constant for hydrolysis among the substituted benzylidene-*tert*-butylamines and the nitro-substituted compound undergoes hydrolysis somewhat more slowly than the others. The effect of substituents in this reaction is clearly not compatible with rate-determining attack of water, which should be facilitated by electron-withdrawing

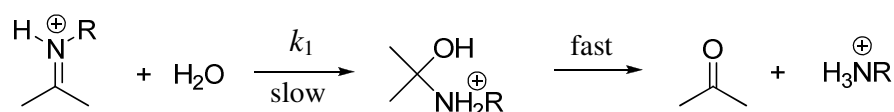
substituents, but suggests that the reaction involves attack of hydroxide on the protonated imine (Scheme 2.29). The observed rate constants for hydrolysis are independent of pH because the concentrations of hydroxide ion and of the protonated imine vary in an equal and opposite manner as the pH is changed.

Scheme 2.29:



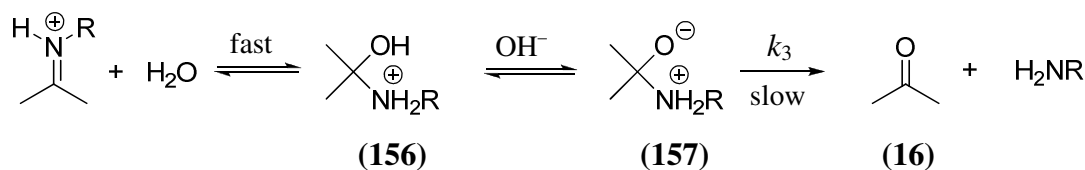
As the pH is decreased and an appreciable amount of iminium ion is formed, the hydroxide ion reaction becomes insignificant and the attack of water on the protonated imine becomes the predominant reaction pathway (Scheme 2.30). A decrease in rate constant is observed for those compounds for which the attack of water on the protonated imine is slow, and an increase in rate constant is observed for those compounds for which the corresponding reaction is fast.

Scheme 2.30:



In this pH region, the reaction shows the expected increase in rate constant with electron-withdrawing substituents. When the imine is completely protonated the rate constant levels off (pH 4-5). At still lower pH values (< 4) the rate constant is observed to decrease because of a change in rate-determining step to rate-determining loss of amine from the carbinolamine intermediate (Scheme 2.31). The decrease in rate constant in strong acid solution results from the requirement that a proton be removed from the hydroxyl group of the carbinolamine intermediate, in order to obtain sufficient driving force to expel the basic amine. In strong acid solution this becomes progressively more difficult.

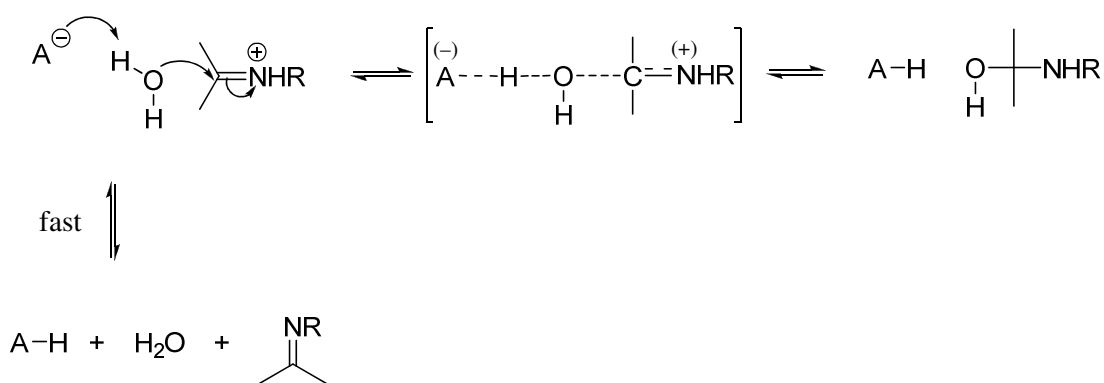
Scheme 2.31:



In order to ensure that the pH-rate behaviour observed for the hydrolysis of benzylidene-*tert*-butylamines is not a consequence, in part, of steric effects due to the bulky *tert*-butyl group, rate constants for the hydrolysis of *N*-ethyl substituted imines were studied as a function of pH. It was found that the behaviour of these imines was quantitatively similar to that of the corresponding benzylidene-*tert*-butylamines. Therefore, substitution of a *tert*-butyl for an ethyl group does not have a large steric effect on the rate constant for hydrolysis.

The potential presence of general catalysis was also investigated. No general catalysis was observed at alkaline pH (> 9). It was found that in the pH range 4-5, the hydrolysis of the imine was subject to general base catalysis by acetate anion. Under these conditions the imine is fully protonated and the role of the catalyst is to aid the removal of a proton from an attacking water molecule as shown in Scheme 2.32.

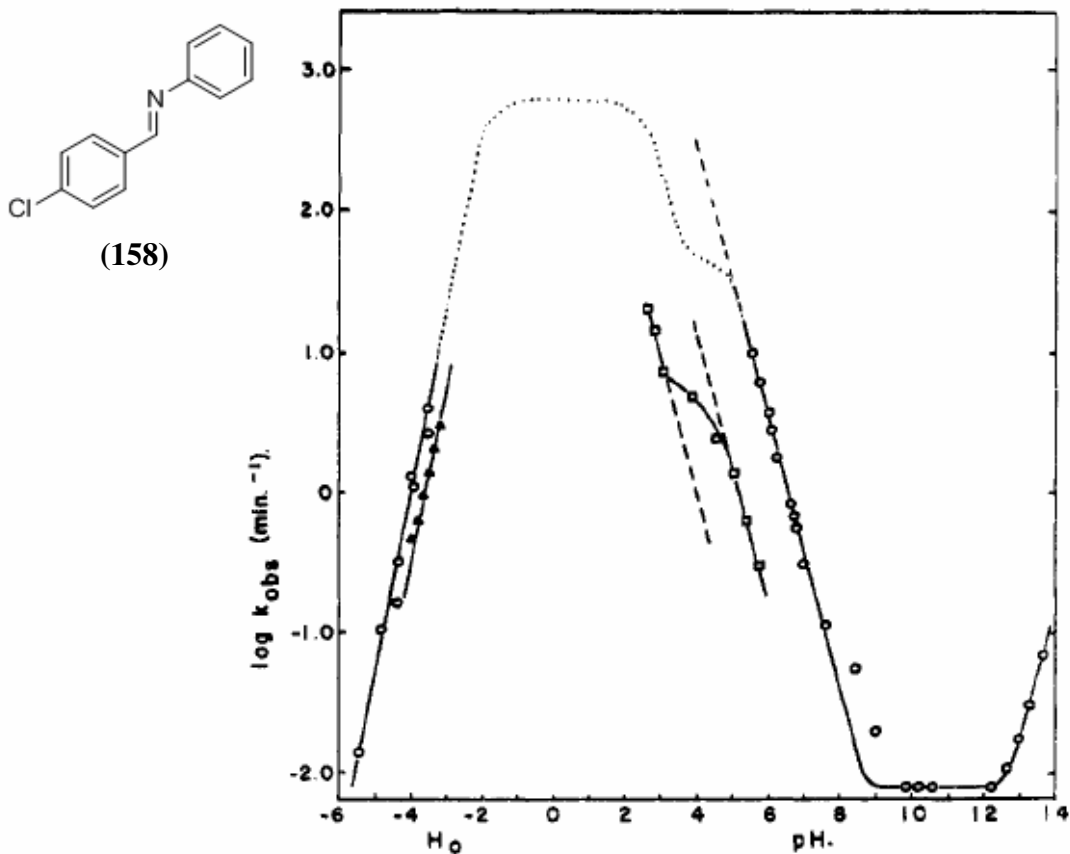
Scheme 2.32:



The $\text{p}K_{\text{a}}$ values of the iminium ions were estimated from the mid-point between the two pH-independent regions, where observed, in the region of the break of the pH-rate profile and also from spectral titration. Results were in agreement to 0.2 units and were in the range 5.40-7.70 (Table 2.26, Section 2.2.4).

The hydrolysis of *N*-*p*-chlorobenzylideneaniline (**158**) was also examined by Jencks. Figure 2.53 shows the pH dependence of the rate of hydrolysis.⁸⁸

Figure 2.53: Rate of hydrolysis of *N*-*p*-chlorobenzylideneaniline (**158**) as a function of pH at 25 °C and $I = 0.5$.



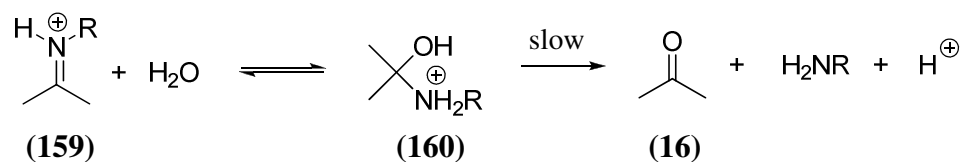
(Reproduced with the permission of ACS publications)

The break in the pH-rate profile due to a change in rate-determining step cannot be directly observed in aqueous solution because of the rapid rate of hydrolysis in this pH region. The break corresponding to a change in rate-determining step was observed at pH 4 by utilising aqueous ethanol as the solvent in order to slow down hydrolysis. The dotted line in Figure 2.52 shows the calculated rate of the reaction in pH region in which it was not possible to measure. This was obtained from rate and equilibrium constants for Schiff base formation and the pK_a of the protonated Schiff base and exhibits a break similar to that found in 80% ethanol.

For the hydrolysis of benzylideneanilines, there is decomposition of the protonated carbinolamine intermediate (**160**) as well as of the dipolar form. The electron-

withdrawing phenyl group on the amine permits amine expulsion with less driving force than in the case of more basic amines (Scheme 2.33).

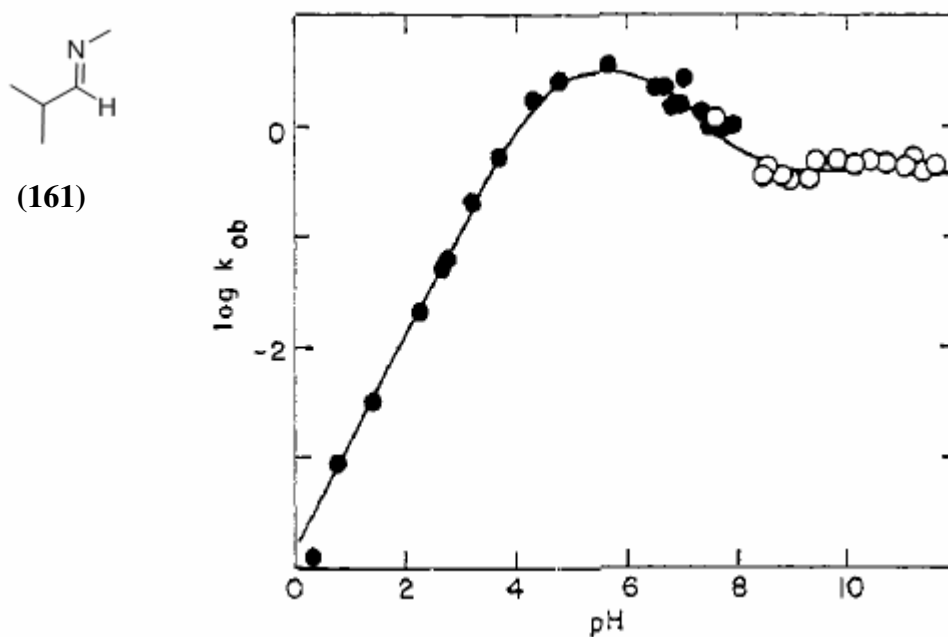
Scheme 2.33:



The rate of hydrolysis decreases rapidly with increasing acid concentration in the H_0 region of the rate profile, corresponding to rate-determining decomposition of the carbinolamine intermediate.

Kinetics of the hydrolysis of imines formed from basic amines and alkyl aldehydes were also examined in the pH range 0.3-8.2 and pH-rate profiles constructed (Figure 2.54).⁸⁹ The hydrolysis of *N-isobutylidenemethylamine* (**161**) is similar to that of the *N-benzylidene-tert-butylamines* which has been investigated by Cordes and Jencks.

Figure 2.54: Plot of k_{obs} for the hydrolysis of *N-isobutylidenemethylamine* (**161**) in water at 35 °C against pH: (●), from the rate of imine hydrolysis; (○), from the rate of imine formation.



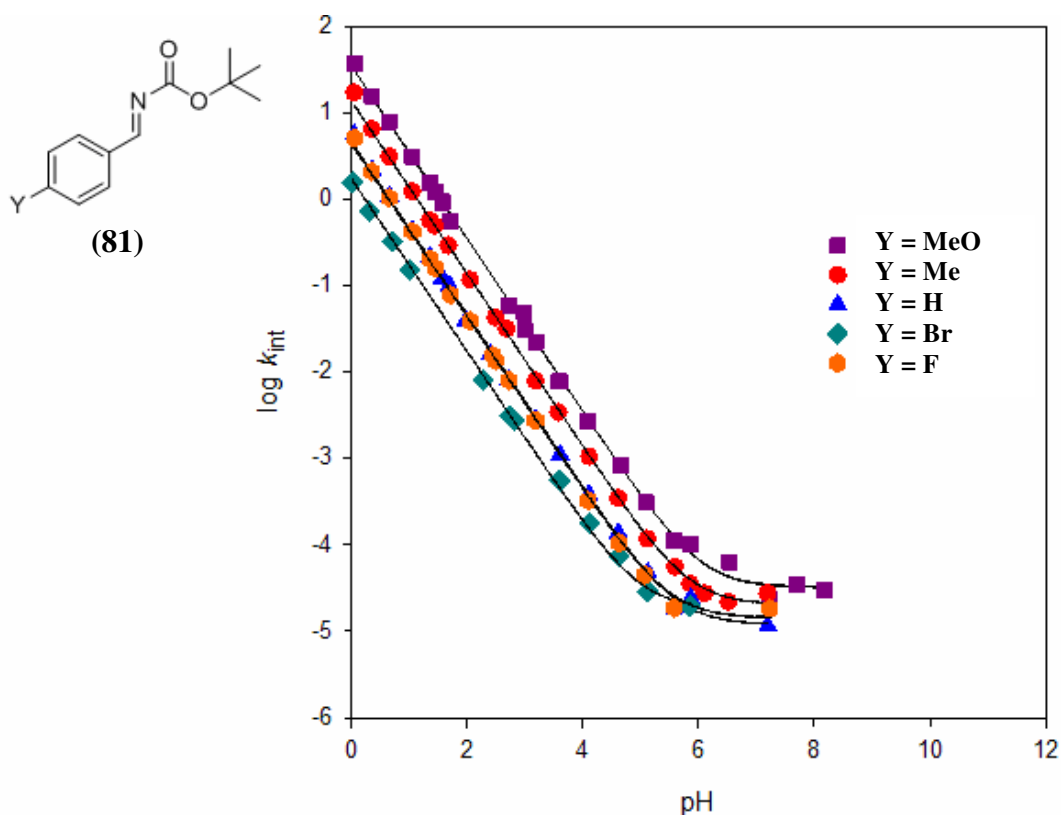
(Reproduced with the permission of ACS publications)

In the acid region of the pH-rate profile (< 4 pH units) the rate-determining step is decomposition of the carbinolamine intermediate. Under these conditions the reactant is mainly present as the protonated forms of the imine and carbinolamine. As the pH increases so too does the fraction of carbinolamine present in the zwitterionic form and hence the rate of hydrolysis is seen to increase. Above pH 4 the rate-determining step becomes attack of water on the iminium ion and a decrease in rate with increasing pH is observed. At alkaline pH (> 9) the hydrolysis reaction is pH-independent and corresponds to rate-determining attack of hydroxide ion on the protonated imine.

No significant general catalysis was observed in the acid region of the rate profile. As general catalysis of imine formation under alkaline conditions was not observed, it was concluded that the reverse hydrolysis reaction would not be susceptible to general catalysis. In view of the kinetic studies of Jencks on benzylidene-*tert*-butylamines, general catalysis would be expected in the intermediate pH range where the rate-determining step is attack of water on the protonated imine. This possibility was not investigated systematically for *N*-isobutylidenemethylamine (**161**).

Our investigations of the hydrolysis reaction of imines formed from substituted benzaldehydes and Boc amine provided the pH-rate profiles shown in Figure 2.55.

Figure 2.55: Logarithm of the rate of hydrolysis of *N*-Boc imines (**81**) as a function of pH at 25 °C and $I = 1.0$ in buffered aqueous solution.



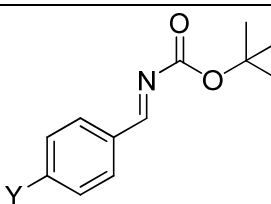
Rate constants for imine hydrolysis were not measured below pH 0. It is clear that the rate constants continue to increase with increasing acidity even at the highest acid concentration used and no pH-independent region is observed at low pH which would correspond to rate-determining attack of water on the fully protonated imine. This is likely to result from the high acidity of the iminium ion produced so that the imine does not become fully protonated and hence the decomposition of the carbinolamine intermediate does not become rate-limiting under our experimental conditions. Above pH 6, the rate-determining step is attack of hydroxide on the iminium ion and a pH-independent region is observed.

The contribution, if any, of general catalysis was assessed by performing the hydrolysis reactions of *N*-Boc imines in aqueous buffers with varying acid/base ratios at constant pH. Values of second-order rate constants for general acid-catalysed hydrolysis k_{HA} ($\text{M}^{-1}\text{s}^{-1}$) were obtained. A small decrease in the value of k_{HA} with

increasing pH was observed for a given buffer with a maximum 6-fold change observed in values of k_{HA} ($\text{M}^{-1}\text{s}^{-1}$) for *p*-methoxy-substituted imine for a range of acetic acid buffers. These results indicate a negligible contribution of general acid catalysis to the rate constant for imine hydrolysis.

The second-order rate constants for acid-catalysed hydrolysis, k_{H} ($\text{M}^{-1}\text{s}^{-1}$), and the first-order rate constants for buffer-independent hydrolysis, k_0 (s^{-1}), obtained for imines (119)-(123) are summarised in Table 2.24.

Table 2.24: Rate constants for the hydrolysis of *N*-Boc imines (119)-(123).

	Imine	k_{H} ($\text{M}^{-1}\text{s}^{-1}$) ^a	k_0 (s^{-1}) ^b
	Y = MeO (119)	3.50×10^1	3.20×10^{-5}
	Y = Me (120)	1.39×10^1	2.03×10^{-5}
	Y = H (121)	4.68	1.19×10^{-5}
	Y = Br (122)	1.74	1.82×10^{-5}
	Y = F (123)	4.39	1.41×10^{-5}

(a) The second-order rate constant for acid-catalysed hydrolysis was obtained from non-linear least-squares analysis of the pH-rate profile for imine hydrolysis. (b) The first-order rate constant for buffer-independent hydrolysis was obtained from non-linear least-squares analysis of the pH-rate profile for imine hydrolysis.

It can be seen from this data that there is no significant substituent effect upon the rate constants for hydrolysis. The value of k_0 (s^{-1}), the first-order rate constant for buffer-independent hydrolysis only varies by 2.5-fold while there is a maximum 20-fold change in k_{H} ($\text{M}^{-1}\text{s}^{-1}$), the second-order rate constant for acid-catalysed hydrolysis. The same general trend of an increase in rate constant with electron-donating substituents is observed for k_{H} . The order of increase in k_{H} ($\text{M}^{-1}\text{s}^{-1}$) as a function of substituent is as follows; Br < F < H < Me < MeO. The presence of electron-donating substituents favours protonation of the imine while electron-withdrawing substituents favour the attack of water on the imine. The fact that a net electron-donating substituent effect is observed suggests that the substituent effect on the imine protonation step outweighs the substituent effect on the step involving attack of water on the protonated imine.

As the rate constants for imine hydrolysis continue to increase at pH 0, the pH-independent region corresponding to attack of water on the fully protonated imine

could not be accessed and as such reliable estimates of iminium ion pK_a values cannot be extracted from these rate profiles. However, an upper limit of 2-3 units can be assigned.

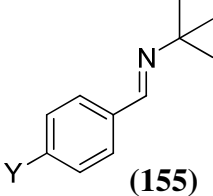
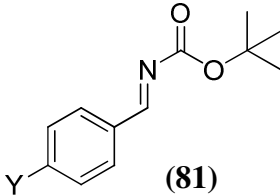
2.2.4 Determination of pK_a values of iminium ions in dimethyl sulfoxide.

The pK_a values of *N*-Boc iminium ions were estimated in dimethyl sulfoxide using a bracketing indicator method and were in the range 0.65-1.61. Equilibrium constants were measured by UV-Vis spectrophotometry with the concentration of neutral and protonated imine in large excess over that of the indicator used. In order to test the validity of this method the literature pK_a value of anilinium ion was reproduced. This has been determined in the DMSO by Crampton ($pK_a = 3.82$)⁷⁷ and Kolthoff ($pK_a = 3.6$)⁸¹. The value of 3.84 ± 0.16 obtained in this study (Appendix B) is in good agreement with those previously reported.

It is important to recognise that pK_a values are solvent dependent, with acid dissociation constants depending on the ability of the solvent to solvate the proton, anion and undissociated acid. It can be seen that for compounds which form highly delocalised anions, acidities do not differ greatly in H₂O and DMSO. For example 4-chloro-2,6-dinitrophenol shows a small increase in pK_a of 0.6 units in going from H₂O to DMSO.⁷⁹ The pK_a values of some ammonium ions, including anilinium ion, are also found to be similar in both media.⁷⁷ However for weaker acids which form more localised anions such as methanol, a large increase in pK_a is observed on going from water pK_a (15.5) to DMSO (29.0)⁷⁹. This is a result of the strong H-bond donor properties of water which achieves maximum stabilising effects towards highly localised ions such as methoxide.

Analysis of pH-rate profiles for hydrolysis indicates that the aqueous pK_a values of the iminium ions are < 2 units, which is consistent with the magnitude of the values determined in DMSO. Thus the observed solvent effect is small in this case. These values can be compared with those determined by Jencks for related *N*-benzylidene-*tert*-butylamines (Table 2.25). The effect of substituting an electron-withdrawing Boc group for the *tert*-butyl group is to lower the iminium ion pK_a by ~ 6 units.

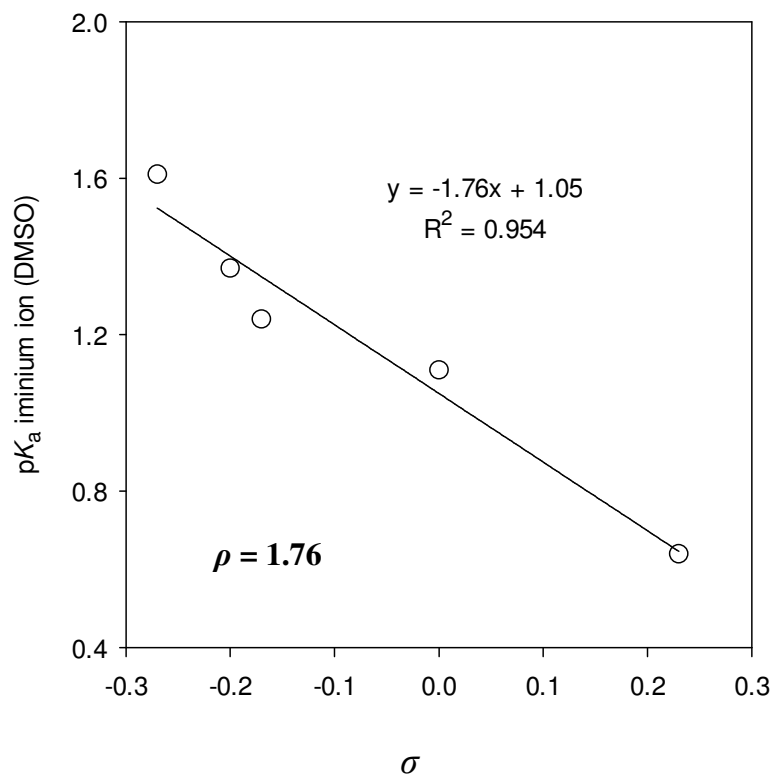
Table 2.25:

	Y	pK _a ^a		Y	pK _a ^b
 (155)	NO ₂	5.40	 (81)	Br	0.65
	Cl	6.50		H	1.11
	H	6.70		Me	1.24
	Me	7.40		^t Bu	1.37
	MeO	7.70		MeO	1.61

(a) Aqueous pK_a values for the protonated benzylidene-*t*-butylamines obtained from pH-rate profiles for hydrolysis. (b) pK_a values of *N*-Boc iminium ions determined in DMSO using a bracketing indicator method.

A Hammett plot of the pK_a values of iminium ions (**119'**)-(**123'**) against σ is presented in Figure 2.55 which gives $-\rho$ as the slope, thus giving a ρ value of 1.76. A positive ρ is consistent with the ionisation of an iminium ion to a neutral imine as there is an increase in electron density near the benzene ring in the product. Jencks observed a better correlation with σ^+ in the Hammett plot of the pK_a values of related benzylidene-*tert*-butylamines. This might be expected if there was some slight carbocation character on the carbon beside the aryl ring. However, with an electron-withdrawing *N*-Boc group this is likely disfavoured and a better correlation was obtained with σ rather than σ^+ in this case.

The magnitude of the ρ value is close to that for benzoic acid so a similar sensitivity to substituent effects is observed. This is reasonable as the atom experiencing a change in electron density is a similar distance from the ring as is the oxyanion of benzoic acid derivatives. The value of ρ is slightly larger in this case which could be a result of the imine nitrogen being closer to the ring.

Figure 2.56: Hammett plot of *N*-Boc iminium ion pK_a against σ .

For an imine formed from a relatively non-basic amine and an aryl aldehyde a decrease in basicity is observed relative to the amine precursor. The pK_a of *N*-*p*-chlorobenzylideneanilinium ion (2.8) is approximately 1.8 units lower than that of anilinium ion. This increase in acidity may be ascribed to two competing factors. The effect of the loss of conjugation of the nitrogen lone pair with the aromatic ring is to increase the pK_a of the Schiff base relative to aniline. Rehybridisation of the orbital containing the lone pair on the nitrogen atom from an sp^3 orbital to an sp^2 orbital results in a decrease in basicity of the Schiff base relative to aniline. As the net effect is a decrease in pK_a , it would appear that the rehybridisation effect dominates in this case. The pK_a ' values of *N*-benzylidene-*tert*-butylamines (**155**) (5.40-7.70) show a decrease relative to that of *tert*-butylamine (10.45)⁹⁰. This is a larger difference than that observed for *N*-*p*-chlorobenzylideneanilinium ion and aniline. As an alkyl amine is used there can be no stabilisation by delocalisation. Therefore the decrease is mainly due to the change in hybridisation.

Unfortunately, the pK_a ' of *tert*-butyl carbamate has not been determined and as such similar comparisons can not be drawn on the pK_a ' difference between *N*-Boc imines and the corresponding amine precursor.

2.2.5 pK_a values of (thio)phosphoric acid catalysts.

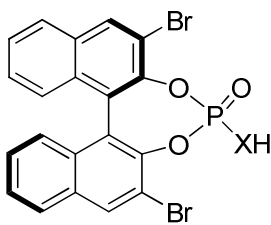
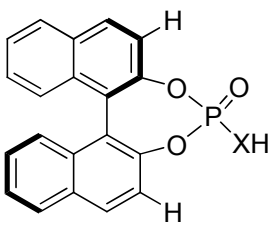
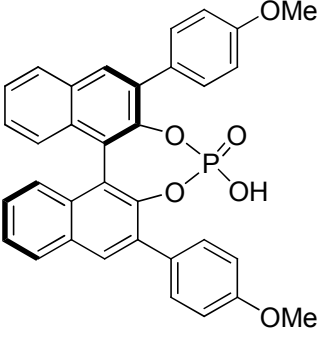
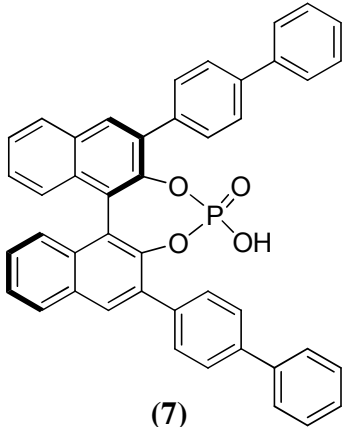
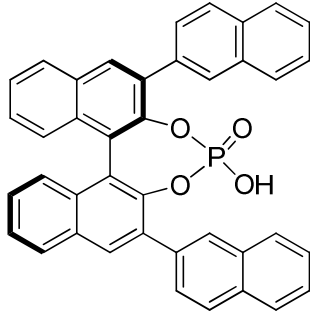
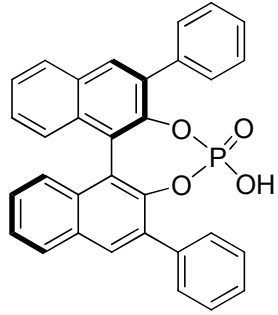
There have been no investigations of the acidity of the phosphoric acid catalysts utilised in this study to date and the aqueous pK_a value of dimethyl phosphate (1.29)⁸⁰ has been quoted in several synthetic studies as an estimate of the pK_a value of these compounds. Unfortunately the BINOL-derived catalysts have extremely limited solubility in water and as such, aqueous values could not be estimated in this work. The catalyst was observed to precipitate out of solution even at the low concentrations required for UV-Vis spectrophotometric studies (< 1 mM). As an alternative, the pK_a values of (thio)phosphoric acids were successfully estimated using the bracketing indicator method in DMSO. This method involved the estimation of equilibrium constants using neutral and anionic forms of the catalyst in large excess over an appropriate indicator in an analogous manner to the measurement of iminium ion pK_a values. The values obtained in this study are summarised in Table 2.26.

There is a dearth of literature pK_a data for phosphate diesters and thiophosphoric analogues. While aqueous pK_a values for dialkyl phosphoric acids have been determined, there are no reports of values for related aryl-substituted (thio)phosphoric acids. In the absence of literature pK_a values for relevant (thio)phosphoric acids, comparisons may be drawn to the relative acidities of thiols and alcohols. The aqueous pK_a value of ethanethiol is 10.5 while that of ethanol is 16. In aqueous solution a negative charge localised on sulfur is preferred generally than one localised on oxygen. This is because the larger size and polarisability of sulfur relative to oxygen allows the charge to density in a thiolate anion to be less than that in an oxyanion. This contributes to the greater acid strengths of thiols relative to alcohols. There is a smaller difference in acidity between thiophenol ($pK_a = 7.8$) and phenol ($pK_a = 9.95$) due to the additional delocalisation provided by the phenyl ring. In this case the negative charge is not fully localised on oxygen or sulfur and the greater polarisability of sulfur is less important.

With this in mind, it could be predicted that the thiophosphate anion will be better able to stabilise the negative charge than the phosphate anion and hence the thiophosphoric

acids would exhibit lower pK_a values. This trend is observed in the results in Table 2.26, although the difference in pK_a is small (≤ 0.7 units).

Table 2.26: Estimates for the pK_a values of (thio)phosphoric acids in DMSO.

 (133) X = O (138) X = S	 (85) X = O (137) X = S	 (136)
$pK_a =$	$pK_a =$	$pK_a =$
2.90 ± 0.03 (X=O) 2.21 ± 0.02 (X=S)	3.37 ± 0.06 (X=O) 3.07 ± 0.09 (X=S)	3.49 ± 0.07
 (7)	 (135)	 (84)
$pK_a =$	$pK_a =$	$pK_a =$
3.54 ± 0.04	3.77 ± 0.08	3.86 ± 0.06

What is surprising from these results is that the substituent at the 3,3'-position has a small effect on the acidity of the phosphoric acids with the range of pK_a values spanning < 1 unit. Although the aryl groups are not directly conjugated it could be predicted that the extended aromatic moieties would have a larger effect on the catalyst pK_a as it could be considered that the phosphoric acid is located in a hydrocarbon cavity. If this were the case, the hydrocarbon environment would destabilise the phosphate anion and increase the pK_a . However as the substituent effect on pK_a is small, it would appear that there is sufficient solvent molecules to mask this

environmental effect. The most acidic catalyst is the bromo-substituted derivative with a pK_a value of 2.90 which is ~ 0.37 units lower than that of the unsubstituted phosphoric acid. The least acidic of the series is the phenyl-substituted catalyst (**84**) with naphthyl- (**135**), biphenyl- (**7**) and *p*-methoxyphenyl-substituted (**136**) catalysts having progressively lower pK_a values, although the differences are very small.

2.2.6 Kinetics of the Mannich reaction

To date there have been no kinetic investigations of the Mannich reaction of *N*-Boc imines with acetylacetone and the effect of imine substituent and solvent on reaction rate has not been addressed. An appropriate $k_{\text{cat}}/k_{\text{uncat}}$ ratio is essential for the success of an asymmetric transformation and as such rate constants for the uncatalysed Mannich reaction were determined using ^1H NMR spectroscopy in this study. The results obtained are summarised in Table 2.27. Of the three solvents utilised, the background Mannich reaction proceeds at the fastest rate in CD_3CN with slower reactions occurring in CD_2Cl_2 and CDCl_3 . This slower background rate could potentially allow for higher enantiomeric excesses to be obtained in the catalysed Mannich reaction in CD_2Cl_2 and CDCl_3 . As such, dichloromethane was chosen as the reaction solvent for the evaluation of the enantioselectivity of (thio)phosphoric acid-catalysed Mannich reactions. Terada also used dichloromethane in the phosphoric acid-catalysed Mannich reaction and achieved high enantiomeric excesses.

Table 2.27: Kinetics of the uncatalysed Mannich reaction.

$\text{Y-C}_6\text{H}_4\text{-CH=N-Boc} + \text{CH}_3\text{COCH}_2\text{COCH}_3 \xrightarrow{\text{solvent}} \text{Y-C}_6\text{H}_4\text{-CH(N-Boc)-CH(Ac)CH}_3$

(10 mM) (82) (100 mM) (83)

Y	$k_{\text{obs}} (\text{s}^{-1})$			$k_{\text{rel}} (\text{max})$
	$\text{CD}_3\text{CN}^{\text{a}}$	$\text{CD}_2\text{Cl}_2^{\text{b}}$	CDCl_3^{b}	
MeO (119)	-	8.24×10^{-5}	2.12×10^{-5}	3.9
Me (120)	3.98×10^{-5}	6.53×10^{-5}	-	1.6
H (121)	3.73×10^{-4}	-	3.43×10^{-5}	10.9
F ^c (122)	6.41×10^{-3}	1.47×10^{-4}	1.71×10^{-4}	44
Br (123)	8.59×10^{-3}	1.56×10^{-4}	-	55

(a) Reactions were performed at 25 °C. (b) Reactions were performed at 22 °C. (c) The concentration of fluoro-substituted imine was 5 mM, with acetylacetone in 10-fold excess.

Rate constants for the Mannich reactions in CD_2Cl_2 and CDCl_3 were measured at 22 °C, while those in CD_3CN were measured at 25 °C. A change in temperature of 3 °C would be expected to bring about a 30-40% change in rate constant. As rate constants in CD_3CN were between 1.6 and 55 times greater than those performed in other solvents the effect cannot be purely a temperature effect. The polar aprotic solvent could effectively stabilise the charged intermediates using the lone pair on the nitrile whereas this stabilisation is not available in the other solvents. This may also be involved in stabilisation of the Mannich product.

It can be seen from these results that there is a relatively small substituent effect on the rate of the Mannich reaction in CDCl_3 and CD_2Cl_2 . A larger substituent effect is observed for the reaction in CD_3CN . The Mannich reaction of the bromo-substituted imine proceeds ~ 216 times faster than that of the methyl-substituted imine in this solvent. A larger solvent effect is observed for the electron-withdrawing substituents, as is illustrated by the k_{rel} values.

Unfortunately, rate constants for the phosphoric acid-catalysed Mannich reaction could not be determined in this study because of a competitive hydrolysis reaction. As previously discussed, *N*-Boc imines are hydrolytically labile and hydrolysis occurs rapidly in acidic solution. It was found that in the presence of (thio)phosphoric acid catalysts in deuterated solvents complete hydrolysis of the imine substrate occurred before the first time point was obtained.

Attempts were made to eliminate the source of adventitious water and the reaction conditions employed were described in Table 2.23 (Section 2.1.5.2). Freshly opened bottles of deuterated solvents were used and solutions were prepared in oven-dried vials fitted with rubber septa and under an argon atmosphere. Efforts at drying the deuterated solvent over molecular sieves or sodium sulfate were ineffective. The concentration of phosphoric acid used was minimised to 0.05 mol%. Samples were also prepared in the absence of acetylacetone in order to ascertain if this was the source of the adventitious water and complete decomposition of the imine was still observed. Ultimately, all attempts to suppress hydrolysis were unsuccessful and as such, rate constants for catalysed Mannich reactions could not be measured.

Chapter 3

Determination of pK_a values of azolium ions

3.0 Foreword.

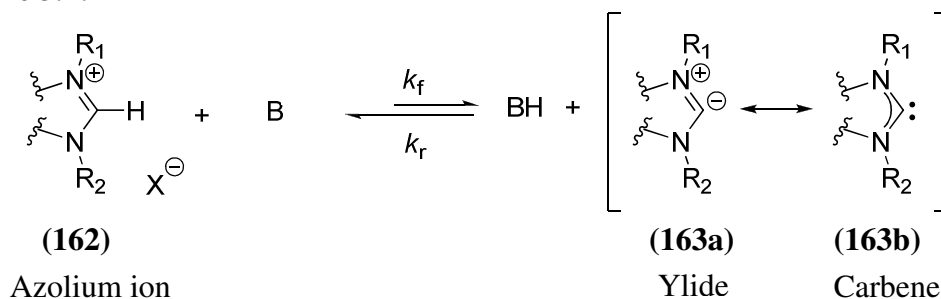
This chapter is divided into four subsections. In Section 3.1, an overview of literature pertaining to the determination of acidity constants of azolium ions is presented. Section 3.2 details the results of our investigations of the second-order rate constants k_{DO} ($\text{M}^{-1}\text{s}^{-1}$) for the deuterium exchange reactions of azolium cations to give the corresponding singlet carbenes at 25 °C and $I = 1.0$ (KCl). Evidence is presented that the reverse rate constant for carbene protonation by solvent water is limited by solvent reorganisation and occurs with a rate constant of $k_{\text{HOH}} = k_{\text{reorg}} = 10^{11} \text{ s}^{-1}$. The data are used to calculate carbon acid pK_a values for ionisation of imidazolium and triazolium cations. The results obtained are discussed in Section 3.3 and summarised in Section 3.4.

3.1 Introduction.

3.1.1 Acid-base chemistry of azolium ions.

While stable carbenes have revealed significant potential in the field of organocatalysis and as ligands in organometallic catalysis, there remains relatively little experimental data pertaining to the carbon acid pK_a values of their conjugate acids. Under basic conditions, azolium ions may be deprotonated to form a resonance hybrid of an ylide and a carbene (Scheme 3.1).

Scheme 3.1:



The acidity constant, K_a , for ionisation of the azolium ion to the carbene, is given by Equation 3.1 (when $B = H_2O$).

$$K_a = \frac{[(163b)] [BH]}{[(162)]} \quad \text{(Equation 3.1)}$$

The negative logarithm of the equilibrium constant or acid dissociation constant K_a is referred to as the pK_a (Equation 3.2).

$$pK_a = -\log K_a \quad \text{(Equation 3.2)}$$

3.1.2 Kinetic acidities of azolium ions.

Conventional methods for the determination of pK_a values of strong acids involve measurement of equilibrium concentrations of the carbon acid and anion in aqueous solution using, for example, UV-Vis spectrophotometry. As azolium ions are weak carbon acids, the equilibrium concentration of ylide is generally too small to be measured directly by conventional spectroscopic and potentiometric techniques.

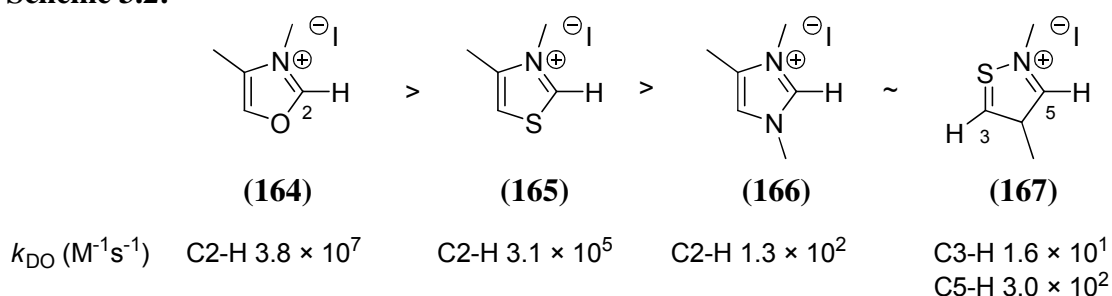
An alternative kinetic approach may be adopted for the determination of pK_a values of these weak acids. The acidity constant, K_a , may be written as the ratio of rate constants for the forward and reverse directions of the acid dissociation equilibrium: the rate constant for deprotonation of the azolium ion ($k_f, M^{-1}s^{-1}$) and the rate constant for reverse protonation of the carbene (k_r, s^{-1}) (Equation 3.3).

$$K_a = \frac{k_f}{k_r} \quad \text{(Equation 3.3)}$$

For weak carbon acids, the rate of the forward reaction is relatively slow and as such it is accessible by means of isotope exchange. The improvement in techniques such as NMR spectroscopy has made it possible to estimate kinetic acidities of azolium ions more precisely. This is a thermodynamically unfavourable process and hence according to the Hammond postulate, the transition state for carbene formation resembles the carbene product rather than the parent imidazolium ion.

Investigations of azolium ions and their ylides were prompted by an interest in the behaviour of the thiazolium moiety of the co-factor thiamine in relation to enzymatic catalysis. A systematic study by Haake in 1967⁹¹ gives the following order of reactivity of azolium ions towards deuterioxide ion-catalysed exchange: oxazolium (**164**) > thiazolium (**165**) > imidazolium ions (**166**) (Scheme 3.2) It has been established that an increase in the rate constant for H/D exchange is observed for azolium ions with more electronegative substituents α to the C-H undergoing exchange.⁹²

Scheme 3.2:

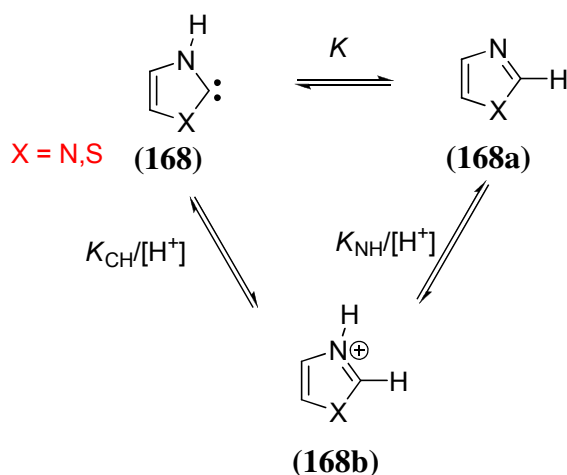


However, these relative rates are the reverse of that expected on the basis of the relative electronegativities of nitrogen and sulfur. Nitrogen, with the higher electronegativity, would be expected to stabilise the conjugate base of the imidazolium ion to a greater extent than sulfur would be expected to stabilise the conjugate base of the thiazolium ion. There have been several attempts to rationalise the apparent greater stability of thiazolium than of imidazolium ylides/carbenes.⁹³

The isolation and characterisation of a range of stable *N*-heterocyclic carbenes has driven several computational studies on the stability of these species. One conclusion that can be drawn from this work is that imidazolyl-2-ylidenes are more stable than thiazolyl-2-ylidenes. Theoretical studies by Scheffers-Sap,⁹⁴ showed that the polarising influence of sulfur in thiazolium ions is the major source of stabilisation of the negative charge at the C2 position rather than a d- σ -orbital overlap.

Amyes *et al.*⁹⁵ compared the thermodynamic rather than kinetic acidities of thiazolium and imidazolium ions using a thermodynamic cycle (Scheme 3.3).

Scheme 3.3:

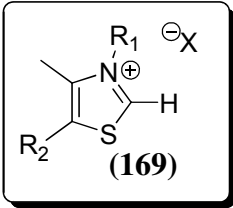
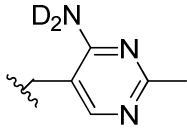
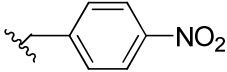
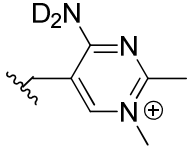
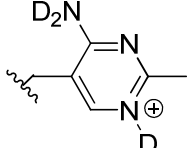
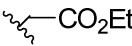


$$\text{Log } K = pK_{\text{CH}} - pK_{\text{NH}} \quad \text{(Equation 3.4)}$$

The substituent effect on the carbon basicity of *N*-heterocyclic carbenes is the sum of the substituent effects on the 1,2- shift at the carbene (**168**) to give the neutral azole (**168a**) and on *N*-protonation of the azole to give the azolium cation (**168b**). It was concluded that the smaller C2 acidity of the imidazolium ion relative to the thiazolium ion in water (3.9 *pK* units) reflects the greater stability of the imidazolium cation relative to the neutral azole by 6.4 kcal/mol and not the greater stability of the thiazol-2-ylidene relative to the imidazol-2-ylidene. Indeed, a 1.1 kcal/mol greater stability of imidazol-2-ylidene than of thiazol-2-ylidene was calculated.

Detailed studies by Washabaugh and Jencks⁹⁶ have provided access to kinetic acidities for a range of thiazolium derivatives (Table 3.1).

Table 3.1:

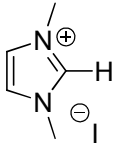
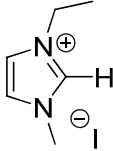
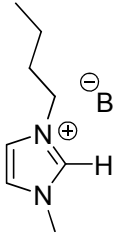
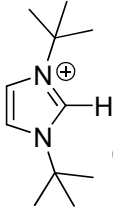
R_1	R_2	X	$k_{DO} (M^{-1}s^{-1})$ 30 °C	
Ethyl	H	Br ⁻	3.24×10^5	
Propyl	H	I ⁻	3.80×10^5	
Methyl	H	Cl ⁻	4.27×10^5	
CH ₂ CH ₂ CO ₂ [⊖]	H	Br ⁻	4.27×10^5	
CH ₂ CH=CH ₂	H	Br ⁻	9.77×10^5	
CH ₂ CO ₂ [⊖]	H	Cl ⁻	1.07×10^6	
Benzyl	H	Cl ⁻	2.14×10^6	
		CH ₂ CH ₂ OH	Cl ⁻	3.39×10^6
		H	Br ⁻	6.03×10^6
		CH ₂ CH ₂ OH	2I ⁻	7.59×10^6
		CH ₂ CH ₂ OH	2I ⁻	8.32×10^6
		H	Br ⁻	8.71×10^6
	CH ₂ CN	H	Cl ⁻	4.68×10^7

Here the relative differences in the rate constants for deuterioxide ion-catalysed exchange of thiazolium ion (**169**) may be assigned to the relative inductive effects of the *N*-substituents. In the case of the ions shown there is no possibility of resonance effects due to an intervening CH₂ group. A quantitative comparison of the effects of structural changes on kinetic acidities of imidazolium, triazolium and thiazolium ions is hampered by the lack of structurally homologous examples and comparable reaction conditions.

The first data on the kinetic acidity of *N*-substituted imidazolium ions in water at room temperature was reported by Amyes *et al.* in 2004.⁹⁵ Further work in our group^{97,98} has significantly extended the range of imidazolium ions investigated by Amyes *et al.* and

provides access to a systematic study of substituent effects on kinetic and thermodynamic acidity. A selection of available values is presented in Table 3.2.

Table 3.2:

Imidazolium ion	Temp °C	k_{DO} ($\text{M}^{-1}\text{s}^{-1}$)	Reference
 (170)	31	3.0×10^2	92
	25	2.47×10^2	95
	25	2.7×10^2	99
 (171)	25	1.84×10^2	97
 (172)	25	1.64×10^2	97
 (173)	25	1.66	97

A decrease in kinetic acidity is observed as the *N*-substituents become more σ electron-donating in the order methyl < ethyl < butyl as the positive charge on the azolium ion is increasingly stabilised. A 150-fold decrease is exhibited in the second-order rate constant for deuterioxide ion-catalysed exchange of the *bis*-^tbutyl substituted ion (**173**) relative to 1,3-dimethylimidazolium iodide (**170**).

As previously mentioned, H/D exchange reactions of azolium ions are accelerated by the introduction of electronegative atoms into the ring. There are considerably fewer studies of the kinetic acidities of 1,2,4-triazolium ions. Second-order rate constants for H/D exchange of 1,2,4-triazolium ions at 31 °C (**174**)-(175) have been reported.¹⁰⁰ This data is described as preliminary and was obtained by communication with another author. No details of the experimental methods employed were published.

Table 3.3:

Triazolium ion	Position	k_{DO} ($M^{-1}s^{-1}$)
 (174)	3	1.9×10^3
	5	8.6×10^7
 (175)	3	1.0×10^7
	5	-

3.1.3 Thermodynamic acidities of azolium ions.

There are limited systematic studies in the literature of aqueous thermodynamic pK_a values of azolium ions determined from H/D exchange studies. Washabaugh and Jencks estimated pK_a values of 17-19 for various substituted thiazolium ions (Table 3.4).

Table 3.4:

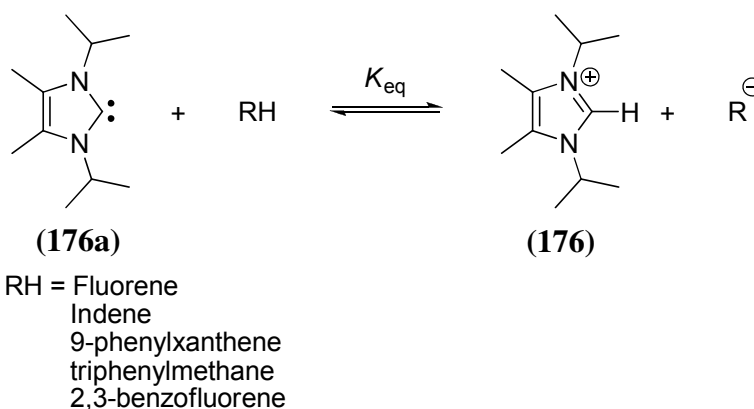
R_1	R_2	X	pK_a (D_2O) ^a	pK_a (DO^-) ^b	
Methyl	H	Cl^-	18.7	18.9	
Benzyl	H	Cl^-	-	18.2	
	H	Br^-	17.8	17.8	
 (169)		CH_2CH_2OH	$2\Gamma^-$	17.7	17.6
	CH_2CN	H	Cl^-	16.9	16.9
	CH_2CH_2OH	$2\Gamma^-$	-	18.0	

(a) Aqueous pK_a values of thiazolium ions were calculated from rate constants for C2 deprotonation by D_2O . (b) Aqueous pK_a values of thiazolium ions were calculated from rate constants for C2 deprotonation by DO^- .

Studies of thermodynamic pK_a values of azolium ions in organic solvent are limited. Alder *et al.* investigated the acidity of 1,3-diisopropyl-4,5-dimethylimidazolium ion (176) in DMSO and THF using a bracketing indicator method.¹⁰¹ This involved

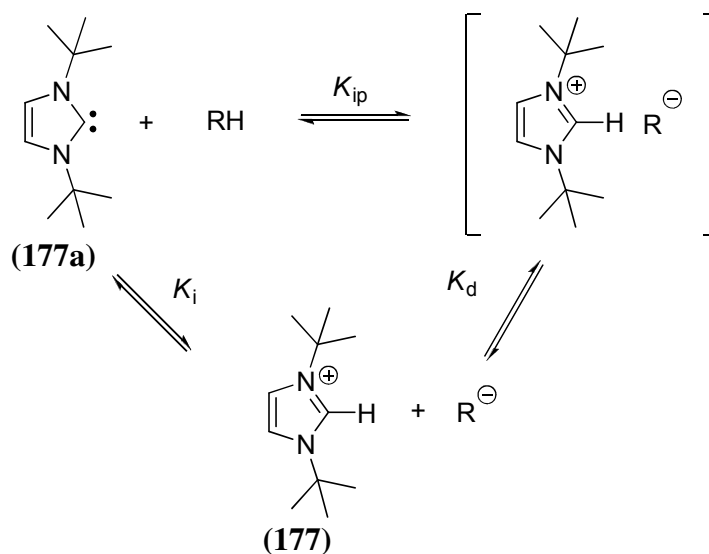
generation of the imidazolium ylide in solution using potassium hydride and subsequently examining the ability of the ylide to deprotonate various acidic hydrocarbon indicators in deuterated DMSO using ^1H NMR spectroscopy (Scheme 3.4). While indene ($pK_{\text{a}}(\text{DMSO}) = 20.1$) was completely converted to the conjugate anion, 9-phenylxanthene ($pK_{\text{a}}(\text{DMSO}) = 27.7$) and triphenylmethane ($pK_{\text{a}}(\text{DMSO}) = 30.6$) were not measurably deprotonated. Spectra of 1:1 mixtures of **(176a)** with fluorene ($pK_{\text{a}}(\text{DMSO}) = 22.9$) and 2,3-benzofluorene ($pK_{\text{a}}(\text{DMSO}) = 23.5$) showed separate peaks for the hydrocarbons and their conjugate bases. Integration of these spectra yielded pK_{a} value of 24.0 for **(176)**. Corrections were not made for ion pairing in DMSO. Similar experiments were performed in THF and showed that **(176a)** could not deprotonate fluorene to a measurable extent, but almost completely deprotonated 9-phenylfluorene ($pK_{\text{a}}(\text{THF}) = 18.5$). This reflects the fact that formation of the azolium ion is less favourable in solvents of lower polarity.

Scheme 3.4:



Kim and Streitwieser investigated the basicity of 1,3-di-*tert*-butylimidazol-2-ylidene (**(177a)**) in THF and DMSO by deducing the dissociation constant of ion pairs to free ions using UV-Vis spectrophotometry.¹⁰² The reaction of the carbene (**(177a)**) with the hydrocarbon indicator first produces an ion pair between the protonated carbene and the indicator anion with equilibrium constant K_{ip} . The ion pair dissociates to the free ions with an equilibrium constant K_{d} . The ion pair may be considered as in equilibrium with the carbene and hydrocarbon ($K_{\text{i}} = K_{\text{ip}}K_{\text{d}}$) (Scheme 3.5).

Scheme 3.5:



RH = Phenyl-2,3-benzofluorene
3,4-benzofluorene
benzylfluorene

It was observed that the carbene is effectively relatively less basic in THF (ion pair $pK_a = 20$) than in DMSO ($pK_a = 22.7$). This may occur as the parent azolium ion may be stabilised by hydrogen bonding in DMSO but not the carbene itself.

Equilibrium acidities of 1,3-dialkylimidazolium ions (**178**) were systematically measured in DMSO solution using overlapping indicators.¹⁰³ The pK_a values were determined using UV-Vis spectrophotometry and were observed to range from 19.7 to 23.4. Substituent effects at the imidazolium ring and counter ion effects were investigated and selected values are presented in Table 3.5.

Table 3.5:

	R	X ⁻	pK_a
<p>(178)</p>	Methyl	(CF ₃ SO ₂) ₂ N ⁻	22.0
	Ethyl	(CF ₃ SO ₂) ₂ N ⁻	22.1
	<i>n</i> Butyl	(CF ₃ SO ₂) ₂ N ⁻	22.0
	<i>n</i> Butyl	Cl ⁻	22.0
	<i>n</i> Butyl	Br ⁻	22.1
	<i>n</i> Butyl	BF ₄ ⁻	22.1
	<i>n</i> Butyl	PF ₆ ⁻	22.1
	<i>n</i> Octyl	(CF ₃ SO ₂) ₂ N ⁻	21.1

The influence of counter ion on the acidity of the imidazolium salts was found to be essentially negligible, with pK_a values ultimately dependant on cation structure. This was not unexpected as previous study on the intermolecular interaction energies in the ion pairs of 1-ⁿbutyl-3-methylimidazolium salts showed that the interaction energies differ by only a few kilocalories per mole in the absence of solvent and the strong solvation effect in DMSO may well level off these small differences of interaction energies. A pK_a value of 22.0 determined for the 1,3-dimethylimidazolium cation (**170**) is similar to the value of 23.0 determined for the same cation in aqueous solution by Amyes *et al.*⁹⁵ The slightly greater acidity in DMSO may be due to the better solvation of the parent azolium ion relative to the carbene/yliide in water rather than DMSO.

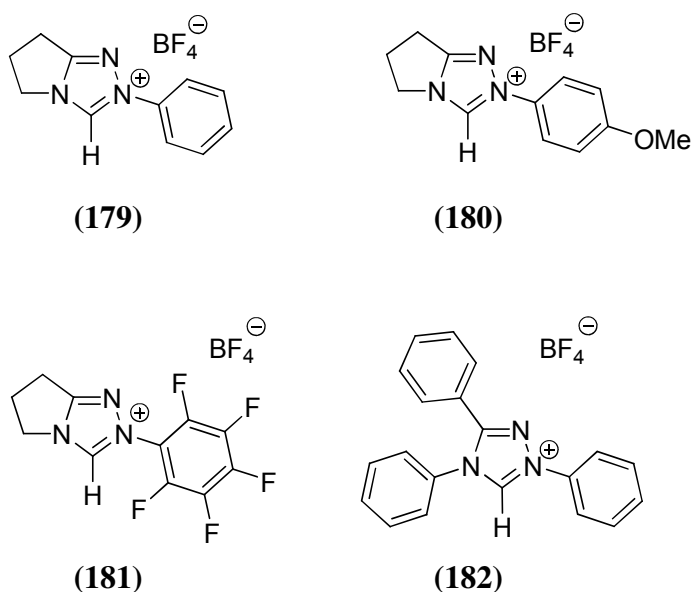
The effects of *N*-substitution on imidazolium ion pK_a values in DMSO, acetonitrile and water were examined in a computational study by Yates.¹⁰⁴ When ranked according to acidity, the azolium ions followed an identical pattern independent of solvent. It was found that computed values were not in reasonable agreement with experimental values where available. For example Yates determined an aqueous pK_a value of 27.4 for 1,3-dimethylimidazolium cation which is significantly higher than that determined by Amyes *et al.* for the same compound (23.0).

Although there have been significant studies of imidazolium ion acidity in both DMSO and water, there have been no systematic investigations of pK_a values of 1,2,4-triazolium ions. It is clear that determination of acidity constants for an increased range of azolium ions in a single solvent is required for the purpose of meaningful comparisons. The aims of this work were to determine pK_a values of *N,N*-dialkyl imidazolium ions and 1,2,4-triazolium ions in aqueous solution using the kinetic approach of Amyes *et al.* A better understanding of the factors affecting the basicity and nucleophilicity of *N*-heterocyclic carbenes and their interrelations would have great potential for future synthetic applications.

3.2. Results.

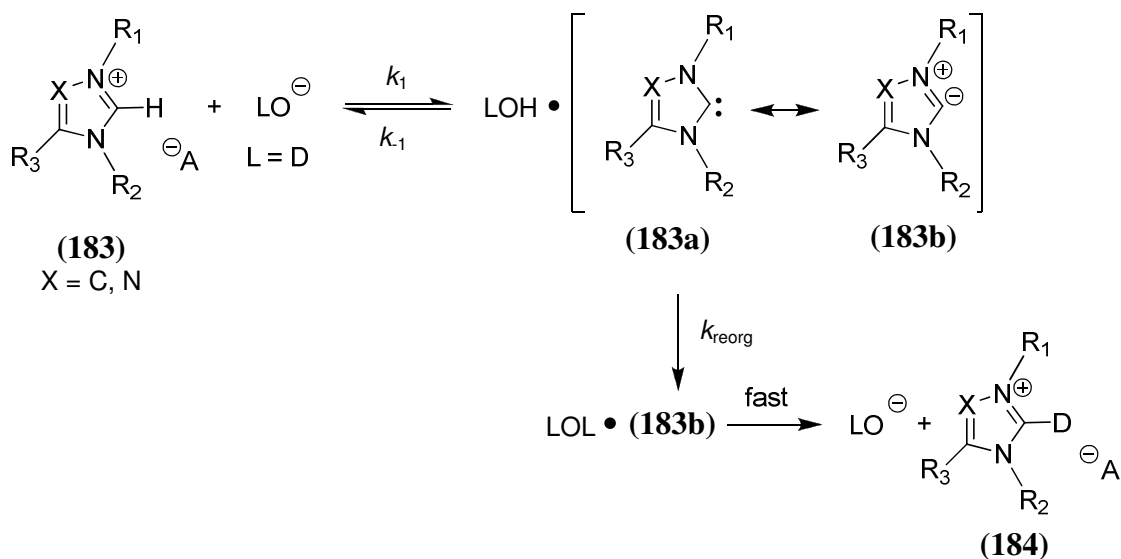
3.2.1 Deuterium exchange reactions of triazolium ions followed by ^1H NMR spectroscopy.

The H/D exchange reactions of triazolium ions **(179)**-**(182)** were analysed by 400 MHz and 500 MHz ^1H NMR spectroscopy at a range of pD values. The disappearance of the C3-H in D_2O solution due to deuterium exchange was monitored at 25 °C and $I = 1.0$ (KCl). From these data, first and second-order rate constants for deprotonation of substrate by deuterioxide ion to give the corresponding carbenes could be estimated.



The mechanism for exchange of the C3-H of triazolium ions **(179)**-**(182)** for deuterium is shown in Scheme 3.6. Triazolium ions **(179)**-**(182)** are represented by general structure **(183)** ($X=\text{N}$). Triazolium ions **(183)** may be deprotonated at the C3 position by a base in D_2O solution to form a carbene **(183a)**, which is more appropriately represented by an ylidic resonance structure **(183b)**. Solvent reorganisation then occurs, which involves replacement of HOD by a DOD molecule. At typical substrate concentrations (5-10 mM), the concentration of the protonated DOH is small relative to that of bulk D_2O solvent. Thus reprotonation of the carbene by DOH to generate the protonated substrate is negligible and effectively irreversible deuteration by D_2O occurs.

Scheme 3.6:



Reactions were initiated by direct addition of the required amount of buffer and internal standard to the solid substrate. For experiments carried out at 500 MHz the sample (0.75 mL) remained in the NMR probe at 25 °C throughout the reaction time course with spectra taken over varying time periods. Each ^1H NMR spectrum was recorded over a period of 12 minutes (32 transients). For reactions monitored directly in the NMR probe, the reaction time t was calculated from the time at the midpoint of the analyses.

Experiments carried out at 400 MHz were performed on a larger scale and incubated in reaction vials at 25 °C in a water bath. The reactions were initiated in the same way and reaction progress was monitored over time by withdrawing aliquots (~ 800 μL) at timed intervals. These aliquots were immediately quenched to pH 0.5-1 by addition of 5 M DCl solution. The samples were analysed immediately by ^1H NMR spectroscopy. A typical ^1H NMR spectrum, obtained during the exchange reaction of a particular triazolium ion substrate (**183**) (X=N) in D_2O at 25 °C and $I = 1.0$ (KCl), consists of a number of peaks. The signal due to the C3-H is visible as a broad singlet at ~10.0 ppm. Over time the area of this signal decays due to the formation of the deuterated product (**184**). The signal due to the twelve methyl hydrogens of the internal standard, tetramethylammonium deuteriosulfate, appears as a broad singlet at 3.02- 3.17 ppm. Coupling to ^{15}N by the hydrogens of the internal standard is evident by triplet splitting

at the top of this broad singlet. The hydrogens of the internal standard do not undergo exchange in the reaction conditions of these experiments. *

The progress of the deuterium exchange reactions for triazolium ions **(179)**-**(182)** was determined from the change in the integrated area of the singlet at ~10.0 ppm, due to the C3-H of the substrate over time in relation to that of a peak at ~3.1 ppm due to the twelve non-exchanging methyl hydrogens of the internal standard. By comparison there was no detectable change in the areas of the peaks due to the protons on the saturated fused carbocycle substituent relative to the standard peak with time.

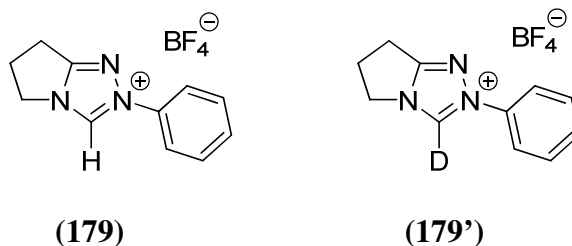
The fraction of substrate remaining $f(s)$, for triazolium ions **(179)**-**(182)** is determined from Equation 3.5.

$$f(s) = \frac{(A_{C3-H}/A_{Std})_t}{(A_{C3-H}/A_{Std})_{t=0}} \quad \text{(Equation 3.5)}$$

The observed pseudo-first-order rate constant for exchange of the C3-H of **(179)**-**(182)** for deuterium was then determined from semi-logarithmic plots of $f(s)$ against time (Equation 3.6). These plots were linear for the half-lives examined with 4 - 12 data points.

$$\ln f(s) = -k_{\text{obs}} t \quad \text{(Equation 3.6)}$$

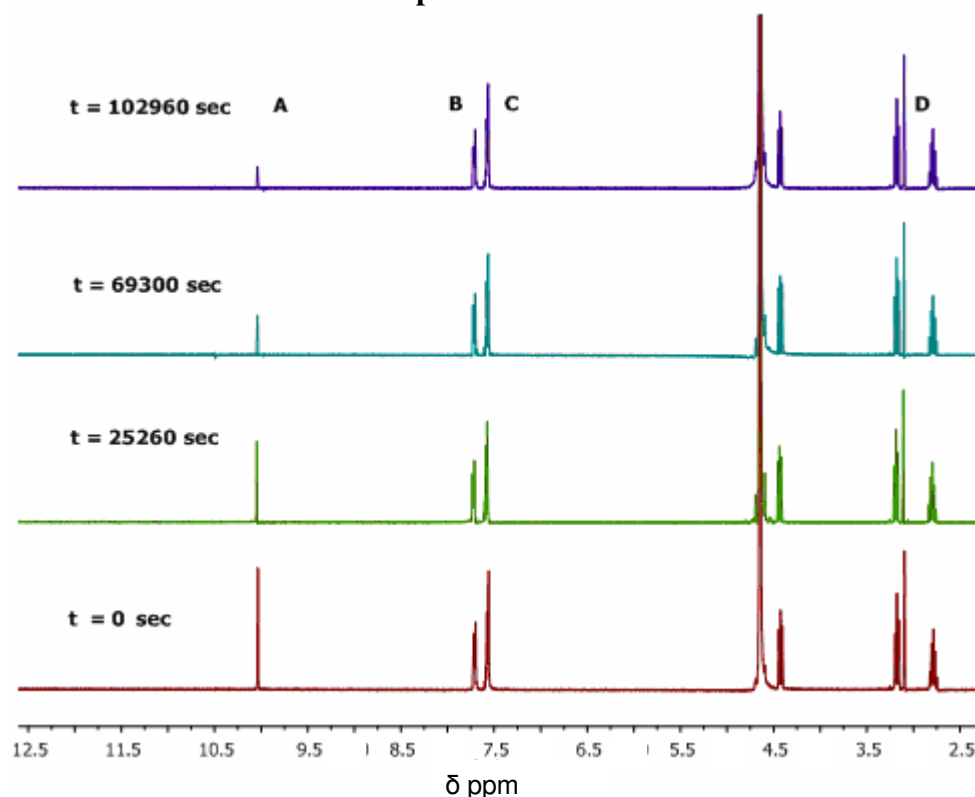
* No H/D exchange of tetramethylammonium hydrogensulfate was observed in 1.0 M KOD in D₂O at 25 °C after 16 days.

3.2.1.1 2-Phenyl-6,7-dihydro-5H-pyrrolo[2,1-c][1,2,4]triazol-2-ium tetrafluoroborate (179).

Rate constants for deuterioxide ion-catalysed exchange of the C3-H of triazolium ion (**179**) to form the corresponding deuterated product (**179'**) were determined by 400 MHz ^1H NMR spectroscopy. The relatively rapid exchange reaction in this case required the reaction to be performed in DCl solutions of different concentrations (pD 0.45-2.37). In the case of the exchange reactions of triazolium ion (**179**), all of the reaction data and subsequent analysis will be included in the main thesis as a representative example. For all subsequent exchange studies for triazolium ions (**180**)-(**182**) (Sections 3.2.1.2 - 3.2.1.4) the majority of the data will be presented in Appendix D.

Figure 3.1 shows representative ^1H NMR spectra of triazolium ion (**179**) (10 mM, pD 2.10), obtained during the exchange for deuterium of the C3-H in D_2O at 25 °C and $I = 1.0$ (KCl). Deuterium exchange at C3 results in the disappearance of the singlet peak due to the C3-H at 10.03 ppm (A). This is measured relative to the internal standard peak (D). The peak due to the *o*-PhHs appears as a multiplet at 7.57 ppm (B). The signals due to the *p*-PhH and *m*-PhHs appear as a multiplet at 7.55 ppm (C). The signals due to the three CH_2 groups on the fused carbocycle appear as two triplets at 4.42 ppm and 3.17 ppm and a multiplet at 2.78 ppm. In the reaction timeframe there is no change in the total integrated area for the signals due to all other protons relative to the constant peak area of the broad triplet at 3.17 ppm (D) due to the internal standard, indicating that H/D exchange is not occurring at any position other than at C3 under these experimental conditions.

Figure 3.1: Representative ^1H NMR spectra at 400 MHz of triazolium ion (179) (10 mM, pD 2.10), obtained during exchange of the C3-H for deuterium in D_2O at 25 °C and $I = 1.0$ (KCl). The time elapsed is indicated above each spectrum in seconds.



Values for experimental first-order rate constants for deuterium exchange (k_{obs} , s^{-1}) were obtained as the slopes of semi-logarithmic plots (Figures 3.2a – 3.2b) of $f(s)$ against time according to Equation 3.6. Reaction data and first-order rate constants k_{obs} (s^{-1}) at different pD values are shown in Table 3.6.

The concentration of deuterioxide ion was calculated using Equation 3.7, where $K_w = 10^{-14.87} \text{ M}^2$ is the ion product of D_2O at 25 °C. A value for the apparent activity coefficient of deuterioxide ion, γ_{DO} , of 0.73 has been determined under our experimental conditions of ionic strength 1.0 maintained with KCl.

$$[\text{DO}^-] = \frac{10^{\text{pD} - \text{p}K_w}}{\gamma_{\text{DO}}} \quad \text{(Equation 3.7)}$$

Figure 3.2a: Semi-logarithmic plot of the fraction of remaining C3-H against time for the deuterium exchange reaction of triazolium ion (179) at different pD values: (●), 0.01 M DCl, pD 2.00; (■), 0.008 M DCl, pD 2.10; (▲), 0.006 M DCl, pD 2.23; (◆), 0.004 M DCl, pD 2.37 in D₂O at 25 °C and I = 1.0 (KCl).

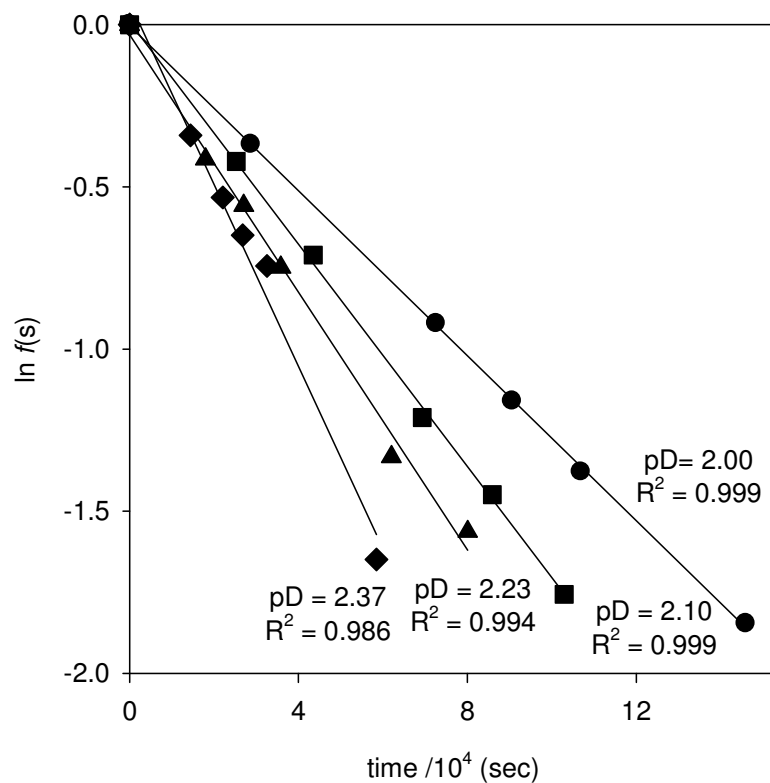


Figure 3.2b: Semi-logarithmic plot of the fraction of remaining C3-H against time for the deuterium exchange reaction of triazolium ion (179) at different pD values: (\blacktriangle), 0.5 M DCl, pD 0.045; (\blacklozenge), 0.3 M DCl, pD 0.61; (\bullet), 0.1 M DCl, pD 1.08 in D_2O at 25 °C and $I = 1.0$ (KCl).

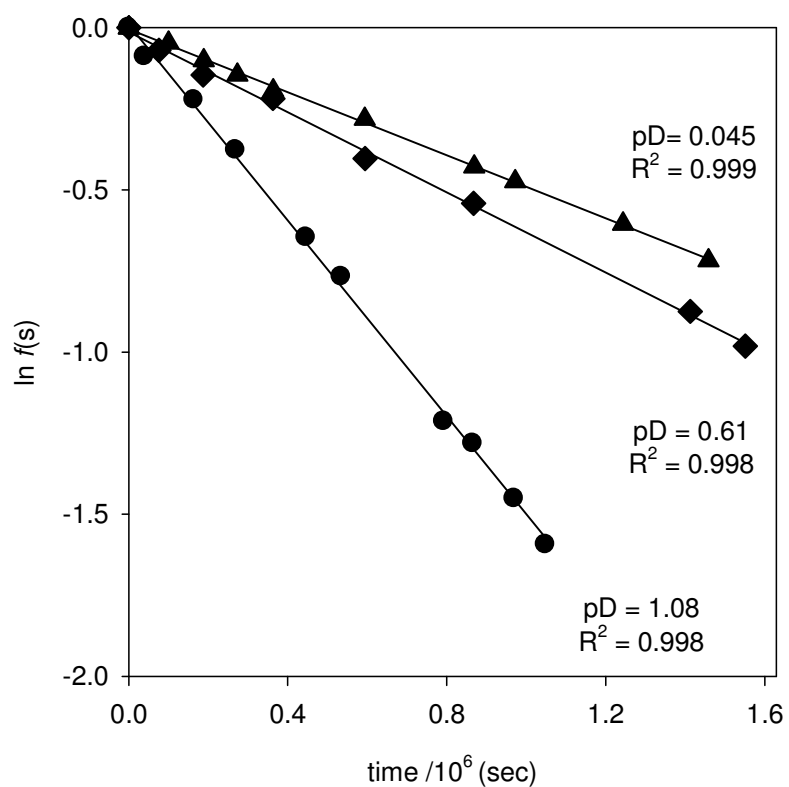


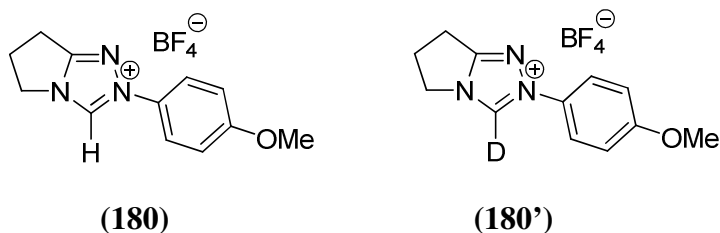
Table 3.6: First-order rate constants for exchange of the C3-H of triazolium ion (179) for deuterium in DCl solution in D₂O at 25 °C and I = 1.0 (KCl).

[DO] ^a (M)	Time (s)	$f(s)^b$	$\ln f(s)$	k_{obs}^c (s ⁻¹)
5.22×10^{-15} (pD 0.45)	0	1.000	0.000	4.86×10^{-7}
	100576	0.953	-0.048	
	188418	0.904	-0.101	
	273512	0.864	-0.146	
	363764	0.824	-0.194	
	593677	0.754	-0.282	
	868885	0.651	-0.429	
	971983	0.622	-0.474	
	1243260	0.546	-0.605	
	1458440	0.488	-0.718	
1663645	0.464	-0.768		
7.59×10^{-15} (pD 0.61)	0	1.000	0.000	6.15×10^{-7}
	76351	0.933	-0.069	
	187127	0.865	-0.145	
	362813	0.804	-0.219	
	594663	0.668	-0.403	
	867479	0.582	-0.541	
	1412427	0.417	-0.875	
	1550881	0.375	-0.981	
2.24×10^{-14} (pD 1.08)	0	1.000	0.000	1.51×10^{-6}
	39582	0.914	-0.089	
	164102	0.800	-0.223	
	268903	0.686	-0.378	
	446182	0.524	-0.647	
	534802	0.464	-0.768	
	792491	0.297	-1.214	
	865629	0.277	-1.283	
	969477	0.234	-1.452	
	1048362	0.203	-1.594	
1.86×10^{-13} (pD 2.00)	0	1.000	0.000	1.27×10^{-5}
	28800	0.691	-0.370	
	72720	0.398	-0.922	
	90720	0.313	-1.161	
	106980	0.252	-1.380	
	146040	0.158	-1.848	
2.33×10^{-13} (pD 2.10)	0	1.000	0.000	1.71×10^{-5}
	25260	0.656	-0.422	
	43500	0.492	-0.710	
	69300	0.298	-1.211	
	85920	0.235	-1.450	
	102960	0.173	-1.757	
0	0	1.000	0.000	
	18000	0.661	-0.415	

3.15×10^{-13} (pD 2.23)	27060	0.572	-0.558	1.98×10^{-5}
	35880	0.473	-0.748	
	62040	0.264	-1.332	
	80100	0.210	-1.563	
4.35×10^{-13} (pD 2.37)	0	1.000	0.000	2.81×10^{-5}
	14460	0.711	-0.341	
	22080	0.587	-0.533	
	26820	0.522	-0.649	
	32580	0.475	-0.744	
	58500	0.192	-1.65	

(a) Measurements were made in deuterium chloride solution in the pD 0.45–2.37 range. $[DO^-]$ was calculated using Equation 3.7. (b) The fraction of un-exchanged substrate remaining, $f(s)$, was calculated according to Equation 3.5. Measurements were made at an initial substrate concentration of 10 mM. (c) The value of the first-order rate constant, (k_{obs}), was obtained as the slope of the plot of $\ln f(s)$ against time in Figures 3.2a–3.2b.

3.2.1.2 4-Methoxyphenyl-6,7-dihydro-5H-pyrrolo[2,1-c][1,2,4]triazol-2-ium tetrafluoroborate (**180**).

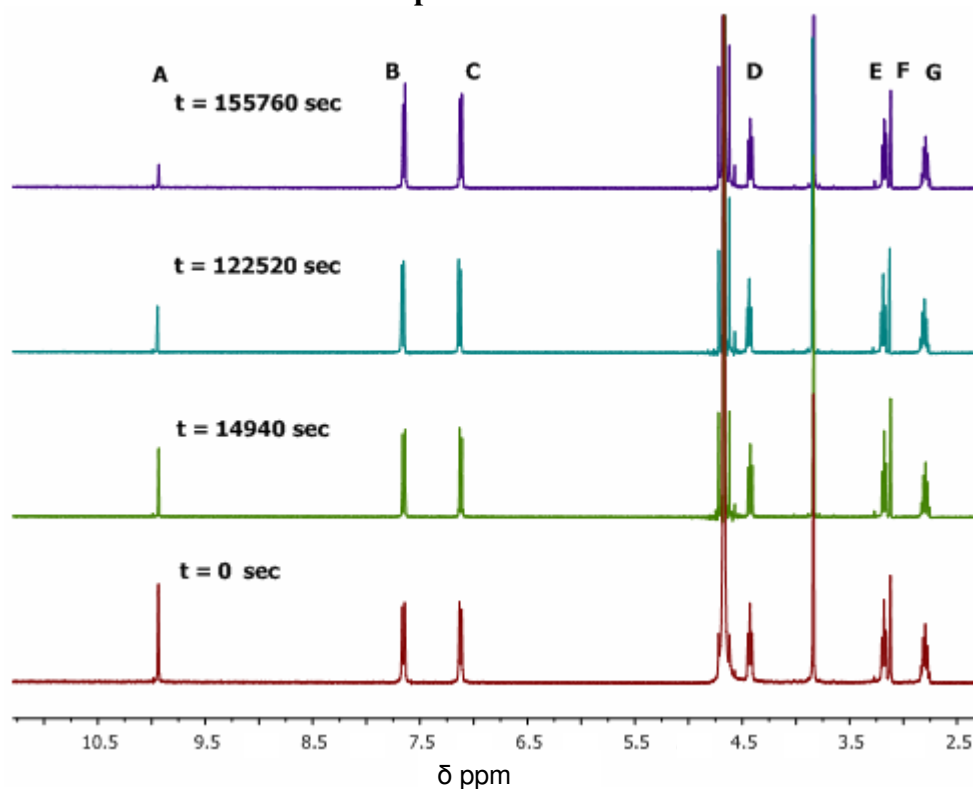


Rate constants for deuterioxide ion-catalysed exchange of the C3-H of triazolium ion (**180**) to form the corresponding deuterated product (**180'**) were determined by 400 MHz 1H NMR spectroscopy. The exchange reactions were performed in DCl and acetic acid buffer solutions.

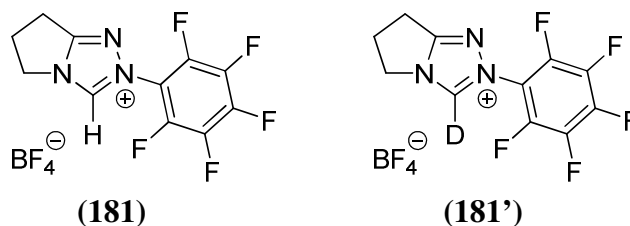
Figure 3.3 shows representative 1H NMR spectra of triazolium ion (**180**) (10 mM substrate, pD 2.01), obtained during the exchange for deuterium of the C3-H in D_2O at 25 °C and $I = 1.0$ (KCl). Deuterium exchange at C3 results in the disappearance of the singlet peak due to the C3-H at 9.85 ppm (A). This is measured relative to the internal standard peak (F). The peak due to the *o*-PhHs appears as doublet at 7.02 ppm (C). The signal due to the *m*-PhHs appears as a doublet at 7.55 ppm (B). The singlet due to the *p*-OCH₃ group appears at 3.74 ppm. The signals due to the three CH₂ groups on the fused carbocycle appear as two triplets at 4.34 ppm (D) and 3.09 ppm (E) and a multiplet at 2.70 ppm (G). In the reaction timeframe there is no change in the total

integrated area for the signals due to all other protons relative to the constant peak area of the broad triplet at 3.03 ppm (F) due to the internal standard. This indicates that H/D exchange is negligible at positions other than C3, under these experimental conditions.

Figure 3.3: Representative ^1H NMR spectra at 400 MHz of triazolium ion (180) (10 mM, pD 2.01), obtained during exchange of the C3-H for deuterium in D_2O at 25 °C and $I = 1.0$ (KCl). The time elapsed is indicated above each spectrum in seconds.



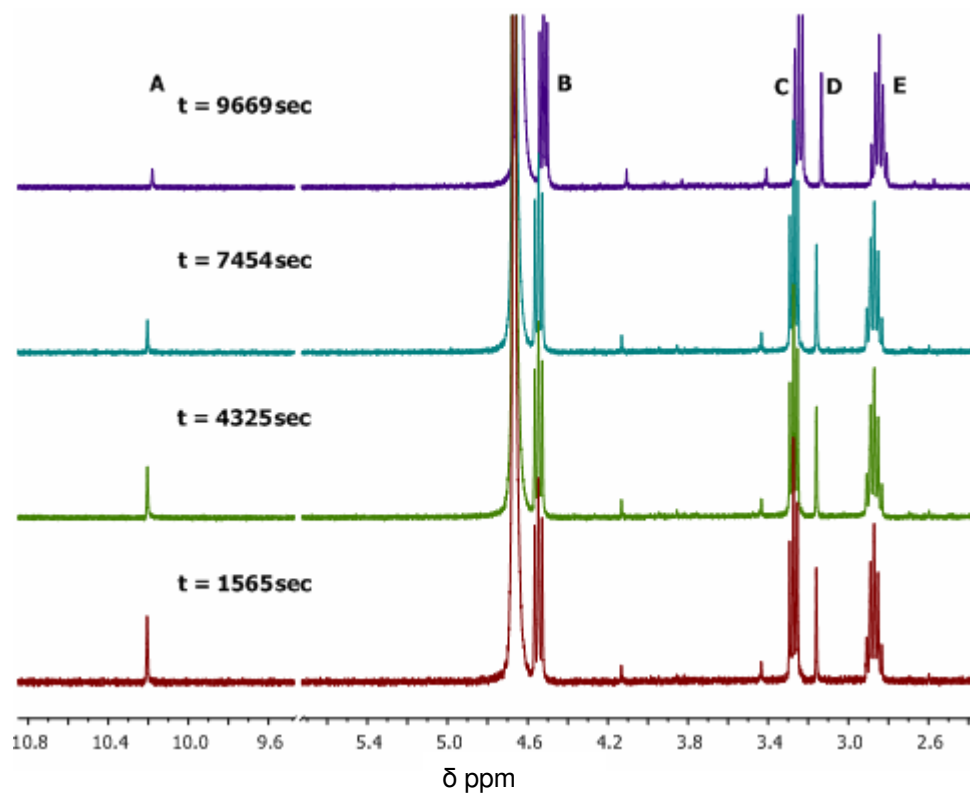
Values for experimental first-order rate constants for deuterium exchange (k_{obs} , s^{-1}) were obtained as the slopes of semi-logarithmic plots (Appendix D, Figures D1a- 1b) of $f(s)$ against time. Reaction data and first-order rate constants k_{obs} (s^{-1}) at different pD values are shown in Appendix D (Table D1).

3.2.1.3 Pentafluorophenyl-6,7-dihydro-5H-pyrrolo[2,1-c][1,2,4]triazol-2-ium tetrafluoroborate (181).

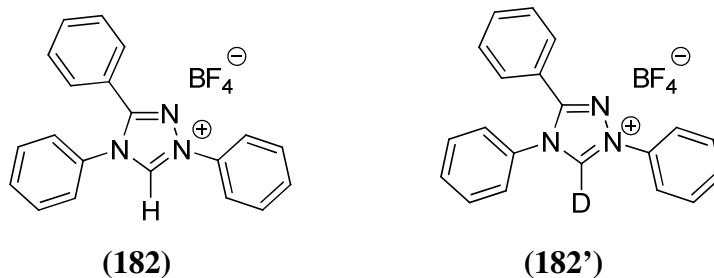
Rate constants for deuterioxide ion-catalysed exchange of the C3-H of triazolium ion (181) to form the corresponding deuterated product (181') were determined by 500 MHz ¹H NMR spectroscopy. The exchange reactions were performed in DCl solution.

Figure 3.4 shows representative ¹H NMR spectra of triazolium ion (181) (5 mM, pD 1.96) obtained during the exchange for deuterium of the C3-H in D₂O at 25 °C and I = 1.0 (KCl). Deuterium exchange results in the disappearance of the singlet peak due to the C3-H at 10.04 ppm (A). This is measured relative to the internal standard peak (D). The signals due to the three CH₂ groups on the fused carbocycle appear as two triplets at 4.52 ppm (B) and 3.32 ppm (C) and a multiplet at 2.78 ppm (E). In the reaction timeframe there is no change in the total integrated area for the signals due to all other protons relative to the constant peak area of the broad triplet at 3.17 ppm (D) due to the internal standard, indicating that H/D exchange is not occurring at any position other than at C3 under these experimental conditions.

Figure 3.4: Representative ^1H NMR spectra at 500 MHz of triazolium ion (181) (5 mM, pD 1.96), obtained during exchange of the C3-H for deuterium in D_2O at 25 °C and $I = 1.0$ (KCl). The time elapsed is indicated above each spectrum in seconds.



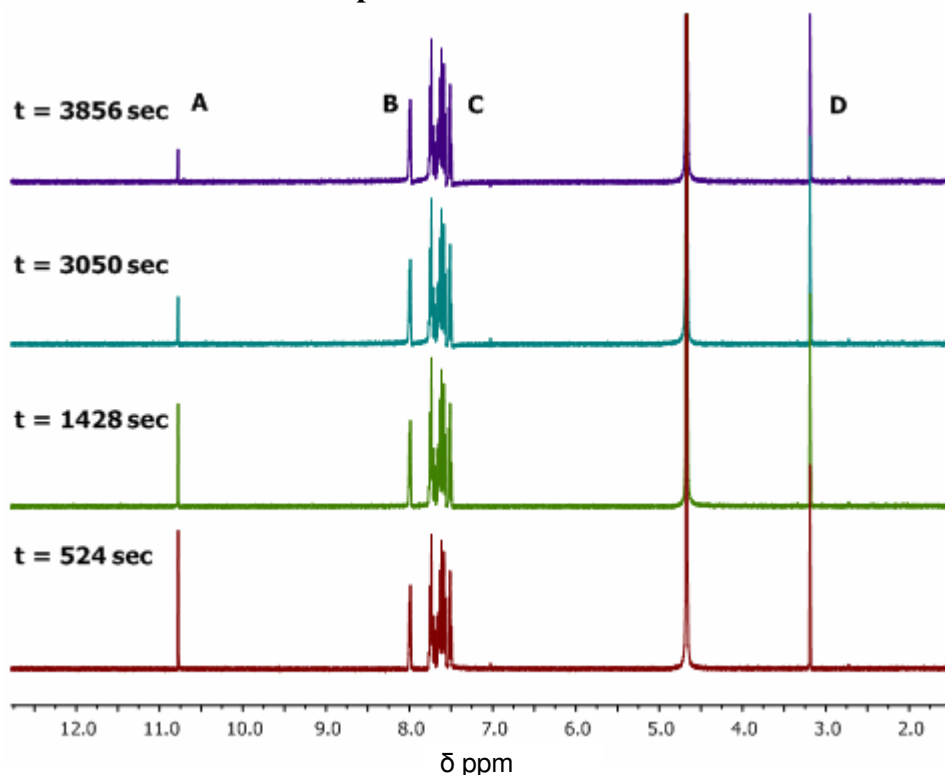
Values for experimental first-order rate constants for deuterium exchange (k_{obs} , s^{-1}) were obtained as the slopes of semi-logarithmic plots (Appendix D, Figure D2) of $f(s)$ against time. Reaction data and first-order rate constants k_{obs} (s^{-1}) at different pD values in deuterium chloride solution are shown in Appendix D Table D2.

3.2.1.4 1,3,4-Triphenyl-4H-1,2,4-triazol-1-ium tetrafluoroborate (182).

Rate constants for deuterioxide ion-catalysed exchange of the C3-H of triazolium ion **(182)** to form the corresponding deuterated product **(182')** were determined by 500 MHz ^1H NMR spectroscopy. The exchange reactions were performed in DCl solutions.

Figure 3.5 shows representative ^1H NMR spectra of triazolium ion **(182)** (5 mM, pD 2.83), obtained during the exchange for deuterium of the C3-H in D_2O at 25 °C and $I = 1.0$ (KCl). Deuterium exchange results in the disappearance of the singlet peak due to the C3-H at 10.75 ppm (A). This is measured relative to the internal standard peak (D). During the reaction timeframe there is no change in the total integrated area for the signals due to all aryl protons (B), (C) (7.6-8.0 ppm) relative to the constant peak area of the broad triplet at 3.17 ppm (D) due to the internal standard, indicating that H/D exchange is not occurring at any position other than at C3 under these experimental conditions.

Figure 3.5: Representative ^1H NMR spectra at 500 MHz of triazolium ion (182) (5 mM, pD 2.83), obtained during exchange of the C3-H for deuterium in D_2O at 25 °C and $I = 1.0$ (KCl). The time elapsed is indicated above each spectrum in seconds.



Values for experimental first-order rate constants for deuterium exchange (k_{obs} , s^{-1}) were obtained as the slopes of semi-logarithmic plots (Appendix D Figure D3) of $f(s)$ against time. Reaction data and the first-order rate constants k_{obs} (s^{-1}) at different pD values in deuterium chloride solution are shown in Appendix D (Table D3).

First-order rate constants for deuterioxide ion-catalysed exchange (k_{obs} s^{-1}) obtained in Sections 3.2.1.1-3.2.1.4 will be used to obtain second-order rate constants for deuterioxide ion-catalysed exchange (k_{DO} $\text{M}^{-1}\text{s}^{-1}$).

As some of these k_{obs} (s^{-1}) values were obtained in buffered solution, the contribution of the buffer species to k_{obs} (s^{-1}) will have to be delineated in order to access k_{DO} ($\text{M}^{-1}\text{s}^{-1}$) values due to deuterioxide catalysis only. This is the subject of the next section. Furthermore, the assessment of buffer contributions, if any, to the observed first-order rate constants for deuterioxide ion-catalysed exchange at fixed pD values will enable a rate constant for the reverse protonation of the carbene to be evaluated.

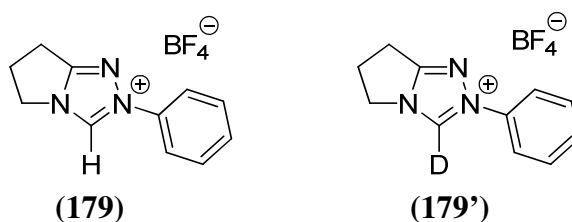
3.2.2 Determination of second-order rate constants for deuterioxide ion-catalysed exchange k_{DO} ($M^{-1}s^{-1}$).

The observed experimental pseudo-first-order rate constant for exchange (k_{obs}) is the sum of the contributions of all potential catalytic species to the exchange reaction, including contributions by solvent (k_{D_2O}), deuterioxide ($k_{DO}[DO^-]$), and buffer base ($k_B[B]$) (Equation 3.8).

$$k_{obs} = k_{D_2O} + k_{DO}[DO^-] + k_B[B] \quad \text{(Equation 3.8)}$$

Buffer catalysis ($k_B[B]$) may be a contributing term where there is general base catalysis of exchange. To assess the contribution of the term for general base catalysis, experiments are performed at a fixed concentration of deuterioxide ion while the concentration of the buffer base is varied. This is achieved by using a constant ratio of buffer acid/base forms whilst varying their absolute concentrations. If there is general base catalysis of exchange then the observed pseudo-first-order rate constant for exchange (k_{obs}) will increase with the increasing concentration of buffer base present in addition to varying with a change in the deuterioxide concentration. For the most part our exchange studies were performed in DCl solution rather than in buffers, however in a few cases acetic acid buffers were employed in which case general base catalysis is a possibility. General base catalysis of exchange can be observed when deprotonation of the substrate by DO^- is rate determining for the overall deuterioxide ion-catalysed exchange reaction. The low reactivity of lyoxide ion in proton transfer to/from carbon for its basicity is termed the lyoxide ion anomaly. As a result of this effect, Brønsted bases result in an increase in the rate constant for this proton-transfer step ($k_B[B]$). However, when reprotonation of the carbene/ylide intermediate by solvent (k_{-1}) is so fast that solvent reorganisation is rate-determining for the overall deuterioxide ion-catalysed reaction (Scheme 3.6), general base catalysis of the overall deuterium exchange reaction is not possible as there is no way for a Brønsted base to lower the barrier to solvent reorganisation. Furthermore, if general base catalysis is not observed then this implies that the reverse protonation of the carbene/ylide is also limited by solvent reorganisation. Thus the absence of general base catalysis of exchange also permits us to assign a value of $k_{reorg} = 10^{11} s^{-1}$ as the rate constant for the reverse protonation of the carbene.

Results of the investigations of potential buffer catalysis of deuterium exchange at the C3 position of a representative triazolium ion (**179**) are now presented.



Rate constants for deuterioxide ion-catalysed exchange of the C3-H of triazolium ion (**179**) to form the corresponding deuterated product (**179'**) in acetic acid buffers at a fixed pD were determined by 400 MHz ^1H NMR spectroscopy. ^1H NMR spectral details in acetate buffers at fixed pD values were exactly as described in Section 3.2.1.1 for analogous exchange reactions in deuterium chloride solution at different pD values.

Values for experimental first-order rate constants for deuterium exchange (k_{obs} , s^{-1}) were obtained as the slopes of the semi-logarithmic plot of $f(s)$ against time (Figure 3.6) at different acetic acid buffer concentrations and at a fixed pD and are shown in Table 3.7.

Figure 3.6: Semi-logarithmic plot of the fraction of remaining C3-H against time for the deuterium exchange reaction of triazolium ion (179) in 10% f_B acetic acid buffer (0.05 M (\diamond), 0.075 M (\circ), 0.1 (\triangle) and 0.15 M (\square)) at 25 °C and $I = 1.0$ (KCl).

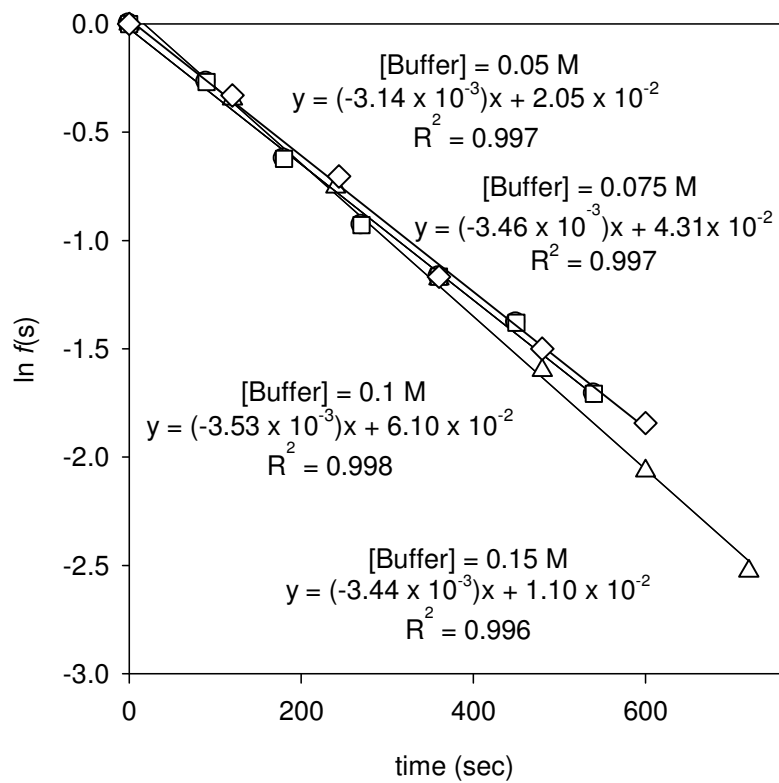


Table 3.7: First-order rate constants for exchange of the C3-H of triazolium ion (**179**) for deuterium in acetic acid buffers (10% f_B) in D_2O at 25 °C and $I = 1.0$ (KCl).

[Buffer] _T ^a (M)	[DO ⁻] ^b (M)	Time (secs)	$f(s)$ ^c	$\ln f(s)$	k_{obs} ^d (s ⁻¹)
0.05	5.23×10^{-11} (pD 4.45)	0	1.000	0.000	3.14×10^{-3}
		120	0.719	-0.331	
		244	0.494	-0.704	
		360	0.311	-1.168	
		480	0.223	-1.500	
		600	0.158	-1.843	
0.075	5.48×10^{-11} (pD 4.47)	0	1.000	0.000	3.46×10^{-3}
		90	0.793	-0.232	
		180	0.573	-0.557	
		270	0.402	-0.911	
		360	0.299	-1.207	
		450	0.232	-1.461	
0.10	5.60×10^{-11} (pD 4.48)	0	1.000	0.000	3.53×10^{-3}
		120	0.707	-0.347	
		240	0.471	-0.753	
		360	0.308	-1.178	
		480	0.202	-1.599	
		600	0.127	-2.064	
0.15	5.60×10^{-11} (pD 4.48)	0	1.000	0.000	3.44×10^{-3}
		90	0.741	-0.300	
		180	0.534	-0.627	
		270	0.407	-0.899	
		360	0.300	-1.204	
		465	0.218	-1.523	
540	0.147	-1.917			

(a) Total concentration of acetic acid buffers ([DOAc] + [KOAc]) (b) Measurements were made in 10% free base acetic acid buffers. The concentration of deuterioxide [DO⁻] was calculated using $[DO^-] = (10^{pD-pK_w})/\gamma_{OL}$ with $pK_w = 14.87$, where $\gamma_{OL} = 0.73$ is the activity correction of lyoxide ion under our experimental conditions. (c) The fraction of un-exchanged substrate remaining, $f(s)$, was calculated according to Equation 3.5. Measurements were made at initial substrate concentration of 10 mM. (d) The value of the first-order rate constant, ($k_{obs} s^{-1}$), was obtained as the slope of the plot of $\ln f(s)$ against time in Figure 3.6.

The first-order rate constants for the exchange reactions in acetic acid buffer of the C3-H of triazolium ion (**179**) are summarised in Table 3.8. Also shown in Table 3.8 are k_{rel} values which are calculated according to Equation 3.9, where k_{DO} is the experimental second-order rate constant for deuterioxide ion-catalysed exchange. The ratio of first-

order rate constants (k_{rel}) is a measure of the relative difference between the observed experimental rate constant (k_{obs}) and the deuterioxide ion-catalysed rate of exchange ($k_{\text{DO}}[\text{DO}^-]$) where k_{DO} is obtained for reactions in un-buffered solution. This equation also corrects for the small changes in pD that occur upon dilution of a buffer solution at constant ionic strength. In a case where there is no general base catalysis of exchange this ratio should be close to unity.

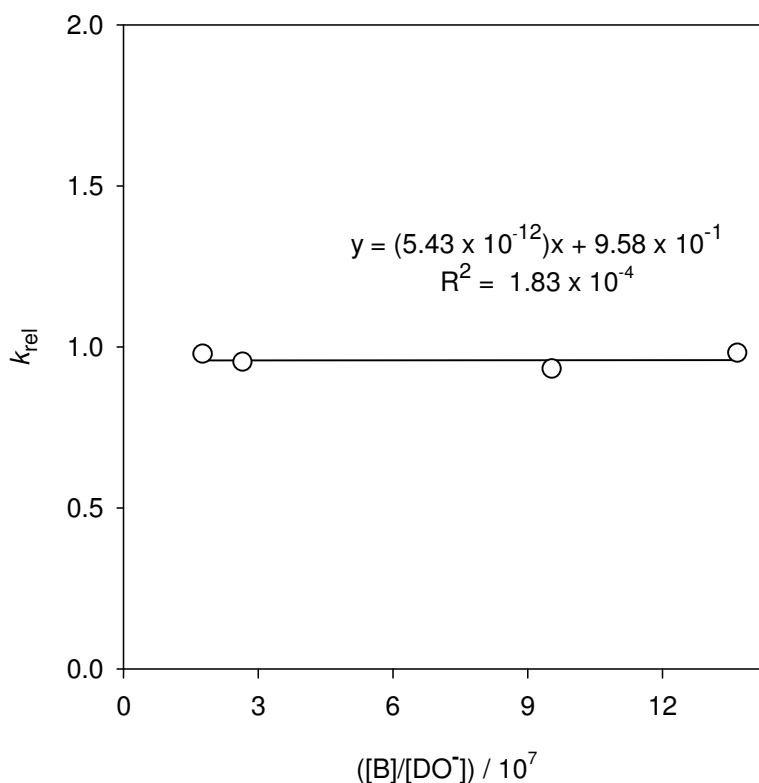
$$k_{\text{rel}} = \frac{k_{\text{obs}}}{k_{\text{DO}}[\text{DO}^-]} = 1 + \frac{k_{\text{B}}[\text{B}]}{k_{\text{DO}}[\text{DO}^-]} \quad \text{(Equation 3.9)}$$

In this case, the values obtained for k_{rel} are approximately unity at each buffer concentration. As the value for k_{rel} changes little over a large range in buffer concentration it can be concluded that there is no buffer catalysis of exchange occurring in the deuterioxide catalysed exchange reaction of triazolium ion (179).

Table 3.8: Ratio of first-order rate constants (k_{rel}) for the deprotonation of triazolium ion (179) in acetic acid buffers relative to un-buffered deuterioxide solution at 25 °C and I = 1.0 (KCl).

$[\text{B}]^{\text{a}}$ (M)	$([\text{B}]/[\text{DO}^-])^{\text{b}}$	$k_{\text{obs}}^{\text{c}}$ (s^{-1})	$k_{\text{rel}}^{\text{d}}$
0.005	9.56×10^7	3.14×10^{-3}	0.929
0.0075	1.37×10^8	3.46×10^{-3}	0.978
0.01	1.78×10^7	3.53×10^{-3}	0.975
0.015	2.68×10^7	3.44×10^{-3}	0.950

(a) The concentration of acetate ion (free base) form of buffer. (b) Ratio of concentrations of acetate free base to deuterioxide ion (c) Observed pseudo first-order rate constant for exchange at a given acetic acid buffer concentration at pD 4.47. (d) k_{rel} is the ratio of observed first-order rate constant for exchange in acetic acid buffer at pD 4.47, (k_{obs}), and the first-order rate of deuterioxide ion-catalysed exchange only ($k_{\text{DO}}[\text{DO}^-]$), calculated using Equation 3.9. In this case $k_{\text{DO}} = 6.46 \times 10^7 \text{ M}^{-1}\text{s}^{-1}$.

Figure 3.7: Plot of the ratio of rate constants k_{rel} against $([B]/[DO^-])$.

Shown in Figure 3.7 is a plot of k_{rel} values against the ratio of buffer to deuterioxide ion concentration. The slope of this plot should be the ratio of the second-order rate constants for the general base and deuterioxide ion-catalysed exchange, k_B/k_{DO} according to Equation 3.9 and the y-axis intercept should be unity. The slope of this plot is small in comparison to the increase in buffer concentration which indicates that general base catalysis of exchange is not significant. This is judged to be the case for all azolium ions (179)-(182) as previous studies on imidazolium ions have shown this to be the case.

As buffer catalysis is not significant Equation 3.8 may be simplified to Equation 3.10.

$$k_{obs} = k_{D_2O} + k_{DO}[DO^-] \quad \text{(Equation 3.10)}$$

The second-order rate constant for deuterioxide ion-catalysed exchange may be obtained as the slope of a plot of k_{obs} values against the concentration of deuterioxide

ion. A significant non-zero y-axis intercept of these plots could be assigned to an uncatalysed solvent reaction.

Second-order plots for triazolium ions (179)-(182) are given in Figures 3.8-3.11. The slopes (k_{DO} values) and intercepts (assigned as k_{D2O} values) are summarised in Table 3.9.

Figure 3.8: Plot of k_{obs} against $[DO^-]$ for the H/D exchange reaction of triazolium ion (179) in D_2O at 25 °C and $I = 1.0$ (KCl).

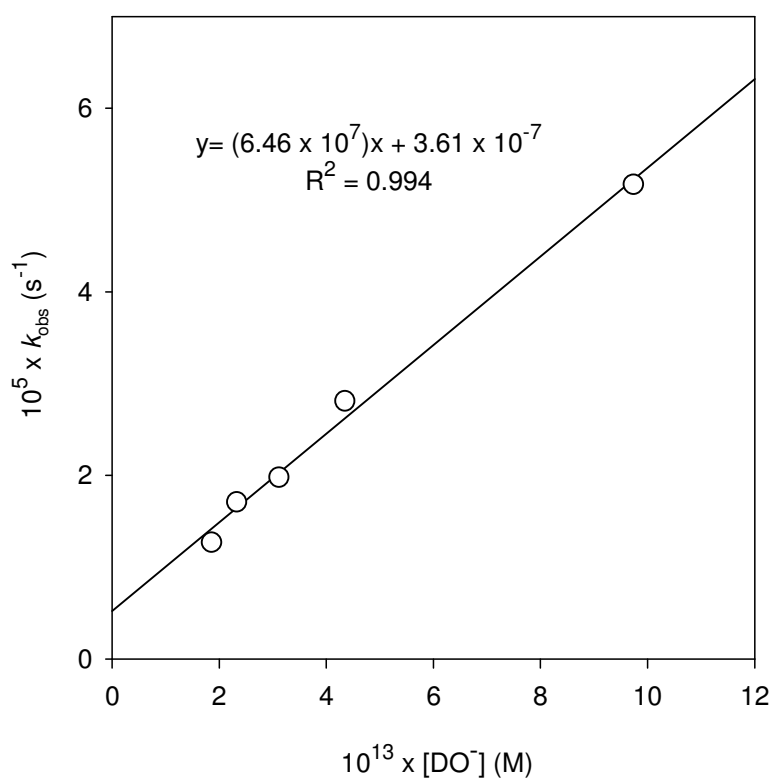


Figure 3.9: Plot of k_{obs} against $[\text{DO}^-]$ for the H/D exchange reaction of triazolium ion (180) in D_2O at 25°C and $I = 1.0$ (KCl).

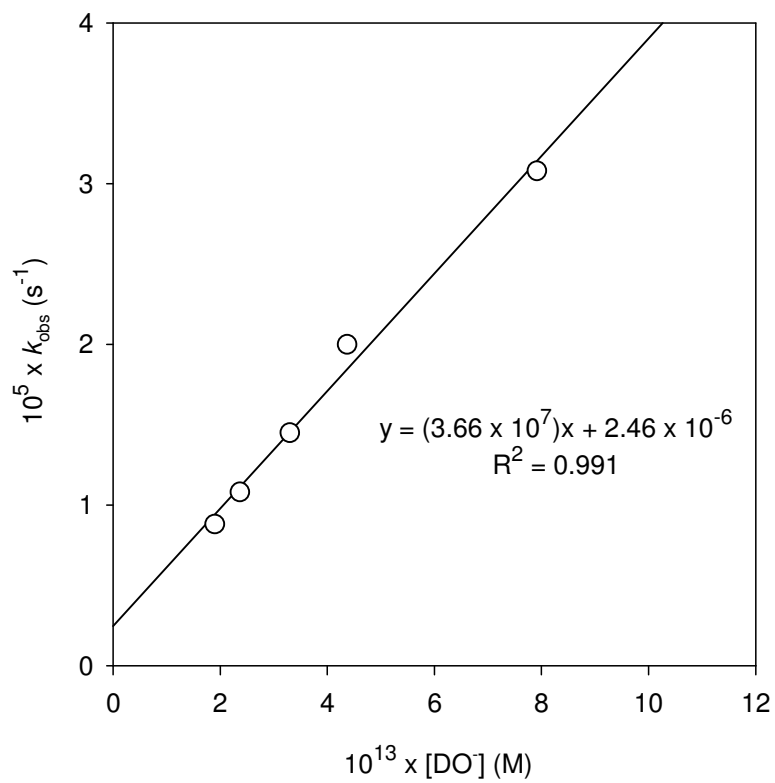


Figure 3.10: Plot of k_{obs} against $[\text{DO}^-]$ for the H/D exchange reaction of triazolium ion (181) in D_2O at $25\text{ }^\circ\text{C}$ and $I = 1.0$ (KCl).

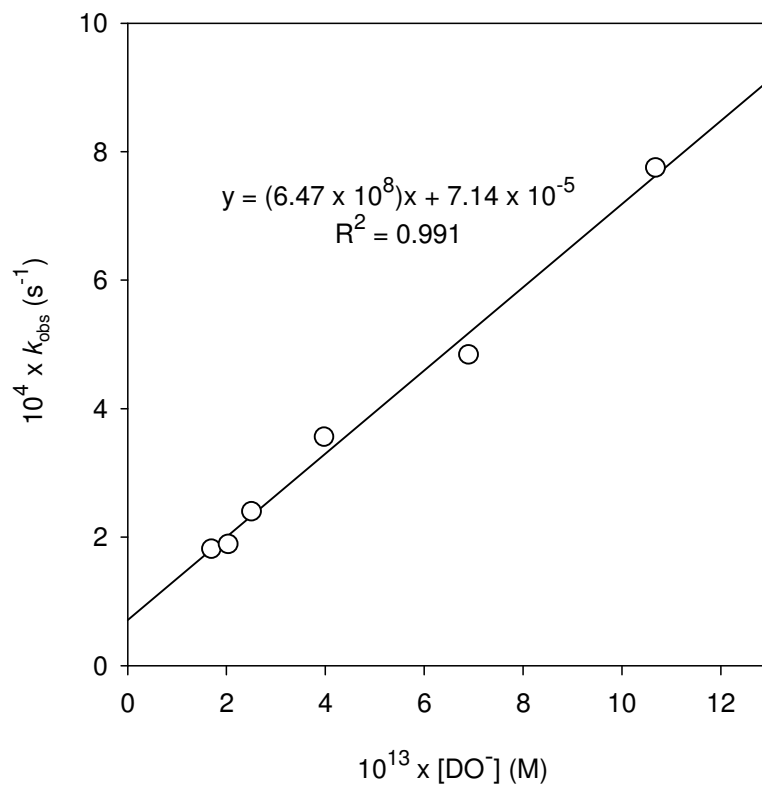
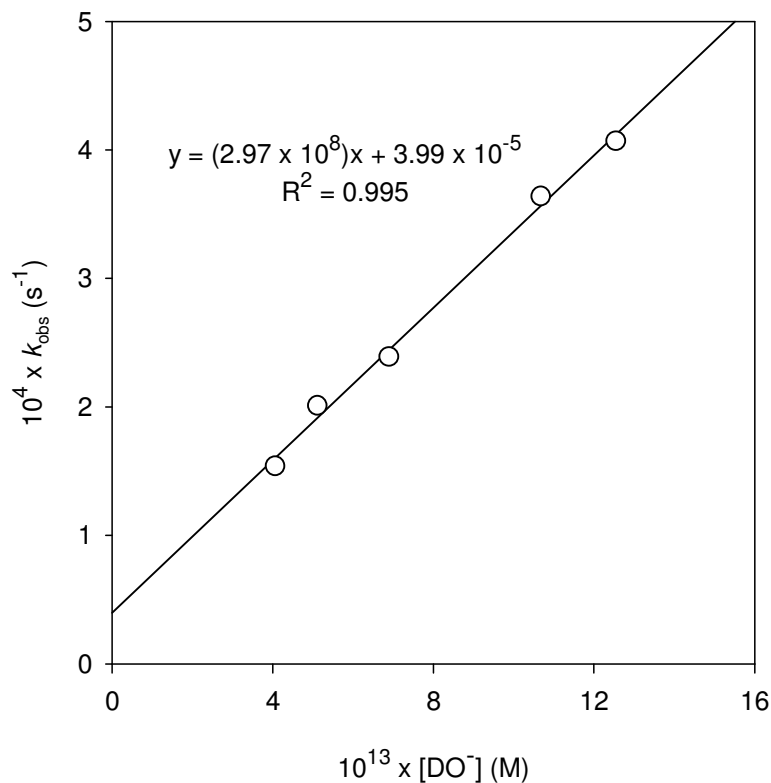


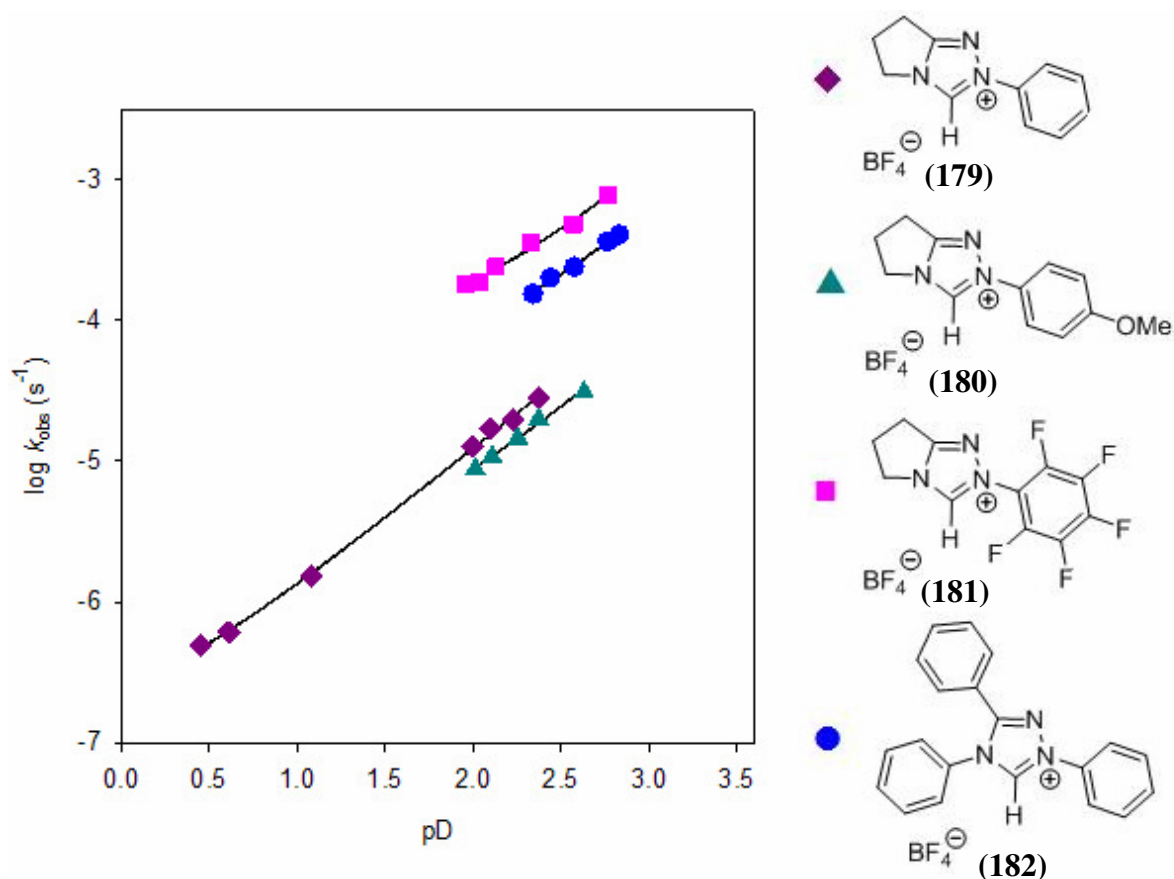
Figure 3.11: Plot of k_{obs} against $[\text{DO}^-]$ for the H/D exchange reaction of triazolium ion (182) in D_2O at 25 °C and $I = 1.0$ (KCl).**Table 3.9:** Rate constants for exchange of the C3-H of triazolium ions (179)-(182) for deuterium in D_2O at 25 °C and $I = 1.0$ (KCl).

	Substrate	$k_{\text{DO}} \text{ (M}^{-1}\text{s}^{-1}\text{)}^{\text{a}}$	$k_{\text{D}_2\text{O}} \text{ (s}^{-1}\text{)}^{\text{b}}$
	$\text{R}^1 = \text{phenyl (179)}$	6.46×10^7	3.61×10^{-7}
	$\text{R}^1 = p\text{-methoxyphenyl (180)}$	3.66×10^7	2.46×10^{-6}
	$\text{R}^1 = \text{pentafluorophenyl (181)}$	6.47×10^8	7.14×10^{-5}
	$\text{R}^2 = \text{phenyl (182)}$	2.97×10^8	3.99×10^{-5}

(a) The value of the second-order rate constant, (k_{DO}), was obtained as the slope of the plot of k_{obs} against $[\text{DO}^-]$ in Figures 3.8-3.11. (b) $k_{\text{D}_2\text{O}}$ was obtained as the y-axis intercept of the plot of k_{obs} against $[\text{DO}^-]$ in Figures 3.8-3.11.

Values of k_{DO} ($\text{M}^{-1}\text{s}^{-1}$) and $k_{\text{D}_2\text{O}}$ (s^{-1}) may also be estimated from pD-rate profiles for deuterioxide ion-catalysed exchange (Figure 3.12)

Figure 3.12: pD-rate profile for the deuterium exchange reaction of triazolium ions (179)-(182) in D_2O at 25°C and $I = 1.0$ (KCl).

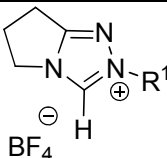
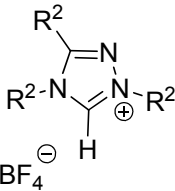


Estimates of the second-order rate constant for deuterioxide ion-catalysed exchange k_{DO} ($\text{M}^{-1}\text{s}^{-1}$), and the first-order rate constant for the solvent reaction, $k_{\text{D}_2\text{O}}$ (s^{-1}), were obtained by non-linear least squares analysis. The experimental data, shown as (◆), (▲), (■), and (●) for triazolium ions (179)-(182) respectively, was fitted to Equation 3.11 where $x = \text{pD} - 14.87$. The pK for the auto-ionisation of D_2O is 14.87.

$$F = \log k_{\text{obs}} = \log[(k_{\text{DO}}10^x/\gamma_{\text{DO}}) + k_{\text{D}_2\text{O}}] \quad (\text{Equation 3.11})$$

Values of k_{DO} ($\text{M}^{-1}\text{s}^{-1}$) and $k_{\text{D}_2\text{O}}$ (s^{-1}) for deuterioxide ion-catalysed exchange obtained from non-linear least squares analysis are shown in Table 3.10. The standard errors of the estimates are quoted in parentheses below each value.

Table 3.10: Rate constants for exchange of the C3-H of triazolium ions (**179**)-(**182**) for deuterium in D_2O at 25 °C and $I = 1.0$ (KCl).

	Substrate	k_{DO} ($M^{-1}s^{-1}$) ^a	k_{D2O} (s^{-1}) ^b
	$R^1 = \text{phenyl}$ (179)	6.58×10^7 (1.92×10^6)	1.28×10^{-7} (2.61×10^{-8})
	$R^1 = p\text{-methoxyphenyl}$ (180)	3.91×10^7 (2.51×10^6)	1.54×10^{-6} (7.45×10^{-7})
	$R^1 = \text{pentafluorophenyl}$ (181)	6.16×10^8 (4.35×10^7)	7.84×10^{-5} (1.36×10^{-5})
	$R^2 = \text{phenyl}$ (182)	2.93×10^8 (1.71×10^7)	4.09×10^{-5} (1.10×10^{-5})

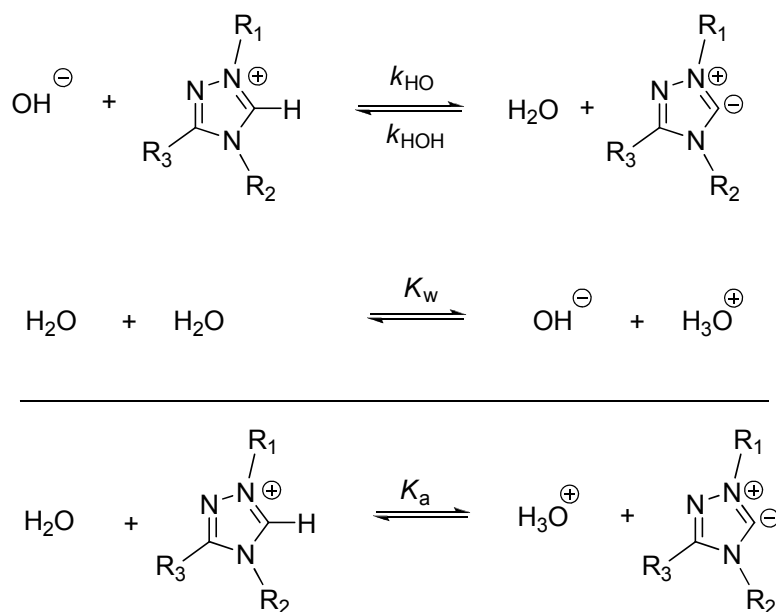
(a) The value of the second-order rate constant, k_{DO} , was obtained from non-linear least squares analysis of pD-rate profiles in Figure 3.12 using Equation 3.11. (b) The value of the first-order rate constant for the solvent reaction, k_{D2O} , was obtained non-linear least squares analysis of pD-rate profiles in Figure 3.12 using Equation 3.11.

3.2.3 Estimation of k_{HO} and pK_a values.

The second-order rate constants for deuterioxide ion-catalysed exchange k_{DO} ($M^{-1}s^{-1}$) in Section 3.2.2 can be used to estimate pK_a values for the triazolium ions studied by providing access to k_{HO} values for hydroxide ion-catalysed deprotonation (Scheme 3.7).

Combining the reaction of triazolium ions and hydroxide ion with the self-ionisation of water, provides us with the acidity of azolium ions relative to hydronium ion. This can then be related to the rate constants k_{HO} , k_{H_2O} and K_a (Equation. 3.12).

Scheme 3.7:



$$pK_a = pK_w + \log\left(\frac{k_{HOH}}{k_{HO}}\right) \quad \text{(Equation 3.12)}$$

Scheme 3.6 highlighted the different microscopic steps for deuterioxide ion-catalysed exchange. The lack of detectable buffer catalysis of exchange indicates that the solvent reorganisation step is rate-determining for the overall deuterioxide ion-catalysed reaction. If the initial proton transfer step was rate-determining, then buffer catalysis of exchange would be observed. However there is no mechanism by which Brønsted bases may lower the barrier to solvent reorganisation. Thus proton transfer occurs as a

pre-equilibrium and is not rate-limiting. The secondary solvent isotope effect relationship, $k_{D_2O}/k_{H_2O} = 2.4$, may thus be applied where proton transfer occurs in a pre-equilibrium. In this way, the values of k_{H_2O} can be obtained from the experimental k_{D_2O} values. This secondary solvent isotope effect results from the higher basicity of deuterioxide ion in D_2O , compared to hydroxide ion in H_2O . Further, the “Principle of microscopic reversibility” dictates that the reverse reprotonation of the carbene by water (Scheme 3.6) is also limited by solvent reorganisation if this step is limiting in the forward direction.

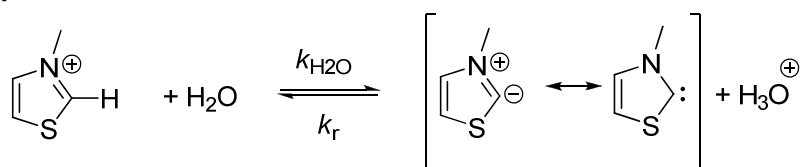
The rate constant for the reorganisation of solvent k_{reorg} , has been estimated to be equal to that for the dielectric relaxation of water, 10^{11} s^{-1} . Thus the rate constant for reprotonation of the carbene or ylide by water, k_{HOH} , may be equated with the rate constant for solvent reorganisation according to Equation 3.13.

$$k_{HOH} = k_{reorg} \approx 10^{11} \text{ s}^{-1} \quad \text{(Equation 3.13)}$$

The pK_a value is estimated by combining the value for the reverse protonation of the carbene by water, k_{H_2O} , with the value for k_{HO} , according to Equation 3.12. The term pK_w is derived from the ion product of water, $K_w = 10^{-14} \text{ M}^2$, and hence $pK_w = 14$.

In an investigation of H/D exchange reactions of thiazolium salts, Washabaugh and Jencks estimated pK_a values using $k_{H_2O} (\text{s}^{-1})$, the first-order rate constant for the solvent reaction (Scheme 3.8).

Scheme 3.8:



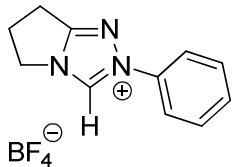
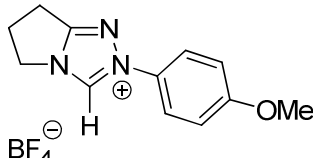
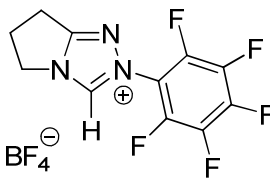
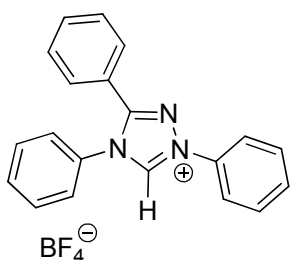
A further estimate of the acidity of triazolium ions could be obtained by using the intercepts of second-order plots for deuterioxide ion-catalysed exchange (assigned as k_{D_2O} values). A secondary solvent isotope effect of $k_{H_2O}/k_{D_2O} = 2.6$ may be applied to obtain values of k_{H_2O} from the experimental k_{D_2O} values.

A value of $k_r = 2 \times 10^{10} \text{ M}^{-1}\text{s}^{-1}$ was assumed for the diffusion-controlled reaction in the reverse direction (Equation 3.14) which is the protonation of the carbene by hydronium ion.

$$K_a = \frac{k_{\text{H}_2\text{O}}}{k_r} \quad \text{(Equation 3.14)}$$

The resulting estimated pK_a values for triazolium ions **(179)**-**(182)** are shown in Table 3.11.

Table 3.11: Kinetic and thermodynamic acidities of the C3-H of triazolium ions (179)-(182) in water at 25 °C and I = 1.0 (KCl).

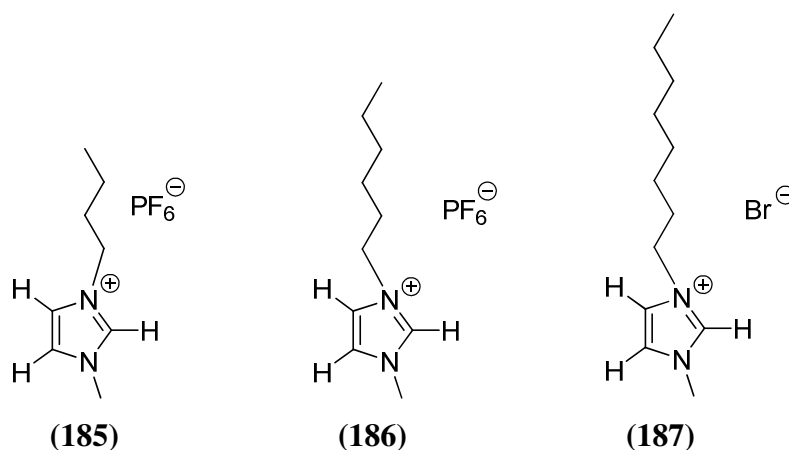
Triazolium ion	k_{DO} ($M^{-1}s^{-1}$)	k_{HO}^c ($M^{-1}s^{-1}$)	pK_a^d (DO^-)	k_{D_2O} (s^{-1})	$k_{H_2O}^g$ (s^{-1})	pK_a^h (D_2O)
 (179)	6.46×10^7 ^a	2.69×10^7	17.6	3.61×10^{-7e}	9.39×10^{-7}	16.3
	6.58×10^7 ^b	2.74×10^7	17.6	1.28×10^{-7f}	3.33×10^{-7}	16.8
 (180)	3.66×10^7 ^a	1.53×10^7	17.8	2.46×10^{-6e}	6.40×10^{-6}	15.5
	3.91×10^7 ^b	1.63×10^7	17.8	1.54×10^{-6f}	4.00×10^{-6}	15.7
 (181)	6.47×10^8 ^a	2.70×10^8	16.6	7.14×10^{-5e}	1.86×10^{-4}	14.0
	6.16×10^8 ^b	2.57×10^8	16.6	7.84×10^{-5f}	2.04×10^{-4}	14.0
 (182)	2.97×10^8 ^a	1.24×10^8	16.9	3.99×10^{-5e}	1.04×10^{-4}	14.3
	2.93×10^8 ^b	1.22×10^8	16.9	4.09×10^{-5f}	1.06×10^{-4}	14.3

(a) Second-order rate constant for deprotonation of the substrate ion at C3 by deuterioxide ion in D_2O obtained as the slope of second-order plots for H/D exchange. (b) Second-order rate constant for deprotonation of the substrate ion at C3 by deuterioxide ion in D_2O obtained from non-linear least squares analysis of the pD-rate profile for H/D exchange. (c) Second-order rate constants for deprotonation of substrate at C3 by hydroxide ion in H_2O , calculated from the experimental value for k_{DO} , using an estimated secondary solvent isotope effect of $k_{DO}/k_{HO} = 2.4$ (see text). (d) Carbon acid pK_a for ionisation of the substrate ion at C3 in H_2O , calculated using Equation 3.12 (see text). The estimated error is ± 0.5 . (e) First-order rate constant for deprotonation of the substrate ion at C3 by solvent D_2O obtained as the intercept of second-order plots for H/D exchange. (f) First-order rate constant for deprotonation of the substrate ion at C3 by solvent D_2O obtained from non-linear least squares analysis of pD-rate profiles for H/D exchange. (g) First-order rate constants for deprotonation of substrate at C3 by solvent H_2O ,

calculated from the experimental value for k_{D_2O} , using an estimated secondary solvent isotope effect of $k_{H_2O}/k_{D_2O} = 2.6$ (see text). (h) Carbon acid pK_a value of substrate ion at C3 in H_2O , calculated using Equation 3.14 (see text).

3.2.4 Deuterium exchange reactions of imidazolium ions followed by 1H NMR spectroscopy.

The H/D exchange reactions of imidazolium ions (**185**)-(**187**) were analysed by 400 MHz 1H spectroscopy in an analogous manner to measurements conducted on triazolium ions as discussed in Section 3.2.1. The disappearance of the C2-H in D_2O solution was monitored at 25 °C and $I = 1.0$ (KCl). From these data, first and second-order rate constants for deprotonation of substrate by deuterioxide ion to give the corresponding carbenes could be estimated.



The mechanism for exchange of the C2-H of imidazolium ions (**185**)-(**187**) for deuterium is shown in Scheme 3.6 ($X = C$).

The progress of the deuterium exchange reactions for imidazolium ions (**185**)-(**187**) was determined from the integrated areas of the singlet at 8.6 ppm, due to the C2-H of the substrate over time in relation to the integration of a peak at 3.15 ppm due to the twelve non-exchanging hydrogens of the internal standard (tetramethylammonium deuteriosulfate). By comparison there was no detectable change in the areas of the peaks due to the protons on the saturated ring relative to the standard peak with time.

The fraction of substrate remaining $f(s)$, and the observed pseudo-first-order rate constant for exchange of the C2-H of imidazolium ions (**185**)-(**187**) is determined from Equation 3.15 and Equation 3.6 respectively.

$$f(s) = \frac{(A_{C2-H}/A_{Std})_t}{(A_{C2-H}/A_{Std})_{t=0}} \quad \text{(Equation 3.15)}$$

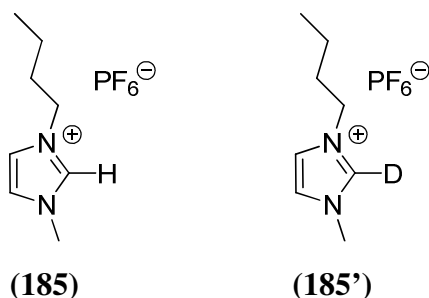
As shown in Section 3.2.2, this pseudo-first-order rate constant for deuterium exchange could be formally the sum of the first-order rate constants for exchange catalysed by solvent, deuterioxide ion and also buffer base for those reactions performed in buffers.

The buffer term, $k_B[\text{Buffer}]$, will be neglected as it has been shown that phosphate buffers do not catalyse the H/D exchange of a range of substituted azolium ions.⁹⁵, Section 3.2.2.

The value for deprotonation by solvent water, k_{D_2O} , is expected to be much lower than the other contributory terms and will also be neglected. For the case of analogous thiazolium ions, a value of $k_{D_2O} \sim 1.5 \times 10^{-8} \text{ s}^{-1}$ was estimated by Washabaugh and Jencks.³ Typically we have found that second-order rate constants for deuterioxide ion-catalysed exchange ($k_{DO} \text{ M}^{-1} \text{ s}^{-1}$) of imidazolium ions are 20 – 8000 fold slower than for the corresponding thiazolium ions. On that basis we could predict that the contribution of k_{D_2O} for imidazolium ions (**185**)-(**187**) to the overall rate of exchange is not significant. Therefore in the present discussion, $k_{\text{obs}} (\text{s}^{-1})$ may be simplified as in Equation 3.16 where $k_{DO} (\text{M}^{-1}\text{s}^{-1})$ is the second-order rate constant for deuterioxide ion-catalysed exchange and $[\text{DO}^-] (\text{M})$ is the concentration of deuterioxide ion.

$$k_{\text{obs}} = k_{DO}[\text{DO}^-] \quad \text{(Equation 3.16)}$$

The second-order rate constant for exchange of the C2-H for deuterium, catalysed by deuterioxide ion, $k_{DO} (\text{M}^{-1}\text{s}^{-1})$, may then be obtained as the slope of the plot of k_{obs} against deuterioxide ion concentration.

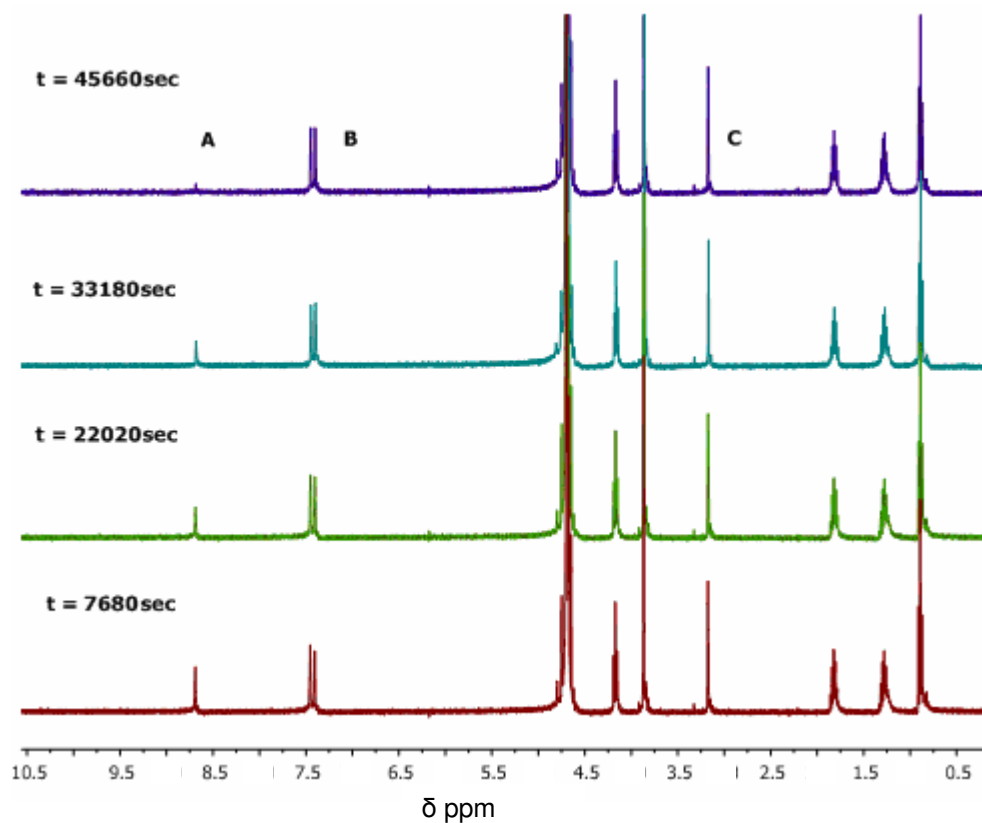
3.2.4.1 1-Butyl-3-methylimidazolium hexafluorophosphate (185).

Rate constants for deuterioxide ion-catalysed H/D exchange of the C2-H of imidazolium ion (**185**) to form the corresponding deuterated product (**185'**) were determined by 400 MHz ^1H NMR spectroscopy.

Figure 3.13 shows representative ^1H NMR spectra of (**185**), obtained during the exchange for deuterium of the C2-H in D_2O at 25 °C and $I = 1.0$ (KCl). Deuterium exchange at C2 of (**185**) results in the disappearance of the singlet peak for the C2-H at 8.68 ppm (A). The signals for the C4-H and C5-H appear at 7.44 ppm and 7.39 ppm respectively (B). H/D exchange at C4-H and C5-H was not observed under these experimental conditions as indicated by comparison of the integrated area of C4-H and C5-H peaks against the internal standard peak at 3.15 ppm (C), which remained constant.

There is no change in the total integrated area for the signals due to the C4-H and C5-H or the butyl and methyl hydrogens, during the time course for complete exchange at C2, which shows that deuterium exchange at these positions is negligible under these conditions.

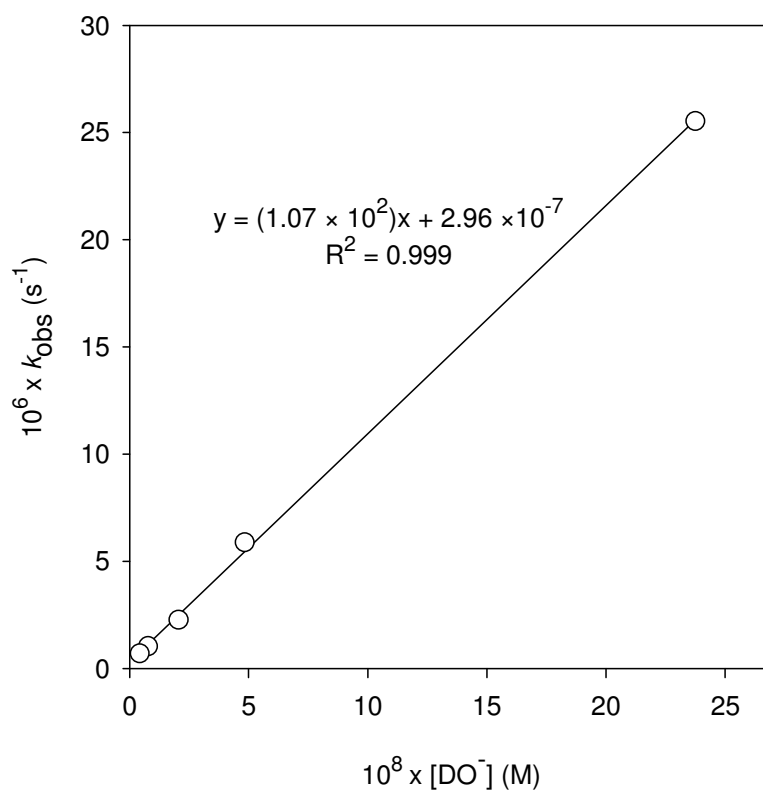
Figure 3.13: Representative ^1H NMR spectra at 400 MHz of imidazolium ion (185) (10 mM, pD 8.12), obtained during exchange of the C2-H for deuterium in D_2O at 25 °C and $I = 1.0$ (KCl). The time elapsed is indicated above each spectrum in seconds.



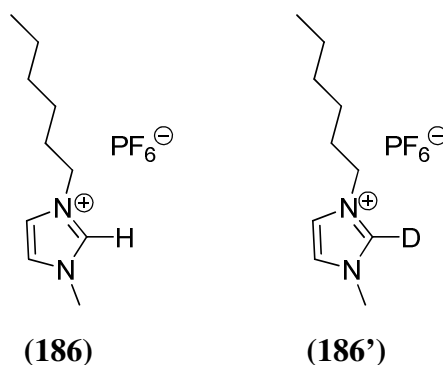
Values for experimental first-order rate constants for deuterium exchange (k_{obs} , s^{-1}) were obtained as the slopes of semi-logarithmic plots of $f(s)$ against time (Appendix D, Figure D4). Reaction data and first-order rate constants k_{obs} (s^{-1}) at different pD values in phosphate buffers are shown in Appendix D (Table D4).

An estimate of $1.07 \times 10^2 \text{ M}^{-1}\text{s}^{-1}$ for k_{DO} , the second-order rate constant for deuterioxide ion-catalysed exchange, was obtained as the slope of the plot of k_{obs} against $[\text{DO}^-]$ (Figure 3.14).

Figure 3.14: Plot of k_{obs} against $[\text{DO}^-]$ for the H/D exchange reaction of imidazolium ion (185) in D_2O at 25°C and $I = 1.0$ (KCl).



3.2.4.2 1-Hexyl-3-methylimidazolium hexafluorophosphate (186).



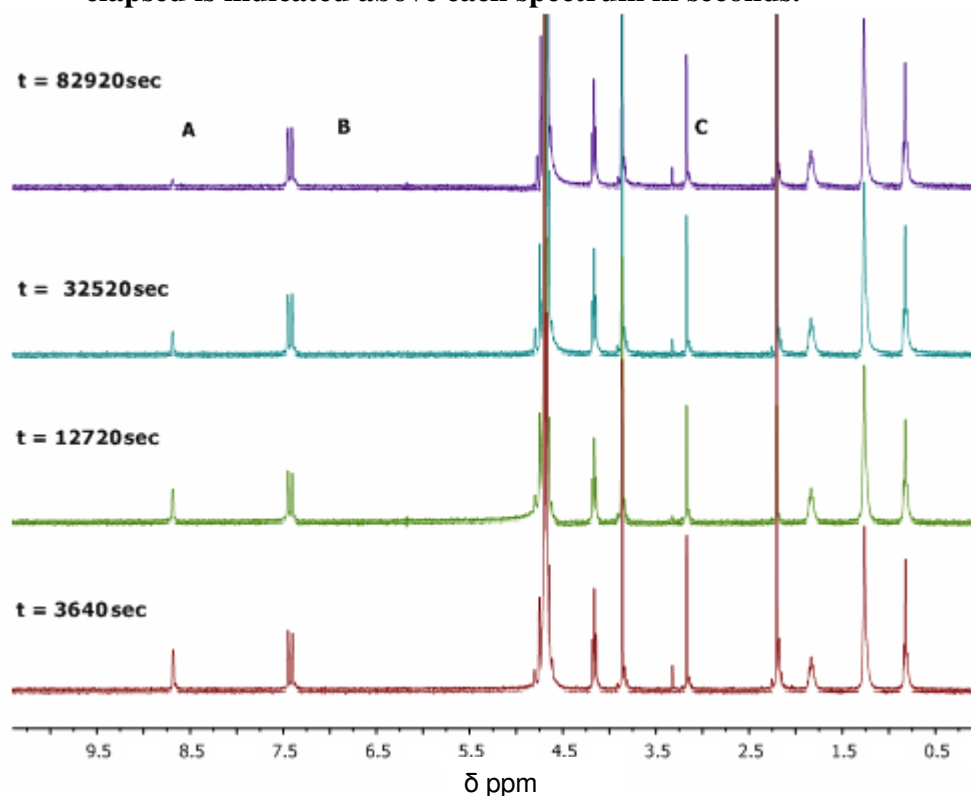
Rate constants for deuterioxide ion-catalysed H/D exchange of the C2-H of imidazolium ion (186) to form the corresponding deuterated product (186') were determined by 400 MHz ^1H NMR spectroscopy.

Figure 3.15 shows representative ^1H NMR spectra of (186) (10 mM, pD 8.12), obtained during the exchange for deuterium of the C2-H in D_2O at 25°C and $I = 1.0$

(KCl). Deuterium exchange at C2 of (**186**) results in the disappearance of the singlet peak for the C2-H at 8.68 ppm (A). The signals for the C4-H and C5-H appear at 7.45 ppm and 7.40 ppm respectively (B). H/D exchange at C4-H and C5-H was not observed under these experimental conditions as indicated by comparison of the C4-H and C5-H against the internal standard peak at 3.16 ppm (C), which remained constant.

There is no change in the total integrated area for the signals due to the C4-H and C5-H or the hexyl and methyl hydrogens, during the time course for almost complete exchange at C2, which shows that deuterium exchange at these positions is negligible under these conditions.

Figure 3.15: Representative ^1H NMR spectra at 400 MHz of imidazolium ion (**186**) (10 mM, pD 8.12), obtained during exchange of the C2-H for deuterium in D_2O at 25 °C and $I = 1.0$ (KCl). The time elapsed is indicated above each spectrum in seconds.

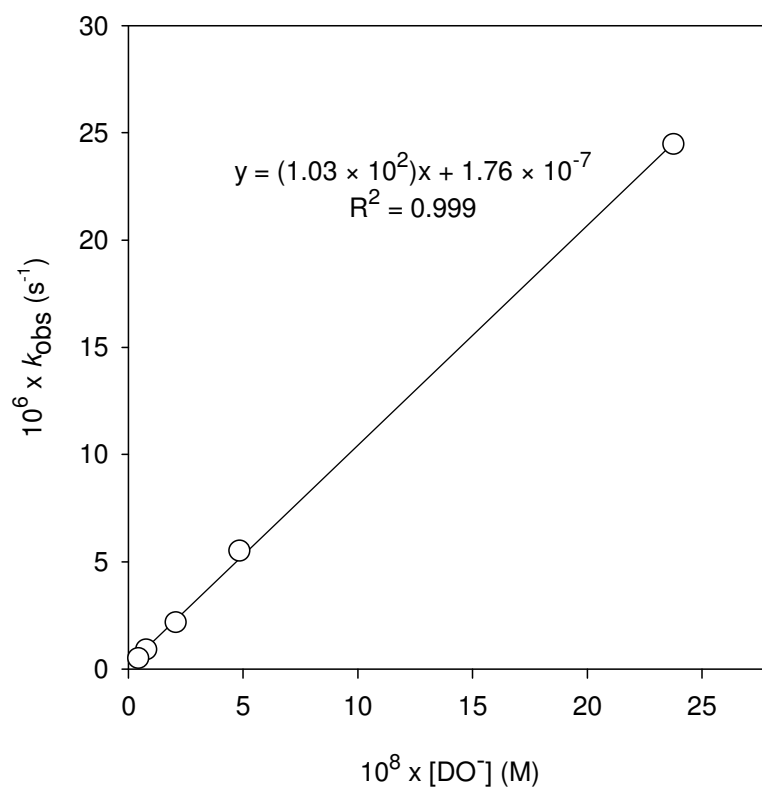


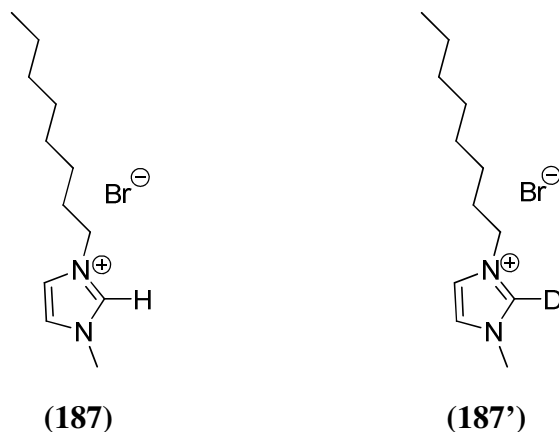
Values for experimental first-order rate constants for deuterium exchange (k_{obs} , s^{-1}) were obtained as the slopes of semi-logarithmic plots of $f(s)$ against time (Appendix D,

Figure D5). Reaction data and first-order rate constants k_{obs} (s^{-1}) at different pD values in phosphate buffers are shown in Appendix D (Table D5).

An estimate of $1.03 \times 10^2 \text{ M}^{-1} \text{ s}^{-1}$ for k_{DO} , the second-order rate constant for deuterioxide ion-catalysed exchange, was obtained as the slope of the plot of k_{obs} against $[\text{DO}^-]$ (Figure 3.16).

Figure 3.16: Plot of k_{obs} against $[\text{DO}^-]$ for the H/D exchange reaction of imidazolium ion (186) in D_2O at 25°C and $I = 1.0$ (KCl).



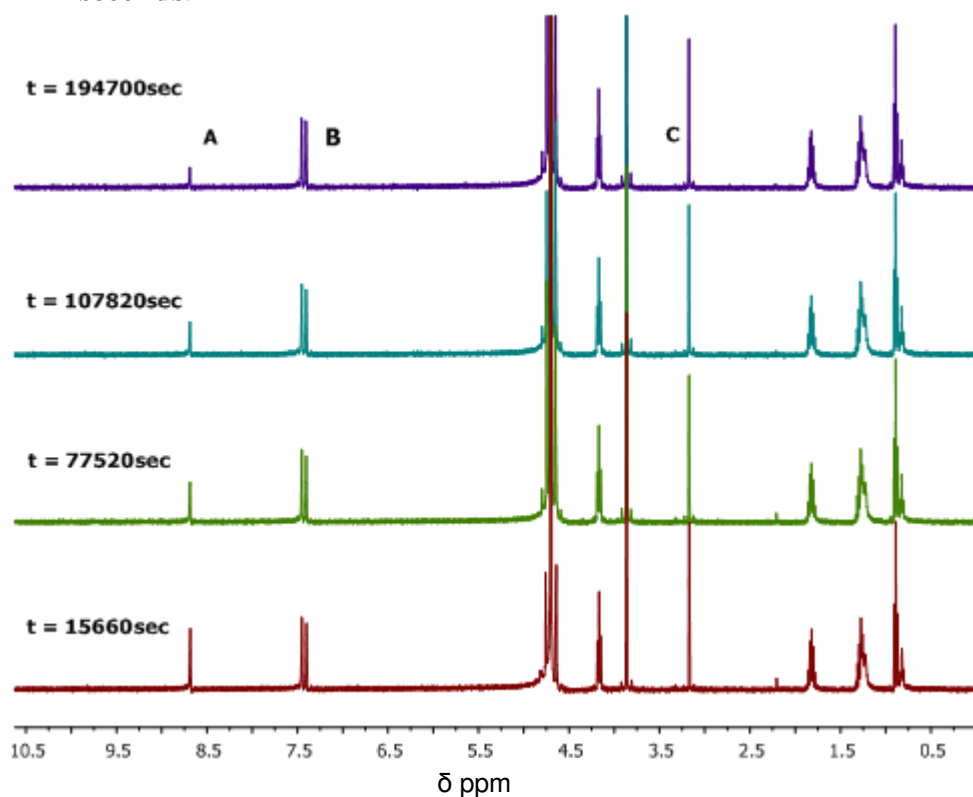
3.2.4.3 1-Octyl-3-methylimidazolium bromide (187).

Rate constants for deuterioxide ion-catalysed H/D exchange of the C2-H of imidazolium ion (**187**) to form the corresponding deuterated product (**187'**) were determined by 400 MHz ^1H NMR spectroscopy.

Figure 3.17 shows representative ^1H NMR spectra of (**187**) (10 mM, pD 7.43), obtained during the exchange for deuterium of the C2-H in D_2O at 25 °C and $I = 1.0$ (KCl). Deuterium exchange at C2 of (**187**) results in the disappearance of the singlet peak for the C2-H at 8.68 ppm (A). The signals for the C4-H and C5-H appear at 7.44 ppm and 7.40 ppm respectively (B). H/D exchange at C4-H and C5-H was not observed under these experimental conditions as indicated by comparison of the C4-H and C5-H against the internal standard peak at 3.17 ppm (C), which remained constant.

There is no change in the total integrated area for the signals due to the C4-H and C5-H or the octyl and methyl hydrogens, during the time course for almost complete exchange at C2, which shows that deuterium exchange at these positions is negligible under these conditions.

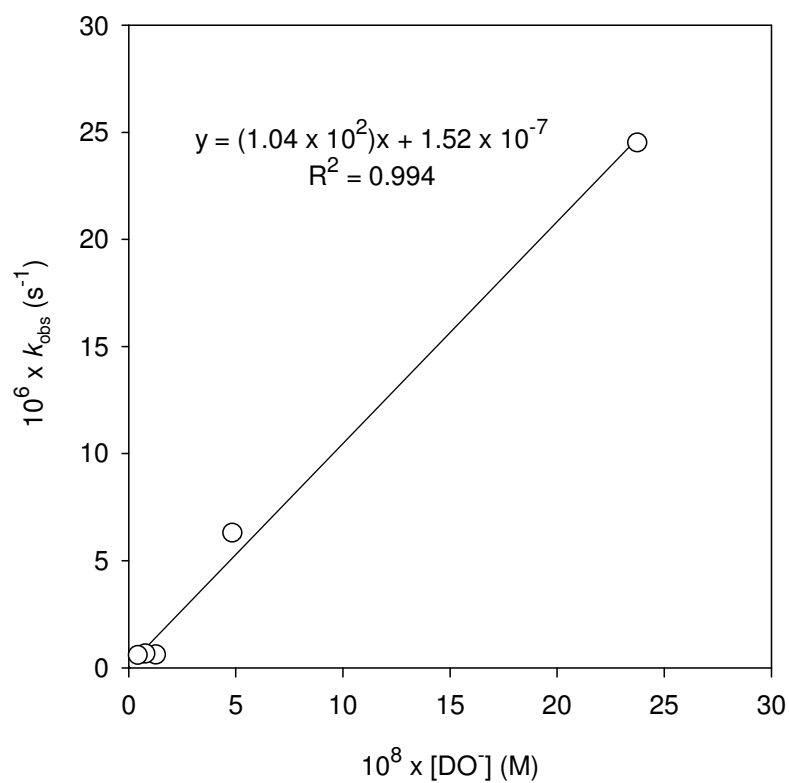
Figure 3.17: Representative ^1H NMR spectra at 400 MHz of imidazolium ion (187) (10 mM, pD 7.43), obtained during exchange of the C2-H for deuterium in phosphate buffers in D_2O at 25 °C and $I = 1.0$ (KCl). The time point elapsed is indicated above each spectrum in seconds.



Values for experimental first-order rate constants for deuterium exchange (k_{obs} , s^{-1}) were obtained as the slopes of semi-logarithmic plots of $f(s)$ against time (Appendix D, Figure D6a-D6b). Reaction data and first-order rate constants k_{obs} (s^{-1}) at different pD values in phosphate buffer are shown in Appendix D (Table D6).

An estimate of $1.04 \times 10^2 \text{ M}^{-1} \text{ s}^{-1}$ for k_{DO} , the second-order rate constant for deuterioxide ion-catalysed exchange, was obtained as the slope of the plot of k_{obs} against $[\text{DO}^-]$ (Figure 3.18).

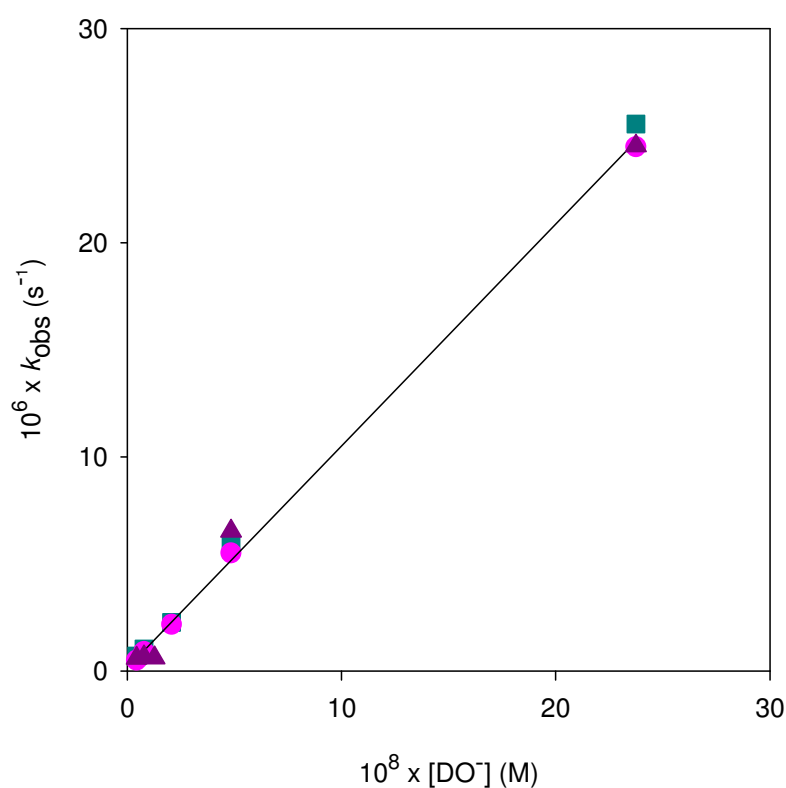
Figure 3.18: Plot of k_{obs} against $[\text{DO}^-]$ for the H/D exchange reaction of imidazolium ion (187) in D_2O at 25°C and $I = 1.0$ (KCl).



3.2.5 Estimation of k_{HO} and pK_a values.

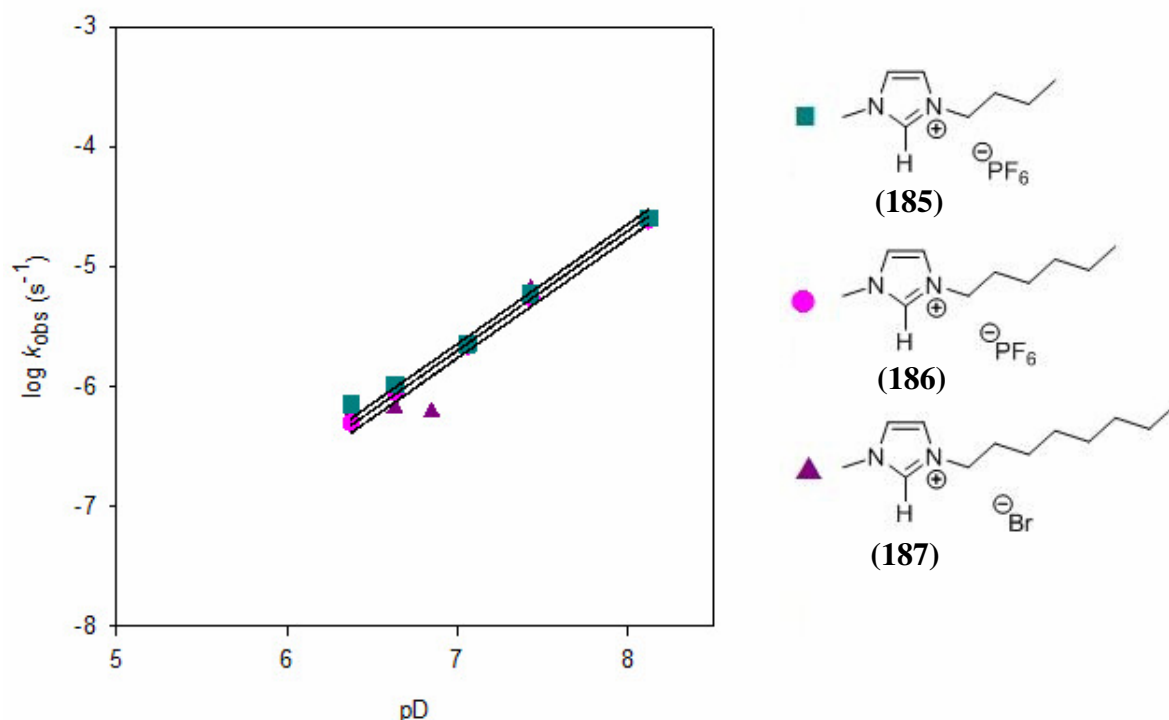
Second-order plots for imidazolium ions (185)-(187) are shown in Figure 3.19. The slopes of these plots give the second-order rate constants, k_{DO} ($M^{-1}s^{-1}$), for deuterioxide ion-catalysed H/D exchange of the C2-H of imidazolium ions (185)-(187).

Figure 3.19: Deuterioxide-rate profile for the deuterium exchange reactions of imidazolium ions (185) (■), (186) (●) and (187) (▲) in D_2O at 25 °C and $I = 1.0$ (KCl).



Values for the second-rate constants for deuterioxide ion-catalysed exchange (k_{DO} $M^{-1}s^{-1}$) may also be estimated by non-linear least squares analysis of pD-rate profiles for deuterium exchange (Figure 3.20).

Figure 3.20: pD-rate profile for deuterium exchange reactions of imidazolium ions (185)-(187) in D_2O at 25 °C and $I = 1$ (KCl).



The experimental data, shown as (■), (●) and (▲) for imidazolium ions (185)-(187) respectively, was fitted to Equation 3.17 where $x = pD - 14.87$.

$$F = \log k_{\text{obs}} = \log(k_{\text{DO}}10^x/\gamma_{\text{DO}}) \quad (\text{Equation 3.17})$$

Values of k_{DO} ($M^{-1}s^{-1}$) obtained from non-linear least squares analysis are shown in Table 3.12 and are in reasonable agreement with those obtained as the slopes of second-order plots for deuterioxide ion-catalysed exchange.

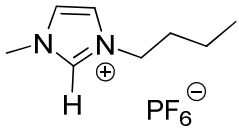
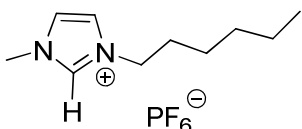
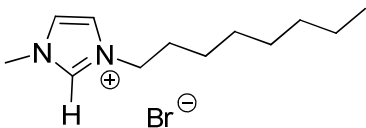
A value for the second-order rate constant for deprotonation of substrate at C3 by hydroxide ion in H_2O , k_{HO} , can be calculated from the corresponding value for deprotonation by deuterioxide ion in D_2O , k_{DO} , using a secondary solvent isotope effect of $k_{\text{DO}}/k_{\text{HO}} = 2.4$ for proton transfer that is limited by the solvent reorganisation step.

As for the triazolium ions, the absence of detectable buffer catalysis of exchange strongly supports the conclusion $k_{\text{HOH}} = k_{\text{reorg}}$ for the protonation of imidazol-2-yl carbenes by solvent water. Investigation into buffer catalysis of exchange for a range of cyclic azolium ions, including imidazolium ions, has shown that the contribution of general base catalysis to the overall exchange reaction is negligible.⁹⁵

Combining values for the second-order rate constant for hydroxide ion-catalysed carbene formation from parent imidazolium ions and the first-order rate constant for the reverse protonation of the carbene conjugate base ($k_{\text{HOH}} = 10^{11} \text{ s}^{-1}$) according to Equation 3.12 yields the pK_a value.

The pK_a values for compounds 1-butyl-3-methylimidazolium hexafluorophosphate (**185**), 1-hexyl-3-methylimidazolium hexafluorophosphate (**186**) and 1-octyl-3-methylimidazolium bromide (**187**) were determined using this method (Table 3.12).

Table 3.12: Kinetic acidities of the C2-H of imidazolium ions (185), (186), and (187) in water at 25 °C and $I = 1.0$ (KCl).

Imidazolium ion	k_{D_2O} ($M^{-1}s^{-1}$)	k_{HO} ($M^{-1}s^{-1}$) ^c	pK_a ^d
 (185)	1.07×10^2 ^a	4.42×10^1	23.3
	1.22×10^2 ^b	5.10×10^1	23.3
 (186)	1.03×10^2 ^a	4.25×10^1	23.4
	1.07×10^2 ^b	4.46×10^1	23.4
 (187)	1.04×10^2 ^a	4.29×10^1	23.4
	9.29×10^1 ^b	3.87×10^1	23.4

(a) Second-order rate constant for deprotonation of the substrate ion at C2 by deuterioxide ion in D_2O obtained as the slope of second-order plots for H/D exchange. (b) Second-order rate constant for deprotonation of the substrate ion at C2 by deuterioxide ion in D_2O obtained from non-linear least squares analysis of pD-rate profiles for H/D exchange. (c) Second-order rate constants for deprotonation of substrate at C2 by hydroxide ion in H_2O , calculated from the experimental value for k_{D_2O} , using an estimated secondary solvent isotope effect of $k_{D_2O}/k_{HO} = 2.4$ (see text). (d) Carbon acid pK_a for ionisation of the substrate ion at C2 in H_2O , calculated using Equation 3.12 (see text). The estimated error is ± 0.5 .

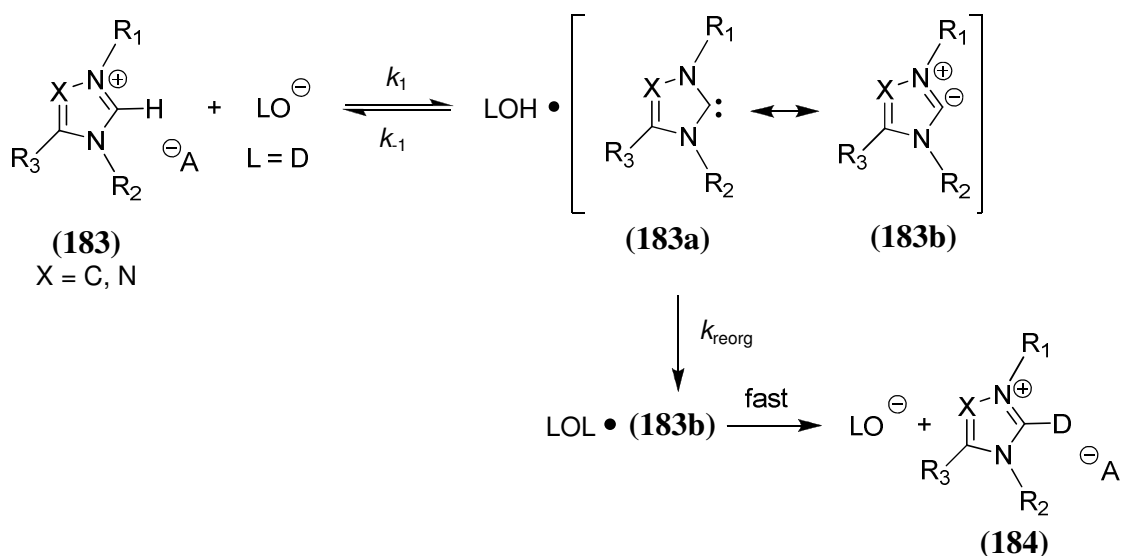
3.3 Discussion.

3.3.1 Deuterium exchange reactions.

Deuterium exchange reactions for all azolium ions were followed by ^1H NMR spectroscopy at 25 °C and ionic strength $I = 1.0$ (KCl) as detailed in Section 3.2. There is no evidence for any hydrolysis of these azolium cations or formation of the corresponding carbene dimers under these experimental conditions.

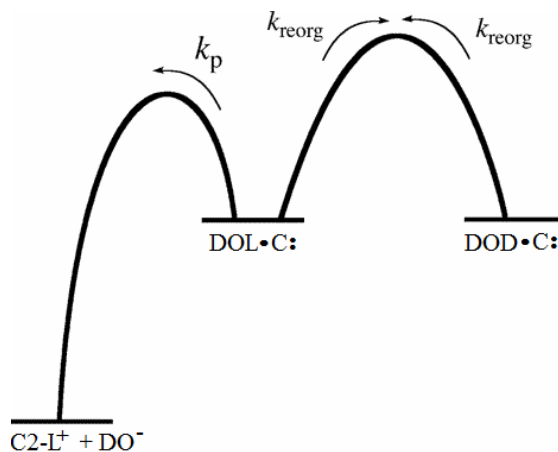
A detailed mechanism for deuterioxide ion-catalysed exchange of azolium ions may be illustrated as in Figure 3.21. In D_2O solution, the deuterioxide base encounters the azolium ion and results in proton abstraction to give an intimate solvated pair.

Figure 3.21:

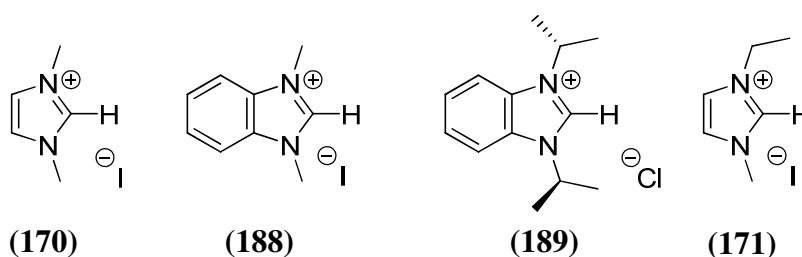


This may react by either of two pathways as shown in Figure 3.22. Firstly, reprotonation by DOH (k_p) may occur, regenerating protonated substrate. A second pathway involves irreversible protonation by D_2O , which initially involves placement of a molecule of DOD in a position to deliver a deuteron to C2 of the carbene complex. The solvent reorganisation step is irreversible and results in an exchange reaction as there is a large excess of solvent deuterium atoms (110 M D in D_2O). The rate constant for solvent reorganisation may be equated to that for the dielectric relaxation of the solvent, $k_{\text{reorg}} \approx 10^{11} \text{ s}^{-1}$.^{95,105,106}

Figure 3.22:



Amyes *et al.*⁹⁵ presented evidence that the solvent reorganisation step is rate-limiting for the above mechanism in the case of deuterium exchange at the C2-H of imidazolium ions. Firstly, no buffer catalysis of deuterium exchange was detected at the C2 of various *N,N*-dialkylated imidazolium ions including (170), (171) and substituted benzimidazolium ions (188) and (189). Rate constants for deuterioxide ion-catalysed exchange at different buffer concentrations and fixed pD were within an estimated 10% experimental error limit, indicating that proton transfer is non-rate-determining. Results from similar buffer catalysis experiments carried out on 1-ethyl-3-methylimidazolium ion (171) in our laboratory⁹⁷ are in agreement with these findings.

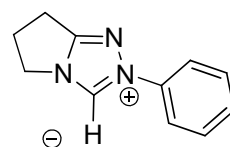


We may also assume that buffer catalysis of exchange will not be observed for the three *N,N*-dialkylated imidazolium ions studied in this work: 1-butyl-3-methylimidazolium hexafluorophosphate (185), 1-hexyl-3-methylimidazolium hexafluorophosphate (186), 1-octyl-3-methylimidazolium bromide (187). The experimental second-order rate constants for deuterioxide ion-catalysed exchange that we determined for imidazolium ions (185)-(187) are lower than the smallest rate constant for 1,3-dimethylimidazolium iodide (170) determined by Amyes *et al.* Thus the reprotonation of the ylides formed from the imidazolium ions (185)-(187) will be

at least as fast as in the case of those formed from the imidazolium ion (**170**) studied by Amyes *et al.*

To date there has been no reported assessment of the presence or extent of buffer catalysis of exchange of 1,2,4-triazolium ions. Our investigation has confirmed the absence of detectable buffer catalysis of exchange for triazolium ions (**179**)-(182) under our experimental conditions Table 3.13.

Table 3.13:

Azolium ion	[Buffer] ^a (M)	pD	[DO ⁻] ^b (M)	k_{obs} ^c (s ⁻¹)	k_{rel} ^d
 (179)	0.005	4.45	5.23×10^{-11}	3.14×10^{-3}	0.929
	0.0075	4.47	5.48×10^{-11}	3.46×10^{-3}	0.978
	0.01	4.48	5.60×10^{-11}	3.53×10^{-3}	0.975
	0.015	4.48	5.60×10^{-11}	3.44×10^{-3}	0.950

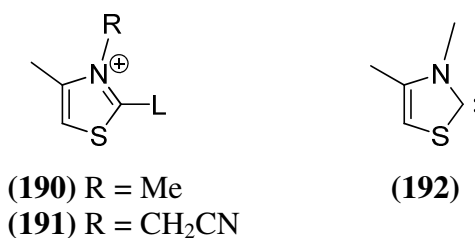
(a) The concentration of acetate anion (free base form of buffer). (b) Concentration of deuterioxide ion at the pD of the experiment, calculated using $[\text{DO}^-] = 10^{(\text{pD} - \text{p}K_w)} / \gamma_{\text{OL}}$ with $\text{p}K_w = 14.87$, where $\gamma_{\text{OL}} = 0.73$ is the activity correction of lyoxide ion under our experimental conditions. (c) k_{obs} is the experimental rate constant for deuterium exchange catalysed by deuterioxide ion at the pD of the experiment in buffered D₂O solution. (d) k_{rel} is the ratio of the observed rate constant for exchange (k_{obs}) and the rate of deuterioxide ion-catalysed exchange only ($k_{\text{DO}}[\text{DO}^-]$), see Equation 3.9 (Section 3.2.2). Using this equation allows for correction for small changes in pD that occur upon dilution at constant ionic strength.

Amyes *et al.*⁹⁵ reported that a two fold increase in the concentration of acetic acid buffer from 50 mM to 100 mM showed a non-significant change ($\pm 10\%$) in k_{ex} (s⁻¹) for 1,3-dimethylimidazolium ion (**170**). The lack of detectable buffer catalysis of exchange indicates that proton transfer occurs in a pre-equilibrium and is not rate-determining.

Similar conclusions may be drawn from the calculated k_{rel} values for triazolium ion (**179**) shown in Table 3.12. There is little variation in the values for k_{rel} for over a large concentration range of acetic acid buffer. This is illustrated by the second-order rate constant of the plot of the ratio of rate constants k_{rel} against ($[\text{B}]/[\text{DO}^-]$) (Figures 3.7). This is good evidence against the presence of buffer catalysis for these azolium ions.

As described in Section 3.2.2, the ratio of first-order rate constants (k_{rel}) is a measure of the relative difference between the observed experimental rate constant (k_{obs}) and the deuterioxide ion-catalysed rate of exchange ($k_{\text{DO}}[\text{DO}^-]$). This ratio should be close to unity in a situation where there is no general base catalysis of exchange. The values obtained for k_{rel} in the cases of the triazolium ion shown in Table 3.12 do not deviate from unity significantly. This confirms the absence of detectable general base catalysis of exchange.

Other significant evidence exists for a rate-determining solvent reorganisation step during H/D exchange of azolium ions. It was concluded in earlier work by Washabaugh and Jencks¹⁰⁷ on analogous deuterium exchange reactions of 3,4-dimethylthiazolium ion (**190**) that reverse protonation by water is limited by the physical encounter of a molecule of HOL (L=H) with the carbene complex. If the proton transfer was rate-determining in deuterioxide ion-catalysed exchange, $k_{\text{H}}/k_{\text{T}}$ and $k_{\text{D}}/k_{\text{T}}$ are maximised and the Swain-Schaad rule is obeyed, a primary kinetic isotope effect of 3.34 would be observed. However, there are only small primary isotope effects of $k_{\text{H}}/k_{\text{T}} = 2.94$ and $k_{\text{D}}/k_{\text{T}} = 1.58$ for hydron transfer from C2 of the 3,4-dimethylthiazolium cation (**190**) (L = H, D, T) to lyoxide ion at 30 °C. These quantities exhibit significant deviation from the Swain-Schaad relationship. As solvent reorganisation becomes more rate-determining relative to deprotonation, internal return of the transferred hydron to the carbon acid becomes more significant and primary kinetic isotope effects deviate from the Swain-Schaad relationship. When solvent reorganisation is entirely rate-determining, k_{-1}/k_{reorg} is high showing that there is significant internal return of the transferred hydron to the carbene ($k_{-1}/k_{\text{reorg}} \approx 3$ for L=H, Scheme 3.22), so the reverse protonation of carbene/ylide by solvent water is limited largely by the physical encounter of a molecule of HOH with the carbene.

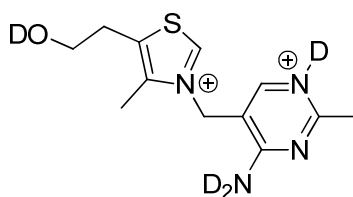


The value of k_{DO} ($\text{M}^{-1}\text{s}^{-1}$) for deprotonation at C2 of the imidazolium analogues of (**190**) in this work and in the work of Amyes *et al.*⁹⁵ are 20 - 8000-fold smaller than

those for deprotonation of thiazolium ions. This implies that imidazol-2-ylidenes are less stable than thiazol-2-ylidenes relative to their azolium ion ground states. Thus deprotonation should be even more limited by the solvent reorganisation step ($k_{-1} > k_{\text{reorg}}$ in Scheme 3.21).

Washabaugh and Jencks¹⁰⁷ also found a systematic increase in the secondary solvent isotope effect for hydron transfer to lyoxide ion from C2 of *N*-substituted 4-methylthiazolium cations with their decreasing reactivity from $k_{\text{DO}}/k_{\text{HO}} = 1.30$ for **(191)** (L = T) to $k_{\text{DO}}/k_{\text{HO}} = 2.35$ for **(190)** (L = T). Therefore, the secondary solvent isotope effect for proton transfer from C2 of the structurally similar but less reactive imidazolium cations to lyoxide ion should be essentially equal to the limiting maximum value of $k_{\text{DO}}/k_{\text{HO}} = 2.4$. This is consistent with proton transfer that is limited by solvent reorganisation with $k_{-1} > k_{\text{reorg}}$ and $k_{\text{HOH}} = k_{\text{reorg}}$.

These studies showed that the second-order rate constants for H/D exchange of related thiazolium ions are on the order of $10^6 \text{ M}^{-1}\text{s}^{-1}$, which is 77-fold slower than the fastest k_{DO} measured for triazolium ion **(181)** in these investigations. Isotope effects have not been measured in this case, however the absence of detectable buffer catalysis for triazolium ion **(179)** is good evidence that the solvent reorganisation step is rate-limiting.

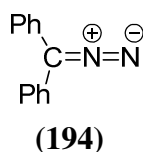


(193)

$$k_{\text{DO}} (\text{M}^{-1}\text{s}^{-1}) = 8.31 \times 10^6$$

Finally, rate constants for proton transfer from several alcohol solvents to singlet diphenylcarbene ($\text{Ph}_2\text{:}$), generated by femtosecond laser flash photolysis of diphenyldiazomethane **(194)**, show a good correlation with solvation time (dielectric reaction time) of the solvent. For example k_{MeOH} was determined to be $1.1 \times 10^{11} \text{ s}^{-1}$ ($\tau = 9 \text{ ps}$) which is very similar to the solvation time of methanol, $\tau_{\text{MeOH}} = 6.8 \text{ ps}$, showing that proton transfer from hydroxylic solvents to highly unstable carbenes is

limited by solvent reorganisation with a rate constant on the order of 10^{11} s^{-1} .

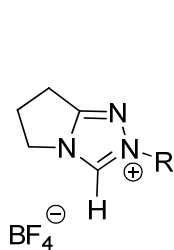


The conclusion that solvent reorganisation is rate-limiting for deuterioxide ion-catalysed exchange at the C2-H of imidazolium ions allows the definition of two vital parameters in the calculation of the corresponding pK_a values. Firstly, the value of k_{HO} may be obtained from the experimental k_{DO} values via the secondary solvent isotope relationship $k_{\text{DO}}/k_{\text{HO}} = 2.4$ where proton transfer is non-rate-determining and occurs in a pre-equilibrium. This solvent isotope effect results from the higher basicity of deuterioxide ion in D_2O compared to hydroxide ion in H_2O . Secondly, the inference that the reverse protonation of these ylides by solvent water is limited by solvent reorganisation permits the assignment of the rate constant for dielectric relaxation of solvent, $k_{\text{reorg}} = 10^{11} \text{ s}^{-1}$ as the rate constant for protonation of the carbenes by water.

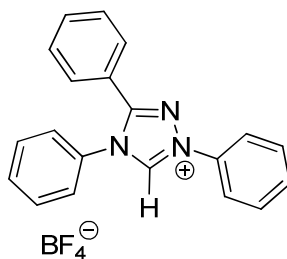
3.3.2 Acidity of 1,2,4-triazolium ions.

3.3.2.1 Substituent effects on kinetic acidities, k_{DO} ($M^{-1}s^{-1}$), of triazolium ions.

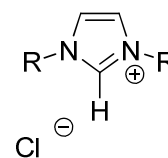
The H/D exchange reactions of azolium ions (**179**)-(**182**) were monitored by 400 MHz and 500 MHz 1H NMR spectroscopy in D_2O solution as described in Section 3.2. The resulting second-order rate constants, k_{DO} ($M^{-1}s^{-1}$) for deuterioxide ion-catalysed exchange of C3-H for deuterium in D_2O solution at 25 °C and $I = 1.0$ (KCl) are as follows: (**179**), 6.46×10^7 ; (**180**), 3.66×10^7 ; (**181**), 6.47×10^8 and (**182**), 2.97×10^8 .



(**179**) R = Ph
 (**180**) R = *p*MeOPh
 (**181**) R = C_6F_5



(**182**)



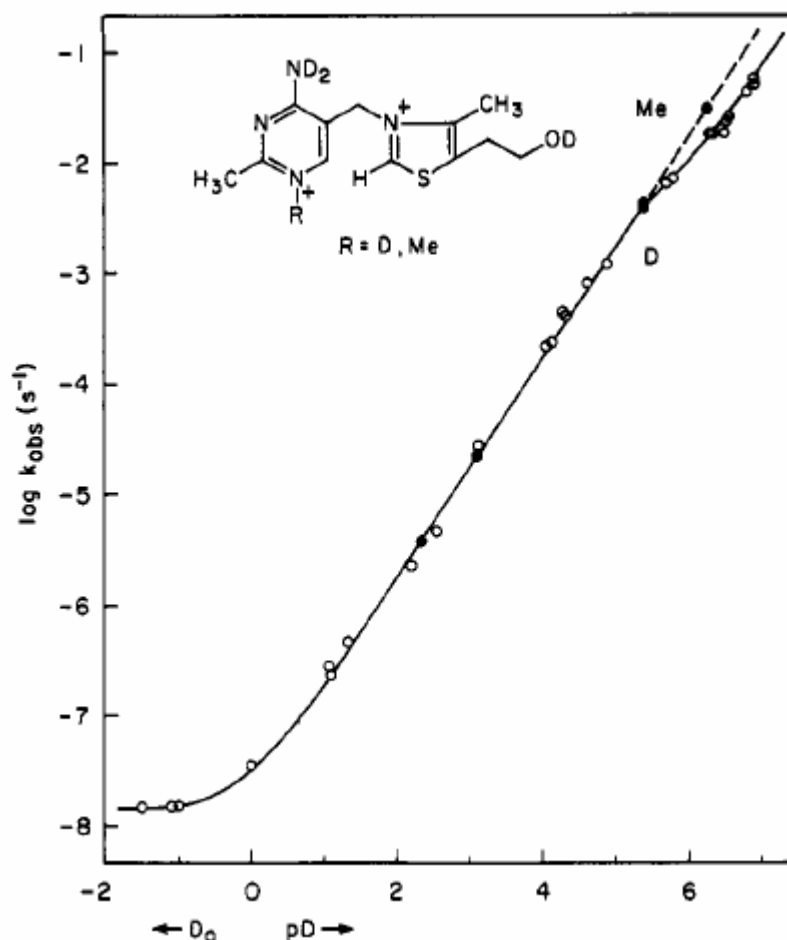
(**195**) R = *p*MeOPh

The second-order rate constant for deuterium exchange of *p*-methoxyphenyl substituted triazolium ion (**180**) shows a 762-fold increase relative to that of 1,3-*bis*(*p*-methoxyphenyl)imidazolium chloride (**195**) ($4.80 \times 10^4 M^{-1}s^{-1}$). This illustrates the increased acidity towards deuterioxide ion observed with more electronegative atoms in the ring. Olofson observed a significant rate enhancement upon introduction of two extra nitrogen atoms to the imidazolium ring such that the rapid base-catalysed exchange reaction of tetrazolium ions had to be monitored in 2 *N* DCl.⁹² This is in accord with our observations of the increased kinetic acidity of triazolium ions (**179**)-(**182**).

Figure 3.23 shows the pD -rate profile obtained by Jencks for H/D exchange reactions of thiamin (**193**) and *N*-methyl thiamin. Upward deviation in the profile at $pD \sim 0$ indicates a change in pathway from pD -independent exchange to deuterioxide ion-catalysed exchange. Use of the Hammett H_0 scale was required to access the pH -independent reaction. Second-order rate constants for deuterioxide ion-catalysed

exchange of triazolium ions measured in this study are ~ 77 -fold greater than rate constants than those determined by Jencks for analogous exchange reactions of thiazolium ions. This is consistent with the trend that introduction of more electronegative atoms into the ring increases kinetic acidity.

Figure 3.23: pD-Rate profile for deuterium exchange of C2-H of thiamin and *N*-methylthiamin in D_2O at 30 °C.

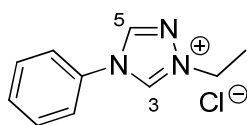


(Reproduced with the permission of ACS publications)

The pD-rate profile for H/D exchange reactions obtained for triazolium ions (**179**)-(**182**) is shown in Figure 3.12. A significant y-axis intercept of second-order plots for deuterioxide ion-catalysed exchange was assigned as k_{D_2O} (s^{-1}), the first-order rate constant for the solvent reaction. There is no clear pD-independent portion as seen by Jencks. However, for triazolium ion (**181**) there is slight levelling off and it is possible that the pD-independent solvent reaction could occur close to this region of the rate profile. Second-order rate constants for deuterioxide ion-catalysed exchange obtained

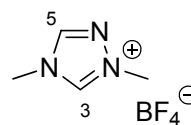
as the slopes of second-order plots for H/D exchange are in excellent agreement with those obtained from non-linear least squares fitting of pD-rate profiles for H/D exchange. First-order rate constants for the solvent reaction obtained as y-axis intercepts of second-order plots differ slightly from those obtained from non-linear least squares analysis of pD-rate profiles. This may be due to the large error involved in extrapolation to the y-axis.

Literature values for the deuterioxide ion-catalysed exchange of the C3-H of 1,2,4-triazolium ions are few. The only relevant values are listed by Schroeder¹⁰⁰ and were obtained through correspondence with another author. The reactions were performed at 31 °C. However no other experimental details were provided and the values were described as preliminary.



(174)

C3	$1.9 \times 10^3 \text{ M}^{-1}\text{s}^{-1}$
C5	$8.6 \times 10^7 \text{ M}^{-1}\text{s}^{-1}$



(175)

C3	$1.0 \times 10^7 \text{ M}^{-1}\text{s}^{-1}$
C5	-

The k_{DO} value obtained for triazolium ion (175) is on the order of those obtained in our studies. In our studies to date, exchange between the positively charged nitrogen and a second nitrogen (C3) has been observed to occur faster than backbone exchange. However, values listed by Schroeder suggest slower exchange at C3 for (174) than that which occurs at C5. The rate constant reported for exchange at C5 for (174) is more consistent with the second-order rate constants we have determined in this study for exchange at C3.

Comparison of the observed k_{DO} values of triazolium ions (179) - (182) shows that the strongly inductively electron-withdrawing pentafluorophenyl increases the k_{DO} value 10-fold compared to relatively weaker inductively electron-withdrawing phenyl group of (179). The effect of increasing the number of phenyl groups on the ring from one (179) to three (182) increases k_{DO} ~5 fold. Electron-withdrawing substituents are

expected to increase to k_{DO} values due to destabilisation of the cationic parent relative to the neutral ylide/carbene. The *p*-methoxyphenyl substituent produces a k_{DO} value which is 1.8 times less than that of the phenyl. The methoxy substituent is electron-donating by resonance but inductively electron-withdrawing. In general, if resonance is possible due to coplanarity, the electron-donating resonance effect will outweigh the inductive electron withdrawing effect of the methoxy substituent. The small decrease in k_{DO} value for the *p*-methoxyphenyl triazolium ion (**180**) relative to the phenyl-substituted triazolium ion (**179**) shows that the resonance effects slightly outweigh inductive effects here although there are no available X-ray crystal structures that could illustrate the degree of planarity between the aryl substituents and the triazole rings.

3.3.2.2 Substituent effects on carbon acid pK_a values of triazolium ions.

Carbon acid pK_a values of triazolium ions (**179**)-(182) were estimated using second-order rate constants for deuterioxide ion-catalysed exchange, k_{DO} ($M^{-1}s^{-1}$), as described in Section 3.2.2. The resulting pK_a values are as follows: (**179**), 17.6; (**180**), 17.8; (**181**), 16.6 and (**182**), 16.9.

The logarithmic pK_a scale reduces the magnitude of substituent effects observed on k_{DO} values. The *p*-methoxyphenyl group has a net electron-donating resonance effect and a small increase in the pK_a value of *p*-methoxy-substituted triazolium ion (**180**) relative to the phenyl-substituted ion (**179**) is observed. This may be due to increased stabilisation of the azolium ion relative to the neutral carbene/ylide. A small decrease in pK_a is observed for the pentafluorophenyl-substituted ion (**181**) relative to the phenyl substituted ion (**179**), which is in accord with an electron-withdrawing substituent effect lowering pK_a values. The pK_a value of (**182**) is lower than that obtained for (**179**). This result is consistent with the trend that aryl substituents decrease the pK_a .

Estimates of the carbon acid pK_a values of triazolium ions were also made using values for k_{D2O} (s^{-1}), the first-order rate constant for C3 deprotonation by D_2O . Although a clear levelling off corresponding to the solvent reaction was not observed in the pD -

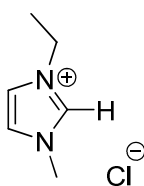
rate profile, significant y-axis intercepts of second-order plots of k_{obs} against the concentration of deuterioxide ion were obtained. These could correspond to a contribution from the solvent reaction and the value of the y-axis intercepts were tentatively assigned as $k_{\text{D}_2\text{O}}$. The resulting estimates of triazolium ion pK_a values differ by 1-2 units from pK_a values derived from $k_{\text{D}_2\text{O}}$ values. There is significant error in extrapolation to the y-axis to obtain $k_{\text{D}_2\text{O}}$ values which is a factor in the large difference in the two estimates. The relative pK_a values along the series (179)-(182) determined from $k_{\text{D}_2\text{O}}$ ($\text{M}^{-1}\text{s}^{-1}$) and $k_{\text{D}_2\text{O}}$ (s^{-1}) values do however exhibit the same trend.

3.3.3 Acidity of imidazolium ions.

3.3.3.1 Substituent effects on kinetic acidities, $k_{\text{D}_2\text{O}}$ ($\text{M}^{-1}\text{s}^{-1}$), of imidazolium ions.

The H/D exchange reactions of imidazolium ions (185)-(187) were monitored by 400 MHz ^1H NMR spectroscopy in D_2O solution as described in Section 3.2.4. The resulting second-order rate constants, $k_{\text{D}_2\text{O}}$ ($\text{M}^{-1}\text{s}^{-1}$) for deuterioxide ion-catalysed exchange of C2-H for deuterium in D_2O solution at 25 °C and $I = 1.0$ (KCl) are as follows: 1-butyl-3-methylimidazolium hexafluorophosphate (185), (1.07×10^2), 1-hexyl-3-methylimidazolium hexafluorophosphate (186), (1.03×10^2) and 1-octyl-3-methylimidazolium bromide (187), (1.04×10^2). These results are essentially identical as they are within experimental error.

There are no literature values for the second-order rate constants for H/D exchange of these azolium salts. The values obtained in this study are, however, consistent with estimates obtained for similar salts.^{95,97} By comparison of these results with the $k_{\text{D}_2\text{O}}$ value for 1-ethyl-3-methylimidazolium chloride (196) ($2.29 \times 10^2 \text{ M}^{-1}\text{s}^{-1}$), the general trend followed is a smaller $k_{\text{D}_2\text{O}}$ value in the presence of longer *N*-alkyl chain substituents.



(196)



(197)

By the Hammond postulate, the transition state for carbene formation should resemble the carbene product for these thermodynamically uphill reactions. Any factor that decreases the stability of the product carbene relative to the conjugate acid imidazolium ion should lead to a decrease in the rate constant for carbene formation. In general, alkyl groups are inductively electron-donating and so are expected to stabilise the positive charge on the nitrogen to which they are attached, so the azolium ion is stabilised relative to the neutral carbene product. This is experimentally evident by a decrease in the k_{DO} value observed upon increasing the length of the alkyl chain. The systematic decrease in observed k_{DO} values appears to correlate with the steric bulk and hydrophobicity of the *N*-substituent. For example, the observed k_{DO} for 1,3-bis(1-adamantyl)imidazolium chloride (**197**) was found to be $1.07 \text{ M}^{-1}\text{s}^{-1}$ which shows a 214-fold decrease relative to that of 1-ethyl-3-methylimidazolium chloride (**196**) ($2.29 \times 10^2 \text{ M}^{-1}\text{s}^{-1}$).⁹⁸ This is potentially a result of the poorer aqueous solvation of the carbene with bulky hydrophobic groups compared with the charged conjugate acid azolium ion. Alternatively, it could be partly a result of the steric repulsion which occurs upon deprotonation at C2, as this would disfavour carbene formation.

3.3.3.2 The effect of counter ion on the kinetic acidity of imidazolium ions.

In non-polar solvents ion pairs are generally closely associated, however in aqueous solution they are fully solvent separated. Thus the effect of the counter ion on the rate constants for H/D exchange is expected to be small as in aqueous solution ion pairs are solvent separated. Also the concentration of counter ion will be hugely diluted by the concentration of chloride ion present to maintain an ionic strength of unity.

Little effect on the second-order rate constant for deuterium exchange was observed upon substitution of counter ion in previous work.^{97,98} For 1-ethyl-3-methylimidazolium ion, a change in counter ion from iodide (**171**) to chloride (**196**) had no effect on the second-order rate constant for deuterium exchange, as the results are identical within the experimental error.

However, upon changing to a larger counter ion such as hexafluorophosphate a small counter ion effect on k_{DO} is observed. Previous work in our laboratory⁹⁷ shows the

value of k_{DO} for 1-butyl-3-methylimidazolium bromide to be $1.64 \times 10^2 \text{ M}^{-1}\text{s}^{-1}$ compared to $1.07 \times 10^2 \text{ M}^{-1}\text{s}^{-1}$ for 1-butyl-3-methylimidazolium hexafluorophosphate (**185**).

3.3.3.3 Substituent effects on carbon acid pK_a values of imidazolium ions.

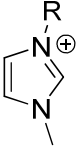
Estimates of the pK_a values of imidazolium ions (**185**)-(**187**) in D_2O solution at 25°C and $I = 1.0$ (KCl) are as follows: 1-butyl-3-methylimidazolium hexafluorophosphate (**185**), (23.3), 1-hexyl-3-methylimidazolium hexafluorophosphate (**186**), (23.4) and 1-octyl-3-methylimidazolium bromide (**187**), (23.4).

As the only variable in Equation 3.12 in the calculation of these pK_a values is k_{HO} , substituent effects that are observed on k_{HO} or k_{DO} will be mirrored in the corresponding pK_a values. The magnitude of the observed substituent effects on pK_a values will be much smaller than on k_{HO} or k_{DO} because of the logarithmic scale of the former. These values are consistent with the general trend that alkyl substituents increase the pK_a .

A pK_a value of 23.0 was determined by Amyes *et al.* for 1,3-dimethylimidazolium iodide (**170**). Previous work in our laboratory gives an estimated pK_a value of 23.0 for 1-ethyl-3-methylimidazolium chloride (**196**) which is identical to that determined for imidazolium ion (**170**), within experimental error. The pK_a values of imidazolium ions (**185**)-(**187**) are essentially identical and show a further increase relative to (**170**). Increasing the steric bulk and hydrophobicity of the *N*-alkyl substituent appears to disfavour carbene formation leading to a decrease in acidity of the imidazolium conjugate acids.

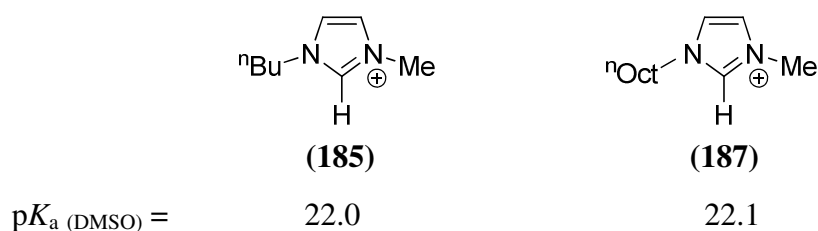
Keeping one *N*-methyl substituent whilst varying the second *N*-substituent from ⁿbutyl, ⁿhexyl to ⁿoctyl has a negligible effect on the value of k_{DO} and resulting pK_a values are identical within experimental error. This is consistent with the findings of Chu *et al.* in a study of the thermodynamic acidities of 1,3-dialkylimidazolium ions in dimethyl sulfoxide (Table 3.14).¹⁰³ By contrast, changing both *N*-substituents to bulkier ^tbutyl or adamantyl substituents decreases k_{DO} values by 200-300 fold and increases the pK_a value by 2-3 units.

Table 3.14: Equilibrium acidities of 1,3-dialkylimidazolium ions in DMSO at 25 °C.

	R	pK_a
 (178)	Me	22.0
	Et	22.1
	ⁿ Bu	22.0
	ⁿ Oct	22.1
	^t Bu	22.6

The aqueous pK_a values determined for imidazolium ions (185)-(187) in this study (23.3-22.4) may be compared to values for *N*-alkyl-substituted thiazolium ions, which are 4-7 units less. Replacement of nitrogen by a less electronegative but more polarisable sulfur increases acidity.

Further comparisons can be made with available literature pK_a values for imidazolium ions in non-aqueous solvents.



The small increase in pK_a value for the ⁿoctyl over ⁿbutyl-substituted imidazolium cation is consistent with our observations of aqueous values. The pK_a values of *N,N*-dialkyl imidazolium cations are similar in water and DMSO with aqueous pK_a values ~ 1 unit higher than the corresponding values determined in DMSO. This increase is likely due to the better stabilisation of the azolium ion in water relative to the carbene/ylide.

3.4 Summary.

As azolium ions are weak carbon acids, the equilibrium concentration of carbene/ylide is too small to adopt conventional methods of measurement of pK_a values. In this study a kinetic approach was used in order to estimate pK_a values of imidazolium and triazolium ions. The reactivity of these ions towards deuterioxide ion was investigated in aqueous solution at various pDs at 25 °C and ionic strength of unity using ^1H NMR spectroscopy. Second-order plots and pD-rate profiles were constructed from which second-order rate constants for deuterioxide ion-catalysed exchange k_{DO} ($\text{M}^{-1}\text{s}^{-1}$) could be estimated.

Kinetic acidities of imidazolium ions (**185**)-(**187**) were identical within experimental error and were consistent with values obtained in previous work in our laboratory and illustrate that substitution of one alkyl group on the imidazolium ring has a small effect on k_{DO} . A small counter ion effect was observed.

Triazolium ions showed increased reactivity towards deuterioxide ion. This required that deuterium exchange reactions were performed in DCl solutions. The acceleration of rates of H/D exchange for azolium ions with more electronegative atoms has been reported and our results are in accord with these findings. In the case of these more reactive triazolium ions, estimates for the first-order rate constants for the solvent reaction, $k_{\text{D}_2\text{O}}$ (s^{-1}), could also be obtained. Each second-order plot for the H/D exchange of azolium ions (**179**)-(**182**) exhibits a significant y-axis intercept which was tentatively assigned as $k_{\text{D}_2\text{O}}$ (s^{-1}). Although there is no clear pD-independent solvent reaction visible in the pD-rate profile for deuterioxide ion-catalysed exchange of triazolium ions (**179**)-(**182**), there is a slight levelling off for azolium ion (**181**) and it is possible that the solvent reaction could occur close to this region of the profile.

Values of the second-order rate constant for hydroxide ion catalysed exchange k_{HO} ($\text{M}^{-1}\text{s}^{-1}$) were estimated from k_{DO} values following application of a secondary solvent isotope relationship ($k_{\text{DO}}/k_{\text{HO}} = 2.4$).

The acid dissociation constant, K_a , for azolium ions may also be written as the ratio of the rate constant for deprotonation of azolium ions and the reverse rate constant for

reprotonation. As there was no detectable general base catalysis of exchange for representative azolium ions, it was concluded that proton transfer occurred in a pre-equilibrium and that k_{reorg} , the solvent reorganisation step, was rate-limiting. As such, a value of 10^{11} s^{-1} may be assigned as the rate constant for reprotonation of the carbene/ylide. This allows pK_a values of azolium ions to be estimated.

Chapter 4

Experimental

4.0 Foreword.

This chapter is divided into five subsections. Section 4.1 describes the general instrumentation utilised. Section 4.2 details the synthesis of imines and catalysts under investigation. Materials used and preparation of solutions are outlined in Section 4.3 and 4.4 respectively. Finally, Section 4.5 describes the kinetic methods used throughout these studies.

4.1 General instrumentation.

NMR samples were prepared in chloroform-d₁, deuterium oxide-d₂, acetone-d₆, dichloromethane-d₂, acetonitrile-d₃ and dimethyl sulfoxide-d₆ (DMSO). Tetramethylsilane (TMS) was used as an internal reference in chloroform-d₁, dichloromethane-d₂ and acetonitrile-d₃. ¹H NMR spectra at 400 and 500 MHz and ¹³C NMR spectra at 100 and 125 MHz were recorded on Bruker Avance 400, Varian Mercury 400 and Varian Inova 500 spectrometers in Durham University. ¹H and ¹³C NMR chemical shifts in deuterated solvents are reported relative to residual solvent peaks as listed in Table 4.1.

Table 4.1: Chemical shifts of residual solvent signals in deuterated solvents used.

Solvent	δ_{H} ppm	δ_{C} ppm
Acetone-d ₆	2.05	29.84, 206.26
Acetonitrile-d ₃	1.94	1.32, 118.36
Chloroform-d ₁	7.26	77.0
Deuterium oxide-d ₂	4.67	-
Dichloromethane-d ₂	5.32	54.0
Dimethylsulfoxide-d ₆	2.50	39.5

Data are presented as follows: chemical shift, integration, multiplicity (br = broad, s = singlet, d = doublet, t = triplet, q = quartet, sep = septet, m = multiplet), coupling constants in Hertz (Hz), and assignment.

Elemental analyses were obtained from the Microanalytical Unit, Chemistry Department, Durham University. Mass spectrometry was performed on a Thermo-

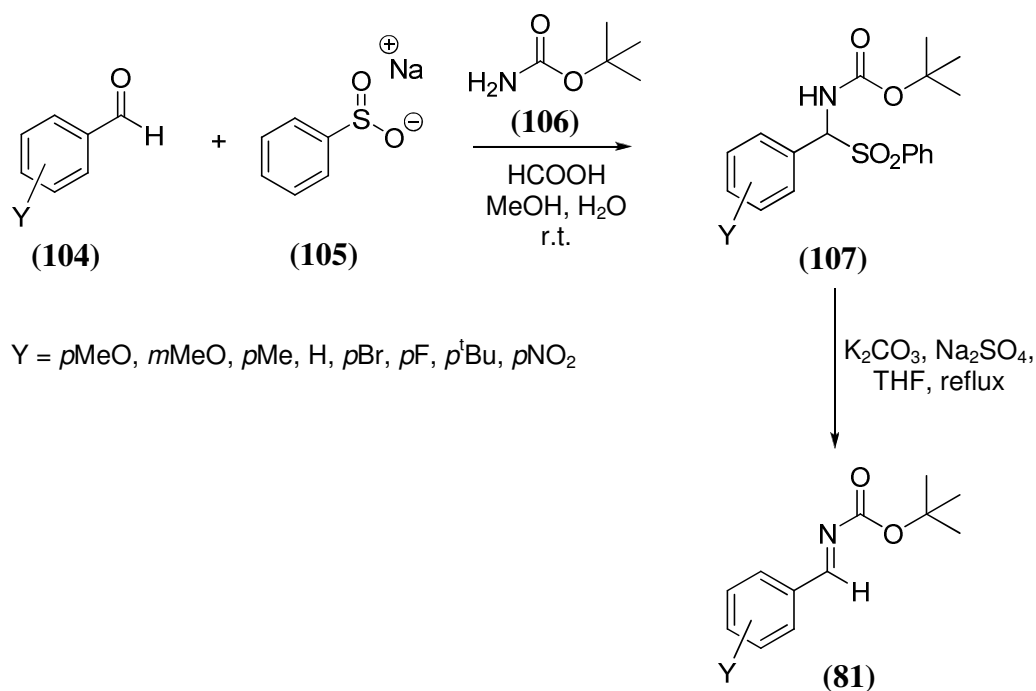
Finnigan *LTQ FT* machine. All UV-Vis measurements were carried out on Cary-100 and Cary-50 UV-VIS spectrophotometers. Stopped-flow spectrophotometry was performed on an Applied Photophysics SX-17MV instrument. Chiral HPLC was performed on a Perkin Elmer instrument using a Daicel Chiralpak IA column. Thin Layer Chromatography was carried out using silica-backed Merck Kieselgel 60 F254 plates. Column chromatography was carried out using silica gel (LC60A40-63 micron). Samples for infrared spectroscopy were prepared as KBr discs and spectra were recorded on Perkin Elmer Spectrum RX1 instrument with an ATR attachment.

All reactions involving air or moisture sensitive reagents were performed under an argon atmosphere using oven-dried glassware. Solvents were dried prior to use using an Innovative Technology Inc. solvent purification system and stored over molecular sieves. Chloroform- d_1 used for taking NMR spectra of imines was stored over potassium carbonate in order to neutralise acid impurities in the solvent and prevent hydrolysis.

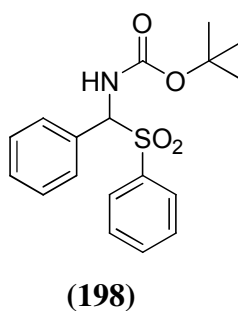
4.2 Synthesis of compounds for kinetic study.

4.2.1 Synthesis of *N*-Boc imines.

Imines were synthesised in two steps according to standard literature procedures.



4.2.1.1 *N*-(*tert*-butoxycarbonyl)- α -(phenylsulfonyl)benzylamine (198)⁵⁵.



A 25 mL flask was charged with *tert*-butyl carbamate (0.500 g, 4.27 mmol, 1 equiv) and benzenesulfinic acid sodium salt (1.40 g, 8.54 mmol, 2 equiv). The solids were suspended in methanol and water (1:2, 15 mL) and benzaldehyde (0.66 mL, 6.40 mmol, 1.5 equiv) was added followed by formic acid (90%, 0.35 mL). The reaction mixture was stirred at room temperature for 48 h. The resulting precipitate was isolated

via Buchner funnel filtration, purified by rinsing well with cold water and diethyl ether and dried *in vacuo* (**198**) (1.01 g, 68%).

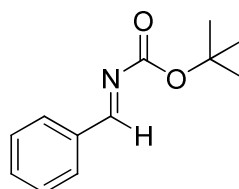
IR (cm⁻¹): ν 2980, 1693, 1508, 1307, 1142.

¹H NMR (400 MHz, CDCl₃) δ 7.92 (2H, d, $J = 7.2$ Hz, ArH), 7.63-7.67 (1H, m, ArH), 7.52-7.56 (2H, m, ArH), 7.38-7.49 (5H, m, ArH), 5.93 (1H, br d, $J = 10.3$ Hz), 5.84 (1H, br d, $J = 10.3$ Hz), 1.26 (9H, s, C(CH₃)₃).

¹³C NMR (125 MHz, CDCl₃) δ 153.7, 137.1, 134.2, 130.1, 129.9, 129.7, 129.3, 129.2, 129.0, 81.5, 74.1, 28.3.

C₁₈H₂₁NO₄S requires: C, 62.23%; H, 6.09%; N, 4.03%. Found; C, 62.36%; H, 6.10%; N, 4.03%.

4.2.1.2 Benzaldehyde *N*-(*tert*-butoxycarbonyl)imine (**121**)⁵⁵.



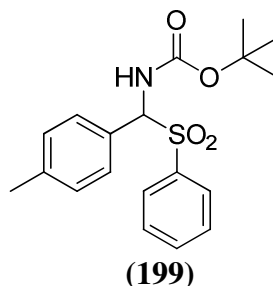
(**121**)

A 50 mL flask was charged with anhydrous potassium carbonate (1.64 g, 11.8 mmol, 6 equiv) and anhydrous sodium sulfate (1.72 g, 12.1 mmol). *N*-(*tert*-butoxycarbonyl)- α -(phenylsulfonyl)benzylamine (**198**) (0.600 g, 1.73 mmol, 1 equiv) was added and the flask was placed under an argon atmosphere. Anhydrous THF (20 mL) was added and the flask was capped with a water-cooled condenser. The reaction mixture was brought to reflux for 15 h and then cooled to room temperature and the solids removed via rapid filtration through a sintered glass funnel. The filtrate was concentrated and dried *in vacuo* to give the imine (**121**) as a colourless oil (0.336 g, 95%).

¹H NMR (400 MHz, CDCl₃) δ 8.88 (1H, s, CH=N), 7.90-7.93 (2H, m, ArH), 7.54-7.57 (1H, m, ArH), 7.43-7.49 (2H, m, ArH), 1.59 (9H, s, C(CH₃)₃).

¹³C NMR (100 MHz, CDCl₃) δ 169.2, 162.4, 133.9, 133.3, 130.0, 128.7, 82.0, 28.0.

MS (ES⁺) m/z : 205.9 [M]⁺.

4.2.1.3 *N*-(*tert*-butoxycarbonyl)- α -(phenylsulfonyl)-4-methylbenzylamine (**199**)⁵⁵.

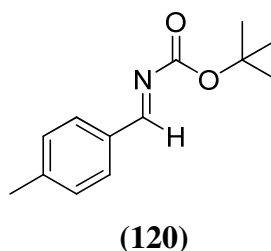
The reaction was performed on a 4.27 mmol scale utilising the same procedure as for the preparation of (**198**) using *p*-tolualdehyde. After 48 h, the sulfone (**199**) was isolated as a white solid (0.987 g, 64%).

IR (cm⁻¹): ν 1698, 1508, 1310, 1142.

¹H NMR (400 MHz, CDCl₃) δ 7.92 (2H, d, $J = 7.6$ Hz, ArH), 7.64 (1H, t, $J = 7.6$ Hz, ArH), 7.55 (2H, t, $J = 7.6$ Hz, ArH), 7.33 (2H, d, $J = 7.7$ Hz, ArH), 7.22 (2H, d, $J = 7.7$ Hz, ArH), 5.88 (1H, br d, $J = 10.7$ Hz), 5.75 (1H, br d, $J = 10.7$ Hz), 2.37 (3H, s, ArCH₃), 1.25 (9H, s, C(CH₃)₃).

¹³C NMR (125 MHz, CDCl₃) δ 153.4, 140.0, 137.0, 133.8, 129.5, 129.4, 129.0, 128.7, 127.0, 81.1, 73.7, 28.0, 21.3.

C₁₉H₂₃NO₄S requires: C, 63.13%; H, 6.41%; N, 3.88%. Found; C, 63.29%; H, 6.43%; N, 3.84%.

4.2.1.4 *p*-Methylbenzaldehyde *N*-(*tert*-butoxycarbonyl)imine (**120**)⁵⁵.

The reaction was performed on a 0.553 mmol scale using the same procedure as for the preparation of (**121**). After 15 h, the product (**120**) was isolated as a colourless oil (0.116 g, 96%).

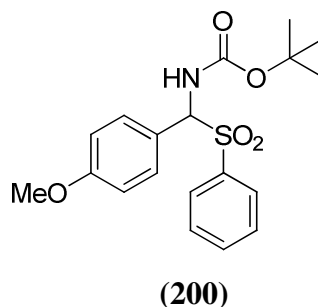
IR (cm⁻¹): ν 2985, 1705, 1600, 1260, 1155.

^1H NMR (400 MHz, CDCl_3) δ 8.87 (1H, s, $\text{CH}=\text{N}$), 7.82 (2H, d, $J = 8.1$ Hz, ArH), 7.28 (2H, d, $J = 8.1$ Hz, ArH), 2.42 (3H, s, ArCH_3), 1.58 (9H, s, $\text{C}(\text{CH}_3)_3$).

^{13}C NMR (100 MHz, CDCl_3) δ 169.8, 162.7, 144.5, 131.5, 130.3, 129.6, 82.0, 27.8, 21.7.

MS (ES^+) m/z : 219.8 $[\text{M}]^+$.

4.2.1.5 *N*-(*tert*-butoxycarbonyl)- α -(phenylsulfonyl)-4-methoxybenzylamine (**200**).



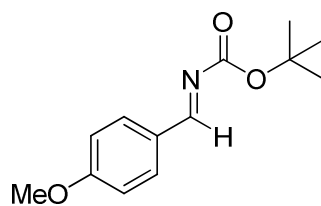
The reaction was performed on a 4.27 mmol scale utilising the same procedure as for the preparation of (**198**) with *p*-methoxybenzaldehyde. After 24 h, the sulfone (**200**) was isolated as a white solid (1.10 g, 68%).

IR (cm^{-1}): ν 2966, 1694, 1504, 1311, 1242, 1149.

^1H NMR (400 MHz, CDCl_3) δ 7.92 (2H, d, $J = 7.1$ Hz, ArH), 7.63 (1H, t, $J = 7.1$ Hz, ArH), 7.48-7.58 (2H, m, ArH), 7.34 (2H, d, $J = 7.9$ Hz, ArH), 7.23 (2H, d, $J = 7.9$ Hz, ArH), 5.87 (1H, br d, $J = 10.9$ Hz), 5.65 (1H, br d, $J = 10.9$ Hz), 3.82 (3H, s, OCH_3), 1.25 (9H, s, $\text{C}(\text{CH}_3)_3$).

^{13}C NMR (100 MHz, CDCl_3) δ 153.5, 140.0, 137.0, 133.8, 129.8, 129.6, 129.0, 128.8, 126.8, 81.1, 73.8, 28.0, 21.3.

$\text{C}_{19}\text{H}_{23}\text{NO}_5\text{S}$ requires C, 60.46%; H, 6.14%; N, 3.71%. Found; C, 60.41%; H, 6.12%; N, 3.64%.

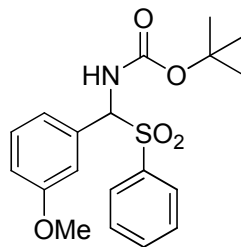
4.2.1.6 *p*-Methoxybenzaldehyde *N*-(*tert*-butoxycarbonyl)imine (**119**)⁵⁵.**(119)**

The reaction was performed on a 0.530 mmol scale using the same procedure as for the preparation of (**121**). After 15 h, the product (**119**) was obtained as a white solid (0.117 g, 94%).

¹H NMR (400 MHz, CDCl₃) δ 8.88 (1H, s, CH=N), 7.90 (2H, d, *J* = 8.3 Hz, ArH), 6.97 (2H, d, *J* = 8.3 Hz, ArH), 3.88 (3H, s, ArOCH₃), 1.58 (9H, s, C(CH₃)₃).

¹³C NMR (100 MHz, CDCl₃) δ 169.5, 164.0, 162.7, 132.3, 126.8, 114.2, 81.6, 55.3, 27.8.

MS (ES⁺) *m/z*: 235.9 [M]⁺.

4.2.1.7 *N*-(*tert*-butoxycarbonyl)- α -(phenylsulfonyl)-3-methoxybenzylamine (**201**).**(201)**

The reaction was performed on a 4.27 mmol scale utilising the same procedure as for the preparation of (**198**) using *m*-methoxybenzaldehyde. After 48 h, the sulfone (**201**) was isolated as a white solid (1.03 g, 64%).

IR (cm⁻¹): ν 2986, 1695, 1505, 1311, 1145.

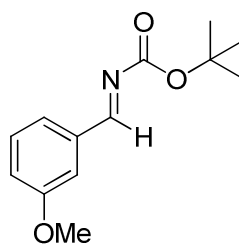
¹H NMR (400 MHz, CDCl₃) δ 7.92 (2H, d, *J* = 7.4 Hz, ArH), 7.64 (1H, t, *J* = 7.4 Hz, ArH), 7.50- 7.59 (2H, m, ArH), 7.28-7.37 (1H, m, ArH), 6.90-7.08 (3H, m, ArH), 5.90

(1H, br d, $J = 11.0$ Hz), 5.70 (1H, br d, $J = 11.0$ Hz), 3.82 (3H, s, ArOCH₃), 1.26 (9H, s, C(CH₃)₃).

¹³C NMR (100 MHz, CDCl₃) 159.7, 153.4, 137.0, 133.9, 131.8, 129.4, 129.0, 128.6, 126.0, 121.5, 114.5, 81.2, 73.9, 55.5, 28.2.

C₁₉H₂₃NO₅S requires C, 60.46%; H, 6.14%; N, 3.71%. Found C, 60.75%; H, 6.21%; N, 3.83%.

4.2.1.8 *m*-Methoxybenzaldehyde *N*-(*tert*-butoxycarbonyl)imine (**202**).



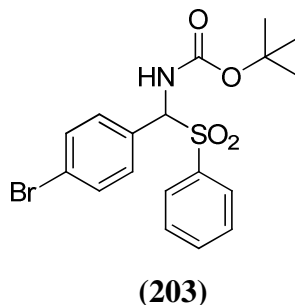
(**202**)

The reaction was performed on a 0.999 mmol scale using the same procedure as for the preparation of (**121**). After 15 h, the product (**202**) was obtained as a white solid (0.220 g, 94%).

¹H NMR (400 MHz, CDCl₃) δ 8.82 (1H, s, CH=N), 7.48 (1H, s, ArH), 7.31-7.42 (2H, m, ArH), 7.06-7.18 (1H, m, ArH), 3.83 (3H, s, ArOCH₃), 1.58 (9H, s, C(CH₃)₃).

¹³C NMR (100 MHz, CDCl₃) δ 169.6, 162.5, 159.9, 135.4, 129.7, 124.2, 120.7, 112.3, 82.3, 55.4, 27.8.

MS (ES⁺) m/z : 235.9 [M]⁺.

4.2.1.9 *N*-(*tert*-butoxycarbonyl)- α -(phenylsulfonyl)-4-bromobenzylamine (**203**)⁵⁵.

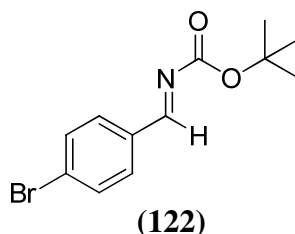
The reaction was performed using the same procedure as for the preparation of (**198**) on a 4.27 mmol scale with *p*-bromobenzaldehyde (1.2 equiv). After 48 h, the product (**203**) was isolated as a white solid (0.964 g, 53%) following extensive trituration with ice-cold water and diethyl ether.

IR (cm⁻¹): ν 2986, 1693, 1512, 1309, 1143.

¹H NMR (400 MHz, CDCl₃) δ 7.91 (2H, d, $J = 7.3$ Hz, ArH), 7.62-7.72 (1H, m, ArH), 7.51-7.58 (4H, m, ArH), 7.32 (2H, d, $J = 8.2$ Hz, ArH), 5.87 (1H, br d, $J = 10.2$ Hz), 5.67 (1H, br d, $J = 10.2$ Hz), 1.25 (9H, s, C(CH₃)₃).

¹³C NMR (100 MHz, CDCl₃) δ 153.4, 136.7, 134.1, 132.0, 130.4, 129.4, 129.1, 128.9, 124.3, 81.4, 73.2, 27.9.

C₁₈H₂₀BrNO₄S requires: C, 50.71%; H, 4.73%; N, 3.29%. Found; C, 50.51%; H, 4.72%; N, 3.20%.

4.2.1.10 *p*-Bromobenzaldehyde *N*-(*tert*-butoxycarbonyl)imine (**122**)⁵⁵.

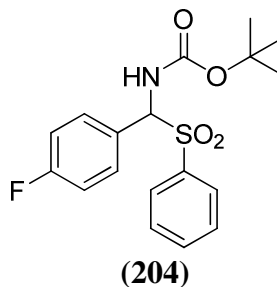
The reaction was performed on a 0.469 mmol scale using the same procedure as for the preparation of (**121**). After 15 h, the imine (**122**) was isolated as a white solid (0.121 g, 91%).

^1H NMR (400 MHz, CDCl_3) δ 8.82 (1H, s, $\text{CH}=\text{N}$), 7.78 (2H, d, $J = 8.8$ Hz, ArH), 7.62 (2H, d, $J = 8.8$ Hz, ArH), 1.58 (9H, s, $\text{C}(\text{CH}_3)_3$).

^{13}C NMR (100 MHz, CDCl_3) δ 168.3, 162.3, 133.0, 132.3, 131.4, 128.5, 82.5, 27.9.

MS (ES^+) m/z : 283.8, 285.8 $[\text{M}]^+$.

4.2.1.11 *N*-(*tert*-butoxycarbonyl)- α -(phenylsulfonyl)-4-fluorobenzylamine (**204**)⁵⁵.



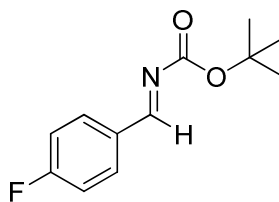
The reaction was performed on a 4.27 mmol scale utilising the same procedure as for the preparation of (**198**). After 72 h, the sulfone (**204**) was isolated as a white solid (0.998 g, 64%).

IR (cm^{-1}): ν 1705, 1507, 1310, 1142.

^1H NMR (400 MHz, CDCl_3) δ 7.92 (2H, d, $J = 7.5$ Hz, ArH), 7.65 (1H, t, $J = 7.5$ Hz, ArH), 7.54 (2H, t, $J = 7.5$ Hz, ArH), 7.40-7.48 (2H, m, ArH), 7.10 (2H, t, $J = 8.6$ Hz, ArH), 5.89 (1H, br d, $J = 10.8$ Hz), 5.67 (1H, br d, $J = 10.8$ Hz), 1.25 (9H, s, $\text{C}(\text{CH}_3)_3$).

^{13}C NMR (100 MHz, CDCl_3) δ 164.9, 162.4, 153.5, 136.8, 134.1, 130.9, 130.8, 129.5, 129.1, 125.9, 116.0, 115.7, 81.4, 73.2, 28.0.

$\text{C}_{18}\text{H}_{20}\text{FNO}_4\text{S}$ requires: C, 59.16%; H, 5.52%; N, 3.83%. Found; C, 58.97%; H, 5.42%; N, 3.72%.

4.2.1.12 *p*-Fluorobenzaldehyde *N*-(*tert*-butoxycarbonyl)imine (**123**)⁵⁵.**(123)**

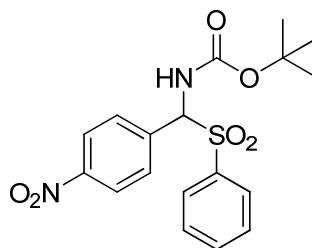
The reaction was performed on a 0.547 mmol scale using the same procedure as for the preparation of (**121**). After 15 h the imine (**123**) was isolated as a white solid (0.116 g, 95%).

IR (cm⁻¹): ν 2980, 1710, 1631, 1362, 1145.

¹H NMR (400 MHz, CDCl₃) δ 8.85 (1H, s, CH=N), 7.90-7.96 (2H, m, ArH), 7.12-7.18 (2H, m, ArH), 1.58 (9H, s, C(CH₃)₃).

¹³C NMR (100 MHz, CDCl₃) δ 168.0, 167.1, 164.6, 162.3, 132.4, 132.3, 130.4, 116.2, 115.9, 82.2, 27.8.

MS (ES⁺) *m/z*: 223.8 [M]⁺.

4.2.1.13 *N*-(*tert*-butoxycarbonyl)- α -(phenylsulfonyl)-4-nitrobenzylamine (**205**).**(205)**

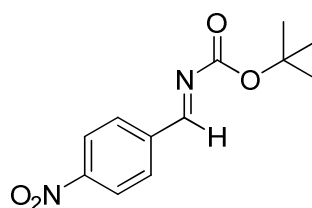
The reaction was performed on a 4.27 mmol scale utilising the same procedure for the preparation of (**198**). After 72 h, the sulfone (**205**) was isolated as a pale yellow solid (1.01 g, 60%).

IR (cm⁻¹): ν 3344, 2966, 1690, 1509, 1348, 1152.

^1H NMR (400 MHz, CDCl_3) δ 8.30 (2H, d, $J = 8.8$ Hz, ArH), 7.95 (2H, d, $J = 7.4$ Hz, ArH), 7.49-7.79 (5H, m, ArH), 6.05 (1H, br d, $J = 10.7$ Hz), 5.78 (1H, br d, $J = 10.7$ Hz), 1.26 (9H, s, $\text{C}(\text{CH}_3)_3$).

$\text{C}_{18}\text{H}_{20}\text{N}_2\text{O}_6\text{S}$ requires: C, 55.09%; H, 5.14%; N, 7.14%. Found; C, 54.87%; H, 5.09%; N, 6.95%.

4.2.1.14 *p*-Nitrobenzaldehyde *N*-(*tert*-butoxycarbonyl)imine (206).



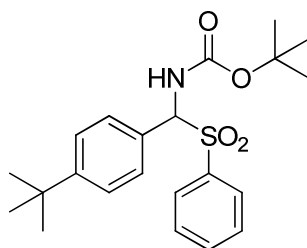
(206)

The reaction was performed on a 0.509 mmol scale using the same procedure as for the preparation of (121). After 15 h, imine (206) was isolated as a yellow solid (0.0950 g, 75%)

^1H NMR (400 MHz, CDCl_3) δ 8.89 (1H, s, $\text{CH}=\text{N}$), 8.34 (2H, d, $J = 8.9$ Hz, ArH), 8.10 (2H, d, $J = 8.9$ Hz, ArH), 1.62 (9H, s, $\text{C}(\text{CH}_3)_3$).

^{13}C NMR (125 MHz, CDCl_3) δ 166.4, 162.0, 139.5, 130.8, 124.2, 123.6, 83.4, 28.2.

4.2.1.15 *N*-(*tert*-butoxycarbonyl)- α -(phenylsulfonyl)-4-*tert*-butylbenzylamine (207).



(207)

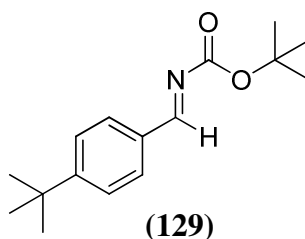
The reaction was performed on a 4.27 mmol scale utilising the same procedure as for the preparation of (198). After 48 h, the sulfone (207) was isolated as a white solid (1.19 g, 69%).

^1H NMR (500 MHz, CDCl_3) δ 7.94 (2H, d, $J = 7.4$ Hz, ArH), 7.64 (1H, t, $J = 7.4$ Hz, ArH), 7.54 (2H, m, ArH), 7.45 (2H, d, 8.3 Hz, ArH), 7.39 (2H, d, $J = 8.3$ Hz, ArH), 5.90 (1H, br d, $J = 10.8$ Hz), 5.73 (1H, br d, $J = 10.8$ Hz), 1.32 (9H, s, $\text{C}(\text{CH}_3)_3$), 1.23 (9H, s, $\text{C}(\text{CH}_3)_3$)

^{13}C NMR (100 MHz, CDCl_3) δ 153.6, 137.3, 134.1, 129.7, 129.3, 128.9, 126.9, 126.1, 81.4, 73.9, 35.0, 31.5, 28.2.

$\text{C}_{22}\text{H}_{29}\text{NO}_4\text{S}$ requires C, 65.48%; H, 7.24%; N, 3.47%. Found; C, 65.26%; H, 7.20%; N, 3.35%.

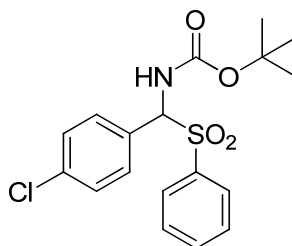
4.2.1.16 4-*tert*-Butylbenzaldehyde *N*-(*tert*-butoxycarbonyl)imine (**129**).



The reaction was performed on a 0.427 mmol scale using the same procedure as for the preparation of (**121**). After 15 h, the imine (**129**) was isolated as a white solid (0.0970 g, 87%).

^1H NMR (400 MHz, CDCl_3) δ 8.87 (1H, s, $\text{CH}=\text{N}$), 7.86 (2H, d, $J = 8.5$ Hz, ArH), 7.48 (2H, d, $J = 8.5$ Hz, ArH), 1.58 (9H, s, $\text{C}(\text{CH}_3)_3$), 1.33 (9H, s, $\text{C}(\text{CH}_3)_3$).

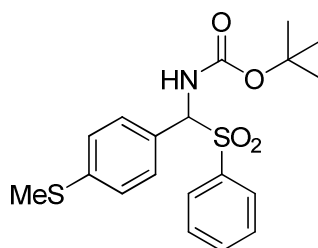
^{13}C NMR (100 MHz, CDCl_3) δ 169.8, 162.8, 157.5, 131.4, 130.2, 125.8, 82.0, 35.2, 31.0, 28.0.

4.2.1.17 ***N*-(*tert*-butoxycarbonyl)- α -(phenylsulfonyl)-4-chlorobenzylamine (208).****(208)**

The reaction was performed on a 4.27 mmol scale utilising the same procedure as for the preparation of **(198)**. After 72 h, the sulfone **(208)** was isolated as a white solid (1.11 g, 68%)

^1H NMR (400 MHz, CDCl_3) δ 7.91 (2H, d, $J = 7.1$ Hz, ArH), 7.66 (1H, t, $J = 7.5$ Hz, ArH), 7.52-7.70 (2H, m, ArH), 7.31-7.49 (4H, m, ArH), 5.88 (1H, br d, $J = 10.7$ Hz), 5.64 (1H, br d, $J = 10.7$ Hz), 1.25 (9H, s, $\text{C}(\text{CH}_3)_3$).

$\text{C}_{18}\text{H}_{20}\text{ClNO}_4\text{S}$ requires: C, 56.61%; H, 5.28%; N, 3.67%. Found; C, 56.39%; H, 5.06%; N, 3.48%.

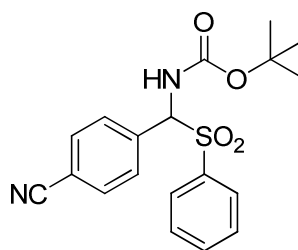
4.2.1.18 ***N*-(*tert*-butoxycarbonyl)- α -(phenylsulfonyl)-4-(methylthio)benzylamine (209).****(209)**

The reaction was performed on a 4.27 mmol scale utilising the same procedure as for the preparation of **(198)**. After 72 h, the sulfone was isolated as a white solid **(209)** (1.03 g, 61%) following extensive trituration with ice cold water and diethyl ether.

^1H NMR (400 MHz, CDCl_3) δ 7.92 (2H, d, $J = 7.2$ Hz, ArH), 7.65 (1H, t, $J = 7.2$ Hz, ArH), 7.56 (2H, t, $J = 7.4$ Hz, ArH), 7.27-7.40 (4H, m, ArH), 5.84 (1H, br d, $J = 10.7$ Hz), 5.67 (1H, br d, $J = 10.7$ Hz), 2.48 (3H, s, SCH_3), 1.25 (9H, s, $\text{C}(\text{CH}_3)_3$)

$\text{C}_{19}\text{H}_{23}\text{NO}_4\text{S}_2$ requires: C, 57.99%; H, 5.89%; N, 3.56%. Found; C, 57.93%; H, 5.88%; N, 3.52%.

4.2.1.19 ***N*-(*tert*-butoxycarbonyl)- α -(phenylsulfonyl)-4-cyanobenzylamine (210).**



(210)

The reaction was performed on a 4.27 mmol scale utilising the same procedure as for the preparation of **(198)**. After 72 h, a white precipitate was isolated and crystallised from diethyl ether to yield the product **(210)** as colourless crystals (0.954 g, 60%).

IR (cm^{-1}): ν 2980, 2230, 1696, 1499, 1305, 1139.

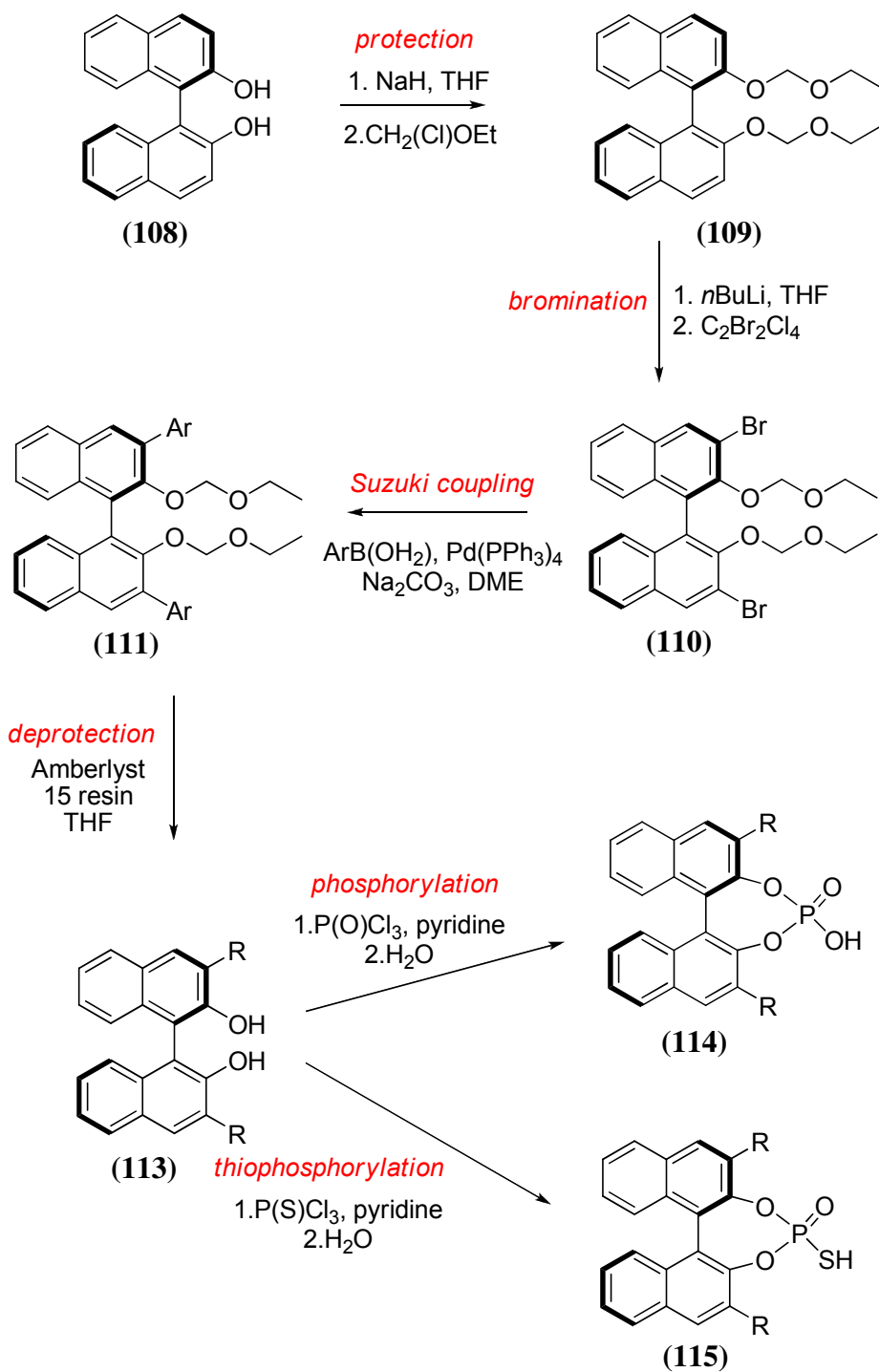
^1H NMR (400 MHz, CDCl_3) δ 7.93 (2H, d, $J = 7.7$ Hz, ArH), 7.63-7.80 (3H, m, ArH), 7.50-7.62 (4H, m, ArH), 5.98 (1H, br d, $J = 10.4$ Hz), 5.72 (1H, br d, $J = 10.4$ Hz), 1.25 (9H, s, $\text{C}(\text{CH}_3)_3$).

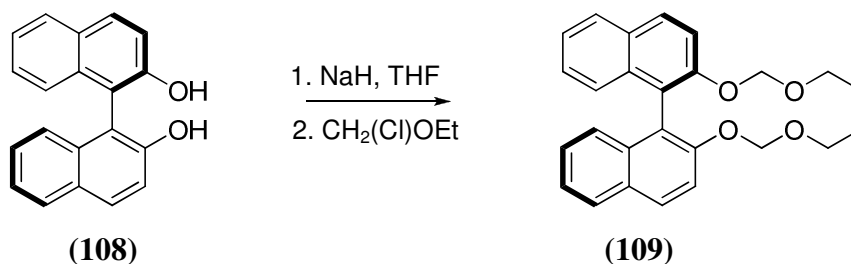
^{13}C NMR (100 MHz, CDCl_3) δ 153.3, 136.3, 135.0, 134.4, 132.3, 129.7, 129.4, 129.3, 118.0, 113.7, 81.7, 73.3, 28.0.

$\text{C}_{19}\text{H}_{20}\text{N}_2\text{O}_4\text{S}$ requires; C, 61.27%; H, 5.41%; N, 7.52%. Found: C, 61.07%; H, 5.33%; N, 7.40%.

4.2.2 Synthesis of phosphoric acid catalysts and thiophosphoryl analogues.

Phosphoric acids and thiophosphoryl analogues were synthesised according to or in analogy with, reported procedures.



4.2.2.1 (R)-2,2'-Bis(ethoxymethoxy)-1,1'-binaphthyl (109).

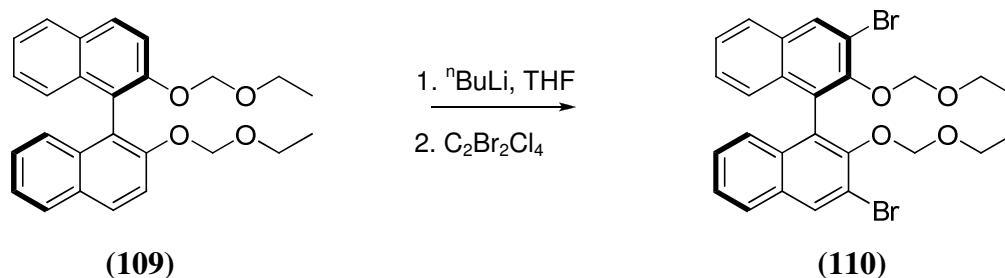
The preparation followed literature procedure¹⁰⁸ with some modifications.

NaH (1.68 g, 60% in oil, 3 equiv) was washed with dry THF (3 × 15 mL) and then stirred in THF (50 mL) at 0 °C under an argon atmosphere. A solution of (R)-2,2'-dihydroxy-1,1'-binaphthyl (**108**) (3.00 g, 10.5 mmol, 1 equiv) in THF (40 mL) was added and the pale yellow mixture was stirred at 0 °C for 1 h, then warmed up to room temperature for 30 mins. The mixture was re-cooled to 0 °C and chloromethyl ethyl ether (3.25 mL, 42.8 mmol) was added slowly. After the addition, the reaction mixture was warmed to room temperature and stirred for 5 h. Saturated aqueous ammonium chloride (50 mL) was added to the flask and the solvent was removed *in vacuo*. The residue was extracted with CH₂Cl₂ (50 mL × 3). The organic layers were combined, washed with brine (50 mL), dried over sodium sulfate and concentrated. Crude product was purified by column chromatography (EtOAc/hexane = 1/10) to give a colourless semi-solid (3.80 g, 90%).

¹H NMR (400 MHz, CDCl₃) δ 7.96 (2H, d, *J* = 9.0 Hz, Ar*H*), 7.88 (2H, d, *J* = 8.9 Hz Ar*H*), 7.61 (2H, d, *J* = 8.0 Hz, Ar*H*), 7.28-7.39 (2H, m, Ar*H*), 7.14-7.24 (2H, m, Ar*H*), 7.15 (2H, d, *J* = 9.0 Hz, Ar*H*), 5.14 (2H, d, *J* = 7.1 Hz, OCH₂O), 5.02 (2H, d, *J* = 7.1 Hz, OCH₂O), 3.24-3.49 (4H, m, CH₂CH₃), 1.00 (6H, t, *J* = 7.1 Hz, CH₂CH₃).

¹³C NMR (100 MHz, CDCl₃) δ 152.8, 134.1, 129.8, 129.3, 127.9, 126.2, 125.6, 124.0, 121.3, 117.5, 93.9, 63.9, 14.9.

MS (EI) *m/z*: 402.1 (M⁺, 88), 342.1 (58), 298.1 (100), 286.1 (74), 269.1 (92), 255.0 (52), 59.0 (96).

4.2.2.2 (*R*)-3,3'-Dibromo-2,2'-Bis(ethoxymethoxy)-1,1'-binaphthyl (**110**)¹⁰⁸.

(*R*)-2,2'-Bis(ethoxymethoxy)-1,1'-binaphthyl (**109**) (5.74 g, 14.3 mmol, 1 equiv) was dissolved in dry Et₂O (200 mL) in a round bottom flask under an argon atmosphere. ⁿBuLi (26.7 mL, 1.6 M in hexane, 3 equiv) was added at room temperature by syringe injection with stirring. After the reaction mixture was stirred for 3 h, THF (130 mL) was injected into the flask and the mixture was stirred for 1 h. The flask was cooled in an ice bath for 5 mins and dibromotetrachloroethane (13.93 g, 42.7 mmol, 3 equiv) was quickly added in one portion giving a bright orange solution. The reaction mixture was stirred overnight and quenched with saturated aqueous ammonium chloride and water. The two phases were separated and the aqueous layer washed with Et₂O twice. All organic layers were combined, washed with brine, dried over sodium sulfate and concentrated. Crude product was purified by column chromatography (EtOAc/hexane = 1/10) and crystallised from Et₂O/hexane to give a white crystalline solid (7.45 g, 94%).

IR (cm⁻¹): ν 1203, 1136, 1005.

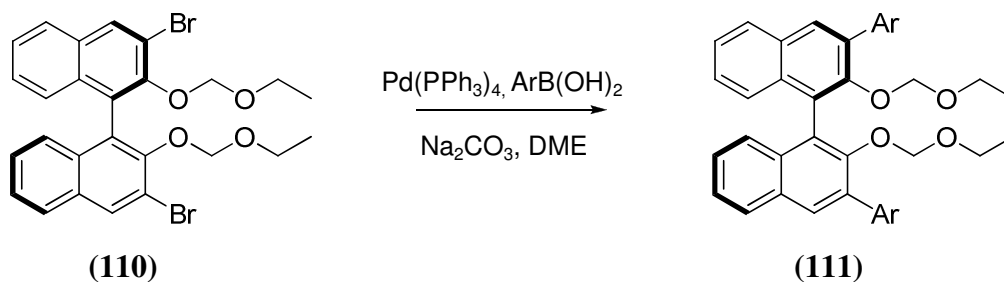
¹H NMR (400 MHz, CDCl₃) δ 8.27 (2H, s, ArH), 7.82 (2H, d, *J* = 8.1 Hz, ArH), 7.39-7.45 (2H, m, ArH), 7.22 - 7.32 (2H, m, ArH), 7.09 (2H, d, *J* = 8.1 Hz, ArH) 4.90 (2H, d, *J* = 5.9 Hz, OCH₂O), 4.83 (2H, d, *J* = 5.9 Hz, OCH₂O), 2.96-3.08 (2H, m, OCH₂CH₃), 2.62-2.72 (2H, m, OCH₂CH₃), 0.60 (6H, t, *J* = 7.2 Hz, CH₂CH₃).

¹³C NMR (100 MHz, CDCl₃) δ 150.3, 133.1, 132.9, 131.5, 127.2, 126.9, 126.9, 126.5, 125.9, 117.5, 97.8, 64.8, 14.3.

C₂₆H₂₄Br₂O₄ requires C, 55.74%; H, 4.32%. Found C, 55.91%; H, 4.34%.

MS (ES⁺) *m/z* 583.1 [M+Na]⁺.

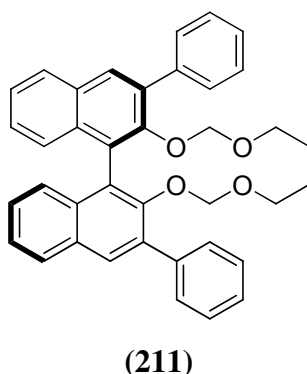
4.2.2.3 General Procedure A: preparation of 3,3'-diaryl-2,2'-bis(ethoxymethoxy)-1,1'-binaphthyls (211)-(214).



The preparation of 3,3'-disubstituted binaphthyl compounds followed literature procedures⁷³ with some modifications.

(*R*)-3,3'-Dibromo-2,2'-bis(ethoxymethoxy)-1,1'-binaphthyl (**110**) (1 equiv) and Pd(PPh₃)₄ (10 mol%) were mixed in DME or toluene in a round bottom flask at room temperature under an argon atmosphere. The mixture was stirred and arylboronic acid (3.5 equiv) and aqueous Na₂CO₃ solution (2 M, 5.2 equiv) was added. The mixture was heated to reflux for 10 h, cooled to room temperature and filtered through a pad of Celite. The filtrate was concentrated *in vacuo* and the resulting residue dissolved in CH₂Cl₂, washed with saturated aqueous NH₄Cl, water, and brine. The organic layer was dried over Na₂SO₄ and concentrated *in vacuo* to give a crude product. Subsequent purification gave the product.

4.2.2.3.1 (*R*)-3,3'-Diphenyl-2,2'-Bis(ethoxymethoxy)-1,1'-binaphthyl (**211**)¹⁰⁸.



Following General Procedure A, (*R*)-3,3'-dibromo-2,2'-bis(ethoxymethoxy)-1,1'-binaphthyl (**110**) (1.50 g, 2.68 mmol, 1 equiv) and Pd(PPh₃)₄ (10 mol%, 0.309 g) were mixed in DME (19 mL) at room temperature under an argon atmosphere giving a dark

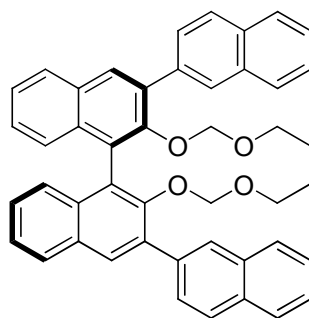
red solution. Phenylboronic acid (1.14 g, 9.37 mmol, 3.5 equiv) and aqueous Na₂CO₃ solution (6.9 mL, 2 M) were added and the resulting mixture was stirred and heated to reflux for 10 h, cooled to room temperature and passed through a bed of Celite. The organic solution was concentrated to give a residue. The residue was dissolved in CH₂Cl₂, washed with saturated aqueous ammonium chloride, water, brine, dried over sodium sulfate and concentrated to give a white foamy product. Crude product was purified by column chromatography (EtOAc/hexane = 1/10) (1.26 g, 85%).

¹H NMR (400 MHz, CDCl₃) δ 7.95 (2H, ArH), 7.89 (2H, d, *J* = 8.1 Hz), 7.70–7.81 (4H, m, ArH), 7.22–7.55 (12H, m, ArH), 4.47 (2H, d, *J* = 5.8 Hz, OCH₂O), 4.44 (2H, d, *J* = 5.8 Hz, OCH₂O), 2.65–2.75 (2H, m, OCH₂CH₃), 2.38–2.49 (2H, m, OCH₂CH₃), 0.40 (6H, t, *J* = 7.1 Hz, OCH₂CH₃).

¹³C NMR (100 MHz, CDCl₃) δ 151.6, 139.1, 135.5, 133.6, 130.8, 130.5, 126.6, 128.3, 127.9, 127.2, 126.4, 126.3, 126.2, 125.0, 97.2, 64.2, 14.2.

MS (ES⁺) *m/z* 577.3 [M+Na]⁺.

4.2.2.3.2 **(*R*)-3,3'-Bis(2-naphthyl)-2,2'-bis(ethoxymethoxy)-1,1'-binaphthyl (212)**¹⁰⁸.



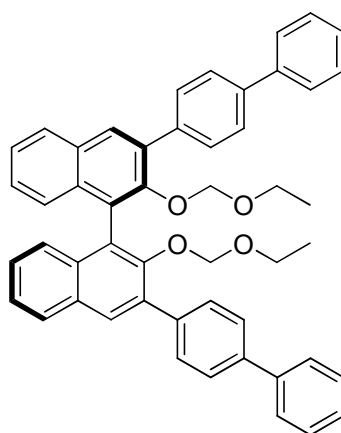
(212)

Following General Procedure A, (*R*)-3,3'-dibromo-2,2'-bis(ethoxymethoxy)-1,1'-binaphthyl (**110**) (1.50 g, 2.68 mmol, 1 equiv) and Pd(PPh₃)₄ (10 mol%, 0.309 g) were mixed in DME (20 mL) at room temperature under an argon atmosphere. 2-Naphthylboronic acid (1.62 g, 9.37 mmol, 3.5 equiv) and aqueous Na₂CO₃ solution (7 mL, 2 M) were added and the resulting mixture was stirred and heated to reflux for 10 h, cooled to room temperature and passed through a bed of Celite. The organic solution was concentrated *in vacuo* to give a residue. The residue was dissolved in CH₂Cl₂, washed with saturated aqueous ammonium chloride, water and brine, dried over

sodium sulfate and concentrated to give a cream solid. Crude product was purified by column chromatography ($\text{CH}_2\text{Cl}_2/\text{hexane} = 1/1$). The product (**212**) (1.57 g, 90%) was used directly for deprotection with only ^1H NMR being examined.

^1H NMR (400 MHz, CDCl_3) δ 8.23 (2H, s, ArH), 8.06 (2H, s, ArH), 7.70-8.01 (10H, m, ArH), 7.22-7.60 (10H, m, ArH), 4.50 (4H, m, OCH_2O), 2.70 (2H, m, OCH_2CH_3), 2.41 (2H, m, OCH_2CH_3) 0.32 (6H, t, CH_2CH_3).

4.2.2.3.3 **(R)-3,3'-Bis(4-biphenyl)-2,2'-bis(ethoxymethoxy)-1,1'-binaphthyl (213).**



(213)

Following General Procedure A, (*R*)-3,3'-dibromo-2,2'-bis(ethoxymethoxy)-1,1'-binaphthyl (**110**) (1.50 g, 2.68 mmol, 1 equiv) and $\text{Pd}(\text{PPh}_3)_4$ (10 mol%, 0.309 g) were mixed in DME (20 mL) at room temperature under an argon atmosphere. 4-Biphenylboronic acid (1.86 g, 9.37 mmol, 3.5 equiv) and aqueous Na_2CO_3 solution (7 mL, 2 M) were added and the resulting mixture was stirred and heated to reflux for 10 h, cooled to room temperature and passed through a bed of Celite. The organic solution was concentrated *in vacuo* to give a residue. The residue was dissolved in CH_2Cl_2 , washed with saturated aqueous ammonium chloride, water and brine, dried over sodium sulfate and concentrated to give a cream solid. Crude product was purified by column chromatography ($\text{EtOAc}/\text{hexane} = 1/10$) and crystallisation from $\text{CH}_2\text{Cl}_2/\text{hexane}$ to give white crystals (**213**) (1.80 g, 95%).

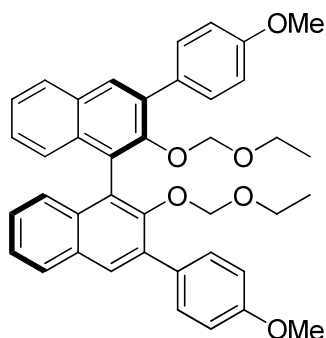
^1H NMR (400 MHz, CDCl_3) δ 8.06 (2H, s, ArH), 7.86-7.98 (6H, m, ArH), 7.65-7.84 (8H, m, ArH), 7.27-7.58 (12H, m, ArH), 4.60 (2H, d, $J = 5.3$ Hz, OCH_2O), 4.55 (2H,

d, $J = 5.3$ Hz, OCH_2O), 2.70-2.88 (2H, m, OCH_2CH_3), 2.45-2.62 (2H, m, OCH_2CH_3), 0.49 (6H, t, $J = 6.5$ Hz, OCH_2CH_3).

^{13}C NMR (100 MHz, CDCl_3) δ 151.6, 140.8, 140.1, 138.1, 135.0, 133.6, 130.9, 130.5, 130.0, 128.8, 127.9, 127.4, 127.1, 127.0, 126.5, 126.4, 125.1, 97.4, 64.3, 14.2.

MS (ES^+) m/z 729.4 $[\text{M}+\text{Na}]^+$.

4.2.2.3.4 (R)-3,3'-Bis(4-methoxyphenyl)-2,2'-bis(ethoxymethoxy)-1,1'-binaphthyl (214).



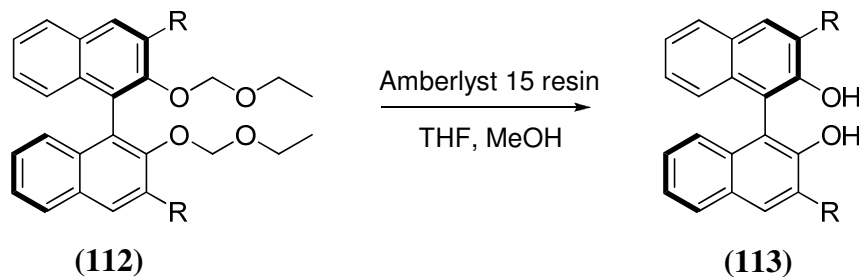
(214)

Following General Procedure A, (*R*)-3,3'-dibromo-2,2'-bis(ethoxymethoxy)-1,1'-binaphthyl (**110**) (1.50 g, 2.68 mmol, 1 equiv) and $\text{Pd}(\text{PPh}_3)_4$ (10 mol%, 0.309 g) were mixed in DME (20 mL) at room temperature under an argon atmosphere. 4-Methoxyphenylboronic acid (1.42 g, 9.37 mmol, 3.5 equiv) and aqueous Na_2CO_3 solution (7 mL, 2 M) were added and the resulting mixture was stirred and heated to reflux for 10 h, cooled to room temperature and passed through a bed of Celite. The organic solution was concentrated *in vacuo* to give a residue. The residue was dissolved in CH_2Cl_2 , washed with saturated aqueous ammonium chloride, water and brine, dried over sodium sulfate and concentrated to give a cream solid. Crude product was purified by column chromatography (EtOAc/hexane = 1/10) and crystallisation from CH_2Cl_2 /hexane to give white crystals (**214**) (1.55 g, 94%).

^1H NMR (400 MHz, CDCl_3) δ 7.98 (2H, s, ArH), 7.92 (2H, d, $J = 8.1$ Hz, ArH), 7.78 (4H, d, $J = 9.0$, ArH), 7.38-7.49 (2H, m, ArH), 7.22-7.36 (4H, m, ArH), 7.07 (4H, d, $J = 9.0$ Hz, ArH), 4.56 (2H, d, $J = 5.8$ Hz, OCH_2O), 4.51 (2H, d, $J = 5.8$ Hz, OCH_2O), 3.90 (6H, s, OCH_3), 2.70-2.85 (2H, m, OCH_2CH_3), 2.42-2.55 (2H, m, OCH_2CH_3), 0.49 (6H, t, $J = 7.0$ Hz, OCH_2CH_3).

^{13}C NMR (100 MHz, CDCl_3) δ 159.0, 151.5, 135.1, 133.3, 131.5, 131.3, 130.6, 130.1, 127.7, 126.4, 126.3, 126.0, 125.0, 113.7, 97.0, 64.2, 55.2, 14.1.

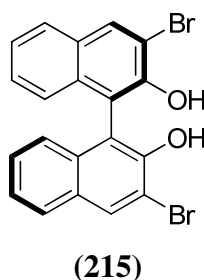
4.2.2.4 General Procedure B: preparation of 3,3'-disubstituted-2,2'-dihydroxy-1,1'-binaphthyls (**146**), (**147**), (**215**)-(217).



R = Br, Ph, Naphth, Biph, *p*MeOPh

A mixture of 3,3'-disubstituted-2,2'-bis(ethoxymethoxy)-1,1'-binaphthyl (2 mmol, 1 equiv) and Amberlyst 15 resin (1.00 g per 2 mmol) in THF/MeOH (1:1) was stirred and heated to reflux under an argon atmosphere for 15 h and cooled to room temperature. The resin was removed by filtration and the filtrate was concentrated. Subsequent purification gave the product.

4.2.2.4.1 (*R*)-3,3'-Dibromo-2,2'-dihydroxy-1,1'-binaphthyl (**215**)¹⁰⁸.



(*R*)-3,3'-Dibromo-2,2'-bis(ethoxymethoxy)-1,1'-binaphthyl (**110**) (1.00 g, 1.78 mmol, 1 equiv) was treated with Amberlyst 15 resin (0.890 g) in THF/MeOH (1:1, 30 mL) as described in General Procedure B. Purification was carried out by crystallisation (CH_2Cl_2 /hexane) to afford a white crystalline product (**215**) (0.688 g, 87%).

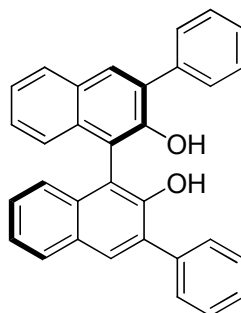
IR (cm^{-1}): ν 3940, 1617, 1578, 1497, 1448, 1422, 1359, 1250, 1203, 1135.

^1H NMR (400 MHz, CDCl_3) δ 8.26 (2H, s, ArH), 7.83 (2H, d, $J = 8.1$ Hz, ArH), 7.27-7.42 (4H, m, ArH), 7.11 (2H, d, $J = 8.5$ Hz, ArH), 5.51 (2H, br s, OH).

^{13}C NMR (CDCl_3) δ 148.1, 132.8, 129.8, 127.6, 127.4, 124.9, 124.6, 114.7, 112.3.

MS (ES^-) m/z 443.9 $[\text{M}-\text{H}]^-$.

4.2.2.4.2 (*R*)-3,3'-Diphenyl-2,2'-dihydroxy-1,1'-binaphthyl (**146**)^{60,109}.



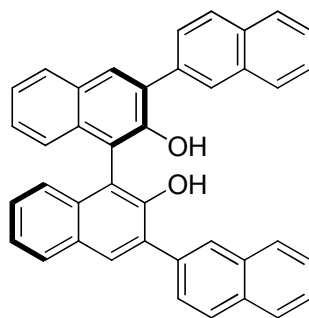
(146)

(*R*)-3,3'-Diphenyl-2,2'-bis(ethoxymethoxy)-1,1'-binaphthyl (**211**) (1.30 g, 2.34 mmol, 1 equiv) was treated with Amberlyst 15 resin (1.17 g) in THF/MeOH (1:1, 40 mL) as described in General Procedure B. Purification was carried out by column chromatography (EtOAc/hexane = 1/10) followed by crystallisation (CH_2Cl_2 /hexane) to afford a white crystalline product (**146**) (0.882 g, 86%).

^1H NMR (400 MHz, CDCl_3) δ 8.03 (2H, s, ArH), 7.93 (2H, s, $J = 8.1$ Hz, ArH), 7.66-7.78 (4H, m, ArH), 7.45-7.55 (4H, m, ArH), 7.36-7.45 (4H, m, ArH), 7.28-7.35 (2H, m, ArH), 7.22-7.27 (2H, m, ArH), 5.38 (2H, s, OH).

^{13}C NMR (100 MHz, CDCl_3) δ 150.2, 137.5, 132.9, 131.4, 130.7, 129.6, 129.4, 128.5, 128.4, 127.8, 127.3, 124.3, 124.3, 112.4.

MS (ES^+) m/z 461.2 $[\text{M}+\text{Na}]^+$.

4.2.2.4.3 **(*R*)-3,3'-Bis(2-naphthyl)-2,2'-dihydroxy-1,1'-binaphthyl (147)**^{108,109}.**(147)**

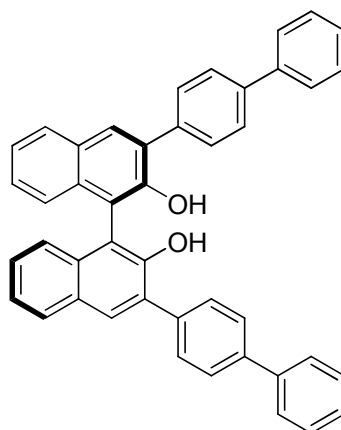
(*R*)-3,3'-Bis(2-naphthyl)-2,2'-bis(ethoxymethoxy)-1,1'-binaphthyl (1.00 g, 1.53 mmol, 1 equiv) was treated with Amberlyst 15 resin (0.764 g) in THF/MeOH (1:1, 40 mL) as described in General Procedure B. Purification was carried out by column chromatography (CH₂Cl₂/hexane = 1/1) followed by crystallisation (CH₂Cl₂/hexane) to afford a light yellow crystalline product (**147**) (0.740 g, 90%).

¹H NMR (400 MHz, CDCl₃) δ 8.22 (2H, s, ArH), 8.14 (2H, s, ArH), 7.82-8.05 (10H, m, ArH), 7.48-7.57 (4H, m, ArH), 7.27-7.46 (6H, m, ArH), 5.46 (2H, s, OH).

¹³C NMR (100 MHz, CDCl₃) δ 150.3, 135.0, 133.5, 133.0, 132.8, 131.7, 130.7, 129.6, 128.5, 128.2, 127.9, 127.7, 127.4, 126.3, 124.4, 124.3, 112.5.

MS (ES⁻) m/z 537.3 [M-H]⁻.

C₄₀H₂₆O₂ requires: C, 89.19%; H, 4.87%. Found: C, 88.98%; H, 4.89%.

4.2.2.4.4 (R)-3,3'-Bis(4-biphenyl)-2,2'-dihydroxy-1,1'-binaphthyl (**216**)¹⁰⁹.**(216)**

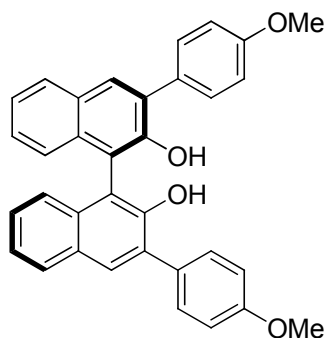
(R)-3,3'-Bis(4-biphenyl)-2,2'-bis(ethoxymethoxy)-1,1'-binaphthyl (1.50 g, 2.12 mmol, 1 equiv) was treated with Amberlyst 15 resin (1.06 g) in THF/MeOH (1:1, 40 mL) as described in General Procedure B. Purification was carried out by column chromatography (CH₂Cl₂/hexane = 1/1) followed by crystallisation (CH₂Cl₂/hexane) to afford a white crystalline product (**216**) (1.20 g, 96%).

¹H NMR (400 MHz, CDCl₃) δ 8.09 (2H, s, ArH), 7.96 (2H, d, *J* = 7.8 Hz, ArH), 7.85 (4H, d, *J* = 8.8 Hz, ArH), 7.74 (4H, d, *J* = 8.2 Hz, ArH), 7.63-7.69 (4H, m, ArH), 7.22-7.49 (12H, m, ArH), 5.41 (2H, s, OH).

¹³C NMR (100 MHz, CDCl₃) δ 150.2, 140.7, 140.5, 136.4, 132.9, 131.4, 130.2, 129.9, 129.5, 128.8, 128.5, 127.4, 127.3, 127.2, 126.1, 124.4, 124.3, 112.3.

MS (ES⁻) *m/z* 589.3 [M-H]⁻.

C₄₄H₃₀O₂ requires: C, 89.46%; H, 5.12%. Found: C, 89.27%; H, 5.20%.

4.2.2.4.5 **(*R*)-3,3'-Bis(4-methoxyphenyl)-2,2'-dihydroxy-1,1'-binaphthyl**
(217)⁶⁰.**(217)**

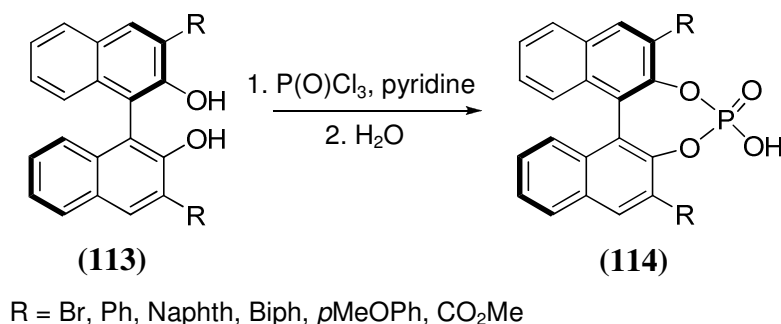
(*R*)-3,3'-Bis(4-methoxyphenyl)-2,2'-bis(ethoxymethoxy)-1,1'-binaphthyl (1.30 g, 2.11 mmol, 1 equiv) was treated with Amberlyst 15 resin (1.06 g) in THF/MeOH (1:1, 40 mL) as described in General Procedure B. Purification was carried out by column chromatography (CH₂Cl₂/hexane = 1/1) followed by crystallisation (CH₂Cl₂/hexane) to afford a white crystalline product **(217)** (1.00 g, 95%).

¹H NMR (400 MHz, CDCl₃) δ 7.99 (2H, s, ArH), 7.92 (2H, d, *J* = 8.0 Hz, ArH), 7.68 (4H, d, *J* = 9.0 Hz, ArH), 7.34-7.42 (2H, m, ArH), 7.25-7.33 (2H, m, ArH), 7.21 (2H, d, *J* = 9.0 Hz, ArH), 7.04 (4H, d, *J* = 9.0 Hz, ArH), 5.35 (2H, s, OH), 3.87 (6H, s, OCH₃).

¹³C NMR (100 MHz, CDCl₃) δ 159.4, 150.2, 132.8, 130.9, 130.7, 130.3, 129.8, 129.5, 128.3, 127.1, 124.3, 124.2, 114.0, 112.4, 55.4.

MS (ES⁻) *m/z* 497.3 [M-H]⁻.

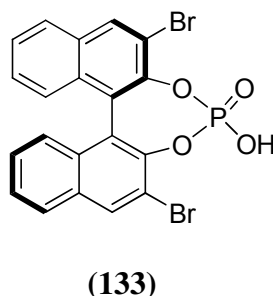
4.2.2.5 General Procedure C: preparation of 3,3'-disubstituted-1,1'-binaphthyl-2,2'-diyl hydrogenphosphates (7), (84), (133), (135), (136) and (218).



The preparation of binaphthyl-derived phosphoric acids (**114**) followed literature procedures.¹¹

The binaphthyl derivative (0.500 mmol) was dissolved into anhydrous pyridine (1 mL) under an argon atmosphere. To the resulting solution was added phosphorus oxychloride (1.5-2 equiv) at room temperature and the reaction mixture was stirred overnight. Water (1 mL) was added and the resulting suspension was stirred for a further 30 mins. Dichloromethane was added and the pyridine was removed by extraction with HCl (1 M). The organic phase was dried over Na₂SO₄ and the product was purified by column chromatography.

4.2.2.5.1 (*R*)-3,3'-Dibromo-1,1'-binaphthyl-2,2'-diyl hydrogenphosphate (133).



(*R*)-3,3'-Dibromo-2,2'-dihydroxy-1,1'-binaphthyl (**215**) (0.200 g, 0.450 mmol, 1 equiv) was treated with phosphorus oxychloride in pyridine as described in General Procedure C. Purification was carried out by column chromatography (ⁱPrOH/CH₂Cl₂ = 1/10) affording a white solid product (**133**) (0.202 g, 89%).

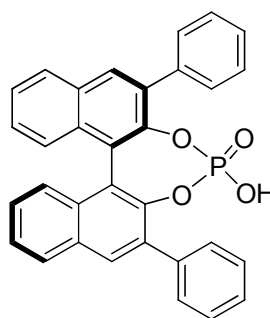
^1H NMR (400 MHz, CDCl_3) δ 8.26 (2H, s, ArH), 7.83 (2H, d, $J = 8.1$ Hz, ArH), 7.49 (2H, t, $J = 7.2$ Hz, ArH), 7.16-7.32 (4H, m, ArH).

^{13}C NMR (100 MHz, $(\text{CD}_3)_2\text{CO}$) δ 144.8 (d, $J_{\text{P-C}} = 9.6$ Hz), 134.8, 132.9, 132.0, 128.6, 128.1, 127.6, 127.3, 123.8 (d, $J_{\text{P-C}} = 2.2$ Hz), 115.2 (d, $J_{\text{P-C}} = 2.9$ Hz).

^{31}P (162 MHz, CDCl_3) δ 5.16.

HRMS (ESI) calculated for $\text{C}_{20}\text{H}_{10}\text{O}_4^{79}\text{Br}_2\text{P}$ ($[\text{M-H}]^-$) requires m/z 502.8685. Found m/z 502.8689.

4.2.2.5.2 **(*R*)-3,3'-Diphenyl-1,1'-binaphthyl-2,2'-diyl hydrogenphosphate (84)**⁶⁰.



(84)

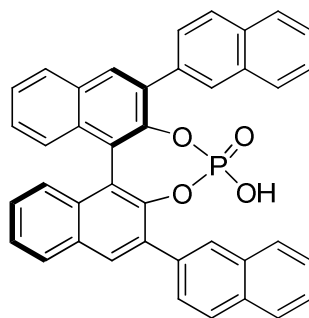
(*R*)-3,3'-Diphenyl-2,2'-dihydroxy-1,1'-binaphthyl (**146**) (0.200 g, 0.456 mmol, 1 equiv) was treated with phosphorus oxychloride in pyridine as described in General Procedure C. Purification was carried out by column chromatography ($i\text{PrOH}/\text{CH}_2\text{Cl}_2 = 1/10$) affording a white solid product (**84**) (0.207 g, 91%).

^1H NMR (400 MHz, CDCl_3) δ 7.72-7.89 (4H, m, ArH), 7.30-7.50 (6H, m, ArH), 7.28 (2H, d, $J = 8.5$ Hz, ArH), 7.11-7.21 (2H, m, ArH), 7.09-6.77 (6H, m, ArH).

^{13}C NMR (CDCl_3) δ 145.4 (d, $J_{\text{P-C}} = 9.6$ Hz), 140.9, 137.4, 134.4, 132.2, 131.4, 131.2, 129.9, 128.4, 128.2, 127.4, 127.1, 126.4, 125.9, 125.7, 122.8.

^{31}P (162 MHz, CDCl_3) δ 2.62.

HRMS (ESI) calculated for $\text{C}_{32}\text{H}_{20}\text{O}_4\text{P}$ ($[\text{M-H}]^-$) requires m/z 499.1105. Found m/z 499.1102.

4.2.2.5.3 **(*R*)-3,3'-Bis(2-naphthyl)-1,1'-binaphthyl-2,2'-diyl hydrogenphosphate (135)**⁸⁵.**(135)**

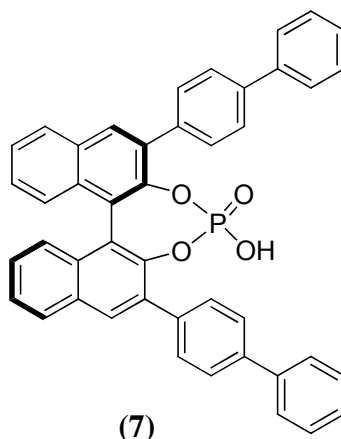
(*R*)-3,3'-Bis(2-naphthyl)-2,2'-dihydroxy-1,1'-binaphthyl (**147**) (0.200 g, 0.371 mmol, 1 equiv) was treated with phosphorus oxychloride in pyridine as described in General Procedure C. Purification was carried out by column chromatography (iPrOH/CH₂Cl₂ = 1/10) affording a white solid product (**135**) (0.198 g, 89%).

¹H NMR (400 MHz, (CD₃)₂SO) δ 8.35 (4H, s, ArH), 8.20 (2H, d, *J* = 8.1 Hz, ArH), 7.94-8.06 (8H, m, ArH), 7.52-7.63 (6H, m, ArH), 7.41 (2H, t, *J* = 7.5 Hz, ArH), 7.26 (2H, d, *J* = 8.5 Hz, ArH).

¹³C NMR (100 MHz, (CDCl₃) δ 144.8 (d, *J*_{P-C} = 9.2 Hz), 134.3, 134.2, 133.2, 132.6, 132.2, 131.6, 128.9, 128.5, 128.2, 127.7 (d, *J*_{P-C} = 4.4 Hz), 127.4, 127.2, 126.6, 126.1, 125.8 (d, *J*_{P-C} = 3.6 Hz), 122.5.

³¹P (162 MHz, (CD₃)₂SO) δ 2.37.

HRMS (ESI) calculated for C₄₀H₂₄O₄P ([M-H]⁻) requires *m/z* 599.1417. Found *m/z* 599.1408.

4.2.2.5.4 *(R)*-3,3'-Bis(4-biphenyl)-1,1'-binaphthyl-2,2'-diyl hydrogenphosphate (**7**)¹¹.

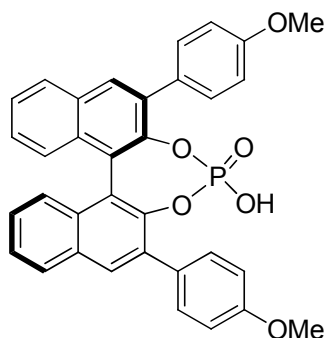
(R)-3,3'-Bis(4-biphenyl)-2,2'-dihydroxy-1,1'-binaphthyl (**216**) (0.200 g, 0.339 mmol, 1 equiv) was treated with phosphorus oxychloride in pyridine as described in General Procedure C. Purification was carried out by column chromatography (¹PrOH/CH₂Cl₂ = 1/10) affording a white solid product (**7**) (0.187 g, 85%).

¹H NMR (400 MHz, (CD₃)₂CO) δ 8.29 (2H, s, *ArH*), 8.20 (2H, d, *J* = 7.6 Hz, *ArH*), 7.94 (4H, d, *J* = 7.2 Hz, *ArH*), 7.68-7.82 (8H, m, *ArH*), 7.52-7.63 (2H, m, *ArH*), 7.28-7.50 (10H, m, *ArH*).

¹³C NMR (100 MHz, (CD₃)₂CO) δ 145.8 (d, *J*_{P-C} = 9.5 Hz), 141.1, 140.8, 137.0, 134.4 (d, *J*_{P-C} = 3.0 Hz), 132.7, 132.4, 132.3, 131.3, 129.6, 129.5, 128.2, 127.6, 127.5, 127.4, 126.9, 123.5 (d, *J*_{P-C} = 2.3 Hz).

³¹P (162 MHz, (CD₃)₂CO) δ 1.44.

HRMS (ESI) calculated for C₄₄H₂₈O₄P ([M-H]⁻) requires *m/z* 651.1730. Found *m/z* 651.1725.

4.2.2.5.5 **(*R*)-3,3'-Bis(4-methoxyphenyl)-1,1'-binaphthyl-2,2'-diyl hydrogenphosphate (136)**⁶⁰.**(136)**

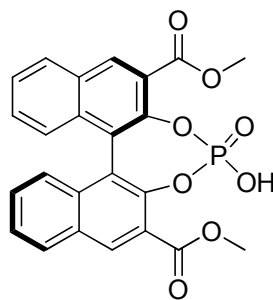
(*R*)-3,3'-Bis(4-methoxyphenyl)-2,2'-dihydroxy-1,1'-binaphthyl (**217**) (0.200 g, 0.401 mmol, 1 equiv) was treated with phosphorus oxychloride in pyridine as described in General Procedure C. Purification was carried out by column chromatography (iPrOH/CH₂Cl₂ = 1/10) affording a white solid product (**136**) (0.202 g, 90%).

¹H NMR (400 MHz, CDCl₃) δ 8.01 (2H, s, ArH), 7.98 (2H, d, *J* = 8.1 Hz, ArH), 7.58 (4H, d, *J* = 8.7 Hz, ArH), 7.45-7.53 (2H, m, ArH), 7.26-7.42 (4H, m, ArH), 6.86 (4H, d, *J* = 8.7 Hz, ArH), 3.52 (6H, s, OCH₃).

¹³C NMR (100 MHz, CDCl₃) δ 159.2, 144.7 (d, *J*_{P-C} = 8.9 Hz), 136.7 (d, *J*_{P-C} = 2.9 Hz), 131.7, 131.5, 131.0, 130.9, 129.0, 128.3, 127.0, 126.3, 125.9, 122.4 (d, *J*_{P-C} = 2.2 Hz), 113.8, 55.0.

³¹P (162 MHz, CDCl₃) δ 4.45.

HRMS (ESI) calculated for C₃₄H₂₄O₆P ([M-H]⁻) requires *m/z* 559.1316. Found *m/z* 559.1308.

4.2.2.5.6 **(*R*)-3,3'-Bis(methoxycarbonyl)-1,1'-binaphthyl-2,2'-diyl hydrogenphosphate (218).****(218)**

(*R*)-Dimethyl-2,2'-dihydroxy-1,1'-binaphthylene-3,3'-dicarboxylate (**116**) (0.200 g, 0.497 mmol, 1 equiv) was treated with phosphorus oxychloride in pyridine as described in General Procedure C. Purification was carried out by column chromatography (¹PrOH/CH₂Cl₂ = 1/10) affording a cream-coloured solid product (**218**) (0.173 g, 75%).

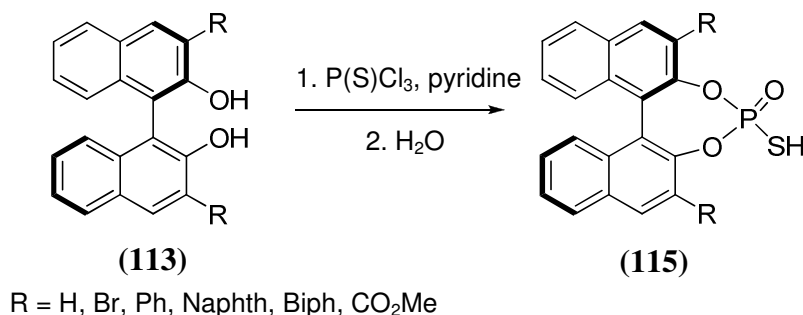
¹H NMR (400 MHz, CDCl₃) δ 8.58 (2H, s, ArH), 7.97 (2H, d, *J* = 8.5, ArH), 7.45 (2H, t, *J* = 7.4, ArH), 7.27 (2H, t, *J* = 7.4, ArH) 7.12 (2H, d, *J* = 8.5, ArH), 3.92 (6H, s, OCH₃).

¹³C NMR (100 MHz, CDCl₃) δ 165.7, 145.2 (d, *J*_{P-C} = 9.1 Hz), 134.7, 134.0, 130.2, 129.5, 128.6, 126.7, 126.2, 123.1 (d, *J*_{P-C} = 2.9 Hz), 122.8 (d, *J*_{P-C} = 2.9 Hz), 52.8.

³¹P (162 MHz, CDCl₃) δ 3.87.

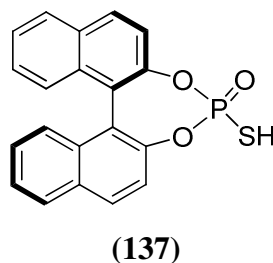
MS (ES⁻) *m/z* 463.2 [M-H]⁻.

4.2.2.6 General Procedure D: preparation of 3,3'-disubstituted-1,1'-binaphthyl-2,2'-diyl thiophosphates (137), (138), (219)-(222).



The binaphthyl derivative (0.500 mmol) was dissolved into anhydrous pyridine (1 mL) under an argon atmosphere. To the resulting solution was added thiophosphoryl chloride (1.5-2 equiv) at room temperature and the reaction mixture was stirred overnight. Water (1 mL) was added and the resulting suspension was stirred for a further 30 mins. Dichloromethane was added and the pyridine was removed by extraction with HCl (1 M). The organic phase was dried over Na₂SO₄ and the product was purified by column chromatography.

4.2.2.6.1 (*R*)-1,1'-Binaphthyl-2,2'-diyl hydrogenthiophosphate (137).



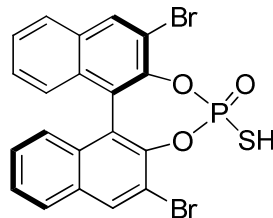
(*R*)-2,2'-dihydroxy-1,1'-binaphthyl (0.200 g, 0.699 mmol, 1 equiv) was treated with thiophosphoryl chloride in pyridine as described in General Procedure D. Purification was carried out by column chromatography (iPrOH/CH₂Cl₂ = 1/10) affording a white solid product (**137**) (0.234 g, 92%).

¹H NMR (400 MHz, CDCl₃) δ 7.92-8.08 (4H, m, ArH), 7.46-7.62 (4H, m ArH), 7.42 (2H, d, *J* = 8.8 Hz, ArH), 7.28-7.36 (2H, m, ArH).

³¹P (162 MHz CDCl₃) δ 66.87

HRMS (ESI) calculated for $C_{20}H_{12}O_3PS$ ($[M-H]^-$) requires m/z 363.0250. Found m/z 363.0247.

4.2.2.6.2 **(*R*)-Dibromo-1,1'-binaphthyl-2,2'-diyl hydrogenthiophosphate (138).**



(138)

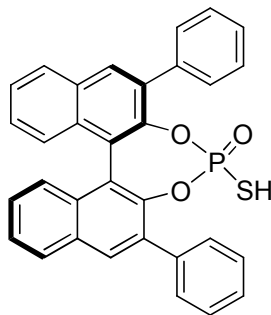
(*R*)-3,3'-Dibromo-2,2'-dihydroxy-1,1'-binaphthyl (**215**) (0.200 g, 0.450 mmol, 1 equiv) was treated with thiophosphoryl chloride in pyridine as described in General Procedure D. Purification was carried out by column chromatography ($iPrOH/CH_2Cl_2 = 1/10$) affording a pale yellow solid product (**138**) (0.199 g, 85%).

1H NMR (400 MHz, $CDCl_3$) δ 8.32 (1H, s, *ArH*), 8.28 (1H, s, *ArH*), 7.82 (2H, t, $J = 7.6$ Hz, *ArH*), 7.44-7.50 (2H, m, *ArH*), 7.23- 7.34 (4H, m, *ArH*).

^{31}P (162 MHz $CDCl_3$) δ 69.85.

HRMS (ESI) calculated for $C_{20}H_{10}O_3^{79}Br_2PS$ ($[M-H]^-$) requires m/z 518.8460. Found m/z 518.8453.

Calculated for $C_{20}H_{10}O^{79}Br^{81}BrPS$ ($[M-H]^-$) requires m/z 520.8440. Found m/z 520.8432.

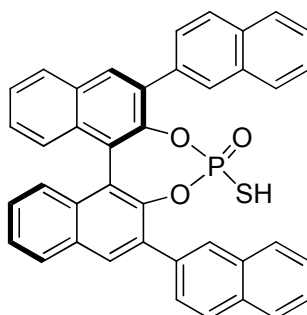
4.2.2.6.3 **(*R*)-3,3'-Diphenyl-1,1'-binaphthyl-2,2'-diyl hydrogenthiophosphate (219).****(219)**

(*R*)-3,3'-Diphenyl-2,2'-dihydroxy-1,1'-binaphthyl (**146**) (0.200 g, 0.456 mmol, 1 equiv) was treated with thiophosphoryl chloride in pyridine as described in General Procedure D. Purification was carried out by column chromatography (iPrOH/CH₂Cl₂ = 1/10) affording a white solid product (**219**) (0.203 g, 86%).

¹H NMR (400 MHz, CDCl₃) δ 8.16-8.26 (4H, m, ArH), 7.68-7.76 (4H, m, ArH), 7.36-7.62 (12H, m, ArH).

³¹P (162 MHz CDCl₃) δ 71.09.

HRMS (ESI) calculated for C₃₂H₂₀O₃PS ([M-H]⁻) requires m/z 515.0876. Found m/z 515.0868.

4.2.2.6.4 **(*R*)-3,3'-Bis(2-naphthyl)-1,1'-binaphthyl-2,2'-diyl hydrogenthiophosphate (220).****(220)**

(*R*)-3,3'-Bis(2-naphthyl)-2,2'-dihydroxy-1,1'-binaphthyl (**147**) (0.150 g, 0.278 mmol, 1 equiv) was treated with thiophosphoryl chloride in pyridine as described in General

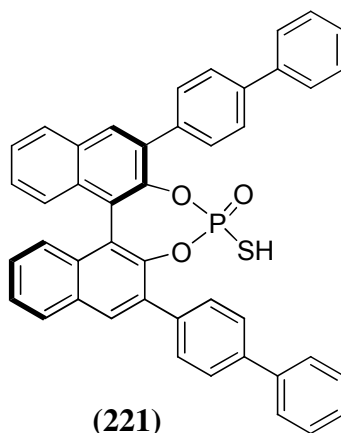
Procedure D. Purification was carried out by column chromatography (i PrOH/CH₂Cl₂ = 1/10) affording a white solid product (**220**) (0.147 g, 86%).

¹H NMR (400 MHz, CDCl₃) δ 8.24 (2H, d, J = 9.2 Hz, ArH), 8.13-8.18 (2H, m, ArH), 8.04-8.09 (2H, m, ArH), 7.85-7.98 (5H, m, ArH), 7.78-7.84 (2H, m, ArH), 7.58-7.64 (2H, t, J = 7.6 Hz, ArH), 7.47-7.55 (5H, m, ArH), 7.37-7.44 (4H, m, ArH).

³¹P (162 MHz CDCl₃) δ 71.03.

HRMS (ESI) calculated for C₄₀H₂₄O₃PS ([M-H]⁻) requires m/z 615.1189. Found m/z 615.1183.

4.2.2.6.5 (*R*)-3,3'-Bis(4-biphenyl)-1,1'-binaphthyl-2,2'-diyl hydrogenthiophosphate (**221**).

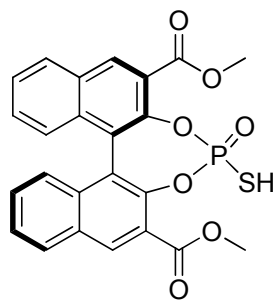


(*R*)-3,3'-Bis(4-biphenyl)-2,2'-dihydroxy-1,1'-binaphthyl (**216**) (0.200 g, 0.339 mmol, 1 equiv) was treated with thiophosphoryl chloride in pyridine as described in General Procedure D. Purification was carried out by column chromatography (i PrOH/CH₂Cl₂ = 1/10) affording a white solid product (**221**) (0.186 g, 82%).

¹H NMR (400 MHz, (CD₃)₂CO) δ 8.27 (2H, d, J = 8.0 Hz, ArH), 8.12-8.20 (2H, m, ArH), 7.81-7.90 (4H, m, ArH), 7.70-7.89 (8H, m, ArH), 7.31-7.59 (12 H, m, ArH).

³¹P (162 MHz (CD₃)₂CO) δ 68.55.

HRMS (ESI) calculated for C₄₄H₂₈O₃PS ([M-H]⁻) requires m/z 667.1502. Found m/z 667.1496.

4.2.2.6.6 **(*R*)-3,3'-Bis(methoxycarbonyl)-1,1'-binaphthyl-2,2'-diyl hydrogen thiophosphate (222).****(222)**

(*R*)-Dimethyl-2,2'-dihydroxy-1,1'-binaphthylene-3,3'-dicarboxylate (**116**) (0.150 g, 0.373 mmol, 1 equiv) was treated with thiophosphoryl chloride in pyridine as described in General Procedure D. Purification was carried out by column chromatography (ⁱPrOH/CH₂Cl₂ = 1/10) affording a pale yellow solid product (**222**) (0.140 g, 78%).

¹H NMR (400 MHz, CDCl₃) δ 8.76 (2H, s, ArH), 7.97 (2H, d, *J* = 8.5, ArH), 7.45 (2H, t, *J* = 7.4, ArH), 7.27 (2H, t, *J* = 7.4, ArH) 7.12 (2H, d, *J* = 8.5, ArH), 3.92 (6H, s, OCH₃).

³¹P (162 MHz CDCl₃) δ 69.31.

HRMS (ESI) calculated for C₂₄H₁₆O₇PS ([M-H]⁻) requires *m/z* 479.0359. Found *m/z* 479.0356.

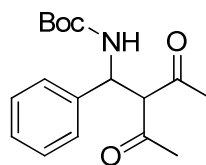
4.2.3 General procedure for phosphoric acid-catalysed direct Mannich reactions.

Catalysed direct Mannich reactions were performed according to literature procedures.¹¹

Catalyst (0.002 mmol, 0.02 equiv), was weighed into an oven dried vial which was then capped with a rubber septum and placed under an argon atmosphere. Dichloromethane was added (1 mL) via syringe injection. *N*-Boc imine (0.100 mmol) was then added quickly under a flow of argon and the mixture was stirred. Acetylacetone (**82**) (11.3 μ L, 0.110 mmol, 1.1 equiv) was added and the resulting solution was stirred for 1h at room temperature. The reaction mixture was poured onto a silica gel column and purified by flash column chromatography ($\text{CH}_2\text{Cl}_2 \rightarrow \text{CH}_2\text{Cl}_2/\text{diethyl ether} = 20/1$). Enantiomeric excess of the β -aminoketone product was determined by HPLC analysis.

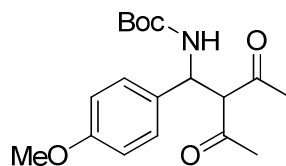
Racemic samples were prepared by reaction of acetylacetone with *N*-Boc imines with no catalyst present. These reactions were monitored by TLC until completion and then purified.

All products of catalysed and uncatalysed reactions were examined by ^1H NMR spectroscopy and mass spectrometry to confirm identity.

4.2.3.1 (2-Acetyl-3-oxo-1-phenyl-butyl)-carbamic acid *tert*-butyl ester (141)¹¹.**(141)**

¹H NMR (400 MHz, CDCl₃) δ 7.24-7.34 (5H, m, ArH), 5.82 (1H, br s, NH), 5.45 (1H, br s, NHCH), 4.20 (1H, d, *J* = 6.8 Hz, NHCHCH), 2.18 (3H, br s, COCH₃), 2.11 (3H, s, COCH₃), 1.39 (9H, s, C(CH₃)₃).

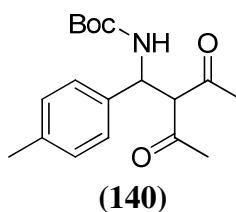
MS (ES⁺) *m/z* 328.2 ([M+Na]⁺).

4.2.3.2 [2-Acetyl-1-(4-methoxyphenyl)-3-oxo-butyl]-carbamic acid *tert*-butyl ester (139)¹¹.**(139)**

HPLC analysis: Chiralpak IA (Hexane: EtOH 90:10, 1 mL/min, 254 nm, 10 °C) 18.4 (major), 24.6 min.

¹H NMR (400 MHz, CDCl₃) δ 7.18 (2H, d, *J* = 8.0 Hz, ArH), 6.85 (2H, d, *J* = 8.0 Hz, ArH), 5.67 (1H, br s, NH), 5.42 (1H, br s, NHCH), 4.17 (1H, d, *J* = 6.9 Hz, NHCHCH), 3.77 (3H, s, PhOCH₃), 2.14 (3H, s, COCH₃), 2.12 (3H, s, COCH₃), 1.41 (9H, s, C(CH₃)₃).

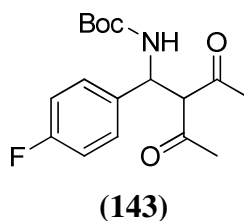
MS (ES⁺) *m/z* 358.2 ([M+Na]⁺).

4.2.3.3 (2-Acetyl-3-oxo-1-(4-tolyl)-butyl)-carbamic acid *tert*-butyl ester (140)¹¹.

HPLC analysis: Chiralpak IA (Hexane: EtOH 90:10, 1 mL/min, 254 nm, 10 °C) 13.3 (major), 18.7 min.

¹H NMR (400 MHz, CDCl₃) δ 7.05-7.17 (4H, m, ArH), 5.70 (1H, br s, NH), 5.44 (1H, br s, NHCH), 4.18 (1H, d, *J* = 7.0 Hz, NHCHCH), 2.31 (3H, s, PhCH₃), 2.18 (3H, s, COCH₃), 2.12 (3H, s, COCH₃), 1.39 (9H, s, C(CH₃)₃).

MS (ES⁺) *m/z* 342.2 ([M+Na]⁺).

4.2.3.4 [2-Acetyl-1-(4-fluorophenyl)-3-oxo-butyl]-carbamic acid *tert*-butyl ester (143)¹¹.

HPLC analysis: Chiralpak IA (Hexane: EtOH 90:10, 1 mL/min, 254 nm, 10 °C) 14.2 (major), 19.1 min.

¹H NMR (400 MHz, CDCl₃) δ 7.15-7.27 (2H, m, ArH), 6.92-7.02 (2H, m, ArH), 5.67 (1H, br s, NH), 5.35 (1H, br s, NHCH), 4.09 (1H, d, *J* = 6.8 Hz, NHCHCH), 2.16 (3H, s, COCH₃), 2.09 (3H, s, COCH₃), 1.36 (9H, s, C(CH₃)₃).

MS (ES⁺) *m/z* 346.2 ([M+Na]⁺).

4.3 Materials.

Deuterium oxide (99.9% D) was purchased from Apollo Scientific Ltd. Potassium deuterioxide (40 wt% 98+% D) and deuterated chloroform (99.8% D) were purchased from Sigma-Aldrich. Deuterium chloride (35%, 99.5% D), dichloromethane-d₂ (99.8% D), acetone-d₆ (99.9% D), acetonitrile-d₃ (99.8% D) and dimethyl sulfoxide-d₆ (99.8% D) were purchased from Goss Scientific.

Dimethyl sulfoxide ($\geq 99.9\%$ ACS reagent for spectrophotometry) was purchased from Sigma-Aldrich. Acetonitrile (HPLC grade, 99.6+%) was purchased from Fisher.

1-Butyl-3-methylimidazolium hexafluorophosphate (**185**) (99%), 1-hexyl-3-methylimidazolium hexafluorophosphate (**186**) (99%) and 1-octyl-3-methylimidazolium bromide (**187**) (99%) were purchased from Solvent Innovation Chemicals Ltd. 2-Phenyl-6,7-dihydro-5H-pyrrolo[2,1-c][1,2,4]triazol-2-ium tetrafluoroborate (**179**), 4-methoxyphenyl-6,7-dihydro-5H-pyrrolo[2,1-c][1,2,4]triazol-2-ium tetrafluoroborate (**180**), pentafluorophenyl-6,7-dihydro-5H-pyrrolo[2,1-c][1,2,4]triazol-2-ium tetrafluoroborate (**181**) and 1,3,4-triphenyl-4H-1,2,4-triazol-1-ium tetrafluoroborate (**182**) were provided by Dr. Andrew Smith, University of St. Andrews. The internal standard, tetramethylammonium deuteriosulfate was a generous gift from Prof. Tina Amyes, University of Buffalo, New York. (*R*)-1,1'-binaphthyl-2,2'-diyl hydrogenphosphate (**85**) was purchased from Sigma-Aldrich.

All other chemicals were reagent grade and were used without further purification unless otherwise stated.

4.4 Preparation of solutions.

4.4.1 Preparation of solutions for ^1H NMR kinetic experiments.

4.4.1.1 ^1H NMR exchange experiments

Stock solutions of potassium deuterioxide and deuterium chloride were prepared by dilution and titration of the commercial concentrated solutions. Stock solutions of buffers, K_2DPO_4 and KD_2PO_4 , were obtained from potassium phosphate monobasic and dibasic by exchanging the hydrogen atoms for deuterium. This was achieved by dissolving the salts in D_2O , followed by removal of solvent under reduced pressure. The process was repeated five times and the salts were freeze dried. Phosphate buffers were prepared by mixing stock solutions of K_2DPO_4 and KD_2PO_4 in D_2O with addition of KCl to give solutions of buffer at various acid/ base ratios and $I = 1.0$ (KCl).

Stock solutions of acetate buffers were prepared by mixing stock solutions of potassium acetate and DCl with addition of KCl when needed to give buffer solutions at various acid/base ratios and $I = 1.0$ (KCl).

4.4.1.2 ^1H NMR studies of the Mannich reaction.

Stock solutions of imines and acetylacetone were prepared in dried vials fitted with rubber septa under an argon atmosphere. Solutions were prepared immediately prior to use.

4.4.2 Preparation of solutions for UV-Vis spectrophotometric experiments.

4.4.2.1 Kinetics of imine hydrolysis.

Stock solutions of potassium hydroxide and hydrogen chloride were prepared by dilution and titration of the commercial concentrated solutions. Acetic acid, chloroacetic acid and imidazole buffers were prepared by mixing stock solutions of the respective basic buffer salts and stock solutions of hydrochloric acid with the addition of KCl when needed to give solutions of buffer at various acid/base ratios and $I = 1.0$

(KCl). Phosphate buffers were prepared by mixing stock solutions of K_2HPO_4 and KH_2PO_4 in H_2O with addition of KCl to give solutions of buffer at various acid/ base ratios and $I = 1.0$ (KCl).

Stock solutions of imines were prepared in spectrophotometric grade acetonitrile and stored in the freezer in dry bags in between kinetic measurements. The final concentration of acetonitrile in the reaction mixture was $< 1\%$.

4.4.2.2 Determination of pK_a values in dimethyl sulfoxide.

Stock solutions of NaOH were prepared by dilution of volumetric standards into DMSO. Upon measurement, the final concentration of water in the cuvette was $< 2\%$. Acid stock solutions were prepared by dilution of a volumetric standard of HCl in ether into DMSO. Upon measurement, the final concentration of ether in the cuvette was $< 1\%$.

4.4.3 Preparation of solutions for stopped-flow spectrophotometric measurements.

HCl solutions were prepared at twice the required concentration to account for dilution upon mixing in the stopped flow apparatus. pH measurements were conducted on diluted samples of HCl solutions to obtain the final pH of reaction mixture. Stock solutions of imine were prepared in acetonitrile (6 mM). These stock solutions were diluted (1/60) into KCl (1M) immediately prior to measurement to minimise decay of the imine substrate.

4.5 Kinetic methods

4.5.1 ^1H NMR exchange reactions.

H/D exchange reactions of imidazolium ions (**185**)-(**187**) and triazolium ions (**179**)-(**180**) were carried out in 12.5 mL vials which were incubated at 25 ± 0.1 °C in a thermostated water bath. All reactions were carried out in D_2O with the ionic strength maintained at $I = 1.0$. Typically, reactions were run on a 5 mL scale and were initiated by injection of buffer and internal standard solution to solid substrate. In general, the final substrate and internal standard concentrations in the reaction solutions were 5 - 10 mM and 0.5 - 1 mM, respectively. This ensured an approximately 1:1 ^1H NMR integration ratio of the singlet due to relevant acidic hydrogen of substrate and the triplet due to the 12 methyl hydrogens of internal standard.

The reaction progress was monitored over time by withdrawing aliquots (~ 800 μL) at timed intervals. These aliquots were quenched to pD 0-1 by addition of 5 M DCl solution. The samples were analysed immediately by ^1H NMR spectroscopy.

H/D exchange reactions of triazolium ions (**181**)-(**182**) were performed in NMR tubes and monitored directly by obtaining back to back scans on the instrument in use. In these cases the temperature of the instrument was calibrated to 25 °C prior to monitoring the reaction. Reactions were initiated by addition of HCl and internal standard solutions directly to solid substrate.

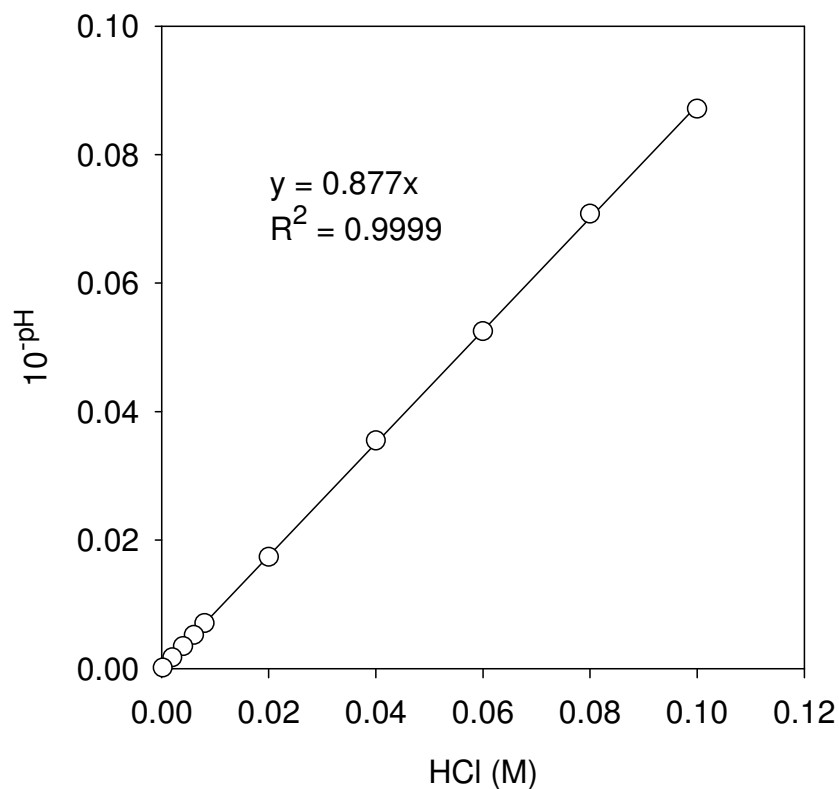
The pD of buffered solutions was determined at 25 °C using a MeterLabTM PHM 290 pH-Stat Controller equipped with a radiometer (pH 4 - 7 - 10 @ 25 °C) combination electrode, that could be standardised between pH 4 - 7 or pH 7 - 10 to encompass the pD of the buffer solution. The pD was calculated by adding 0.4 to the observed reading of the pH meter.

The hydronium ion concentration at any pH was calculated from $[\text{H}_3\text{O}^+] = 10^{-\text{pH}}/\gamma_{\text{H}}$, where $\gamma_{\text{H}} = 0.877$ is the apparent activity coefficient of hydronium ion under our experimental conditions. To determine a value for γ_{H} , a series of dilutions of standardised 1M HCl were made to give a titrimetrically known series of HCl

solutions in the concentration range 0.001 – 0.1 M and the pHs of these solutions measured. The fit of the data to Equation 4.1 gave $\gamma_{\text{H}} = 0.877$ (Figure 4.1)

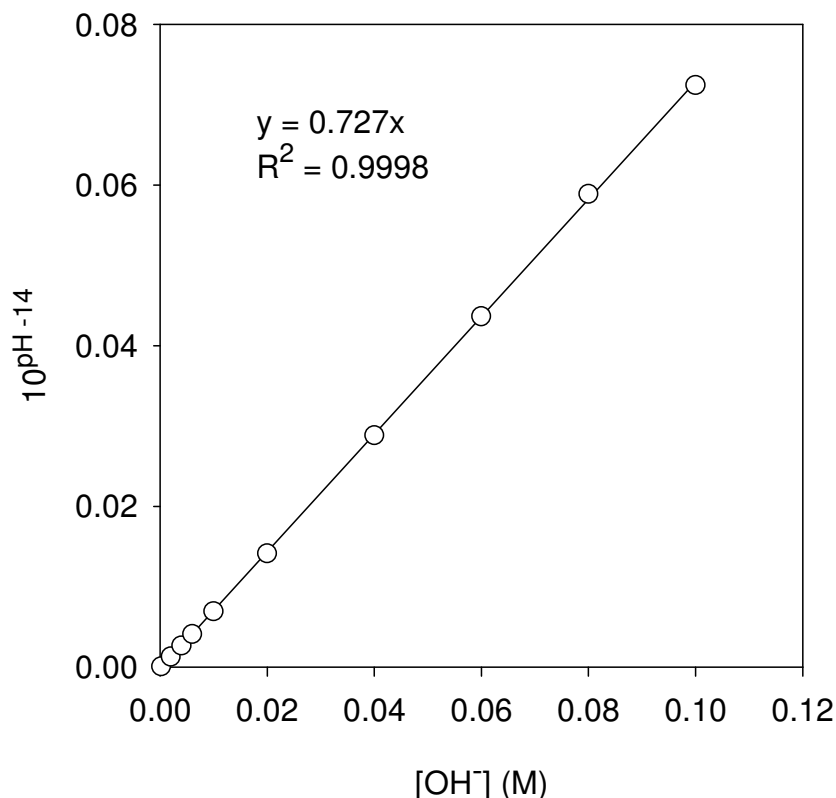
$$10^{-\text{pH}} = \gamma_{\text{H}} [\text{H}^+] \quad (\text{Equation 4.1})$$

Figure 4.1: Determination of the activity coefficient for hydronium ion.



Similarly, the activity coefficient for hydroxide ion was determined from the fit of the observed pH of a series of solutions of known hydroxide concentration at constant ionic strength to Equation 4.2 as shown in Figure 4.2.

$$10^{(\text{pH}-\text{p}K_{\text{w}})} = \gamma_{\text{OH}} [\text{HO}^-] \quad (\text{Equation 4.2})$$

Figure 4.2: Determination of the activity coefficient for hydroxide ion.

The deuterioxide concentration was calculated from the equation $[\text{DO}^-] = (10^{\text{pD}} - \text{p}K_w)/\gamma_{\text{DO}}$, where $K_w = 10^{-14.87} \text{ M}^2$ is the ion product of D_2O at 25 °C and $\gamma_{\text{DO}} = 0.727$ is the apparent activity coefficient of deuterioxide ion under our experimental conditions. The estimated error on the observed pseudo-first-order rate constant (k_{obs} , s^{-1}) is $\pm 5\%$ based on the error of the ^1H NMR measurement. Although the measurements of k_{obs} and the calculation of $\text{p}K_a$ are single determinations, the calculated error in similar measurements and calculations performed by Richard *et al.*¹¹⁰ is $\pm 5\%$ for k_{obs} and ± 0.5 units for the $\text{p}K_a$.

^1H NMR spectra of 1-butyl-3-methylimidazolium hexafluorophosphate (**185**), 1-hexyl-3-methylimidazolium hexafluorophosphate (**186**), 1-octyl-3-methylimidazolium bromide (**187**) were recorded on a Bruker 400 Ultrashield spectrometer. The relaxation delay between pulses was set to 1 s on this spectrometer. Spectra were recorded at a pulse angle of 90° , a sweep width of 8278.1 Hz, an acquisition time of 7.899 sec, and

16 transients (total running time 5-10 min). Baselines were subject to first-order drift correction before integration of the peak areas.

^1H NMR spectra of triazolium ions (**179**) and (**180**) were recorded on a Varian 400 spectrometer with a relaxation delay of 20 s, sweep width of 7996.8 Hz, and acquisition time of 4 sec and a 90° pulse angle. Spectra were run with 32 transients with a total running time of 12 minutes.

^1H NMR spectra of triazolium ions (**181**)-(**182**) were recorded on an Oxford Varian Inova 500 spectrometer with a relaxation delay of 20 s, sweep width of 7996.8 Hz, an acquisition time of 4 sec and a 90° pulse angle. Spectra were run with 32 transients with a total running time of 12 minutes.

4.5.2 ^1H NMR studies of the Mannich reaction.

Mannich reactions were conducted in NMR tubes which had been thoroughly dried and flushed with argon. Reactions were initiated by injection of imine stock solution to a solution containing a 10-fold excess of acetylacetone.

For reactions performed at 22°C , the NMR tubes were kept in a thermostated water bath between NMR spectroscopic measurements. Spectra were recorded on a Varian 400 MHz instrument with a relaxation delay of 20 sec, sweep width of 7996.8 Hz, an acquisition time of 4 sec, a 90° pulse angle and 16 transients with a total running time of 6 minutes.

For reactions performed at 25°C , the reaction was monitored in NMR tubes by taking back to back spectra on an Oxford Varian Inova 500 spectrometer with a relaxation delay of 20 s, sweep width of 7996.8 Hz, an acquisition time of 4 sec and a 90° pulse angle. Spectra were run with 16 transients with a total running time of 6 minutes. In these cases the temperature of the instrument was calibrated to 25°C prior to monitoring the reaction.

4.5.3 UV-Vis spectrophotometric measurements.

4.5.3.1 Kinetics of imine hydrolysis

Measurements were performed on Cary 50 and Cary 100 spectrometers. Both were equipped with Peltier thermostated multi-cell holders which maintained the temperature at 25 °C. Buffer solutions were delivered to quartz cuvettes (3 mL) using glass pipettes. The solutions were equilibrated for at least ten minutes prior to the addition of 25 μ L of imine stock solution using Hamilton syringes. The reactions were followed at a single analytical wavelength.

4.5.3.2 Determination of pK_a values.

Measurements were conducted on a Cary 100 instrument using matching quartz cuvettes (1 mL). The absorbance was zeroed on a sample containing DMSO only. Acid or base solutions were added to cuvettes already containing the relevant compound and indicator solutions. For investigations involving BINOL-derived phosphoric acids, the absorbance was recorded at a single wavelength for ten minutes and a UV-Vis scan was then obtained. For determination of pK_a values of iminium ions, a scan was recorded rapidly (30 sec) followed by absorbance measurement at a single analytical wavelength. Decomposition of the compound did not induce a large change in absorbance at the analytical wavelength chosen.

4.5.4 Stopped-flow spectrophotometric measurements.

Stopped-flow spectrophotometry was used to measure rates of imine hydrolysis in acid solution. This was achieved using two syringes (2.5 mL) in a 1:1 mixing arrangement. One syringe contained acid solution (at twice the required concentration) and the second syringe contained imine solution (1/60 dilution of a 6 mM stock in acetonitrile into KCl (1 M)). The solutions were incubated at 25 °C for several minutes and the lines were flushed thoroughly with these solutions before data was acquired. These reactions were monitored at a single analytical wavelength.

Chapter 5

Summary and future work

In order to probe the mechanism of the phosphoric acid-catalysed Mannich reaction, a series of substituted *N*-Boc imine substrates were synthesised as well as a range of phosphoric acid catalysts. Thiophosphoric acid catalysts were also prepared. It is generally assumed in the literature that chirality transfer occurs by proton transfer from the catalyst to a single enantiotopic face of substrate, however the extent of proton transfer, if any, has not been experimentally quantified to date. It was therefore considered important to investigate the relative acidities of the catalysts and substrates. The pK_a values of iminium ions and (thio)phosphoric acids were investigated in water and organic solvent.

The hydrolytic lability of *N*-Boc imines complicated the determination of aqueous pK_a values as conventional techniques could not be used. The approach adopted in this work involved the construction of pH-rate profiles for imine hydrolysis. This was achieved by measuring rates of hydrolysis in aqueous buffered solution at 25 °C and ionic strength of unity. Unfortunately pK_a values could not be estimated from these rate profiles as a pH-independent region at low pH could not be accessed. Values for k_H ($M^{-1}s^{-1}$) the second-order rate constant for acid catalysed hydrolysis and k_0 (s^{-1}) the first-order rate constant for uncatalysed hydrolysis were extracted from the rate profiles. The values for k_H were in the range $4.39 - 3.50 \times 10^1 M^{-1}s^{-1}$ while the values for k_0 showed a smaller variation and were in the range $1.19 \times 10^{-5} - 3.20 \times 10^{-5} s^{-1}$. It was possible to estimate from these rate-profiles that the aqueous pK_a values of the iminium ions are < 2 units. The pK_a values of iminium ions were successfully determined in dimethyl sulfoxide using a bracketing indicator method and were in the range 0.65-1.61. The determination of aqueous pK_a values of (thio)phosphoric acids could not be achieved due to the poor solubility of the catalysts in water. However, values were successfully determined in DMSO utilising a bracketing indicator method and were in the range 2.21-3.86. There was a surprisingly small variation in acidity with a range of substituents in the 3,3'-positions.

There is a relatively small difference in iminium ion and catalyst pK_a of 1-3 units which suggests that complete proton transfer from the phosphoric acid to the imine does not occur. This is consistent with the observation of H-bonded associates in the 1H NMR spectra of 1:1 mixtures of both species by Terada.⁶²

The catalysts synthesised in this work were applied in the Mannich reaction and the products were analysed by chiral HPLC. It is clear from our results that all (thio)phosphoric acids investigated in this work are good catalysts of the Mannich reaction, achieving 100% conversion after 1 hour (~70% conversion to Mannich product with remaining material identified as imine hydrolysis product). It was found that catalysts with aromatic moieties in the 3,3'-positions achieved the highest *ees* which is consistent with the observations of Terada.¹¹ To date, thiophosphoryl analogues of BINOL-derived phosphoric acids have not been applied to the asymmetric Mannich reaction. During these investigations it was observed that use of these catalysts dramatically reduced the enantioselectivity. The extent of hydrogen bonding/proton transfer should be similar to that which occurs for phosphoric acids as the difference in pK_a between the thiophosphoryl and phosphoric acid catalysts was found to be small (< 0.7 units). The decrease in enantioselectivity may thus be attributed to the larger size of sulfur relative to oxygen which could potentially allow more flexibility or rotation in the H-bonded associates. In this case, a single face of imine substrate may not be as effectively blocked from nucleophilic attack and hence a single enantiomer is not selectively formed.

Rate constants for the background Mannich reaction of *N*-Boc imines and acetylacetone were measured in CD_3CN , CD_2Cl_2 and $CDCl_3$ using 1H NMR spectroscopy. It was observed that the background reaction occurs more slowly in CD_2Cl_2 and $CDCl_3$, making these solvents appropriate for use in the catalysed Mannich reaction. Measurement of rate constants for the catalysed Mannich reaction was not possible due to a competing hydrolysis reaction. Attempts at suppressing this hydrolysis were unsuccessful. Further approaches to eliminating decomposition of the *N*-Boc imines could include use of different techniques for drying solvents and reagents and use of a glove box for preparation of solutions. Low temperatures could be employed for monitoring the reaction rate.

Providing the rate constants can be measured for catalysed Mannich reactions, a Brønsted plot could be constructed. Correlation of the catalytic constants with pK_a values of iminium ions and phosphoric acid catalysts would provide access to Brønsted coefficients α and β , the magnitude of which could indicate the extent of proton transfer in the transition state for the rate-determining step of the reaction, in the

simplest cases. Comparison of the α or β value with the reaction enantioselectivity where relevant could suggest the extent of proton transfer necessary for optimal selectivities and aid the rational design of better and more broadly applicable Brønsted acid catalysts.

This work also encompassed *N*-heterocyclic carbenes, an important class of organocatalyst. These NHCs are generally formed *in situ* from azolium ion precursors and so knowledge of the carbon acid pK_a values of azolium ions is much sought after. As such we utilised a kinetic approach to investigate the carbon acid pK_a values of *N,N*-dialkylimidazolium ions and triazolium ions in aqueous solution. The reactivity of these ions towards deuterioxide ion was investigated in aqueous solution at various pDs at 25 °C and ionic strength of unity using ^1H NMR spectroscopy. Second-order plots and pD-rate profiles were constructed from which second-order rate constants for deuterioxide ion-catalysed exchange k_{DO} ($\text{M}^{-1}\text{s}^{-1}$) could be estimated.

The values of k_{DO} ($\text{M}^{-1}\text{s}^{-1}$), the second-order rate constants for deuterioxide ion-catalysed exchange of *N,N*-dialkylimidazolium ions (**185**)-(b187) were found to be identical within experimental error (1.03 - $1.07 \text{ M}^{-1}\text{s}^{-1}$). A small counter ion effect was observed. This was not unexpected considering that in aqueous solution the ion pairs are fully solvent separated.

Triazolium ions showed increased reactivity towards deuterioxide ion and so deuterium exchange reactions were performed in DCl solutions. The values of k_{DO} ($\text{M}^{-1}\text{s}^{-1}$), the second-order rate constants for deuterioxide ion-catalysed exchange of triazolium ions (**179**)-(b182) were found to be in the range 3.66×10^7 - $2.80 \times 10^8 \text{ M}^{-1}\text{s}^{-1}$. It was found that altering the aromatic substituent on the triazolium ring had a small effect upon k_{DO} which may be attributed to a lack of inter-ring conjugation. In the case of these more reactive triazolium ions, estimates for the first-order rate constants for the solvent reaction, $k_{\text{D}_2\text{O}}$ (s^{-1}), could also be obtained. Each second-order plot for the H/D exchange of azolium ions (**179**)-(b182) exhibits a significant y-axis intercept which was tentatively assigned as $k_{\text{D}_2\text{O}}$ (s^{-1}) and were in the range 3.77×10^{-5} – $1.28 \times 10^{-7} \text{ s}^{-1}$. Although there is no clear pD-independent solvent reaction visible in the pD-rate profile for deuterioxide ion-catalysed exchange of triazolium ions (**179**)-(b182), there is a slight levelling off for azolium ion (**181**) and it is possible that the solvent reaction

could occur close to this region of the profile. The highest acid concentration used in the exchange reactions of azolium ion (**181**) was 500 mM. The pD-independent portion of the rate profile for this ion may be observed by measuring rate constants for C3 deprotonation by deuterioxide ion at higher acid concentrations.

Application of a secondary solvent isotope relationship ($k_{\text{DO}}/k_{\text{HO}} = 2.4$) to k_{DO} values provided values for the second-order rate constant for hydroxide ion catalysed exchange k_{HO} ($\text{M}^{-1}\text{s}^{-1}$). The acid dissociation constant, K_{a} , for azolium ions may also be written as the ratio of the rate constant for deprotonation of azolium ions and the reverse rate constant for reprotonation. As there was no detectable general base catalysis of exchange for representative azolium ions, it was concluded that proton transfer occurred in a pre-equilibrium and that k_{reorg} , the solvent reorganisation step, was rate-limiting. As such, a value of 10^{11} s^{-1} may be assigned as the rate constant for reprotonation of the carbene/yliide. This allows $\text{p}K_{\text{a}}$ values of azolium ions to be estimated. The resulting values of *N,N*-dialkylimidazolium ions (**185**)-(**187**) were 23.3-22.4. The $\text{p}K_{\text{a}}$ values of triazolium ions (**179**)-(**182**) were in the range 16.6-17.6 which is accord with the observation that increasing the number of electronegative atoms in the azolium ring results in an increase in acidity.

Further evidence for rate-limiting solvent reorganisation could be provided by performing buffer catalysis experiments on the most acidic azolium ion examined in this work (**181**). However, in this case exchange occurs rapidly above pD 3 and acetic acid buffers could not be used to this end. Alternatively, isotope effects on exchange could be measured. Significant deviation from the Swain-Schaad relationship would indicate that the solvent reorganisation step is rate-limiting. This would involve preparation of deuterated and tritiated azolium ions and could be potentially quite difficult.

References

- (1) Dalko, P. I.; Moisan, L. *Angew. Chem., Int. Ed.* **2004**, *43*, 5138-5175.
- (2) Houk, K. N.; List, B. *Acc. Chem. Res.* **2004**, *37*, 487-631.
- (3) Dalko, P. I.; Moisan, L. *Angew. Chem., Int. Ed.* **2001**, *40*, 3726-3748.
- (4) Seayad, J.; List, B. *Org. Biomol. Chem.* **2005**, *3*, 719-724.
- (5) Berkessel, A.; Gröger, H. *Asymmetric organocatalysis: From biomimetic concepts to applications in asymmetric synthesis* **2005**, Wiley-VCH, Weinheim.
- (6) List, B.; Lerner, R. A.; Barbas, C. F. *J. Am. Chem. Soc.* **2000**, *122*, 2395.
- (7) List, B. *Tetrahedron* **2002**, *58*, 5573.
- (8) Jen, W. S.; Wiener, J. J. M.; MacMillan, D. W. C. *J. Am. Chem. Soc.* **2000**, *122*, 9874.
- (9) Sigman, M. S.; Jacobsen, E. N. *J. Am. Chem. Soc.* **1998**, *120*, 4901.
- (10) Huang, Y.; Unni, A. K.; Thadani, A. N.; Rawal, V. H. *Nature* **2003**, *424*, 146.
- (11) Uraguchi, D.; Terada, M. *J. Am. Chem. Soc.* **2004**, *126*, 5356-5357.
- (12) Nakashima, D.; Yamamoto, H. *J. Am. Chem. Soc.* **2006**, *128*, 9626.
- (13) Bredig G.; P.S., F. *Biochem. Z.* **1912**, *46*, 7.
- (14) Pracejus, H. *Justus Liebigs Ann. Chem.* **1960**, *634*, 9.
- (15) Hajos, Z. G.; Parrish, D. R. *J. Org. Chem.* **1974**, *39*, 1615.
- (16) Eder, U.; Sauer, G.; Wiechert, R. *Angew. Chem., Int. Ed.* **1971**, *10*, 496-497.
- (17) Eder, U.; Sauer, G.; Wiechert, R. *Angew. Chem., Int. Ed.* **1971**, *83*, 492-493.
- (18) Ahrendt, K. A.; Borths, C. J.; MacMillan, D. W. C. *J. Am. Chem. Soc.* **2000**, *122*, 4243-4244.
- (19) Wolfgang, A. H. *Angew. Chem., Int. Ed.* **2002**, *41*, 1290-1309.
- (20) Marion, N.; Díez-González, S.; Nolan, S. P. *Angew. Chem., Int. Ed.* **2007**, *46*, 2988-3000.
- (21) Breslow, R. *J. Am. Chem. Soc.* **1958**, *80*, 3719.
- (22) Wanzlick, H. W. *Angew. Chem., Int. Ed. Engl.* **1962**, *1*, 75-80.
- (23) Bourissou, D.; Guerret, O.; Gabbai, F. P.; Bertrand, G. *Chem. Rev.* **2000**, *100*, 39.
- (24) Herrmann, W. A.; Kocher, C. *Angew. Chem., Int. Ed. Engl.* **1997**, *36*, 2162.
- (25) Igau, A.; Grutzmacher, H.; Baceiredo, A.; Bertrand, G. *J. Am. Chem. Soc.* **1988**, *110*, 6463.
- (26) Arduengo, A. J.; Harlow, R. L.; Kline, M. *J. Am. Chem. Soc.* **1991**, *113*, 361.
- (27) Breslow, R. *J. Am. Chem. Soc.* **1958**, *80*, 3719-3726.
- (28) Sheehan, J. C.; Hunneman, D. H. *J. Am. Chem. Soc.* **1966**, *88*, 3666.
- (29) Sheehan, J. C.; Hara, T. *J. Org. Chem.* **1974**, *39*, 1196.
- (30) Dvorak, C. A.; Rawal, V. H. *Tetrahedron Lett.* **1998**, *39*, 2925-2928.
- (31) Enders, D.; Breuer, K.; Raabe, G.; Runsink, J.; Teles, J. H.; Melder, J. P.; Ebel, K.; Brode, S. *Angew. Chem., Int. Ed. Engl.* **1995**, *34*, 1021-1023.
- (32) Enders, D.; Breuer, K.; Teles, J. H. *Helv. Chim. Acta* **1996**, *79*, 1217-1221.
- (33) Knight, R. L.; Leeper, F. J. *Tetrahedron Lett.* **1997**, *38*, 3611.
- (34) Knight, R. L.; Leeper, F. J. *J. Chem. Soc., Perkin Trans.* **1998**, *1*, 1891.

- (35) Enders, D.; Kallfass, U. *Angew. Chem., Int. Ed.* **2002**, *41*, 1743-1745.
- (36) Teles, J. H.; Melder, J. P.; Ebel, K.; Schneider, R.; Gehrler, E.; Harder, W.; Brode, S.; Enders, D.; Breuer, K.; Raabe, G. *Helv. Chim. Acta* **1996**, *79*, 61.
- (37) Stetter, H. *Angew. Chem., Int. Ed.* **1976**, *15*, 639-648.
- (38) Enders, D.; Breuer, K.; Runsink, J. *Helv. Chim. Acta* **1996**, *79*, 1899.
- (39) Kerr, M. S.; Read de Alaniz, J.; Rovis, T. *J. Am. Chem. Soc.* **2002**, *124*, 10298.
- (40) Read de Alaniz, J.; Rovis, T. *J. Am. Chem. Soc.* **2005**, *127*, 6284.
- (41) Vachal, P.; Jacobsen, E. N. *J. Am. Chem. Soc.* **2002**, *124*, 10012.
- (42) Dieter, S.; Albert, K. B.; Alexander, H. *Angew. Chem., Int. Ed.* **2001**, *40*, 92-138.
- (43) Gondi, V. B.; Gravel, M.; Rawal, V. H. *Org. Lett.* **2005**, *7*, 5657.
- (44) Unni, A. K.; Takenaka, N.; Yamamoto, H.; Rawal, V. H. *J. Am. Chem. Soc.* **2005**, *127*, 1336.
- (45) Akiyama, T.; Itoh, J.; Yokota, K.; Fuchibe, K. *Angew. Chem., Int. Ed.* **2004**, *43*, 1566-1568.
- (46) Cheon, C. H.; Yamamoto, H. *J. Am. Chem. Soc.* **2008**, *130*, 9246.
- (47) Verkade, J. M. M.; van Hemert, L. J. C.; Quaedflieg, P. J. L. M.; Rutjes, F. P. J. T. *Chem. Soc. Rev.* **2007**, *37*, 29-41.
- (48) List, B. *J. Am. Chem. Soc.* **2000**, *122*, 9336.
- (49) Notz, W.; Sakthivel, K.; Bui, T.; Zhong, G.; Barbas Iii, C. F. *Tetrahedron Lett.* **2001**, *42*, 199.
- (50) Vesely, J.; Rios, R.; Ibrahim, I.; Córdova, A. *Tetrahedron Lett.* **2007**, *48*, 421.
- (51) Yang, J. W.; Stadler, M.; List, B. *Angew. Chem., Int. Ed.* **2007**, *46*, 609-611.
- (52) Cobb, A. J. A.; Shaw, D. M.; Longbottom, D. A.; Gold, J. B.; Ley, S. V. *Org. Biomol. Chem.* **2005**, *3*, 84-96.
- (53) Lou, S.; Taoka, B. M.; Ting, A.; Schaus, S. E. *J. Am. Chem. Soc.* **2005**, *127*, 11256.
- (54) Song, J.; Wang, Y.; Deng, L. *J. Am. Chem. Soc.* **2006**, *128*, 6048.
- (55) Wenzel, A. G.; Jacobsen, E. N. *J. Am. Chem. Soc.* **2002**, *124*, 12964-12965.
- (56) Wenzel, A. G.; Lalonde, M. P.; Jacobsen, E. N. *Synlett* **2003**, *12*, 1919-1922.
- (57) Bordwell, F. G.; Algrim, D. J.; Harrelson, J. A. *J. Am. Chem. Soc.* **1988**, *110*, 5903.
- (58) Olmstead, W. N.; Margolin, Z.; Bordwell, F. G. *J. Org. Chem.* **1980**, *45*, 3295.
- (59) Akiyama, T.; Takaya, J.; Kagoshima, H. *Tetrahedron Lett.* **2001**, *42*, 4025.
- (60) Yamanaka, M.; Itoh, J.; Fuchibe, K.; Akiyama, T. *J. Am. Chem. Soc.* **2007**, *129*, 6756.
- (61) Akiyama, T. *Chem. Rev.* **2007**, *107*, 5744.
- (62) Gridnev, I. D.; Kouchi, M.; Sorimachi, K.; Terada, M. *Tetrahedron Lett.* **2007**, *48*, 497-500.
- (63) Akiyama, T.; Saitoh, Y.; Morita, H.; Fuchibe, K. *Adv. Synth. Catal.* **2005**, *347*, 1523-1526.

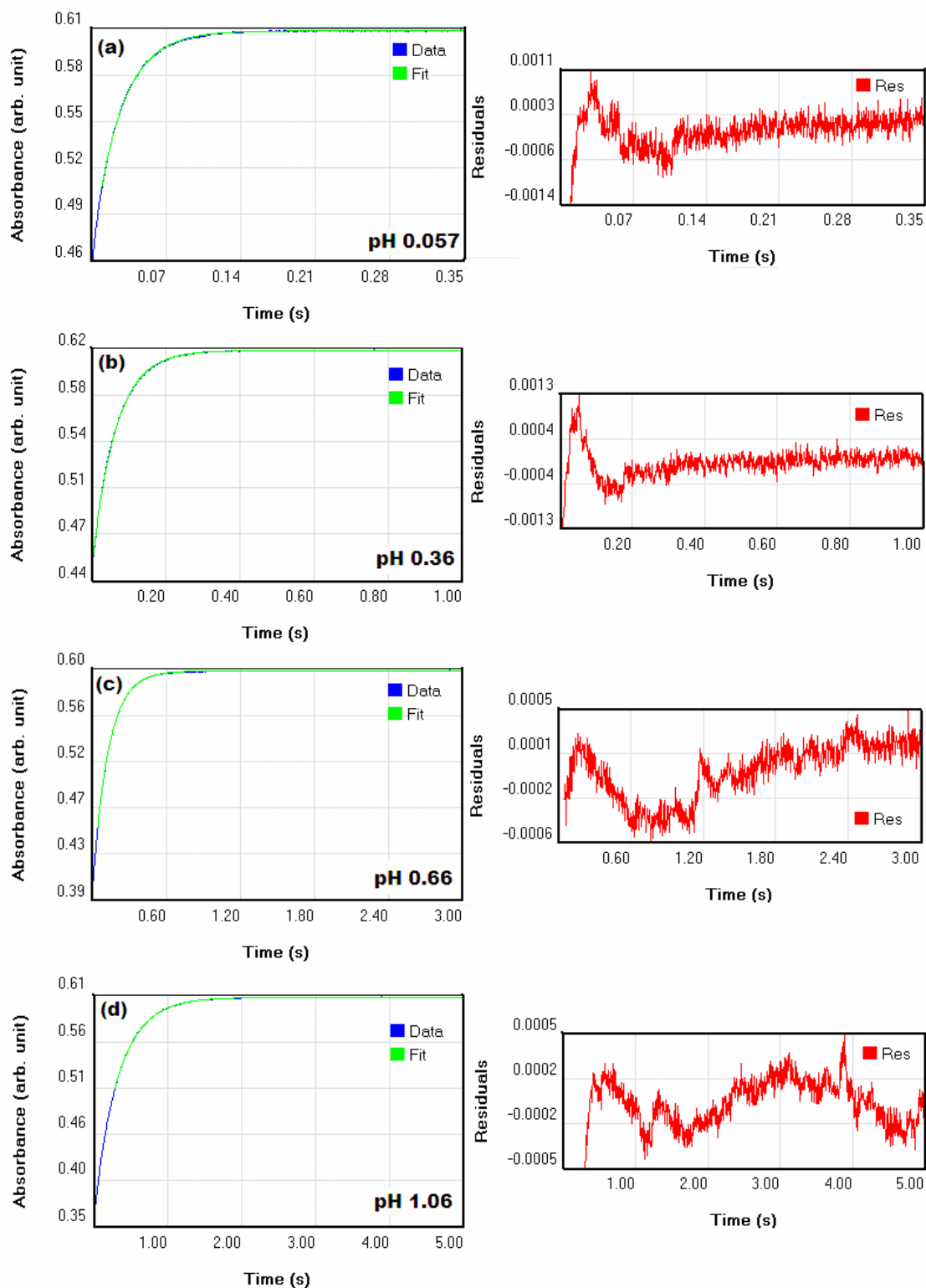
- (64) Arend, M.; Westermann, B.; Risch, N. *Angew. Chem., Int. Ed.* **1998**, *37*, 1044-1070.
- (65) Tramontini, M.; Angiolini, L. *Tetrahedron* **1990**, *46*, 1791-1837.
- (66) Kleinman, E. F. *Comprehensive Organic Synthesis* **1991**, 893.
- (67) Cummings, T. F.; Shelton, J. R. *J. Org. Chem.* **1960**, *25*, 419.
- (68) Fernandez, J. E.; Butler, G. B. *J. Org. Chem.* **1963**, *28*, 3258.
- (69) Burckhalter, J. H.; Wells, J. N.; Mayer, W. J. *Tetrahedron Lett.* **1964**, *21*, 1353.
- (70) Alexander, E. R.; Underhill, E. J. *J. Am. Chem. Soc.* **1949**, *71*, 4014.
- (71) Thompson, B. B. *J. Pharm. Sci.* **1968**, *57*, 715-733.
- (72) Wenzel, A. G.; Jacobsen, E. N. *J. Am. Chem. Soc.* **2002**, *124*, 12964.
- (73) Wu, T. R.; Shen, L.; Chong, J. M. *Org. Lett.* **2004**, *6*, 2701-2704.
- (74) Uraguchi, D.; Terada, M. *J. Am. Chem. Soc.* **2004**, *126*, 5356.
- (75) Frey, P. A.; Sammons, R. D. *Science (Washington, DC, U. S.)* **1985**, *228*, 541.
- (76) Cordes, E. H.; Jencks, W. P. *J. Am. Chem. Soc.* **1963**, *85*, 2843-2848.
- (77) Crampton, M. R.; Robotham, I. A. *J. Chem. Research (S)* **1997**, 22-23.
- (78) Bordwell, F. G.; Branca, J. C.; Hughes, D. L.; Olmstead, W. N. *J. Org. Chem.* **1980**, *45*, 3305-3313.
- (79) Bordwell, F. G. *Acc. Chem. Res.* **1988**, *21*, 456-463.
- (80) Kumler, W. D.; Eiler, J. J. *J. Am. Chem. Soc.* **1943**, *65*, 2355.
- (81) Kolthoff, I. M.; Chantooni, M. K.; Bhowmik, S. *J. Am. Chem. Soc.* **1968**, *90*, 23-28.
- (82) Kutt, A.; Leito, I.; Kaljurand, I.; Soovali, L.; Vlasov, V. M.; Yagupolskii, L. M.; Koppel, I. A. *J. Org. Chem.* **2006**, *71*, 2829.
- (83) Cox, P. J.; Wang, W.; Snieckus, V. *Tetrahedron Lett.* **1992**, *33*, 2253-2256.
- (84) Simonsen, K. B.; Gothelf, K. V.; Jørgensen, K. A. *J. Org. Chem.* **1998**, *63*, 7536-7538.
- (85) Storer, R. I.; Carrera, D. E.; Ni, Y.; MacMillan, D. W. C. *J. Am. Chem. Soc.* **2005**, *128*, 84.
- (86) Akiyama, T.; Morita, H.; Itoh, J.; Fuchibe, K. *Org. Lett.* **2005**, *7*, 2583.
- (87) Cordes, E. H.; Jencks, W. P. *J. Am. Chem. Soc.* **2002**, *84*, 832.
- (88) Cordes, E. H.; Jencks, W. P. *J. Am. Chem. Soc.* **1961**, *84*, 832.
- (89) Hine, J.; Craig, J. C.; Underwood, J. G.; Via, F. A. *J. Am. Chem. Soc.* **1970**, *92*, 5194.
- (90) Hall, H. K. *J. Am. Chem. Soc.* **1957**, *79*, 5441.
- (91) Haake, P.; Bausher, L. P.; Miller, W. B. *J. Am. Chem. Soc.* **1969**, *91*, 1113.
- (92) Olofson, R. A.; Thompson, W. R.; Michelman, J. S. *J. Am. Chem. Soc.* **1964**, *86*, 1865-1866.
- (93) Aldrich, H. S.; Alworth, W. L.; Clement, N. R. *J. Am. Chem. Soc.* **1978**, *100*, 2362.
- (94) Scheffers-Sap, M. M. E.; Buck, H. M. *J. Am. Chem. Soc.* **1979**, *101*, 4807-4811.
- (95) Amyes, T. L.; Diver, S. T.; Richard, J. P.; Rivas, F. M.; Toth, K. *J. Am. Chem. Soc.* **2004**, *126*, 4366.
- (96) Washabaugh, M.; Jencks, W. P. *Biochemistry* **1988**, *27*, 5044.
- (97) Higgins, E. M. *Ph. D thesis, Durham University* **2007**.
- (98) Sherwood, J. A. *M. Sc. thesis, University College Dublin* **2004**.

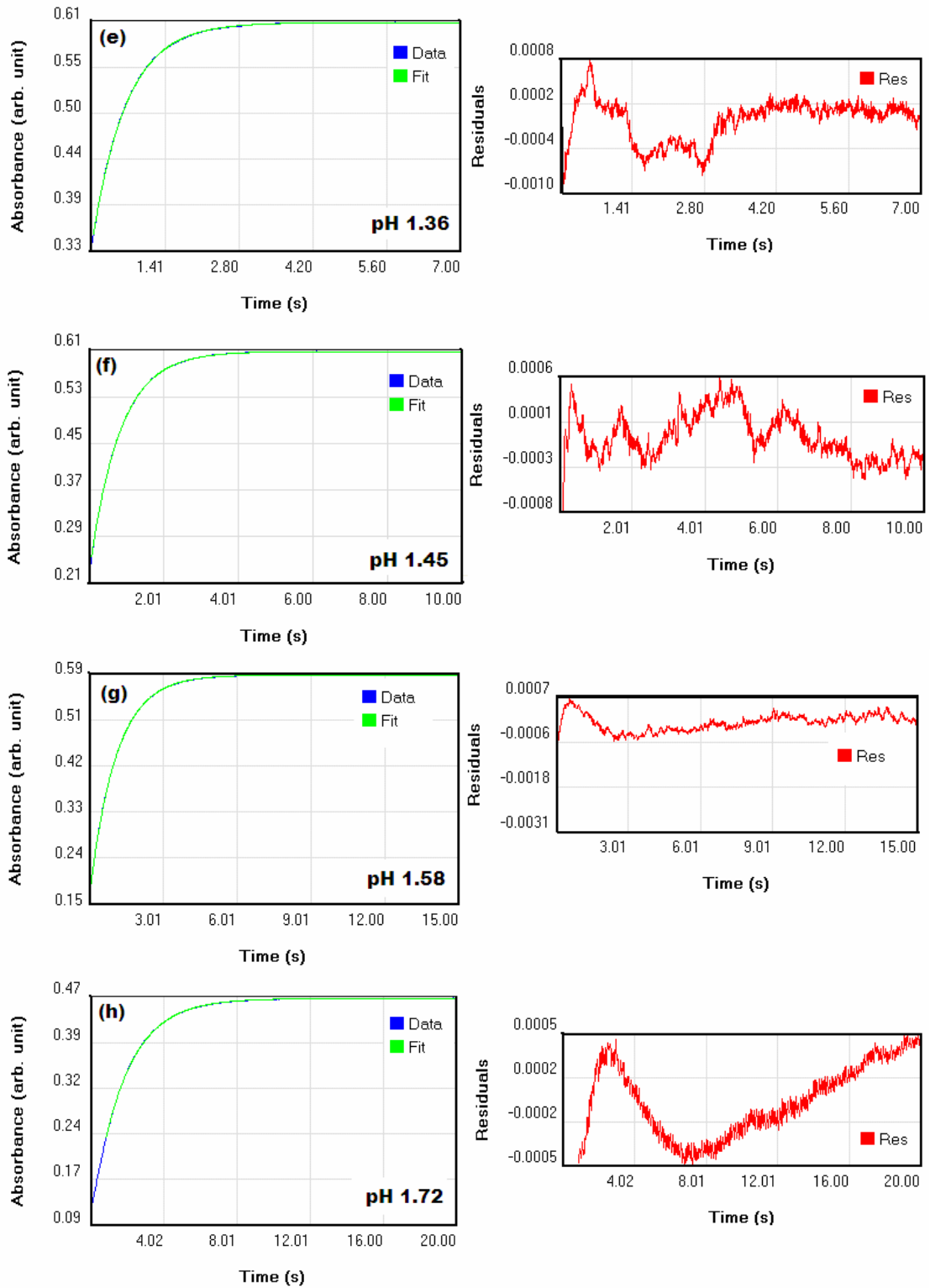
-
- (99) Wong, J. L.; Keck, J. H. *J. Org. Chem.* **1974**, *39*, 2398-2403.
- (100) Schroeder, M. A.; Makino, R. C. *Tetrahedron* **1973**, *29*, 3469.
- (101) Alder, R. W.; Allen, P. R.; Williams, S. J. *J. Chem. Soc., Chem. Commun.* **1995**, 1267-1268.
- (102) Kim, Y.-J.; Streitwieser, A. *J. Am. Chem. Soc.* **2002**, *124*, 5757-5761.
- (103) Chu, Y.; Deng, H.; Cheng, J.-P. *J. Org. Chem.* **2007**, *72*, 7790.
- (104) Magill, A. M.; Cavell, K. J.; Yates, B. F. *J. Am. Chem. Soc.* **2004**, *126*, 8717-8724.
- (105) Richard, J. P.; Williams, G.; O'Donoghue, A. C.; Amyes, T. L. *J. Am. Chem. Soc.* **2002**, *124*, 2957-2968.
- (106) Kaatze, U. *J. Chem. Eng. Data* **1989**, *34*, 371-374.
- (107) Washabaugh, M. W.; Jencks, W. P. *J. Am. Chem. Soc.* **1989**, *111*, 683-692.
- (108) Wu, T. R.; Shen, L.; Chong, J. M. *Org. Lett.* **2004**, *6*, 2701-2704.
- (109) Simonsen, K. B.; Gothelf, K. V.; Jorgensen, K. A. *J. Org. Chem.* **1998**, *63*, 7536.
- (110) Richard, J. P.; Williams, G.; Gao, J. *J. Am. Chem. Soc.* **1999**, *121*, 715.

Appendices

Appendix A Kinetics of imine hydrolysis

Figure A1: Hydrolysis of *p*-methoxybenzaldehyde *N*-(*tert*-butoxycarbonyl)imine (119) in HCl solution (pH 0.057-3.00) at 284 nm, 25 °C and I = 1.0 (KCl); plots of absorbance against time (a)-(k), with corresponding residuals.





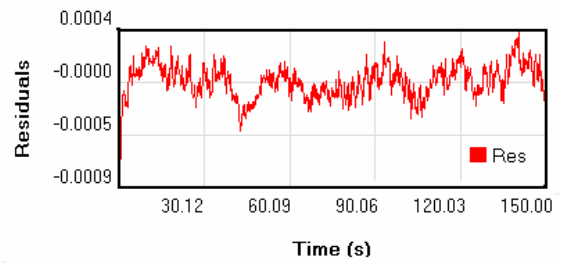
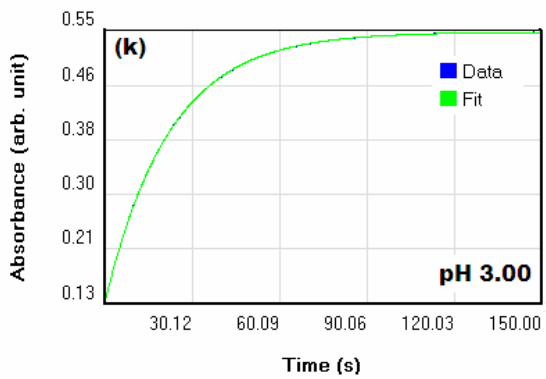
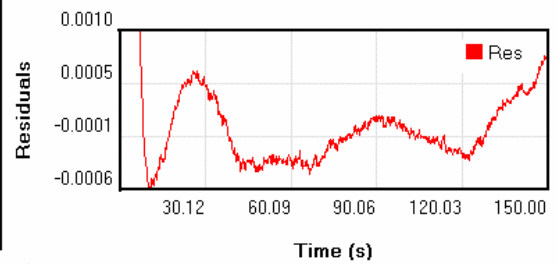
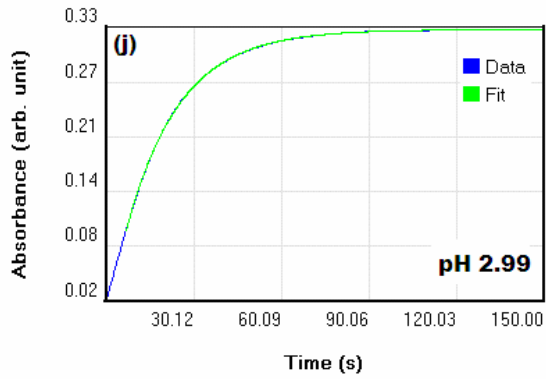
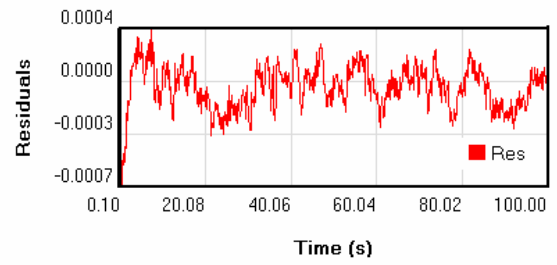
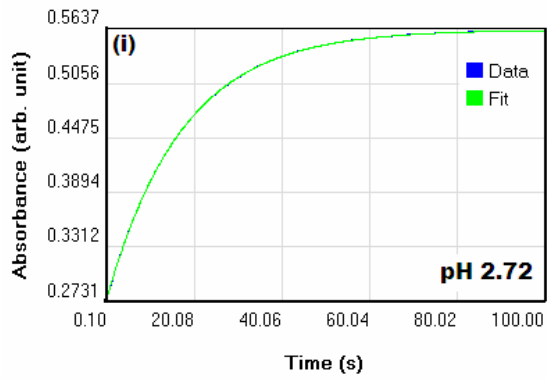


Table A1: Summary of first-order rate constants for the hydrolysis of *p*-methoxybenzaldehyde *N*-(*tert*-butoxycarbonyl)imine (119) in HCl solution at 284 nm, 25 °C and $I = 1.0$ (KCl) obtained using stopped-flow spectrophotometry.^a

pH ^b	k_{hyd}^c (s ⁻¹)	n ^d	log k_{hyd}
0.057	3.67×10^1	14	1.56
0.36	1.57×10^1	12	1.20
0.66	7.87	11	8.96×10^{-1}
1.06	3.09	13	4.90×10^{-1}
1.36	1.55	11	1.90×10^{-1}
1.45	1.23	11	8.99×10^{-2}
1.58	9.25×10^{-1}	9	-3.38×10^{-2}
1.72	5.60×10^{-1}	5	-2.52×10^{-1}
2.72	5.80×10^{-2}	5	-1.24
2.99	3.57×10^{-2}	5	-1.45
3.00	3.01×10^{-2}	5	-1.52

(a) Measurements were made at an initial substrate concentration of 5×10^{-5} M. (b) HCl solutions were diluted by 50% and the pH of the resulting solution measured in order to account for the dilution upon mixing in the stopped-flow apparatus. (c) The value of the first-order rate constant, k_{hyd} (s⁻¹), was obtained from least-squares analysis of absorbance versus time data in Figure A1 (a)-(k). (d) The number of runs averaged to give the value of k_{hyd} .

Figure A2: Hydrolysis of *p*-methoxybenzaldehyde *N*-(*tert*-butoxycarbonyl)imine (119) in chloroacetic acid buffer (75% f_B , pH 3.19); (a) plot of $\ln(A_\infty - A_t)$ against time, (b) plot of k_{obs} against the concentration of chloroacetic acid, $[\text{CH}_2\text{ClCOOH}]$.

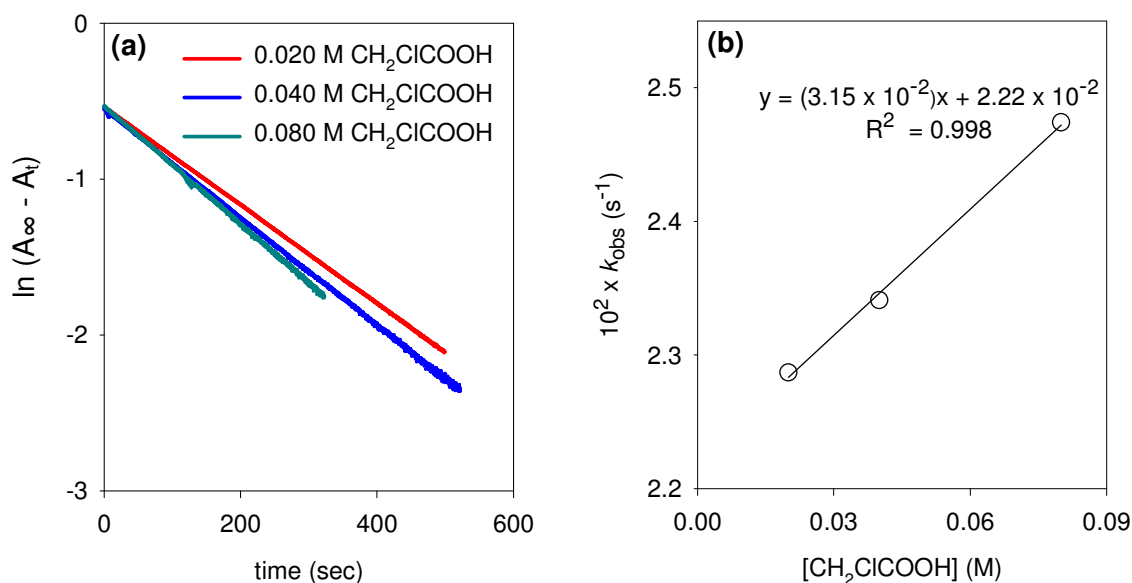


Figure A3: Hydrolysis of *p*-methoxybenzaldehyde *N*-(*tert*-butoxycarbonyl)imine (119) in acetic acid buffer (10% f_B , pH 3.61); (a) plot of $\ln(A_\infty - A_t)$ against time, (b) plot of k_{obs} against the concentration of acetic acid, $[CH_3COOH]$.

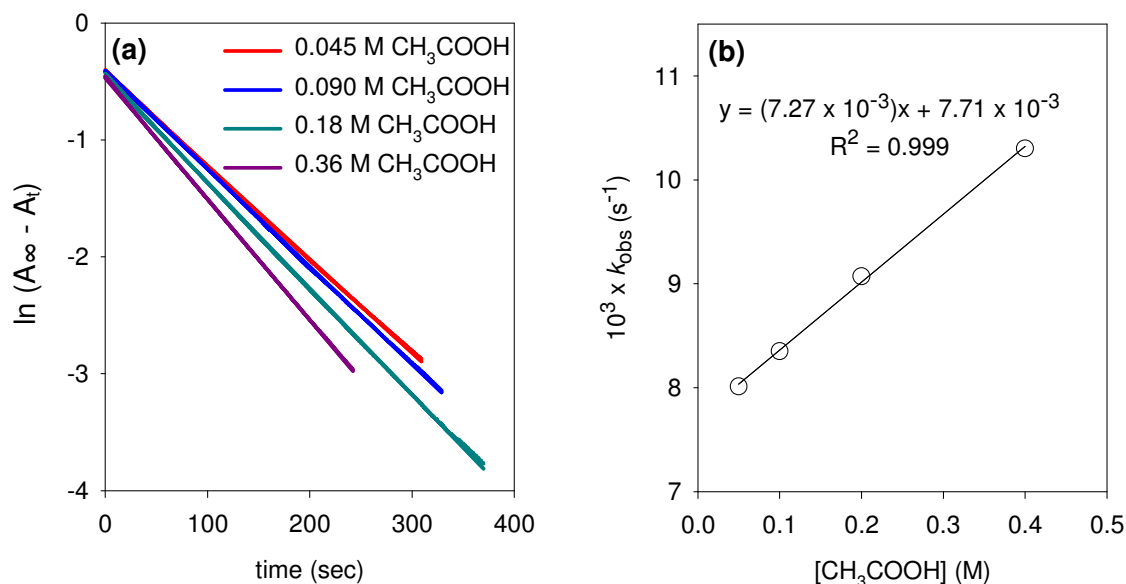


Figure A4: Hydrolysis of *p*-methoxybenzaldehyde *N*-(*tert*-butoxycarbonyl)imine (119) in acetic acid buffer (25% f_B , pH 4.10); (a) plot of $\ln(A_\infty - A_t)$ against time, (b) plot of k_{obs} against the concentration of acetic acid, $[CH_3COOH]$.

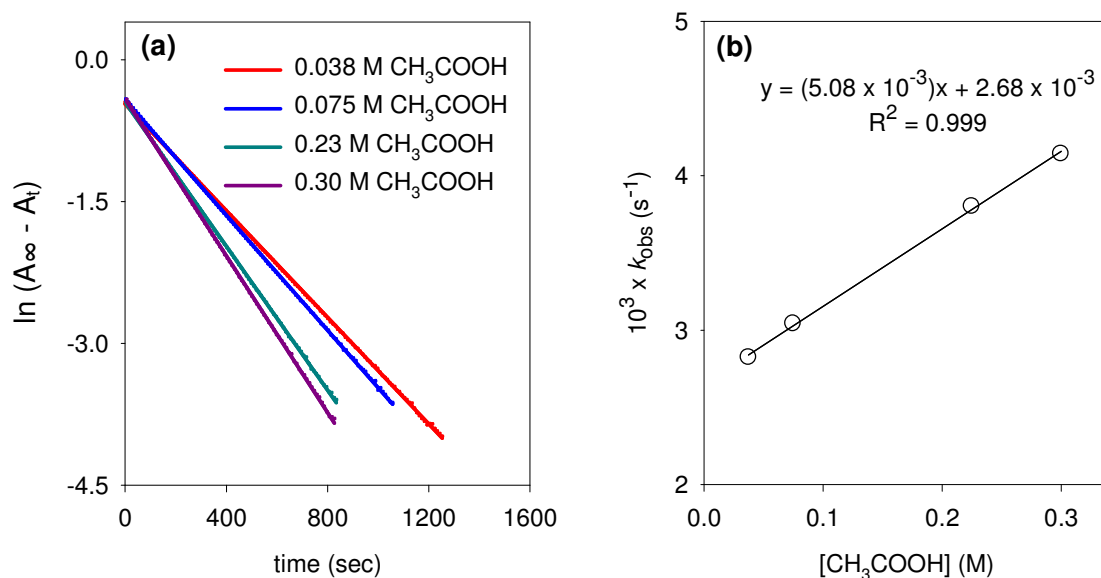


Figure A5: Hydrolysis of *p*-methoxybenzaldehyde *N*-(*tert*-butoxycarbonyl)imine (119) in acetic acid buffer (50% f_B , pH 4.65); (a) plot of $\ln(A_\infty - A_t)$ against time, (b) plot of k_{obs} against the concentration of acetic acid, $[CH_3COOH]$.

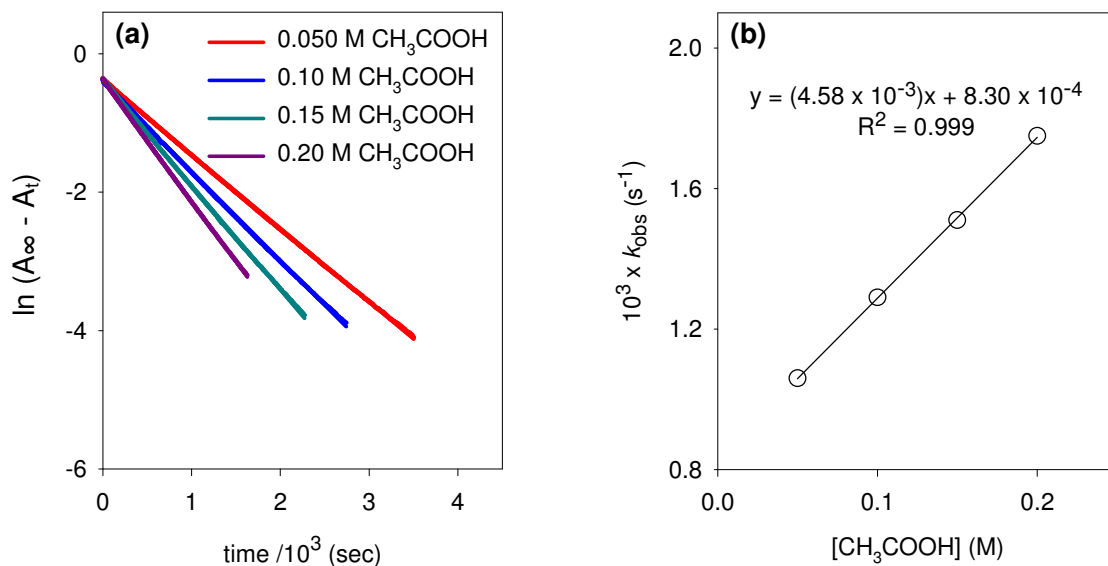


Figure A6: Hydrolysis of *p*-methoxybenzaldehyde *N*-(*tert*-butoxycarbonyl)imine (119) in acetic acid buffer (90% f_B , pH 5.58); (a) plot of $\ln(A_\infty - A_t)$ against time, (b) plot of k_{obs} against the concentration of acetic acid, $[CH_3COOH]$.

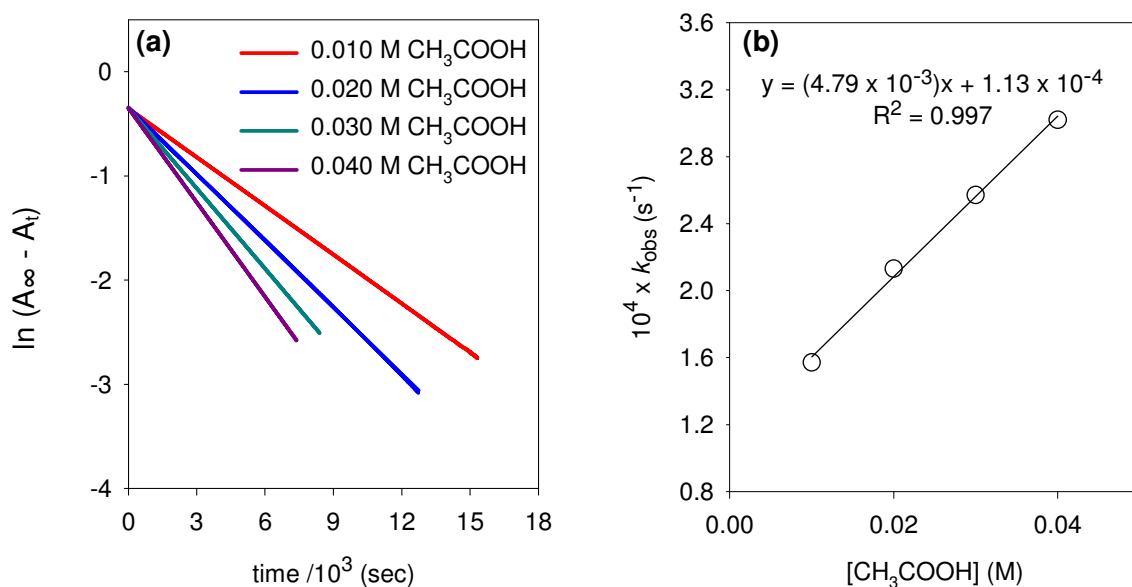


Table A2: First-order rate constants for the hydrolysis of *p*-methoxybenzaldehyde *N*-(*tert*-butoxycarbonyl)imine (119) in acetic acid and chloroacetic acid buffers* at 284 nm, 25 °C and I = 1.0 (KCl).^a

[Buffer] _T ^b (M)	[CH ₃ COOH] ^c (M)	pH	k_{obs} ^d (s ⁻¹)	R ²	k_{HA} ^e (M ⁻¹ s ⁻¹)	k_{hyd} ^f (s ⁻¹)
75% f_{B} [*]	[CH ₂ ClCOOH]					
0.08	0.020	3.19	2.29×10^{-2}	0.999		
0.16	0.040	3.19	2.34×10^{-2}	0.999	3.15×10^{-2}	2.22×10^{-2}
0.32	0.080	3.19	2.47×10^{-2}	0.999		
10% f_{B}						
0.05	0.045	3.62	8.01×10^{-3}	0.999		
0.10	0.090	3.61	8.35×10^{-3}	0.999	7.27×10^{-3}	7.71×10^{-3}
0.20	0.18	3.60	9.07×10^{-3}	0.999		
0.40	0.36	3.60	1.03×10^{-2}	0.999		
25% f_{B}						
0.05	0.038	4.10	2.86×10^{-3}	0.999		
0.10	0.075	4.10	3.08×10^{-3}	0.999	5.08×10^{-3}	2.68×10^{-3}
0.30	0.23	4.10	3.84×10^{-3}	0.999		
0.40	0.30	4.10	4.20×10^{-3}	0.999		
50% f_{B}						
0.10	0.050	4.65	1.06×10^{-3}	0.999		
0.20	0.10	4.65	1.29×10^{-3}	0.999	4.58×10^{-3}	8.30×10^{-4}
0.30	0.15	4.64	1.51×10^{-3}	0.999		
0.40	0.20	4.65	1.75×10^{-3}	0.999		
75% f_{B} ^g						
0.10	0.025	5.06	4.28×10^{-4}	0.999		
0.20	0.050	5.09	5.54×10^{-4}	0.999	4.74×10^{-3}	3.09×10^{-4}
0.30	0.075	5.10	6.70×10^{-4}	0.999		
0.40	0.10	5.11	7.85×10^{-4}	0.999		
90% f_{B}						
0.10	0.010	5.55	1.57×10^{-4}	0.999		
0.20	0.020	5.57	2.13×10^{-4}	0.999	4.79×10^{-3}	1.13×10^{-4}
0.30	0.030	5.59	2.57×10^{-4}	0.999		
0.40	0.040	5.61	3.02×10^{-4}	0.999		

(a) Measurements were made at an initial substrate concentration of 5×10^{-5} M. (b) Total buffer concentration. (c) The concentration of buffer in the acid form. (d) The value of the first-order rate constant, k_{obs} (s⁻¹), was obtained as the slope the plot of $\ln(A_{\infty} - A_t)$ against time in Figures A2-A6. (e) The value of the second-order rate constant, k_{HA} (M⁻¹s⁻¹), was obtained as the slope of the plot of k_{obs} (s⁻¹) against the concentration of general acid in Figures A2-A6. (f) The value of k_{hyd} (s⁻¹) was obtained as the y-axis intercept of the plot of k_{obs} against the concentration of general acid in Figures A2-A6. (g) Values of k_{obs} , k_{hyd} and k_{HA} were obtained from Figures 2.2 and 2.3 shown in Chapter 2, Section 2.1.3.1.1.

Figure A7: Hydrolysis of *p*-methoxybenzaldehyde *N*-(*tert*-butoxycarbonyl)imine (119) in phosphate buffer (20% f_B , pH 5.86); (a) plot of $\ln(A_\infty - A_t)$ against time, (b) plot of k_{obs} against the concentration of dihydrogen phosphate, $[\text{H}_2\text{PO}_4^-]$.

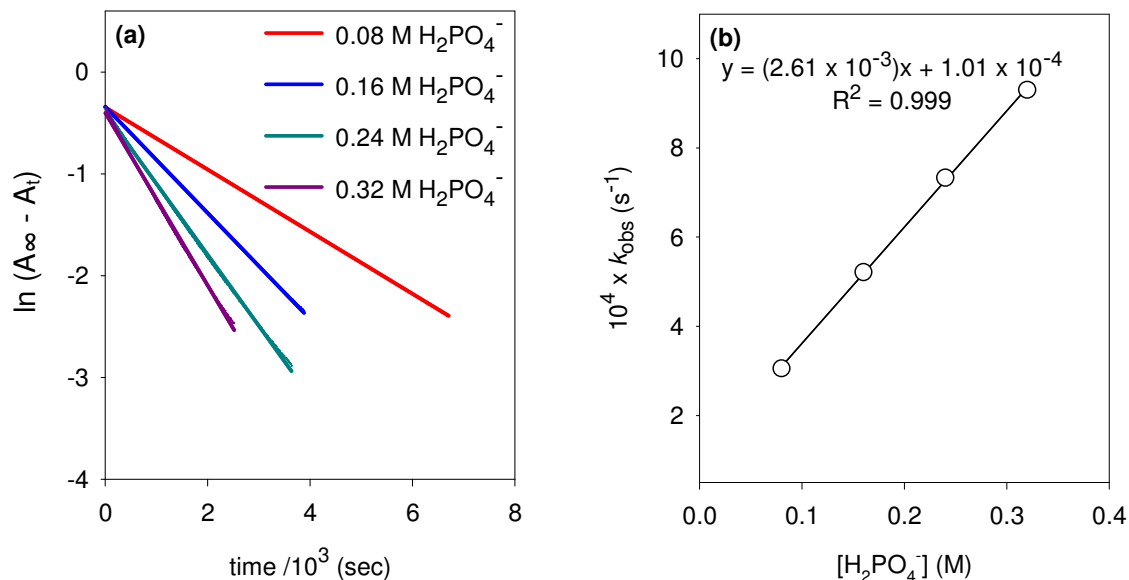


Figure A8: Hydrolysis of *p*-methoxybenzaldehyde *N*-(*tert*-butoxycarbonyl)imine (119) in phosphate buffer (50% f_B , pH 6.54); (a) plot of $\ln(A_\infty - A_t)$ against time, (b) plot of k_{obs} against the concentration of dihydrogen phosphate $[\text{H}_2\text{PO}_4^-]$.

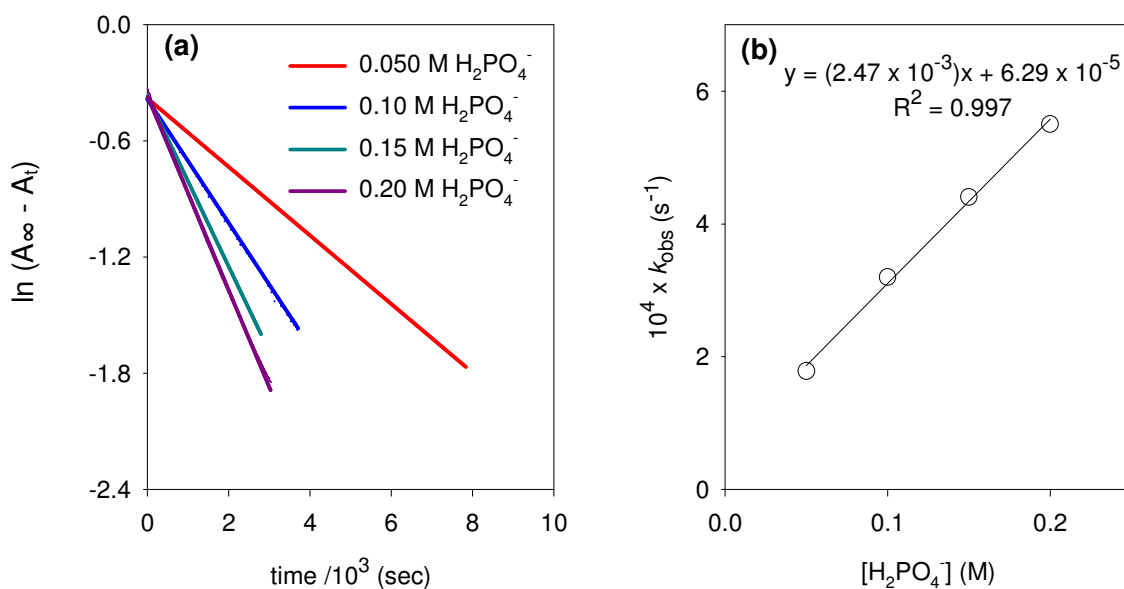


Table A3: First-order rate constants for the hydrolysis of *p*-methoxybenzaldehyde *N*-(*tert*-butoxycarbonyl)imine (119) in phosphate buffers at 284 nm, 25 °C and I = 1.0 (KCl).^a

[Buffer] _T ^b (M)	[H ₂ PO ₄ ⁻] ^c (M)	pH	<i>k</i> _{obs} ^d (s ⁻¹)	R ²	<i>k</i> _{HA} ^e (M ⁻¹ s ⁻¹)	<i>k</i> _{hyd} ^f (s ⁻¹)
20% <i>f</i> _B						
0.10	0.08	5.87	3.05 × 10 ⁻⁴	0.999	2.61 × 10 ⁻³	1.01 × 10 ⁻⁴
0.20	0.16	5.85	5.21 × 10 ⁻⁴	0.999		
0.30	0.24	5.85	7.33 × 10 ⁻⁴	0.999		
0.40	0.32	5.87	9.30 × 10 ⁻⁴	0.999		
50% <i>f</i> _B						
0.10	0.05	6.54	1.78 × 10 ⁻⁴	0.999	2.47 × 10 ⁻³	6.29 × 10 ⁻⁵
0.20	0.10	6.54	3.20 × 10 ⁻⁴	0.999		
0.30	0.15	6.55	4.41 × 10 ⁻⁴	0.999		
0.40	0.20	6.53	5.50 × 10 ⁻⁴	0.999		

(a) Measurements were made at an initial substrate concentration of 5 × 10⁻⁵ M. (b) Total concentration of buffer. (c) Concentration of buffer in acid form. (d) The value of the first-order rate constant, *k*_{obs}, (s⁻¹) was obtained as the slope of the plot of ln (*A*_∞ - *A*_{*t*}) against time in Figures A7-A8. (e) The value of the second-order rate constant, *k*_{HA} (M⁻¹s⁻¹), was obtained as the slope of the plot of *k*_{obs} against the concentration of dihydrogen phosphate in Figures A7-A8. (f) The value of *k*_{hyd} (s⁻¹) was obtained as the y-axis intercept of the plot of *k*_{obs} against dihydrogen phosphate concentration in Figures A7-A8.

Figure A9: Hydrolysis of *p*-methoxybenzaldehyde *N*-(*tert*-butoxycarbonyl)imine (119) in imidazole buffer (50% *f*_B, pH 7.24); (a) plot of ln (*A*_∞ - *A*_{*t*}) against time, (b) plot of *k*_{obs} against the concentration of imidazolium ion, [ImH⁺].

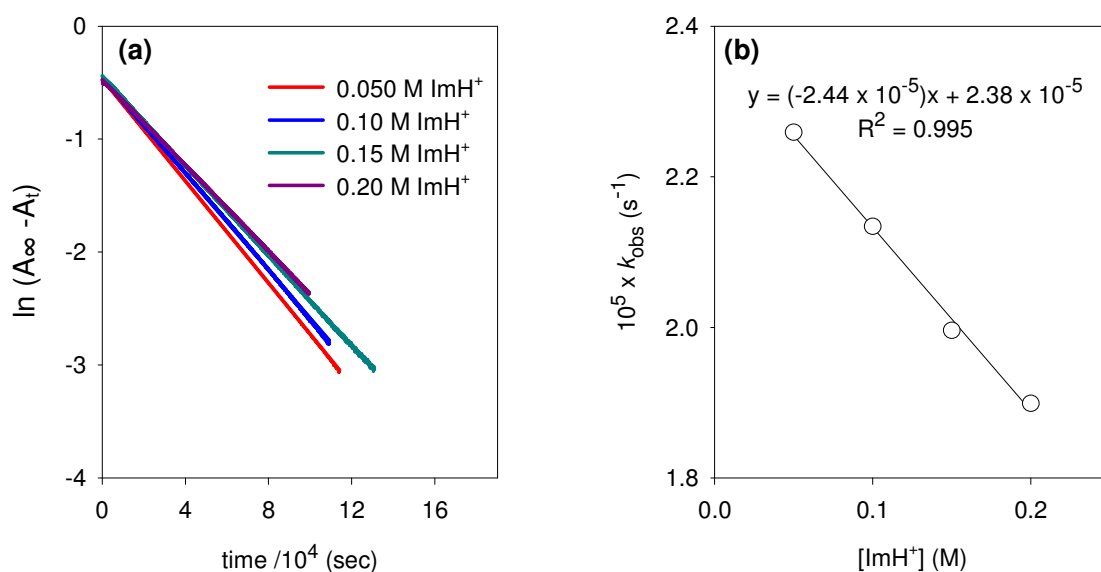


Figure A10: Hydrolysis of *p*-methoxybenzaldehyde *N*-(*tert*-butoxycarbonyl)imine (119) in imidazole buffer (75% f_B , pH 7.71); (a) plot of $\ln(A_\infty - A_t)$ against time, (b) plot of k_{obs} against the concentration of imidazolium ion $[\text{ImH}^+]$.

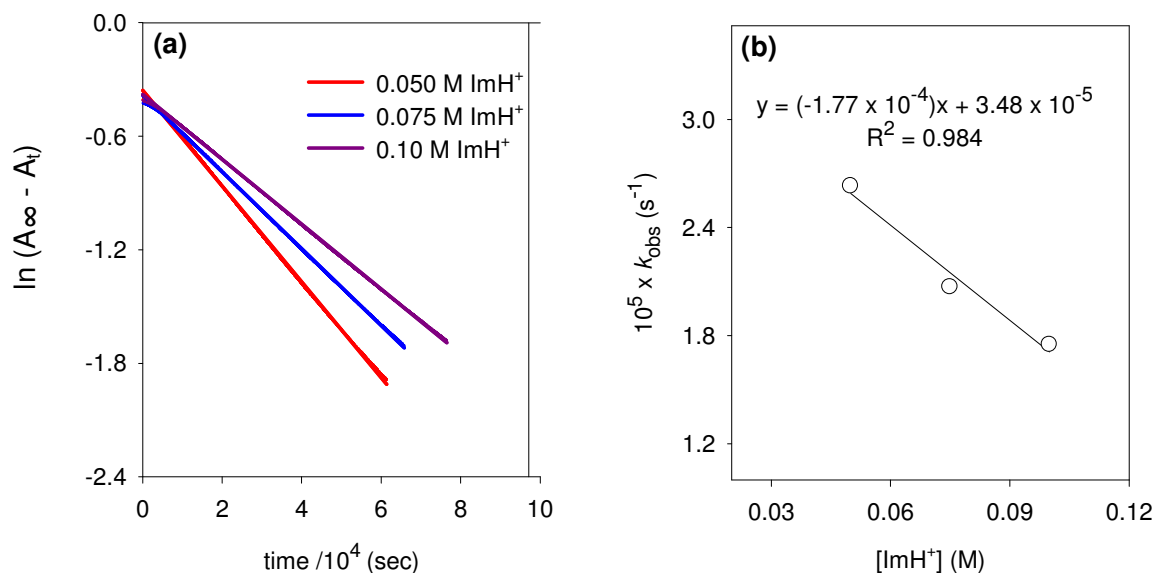


Figure A11: Hydrolysis of *p*-methoxybenzaldehyde *N*-(*tert*-butoxycarbonyl)imine (119) in imidazole buffer (90% f_B , pH 8.18); (a) plot of $\ln(A_\infty - A_t)$ against time with slope equal to k_{obs} , (b) plot of k_{obs} against the concentration of imidazolium ion, $[\text{ImH}^+]$.

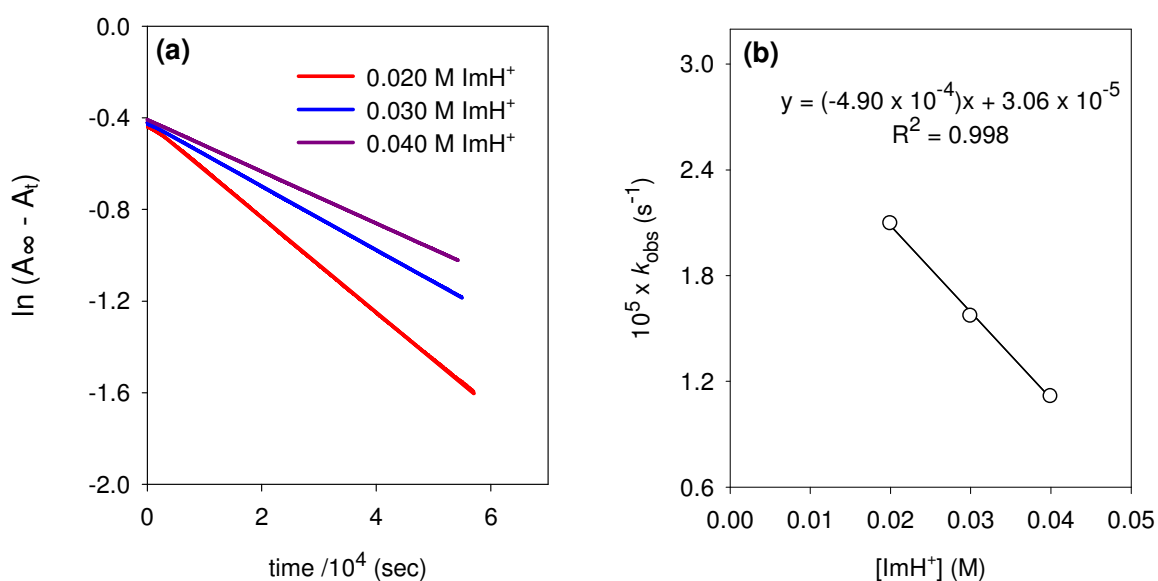
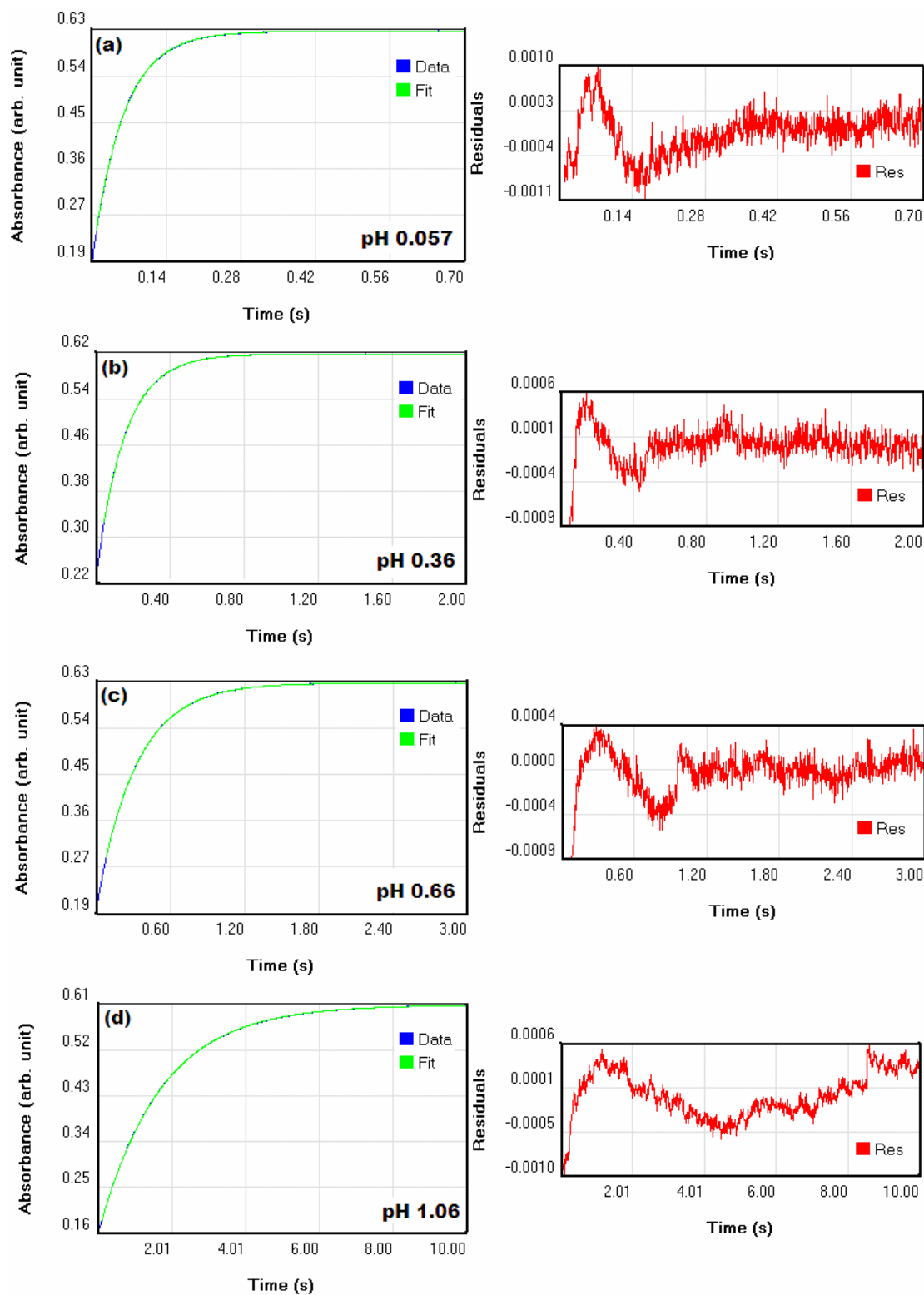


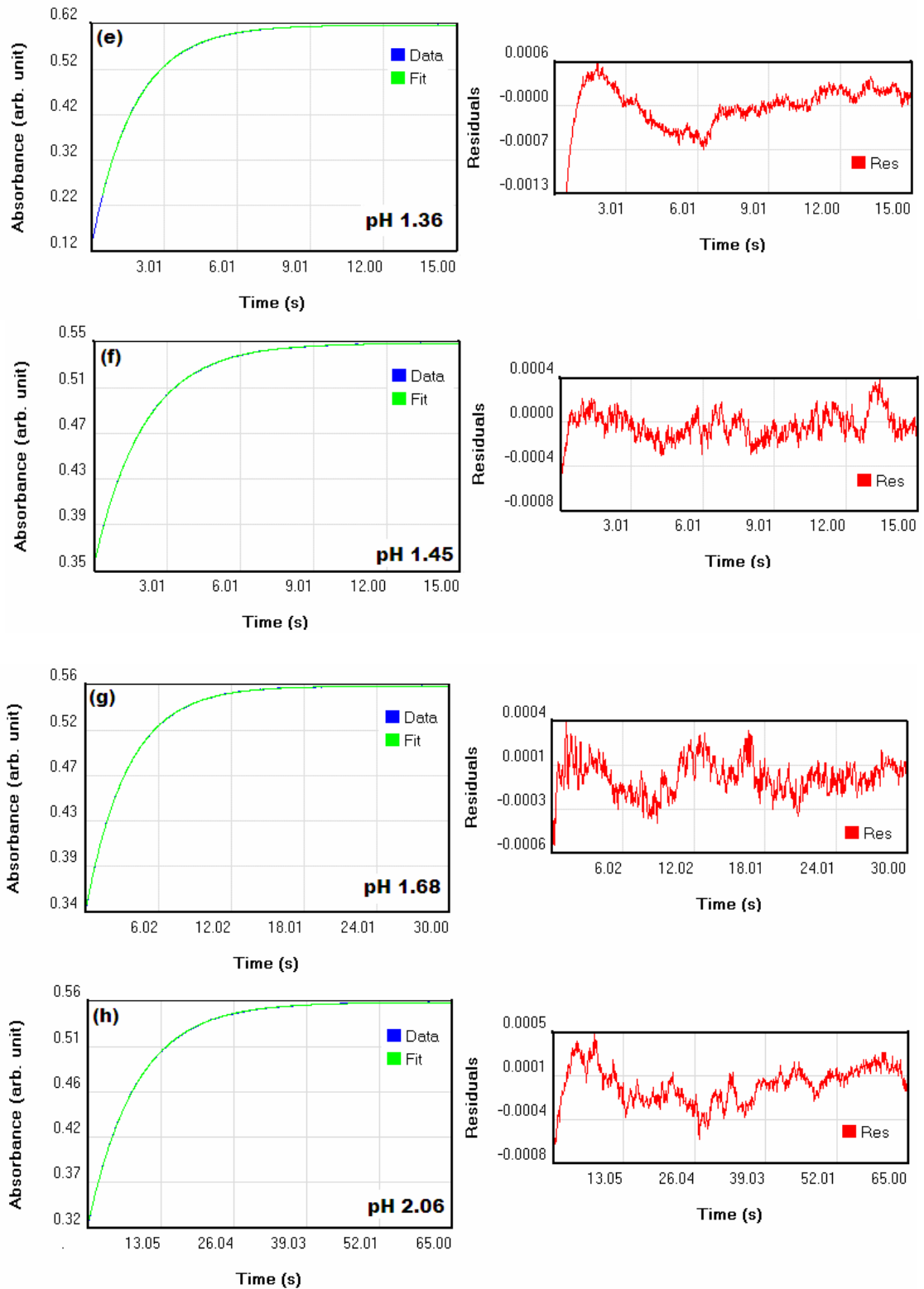
Table A4: First-order rate constants for the hydrolysis of *p*-methoxybenzaldehyde *N*-(*tert*-butoxycarbonyl)imine (119) in imidazole buffers at 284 nm, 25 °C and I = 1.0 (KCl).^a

[Buffer] _T ^b (M)	[ImH ⁺] ^c (M)	pH	k_{obs} ^d (s ⁻¹)	R ²	k' ^e (M ⁻¹ s ⁻¹)	k_{hyd} ^f (s ⁻¹)
50% f_B						
0.10	0.05	7.25	2.26×10^{-5}	0.999		
0.20	0.10	7.25	2.13×10^{-5}	0.999	2.44×10^{-5}	2.38×10^{-5}
0.30	0.15	7.24	2.00×10^{-5}	0.999		
0.40	0.20	7.23	1.90×10^{-5}	0.999		
75% f_B						
0.20	0.050	7.72	2.63×10^{-5}	0.999		
0.30	0.075	7.70	2.07×10^{-5}	0.999	1.77×10^{-4}	3.48×10^{-5}
0.40	0.10	7.72	1.75×10^{-5}	0.999		
90% f_B						
0.20	0.020	8.18	2.10×10^{-5}	0.999		
0.30	0.030	8.18	1.57×10^{-5}	0.999	4.90×10^{-4}	3.06×10^{-5}
0.40	0.040	8.18	1.11×10^{-5}	0.999		

(a) Measurements were made at an initial substrate concentration of 5×10^{-5} M. (b) Total buffer concentration. (c) The concentration of buffer in the acid form. (d) The value of the first-order rate constant, k_{obs} (s⁻¹), was obtained as the slope the plot of $\ln(A_{\infty} - A_t)$ against time in Figures A9-A11. (e) The observed effect of an increase in total buffer concentration is a decrease in k_{obs} . The dependency of k_{obs} on [ImH⁺] appears to be linear, yielding a negative slope, k' (Figures A9-A11). (f) The value of k_{hyd} (s⁻¹) was obtained as the y-axis intercept of the plot of k_{obs} against imidazolium ion concentration in Figures A9-A11.

Figure A12: Hydrolysis of *p*-methylbenzaldehyde *N*-(*tert*-butoxycarbonyl)imine (120) in HCl solution (pH 0.057- 2.69) at 260 nm, 25 °C and I = 1.0 (KCl); plots of absorbance against time (a)-(j) with corresponding residuals.





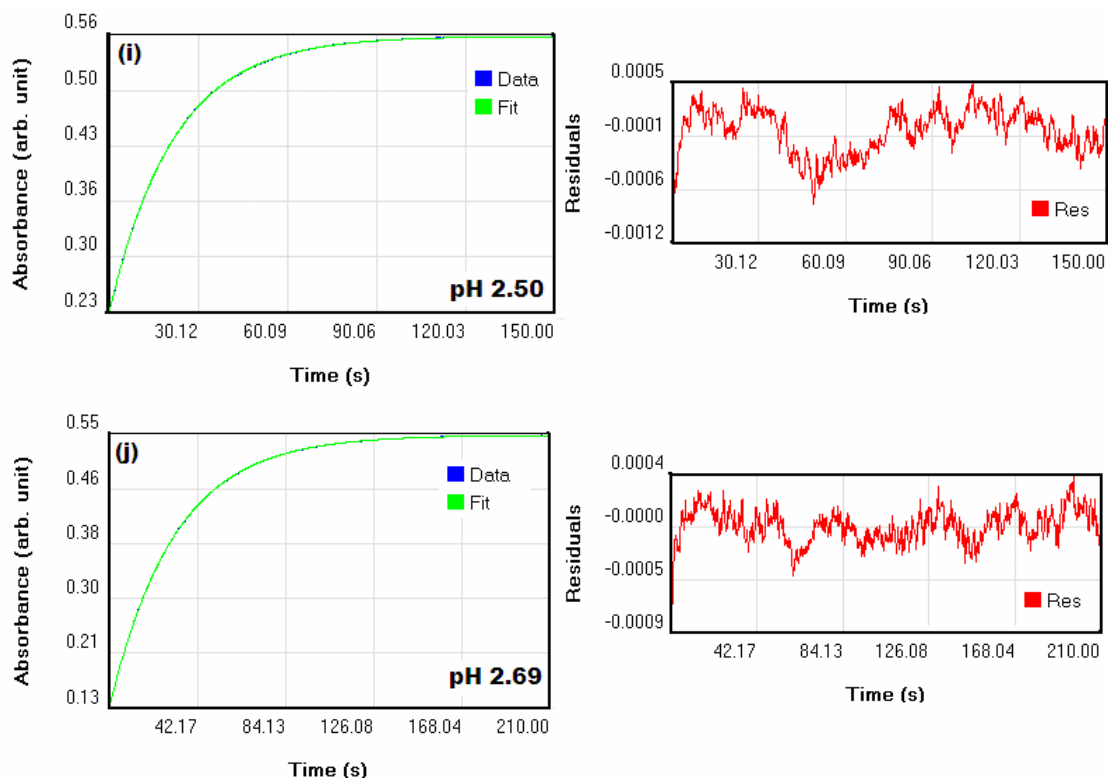


Table A5: Summary of first-order rate constants for the hydrolysis of *p*-methylbenzaldehyde *N*-(*tert*-butoxycarbonyl)imine (120) in HCl solution at 250 nm, 25 °C and *I* = 1.0 (KCl) obtained using stopped-flow spectrophotometry.^a

pH ^b	k_{hyd}^c (s ⁻¹)	<i>n</i> ^d	log k_{hyd}
0.057	1.69×10^1	10	1.23
0.36	6.49	10	8.12×10^{-1}
0.66	3.10	10	4.91×10^{-1}
1.06	1.23	10	8.99×10^{-2}
1.36	5.66×10^{-1}	10	-2.47×10^{-1}
1.45	4.90×10^{-1}	10	-3.10×10^{-1}
1.68	2.88×10^{-1}	10	-5.40×10^{-1}
2.06	1.17×10^{-1}	10	-9.32×10^{-1}
2.50	4.30×10^{-2}	10	-1.37
2.69	3.13×10^{-2}	8	-1.50

(a) Measurements were made at an initial substrate concentration of 5×10^{-5} M. (b) HCl solutions were diluted by 50% and the pH of the resulting solution measured in order to account for the dilution upon mixing in the stopped-flow apparatus. (c) The value of the first-order rate constant, k_{hyd} (s⁻¹), was obtained from least-squares analysis of absorbance versus time data in Figure A12 (a)-(j). (d) The number of runs averaged to give the value of k_{hyd} .

Figure A13: Hydrolysis of *p*-methylbenzaldehyde *N*-(*tert*-butoxycarbonyl)imine (120) in chloroacetic acid buffer (75% f_B , pH 3.19); (a) plot of $\ln(A_\infty - A_t)$ against time, (b) plot of k_{obs} against the concentration of chloroacetic acid, $[\text{CH}_2\text{ClCOOH}]$.

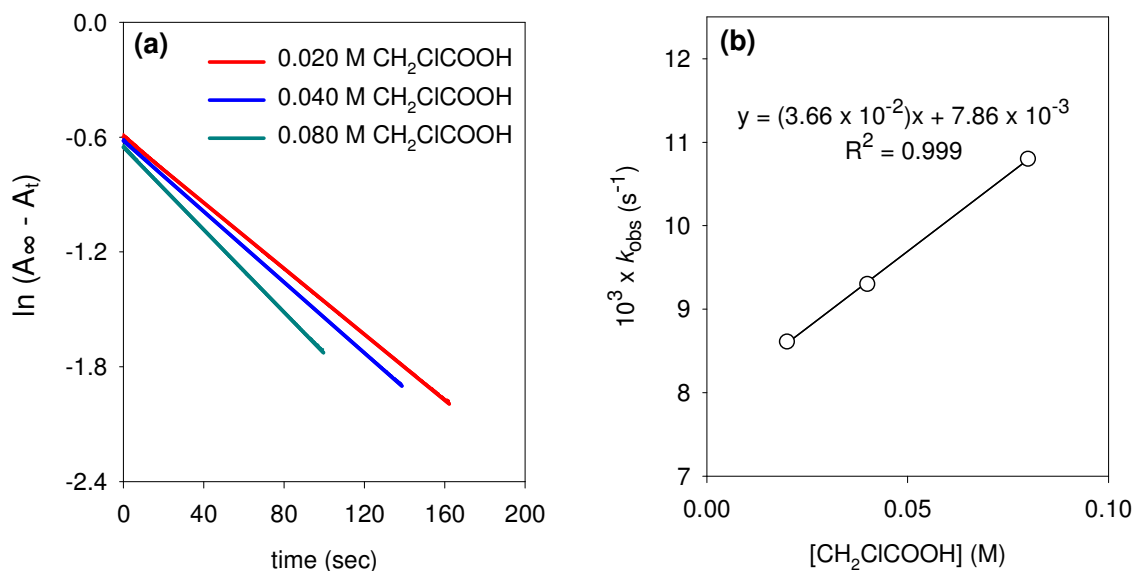


Figure A14: Hydrolysis of *p*-methylbenzaldehyde *N*-(*tert*-butoxycarbonyl)imine (120) in acetic acid buffer (10% f_B , pH 3.58); (a) plot of $\ln(A_\infty - A_t)$ against time, (b) plot of k_{obs} against the concentration of acetic acid, $[\text{CH}_3\text{COOH}]$.

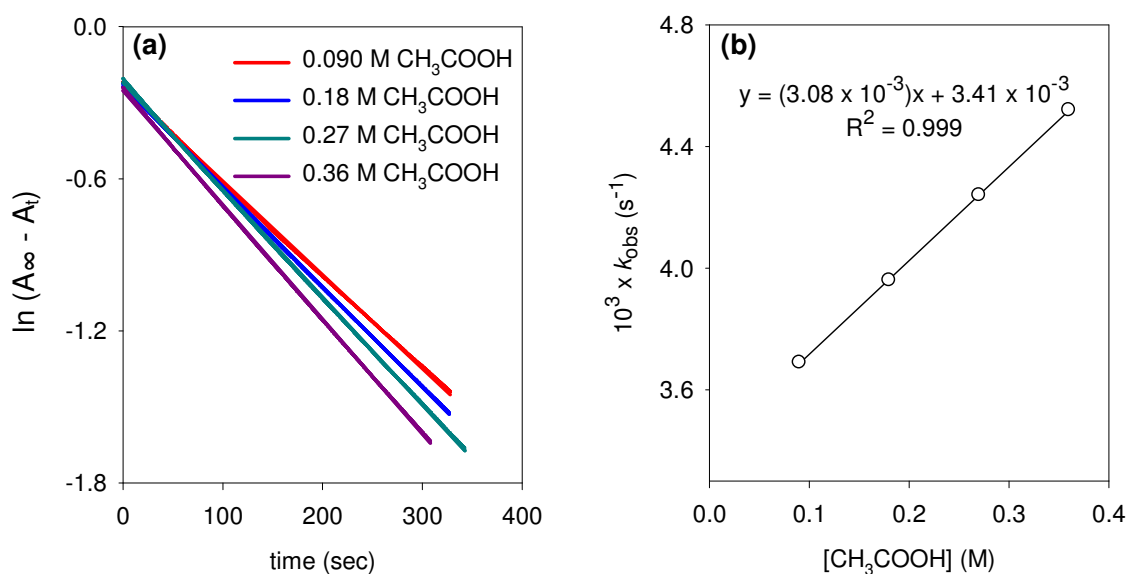


Figure A15: Hydrolysis of *p*-methylbenzaldehyde *N*-(*tert*-butoxycarbonyl)imine (120) in acetic acid buffer (25% f_B , pH 4.12); (a) plot of $\ln(A_\infty - A_t)$ against time, (b) plot of k_{obs} against the concentration of acetic acid, $[CH_3COOH]$.

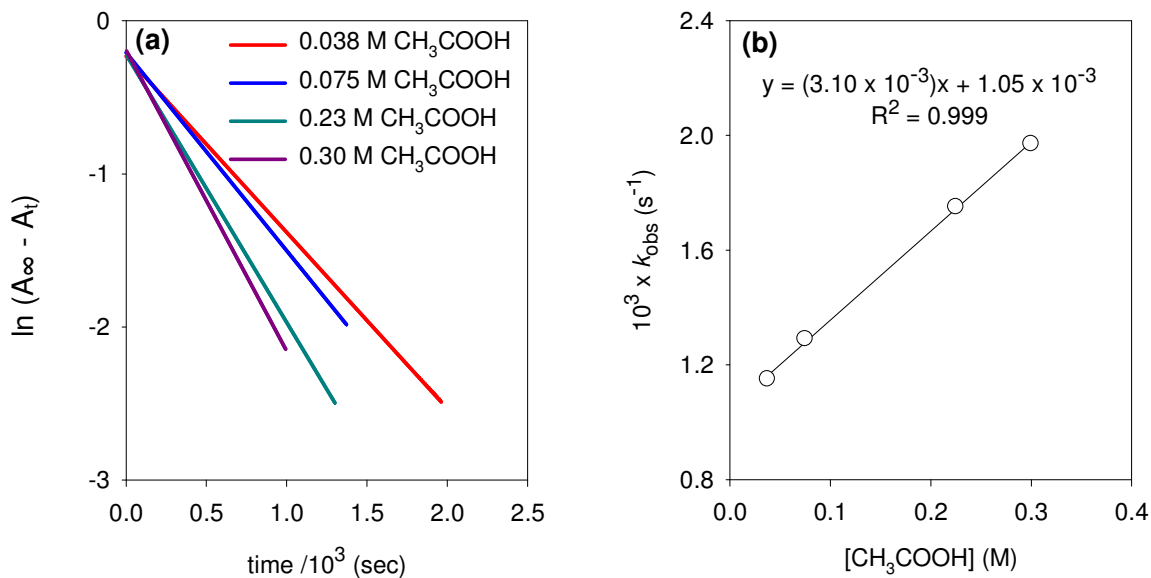


Figure A16: Hydrolysis of *p*-methylbenzaldehyde *N*-(*tert*-butoxycarbonyl)imine (120) in acetic acid buffer (50% f_B , pH 4.62); (a) plot of $\ln(A_\infty - A_t)$ against time, (b) plot of k_{obs} against the concentration of acetic acid, $[CH_3COOH]$.

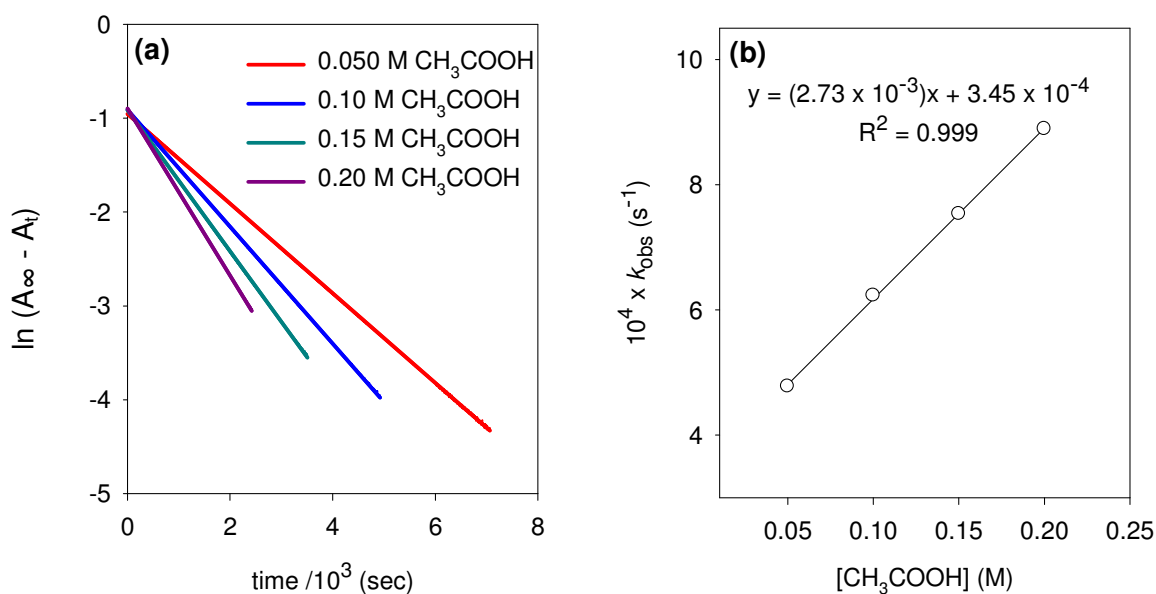


Figure A17: Hydrolysis of *p*-methylbenzaldehyde *N*-(*tert*-butoxycarbonyl)imine (120) in acetic acid buffer (75% f_B , pH 5.12); (a) plot of $\ln(A_\infty - A_t)$ against time, (b) plot of k_{obs} against the concentration of acetic acid, $[CH_3COOH]$.

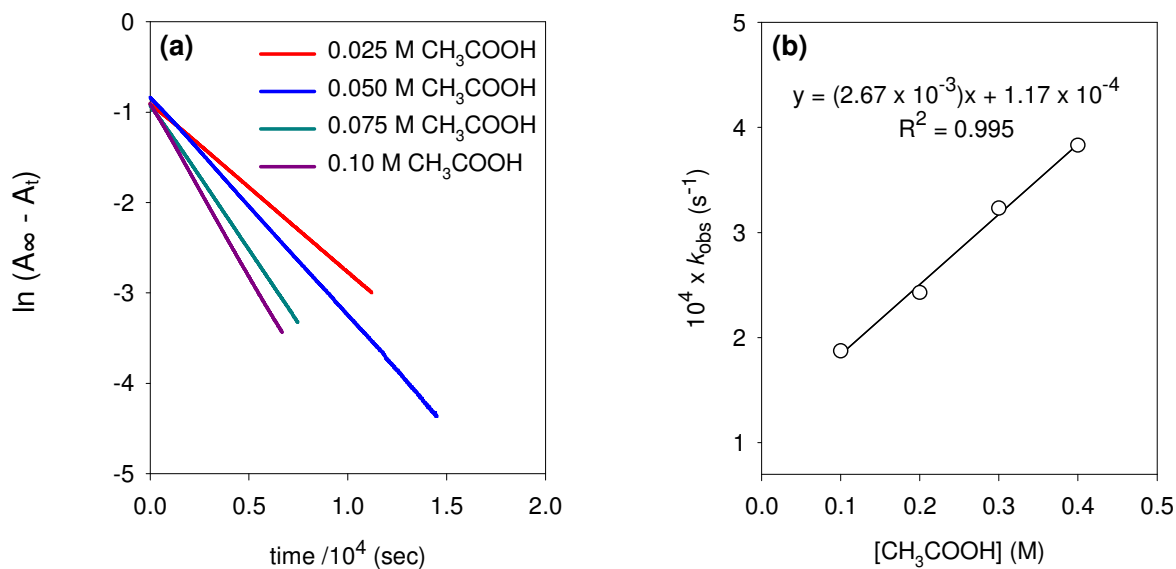


Figure A18: Hydrolysis of *p*-methylbenzaldehyde *N*-(*tert*-butoxycarbonyl)imine (120) in acetic acid buffer (90% f_B , pH 5.60); (a) plot of $\ln(A_\infty - A_t)$ against time, (b) plot of k_{obs} against the concentration of acetic acid, $[CH_3COOH]$.

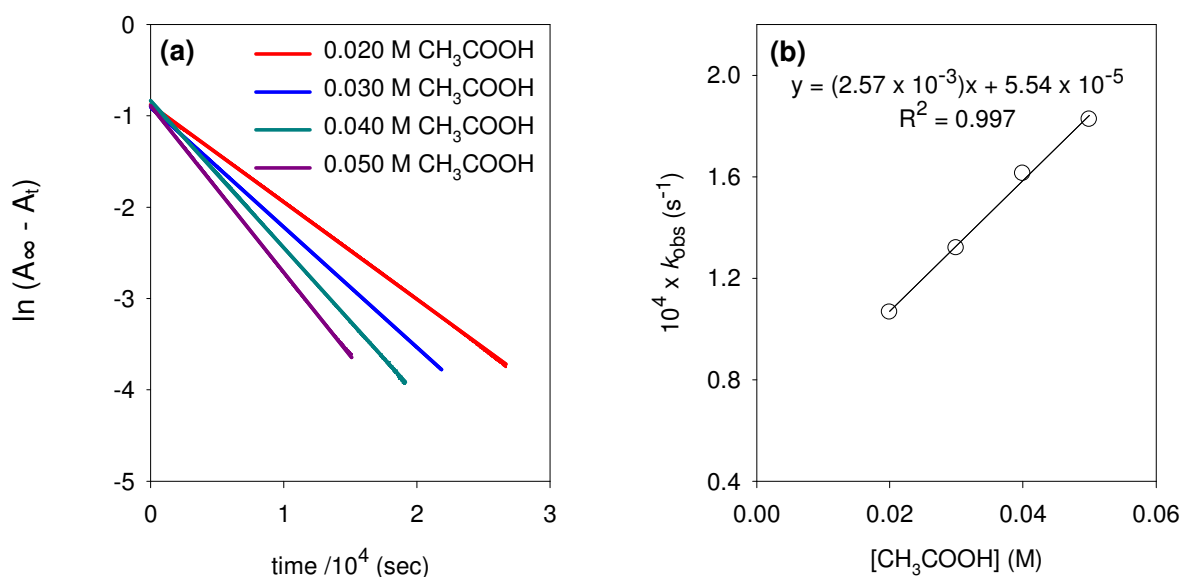


Table A6: First-order rate constants for the hydrolysis of *p*-methylbenzaldehyde *N*-(*tert*-butoxycarbonyl)imine (120) in acetic acid and chloroacetic acid* buffers at 260 nm, 25 °C and I = 1.0 (KCl).^a

[Buffer] _T ^b (M)	[CH ₃ COOH] ^c (M)	pH	$k_{\text{obs}}^{\text{d}}$ (s ⁻¹)	R ²	k_{HA}^{e} (M ⁻¹ s ⁻¹)	$k_{\text{hyd}}^{\text{f}}$ (s ⁻¹)
75% f_{B}^*						
0.080	0.020	3.19	8.61×10^{-3}	0.999		
0.16	0.040	3.19	9.30×10^{-3}	0.999	3.66×10^{-2}	7.86×10^{-3}
0.32	0.080	3.19	1.08×10^{-2}	0.999		
10% f_{B}						
0.10	0.090	3.58	3.69×10^{-3}	0.999		
0.20	0.18	3.57	3.96×10^{-3}	0.999	3.08×10^{-3}	3.41×10^{-3}
0.30	0.27	3.58	4.24×10^{-3}	0.999		
0.40	0.36	3.59	4.52×10^{-3}	0.999		
25% f_{B}						
0.050	0.038	4.12	1.15×10^{-3}	0.999		
0.10	0.075	4.12	1.29×10^{-3}	0.999	3.10×10^{-3}	1.05×10^{-3}
0.30	0.23	4.12	1.75×10^{-3}	0.999		
0.40	0.30	4.11	1.97×10^{-3}	0.999		
50% f_{B}						
0.10	0.050	4.60	4.78×10^{-4}	0.999		
0.20	0.10	4.61	6.23×10^{-4}	0.999	2.73×10^{-3}	3.45×10^{-4}
0.30	0.15	4.62	7.53×10^{-4}	0.999		
0.40	0.20	4.63	8.89×10^{-4}	0.999		
75% f_{B}						
0.10	0.025	5.11	1.87×10^{-4}	0.999		
0.20	0.050	5.10	2.43×10^{-4}	0.999	2.67×10^{-3}	1.17×10^{-4}
0.30	0.075	5.12	3.23×10^{-4}	0.999		
0.40	0.10	5.12	3.83×10^{-4}	0.999		
90% f_{B}						
0.20	0.020	5.57	1.07×10^{-4}	0.999		
0.30	0.030	5.59	1.32×10^{-4}	0.999	2.57×10^{-3}	5.54×10^{-5}
0.40	0.040	5.61	1.61×10^{-4}	0.999		
0.50	0.050	5.63	1.83×10^{-4}	0.999		

(a) Measurements were made at an initial substrate concentration of 5×10^{-5} M. (b) Total buffer concentration. (c) The concentration of buffer in the acid form. (d) The value of the first-order rate constant, k_{obs} (s⁻¹), was obtained as the slope the plot of $\ln(A_{\infty} - A_t)$ against time in Figures A13-A18. (e) The value of the second-order rate constant, k_{HA} (M⁻¹s⁻¹), was obtained as the slope of the plot of k_{obs} against general acid concentration in Figures A13- A18. (f) The value of k_{hyd} (s⁻¹) was obtained as the y-axis intercept of the plot of k_{obs} against general acid concentration in Figures A13-A18.

Figure A19: Hydrolysis of *p*-methylbenzaldehyde *N*-(*tert*-butoxycarbonyl)imine (120) in phosphate buffer (20% f_B , pH 5.86); (a) plot of $\ln(A_\infty - A_t)$ against time, (b) plot of k_{obs} against the concentration of dihydrogen phosphate, $[\text{H}_2\text{PO}_4^-]$.

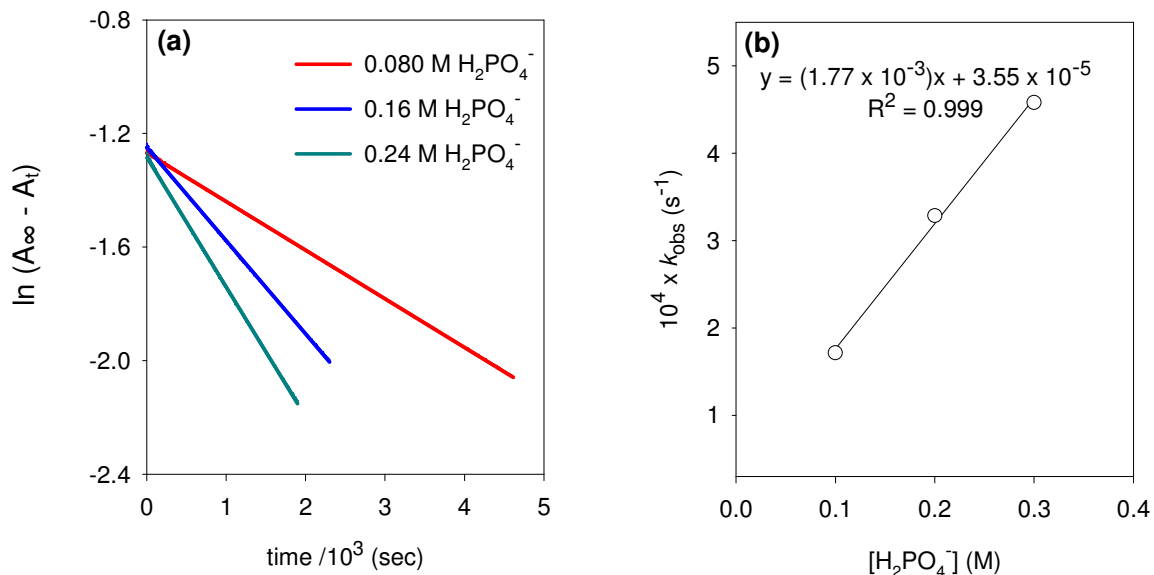


Figure A20: Hydrolysis of *p*-methylbenzaldehyde *N*-(*tert*-butoxycarbonyl)imine (120) in phosphate buffer (30% f_B , pH 6.11); (a) plot of $\ln(A_\infty - A_t)$ against time, (b) plot of k_{obs} against the concentration of dihydrogen phosphate, $[\text{H}_2\text{PO}_4^-]$.

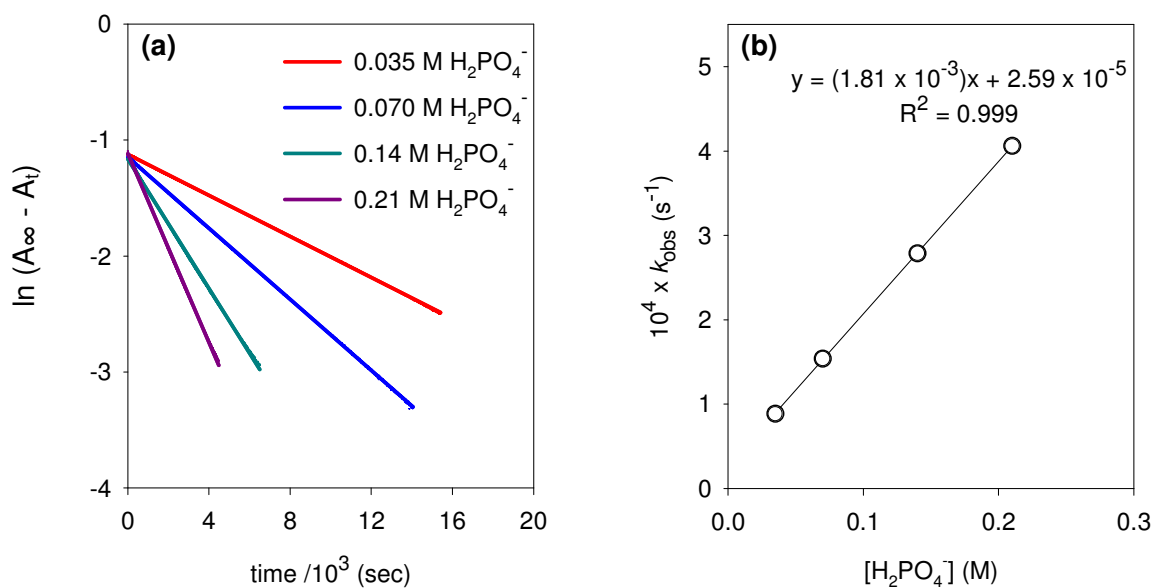


Figure A21: Hydrolysis of *p*-methylbenzaldehyde *N*-(*tert*-butoxycarbonyl)imine (120) in phosphate buffer (50% f_B , pH 6.52); (a) plot of $\ln(A_\infty - A_t)$ against time, (b) plot of k_{obs} against the concentration of dihydrogen phosphate, $[H_2PO_4^-]$.

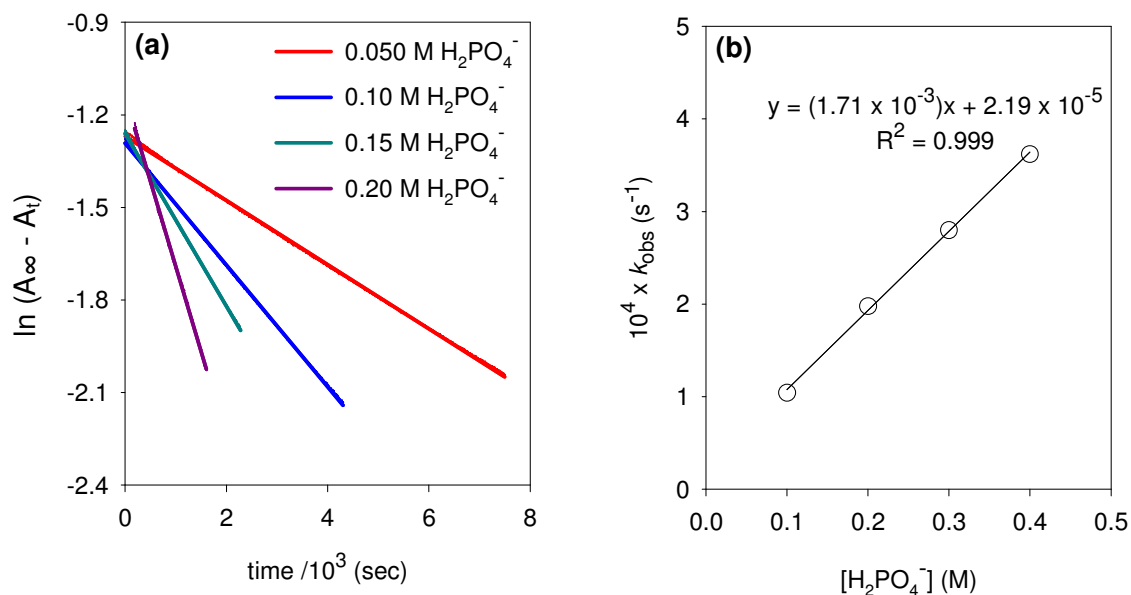


Figure A22: Hydrolysis of *p*-methylbenzaldehyde *N*-(*tert*-butoxycarbonyl)imine (120) in phosphate buffer (80% f_B , pH 7.19); (a) plot of $\ln(A_\infty - A_t)$ against time, (b) plot of k_{obs} against the concentration of dihydrogen phosphate, $[H_2PO_4^-]$.

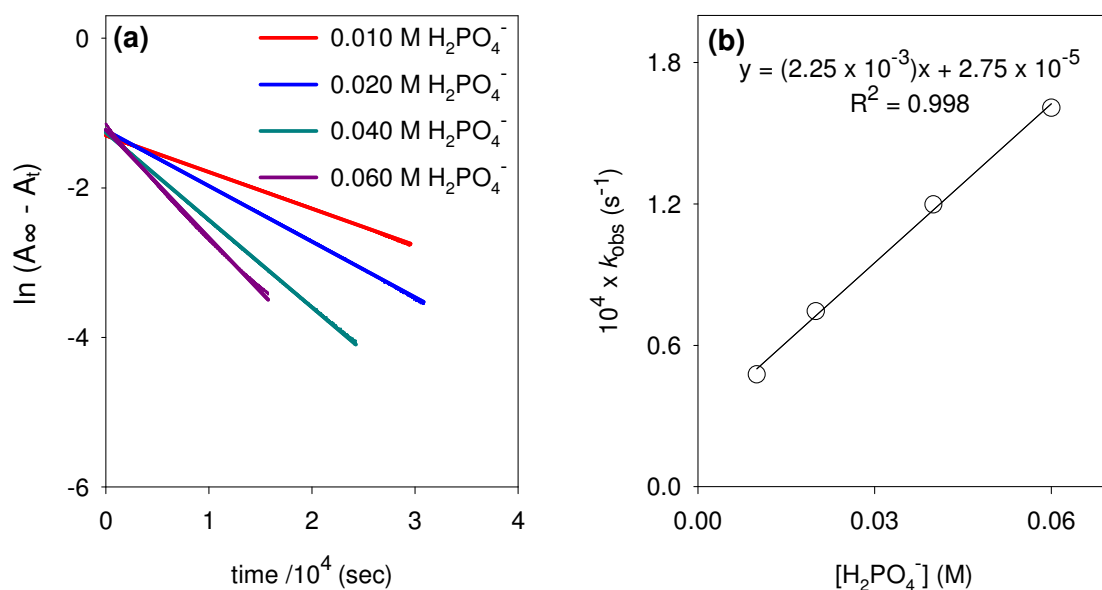
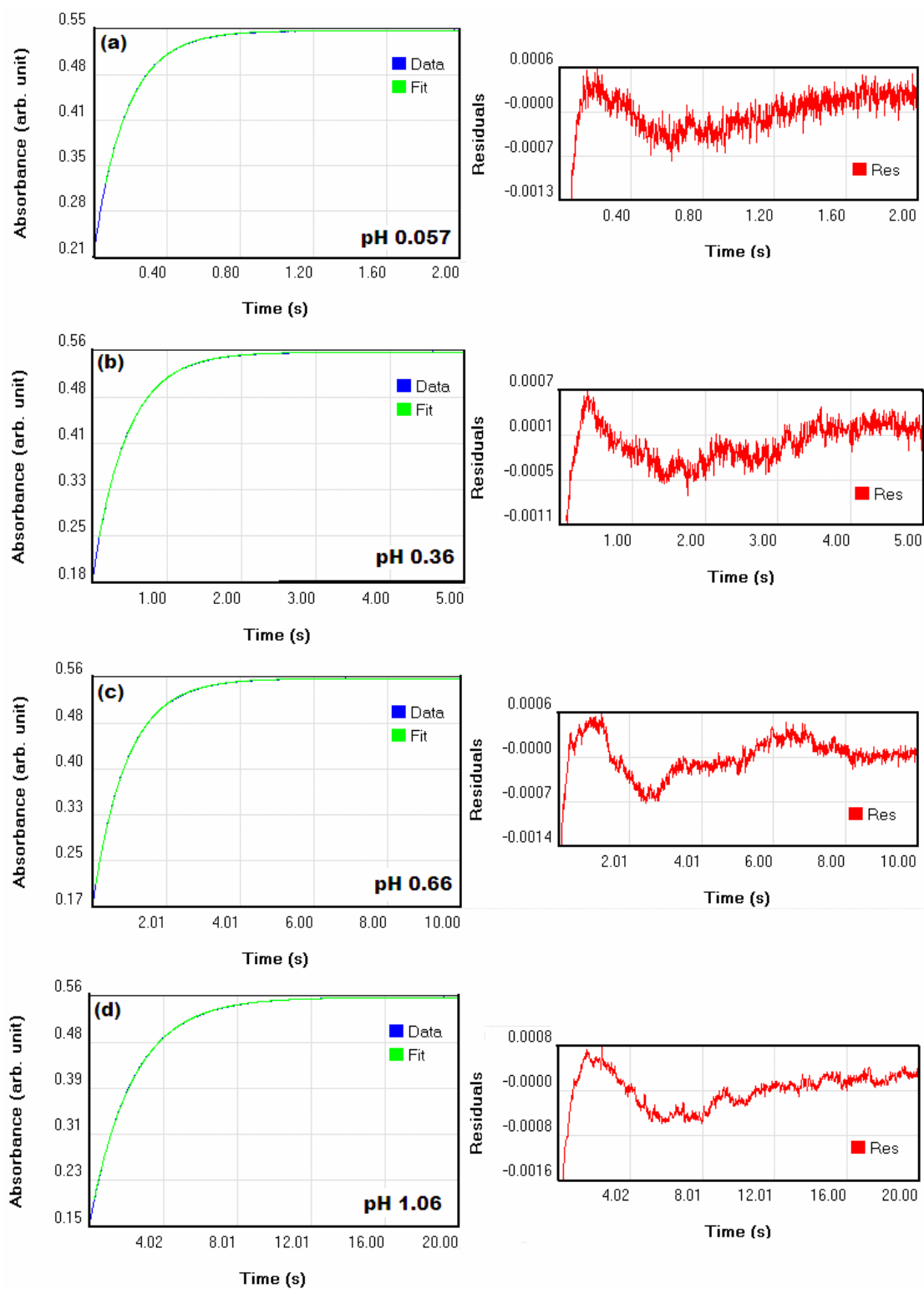


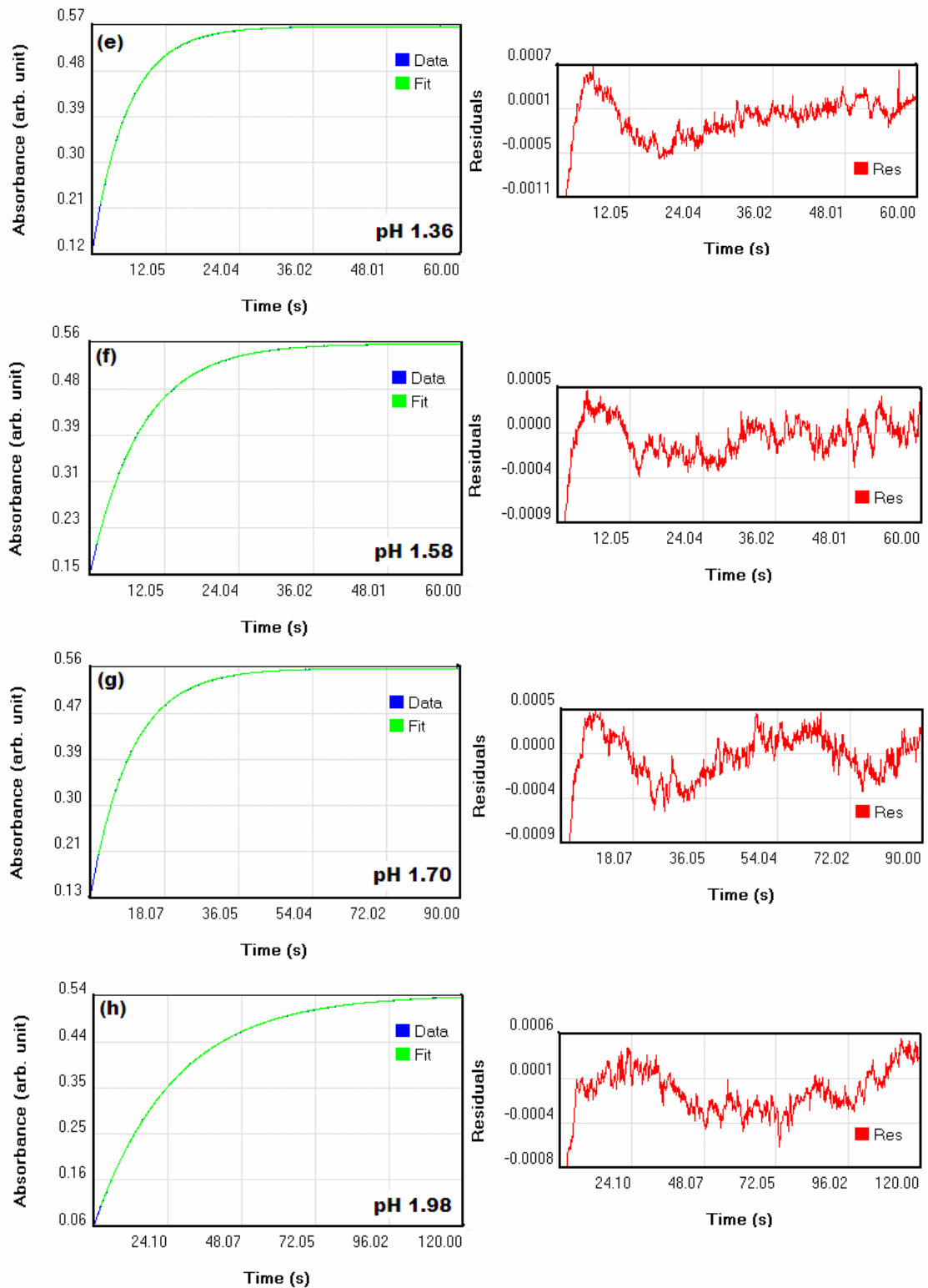
Table A7: First-order rate constants for the hydrolysis of *p*-methylbenzaldehyde *N*-(*tert*-butoxycarbonyl)imine (120) in phosphate buffers at 260 nm, 25 °C and I = 1.0 (KCl).^a

[Buffer] _T ^b (M)	[H ₂ PO ₄ ⁻] ^c (M)	pH	<i>k</i> _{obs} ^d (s ⁻¹)	R ²	<i>k</i> _{HA} ^e (M ⁻¹ s ⁻¹)	<i>k</i> _{hyd} ^f (s ⁻¹)
20% <i>f</i> _B						
0.10	0.080	5.86	1.72 × 10 ⁻⁴	0.999		
0.20	0.16	5.85	3.29 × 10 ⁻⁴	0.999	1.77 × 10 ⁻³	3.55 × 10 ⁻⁵
0.30	0.24	5.86	4.58 × 10 ⁻⁴	0.999		
30% <i>f</i> _B						
0.05	0.035	6.13	8.85 × 10 ⁻⁵	0.999		
0.10	0.070	6.10	1.54 × 10 ⁻⁴	0.999	1.81 × 10 ⁻³	2.59 × 10 ⁻⁵
0.20	0.14	6.10	2.79 × 10 ⁻⁴	0.999		
0.30	0.21	6.12	4.06 × 10 ⁻⁴	0.999		
50% <i>f</i> _B						
0.10	0.050	6.54	1.04 × 10 ⁻⁴	0.999		
0.20	0.10	6.52	1.98 × 10 ⁻⁴	0.999	1.71 × 10 ⁻³	2.19 × 10 ⁻⁵
0.30	0.15	6.50	2.80 × 10 ⁻⁴	0.999		
0.40	0.20	6.50	3.62 × 10 ⁻⁴	0.999		
80% <i>f</i> _B						
0.05	0.010	7.11	4.76 × 10 ⁻⁵	0.999		
0.10	0.020	7.15	7.44 × 10 ⁻⁵	0.999	2.25 × 10 ⁻³	2.75 × 10 ⁻⁵
0.20	0.040	7.23	1.20 × 10 ⁻⁴	0.999		
0.30	0.060	7.29	1.61 × 10 ⁻⁴	0.999		

(a) Measurements were made at an initial substrate concentration of 5 × 10⁻⁵ M. (b) Total buffer concentration. (c) The concentration of buffer in the acid form. (d) The value of the first-order rate constant, *k*_{obs} (s⁻¹), was obtained as the slope the plot of ln (A_∞ - A_t) against time in Figures A19-A22. (e) The value of the second-order rate constant, *k*_{HA} (M⁻¹s⁻¹), was obtained as the slope of the plot of *k*_{obs} (s⁻¹) against the concentration of dihydrogen phosphate in Figures A19-A22. (f) The value of *k*_{hyd} (s⁻¹) was obtained as the y-axis intercept of the plot of *k*_{obs} against the concentration of dihydrogen phosphate in Figures A19-A22.

Figure A23: Hydrolysis of benzaldehyde *N*-(*tert*-butoxycarbonyl)imine (121) in HCl solution (pH 0.057-2.71) at 249 nm, 25 °C and I = 1.0 (KCl); plots of absorbance against time (a)-(j) with corresponding residuals.





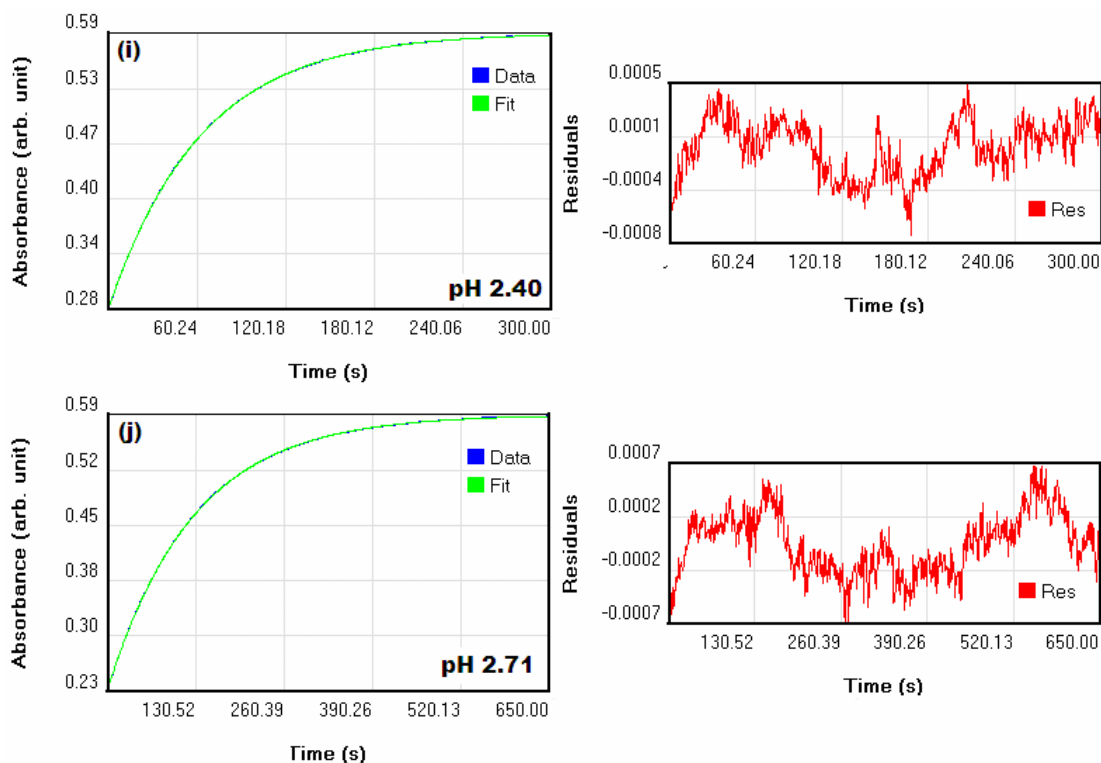


Table A8: Summary of first-order rate constants for the hydrolysis of benzaldehyde *N*-(*tert*-butoxycarbonyl)imine (121) in HCl solution at 249 nm, 25 °C and I = 1.0 (KCl) obtained using stopped-flow spectrophotometry.^a

pH ^b	$k_{\text{hyd}}^{\text{c}}$ (s ⁻¹)	n ^d	log k_{hyd}
0.057	5.58	13	7.47×10^{-1}
0.36	2.15	10	3.32×10^{-1}
0.66	1.08	10	3.34×10^{-2}
1.06	4.28×10^{-1}	10	-3.68×10^{-1}
1.36	2.12×10^{-1}	10	-6.74×10^{-1}
1.58	1.22×10^{-1}	10	-9.15×10^{-1}
1.70	1.01×10^{-1}	10	-9.96×10^{-1}
1.98	3.88×10^{-2}	10	-1.41
2.40	1.59×10^{-2}	10	-1.80
2.71	8.00×10^{-3}	9	-2.10

(a) Measurements were made at an initial substrate concentration of 5×10^{-5} M. (b) HCl solutions were diluted by 50% and the pH of the resulting solution measured in order to account for the dilution upon mixing in the stopped-flow apparatus. (c) The value of the first-order rate constant, k_{hyd} (s⁻¹), was obtained from least-squares analysis of absorbance versus time data in Figure A23 (a)-(j). (d) The number of runs averaged to give the value of k_{hyd} .

Figure A24: Hydrolysis of benzaldehyde *N*-(*tert*-butoxycarbonyl)imine (**121**) in chloroacetic acid buffer (75% f_B , pH 3.19); (a) plot of $\ln(A_\infty - A_t)$ against time, (b) plot of k_{obs} against the concentration of chloroacetic acid, $[CH_2ClCOOH]$.

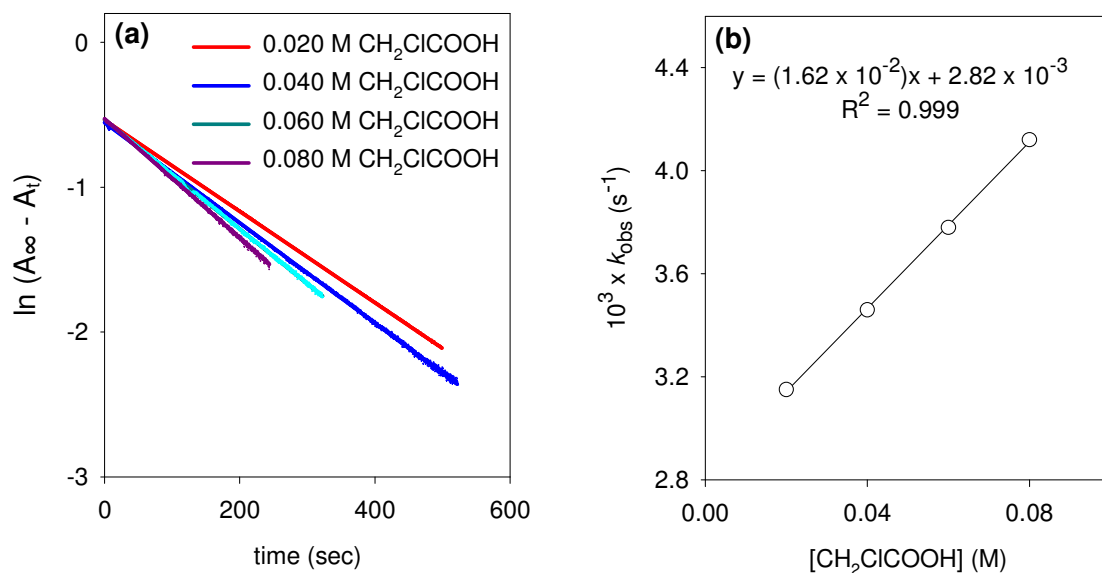


Figure A25: Hydrolysis of benzaldehyde *N*-(*tert*-butoxycarbonyl)imine (**121**) in acetic acid buffer (10% f_B , pH 3.61); (a) plot of $\ln(A_\infty - A_t)$ against time, (b) plot of k_{obs} against the concentration of acetic acid, $[CH_3COOH]$.

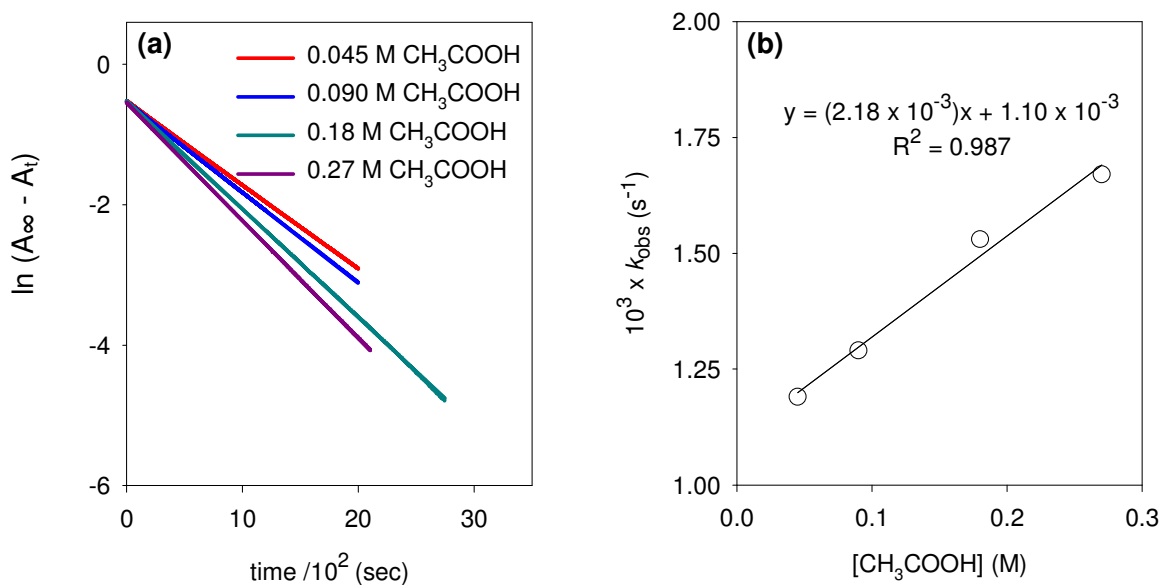


Figure A26: Hydrolysis of benzaldehyde *N*-(*tert*-butoxycarbonyl)imine (**121**) in acetic acid buffer (25% f_B , pH 4.11); (a) plot of $\ln(A_\infty - A_t)$ against time, (b) plot of k_{obs} against the concentration of acetic acid, $[\text{CH}_3\text{COOH}]$.

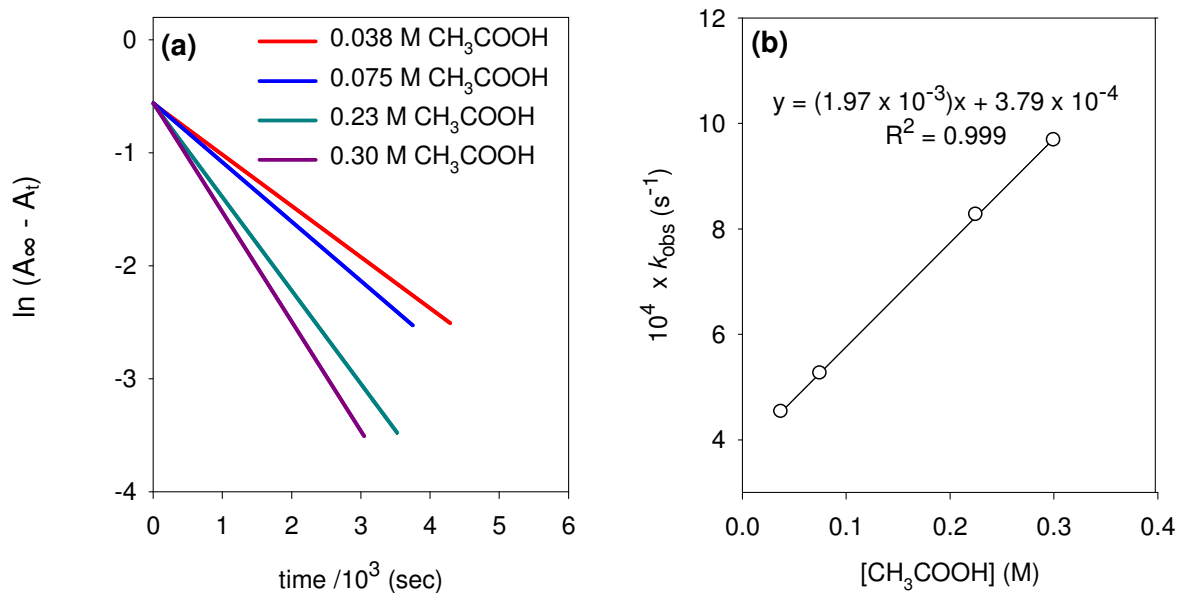


Figure A27: Hydrolysis of benzaldehyde *N*-(*tert*-butoxycarbonyl)imine (**121**) in acetic acid buffer (50% f_B , pH 4.62); (a) plot of $\ln(A_\infty - A_t)$ against time, (b) plot of k_{obs} against the concentration of acetic acid, $[\text{CH}_3\text{COOH}]$.

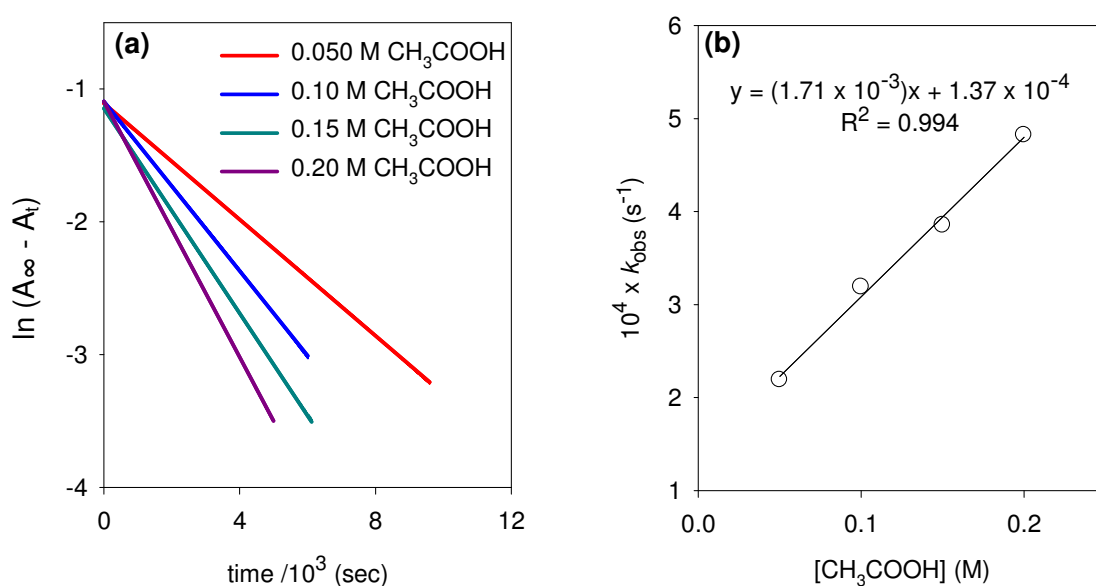


Figure A28: Hydrolysis of benzaldehyde *N*-(*tert*-butoxycarbonyl)imine (**121**) in acetic acid buffer (75% f_B , pH 5.12); (a) plot of $\ln(A_\infty - A_t)$ against time, (b) plot of k_{obs} against the concentration of acetic acid, $[\text{CH}_3\text{COOH}]$.

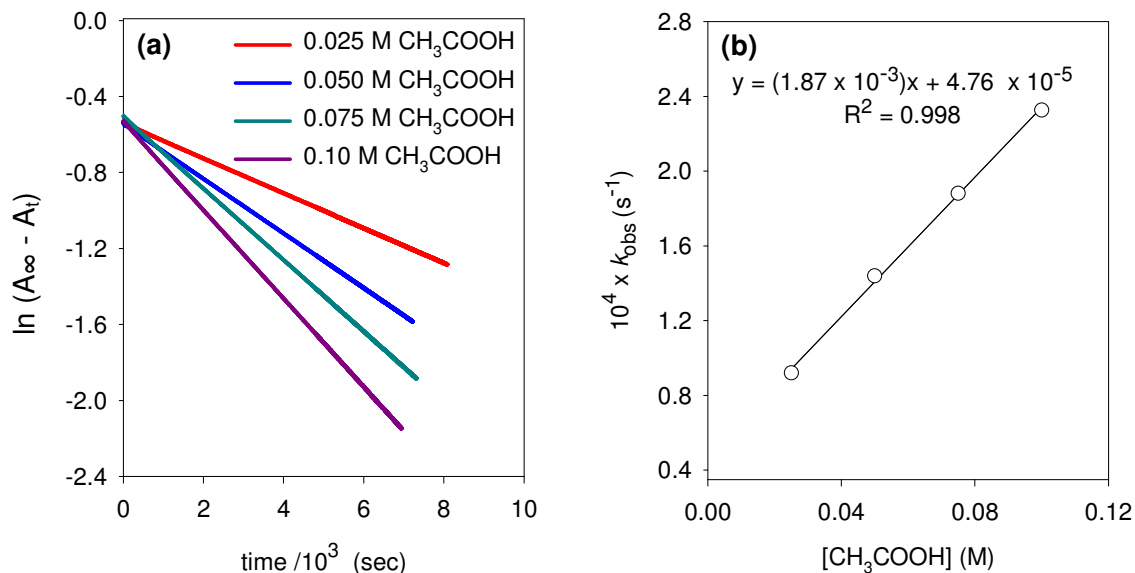


Figure A29: Hydrolysis of benzaldehyde *N*-(*tert*-butoxycarbonyl)imine (**121**) in acetic acid buffer (90% f_B , pH 5.58); (a) plot of $\ln(A_\infty - A_t)$ against time, (b) plot of k_{obs} against the concentration of acetic acid, $[\text{CH}_3\text{COOH}]$.

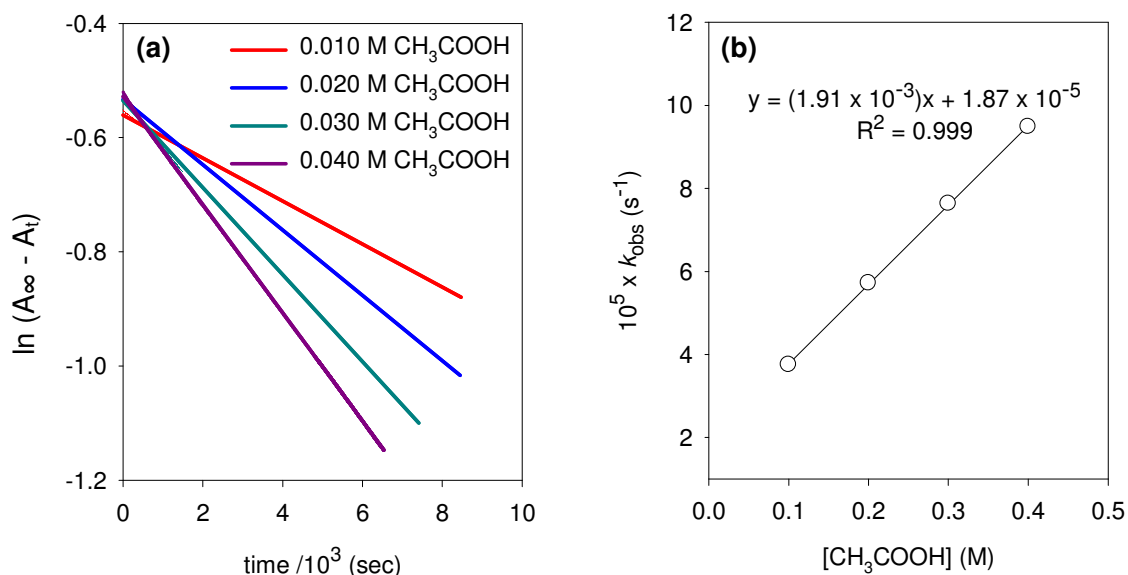


Table A9: First-order rate constants for the hydrolysis of benzaldehyde *N*-(*tert*-butoxycarbonyl)imine (121) in acetic acid and chloroacetic acid* buffers at 249 nm, 25 °C and I = 1.0 (KCl).^a

[Buffer] _T ^b (M)	[CH ₃ COOH] ^c	pH	k_{obs} ^d (s ⁻¹)	R ²	k_{HA} ^e (M ⁻¹ s ⁻¹)	k_{hyd} ^f (s ⁻¹)
75% f_{B} [*]	[CH ₂ ClCOOH]					
0.080	0.020	3.19	3.15×10^{-3}	0.999		
0.16	0.040	3.19	3.46×10^{-3}	0.999	1.62×10^{-2}	2.82×10^{-3}
0.24	0.060	3.19	3.78×10^{-3}	0.999		
0.32	0.080	3.20	4.12×10^{-3}	0.999		
10% f_{B}						
0.050	0.045	3.62	1.19×10^{-3}	0.999		
0.10	0.090	3.61	1.29×10^{-3}	0.999	2.18×10^{-3}	1.10×10^{-3}
0.20	0.18	3.60	1.53×10^{-3}	0.999		
0.30	0.27	3.60	1.67×10^{-3}	0.999		
25% f_{B}						
0.050	0.0375	4.12	4.53×10^{-4}	0.999		
0.10	0.075	4.11	5.26×10^{-4}	0.999	1.97×10^{-3}	3.79×10^{-4}
0.30	0.225	4.11	8.27×10^{-4}	0.999		
0.40	0.30	4.11	9.68×10^{-4}	0.999		
50% f_{B}						
0.10	0.050	4.61	2.19×10^{-4}	0.999		
0.20	0.10	4.61	3.19×10^{-4}	0.999	1.71×10^{-3}	1.37×10^{-4}
0.30	0.15	4.62	3.85×10^{-4}	0.999		
0.40	0.20	4.63	4.82×10^{-4}	0.999		
75% f_{B}						
0.10	0.025	5.11	9.20×10^{-5}	0.999		
0.20	0.050	5.12	1.44×10^{-4}	0.999	1.87×10^{-3}	4.76×10^{-5}
0.30	0.075	5.12	1.88×10^{-4}	0.999		
0.40	0.10	5.14	2.33×10^{-4}	0.999		
90% f_{B}						
0.10	0.010	5.55	3.75×10^{-5}	0.999		
0.20	0.020	5.57	5.72×10^{-5}	0.999	1.91×10^{-3}	1.87×10^{-5}
0.30	0.030	5.59	7.63×10^{-5}	0.999		
0.40	0.040	5.61	9.48×10^{-5}	0.999		

(a) Measurements were made at an initial substrate concentration of 5×10^{-5} M. (b) Total buffer concentration. (c) The concentration of buffer in the acid form. (d) The value of the first-order rate constant, k_{obs} (s⁻¹), was obtained as the slope the plot of $\ln(A_{\infty} - A_t)$ against time in Figures A24-A29. (e) The value of the second-order rate constant, k_{HA} (M⁻¹s⁻¹), was obtained as the slope of the plot of k_{obs} (s⁻¹) against the concentration of general acid in Figures A24-A29. (f) The value of k_{hyd} (s⁻¹) was obtained as the y-axis intercept of the plot of k_{obs} against general acid concentration in Figures A24-A29.

Figure A30: Hydrolysis of benzaldehyde *N*-(*tert*-butoxycarbonyl)imine (**121**) in phosphate buffer (20% f_B , pH 5.87); (a) plot of $\ln(A_\infty - A_t)$ against time, (b) plot of k_{obs} against the concentration of dihydrogen phosphate, $[\text{H}_2\text{PO}_4^-]$.

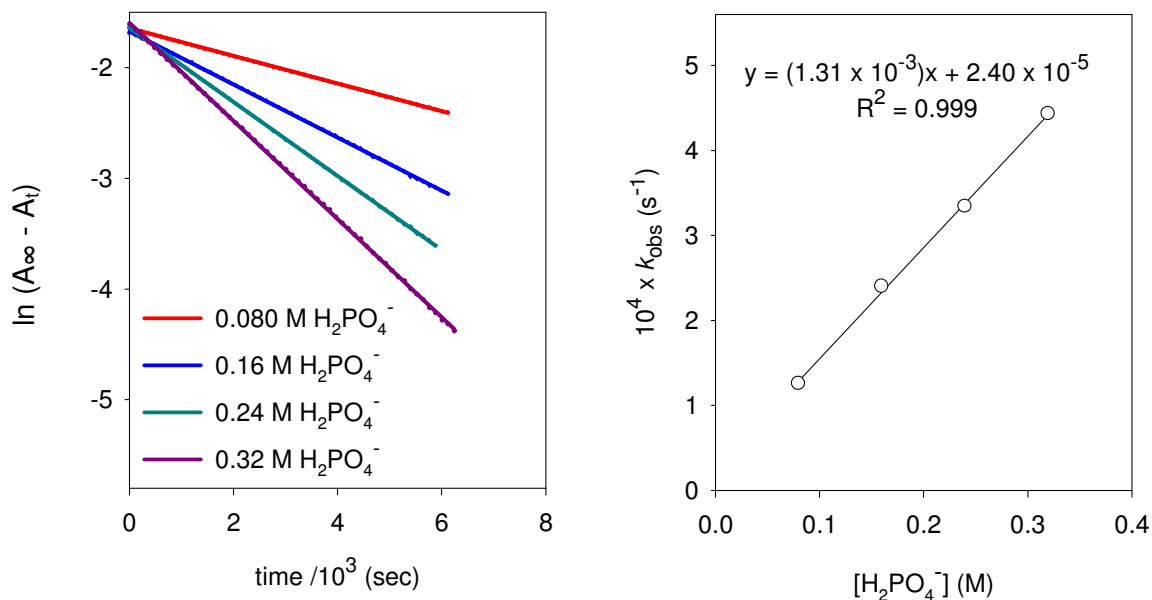


Figure A31: Hydrolysis of benzaldehyde *N*-(*tert*-butoxycarbonyl)imine (**121**) in phosphate buffer (80% f_B , pH 6.55); (a) plot of $\ln(A_\infty - A_t)$ against time, (b) plot of k_{obs} against the concentration of dihydrogen phosphate, $[\text{H}_2\text{PO}_4^-]$.

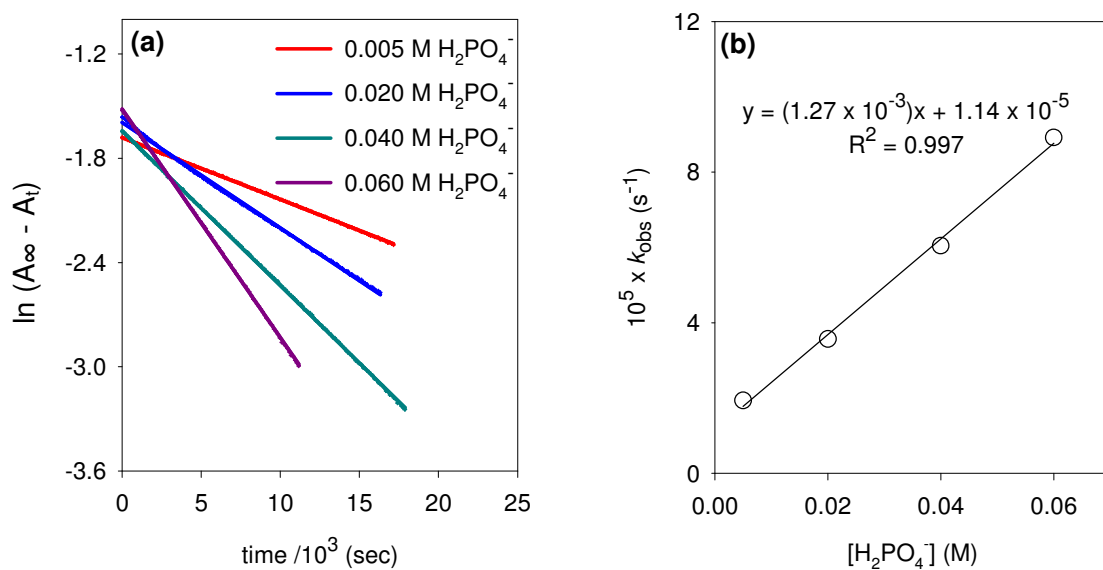
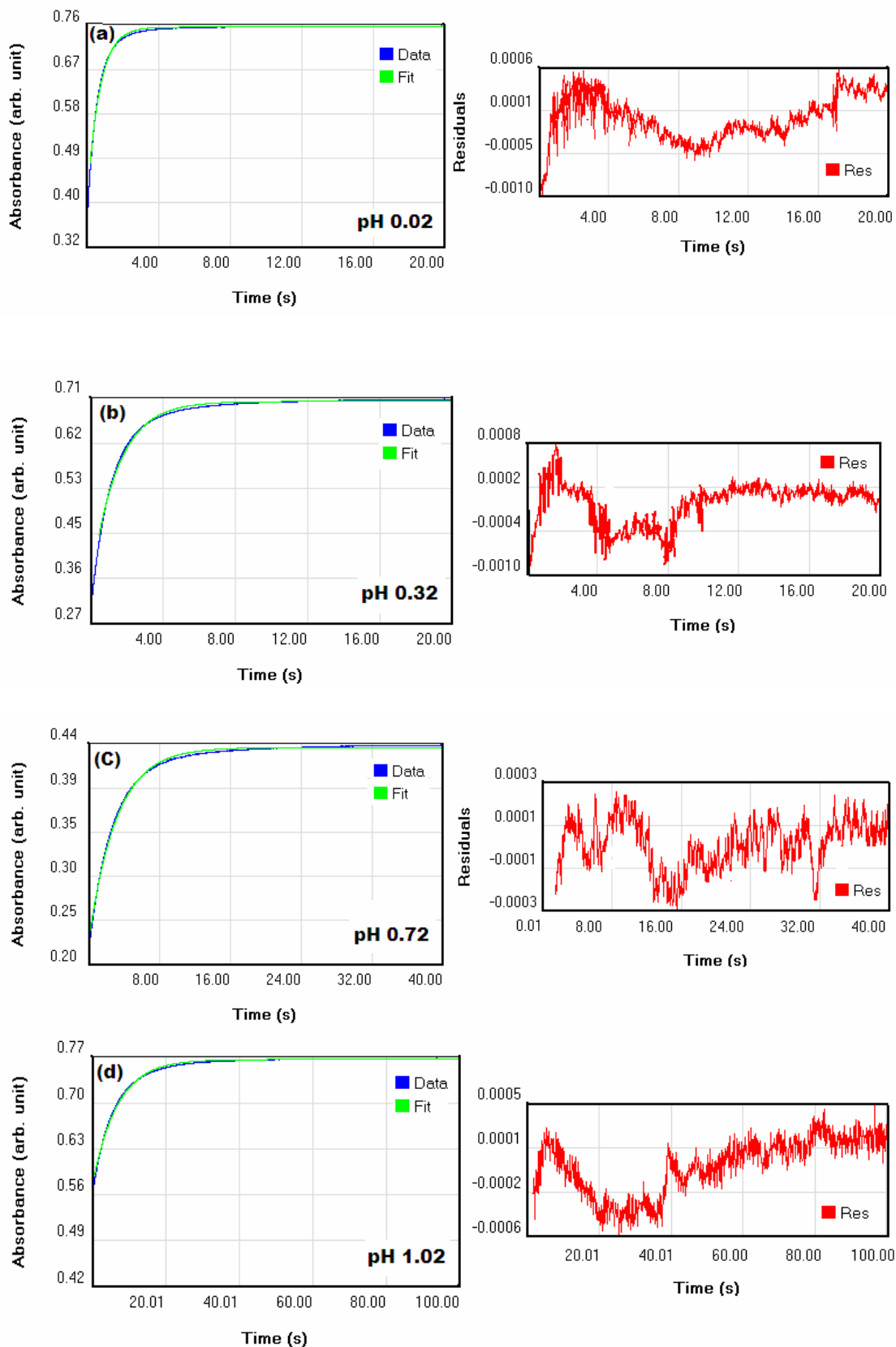


Table A10: First-order rate constants for the hydrolysis of benzaldehyde *N*-(*tert*-butoxycarbonyl)imine (121) in phosphate buffers at 249 nm, 25 °C and I = 1.0 (KCl).^a

[Buffer] _T ^b (M)	[H ₂ PO ₄ ⁻] ^c (M)	pH	k_{obs} ^d (s ⁻¹)	R ²	k_{HA} ^e (M ⁻¹ s ⁻¹)	k_{hyd} ^f (s ⁻¹)
20% f_B						
0.10	0.080	5.87	1.26×10^{-4}	0.999	1.31×10^{-3}	2.40×10^{-5}
0.20	0.16	5.86	2.40×10^{-4}	0.999		
0.30	0.24	5.87	3.34×10^{-4}	0.999		
0.40	0.32	5.87	4.43×10^{-4}	0.999		
80% f_B						
0.025	0.005	6.55	1.93×10^{-5}	0.999	1.27×10^{-3}	1.14×10^{-5}
0.10	0.020	6.55	3.57×10^{-5}	0.999		
0.20	0.040	6.55	6.05×10^{-5}	0.999		
0.30	0.060	6.55	8.92×10^{-5}	0.999		

(a) Measurements were made at an initial substrate concentration of 5×10^{-5} M. (b) Total buffer concentration. (c) The concentration of buffer in the acid form. (d) The value of the first-order rate constant, k_{obs} (s⁻¹), was obtained as the slope the plot of $\ln(A_{\infty} - A_t)$ against time in Figures A30-A31. (e) The value of the second-order rate constant, k_{HA} (M⁻¹s⁻¹) was obtained as the slope of the plot of k_{obs} (s⁻¹) against the concentration of dihydrogen phosphate in Figures A30-A31. (f) The value of k_{hyd} (s⁻¹) was obtained as the y-axis intercept of the plot of k_{obs} against dihydrogen phosphate concentration in Figures A30-A31.

Figure A32: Stopped-flow data for the hydrolysis of *p*-bromobenzaldehyde *N*-(*tert*-butoxycarbonyl)imine (122) in HCl solution (pH 0.02-2.82) at 262 nm, 25 °C and I = 1 (KCl); plots of absorbance against time (a)-(g) with corresponding residuals.



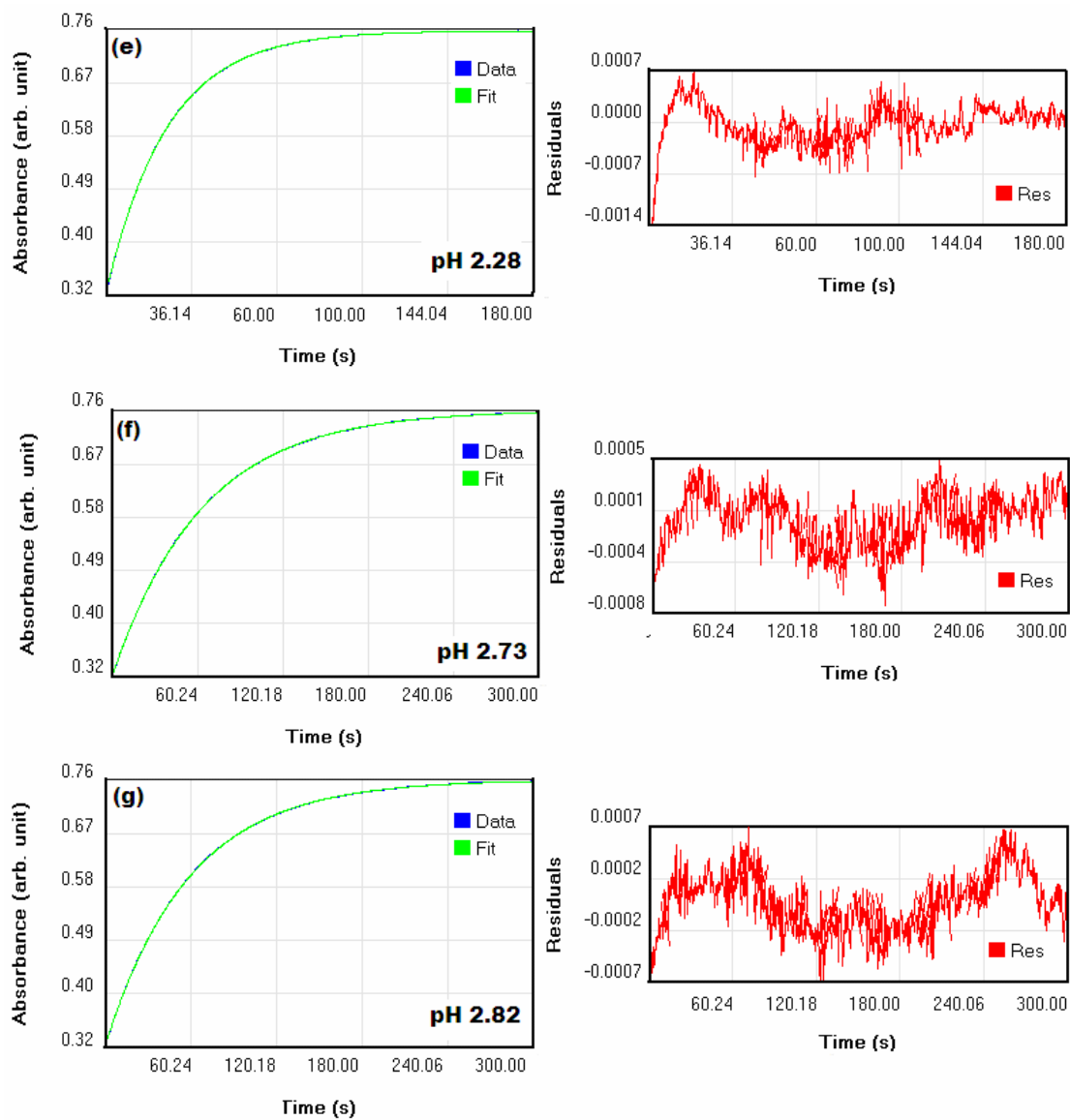


Table A11: Summary of first-order rate constants for the hydrolysis of *p*-bromobenzaldehyde *N*-(*tert*-butoxycarbonyl)imine (122) in HCl solution at 262 nm, 25 °C and I = 1.0 (KCl) obtained using stopped-flow spectrophotometry.^a

pH ^b	k_{hyd}^c (s ⁻¹)	n ^d	log k_{hyd}
0.02	1.57	7	1.96×10^{-1}
0.32	7.35×10^{-1}	6	-1.34×10^{-1}
0.72	3.21×10^{-1}	6	-4.93×10^{-1}
1.02	1.50×10^{-1}	6	-8.24×10^{-1}
2.28	7.96×10^{-3}	6	-2.10
2.73	3.10×10^{-3}	6	-2.51
2.82	2.78×10^{-3}	6	-2.56

(a) Measurements were made at an initial substrate concentration of 5×10^{-5} M. (b) HCl solutions used were diluted by 50% and the pH of the resulting solution measured in order to account for the dilution upon mixing in the stopped-flow apparatus. (c) The value of the first-order rate constant, k_{hyd} (s⁻¹), was obtained from least-squares analysis of absorbance versus time data in Figure A32 (a)-(g). (d) The number of runs averaged to give the value of k_{hyd} .

Figure A33: Hydrolysis of *p*-bromobenzaldehyde *N*-(*tert*-butoxycarbonyl)imine (122) in acetic acid buffer (10% f_B , pH 3.61); (a) plot of $\ln(A_\infty - A_t)$ against time, (b) plot of k_{obs} against the concentration of acetic acid, [CH₃COOH].

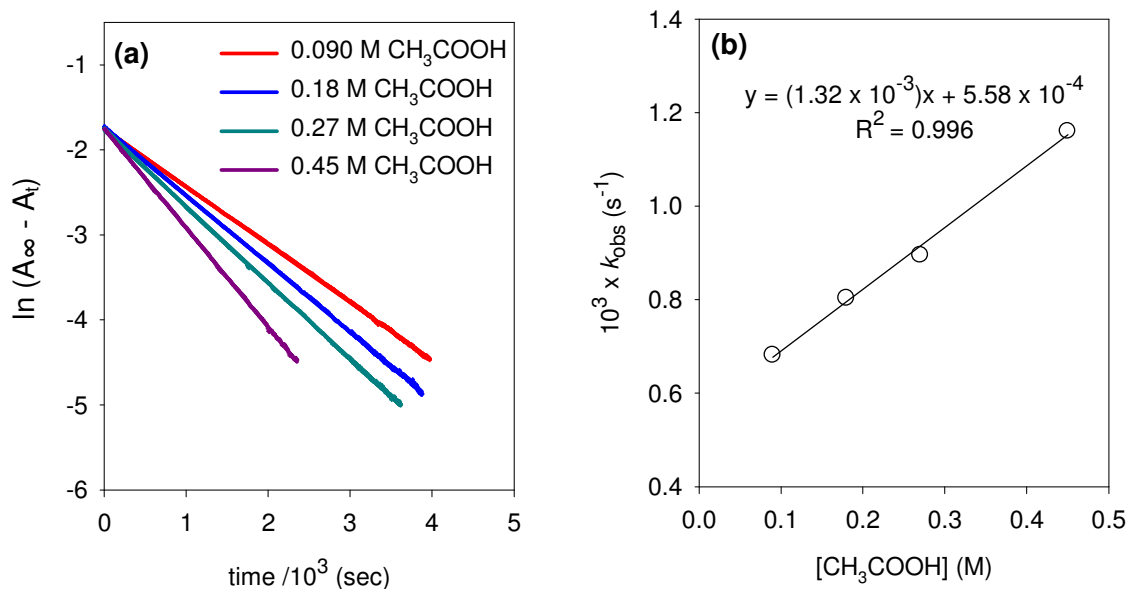


Figure A34: Hydrolysis of *p*-bromobenzaldehyde *N*-(*tert*-butoxycarbonyl)imine (122) in acetic acid buffer (25% f_B , pH 4.12); (a) plot of $\ln(A_\infty - A_t)$ against time, (b) plot of k_{obs} against the concentration of acetic acid, $[CH_3COOH]$.

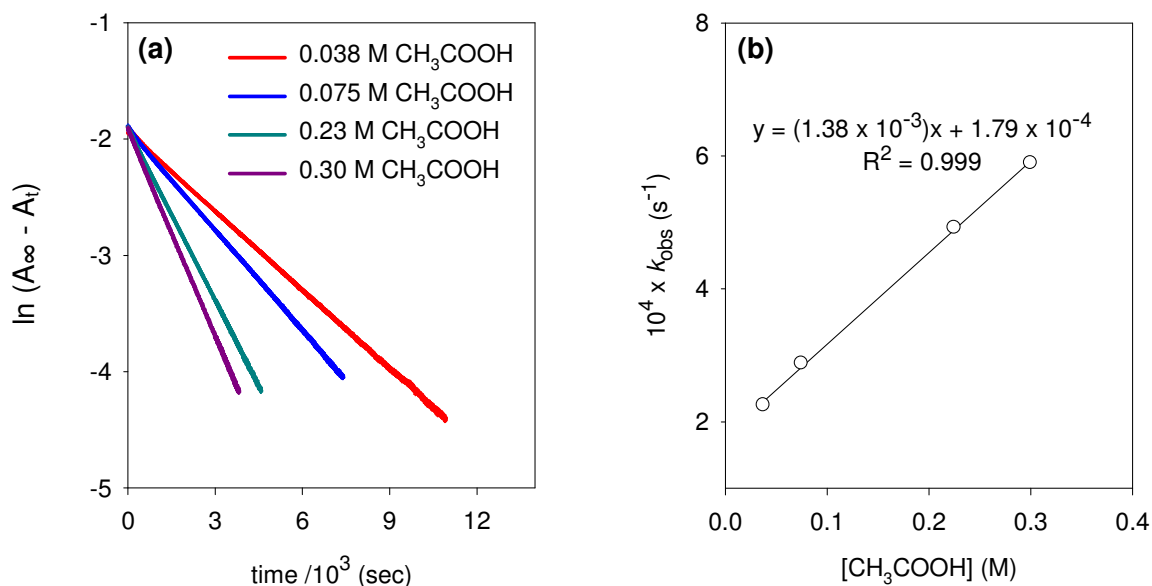


Figure A35: Hydrolysis of *p*-bromobenzaldehyde *N*-(*tert*-butoxycarbonyl)imine (122) in acetic acid buffer (50% f_B , pH 4.63); (a) plot of $\ln(A_\infty - A_t)$ against time, (b) plot of k_{obs} against the concentration of acetic acid, $[CH_3COOH]$.

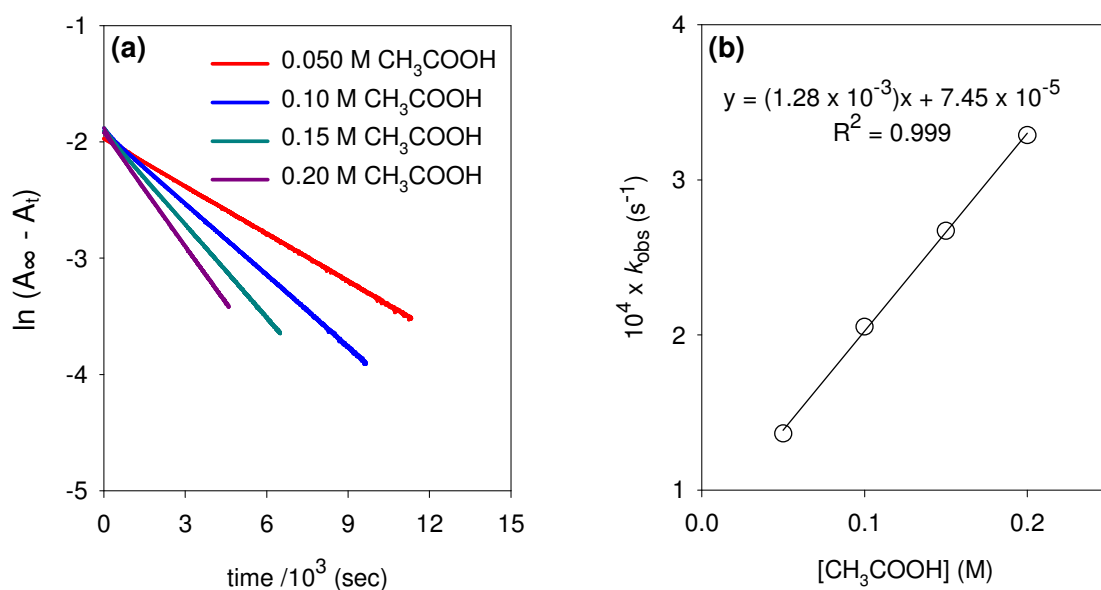


Figure A36: Hydrolysis of *p*-bromobenzaldehyde *N*-(*tert*-butoxycarbonyl)imine (122) in acetic acid buffer (75% f_B , pH 5.13); (a) plot of $\ln(A_\infty - A_t)$ against time, (b) plot of k_{obs} against the concentration of acetic acid, $[CH_3COOH]$.

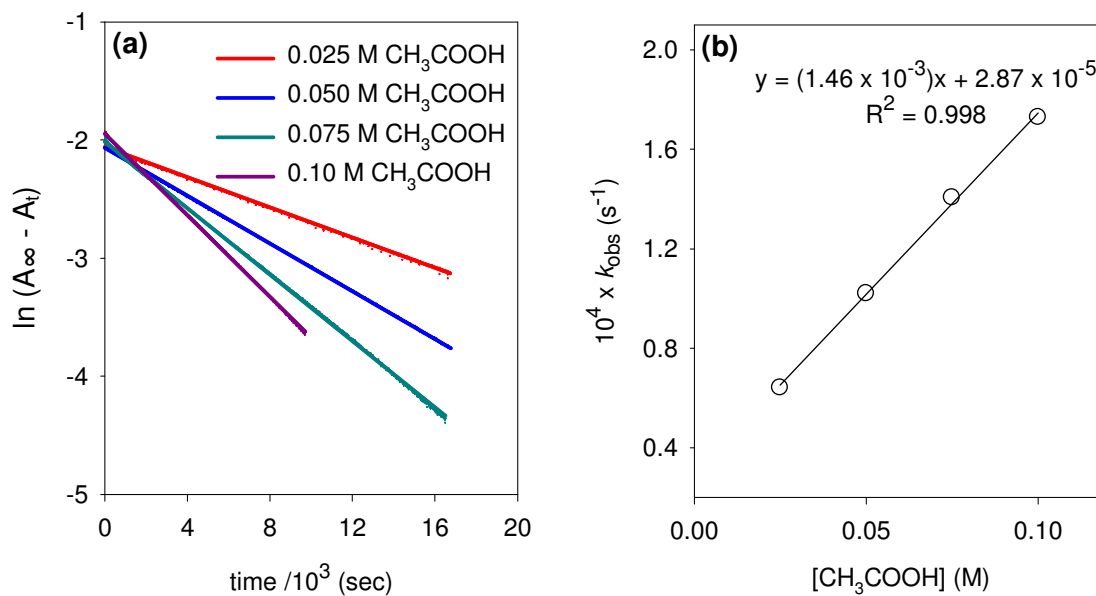


Table A12: First-order rate constants for the hydrolysis of *p*-bromobenzaldehyde *N*-(*tert*-butoxycarbonyl)imine (122) in acetic acid buffers at 262 nm, 25 °C and I = 1.0 (KCl).^a

[Buffer] _T ^b (M)	[CH ₃ COOH] ^c (M)	pH	k_{obs} ^d (s ⁻¹)	R ²	k_{HA} ^e (M ⁻¹ s ⁻¹)	k_{hyd} ^f (s ⁻¹)
10% f_{B}						
0.10	0.090	3.62	6.81×10^{-4}	0.999	1.32×10^{-3}	5.58×10^{-4}
0.20	0.18	3.61	8.03×10^{-4}	0.999		
0.30	0.27	3.60	8.95×10^{-4}	0.999		
0.50	0.45	3.60	1.16×10^{-3}	0.999		
25% f_{B}						
0.050	0.038	4.13	2.25×10^{-4}	0.999	1.38×10^{-3}	1.79×10^{-4}
0.10	0.075	4.12	2.88×10^{-4}	0.999		
0.30	0.23	4.12	4.92×10^{-4}	0.999		
0.40	0.30	4.13	5.89×10^{-4}	0.999		
50% f_{B}						
0.10	0.050	4.62	1.36×10^{-4}	0.999	1.28×10^{-3}	7.45×10^{-5}
0.20	0.10	4.61	2.05×10^{-4}	0.999		
0.30	0.15	4.64	2.67×10^{-4}	0.999		
0.40	0.20	4.63	3.29×10^{-4}	0.999		
75% f_{B}						
0.10	0.025	5.13	6.41×10^{-5}	0.999	1.46×10^{-3}	2.87×10^{-5}
0.20	0.050	5.13	1.02×10^{-4}	0.999		
0.30	0.075	5.13	1.41×10^{-4}	0.999		
0.40	0.10	5.12	1.73×10^{-4}	0.999		

(a) Measurements were made at an initial substrate concentration of 5×10^{-5} M. (b) Total buffer concentration. (c) The concentration of buffer in the acid form. (d) The value of the first-order rate constant, k_{obs} (s⁻¹), was obtained as the slope the plot of $\ln(A_{\infty} - A_t)$ against time in Figures A33-A36. (e) The value of the second-order rate constant, k_{HA} (M⁻¹s⁻¹), was obtained as the slope of the plot of k_{obs} (s⁻¹) against the concentration of acetic acid in Figures A33-A36. (f) The value of k_{hyd} (s⁻¹) was obtained as the y-axis intercept of the plot of k_{obs} against acetic acid concentration in Figures A33-A36.

Figure A37: Hydrolysis of *p*-bromobenzaldehyde *N*-(*tert*-butoxycarbonyl)imine (122) in phosphate buffer (20% f_B , pH 5.86); (a) plot of $\ln(A_\infty - A_t)$ against time, (b) plot of k_{obs} against the concentration of dihydrogen phosphate, $[\text{H}_2\text{PO}_4^-]$.

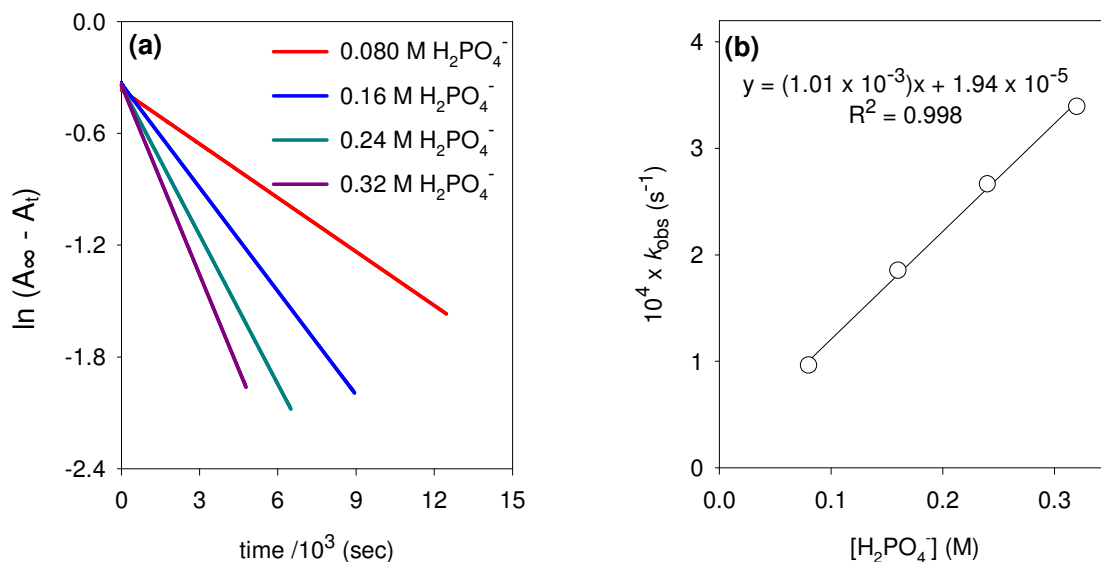
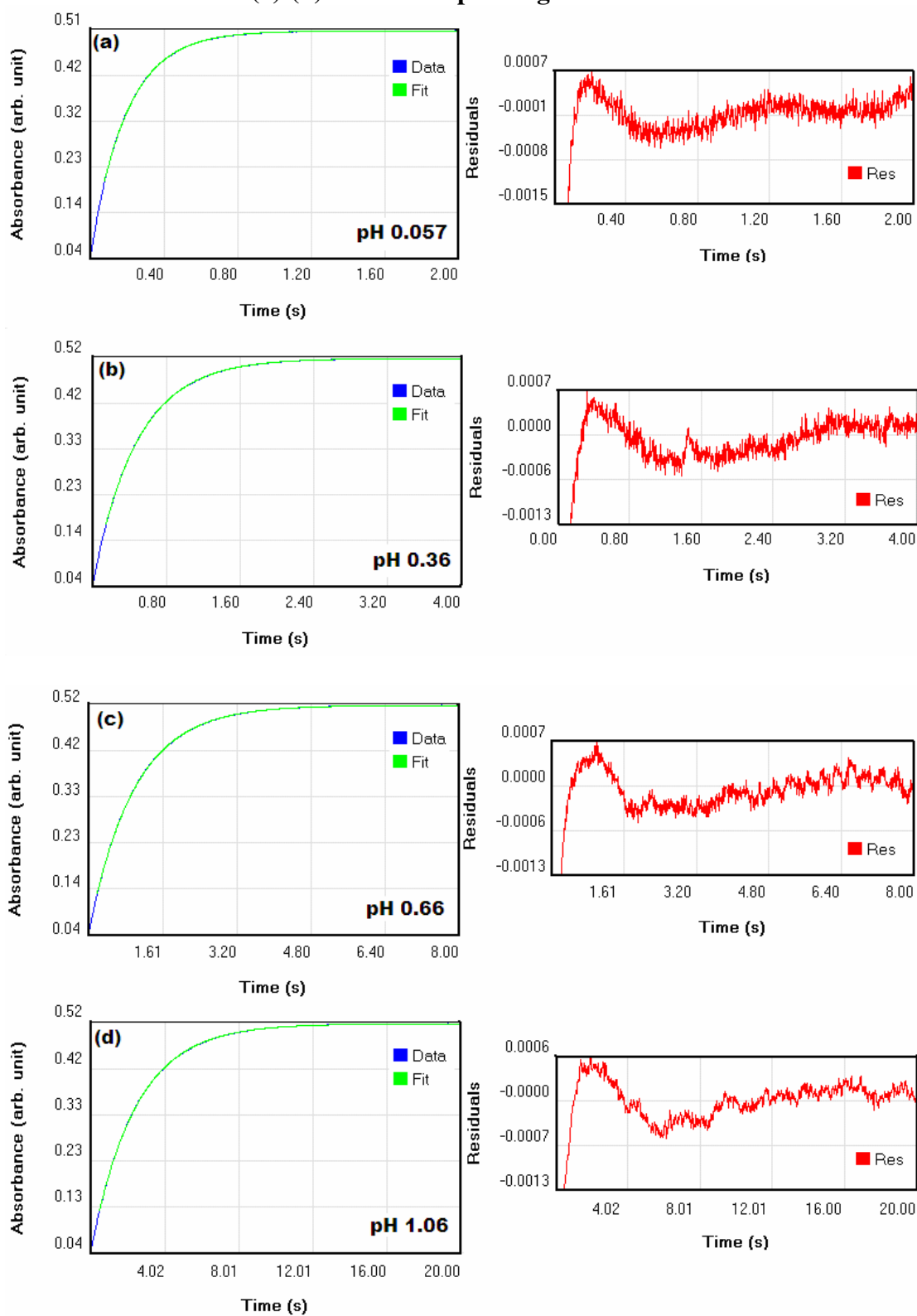


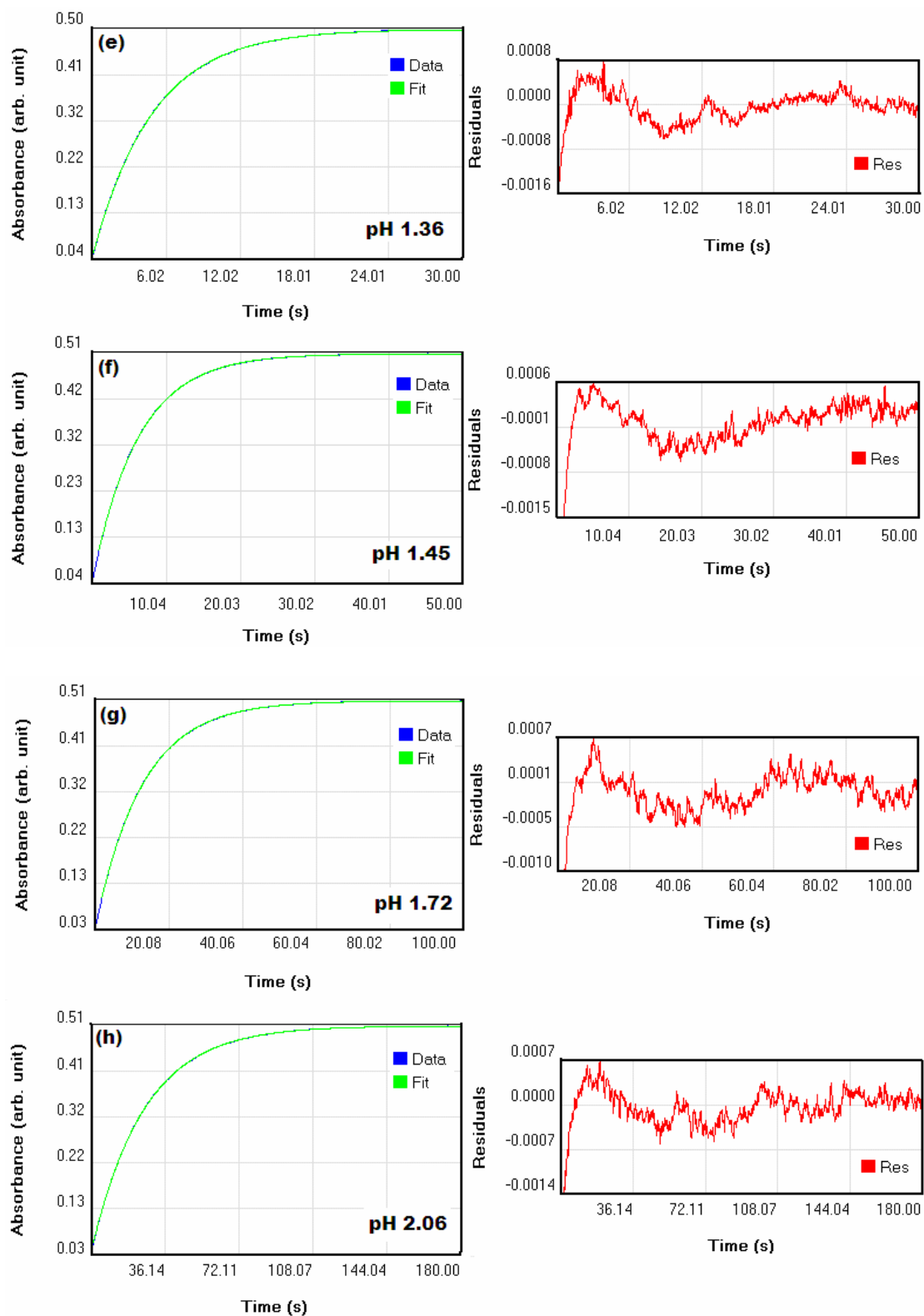
Table A13: First-order rate constants for the hydrolysis of *p*-bromobenzaldehyde *N*-(*tert*-butoxycarbonyl)imine (122) in phosphate buffer at 262 nm, 25 °C and $I = 1.0$ (KCl).^a

[Buffer] _T ^b (M)	[H ₂ PO ₄ ⁻] ^c (M)	pH	k_{obs} ^d (s ⁻¹)	R ²	k_{HA} ^e (M ⁻¹ s ⁻¹)	k_{hyd} ^f (s ⁻¹)
20% f_B						
0.10	0.080	5.86	9.64×10^{-5}	0.999		
0.20	0.16	5.86	1.85×10^{-4}	0.999	1.01×10^{-3}	1.94×10^{-5}
0.30	0.24	5.85	2.67×10^{-4}	0.999		
0.40	0.32	5.86	3.39×10^{-4}	0.999		

(a) Measurements were made at an initial substrate concentration of 5×10^{-5} M. (b) Total buffer concentration. (c) The concentration of buffer in the acid form. (d) The value of the first-order rate constant, k_{obs} (s⁻¹), was obtained as the slope the plot of $\ln(A_\infty - A_t)$ against time in Figure A37. (e) The value of the second-order rate constant, k_{HA} (M⁻¹s⁻¹), was obtained as the slope of the plot of k_{obs} (s⁻¹) against the concentration of dihydrogen phosphate in Figure A37. (f) The value of k_{hyd} (s⁻¹) was obtained as the y-axis intercept of the plot of k_{obs} against dihydrogen phosphate concentration in Figure A37.

Figure A38: Stopped-flow data for the hydrolysis of *p*-fluorobenzaldehyde *N*-(*tert*-butoxycarbonyl)imine (123) in HCl solution (pH 0.057-2.73) at 250 nm, 25 °C and I = 1.0 (KCl); plots of absorbance against time (a)-(k) with corresponding residuals for the fit.





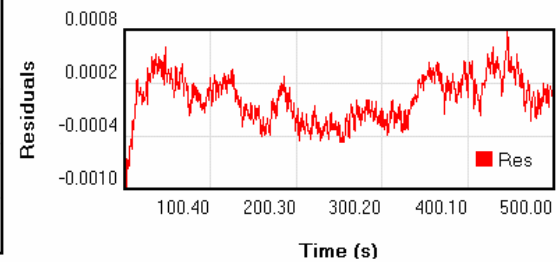
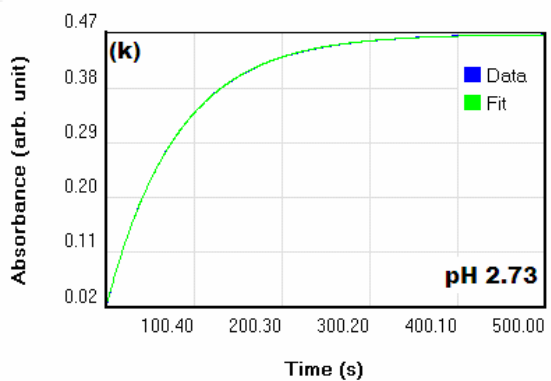
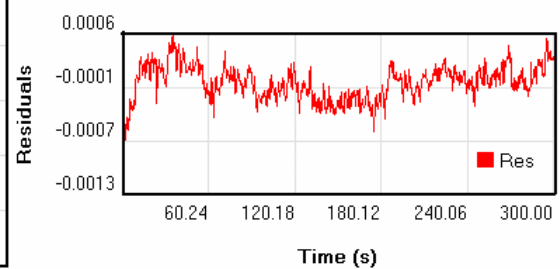
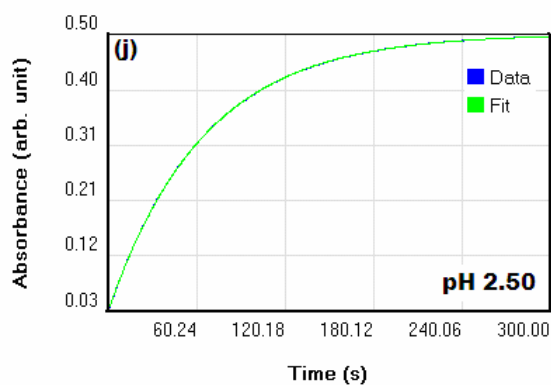
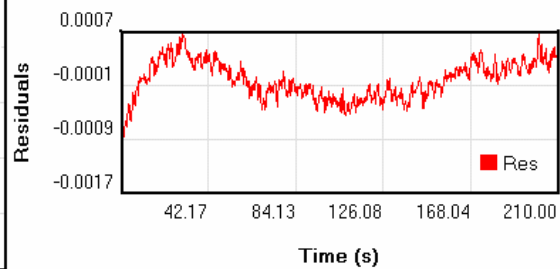
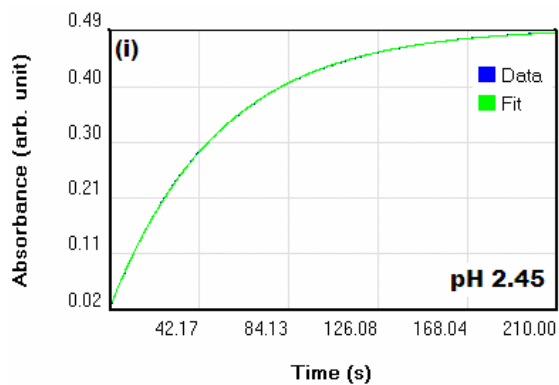


Table A14: Summary of first-order rate constants for the hydrolysis of *p*-fluorobenzaldehyde *N*-(*tert*-butoxycarbonyl)imine (123) in HCl solution at 250 nm, 25 °C and I = 1.0 (KCl) obtained using stopped-flow spectrophotometry.^a

pH ^b	$k_{\text{hyd}}^{\text{c}}$ (s ⁻¹)	n ^d	log k_{hyd}
0.057	5.09	5	7.07×10^{-1}
0.36	2.08	5	3.18×10^{-1}
0.66	1.03	8	1.28×10^{-2}
1.06	4.19×10^{-1}	8	-3.77×10^{-1}
1.36	2.03×10^{-1}	8	-6.93×10^{-1}
1.45	1.60×10^{-1}	8	-7.96×10^{-1}
1.72	7.78×10^{-2}	7	-1.11
2.06	3.89×10^{-2}	5	-1.41
2.45	1.54×10^{-2}	5	-1.81
2.50	1.35×10^{-2}	5	-1.87
2.73	8.00×10^{-3}	5	-2.10

(a) Measurements were made at an initial substrate concentration of 5×10^{-5} M. (b) HCl solutions were diluted by 50% and the pH of the resulting solution measured in order to account for the dilution upon mixing in the stopped-flow apparatus. (c) The value of the first-order rate constant, k_{hyd} (s⁻¹), was obtained from least-squares analysis of absorbance versus time data in Figure A38 (a)-(k). (d) The number of runs averaged to give the value of k_{hyd} .

Figure A39: Hydrolysis of *p*-fluorobenzaldehyde *N*-(*tert*-butoxycarbonyl)imine (123) in chloroacetic acid buffer (75% f_{B} , pH 3.19); (a) plot of $\ln(A_{\infty} - A_t)$ against time, (b) plot of k_{obs} against the concentration of chloroacetic acid, [CH₂ClCOOH].

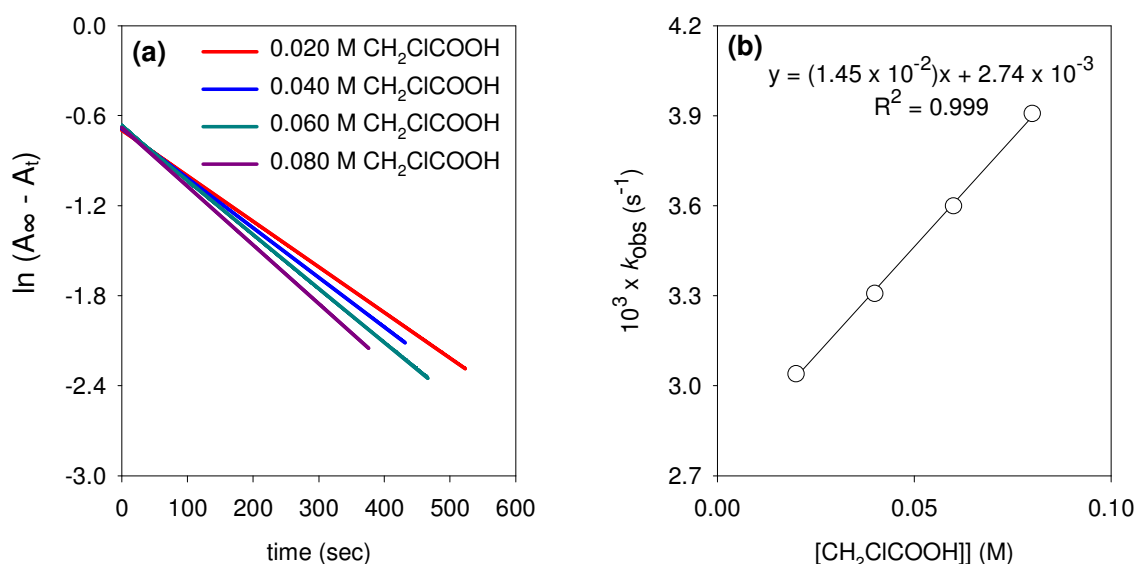


Figure A40: Hydrolysis of *p*-fluorobenzaldehyde *N*-(*tert*-butoxycarbonyl)imine (123) in acetic acid buffer (25% f_B , pH 4.10); (a) plot of $\ln(A_\infty - A_t)$ against time, (b) plot of k_{obs} against the concentration of acetic acid, $[CH_3COOH]$.

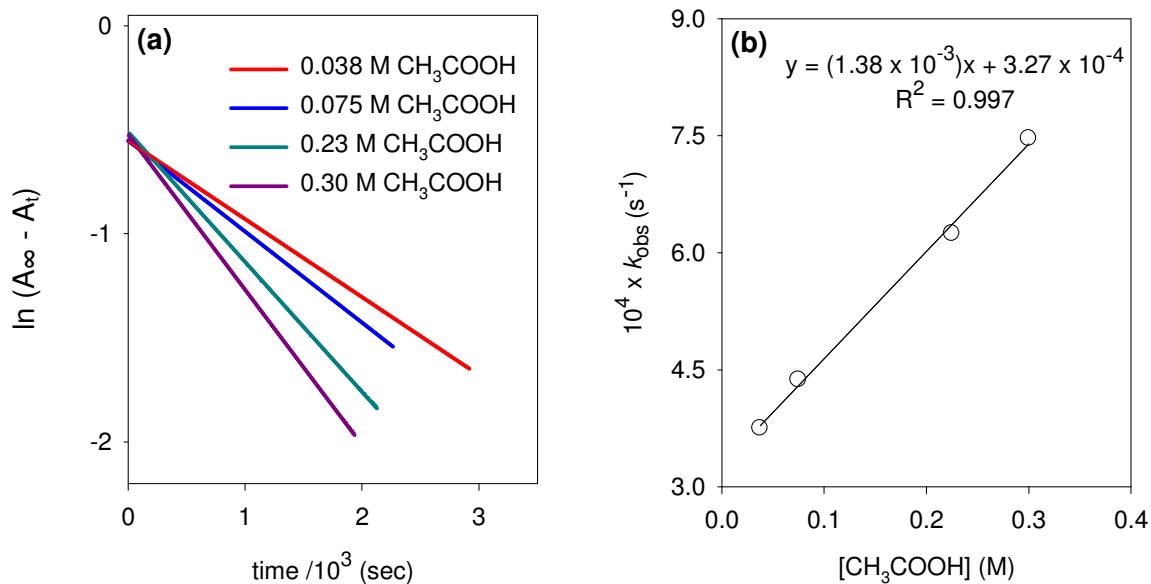


Figure A41: Hydrolysis of *p*-fluorobenzaldehyde *N*-(*tert*-butoxycarbonyl)imine (123) in acetic acid buffer (50% f_B , pH 4.63); (a) plot of $\ln(A_\infty - A_t)$ against time, (b) plot of k_{obs} against the concentration of acetic acid, $[CH_3COOH]$.

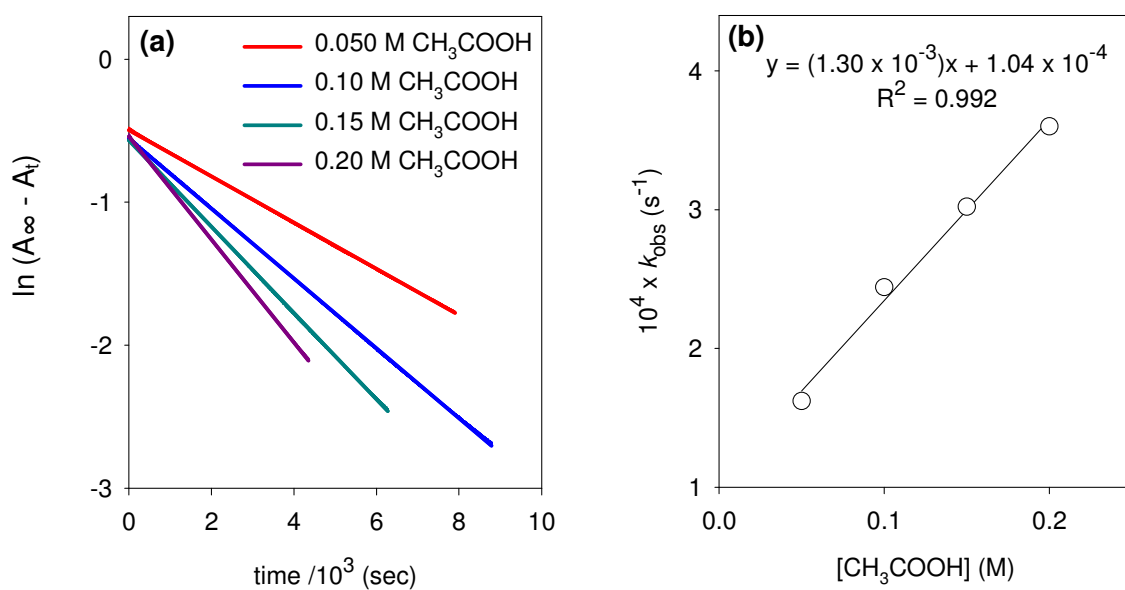


Figure A42: Hydrolysis of *p*-fluorobenzaldehyde *N*-(*tert*-butoxycarbonyl)imine (123) in acetic acid buffer (75% f_B , pH 5.08); (a) plot of $\ln(A_\infty - A_t)$ against time, (b) plot of k_{obs} against the concentration of acetic acid buffer, $[\text{CH}_3\text{COOH}]$.

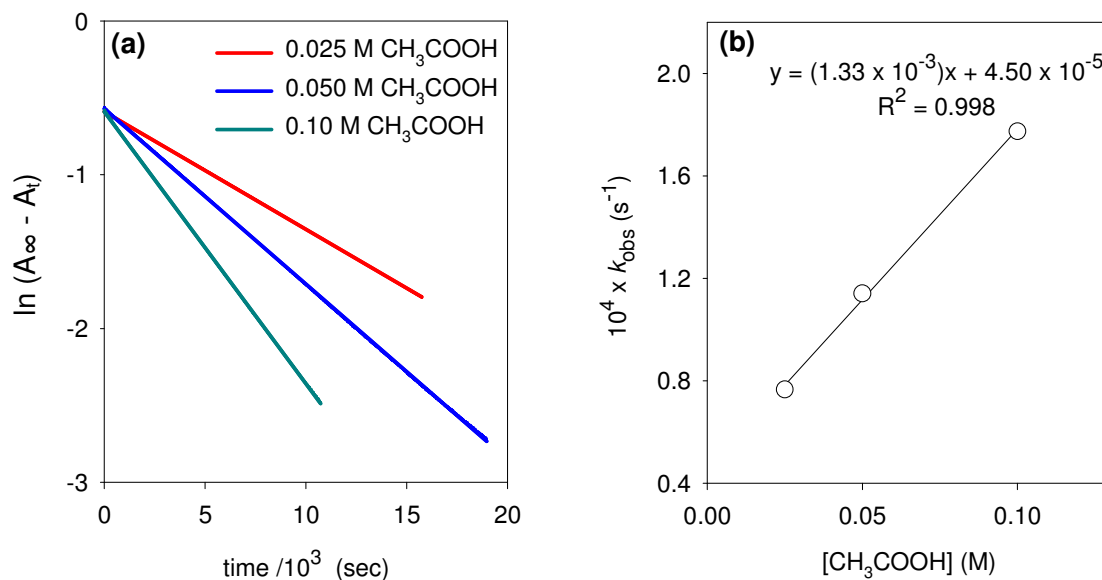


Figure A43: Hydrolysis of *p*-fluorobenzaldehyde *N*-(*tert*-butoxycarbonyl)imine (123) in acetic acid buffer (90% f_B , pH 5.58); (a) plot of $\ln(A_\infty - A_t)$ against time, (b) plot of k_{obs} against the concentration of acetic acid, $[\text{CH}_3\text{COOH}]$.

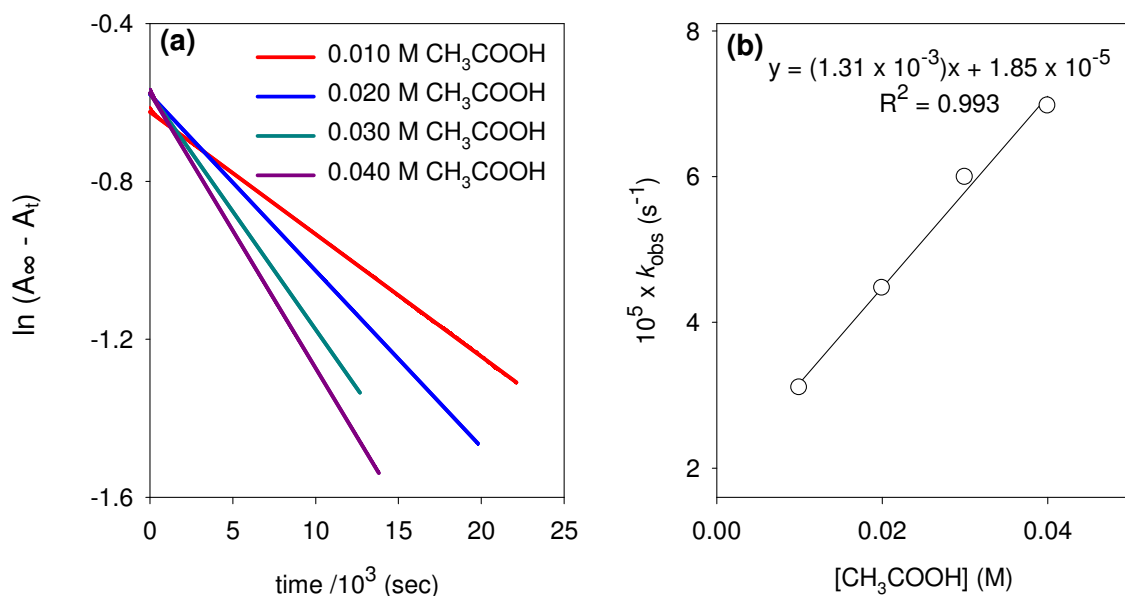


Table A15: First-order rate constants for the hydrolysis of *p*-fluorobenzaldehyde *N*-(*tert*-butoxycarbonyl)imine (123) in acetic acid and chloroacetic acid* buffers at 250 nm, 25 °C and I = 1.0 (KCl).^a

[Buffer] _T ^b (M)	[CH ₃ COOH] ^c (M)	pH	k_{obs} ^d (s ⁻¹)	R ²	k_{HA} ^e (M ⁻¹ s ⁻¹)	k_{hyd} ^f (s ⁻¹)
75% f_{B} [*] [CH ₂ ClCOOH]						
0.080	0.020	3.19	3.04×10^{-3}	0.999	1.45×10^{-2}	2.74×10^{-3}
0.16	0.040	3.20	3.31×10^{-3}	0.999		
0.24	0.060	3.19	3.60×10^{-3}	0.999		
0.32	0.080	3.19	3.91×10^{-3}	0.999		
25% f_{B}						
0.050	0.038	4.09	3.75×10^{-4}	0.999	1.38×10^{-3}	3.27×10^{-4}
0.10	0.075	4.10	4.37×10^{-4}	0.999		
0.30	0.23	4.10	6.25×10^{-4}	0.999		
0.40	0.30	4.11	7.47×10^{-4}	0.999		
50% f_{B}						
0.10	0.050	4.62	1.62×10^{-4}	0.999	1.30×10^{-3}	1.04×10^{-4}
0.20	0.10	4.62	2.44×10^{-4}	0.999		
0.30	0.15	4.63	3.02×10^{-4}	0.999		
0.40	0.20	4.64	3.60×10^{-4}	0.999		
75% f_{B}						
0.10	0.025	5.08	7.66×10^{-5}	0.999	1.33×10^{-3}	4.50×10^{-5}
0.20	0.050	5.08	1.14×10^{-4}	0.999		
0.40	0.10	5.09	1.77×10^{-4}	0.999		
90% f_{B}						
0.10	0.010	5.58	3.10×10^{-5}	0.999	1.31×10^{-3}	1.85×10^{-5}
0.20	0.020	5.58	4.47×10^{-5}	0.999		
0.30	0.030	5.60	5.99×10^{-5}	0.999		
0.40	0.040	5.58	6.97×10^{-5}	0.999		

(a) Measurements were made at an initial substrate concentration of 5×10^{-5} M. (b) Total buffer concentration. (c) The concentration of buffer in the acid form. (d) The value of the first-order rate constant, k_{obs} (s⁻¹), was obtained as the slope the plot of $\ln(A_{\infty} - A_t)$ against time in Figures A39-A43. (e) The value of the second-order rate constant, k_{HA} (M⁻¹s⁻¹), was obtained as the slope of the plot of k_{obs} (s⁻¹) against the concentration of general acid in Figures A39-A43. (f) The value of k_{hyd} (s⁻¹) was obtained as the y-axis intercept of the plot of k_{obs} against general acid concentration in Figures A39-A43.

Figure A44: Hydrolysis of *p*-fluorobenzaldehyde *N*-(*tert*-butoxycarbonyl)imine (123) in imidazole buffer (50% f_B , pH 7.24); (a) plot of $\ln(A_\infty - A_t)$ against time, (b) plot of k_{obs} against the concentration of imidazolium ion, $[\text{ImH}^+]$.

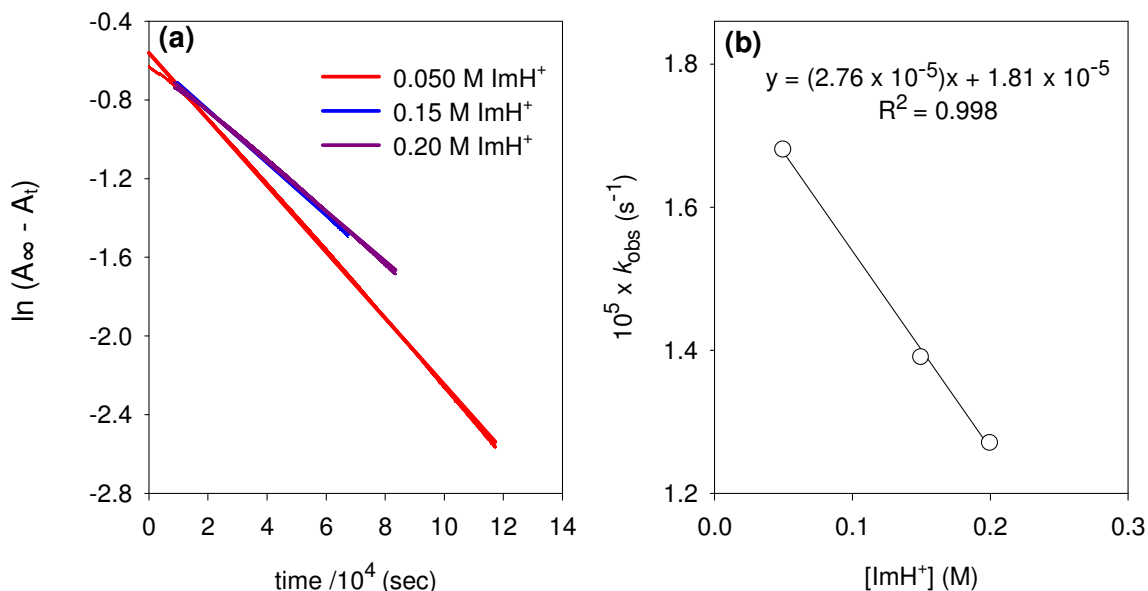
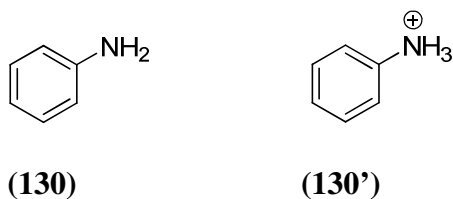


Table A16: First-order rate constants for the hydrolysis of *p*-fluorobenzaldehyde *N*-(*tert*-butoxycarbonyl)imine (123) in imidazole buffer at 250 nm, 25 °C and $I = 1.0$ (KCl).^a

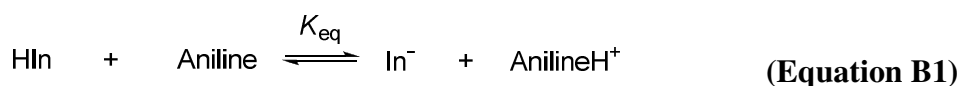
$[\text{Buffer}]_T^b$ (M)	$[\text{ImH}^+]^c$ (M)	pH	k_{obs}^d (s^{-1})	R^2	k'^e ($\text{M}^{-1}\text{s}^{-1}$)	k_{hyd}^f (s^{-1})
50% f_B						
0.10	0.050	7.24	1.68×10^{-5}	0.998		
0.30	0.15	7.24	1.39×10^{-5}	0.999	2.76×10^{-5}	1.81×10^{-5}
0.40	0.20	7.24	1.27×10^{-5}	0.999		

(a) Measurements were made at an initial substrate concentration of 5×10^{-5} M. (b) Total buffer concentration. (c) The concentration of buffer in the acid form. (d) The value of the first-order rate constant, k_{obs} (s^{-1}), was obtained as the slope the plot of $\ln(A_\infty - A_t)$ against time in Figure A44. (e) The observed effect of an increase in total buffer concentration is a decrease in k_{obs} . The dependency of k_{obs} on $[\text{ImH}^+]$ appears to be linear, yielding a negative slope, k' (Figure A44). (f) The value of k_{hyd} (s^{-1}) was obtained as the y-axis intercept of the plot of k_{obs} against imidazolium ion concentration in Figure A44.

Appendix B Determination of the pK_a value of anilinium ion (130') in DMSO.



The measurement was performed as in an analogous manner to that described in Section 2.1.3.2 for the determination of iminium ion pK_a values in DMSO. The equilibrium between aniline and a reference indicator may be described as in Equation B1, where HIn is 4-chloro-2,4-dinitrophenol (134) and In^- (134') is the deprotonated form of the indicator.



UV-Visible spectra of 4-chloro-2,6-dinitrophenol (134) (3×10^{-5} M) in DMSO solutions containing aniline (130) and anilinium ion (130') were recorded at 25 °C.

These are shown in Figure B1, with scans 1-8 corresponding to the conditions given in Table B1.

Figure B1: UV-Visible spectra of 4-chloro-2,6-dinitrophenol (134) in DMSO containing aniline (130) and anilinium ion (130') at 25 °C.

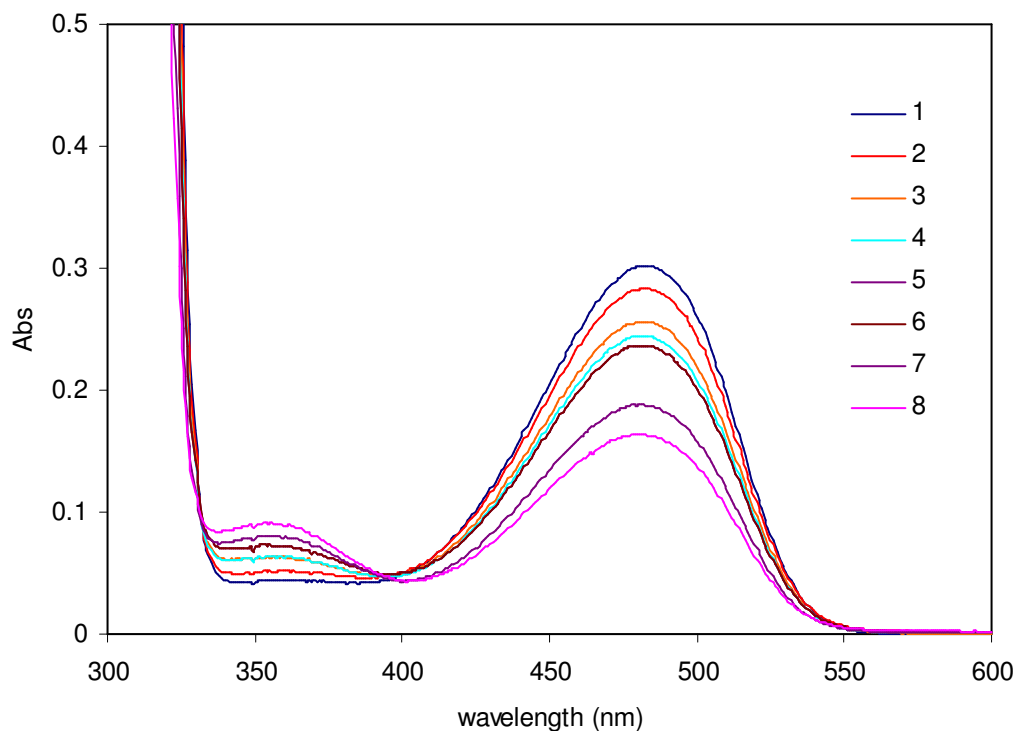


Table B1: Absorbance data for 4-chloro-2,6-dinitrophenol^a (**134**) in DMSO containing aniline (**130**) and anilinium ion^b (**130'**) at 480 nm and 25 °C.

Spectrum number	[AnilineH ⁺] (M)	[Aniline] (M)	Abs	[In ⁻]/[HIn] ^c	K_{eq} ^d
1.	1.50×10^{-3}	8.50×10^{-3}	0.302	5.53	0.98
2.	2.50×10^{-3}	7.50×10^{-3}	0.283	3.81	1.27
3.	4.00×10^{-3}	6.00×10^{-3}	0.256	2.49	1.66
4.	4.50×10^{-3}	5.50×10^{-3}	0.245	2.15	1.76
5.	5.00×10^{-3}	5.00×10^{-3}	0.236	1.91	1.91
6.	6.00×10^{-3}	4.00×10^{-3}	0.215	1.47	2.21
7.	7.00×10^{-3}	3.00×10^{-3}	0.185	1.04	2.42
8.	8.00×10^{-3}	2.00×10^{-3}	0.162	0.79	3.17

(a) The final concentration of 4-chloro-2,6-dinitrophenol (**134**) was 3×10^{-5} M. (b) Anilinium ion was generated by addition of HCl in ether solution in DMSO such that the final concentration of ether was < 2%. (c) The ratio of phenolate to phenol was obtained using the relationship $Abs - A_{min} / A_{max} - Abs$.

(d) Calculated as
$$\frac{[AnilineH^+]}{[Aniline]} \cdot \frac{(Abs - 0.009)}{(0.355 - Abs)}$$

An average value of K_{eq} was calculated, $K_{eq} = 1.92 \pm 0.69$

The pK_a value was calculated using Equation B2.

$$pK_a (AnilineH^+) = \log_{10} K_{eq} + pK_a (4\text{-chloro-2,6-dinitrophenol}) \quad \text{(Equation B2)}$$

In this case, $pK_a = 3.84 \pm 0.16$.

Appendix C Kinetics of the uncatalysed Mannich reaction

Table C1: First-order rate constants for the uncatalysed Mannich reaction of imine (119) (10 mM) with acetylacetone (100 mM) at 22 °C.

Solvent	Time (s)	$f(s)^a$	$\ln f(s)$	k_{obs}^b (s ⁻¹)
CDCl ₃	0	1.000	0.000	2.12×10^{-5}
	1117	0.903	-0.102	
	6574	0.824	-0.194	
	9184	0.757	-0.278	
	11438	0.736	-0.306	
	18255	0.663	-0.410	
	26712	0.480	-0.734	
	83851	0.160	-1.831	
	90540	0.139	-1.971	
CD ₂ Cl ₂	0	1.000	0.000	8.24×10^{-5}
	5402	0.700	-0.357	
	8434	0.502	-0.689	
	10805	0.427	-0.851	
	14586	0.312	-1.165	
	17317	0.253	-1.376	
	20895	0.180	-1.714	

(a) The fraction of substrate remaining, $f(s)$, was calculated according to Equation 2.19. (b) The value of the first-order rate constant (k_{obs} , s⁻¹) was obtained as the slope of the plot of $\ln f(s)$ against time in Figure 2.40.

Table C2: First-order rate constants for the uncatalysed Mannich reaction of imine (120) (10 mM) with acetylacetone (100 mM) at 22 °C.

Solvent	Time (s)	$f(s)^a$	$\ln f(s)$	k_{obs}^b (s ⁻¹)
CD ₂ Cl ₂	0	1.000	0.000	6.53×10^{-5}
	4159	0.784	-0.243	
	7363	0.662	-0.412	
	9269	0.574	-0.555	
	11747	0.472	-0.751	
	13290	0.446	-0.808	
	16036	0.346	-1.060	

(a) The fraction of substrate remaining, $f(s)$, was calculated according to Equation 2.19. (b) The value of the first-order rate constant, k_{obs} (s⁻¹), was obtained as the slope of the plot of $\ln f(s)$ against time in Figure 2.42.

Table C3: First-order rate constants for the uncatalysed Mannich reaction of imine (121) (10 mM) with acetylacetone (100 mM) at 22 °C.

Solvent	Time (s)	$f(s)^a$	$\ln f(s)$	k_{obs}^b (s^{-1})
CDCl ₃	0	1.000	0.000	3.43×10^{-5}
	3355	0.817	-0.202	
	8374	0.646	-0.437	
	10403	0.581	-0.543	
	13387	0.517	-0.659	
	18222	0.440	-0.822	
	25838	0.311	-1.169	
	73500	0.074	-2.597	
	79550	0.057	-2.867	

(a) The fraction of substrate remaining, $f(s)$, was calculated according to Equation 2.19. (b) The value of the first-order rate constant, k_{obs} (s^{-1}), was obtained as the slope of the plot of $\ln f(s)$ against time in Figure 2.44.

Table C4: First-order rate constants for the uncatalysed Mannich reaction of imine (122) (10 mM) with acetylacetone (100 mM) at 22 °C.

Solvent	Time (s)	$f(s)^a$	$\ln f(s)$	k_{obs}^b (s^{-1})
CD ₂ Cl ₂	0	1.000	0.000	1.56×10^{-4}
	1581	0.782	-0.246	
	3505	0.590	-0.528	
	4936	0.429	-0.847	
	6457	0.370	-0.994	
	7447	0.306	-1.185	
	10578	0.194	-1.639	

(a) The fraction of substrate remaining, $f(s)$, was calculated according to Equation 2.19. (b) The value of the first-order rate constant, k_{obs} (s^{-1}), was obtained as the slope of the plot of $\ln f(s)$ against time in Figure 2.46.

Table C5: First-order rate constants for the uncatalysed Mannich reaction of imine (123) (5 mM) with acetylacetone (50 mM) at 22 °C.

Solvent	Time (s)	$f(s)^a$	$\ln f(s)$	k_{obs}^b (s^{-1})
CD ₂ Cl ₂	0	1.000	0.000	1.47×10^{-4}
	1941	0.737	-0.305	
	3865	0.563	-0.575	
	5827	0.414	-0.882	
	7848	0.340	-1.078	
	9761	0.226	-1.485	
CDCl ₃	0	1.000	0.000	1.71×10^{-4}
	3400	0.542	-0.613	
	6795	0.285	-1.255	
	7885	0.239	-1.430	
	9640	0.204	-1.588	

(a) The fraction of substrate remaining, $f(s)$, was calculated according to Equation 2.19. (b) The value of the first-order rate constant, k_{obs} (s^{-1}), was obtained as the slope of the plot of $\ln f(s)$ against time in Figure 2.48.

Appendix D Determination of pK_a values of azolium ions

Figure D1a: Semi-logarithmic plot of the fraction of remaining C3-H against time for the deuterium exchange reaction of triazolium ion (180) in D_2O at 25 °C and $I = 1.0$ (KCl): ●, 0.01 M DCl, pD 2.01; ■, 0.008 M DCl, pD 2.10; ▲, 0.006 M DCl, pD 2.25; ◆, 0.004 M DCl, pD 2.37; ✕, 0.002 M DCl, pD 2.63.

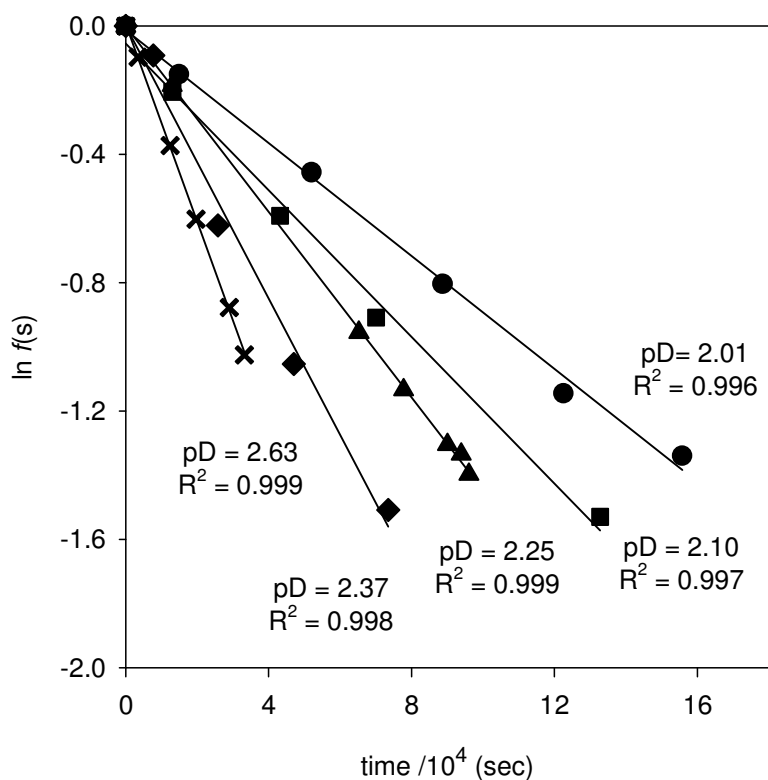


Figure D1b: Semi-logarithmic plot of the fraction of remaining C3-H against time for the deuterium exchange reaction of triazolium ion (180) in D_2O at 25 °C and $I = 1.0$ (KCl):●, acetic acid buffer 10% f_B , pD 4.46.

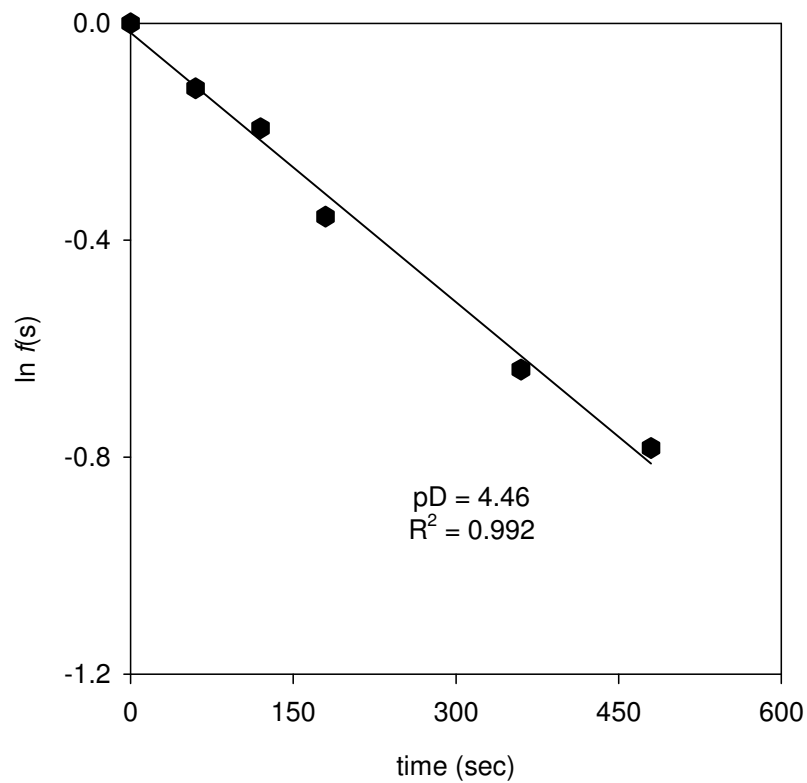


Table D1: First-order rate constants for exchange of the C3-H of triazolium ion (180) for deuterium in DCl and acetic acid buffer solutions in D_2O at 25 °C and $I = 1.0$ (KCl).

$[DO^-]^a$ (M)	Time (s)	$f(s)^b$	$\ln f(s)$	k_{obs}^c (s^{-1})
1.90×10^{-13} (pD 2.01)	0	1.000	0.000	8.80×10^{-6}
	14940	0.860	-0.151	
	52020	0.633	-0.457	
	88680	0.448	-0.804	
	122520	0.318	-1.145	
	155760	0.262	-1.340	
2.37×10^{-13} (pD 2.10)	0	1.000	0.000	1.08×10^{-5}
	13020	0.893	-0.113	
	43200	0.605	-0.503	
	70080	0.472	-0.750	
	100560	0.326	-1.122	
	132780	0.246	-1.404	
3.30×10^{-13} (pD 2.25)	0	1.000	0.000	1.45×10^{-5}
	13020	0.831	-0.185	
	65280	0.385	-0.955	
	77760	0.322	-1.134	
	90060	0.271	-1.304	
	93900	0.263	-1.334	
4.37×10^{-13} (pD 2.37)	0	1.000	0.000	2.00×10^{-5}
	7740	0.882	-0.126	
	25860	0.610	-0.494	
	47040	0.376	-0.977	
	73440	0.238	-1.435	
7.92×10^{-13} (pD 2.63)	0	1.000	0.000	3.08×10^{-5}
	3480	0.907	-0.097	
	12480	0.689	-0.373	
	19680	0.547	-0.602	
	28980	0.416	-0.878	
	33240	0.359	-1.025	
5.35×10^{-11} (pD 4.46)	0	1.000	0.000	1.66×10^{-3}
	60	0.887	-0.120	
	120	0.824	-0.194	
	180	0.700	-0.357	
	360	0.528	-0.639	
	480	0.457	-0.783	

(a) Measurements were made in deuterium chloride and acetic acid buffer solutions in the pD 2.01-4.46 range. $[DO^-]$ was calculated using Equation 3.7 (b) The fraction of un-exchanged substrate remaining $f(s)$, was calculated according to Equation 3.5. Measurements were made at an initial substrate concentration of 10 mM. (c) The value of the first-order rate constant, k_{obs} (s^{-1}), was obtained as the slope of the plot of $\ln f(s)$ against time in Figures D1a-D1b.

Figure D2: Semi-logarithmic plot of the fraction of remaining C3-H against time for the deuterium exchange reaction of triazolium ion (181) in D_2O at 25 °C and $I = 1.0$ (KCl): ●, 0.012 M DCl, pD 1.96; ■, 0.010 M DCl, pD 2.04; ▲, 0.008 M DCl, pD 2.13; ◆, 0.006 M DCl, pD 2.33; ✕, 0.004 M DCl, pD 2.57; ●, 0.003 M DCl, pD 2.77

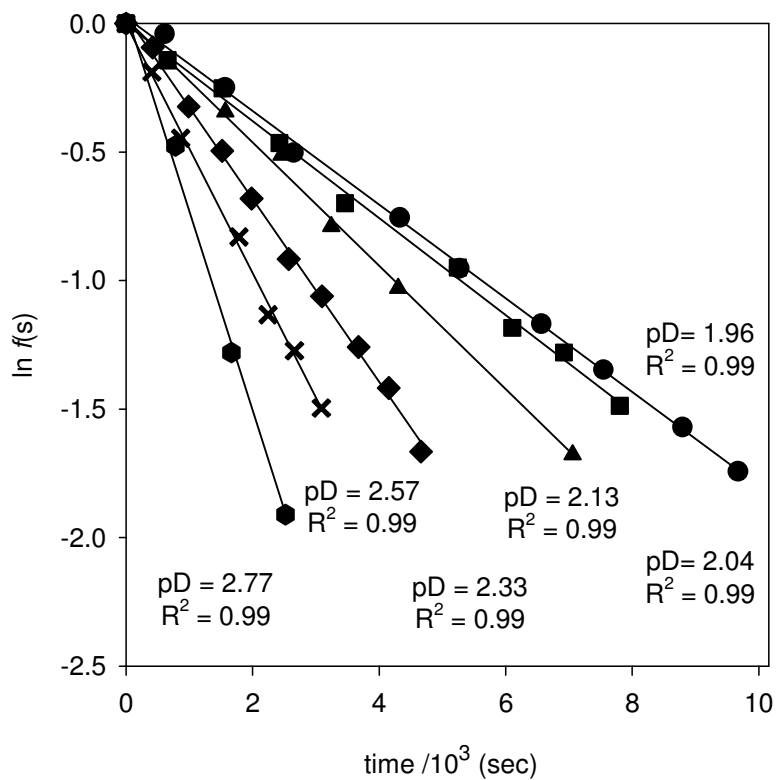


Table D2: First-order rate constants for exchange of the C3-H of triazolium (181) for deuterium in DCl solution in D₂O at 25 °C and I = 1.0 (KCl).

$[\text{DO}^-]^a$ (M)	Time (s)	$f(s)^b$	$\ln f(s)$	k_{obs}^c (s ⁻¹)
1.69×10^{-13} (pD 1.96)	0	1.000	0.000	1.82×10^{-4}
	612	0.961	-0.040	
	1565	0.780	-0.248	
	2650	0.605	-0.503	
	4325	0.470	-0.755	
	5265	0.386	-0.952	
	6563	0.311	-1.168	
	7545	0.260	-1.347	
	8791	0.208	-1.570	
	9669	0.175	-1.743	
2.03×10^{-13} (pD 2.04)	0	1.000	0.000	1.89×10^{-4}
	658	0.868	-0.142	
	1525	0.777	-0.252	
	2426	0.628	-0.465	
	3461	0.497	-0.699	
	5244	0.387	-0.949	
	6104	0.306	-1.184	
	6920	0.278	-1.280	
	7801	0.226	-1.487	
2.50×10^{-13} (pD 2.13)	0	1.000	0.000	2.40×10^{-4}
	671	0.855	-0.157	
	1570	0.709	-0.344	
	2459	0.599	-0.512	
	3246	0.454	-0.790	
	4301	0.357	-1.030	
	7057	0.187	-1.677	
	8250	0.169	-1.778	
	3.97×10^{-13} (pD 2.33)	0	1.000	
424		0.911	-0.093	
992		0.724	-0.323	
1521		0.609	-0.496	
1986		0.506	-0.681	
2573		0.400	-0.916	
3097		0.346	-1.061	
3677		0.284	-1.259	
4152		0.242	-1.419	
4663		0.189	-1.666	
6.89×10^{-13} (pD 2.57)	0	1.000	0.000	4.84×10^{-4}
	409	0.828	-0.189	
	865	0.640	-0.446	
	1786	0.436	-0.830	
	2247	0.322	-1.133	
	2664	0.280	-1.273	

	3088	0.224	-1.496	
	0	1.000	0.000	
1.07×10^{-12}	780	0.621	-0.476	7.75×10^{-4}
(pD 2.77)	1668	0.278	-1.280	
	2520	0.148	-1.911	

(a) Measurements were made in deuterium chloride solution in the pD 1.96– 2.77 range. $[DO]$ was calculated using Equation 3.7. (b) The fraction of un-exchanged substrate remaining $f(s)$, was calculated according to Equation 3.5. Measurements were made at an initial substrate concentration of 10 mM. (c) The value of the first-order rate constant, k_{obs} (s^{-1}), was obtained as the slope of the plot of $\ln f(s)$ against time in Figure D2.

Figure D3: Semi-logarithmic plot of the fraction of remaining C3-H against time for the deuterium exchange reaction of triazolium ion (182) in D_2O at 25 °C and $I = 1.0$ (KCl): ●, 0.006 M DCl, pD 2.34; ■, 0.005 M DCl, pD 2.44 ; ▲, 0.004 M DCl, pD 2.57; ◆, 0.003 M DCl, pD 2.76; ✕, 0.002 M DCl, pD 2.83.

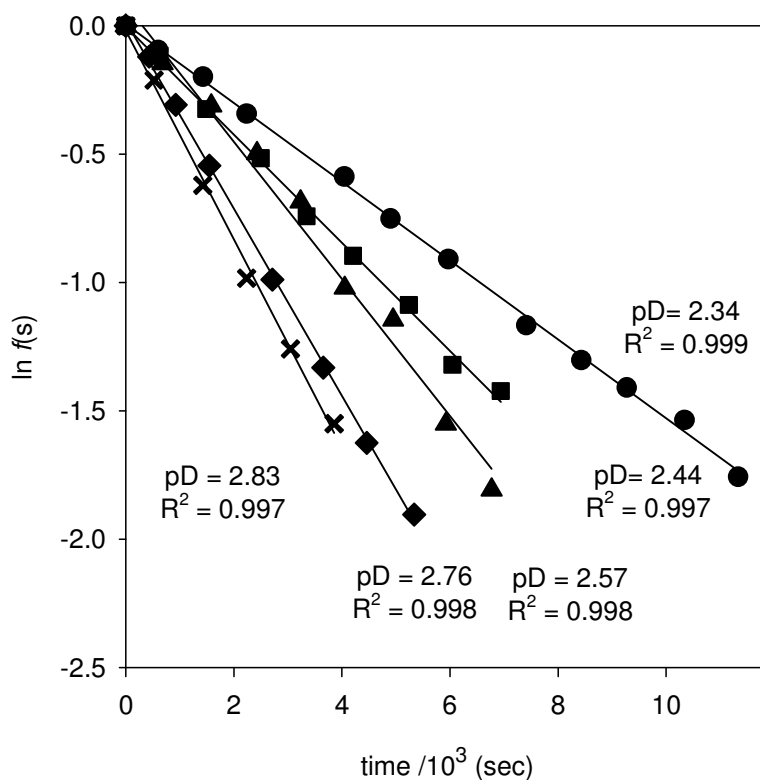


Table D3: First-order rate constants for exchange of the C3-H of triazolium ion (182) in deuterium chloride solution in D_2O at 25 °C and $I=1.0$ (KCl).

$[DO^+]^a$ (M)	Time (s)	$f(s)^b$	$\ln f(s)$	k_{obs}^c (s^{-1})
4.06×10^{-13} (pD 2.34)	0	1.000	0.000	1.54×10^{-4}
	604	0.910	-0.094	
	1431	0.820	-0.199	
	2239	0.710	-0.343	
	4047	0.556	-0.587	
	4902	0.472	-0.751	
	5970	0.403	-0.909	
	7414	0.311	-1.167	
	8432	0.272	-1.303	
	9269	0.244	-1.409	
	10341	0.215	-1.536	
11334	0.173	-1.757		
5.11×10^{-13} (pD 2.44)	0	1.000	0.000	2.01×10^{-4}
	629	0.890	-0.117	
	1493	0.723	-0.324	
	2500	0.597	-0.516	
	3347	0.476	-0.742	
	4206	0.408	-0.896	
	5241	0.337	-1.088	
	6044	0.267	-1.321	
	6942	0.241	-1.423	
6.89×10^{-13} (pD 2.57)	0	1.000	0.000	2.39×10^{-4}
	682	0.863	-0.147	
	1586	0.732	-0.312	
	2426	0.608	-0.498	
	3235	0.504	-0.685	
	4052	0.360	-1.022	
	4948	0.318	-1.146	
	0	1.000	0.000	
437	0.886	-0.121		
927	0.735	-0.308		
1546	0.580	-0.545		
2716	0.372	-0.989		
3656	0.264	-1.332		
4460	0.197	-1.625		
5336	0.149	-1.904		
1.07×10^{-12} (pD 2.76)	0	1.000	0.000	4.07×10^{-4}
	524	0.809	-0.212	
	1428	0.537	-0.621	
	2239	0.374	-0.983	
	3050	0.284	-1.259	
	3856	0.212	-1.550	

(a) Measurements were made deuterium chloride solution in the pD 2.34 – 2.83 range. $[DO^-]$ was calculated using Equation 3.7. (b) The fraction of un-exchanged substrate remaining $f(s)$, was calculated according to Equation 3.5. Measurements were made at an initial substrate concentration of 10 mM. (c) The value of the first-order rate constant, (k_{obs}), was obtained as the slope of the plot of $\ln f(s)$ against time in Figure D3.

Figure D4: Semi-logarithmic plot of the fraction of remaining C2-H against time for the deuterium exchange reaction of imidazolium ion (185) in phosphate buffers at 25 °C and $I = 1.0$ (KCl): ●, 20% f_B , pD 6.38; ▼, 30% f_B , pD 6.63; ■, 50% f_B , pD 7.06; ✕, 70% f_B , pD 7.43; ◆, 90% f_B , pD 8.12.

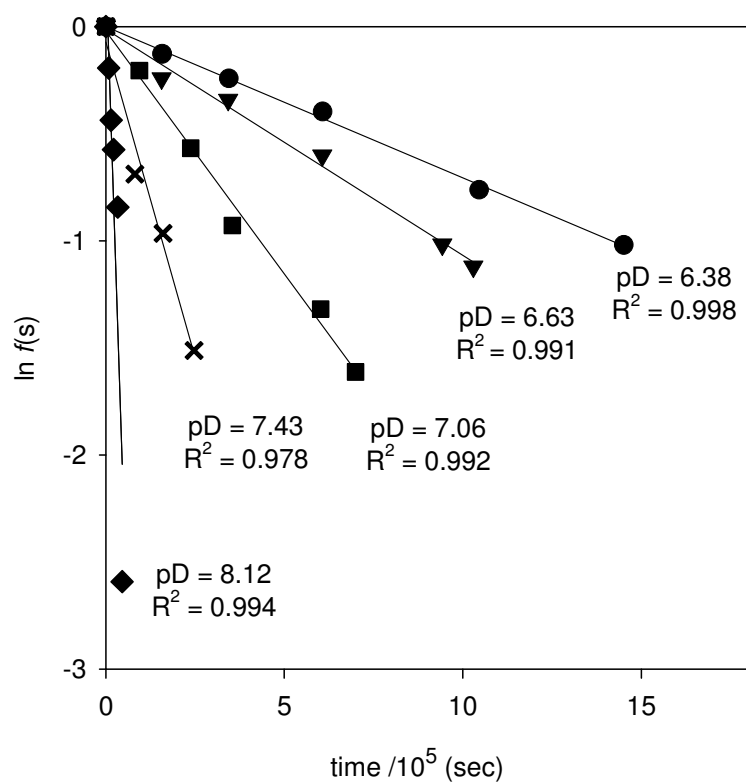


Table D4: First-order rate constants for exchange of the C2-H of imidazolium ion (185) for deuterium in phosphate buffers in D_2O at 25 °C and $I = 1.0$ (KCl).

$[DO^-]^a$ (M)	Time (s)	$f(s)^b$	$\ln f(s)$	k_{obs}^c (s^{-1})
4.30×10^{-9} (pD 6.38)	0	1.000	0.000	7.05×10^{-7}
	157793	0.880	-0.128	
	344777	0.785	-0.242	
	607397	0.672	-0.398	
	1046237	0.467	-0.762	
	1451237	0.361	-1.020	
7.75×10^{-9} (pD 6.63)	0	1.000	0.000	1.05×10^{-6}
	156286	0.785	-0.242	
	342454	0.710	-0.342	
	606274	0.548	-0.602	
	942154	0.361	-1.018	
	1029214	0.326	-1.120	
2.06×10^{-8} (pD 7.06)	0	1.000	0.000	2.26×10^{-6}
	94007	0.814	-0.206	
	237862	0.567	-0.568	
	354382	0.395	-0.929	
	601882	0.267	-1.320	
	699742	0.199	-1.612	
4.83×10^{-8} (pD 7.43)	0	1.000	0.000	5.87×10^{-6}
	81707	0.502	-0.689	
	160117	0.381	-0.966	
	247064	0.220	-1.512	
2.37×10^{-7} (pD 8.12)	0	1.000	0.000	2.55×10^{-5}
	7680	0.824	-0.194	
	14880	0.646	-0.437	
	22020	0.563	-0.575	
	33180	0.430	-0.844	
	45660	0.075	-2.592	

(a) Measurements were made in 250 mM phosphate buffer (total concentration of acidic $D_2PO_4^-$ and basic DPO_4^{2-} components). $[DO^-]$ was calculated using Equation 3.7. (b) The fraction of un-exchanged substrate remaining $f(s)$, was calculated according to Equation 3.15. Measurements were made at an initial substrate concentration of 10 mM. (c) The value of the first-order rate constant, k_{obs} (s^{-1}), was obtained as the slope of the plot of $\ln f(s)$ against time in Figure D4.

Figure D5: Semi-logarithmic plot of the fraction of remaining C2-H against time for the deuterium exchange reaction of imidazolium ion (186) in phosphate buffers in D_2O at 25 °C and $I = 1.0$ (KCl): ●, 20% f_B , pD 6.38; ▼, 30% f_B , pD 6.63; ■, 50% f_B , pD 7.06; ✕, 70% f_B , pD 7.43; ◆, 90% f_B , pD 8.12.

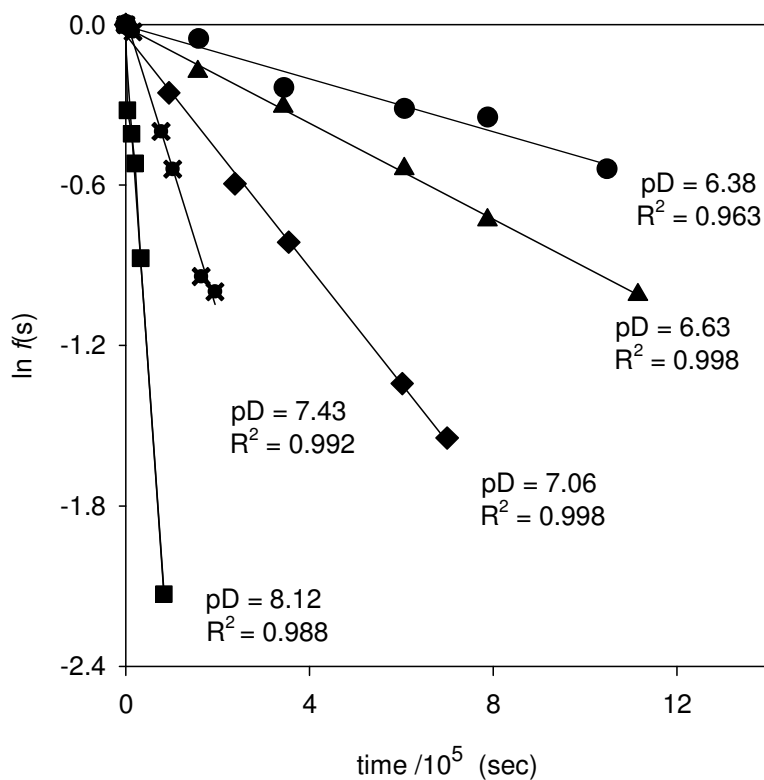


Table D5: First-order rate constants for exchange of the C2-H of imidazolium ion (186) for deuterium in phosphate buffers in D_2O at 25 °C and $I = 1.0$ (KCl).

$[DO^-]^a$ (M)	Time (s)	$f(s)^b$	$\ln f(s)$	k_{obs}^c (s^{-1})
4.30×10^{-9} (pD 6.38)	0	1.000	0.000	4.94×10^{-7}
	158643	0.949	-0.053	
	344639	0.790	-0.236	
	607019	0.730	-0.315	
	788159	0.707	-0.347	
	1048079	0.583	-0.540	
7.75×10^{-9} (pD 6.63)	0	1.000	0.000	8.97×10^{-7}
	157083	0.838	-0.176	
	342979	0.737	-0.306	
	606469	0.583	-0.538	
	787039	0.482	-0.730	
	1115239	0.364	-1.010	
2.06×10^{-8} (pD 7.06)	0	1.000	0.000	2.17×10^{-6}
	94077	0.775	-0.255	
	237867	0.551	-0.595	
	354477	0.443	-0.814	
	601947	0.261	-1.342	
	699927	0.213	-1.546	
4.83×10^{-8} (pD 7.43)	0	1.000	0.000	5.51×10^{-6}
	15600	0.973	-0.027	
	76980	0.670	-0.400	
	102300	0.582	-0.541	
	164160	0.390	-0.942	
	194160	0.368	-0.999	
2.37×10^{-7} (pD 8.12)	0	1.000	0.000	2.44×10^{-5}
	3640	0.726	-0.320	
	12720	0.665	-0.408	
	20160	0.595	-0.519	
	32520	0.418	-0.873	
	82920	0.119	-2.130	

(a) Measurements were made in 250 mM phosphate buffer (total concentration of acidic $D_2PO_4^-$ and basic DPO_4^{2-} components). $[DO^-]$ was calculated using Equation 3.7. (b) The fraction of unexchanged substrate remaining $f(s)$, was calculated according to Equation 3.15. Measurements were made at an initial substrate concentration of 10 mM. (c) The value of the first-order rate constant, k_{obs} (s^{-1}), was obtained as the slope of the plot of $\ln f(s)$ against time in Figure D5.

Figure D6a: Semi-logarithmic plot of the fraction of remaining C2-H against time for the exchange reaction of imidazolium ion (187) in phosphate buffers in D_2O at 25 °C and $I = 1.0$ (KCl): ●, 20% f_B , pD 6.38; ■, 30% f_B , pD 6.63; ◆, 70% f_B , pD 7.43; ▲, 90% f_B , pD 8.12.

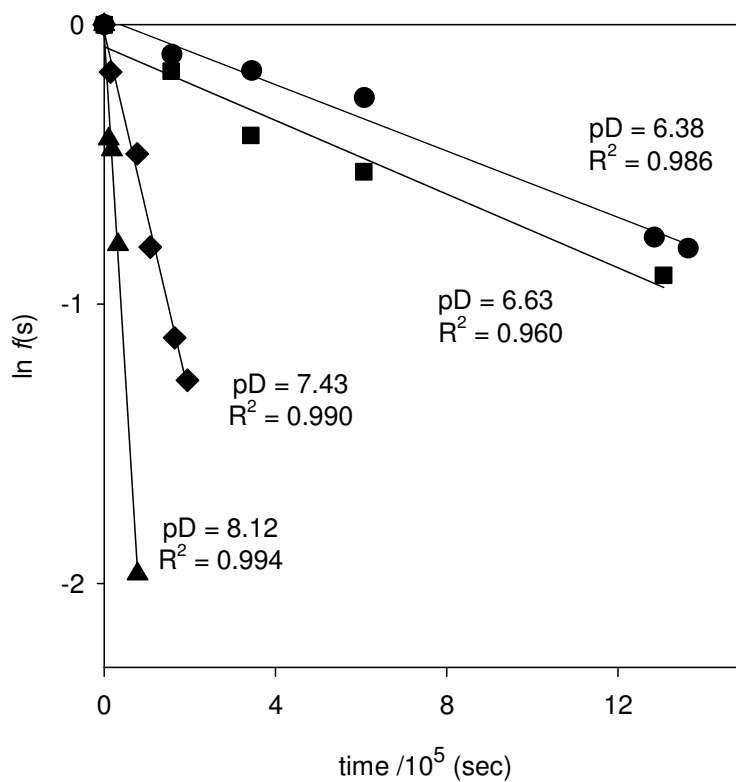


Figure D6b: Semi-logarithmic plot of the fraction of remaining C2-H against time for the deuterium exchange reaction of imidazolium ion (187) in phosphate buffer (50% f_B) at pD 6.85 in D_2O at 25 °C and $I = 1.0$ (KCl).

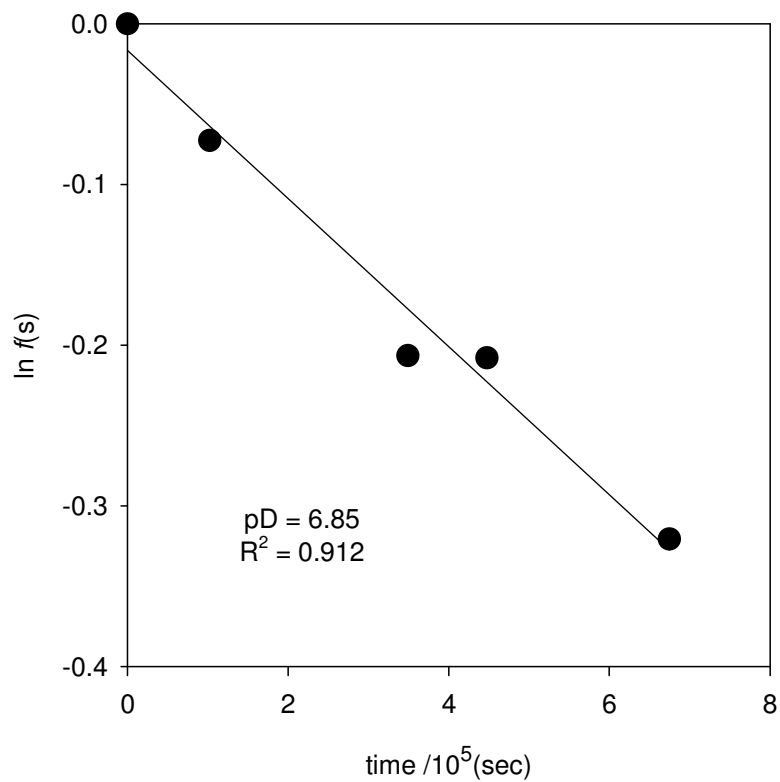
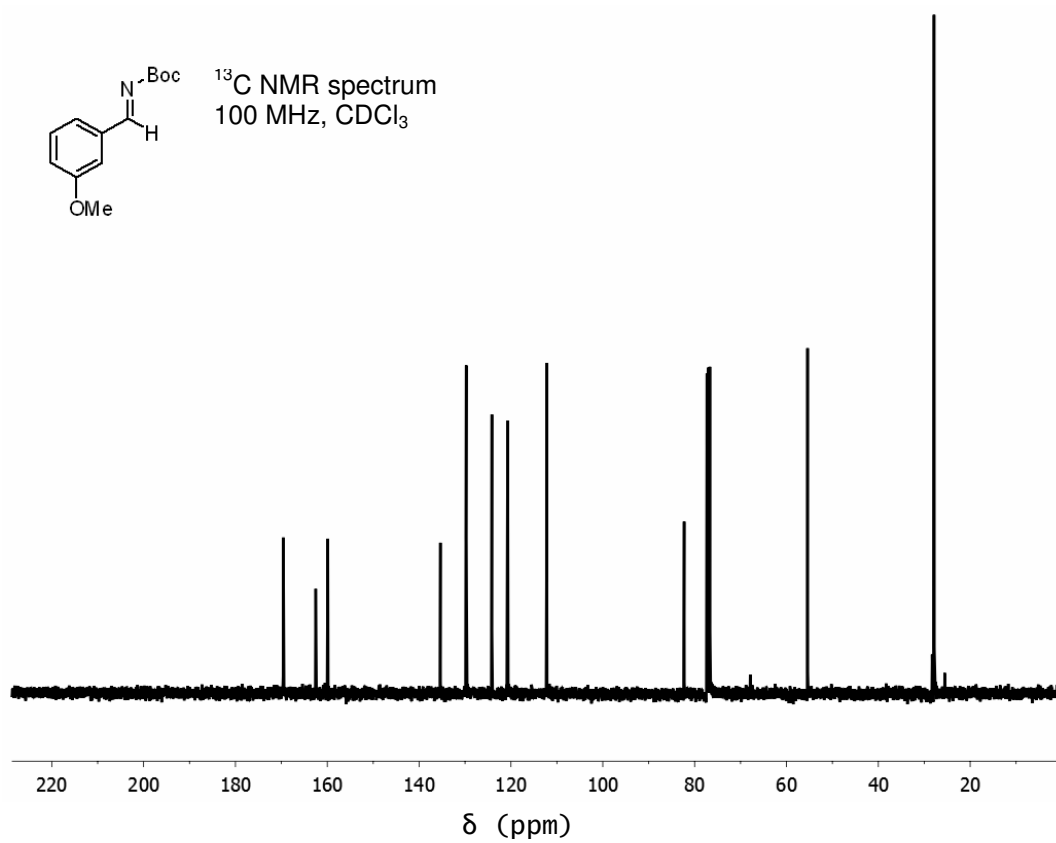
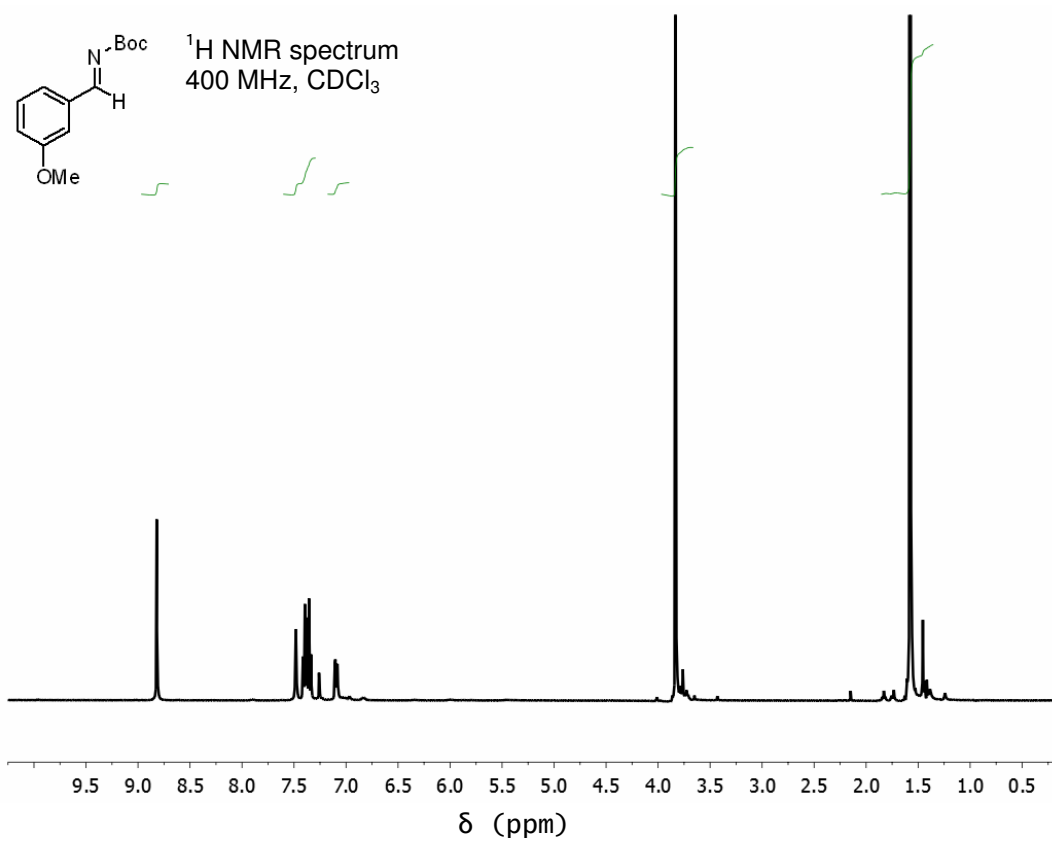


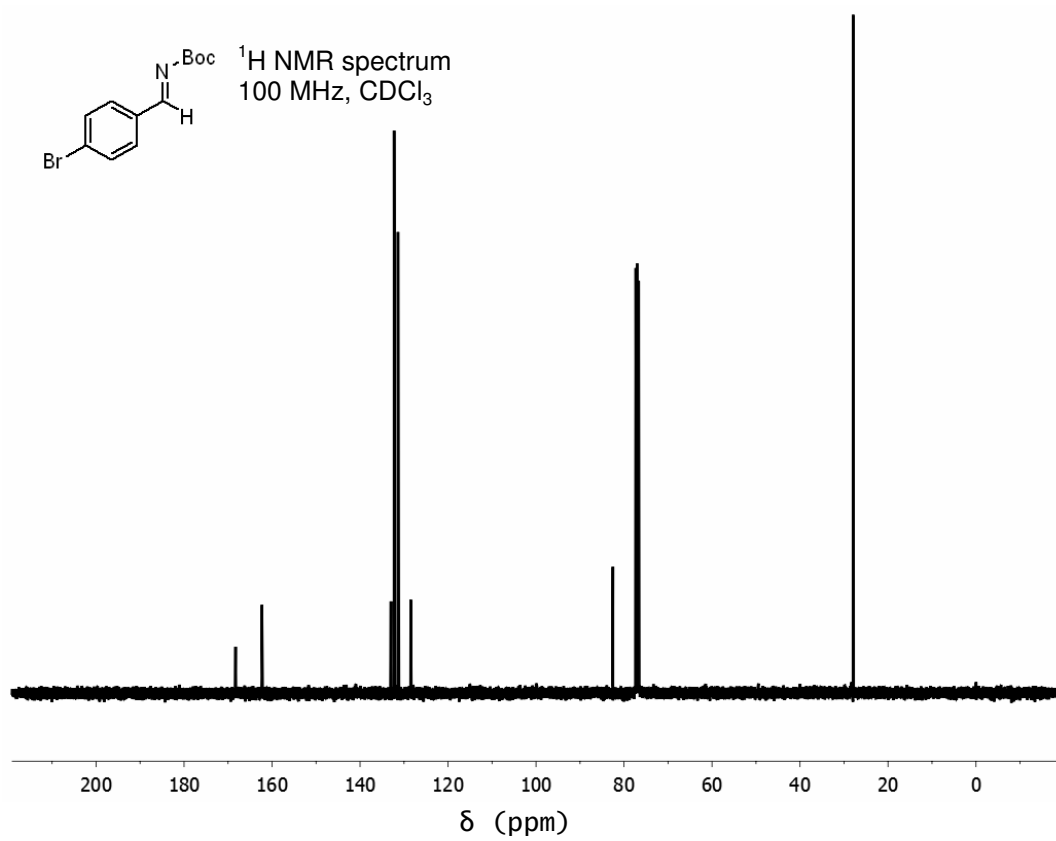
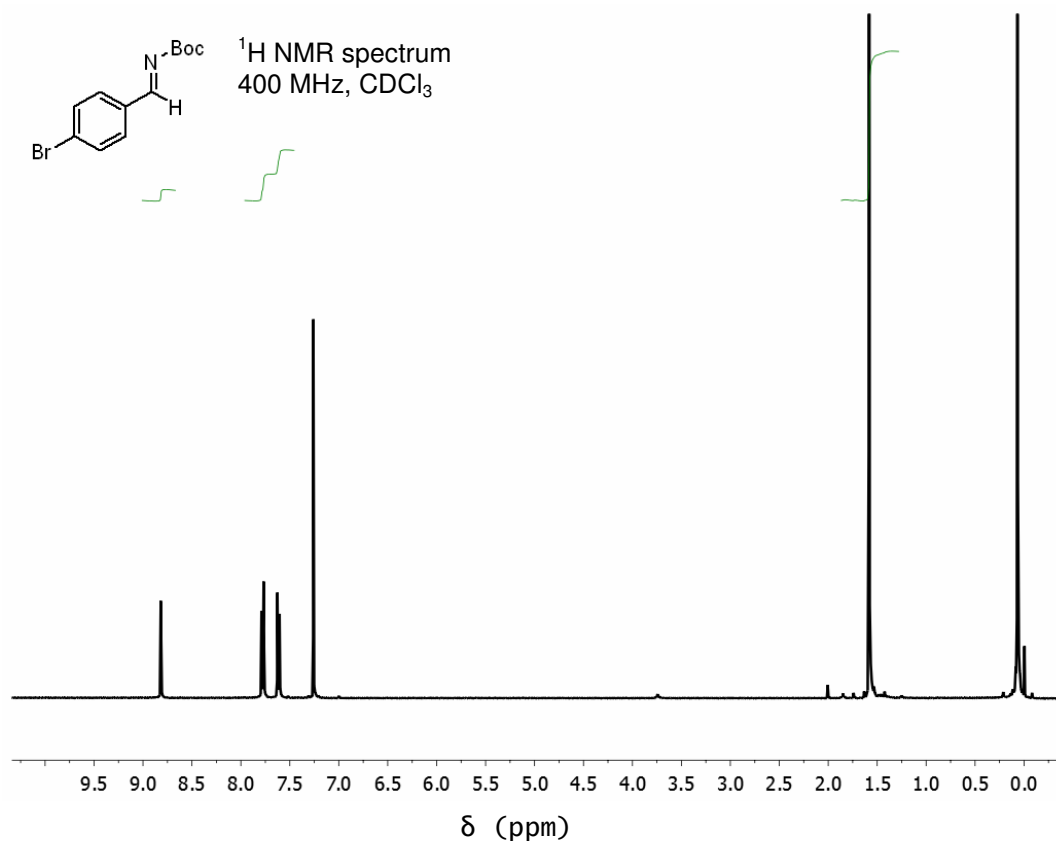
Table D6: First-order rate constants for exchange of the C2-H of imidazolium ion (187) for deuterium in phosphate buffers in D₂O at 25 °C and I = 1.0 (KCl).

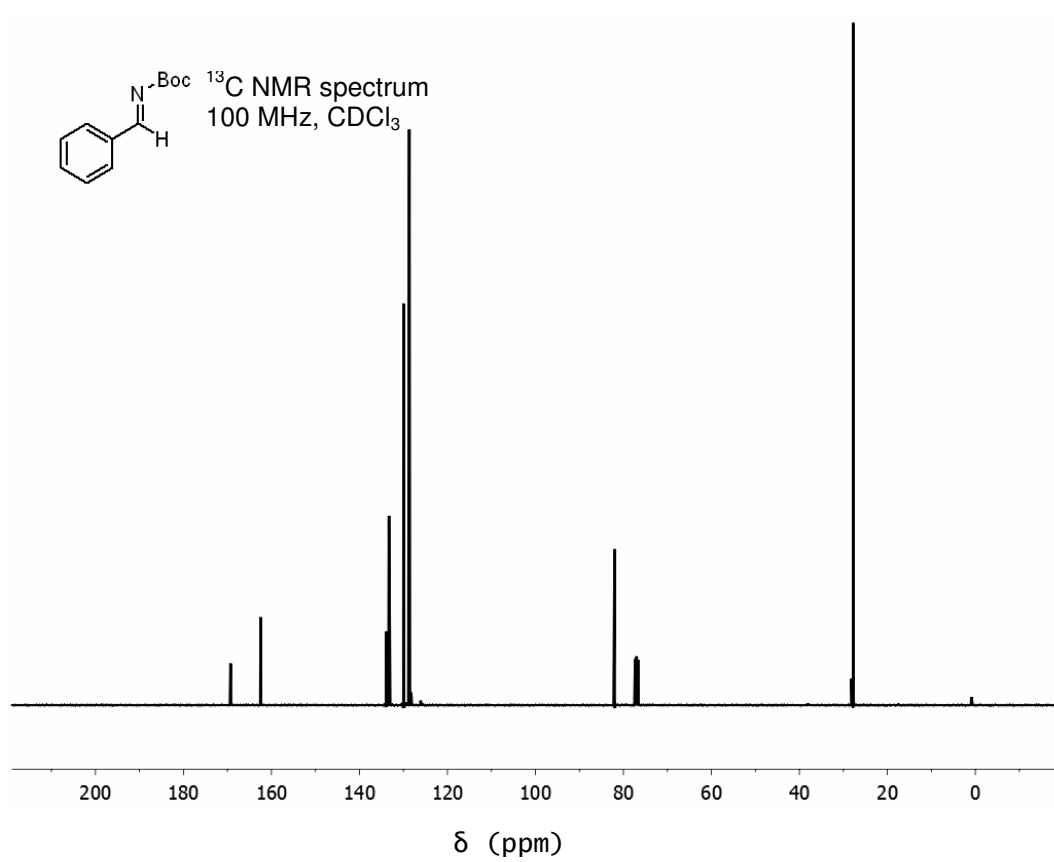
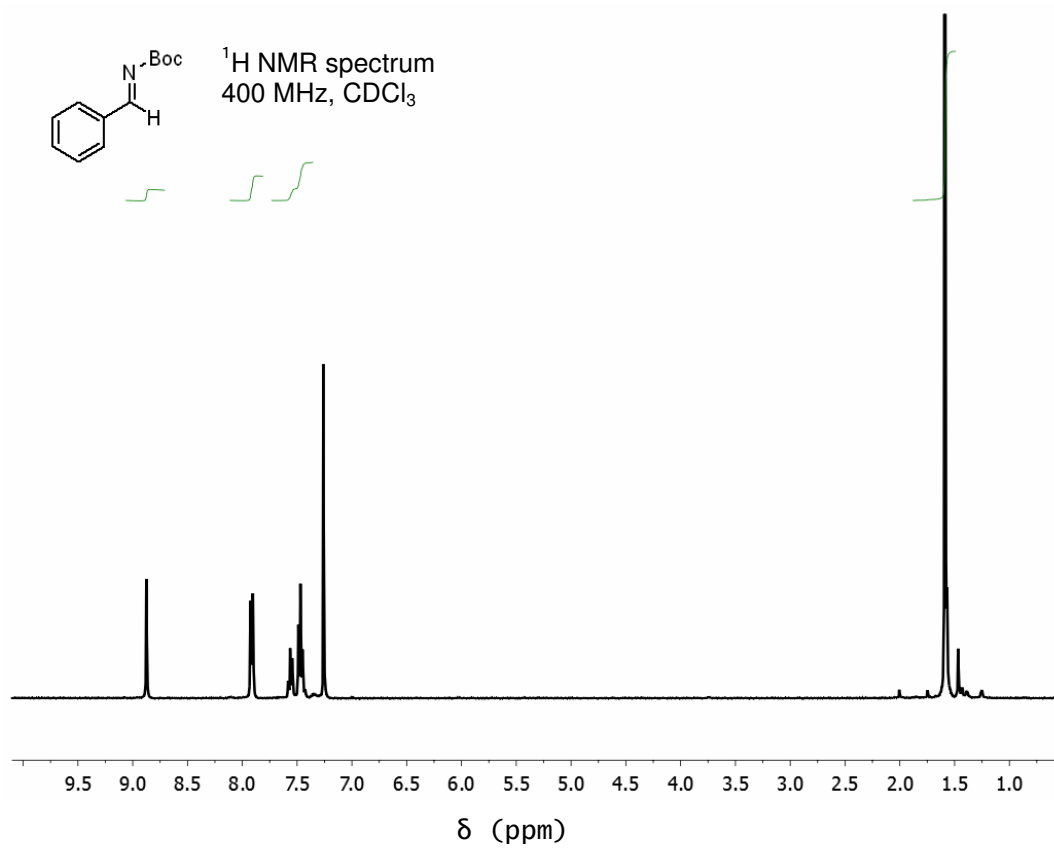
[DO ⁻] ^a (M)	Time (s)	$f(s)$ ^b	$\ln f(s)$	k_{obs} ^c (s ⁻¹)
4.30×10^{-9} (pD 6.38)	0	1.000	0.000	5.93×10^{-7}
	158357	0.899	-0.106	
	344562	0.848	-0.165	
	607122	0.770	-0.261	
	1284342	0.467	-0.761	
	1363362	0.449	-0.801	
7.75×10^{-9} (pD 6.63)	0	1.000	0.000	6.59×10^{-7}
	156886	0.847	-0.166	
	342591	0.673	-0.396	
	606111	0.591	-0.526	
	1306311	0.408	-0.897	
1.27×10^{-8} (pD 6.85)	0	1.000	0.000	6.17×10^{-6}
	102360	0.837	-0.178	
	349200	0.732	-0.312	
	447660	0.731	-0.313	
	594300	0.623	-0.473	
	674940	0.653	-0.426	
4.83×10^{-8} (pD 7.43)	0	1.000	0.000	6.53×10^{-5}
	15660	0.844	-0.170	
	77520	0.630	-0.462	
	107820	0.451	-0.796	
	164700	0.326	-1.121	
2.37×10^{-7} (pD 8.12)	0	1.000	0.000	2.45×10^{-2}
	11100	0.664	-0.409	
	18300	0.639	-0.448	
	32400	0.455	-0.788	
	78300	0.140	-1.966	

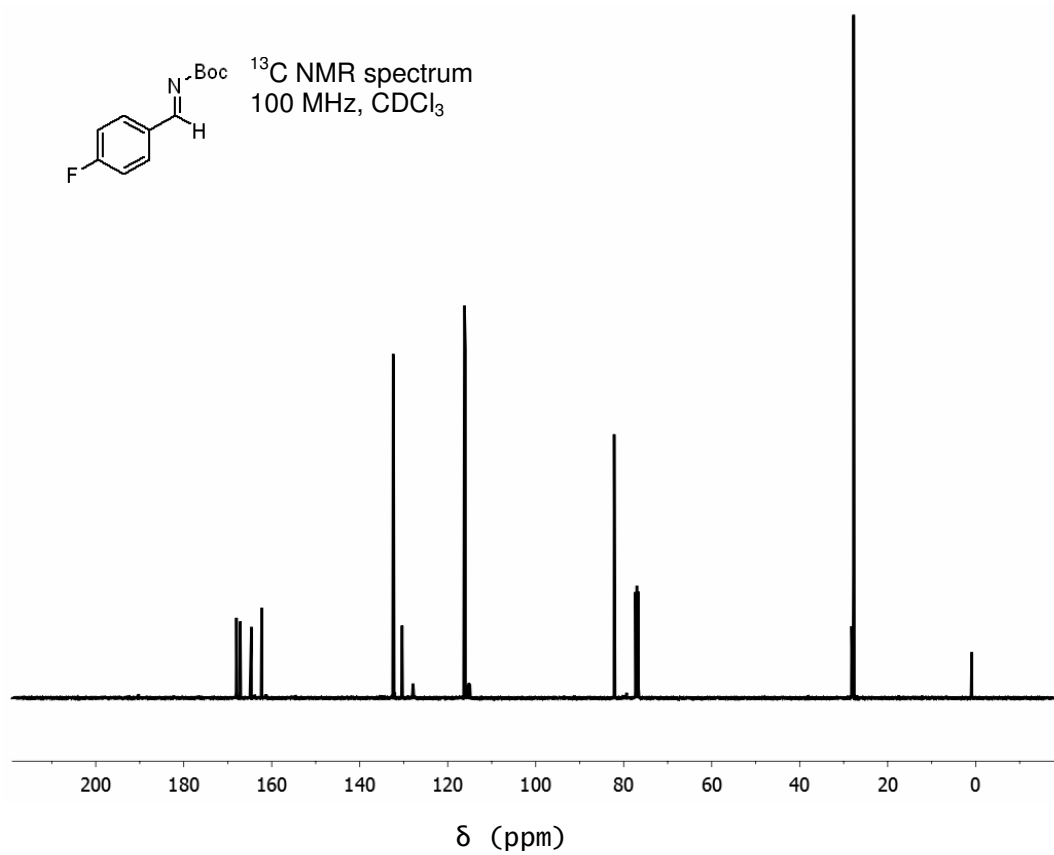
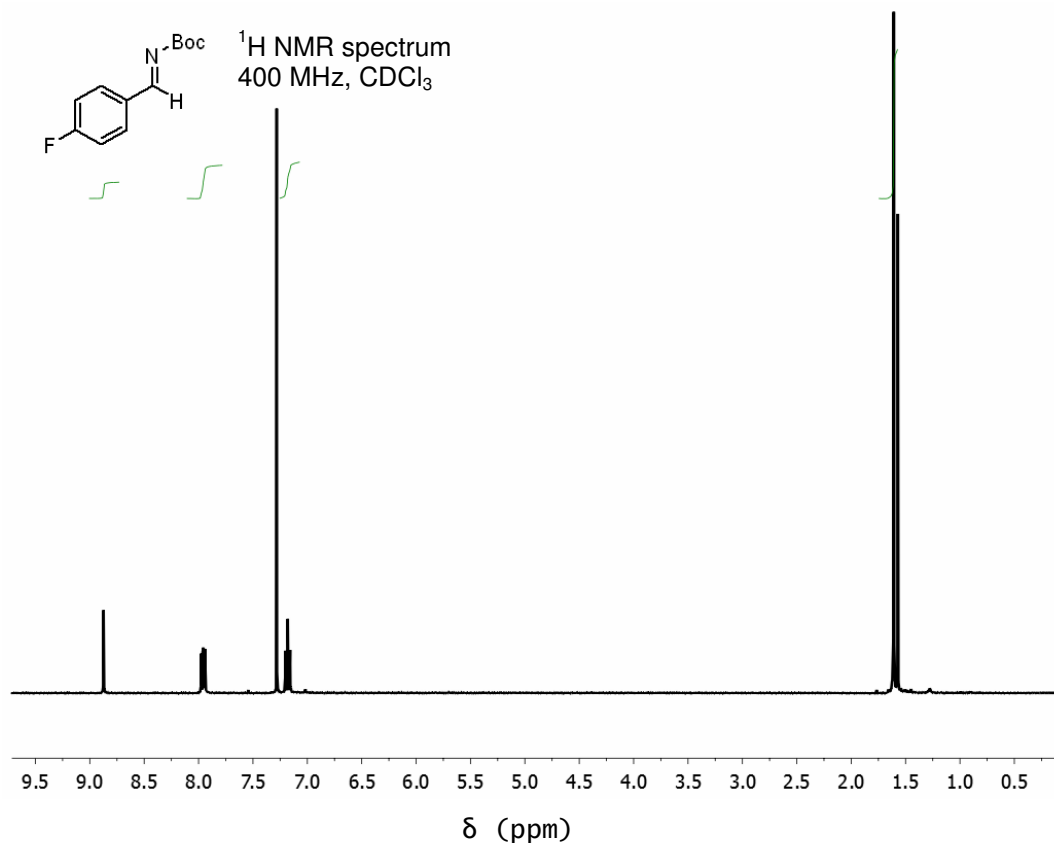
(a) Measurements were made in 250 mM phosphate buffer (total concentration of acidic D₂PO₄⁻ and basic DPO₄²⁻ components). [DO⁻] was calculated using Equation 3.7. (b) The fraction of un-exchanged substrate remaining $f(s)$, was calculated according to Equation 3.15. Measurements were made at an initial substrate concentration of 10 mM. (c) The value of the first-order rate constant, k_{obs} (s⁻¹), was obtained as the slope of the plot of $\ln f(s)$ against time in Figures D6a and D6b.

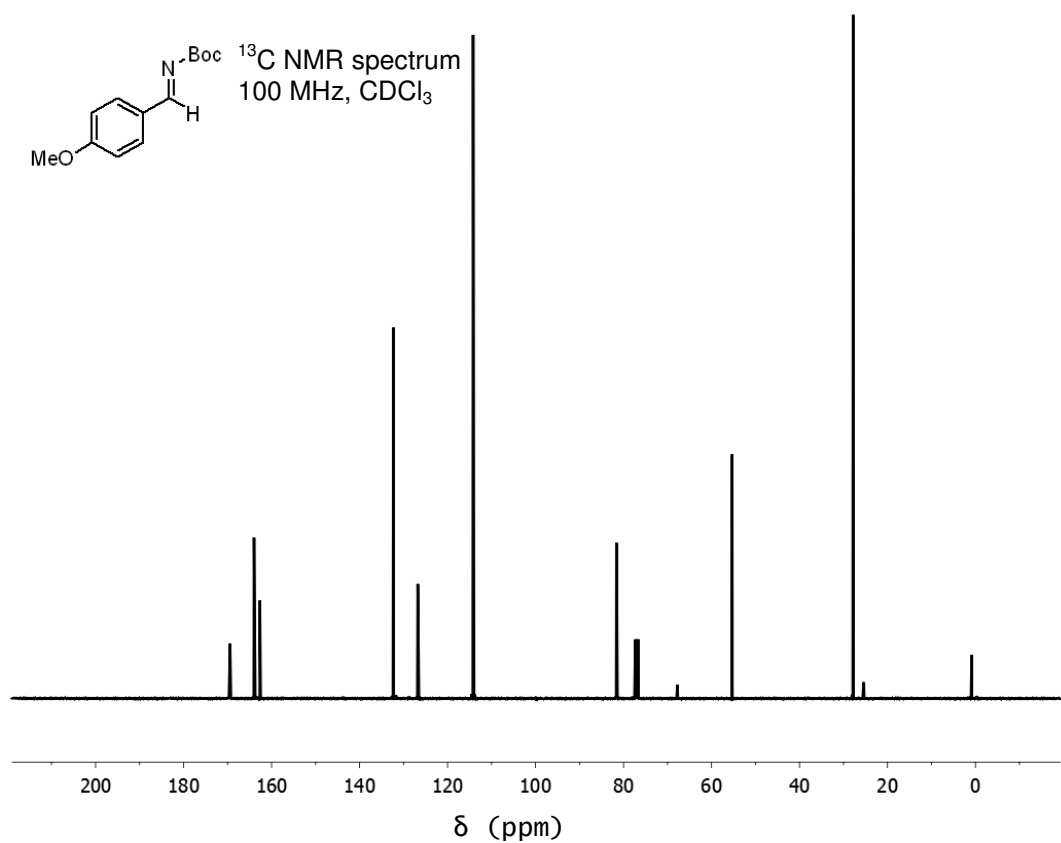
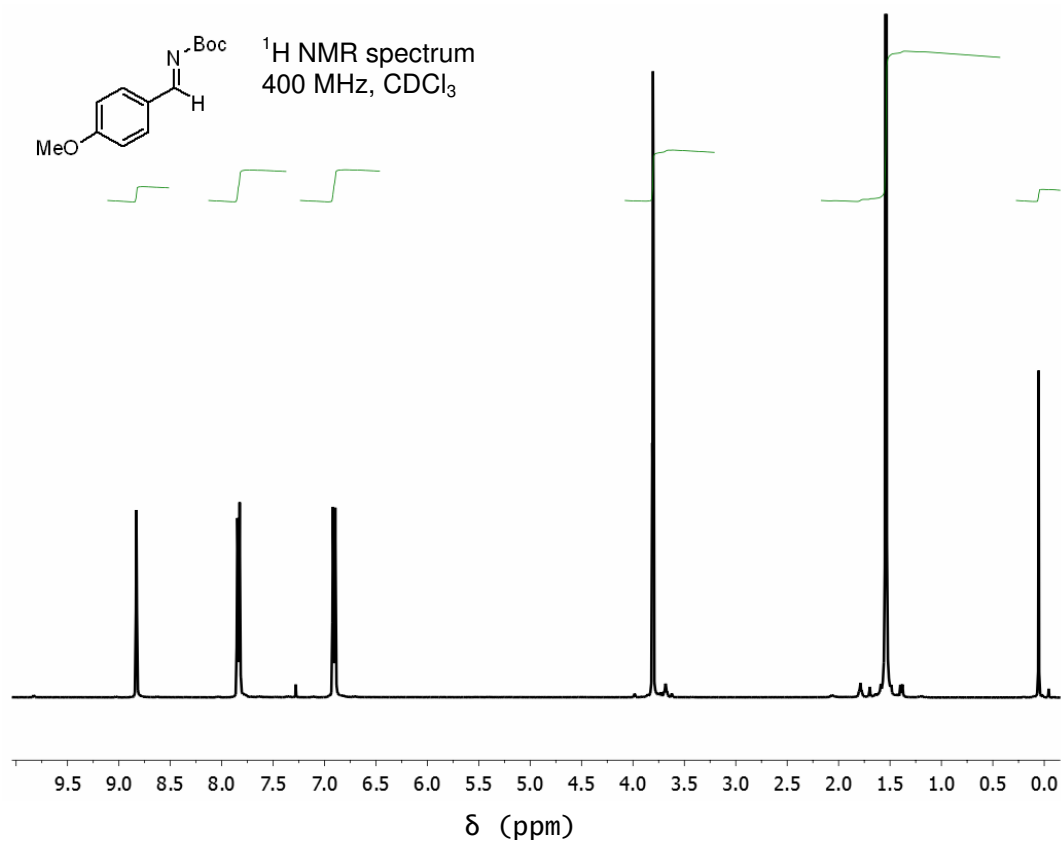
Appendix E Supplementary NMR spectra

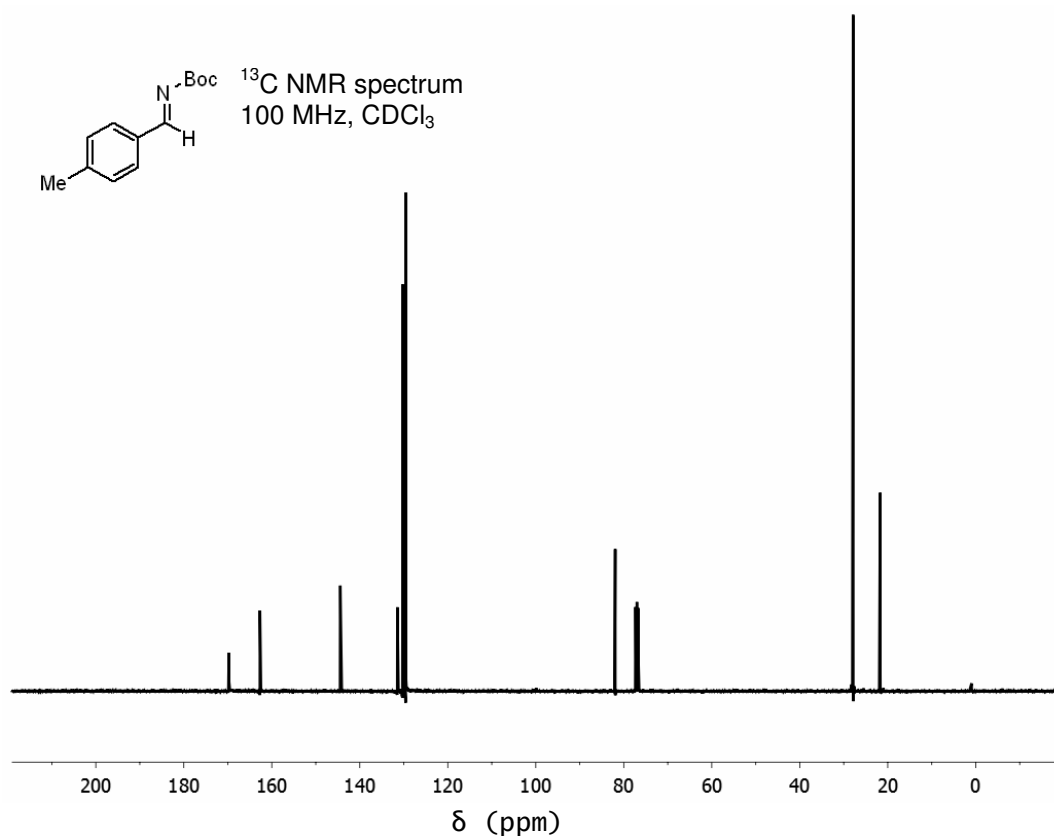
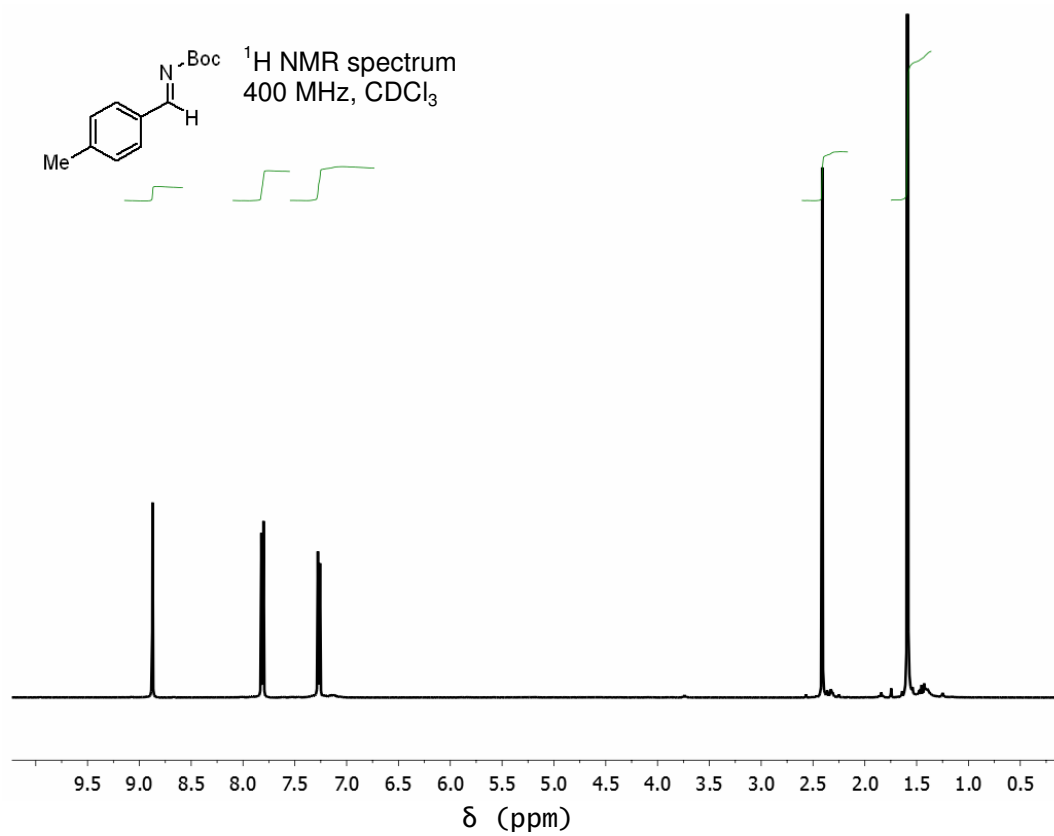


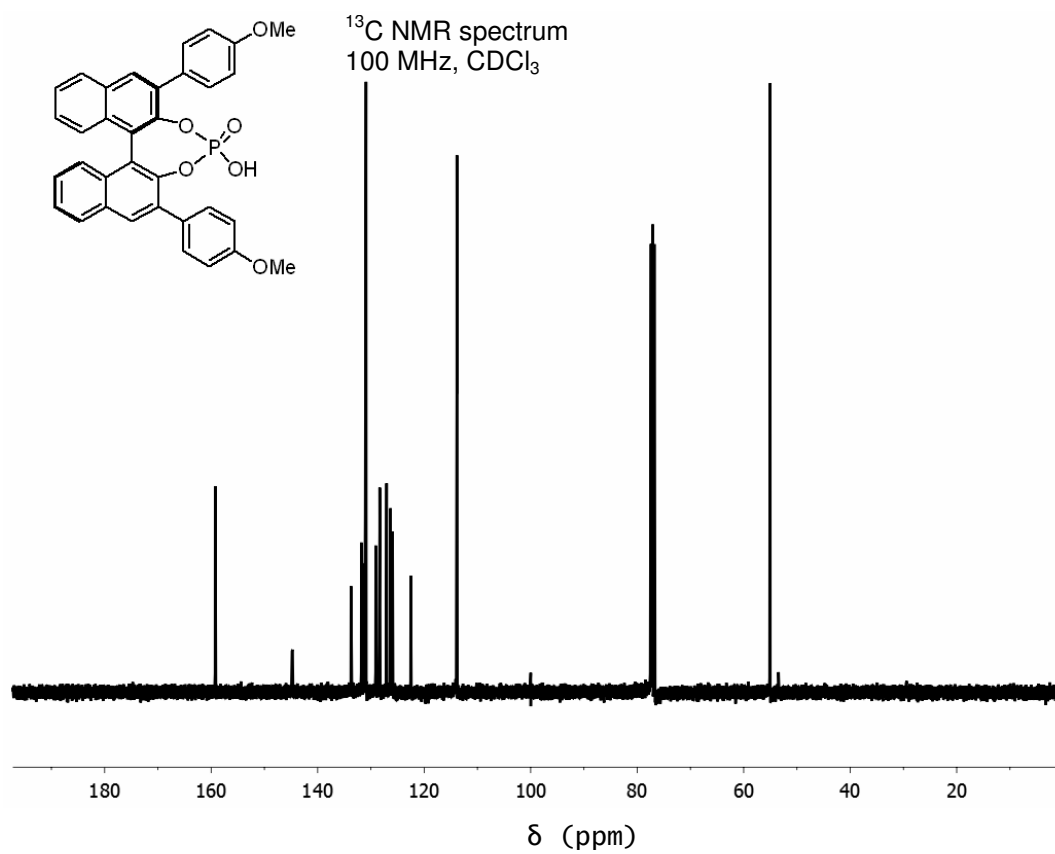
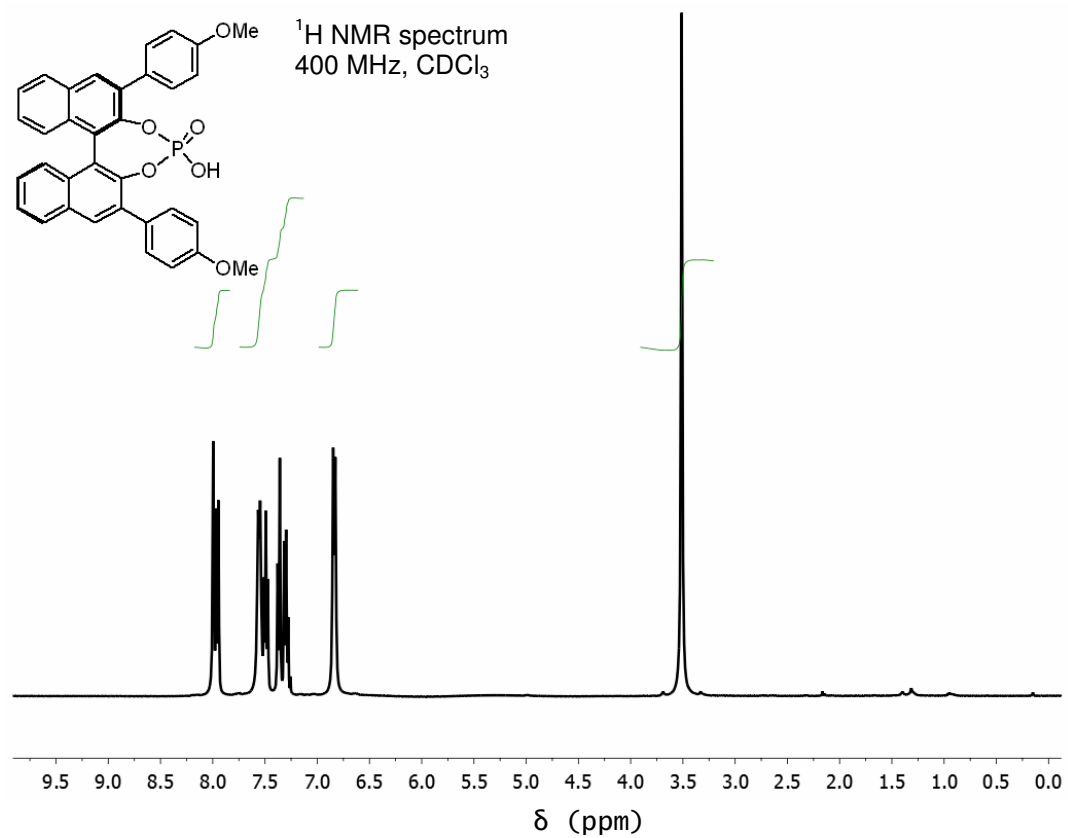


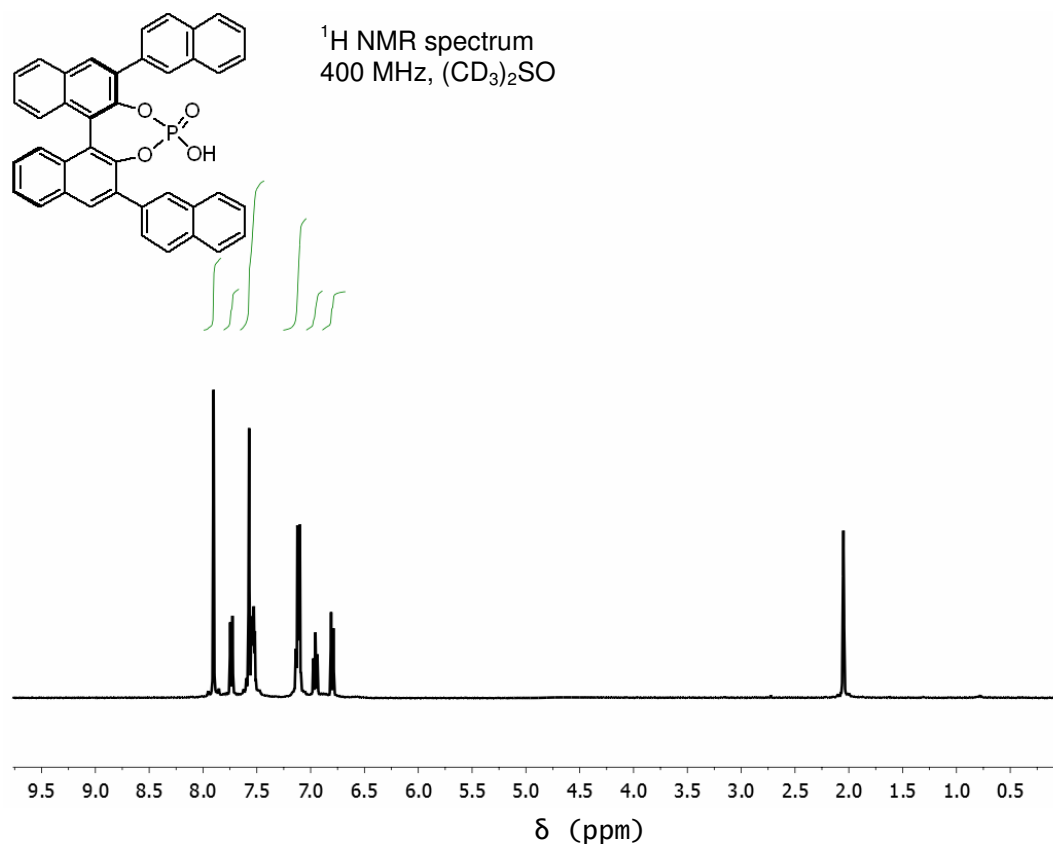
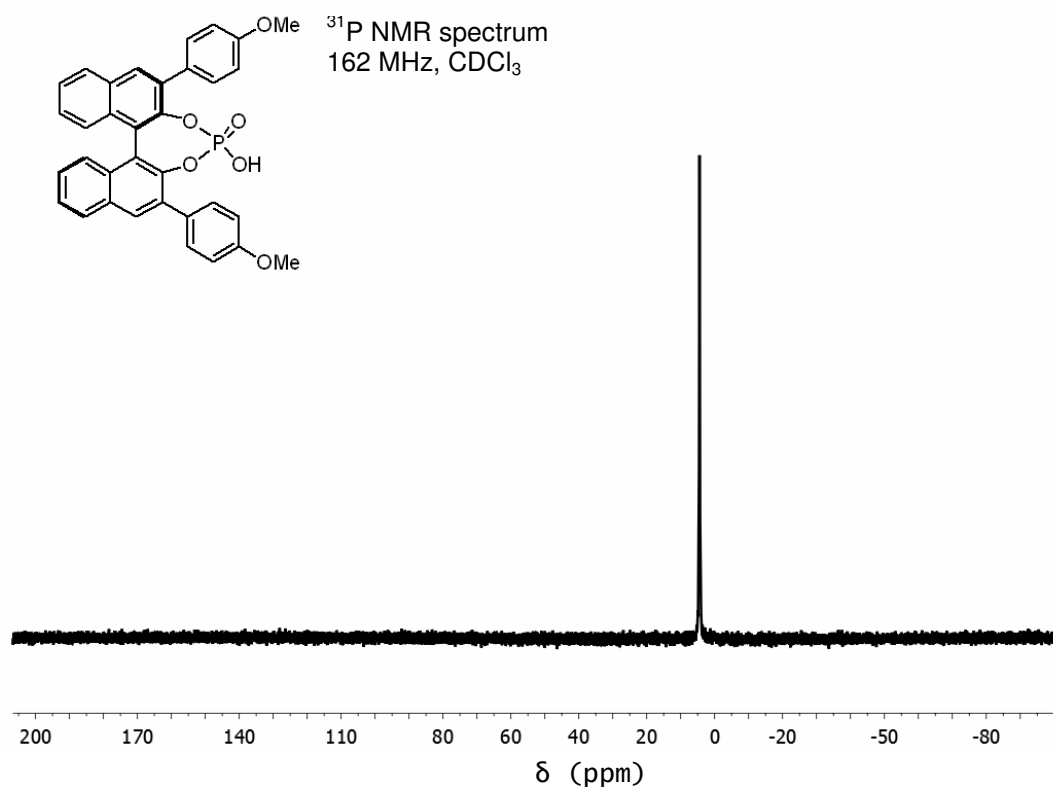


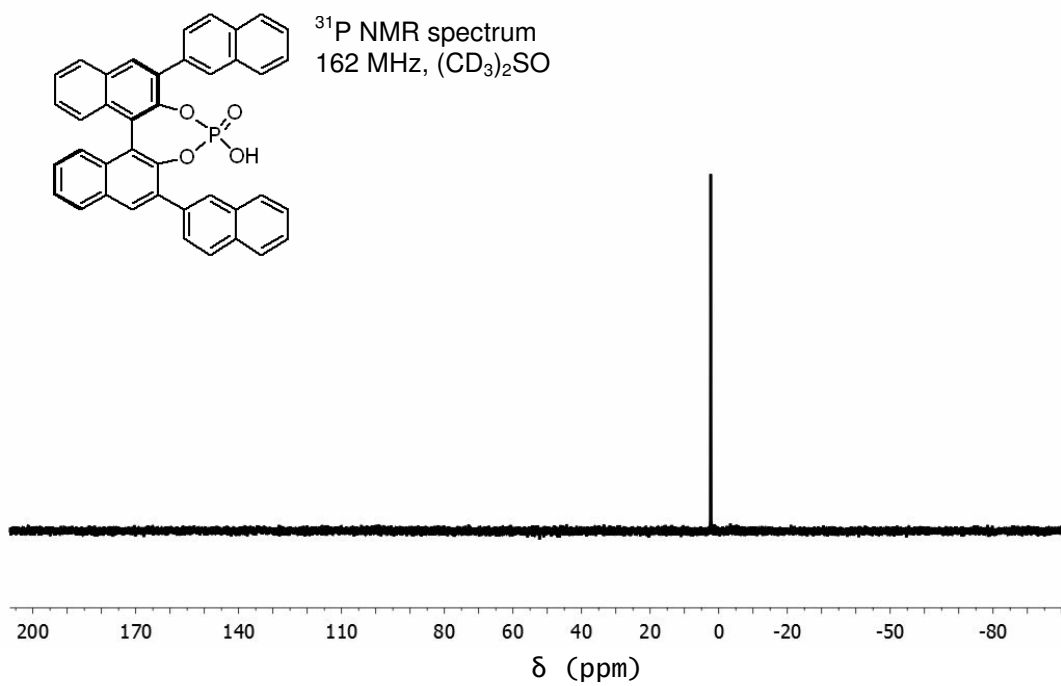
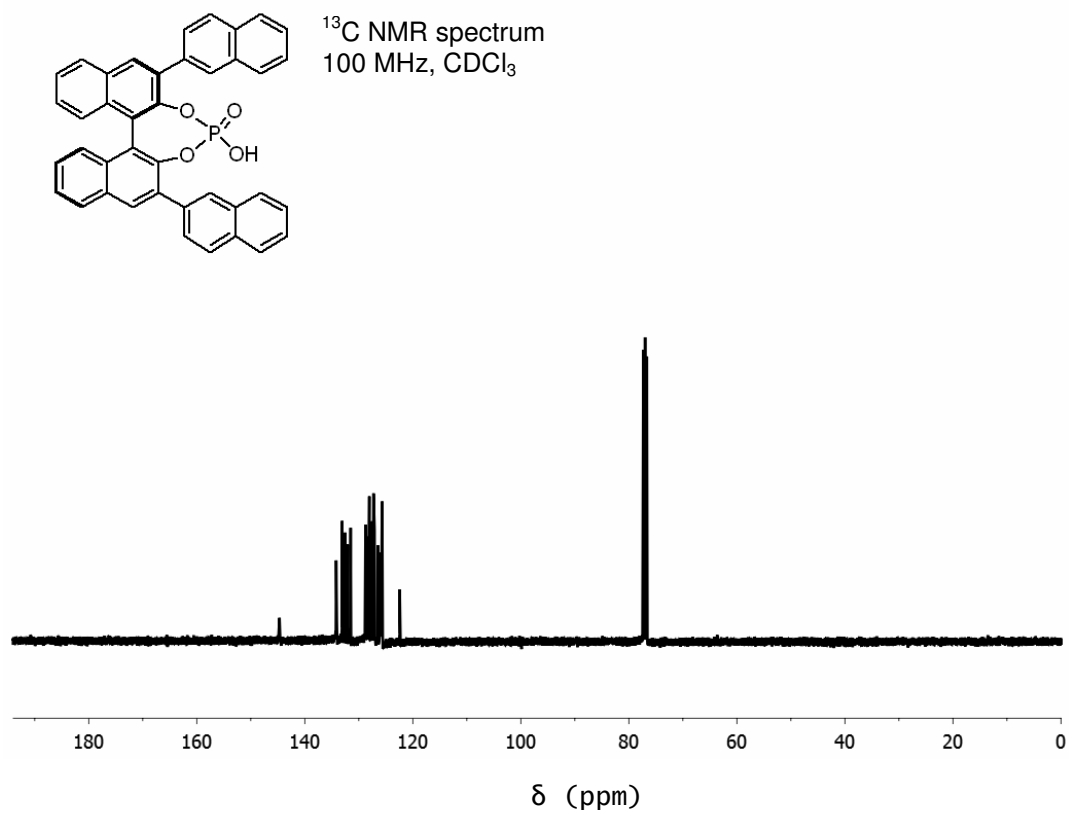


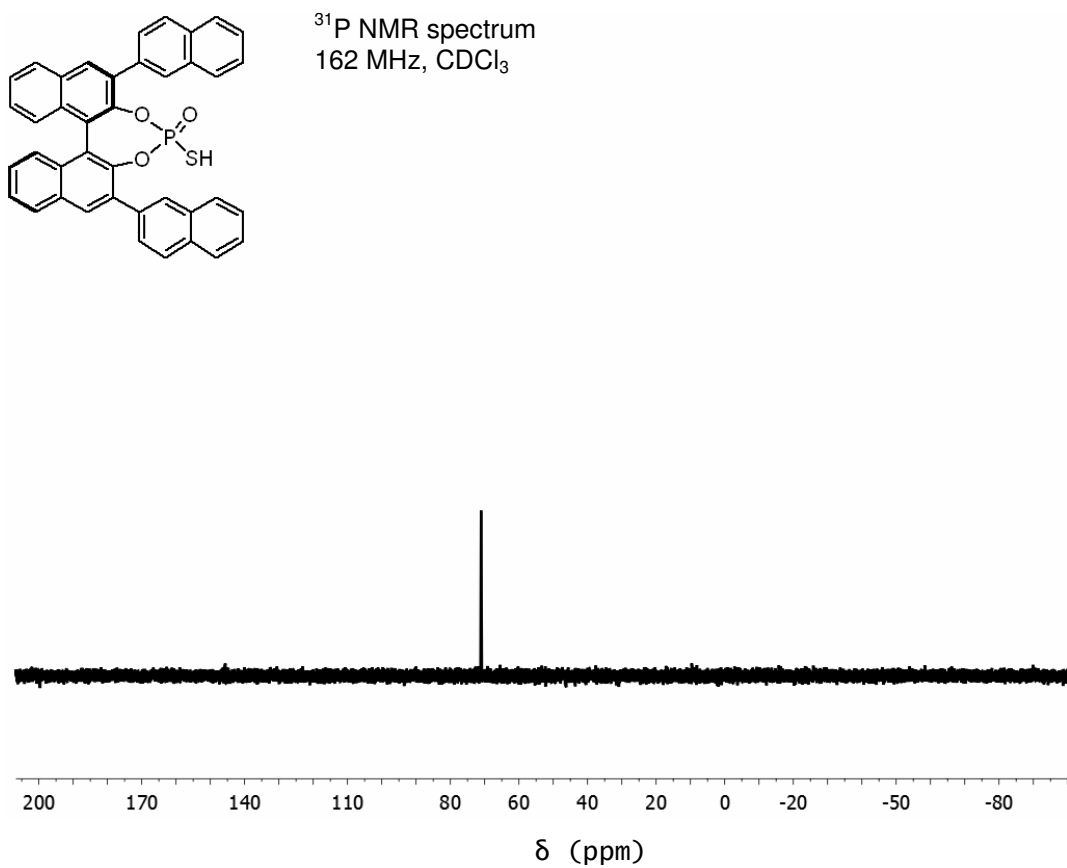
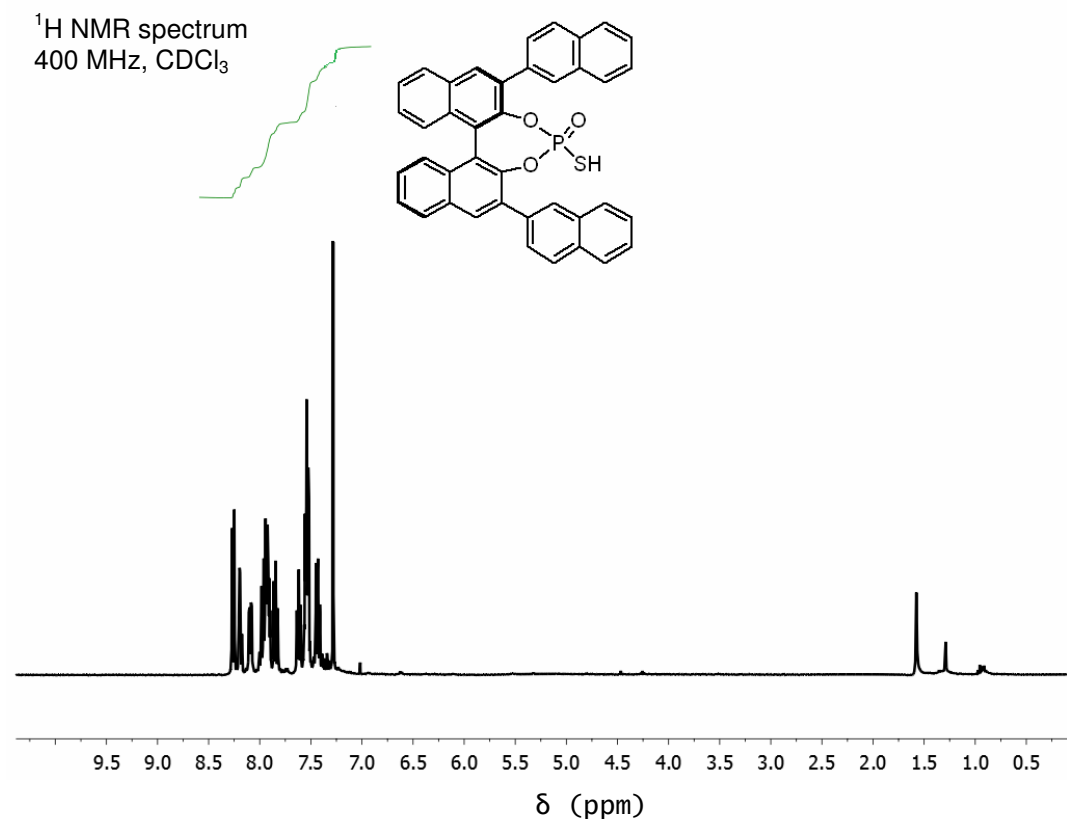




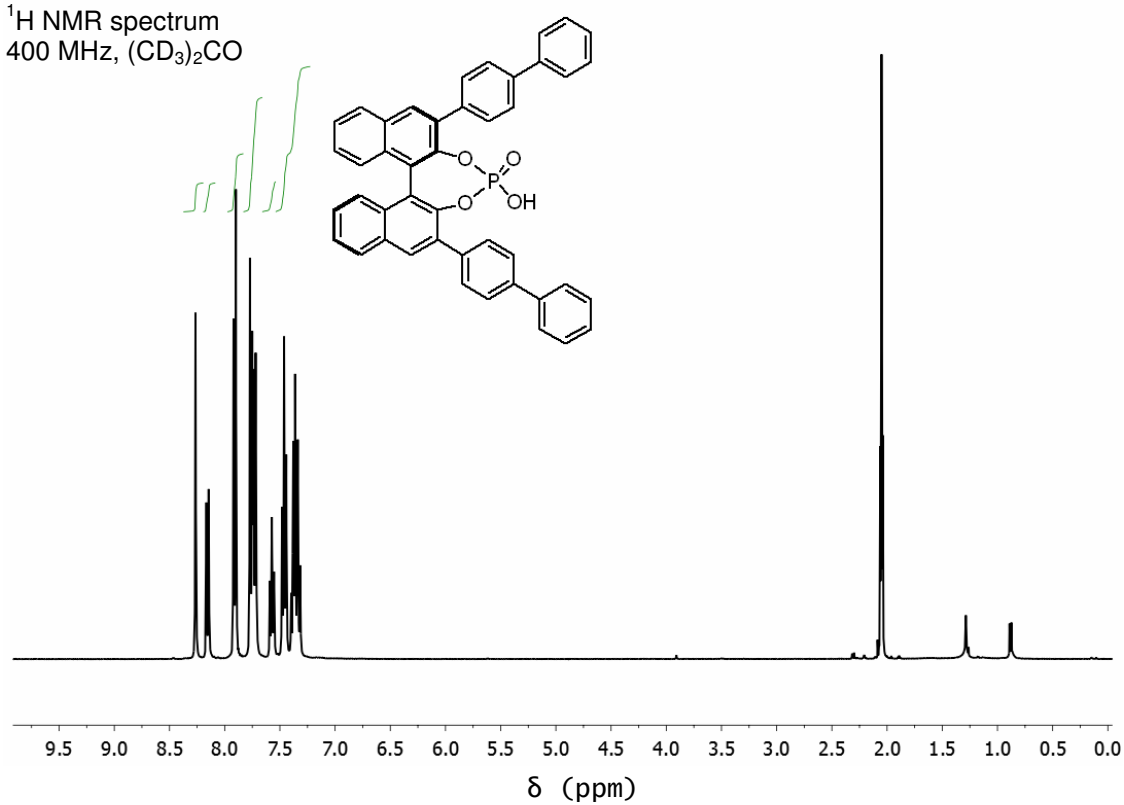




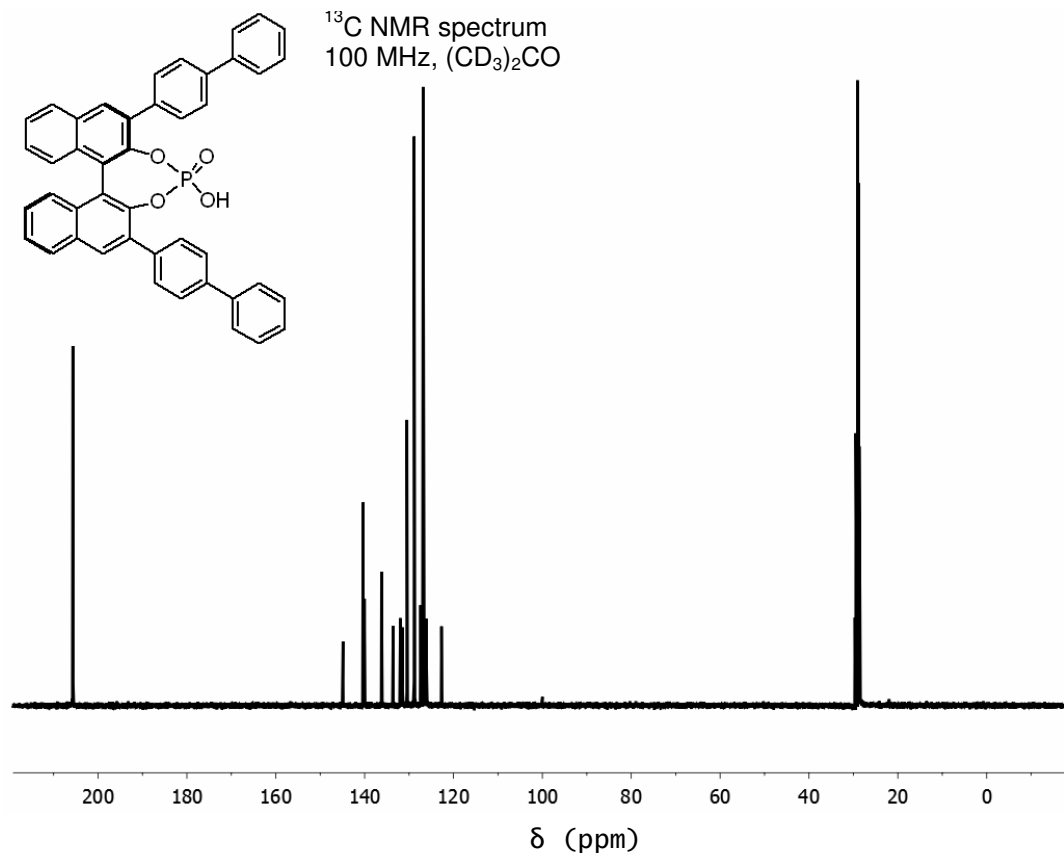


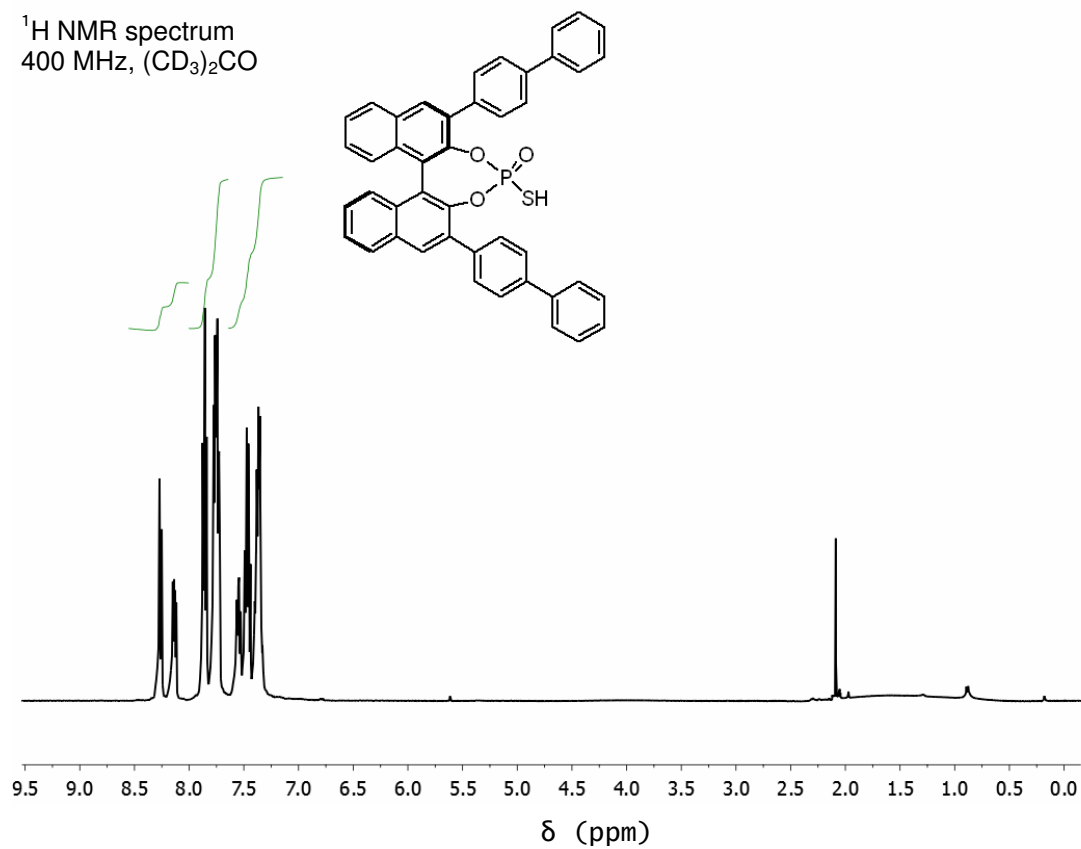
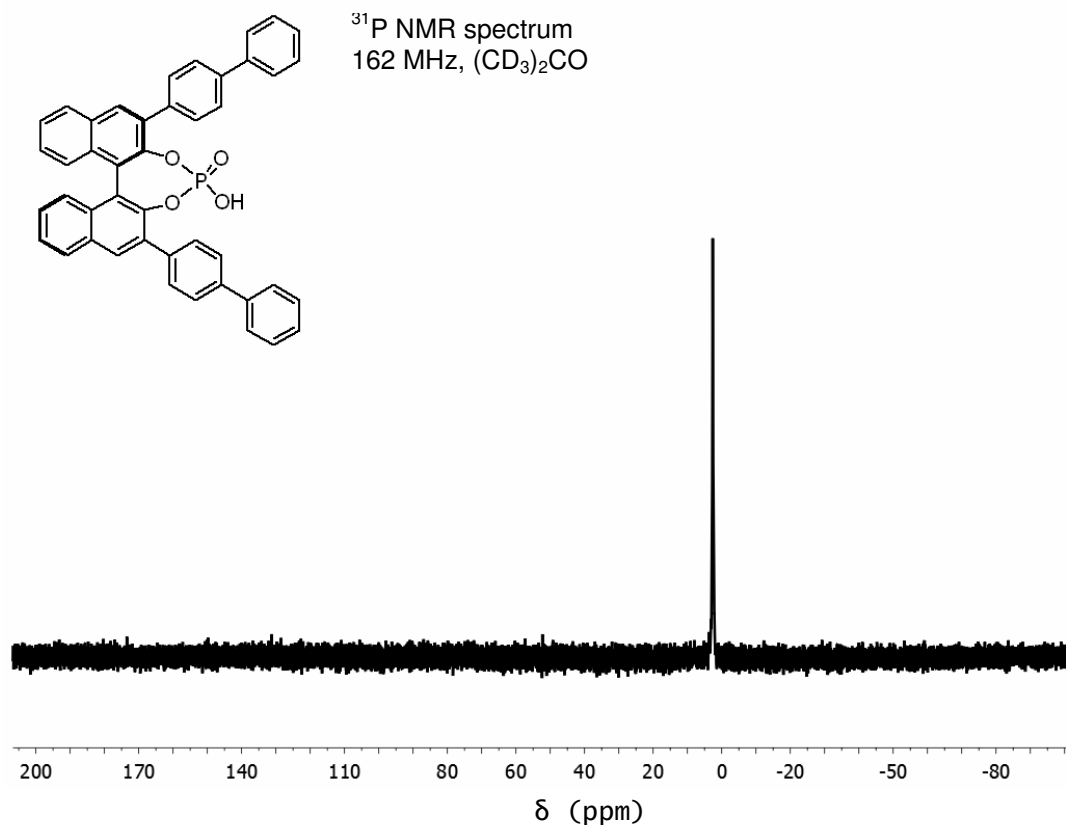


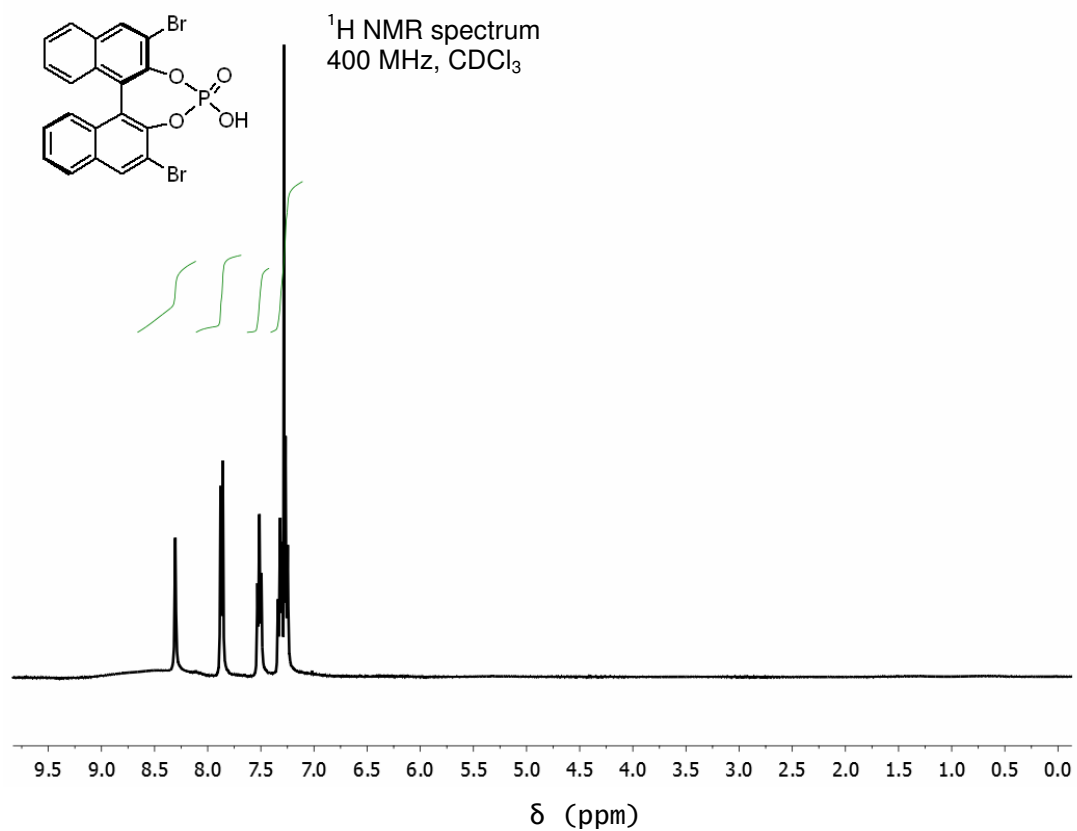
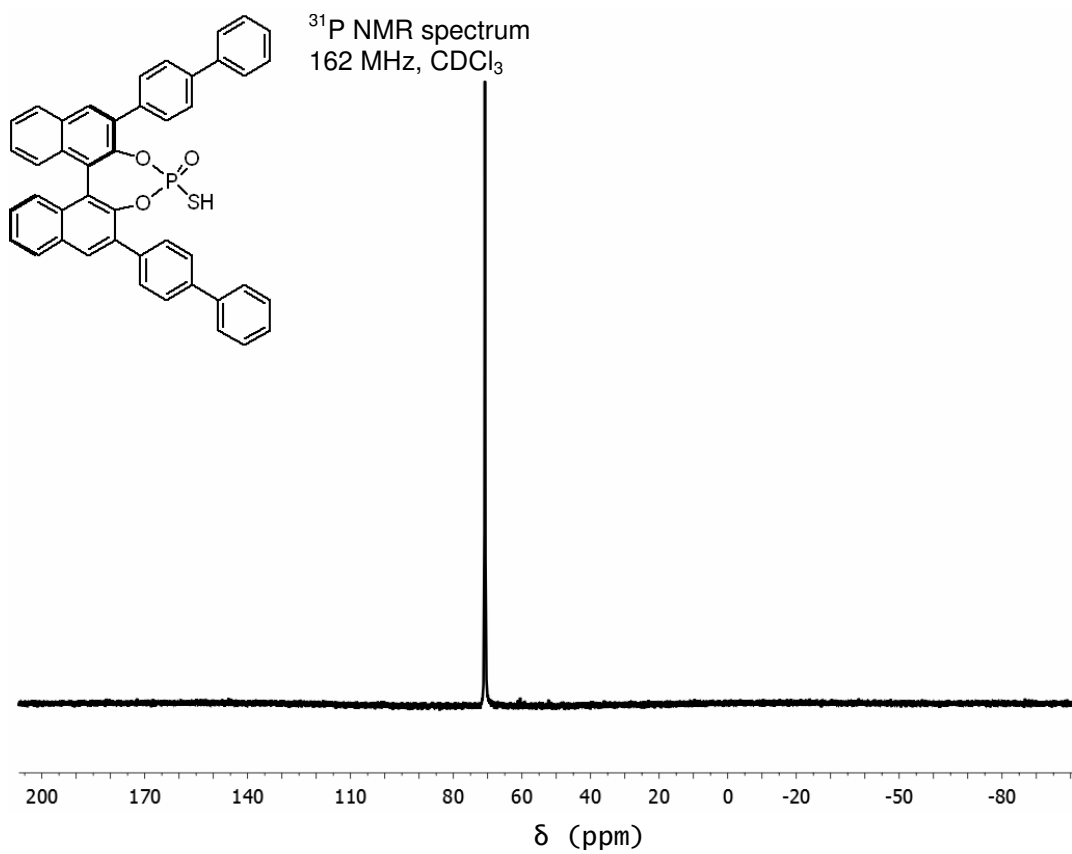
^1H NMR spectrum
400 MHz, $(\text{CD}_3)_2\text{CO}$

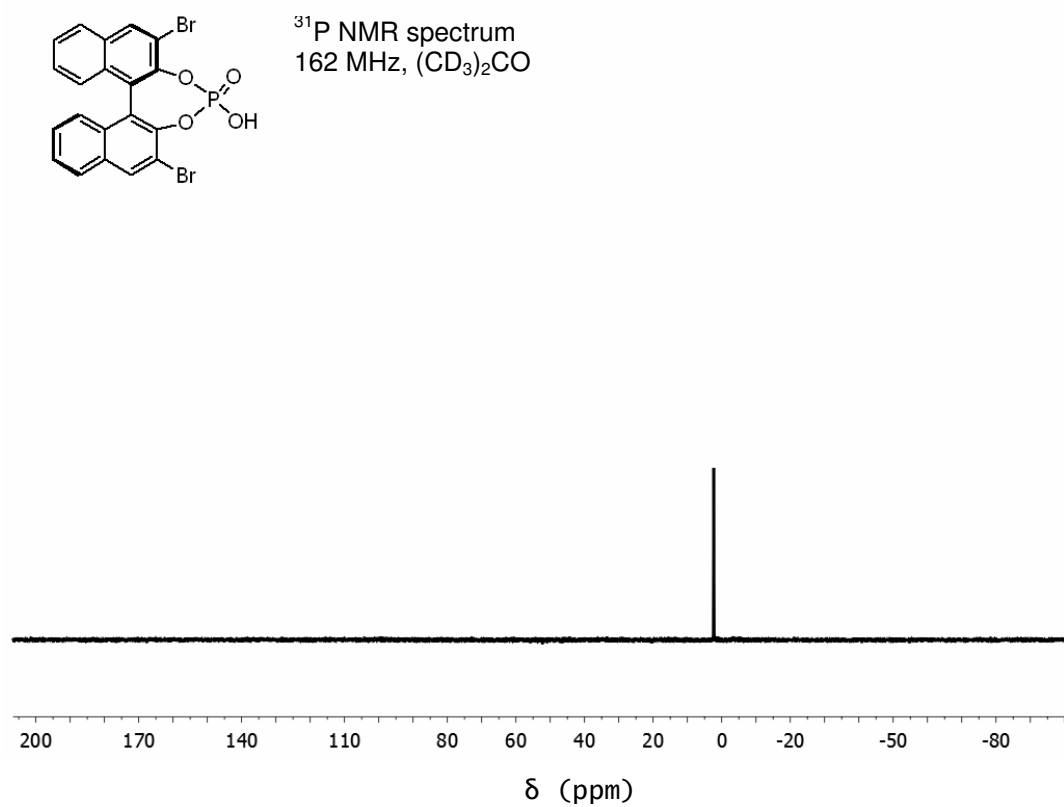
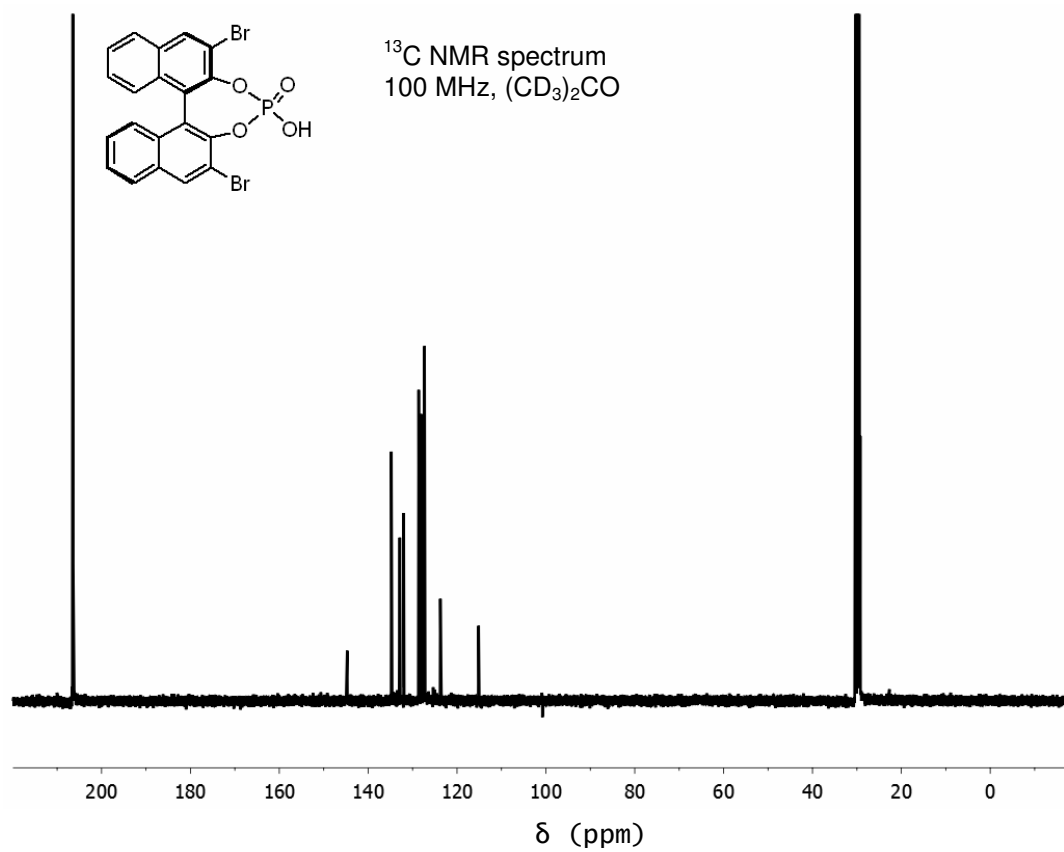


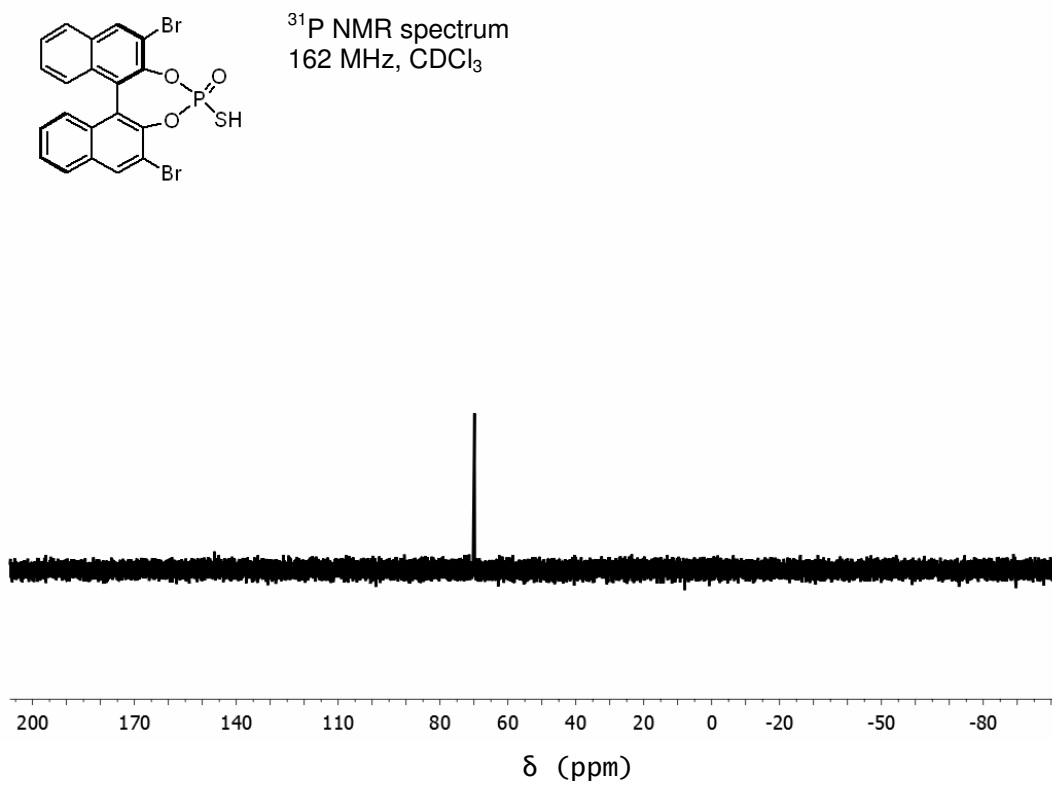
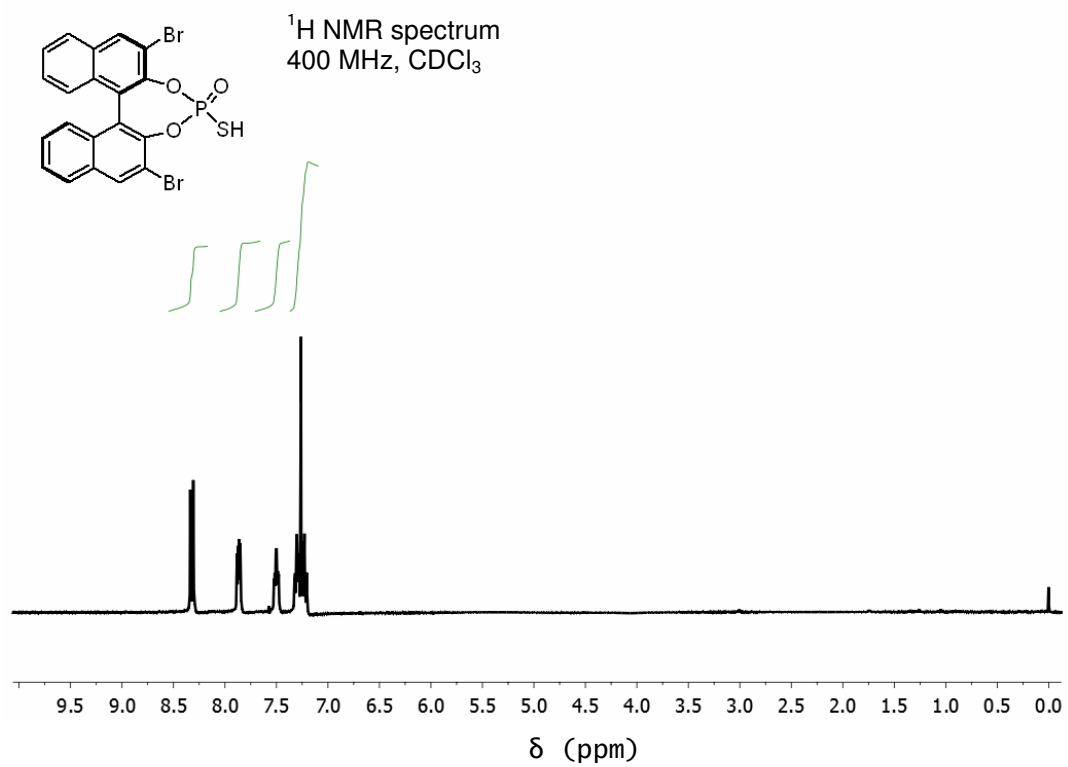
^{13}C NMR spectrum
100 MHz, $(\text{CD}_3)_2\text{CO}$

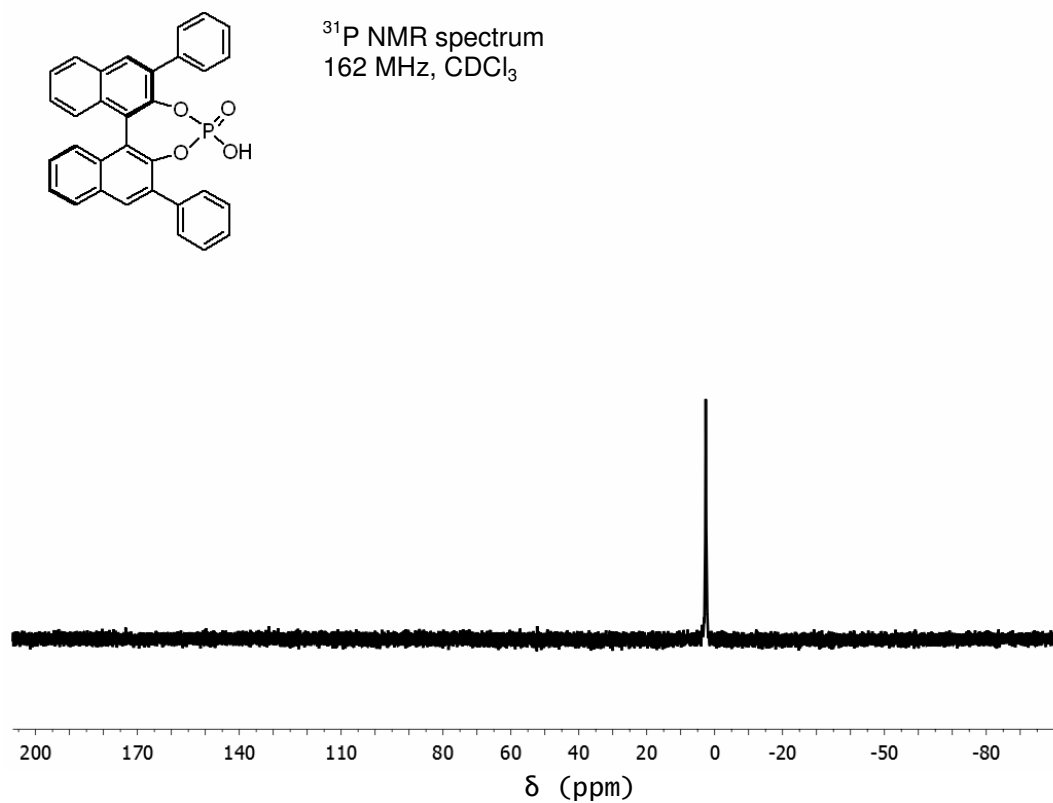
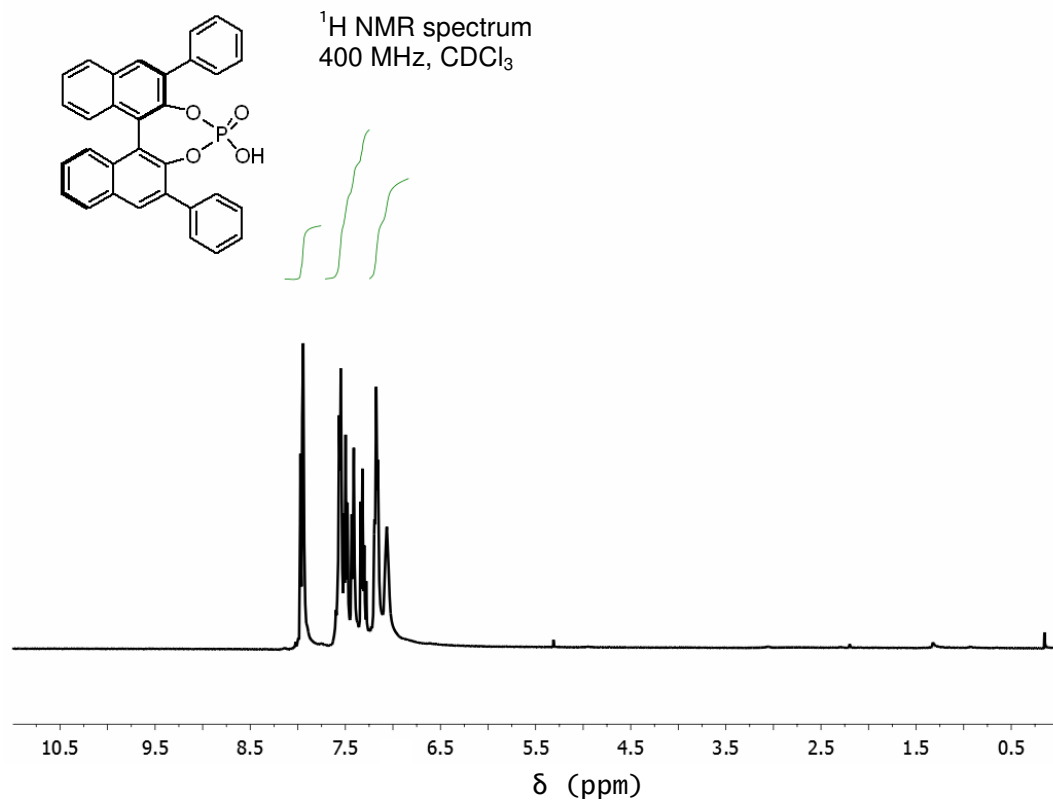


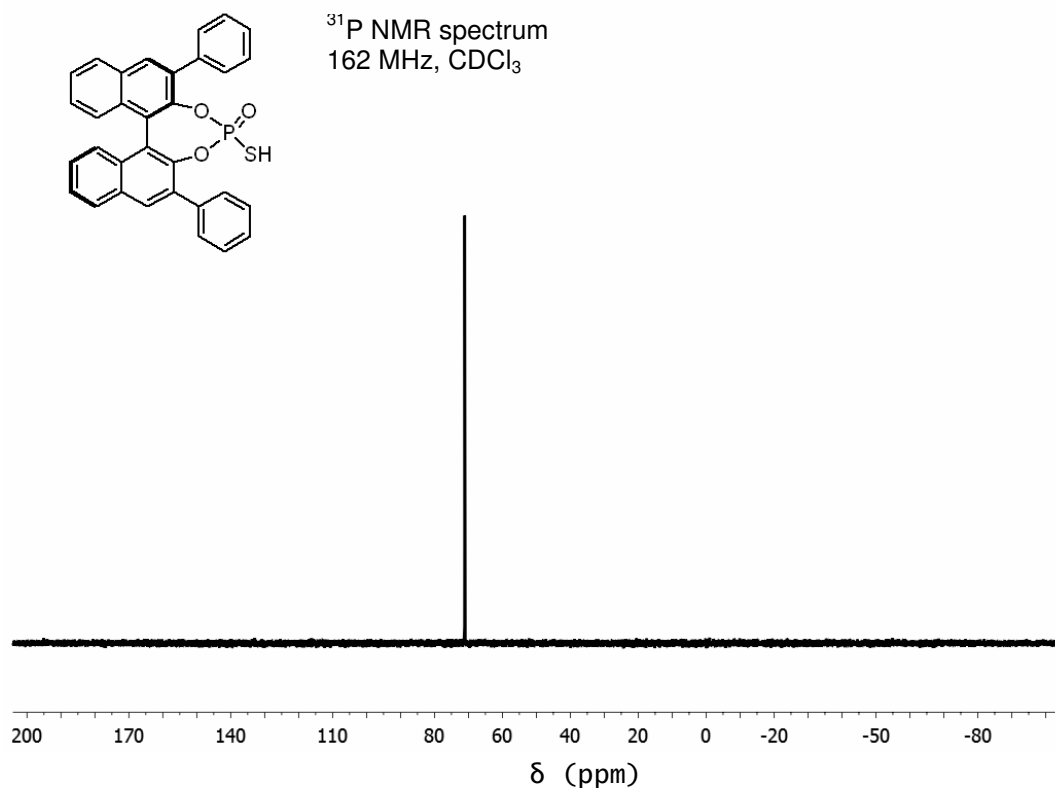
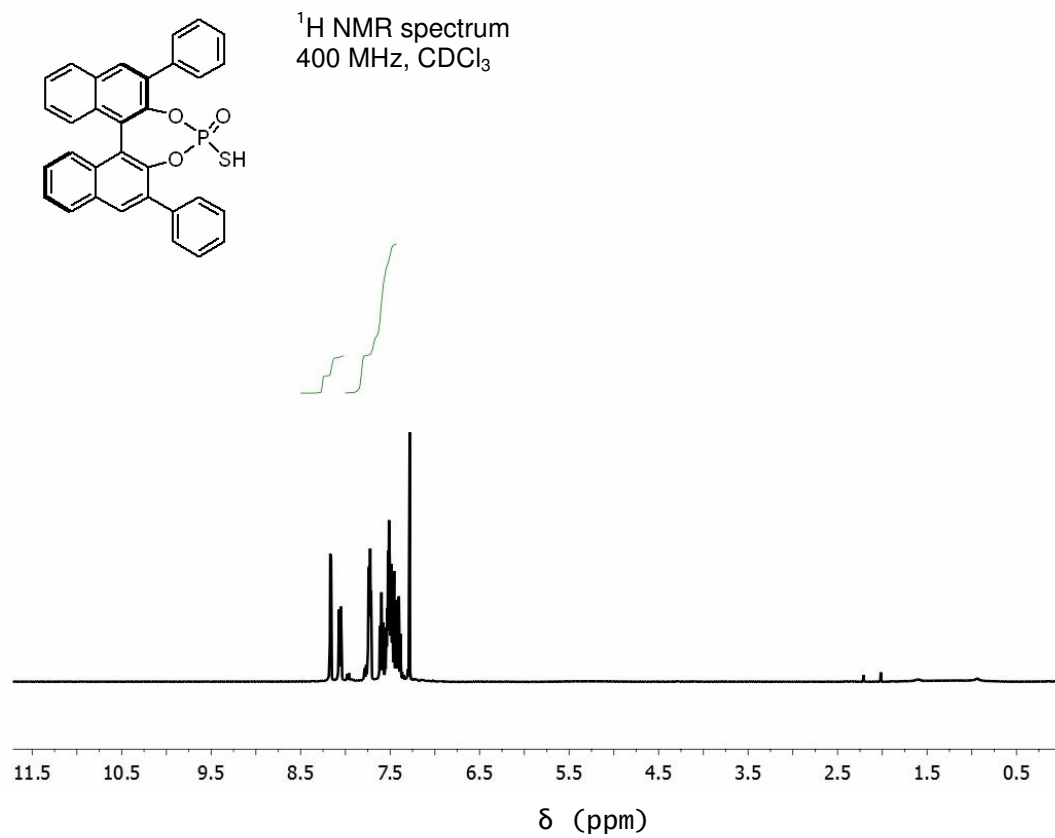


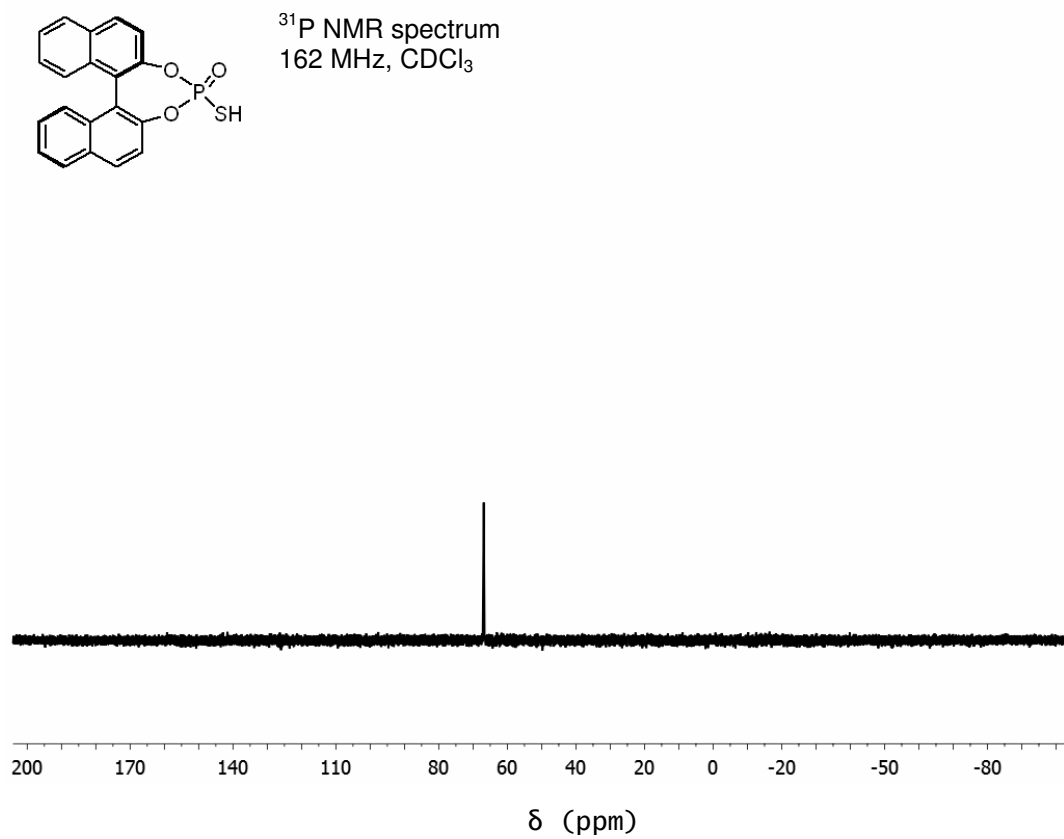
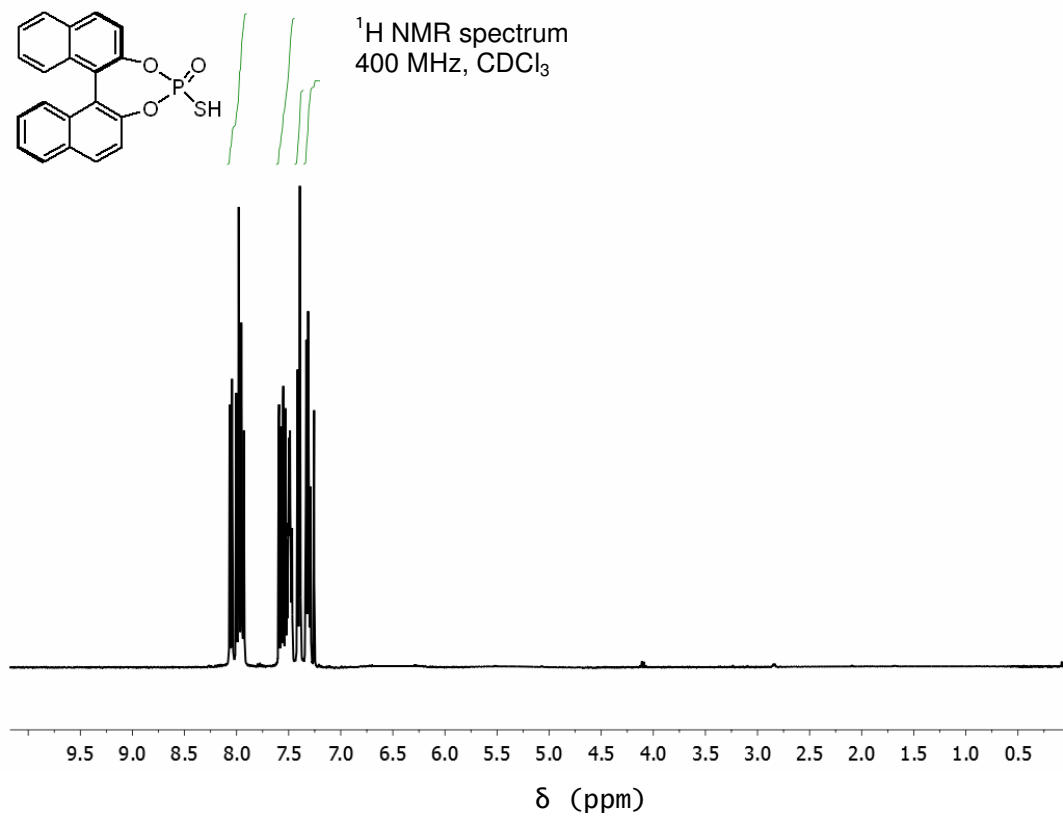


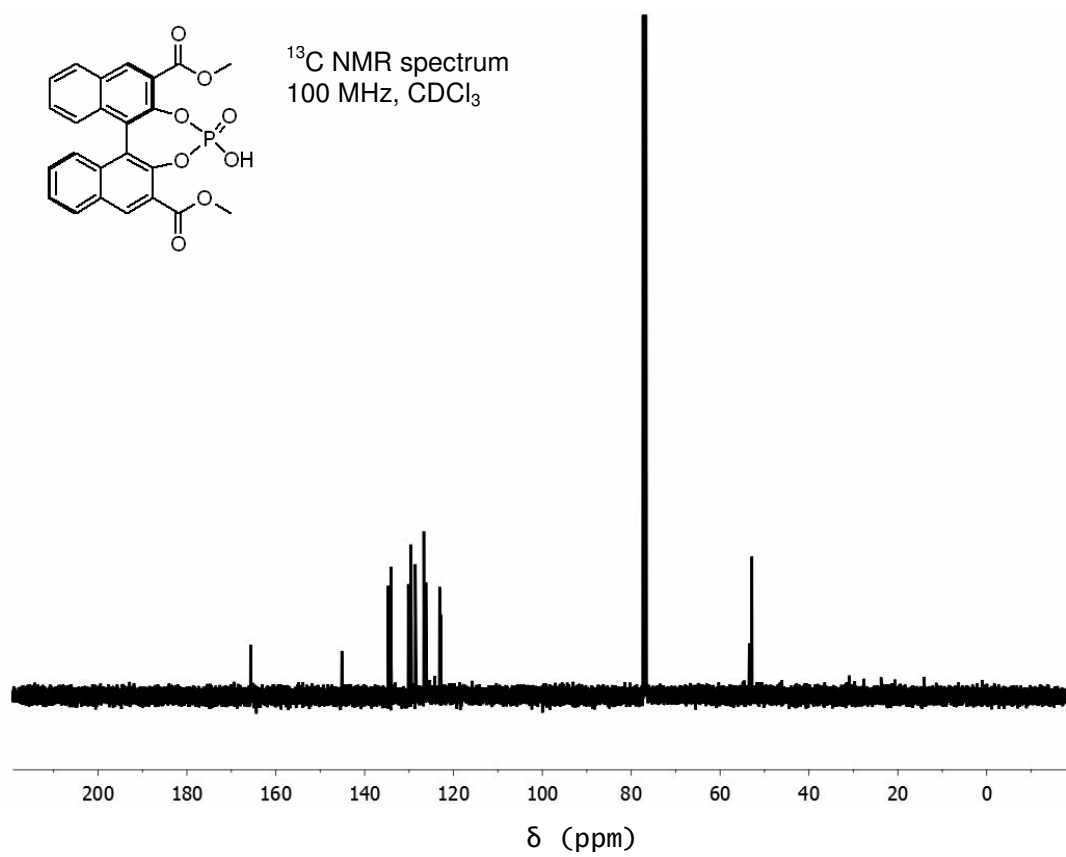
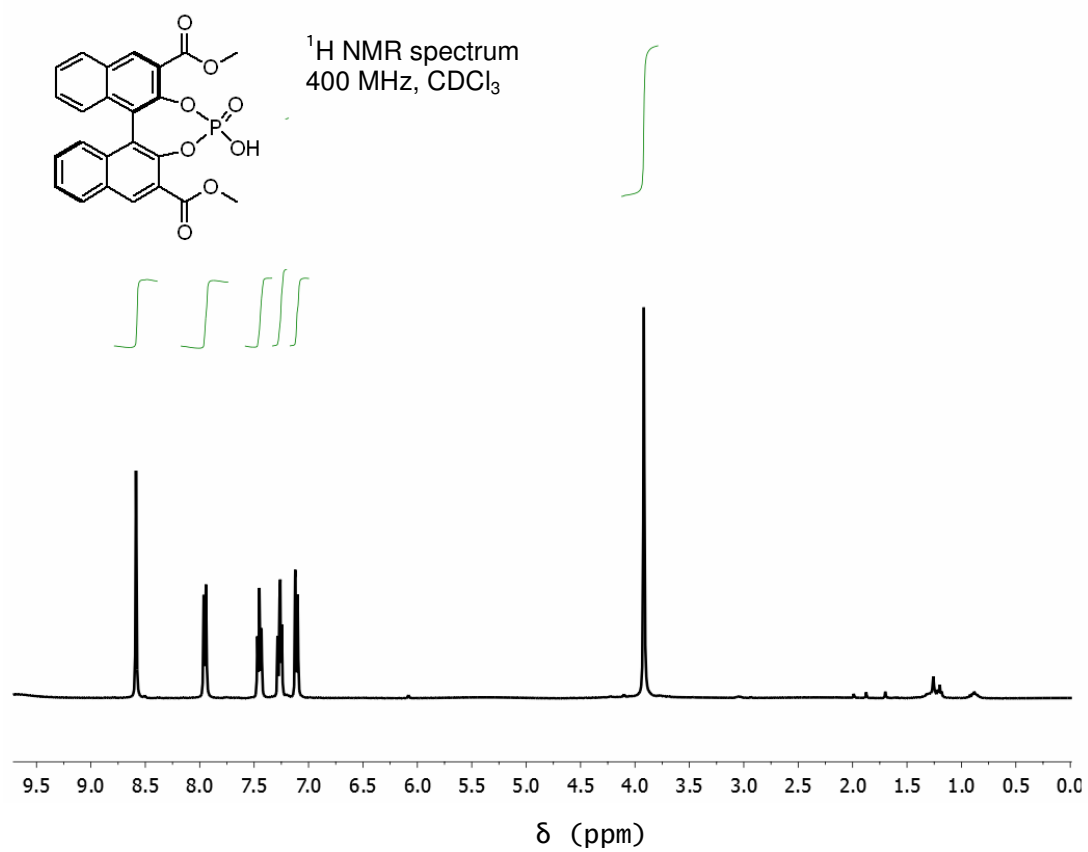


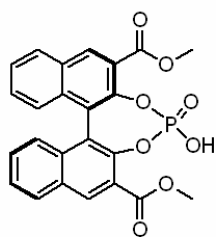












³¹P NMR spectrum
162 MHz, CDCl₃

